(12) INTERNATIONAL APPLICATION PUBLISHED UNDER THE PATENT COOPERATION TREATY (PCT)

(19) World Intellectual Property Organization
International Bureau

(43) International Publication Date
16 May 2019 (16.05.2019)

WIPO | PCT

(10) International Publication Number
WO 2019/094830 A1

(51) International Patent Classification:
A61K 38/04 (2006.01) *C07K 7/00* (2006.01)
A61K 38/08 (2019.01) *C07K 7/02* (2006.01)
A61K 38/10 (2006.01) *C07K 7/06* (2006.01)
A61P 25/00 (2006.01)

(21) International Application Number:
PCT/US2018/060177

(22) International Filing Date:
09 November 2018 (09.11.2018)

(25) Filing Language: English

(26) Publication Language: English

(30) Priority Data:
62/584,530 10 November 2017 (10.11.2017) US
62/584,515 10 November 2017 (10.11.2017) US
PCT/US2018/028514
20 April 2018 (20.04.2018) US

(71) Applicant *(for all designated States except US)*: **WASHINGTON UNIVERSITY** [US/US]; One Brookings Drive, St. louis, Missouri 63130 (US).

(72) Inventor; and
(71) Applicant: **DORN, II, Gerald W.** [US/US]; C/O WASHINGTON UNIVERSITY, One Brookings Drive, St. Louis, Missouri 63130 (US).

(74) Agent: **ROBERTS, Brett J.** et al.; POLSINELLI PC, 100 South Fourth Street, Suite 1000, St. Louis, Missouri 63102 (US).

(81) Designated States *(unless otherwise indicated, for every kind of national protection available)*: AE, AG, AL, AM, AO, AT, AU, AZ, BA, BB, BG, BH, BN, BR, BW, BY, BZ, CA, CH, CL, CN, CO, CR, CU, CZ, DE, DJ, DK, DM, DO, DZ, EC, EE, EG, ES, FI, GB, GD, GE, GH, GM, GT, HN, HR, HU, ID, IL, IN, IR, IS, JO, JP, KE, KG, KH, KN, KP, KR, KW, KZ, LA, LC, LK, LR, LS, LU, LY, MA, MD, ME, MG, MK, MN, MW, MX, MY, MZ, NA, NG, NI, NO, NZ, OM, PA, PE, PG, PH, PL, PT, QA, RO, RS, RU, RW, SA, SC, SD, SE, SG, SK, SL, SM, ST, SV, SY, TH, TJ, TM, TN, TR, TT, TZ, UA, UG, US, UZ, VC, VN, ZA, ZM, ZW.

(84) Designated States *(unless otherwise indicated, for every kind of regional protection available)*: ARIPO (BW, GH, GM, KE, LR, LS, MW, MZ, NA, RW, SD, SL, ST, SZ, TZ, UG, ZM, ZW), Eurasian (AM, AZ, BY, KG, KZ, RU, TJ, TM), European (AL, AT, BE, BG, CH, CY, CZ, DE, DK, EE, ES, FI, FR, GB, GR, HR, HU, IE, IS, IT, LT, LU, LV, MC, MK, MT, NL, NO, PL, PT, RO, RS, SE, SI, SK, SM, TR), OAPI (BF, BJ, CF, CG, CI, CM, GA, GN, GQ, GW, KM, ML, MR, NE, SN, TD, TG).

(54) **Title:** MITOFUSIN MODULATION AGENTS AND METHODS OF USE THEREOF

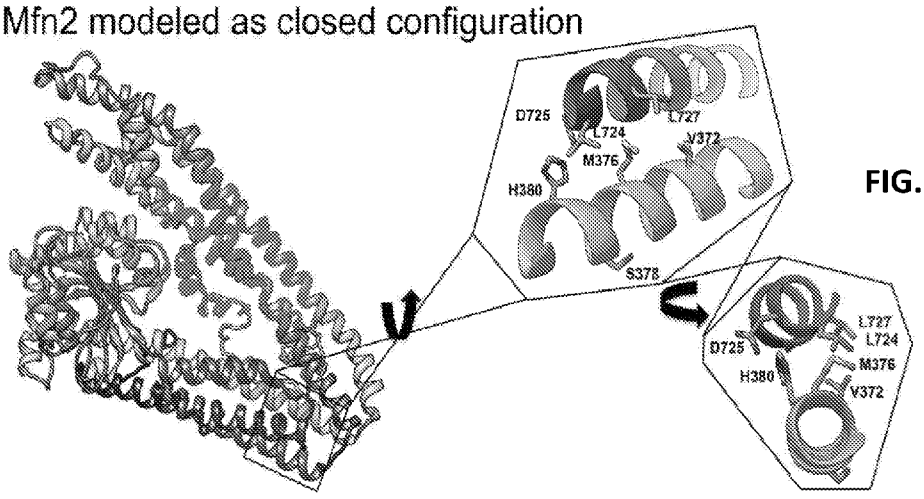

FIG. 1A

(57) **Abstract:** Compositions comprising small molecule modulatory regulators (mitofusin modulatory agents) are described. The mitofusin modulatory agents are useful for treating diseases or disorders associated with a mitochondria-associated disease, disorder, or condition such as diseases or disorders associated with mitofusin 1 (Mfn1) and/or mitofusin 2 (Mfn2), or mitochondrial dysfunction. Methods of treatment, pharmaceutical formulations, and screening methods for identifying compounds that regulate mitochondrial function are also described.

WO 2019/094830 A1

[Continued on next page]

Published:

— *with international search report (Art. 21(3))*
— *before the expiration of the time limit for amending the claims and to be republished in the event of receipt of amendments (Rule 48.2(h))*
— *with sequence listing part of description (Rule 5.2(a))*

MITOFUSIN MODULATION AGENTS AND METHODS OF USE THEREOF

CROSS-REFERENCE TO RELATED APPLICATIONS

[0001] This application claims the benefit of PCT application number PCT/US2018/028514 filed on April 20, 2018, which claims priority from U.S. Provisional Application Serial No. 62/488,787 filed on 23 April 2017, U.S. Provisional Application Serial No. 62/584,530 filed on 10 November 2017 and U.S. Provisional Application Serial No. 62/584,515 filed on 10 November 2017, each of the disclosures of which are incorporated herein by reference in their entirty.

STATEMENT REGARDING FEDERALLY SPONSORED RESEARCH OR DEVELOPMENT

[0002] This invention was made with government support under grant number HL 135736 awarded by National Institutes of Health. The government has certain rights in the invention.

MATERIAL INCORPORATED-BY-REFERENCE

[0003] The Sequence Listing, which is a part of the present disclosure, includes a computer readable form comprising nucleotide and/or amino acid sequences of the present invention. The subject matter of the Sequence Listing is incorporated herein by reference in its entirety.

FIELD OF THE INVENTION

[0004] The present disclosure generally relates to compositions and methods for treating mitochondria-associated diseases, disorders, or conditions. Also provided are methods for screening compositions.

SUMMARY

[0005] Among the various aspects of the present disclosure is the provision of a small molecule regulator of mitochondrial fusion and methods of use thereof.

[0006] One aspect of the present disclosure provides for a method of treating a mitochondria-associated disease, disorder, or condition. In some embodiments, the method comprises administering to a subject a therapeutically

effective amount of a composition comprising one or more of a mitofusin modulating agent or a pharmaceutically acceptable salt thereof, wherein the mitofusin modulating agent is a mitofusin agonist; the mitofusin modulating agent regulates mitochondrial fusion.

[0007] Another aspect of the present disclosure provides for a method of modulating mitofusin in a subject in need thereof. In some embodiments, the method comprises administering to a subject a composition comprising a mitofusin modulating agent or a pharmaceutically acceptable salt thereof; wherein, the mitofusin modulating agent is a mitofusin agonist; the mitofusin modulating agent regulates mitochondrial fusion; the subject has a mitochondria-associated disease, disorder, or condition; or the mitofusin modulating agent is not a compound of TABLE 4.

[0008] Another aspect of the present disclosure provides for a method of enhancing mitochondrial trafficking in nerve axons in a subject in need thereof. In some embodiments, the method comprises administering to a subject a composition comprising a mitofusin modulating agent or a pharmaceutically acceptable salt thereof; wherein, the mitofusin modulating agent is a mitofusin agonist; the mitofusin modulating agent regulates mitochondrial fusion; the subject has a mitochondria-associated disease, disorder, or condition; or the mitofusin modulating agent is not a compound of TABLE 4.

[0010] In some embodiments, the mitofusin modulating agent is a small molecule mimetic of a Mfn2 peptide-peptide interface.

[0011] In some embodiments, the mitofusin modulating agent: has substantially similar functional potency and specificity of both 1-[2-(benzylsulfanyl)ethyl]-3-(2-methylcyclohexyl)urea (Cpd A) and 2-{2-[(5-cyclopropyl-4-phenyl-4H-1,2,4-triazol-3-yl)sulfanyl]propanamido}-4H,5H,6H-cyclopenta[b]thiophene-3-carboxamide (Cpd B); targets at least two phosphorylated forms of MFN; or stimulates mitofusin activity (e.g., fusion and trafficking).

[0012] In some embodiments, the mitofusin modulating agent: enhances mitochondrial trafficking in nerve axons; increases microsomal stability; corrects cell and organ dysfunction caused by primary abnormalities in mitochondrial fission or fusion; reverses mitochondrial defects (e.g., dysmorphometry); restores, activates, regulates, modulates, promotes, or enhances the fusion, function, tethering,

transport, trafficking (e.g., axonal mitochondrial trafficking), mobility, or movement of mitochondria (in, optionally, a nerve or a neuron); enhances mitochondrial elongation or mitochondrial elongation aspect ratio; disrupts intramolecular restraints in Mfn2; allosterically activates Mfn2; corrects mitochondrial dysfunction and cellular dysfunction; repairs defects in neurons with mitochondrial mutations; or targets Mfn1 or Mfn2.

[0013] In some embodiments, the mitofusin modulating agent is selected from a compound of formula: 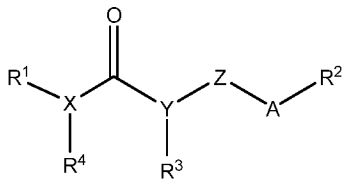 (I); 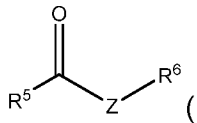 (II); or 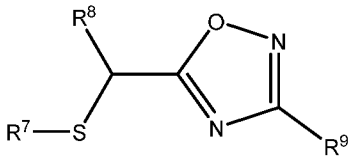 (III), or a pharmaceutically acceptable salt, tautomer, or stereoisomer thereof wherein, R^1 is selected from the group consisting of C_{1-8} alkyl, C_{1-8} alkyl substituted with S, S, thiophene, C_{3-8} cycloalkyl, C_{3-8} heteroaryl, C_{3-8} heterocyclyl, thiophene, and thiophene carboxamide; R^2 is selected from the group consisting of C_{3-8} cycloalkyl, C_{3-8} heteroaryl, C_{3-8} heterocyclyl, imidazole, thiophene, thiophene carboxamide, and triazole; R3 is absent or selected from the group consisting of hydrogen (H) and C1-8 alkyl; R4 is absent or selected form the group consisting of hydrogen (H) and C1-8 alkyl; R^5 is selected from the group consisting of C_{1-8} alkyl, C_{1-8} alkyl substituted with S, S, thiophene, C_{3-8} cycloalkyl, C_{3-8} heteroaryl, C_{3-8} heterocyclyl, thiophene, thiophene carboxamide, and triazole; R^6 is selected from the group consisting of bicyclononanone, pyrrole, benzimidizole, pyrrole substituted pyrrole, and substituted benzimidizole; R^7 is selected from the group consisting of C_{1-8} alkyl, pyrrole, pyrrole substituted pyrrole, benzimidizole, and substituted benzimidizole; R^8 is selected from the group consisting of hydrogen (H); R^9 is selected from the group consisting of C_{1-8} alkyl, pyrrole, substituted pyrrole, pyrrole substituted pyrrole, benzimidizole, and substituted benzimidizole; A is selected from the group consisting of a bond, S, C, O, and N; X is selected from the group consisting of O, C, and N;

[0014] Y is selected from the group consisting of O, C, and N; and Z is a linker group selected from the group consisting of a bond or C_{1-6} alkyl; and optionally, R^1 and R^2 form a cyclic group, R^1 and R^4 form a cyclic group, R^2 and R^3 form a cyclic group, R^4 and R^3 form a cyclic group; or R^8 and R^7 form a cyclic group, wherein, the bicyclononanone optionally comprises one or more N atoms.

[0015] In some embodiments, the mitofusin modulating agent is selected from a compound of 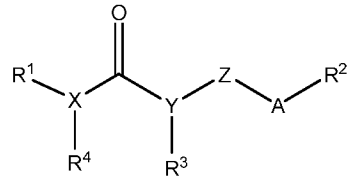 (I), wherein, R^1 is selected from the group consisting of 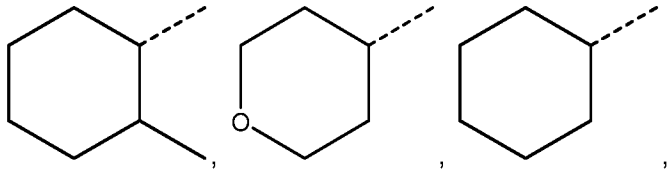 , and 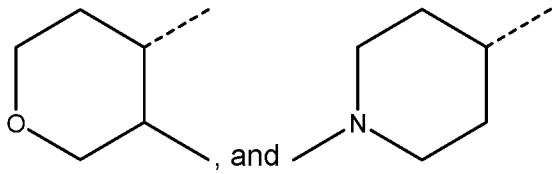 ; R^2 is selected from the group consisting of 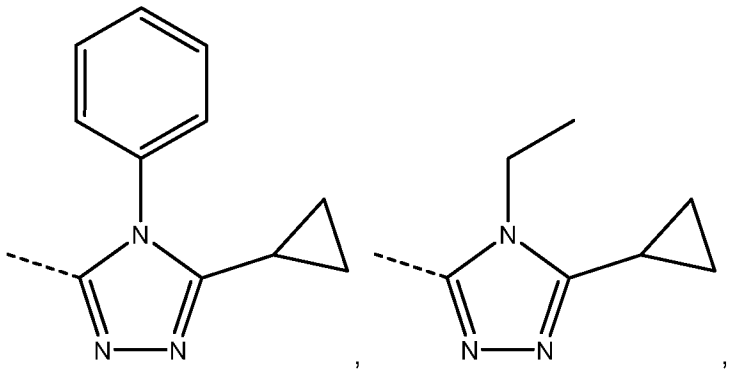 , and 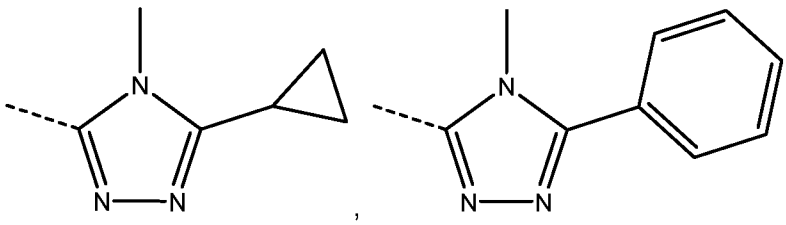 .

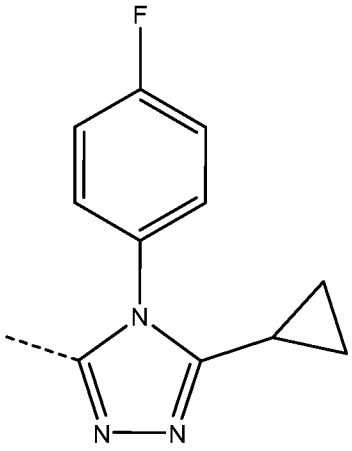

; R^3 is selected from the group consisting of hydrogen (H) and C_{1-8} alkyl; R^4 is selected form the group consisting of hydrogen (H) and C_{1-8} alkyl; A is a bond, S, SO, SO_2, C, or O;

X is N; Y is N; and Z is a linker group selected from the group consisting of a bond or C_{1-6} alkyl.

[0016] In some embodiments, R^1, R^2, R^3, or R^4 are optionally substituted by one or more of: acetamide, C_{1-8} alkoxy, amino, azo, Br, C_{1-8} alkyl, carbonyl, carboxyl, Cl, cyano, C_{3-8} cycloalkyl, C_{3-8} heteroaryl, C_{3-8} heterocyclyl, hydroxyl, F, halo, indole, N, nitrile, O, phenyl, S, sulfoxide, sulfur dioxide, or thiophene; and optionally further substituted with one or more acetamide, alkoxy, amino, azo, Br, C_{1-8} alkyl, carbonyl, carboxyl, Cl, cyano, C_{3-8} cycloalkyl, C_{3-8} heteroaryl, C_{3-8} heterocyclyl, hydroxyl, F, halo, indole, N, nitrile, O, phenyl, S, sulfoxide, sulfur dioxide, or thiophene; wherein, the alkyl, cycloalkyl, heteroaryl, heterocyclyl, indole, or phenyl, is optionally further substituted with one or more selected from the group consisting of acetamide, alkoxy, amino, azo, Br, C_{1-8} alkyl, carbonyl, carboxyl, Cl, cyano, C_{3-8} cycloalkyl, C_{3-8} heteroaryl, C_{3-8} heterocyclyl, hydroxyl, F, halo, indole, N, nitrile, O, phenyl, S, sulfoxide, sulfur dioxide, or thiophene.

[0017] In some embodiments, the compound is selected from the group consisting of:

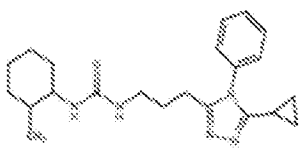

1-(3-(5-cyclopropyl-4-phenyl-4H-1,2,4-triazol-3-

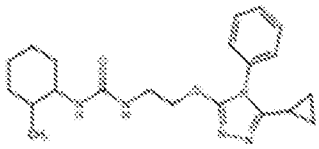

yl)propyl)-3-(2-methylcyclohexyl)urea; 1-(2-((5-cyclopropyl-4-phenyl-4H-1,2,4-triazol-3-yl)oxy)ethyl)-3-(2-methylcyclohexyl)urea;

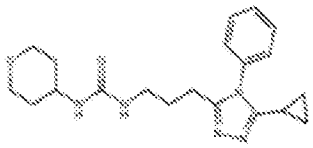

1-(3-(5-cyclopropyl-4-phenyl-4H-1,2,4-triazol-3-yl)propyl)-3-

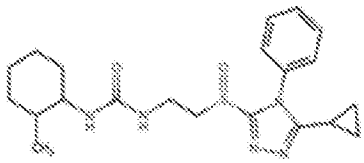

(tetrahydro-2H-pyran-4-yl)urea; 1-(2-((5-cyclopropyl-4-phenyl-4H-1,2,4-triazol-3-yl)sulfinyl)ethyl)-3-(2-methylcyclohexyl)urea;

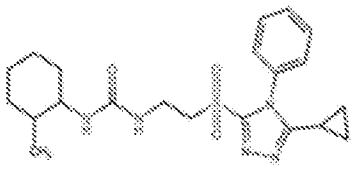

1-(2-((5-cyclopropyl-4-phenyl-4H-1,2,4-triazol-3-

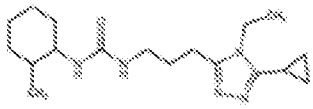

yl)sulfonyl)ethyl)-3-(2-methylcyclohexyl)urea; 1-(3-(5-cyclopropyl-4-ethyl-4H-1,2,4-triazol-3-yl)propyl)-3-(2-methylcyclohexyl)urea;

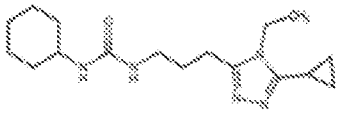

1-cyclohexyl-3-(3-(5-cyclopropyl)-4-ethyl-4H-1,2,4-

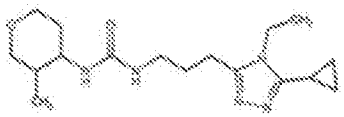

triazol-3-yl)propyl)urea; 1-(3-(5-cyclopropyl-4-ethyl-4H-1,2,4-triazol-3-yl)propyl)-3-(3-methyltetrahydro-2H-pyran-4-yl)urea;

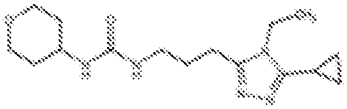

1-(3-(5-cyclopropyl-4-ethyl-4H-1,2,4-triazol-3-yl)propyl)-3-

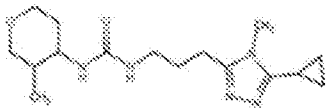

(tetrahydro-2H-pyran-4-yl)urea; 1-(3-(5-cyclopropyl-4-methyl-4H-1,2,4-triazol-3-yl)propyl)-3-(3-methyltetrahydro-2H-pyran-4-yl)urea;

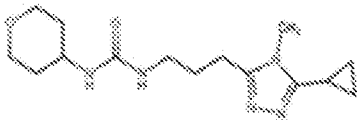

1-(3-(5-cyclopropyl-4-methyl-4H-1,2,4-triazol-3-yl)propyl)-3-(tetrahydro-2H-pyran-4-yl)urea;

1-(3-(4-methyl-5-phenyl-4H-1,2,4-triazol-3-yl)propyl)-3-(2-methylcyclohexyl)urea;

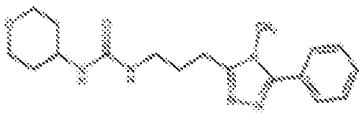

1-(3-(4-methyl-5-phenyl-4H-1,2,4-triazol-3-yl)propyl)-3-(tetrahydro-2H-pyran-4-yl)urea; or

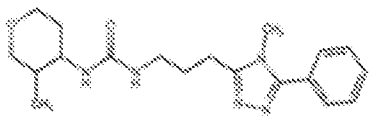

1-(3-(4-methyl-5-phenyl-4H-1,2,4-triazol-3-yl)propyl)-3-(3-methyltetrahydro-2H-pyran-4-yl)urea.

[0018] In some embodiments, the compound is selected from the group consisting of:

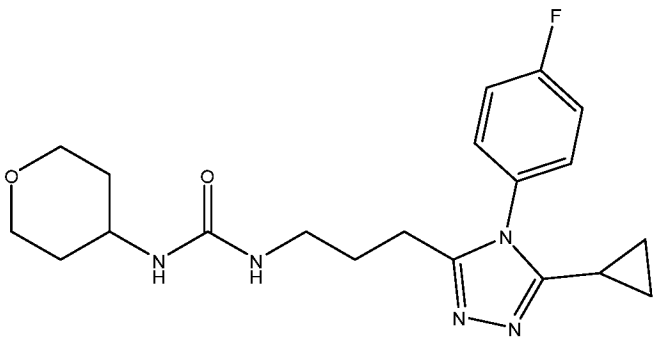

1-(3-(5-cyclopropyl-4-(4-fluorophenyl)-4H-1,2,4-triazol-3-yl)propyl)-3-(tetrahydro-2H-pyran-4-yl)urea;

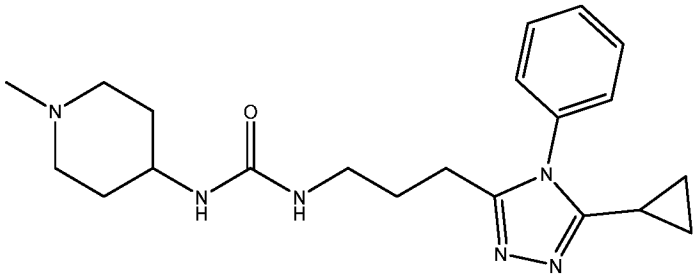

1-(3-(5-cyclopropyl-4-phenyl-4H-1,2,4-triazol-3-yl)propyl)-3-(1-methylpiperidin-4-yl)urea;

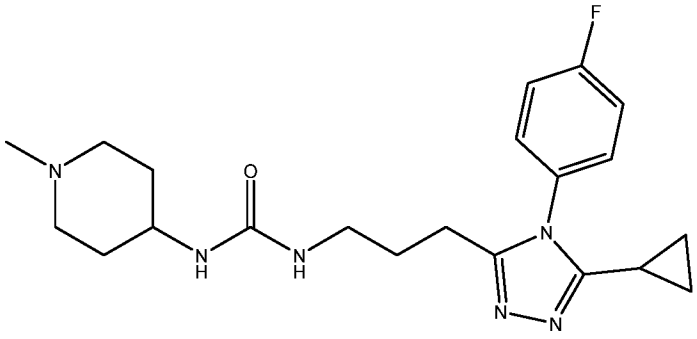

1-(3-(5-cyclopropyl-4-(4-fluorophenyl)-4H-1,2,4-triazol-3-yl)propyl)-3-(1-methylpiperidin-4-yl)urea;

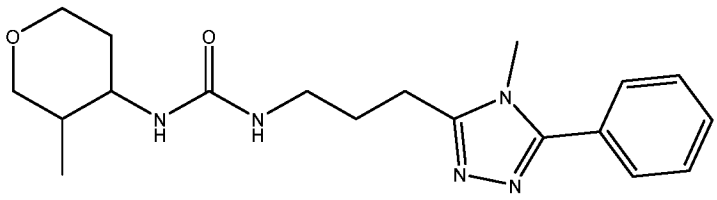

1-(3-(4-methyl-5-phenyl-4H-1,2,4-triazol-3-yl)propyl)-3-(3-methyltetrahydro-2H-pyran-4-yl)urea; and

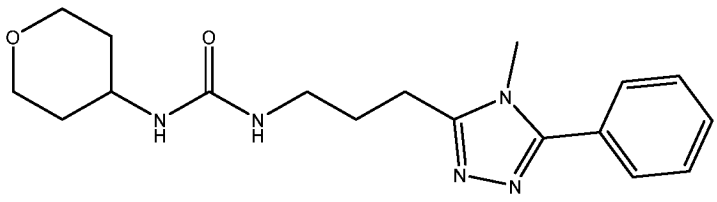

1-(3-(4-methyl-5-phenyl-4H-1,2,4-triazol-3-yl)propyl)-3-(tetrahydro-2H-pyran-4-yl)urea.

[0019] Yet another aspect of the present disclosure provides for a compound of formula:

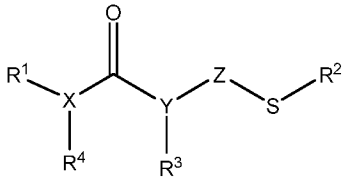

(I);

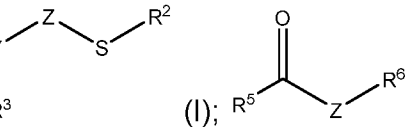

(II); or

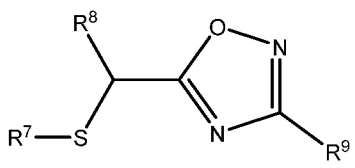

(III),

or a pharmaceutically acceptable salt, tautomer, or stereoisomer thereof

wherein, R^1 is selected from the group consisting of C_{1-8} alkyl, C_{1-8} alkyl substituted with S, S, thiophene, C_{3-8} cycloalkyl, C_{3-8} heteroaryl, C_{3-8} heterocyclyl, thiophene, and thiophene carboxamide; R^2 is selected from the group consisting of C_{3-8} cycloalkyl, C_{3-8} heteroaryl, C_{3-8} heterocyclyl, imidazole, thiophene, thiophene carboxamide, and triazole; R3 is absent or selected from the group consisting of hydrogen (H) and C1-8 alkyl; R4 is absent or selected form the group consisting of hydrogen (H) and C1-8 alkyl; R^5 is selected from the group consisting of C_{1-8} alkyl, C_{1-8} alkyl substituted with S, S, thiophene, C_{3-8} cycloalkyl, C_{3-8} heteroaryl, C_{3-8} heterocyclyl, thiophene, thiophene carboxamide, and triazole; R^6 is selected from the group consisting of bicyclononanone, pyrrole, benzimidizole, pyrrole substituted pyrrole, and substituted benzimidizole; R^7 is selected from the group consisting of C_{1-8} alkyl, pyrrole, pyrrole substituted pyrrole, benzimidizole, and substituted benzimidizole; R^8 is selected from the group consisting of hydrogen (H); R^9 is selected from the group consisting of C_{1-8} alkyl, pyrrole, substituted pyrrole, pyrrole substituted pyrrole, benzimidizole, and substituted benzimidizole; X is selected from the group consisting of O, C, and N; Y is selected from the group consisting of O, C, and N; or Z is a linker group selected from the group consisting of a bond or C_{1-6} alkyl.

[0020] In some embodiments, R^1 and R^2 form a cyclic group, R^1 and R^4 form a cyclic group, R^2 and R^3 form a cyclic group, R^4 and R^3 form a cyclic group; or R^8 and R^7 form a cyclic group, wherein, the bicyclononanone optionally comprises one or more N atoms; or formula (I), (II), or (III) is not a compound of TABLE 4, TABLE 5, TABLE 7, or 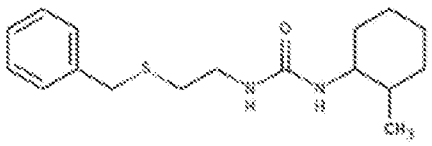 1-[2-(benzylsulfanyl)ethyl]-3-(2-methylcyclohexyl)urea; 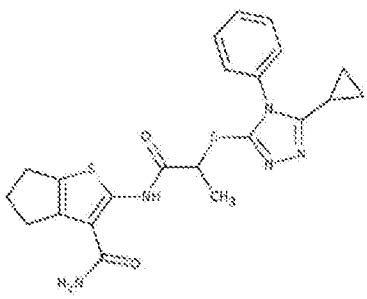 2-{2-[(5-cyclopropyl-4-phenyl-4H-1,2,4-triazol-3-yl)sulfanyl]propanamido}-4H,5H,6H-

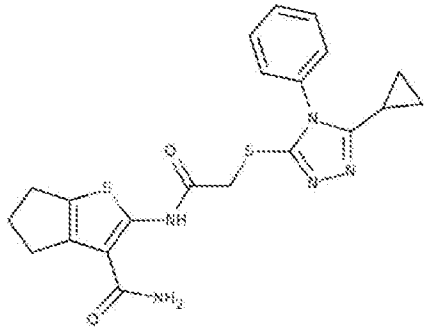

cyclopenta[b]thiophene-3-carboxamide; 2-{2-[(5-cyclopropyl-4-phenyl-4H-1,2,4-triazol-3-yl)sulfanyl]acetamido}-4H,5H,6H-

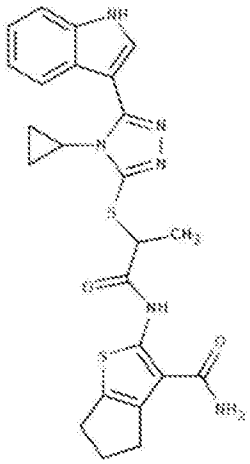

cyclopenta[b]thiophene-3-carboxamide; 2-(2-{[4-cyclopropyl-5-(1H-indol-3-yl)-4H-1,2,4-triazol-3-yl]sulfanyl}propanamido)-4H,5H,6H-

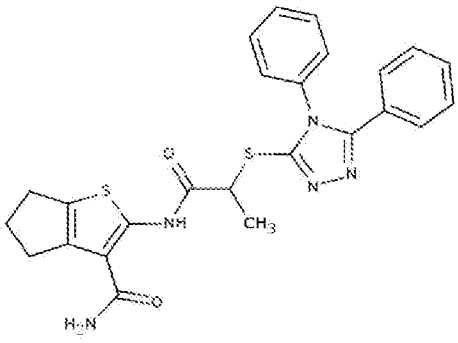

cyclopenta[b]thiophene-3-carboxamide; 2-{2-[(diphenyl-4H-1,2,4-triazol-3-yl)sulfanyl]propanamido}-4H,5H,6H-

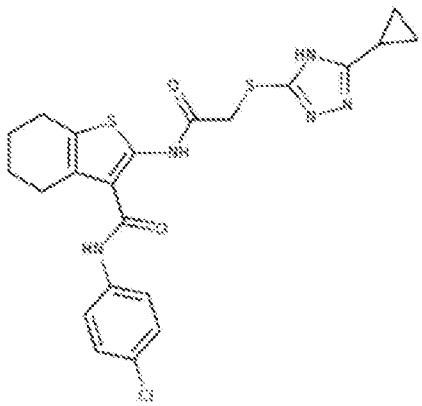

cyclopenta[b]thiophene-3-carboxamide; N-(4-chlorophenyl)-2-{2-[(5-cyclopropyl-4H-1,2,4-triazol-3-yl)sulfanyl]acetamido}-4,5,6,7-tetrahydro-1-benzothiophene-3-carboxamide;

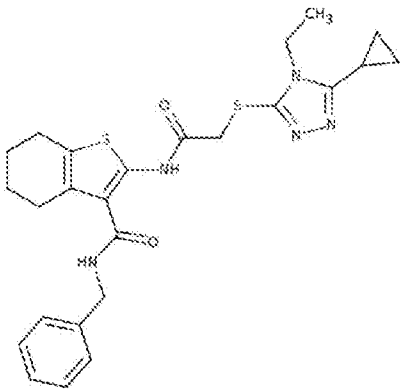

N-benzyl-2-{2-[(5-cyclopropyl-4-ethyl-4H-1,2,4-triazol-3-yl)sulfanyl]acetamido}-4,5,6,7-tetrahydro-1-benzothiophene-3-

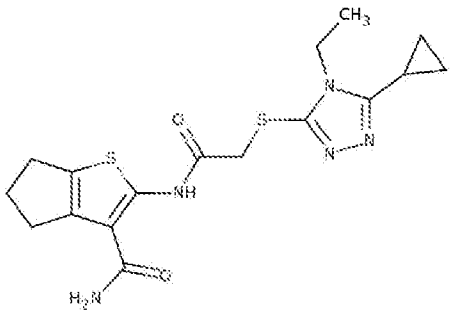

carboxamide; 2-{2-[(5-cyclopropyl-4-ethyl-4H-1,2,4-triazol-3-yl)sulfanyl]acetamido}-4H,5H,6H-cyclopenta[b]thiophene-3-

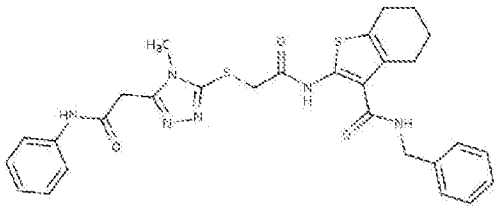

carboxamide; N-benzyl-2-[2-({4-methyl-5-[(phenylcarbamoyl)methyl]-4H-1,2,4-triazol-3-yl}sulfanyl)acetamido]-4,5,6,7-

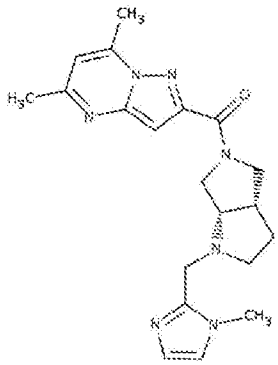

tetrahydro-1-benzothiophene-3-carboxamide; 2-{[(3aS,6aS)-5-{5,7-dimethylpyrazolo[1,5-a]pyrimidine-2-carbonyl}-octahydropyrrolo[3,4-b]pyrrol-1-yl]methyl}-1-methyl-1H-imidazole;

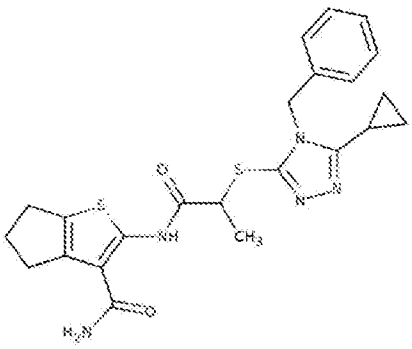

2-{2-[(4-benzyl-5-cyclopropyl-4H-1,2,4-triazol-3-yl)sulfanyl]propanamido}-4H,5H,6H-cyclopenta[b]thiophene-3-carboxamide;

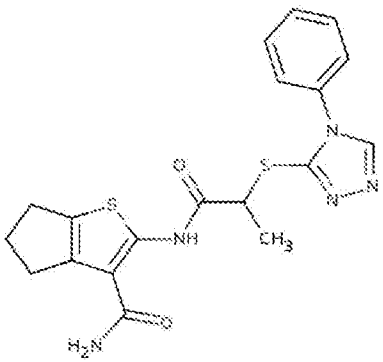

2-{2-[(4-phenyl-4H-1,2,4-triazol-3-

yl)sulfanyl]propanamido}-4H,5H,6H-cyclopenta[b]thiophene-3-carboxamide;

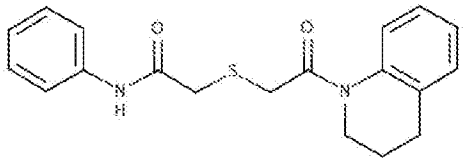

2-{[2-oxo-2-(1,2,3,4-tetrahydroquinolin-1-

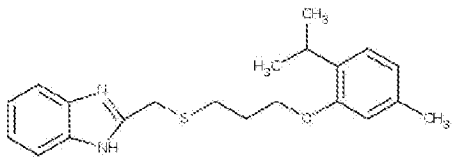

yl)ethyl]sulfanyl}-N-phenylacetamide; 2-[({3-[5-methyl-2-(propan-2-yl)phenoxy]propyl}sulfanyl)methyl]-1H-1,3-benzodiazole;

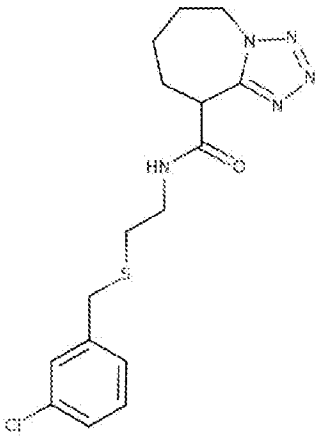

N-(2-{[(3-chlorophenyl)methyl]sulfanyl}ethyl)-5H,6H,7H,8H,9H-[1,2,3,4]tetrazolo[1,5-a]azepine-9-carboxamide; or

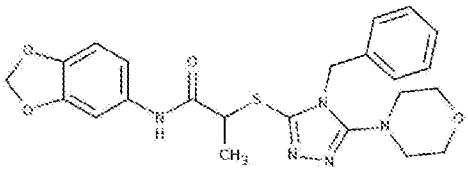

N-(2H-1,3-benzodioxol-5-yl)-2-{[4-benzyl-5-(morpholin-4-yl)-4H-1,2,4-triazol-3-yl]sulfanyl}propanamide.

[0021] In some embodiments, R^1, R^2, R^3, R^4, R^5, R^6, R^7, R^8, or R^9 are optionally substituted by one or more of: acetamide, C_{1-8} alkoxy, amino, azo, Br, C_{1-8} alkyl, carbonyl, carboxyl, Cl, cyano, C_{3-8} cycloalkyl, C_{3-8} heteroaryl, C_{3-8} heterocyclyl, hydroxyl, F, halo, indole, N, nitrile, O, phenyl, S, sulfoxide, sulfur dioxide, or thiophene; or optionally further substituted with one or more acetamide, alkoxy, amino, azo, Br, C_{1-8} alkyl, carbonyl, carboxyl, Cl, cyano, C_{3-8} cycloalkyl, C_{3-8}

heteroaryl, C_{3-8} heterocyclyl, hydroxyl, F, halo, indole, N, nitrile, O, phenyl, S, sulfoxide, sulfur dioxide, or thiophene; wherein, the alkyl, cycloalkyl, heteroaryl, heterocyclyl, indole, or phenyl, is optionally further substituted with one or more selected from the group consisting of acetamide, alkoxy, amino, azo, Br, C_{1-8} alkyl, carbonyl, carboxyl, Cl, cyano, C_{3-8} cycloalkyl, C_{3-8} heteroaryl, C_{3-8} heterocyclyl, hydroxyl, F, halo, indole, N, nitrile, O, phenyl, S, sulfoxide, sulfur dioxide, or thiophene.

[0022] In some embodiments, the compound is of formula

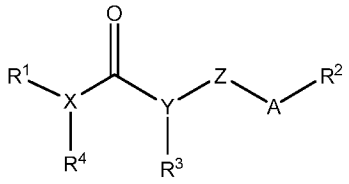

(I), wherein,

R^1 is selected from the group consisting of 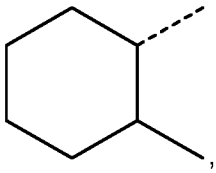 , 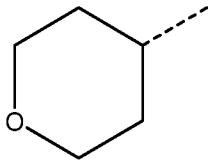 , 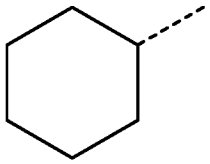 , and 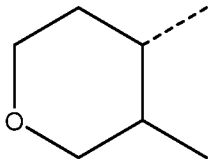 ;

R^2 is selected from the group consisting of 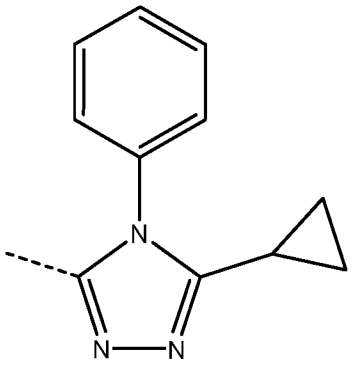 , 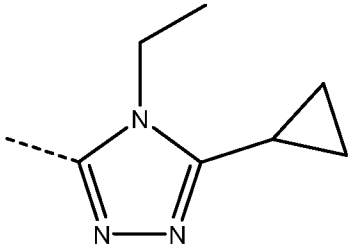 , 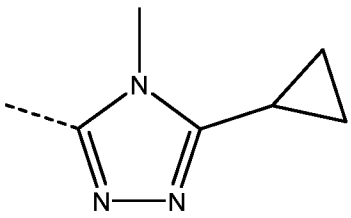 ,

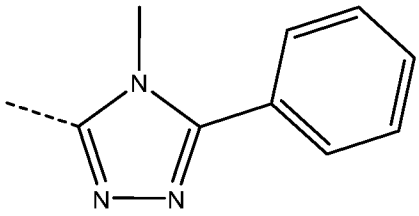

; R^3 is selected from the group consisting of hydrogen (H) and C_{1-8} alkyl; R^4 is selected form the group consisting of hydrogen (H) and C_{1-8} alkyl; A is a bond, S, SO, SO_2, C, or O;

[0023] X is N; Y is N; or Z is a linker group selected from the group consisting of a bond or C_{1-6} alkyl.

[0024] In some embodiments, R^1, R^2, R^3, or R^4 are optionally substituted by one or more of: acetamide, C_{1-8} alkoxy, amino, azo, Br, C_{1-8} alkyl, carbonyl, carboxyl, Cl, cyano, C_{3-8} cycloalkyl, C_{3-8} heteroaryl, C_{3-8} heterocyclyl, hydroxyl, F, halo, indole, N, nitrile, O, phenyl, S, sulfoxide, sulfur dioxide, or thiophene; and optionally further substituted with one or more acetamide, alkoxy, amino, azo, Br, C_{1-8} alkyl, carbonyl, carboxyl, Cl, cyano, C_{3-8} cycloalkyl, C_{3-8} heteroaryl, C_{3-8} heterocyclyl, hydroxyl, F, halo, indole, N, nitrile, O, phenyl, S, sulfoxide, sulfur dioxide, or thiophene; wherein, the alkyl, cycloalkyl, heteroaryl, heterocyclyl, indole, or phenyl, is optionally further substituted with one or more selected from the group consisting of acetamide, alkoxy, amino, azo, Br, C_{1-8} alkyl, carbonyl, carboxyl, Cl, cyano, C_{3-8} cycloalkyl, C_{3-8} heteroaryl, C_{3-8} heterocyclyl, hydroxyl, F, halo, indole, N, nitrile, O, phenyl, S, sulfoxide, sulfur dioxide, or thiophene.

[0025] In some embodiments, the compound is selected from:

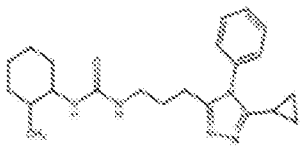

1-(3-(5-cyclopropyl-4-phenyl-4H-1,2,4-triazol-3-yl)propyl)-3-(2-methylcyclohexyl)urea;

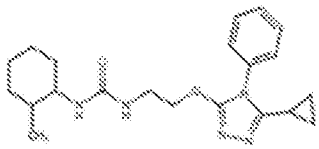

1-(2-((5-cyclopropyl-4-phenyl-4H-1,2,4-triazol-3-yl)oxy)ethyl)-3-(2-methylcyclohexyl)urea;

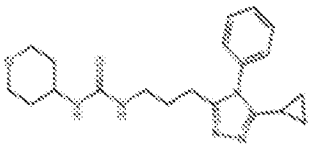

1-(3-(5-cyclopropyl-4-phenyl-4H-1,2,4-triazol-3-yl)propyl)-3-(tetrahydro-2H-pyran-4-yl)urea;

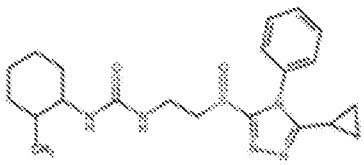

1-(2-((5-cyclopropyl-4-phenyl-4H-1,2,4-triazol-3-yl)sulfinyl)ethyl)-3-(2-methylcyclohexyl)urea;

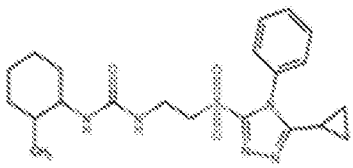

1-(2-((5-cyclopropyl-4-phenyl-4H-1,2,4-triazol-3-yl)sulfonyl)ethyl)-3-(2-methylcyclohexyl)urea;

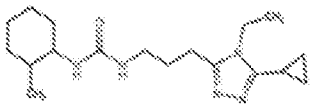

1-(3-(5-cyclopropyl-4-ethyl-4H-1,2,4-triazol-3-yl)propyl)-3-(2-methylcyclohexyl)urea;

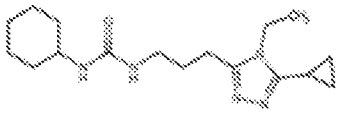

1-cyclohexyl-3-(3-(5-cyclopropyl)-4-ethyl-4H-1,2,4-triazol-3-yl)propyl)urea;

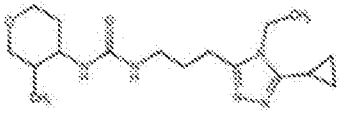

1-(3-(5-cyclopropyl-4-ethyl-4H-1,2,4-triazol-3-yl)propyl)-3-(3-methyltetrahydro-2H-pyran-4-yl)urea;

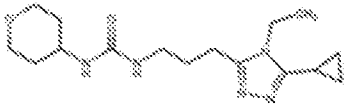

1-(3-(5-cyclopropyl-4-ethyl-4H-1,2,4-triazol-3-yl)propyl)-3-(tetrahydro-2H-pyran-4-yl)urea;

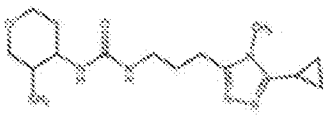

1-(3-(5-cyclopropyl-4-methyl-4H-1,2,4-triazol-3-yl)propyl)-3-(3-methyltetrahydro-2H-pyran-4-yl)urea;

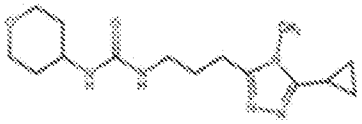

1-(3-(5-cyclopropyl-4-methyl-4H-1,2,4-triazol-3-yl)propyl)-3-(tetrahydro-2H-pyran-4-yl)urea;

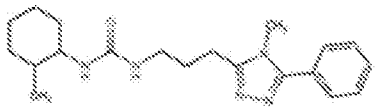

1-(3-(4-methyl-5-phenyl-4H-1,2,4-triazol-3-yl)propyl)-3-(2-methylcyclohexyl)urea;

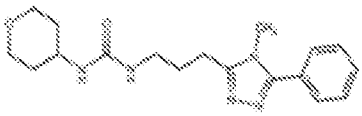

1-(3-(4-methyl-5-phenyl-4H-1,2,4-triazol-3-yl)propyl)-3-(tetrahydro-2H-pyran-4-yl)urea; or

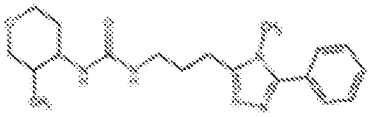

1-(3-(4-methyl-5-phenyl-4H-1,2,4-triazol-3-yl)propyl)-3-(3-methyltetrahydro-2H-pyran-4-yl)urea.

[0026] In some embodiments, the compound is selected from:

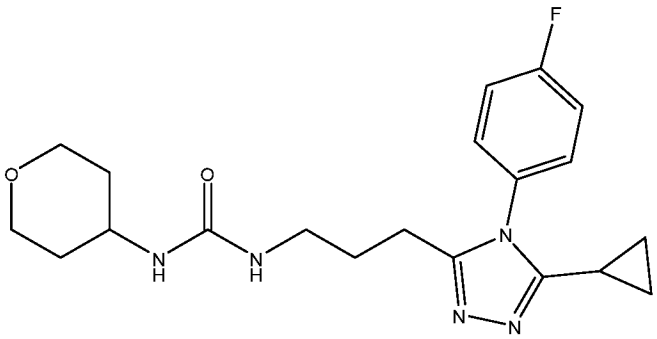

1-(3-(5-cyclopropyl-4-(4-fluorophenyl)-4H-1,2,4-triazol-3-yl)propyl)-3-(tetrahydro-2H-pyran-4-yl)urea;

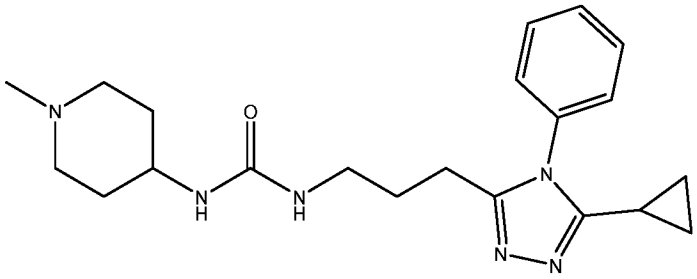

1-(3-(5-cyclopropyl-4-phenyl-4H-1,2,4-triazol-3-yl)propyl)-3-(1-methylpiperidin-4-yl)urea;

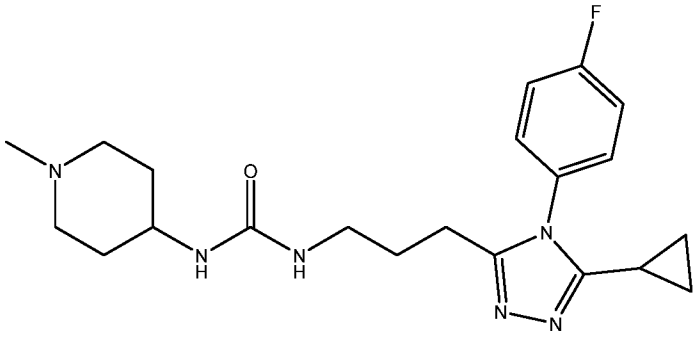

1-(3-(5-cyclopropyl-4-(4-fluorophenyl)-4H-1,2,4-triazol-3-yl)propyl)-3-(1-methylpiperidin-4-yl)urea;

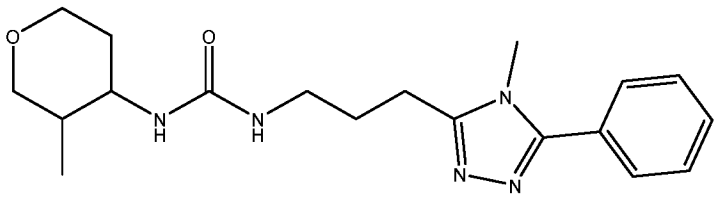

1-(3-(4-methyl-5-phenyl-4H-1,2,4-triazol-3-yl)propyl)-3-(3-methyltetrahydro-2H-pyran-4-yl)urea; or

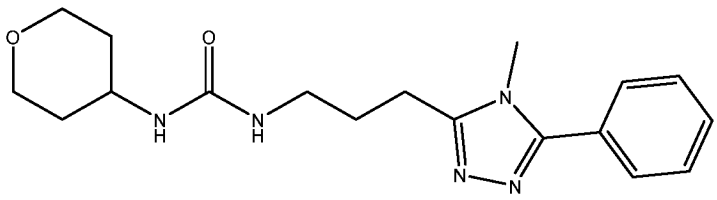

1-(3-(4-methyl-5-phenyl-4H-1,2,4-triazol-3-yl)propyl)-3-(tetrahydro-2H-pyran-4-yl)urea.

[0027] In some embodiments, the compound is a small molecule mimetic of a Mfn2 peptide-peptide interface.

[0028] In some embodiments, the compound targets at least two phosphorylated forms of MFN; enhances mitochondrial trafficking in nerve axons; increases microsomal stability; corrects cell and organ dysfunction caused by primary abnormalities in mitochondrial fission or fusion; reverses mitochondrial defects (e.g., dysmorphometry); restores, activates, regulates, modulates, promotes, or enhances the fusion, function, tethering, transport, trafficking (e.g., axonal

mitochondrial trafficking), mobility, or movement of mitochondria (in, optionally, a nerve or a neuron); enhances mitochondrial elongation or mitochondrial elongation aspect ratio; disrupts intramolecular restraints in Mfn2; allosterically activates Mfn2; corrects mitochondrial dysfunction and cellular dysfunction; repairs defects in neurons with mitochondrial mutations; or targets Mfn1 or Mfn2.

[0029] Yet another aspect of the present disclosure provides for a pharmaceutical composition comprising a compound of formula (I), (II), or (III), optionally in combination with one or more therapeutically acceptable diluents or carriers.

[0030] In some embodiments, the pharmaceutical composition comprises a pharmaceutically acceptable excipient.

[0031] In some embodiments, the pharmaceutical composition comprises a at least one compound selected from the group consisting of neuroprotectants, antiparkinsonian drugs, amyloid protein deposition inhibitors, beta amyloid synthesis inhibitors, antidepressants, anxiolytic drugs, antipsychotic drugs, anti-amyotrophic lateral sclerosis drugs, anti-Huntington's drugs, anti-Alzheimer's drugs, anti-epileptic drugs, or steroids.

[0032] Yet another aspect of the present disclosure provides for a method of treating a mitochondria-associated disease, disorder, or condition in a subject comprising administering to the subject a therapeutically effective amount of a mitofusin modulating agent comprising the compound of formula (I), (II), or (III).

[0033] In some embodiments, the subject is diagnosed with or is suspected of having a mitochondria-associated diseases, disorders, or conditions.

[0034] In some embodiments, the mitochondria-associated disease, disorder, or condition is selected from one or more of the group consisting of: a CNS or PNS injury or trauma, such as trauma to the CNS or PNS, crush injury, spinal cord injury (SCI), traumatic brain injury, stroke, optic nerve injury, or related conditions that involve axonal disconnection; a chronic neurodegenerative condition wherein mitochondrial fusion, fitness, or trafficking are impaired; a disease or disorder associated with mitofusin 1 (Mfn1) or mitofusin 2 (Mfn2) or mitochondrial dysfunction, fragmentation, or fusion; dysfunction in Mfn1 or Mfn2 unfolding; mitochondria dysfunction caused by mutations; a degenerative neurological condition, such as Alzheimer's, Parkinson's, Charcot Marie Tooth Disease, or Huntington's diseases; or

hereditary motor and sensory neuropathy, autism, autosomal dominant optic atrophy (ADOA), muscular dystrophy, Lou Gehrig's disease, cancer, mitochondrial myopathy, Diabetes mellitus and deafness (DAD), Leber's hereditary optic neuropathy (LHON), Leigh syndrome, subacute sclerosing encephalopathy, Neuropathy, ataxia, retinitis pigmentosa, and ptosis (NARP), Myoneurogenic gastrointestinal encephalopathy (MNGIE), Myoclonic Epilepsy with Ragged Red Fibers (MERRF), Mitochondrial myopathy, encephalomyopathy, lactic acidosis, stroke-like symptoms (MELAS), mtDNA depletion, mitochondrial neurogastrointestinal encephalomyopathy (MNGIE), Dysautonomic Mitochondrial Myopathy, Mitochondrial Channelopathy, or pyruvate dehydrogenase complex deficiency (PDCD/PDH).

[0035] Other objects and features will be in part apparent and in part pointed out hereinafter.

DESCRIPTION OF THE DRAWINGS

[0036] Those of skill in the art will understand that the drawings, described below, are for illustrative purposes only. The drawings are not intended to limit the scope of the present teachings in any way.

[0037] The application file contains at least one photograph executed in color. Copies of this patent application publication with color photographs will be provided by the Office upon request and payment of the necessary fee.

[0038] **FIG. 1A** and **FIG. 1B** are a series of hypothetical structures of human MFN2 modeled using I-TASSER. (top) MFN2 modeled in a closed configuration based on structural homology with *Homo sapiens* MFN1 and *Arabidopsis thaliana* dynamin-related protein. (bottom) MFN2 modeled in an open configuration based on structural homology with *Homo sapiens* Opa1. Exploded views show critical HR1 (green)-HR2 (red) interactions in orthogonal views. **FIG. 1C** and **FIG. 1D** are a set of ribbon models depicting the human Mfn2 protein in its folded (inactive) conformation. Major domains are labeled on top. Note the magnified image displaying the interaction of the first and second heptad repeat domains, HR1 and HR2 is on the bottom (see e.g., Example 1).

[0039] **FIG. 2A, FIG. 2B, FIG. 2C, FIG. 2D, FIG. 2E, FIG. 2F, FIG. 2G** and **FIG. 2H** are a series of images and graphs showing MFN2 Ser^{378} phosphorylation by

PINK1 regulates mitochondrial fusion. (**FIG. 2A**) Amino acid sequence surrounding fusion-promoting MFN2 peptide (SEQ ID NO:6). Side chain characteristics (H, hydrophobic; +, basic; -, acidic) are above. (**FIG. 2B**) Mitochondrial fusion stimulated by N- and C-terminal minipeptides. Aspect ratio is mitochondrial long axis/short axis. *Inset*: Fusion in MFN1- and MFN2-null MEFs. (**FIG. 2C**) Alanine (A) scanning of minipeptide 374-384 fusion activity. (**FIG. 2D**) Ser378 substitution analysis of minipeptide 374-384 fusion activity. p values in D and E are vs parent minipeptide 374-384 (ANOVA). (**FIG. 2E**) Binding of minipeptides with Ser378 substitutions to HR2 target sequence (n=6). (**FIG. 2F**) Binding of Asp378 minipeptide to HR2 target sequence before (left) and after (right) Ala substitution for putative interacting amino acids. (**FIG. 2G**) Ion chromatograms from assigned MFN2 Ser378 phosphopeptide fragment ions after incubation with PINK1 kinase (top) and stable isotope-labeled synthetic counterpart (bottom); proportional intensities are in adjacent stack plots. (H) Mitochondrial fusion promoted by MFN2 Ser378 mutants with and without PINK1 kinase; immunoblot of protein expression at bottom. p values are by ANOVA.

[0040] **FIG. 3A** and **FIG. 3 B** shows the purification of mitofusin agonist compounds A and B. At the top are high performance liquid chromatography and mass spectra of compounds as they were obtained from the commercial vendor. On the bottom are spectra after in-house purification. Cpd A: expected m/z 306.18, exact mass found 307.3 $[M + H]^+$; Cpd B: expected m/z 453.15, exact mass found 454.3 $[M + H]^+$.

[0041] **FIG. 4A, FIG. 4B, FIG. 4C, FIG. 4D, FIG. 4E** and **FIG. 4F** are a series of chemical structures and a bar graph that shows the structure and function of compounds A and B, more specifically, the mitofusin-dependent mitochondrial elongation provoked by prototype Mfn agonist peptide mimetics (compounds A and B). **FIG. 4A** shows 3D structures of 1-[2-(benzylsulfanyl)ethyl]-3-(2-methylcyclohexyl)urea, designated compound A, and 2-{2-[(5-cyclopropyl-4-phenyl-4H-1,2,4-triazol-3yl)sulfanyl] propanamido}-4H,5H,6H-cyclopenta[b]thiophene-3-carboxamide, designated compound B (**FIG. 4B). FIG. 4C and FIG. 4D** shows that mitochondrial elongation (increased mitochondrial aspect ratio) evoked by compounds A and B requires either Mfn1 or Mfn2 and each of compound A and compound B inhibited Mfn1 or Mfn2. Note that there was no effect on mitochondrial elongation when both Mfn1 and Mfn2 were absent (see e.g., Example 2). Black bars

are compound-treated cells and white bars are vehicle (DMSO) treated. * = P<0.05 vs control (white). **FIG. 4E** is a schematic of compound B and the moieties subjugated to iterative modification. **FIG. 4F** is a bar graph showing the results of activity studies (increase in aspect ratio is mitochondrial elongation, reflecting increased Mfn-mediated mitochondrial fusion. Structures of derivatives are shown below the bar graph.

[0042] **FIG. 5A, FIG. 5B, FIG. 5C,** and **FIG. 5D** are a series of bar graphs, structures, graphs, and images showing that small molecule HR1 MP374-384 mimetics can be mitofusin agonists. (**FIG. 5A**) Functional screening for class A and B small mitofusin agonists. 1μM of each candidate compound was added to MFN2-deficient MEFs overnight. Mitochondrial aspect ratio is on left and cell viability on right. Structures of the class A and B chemosimilars are shown below (n=3; p values are by ANOVA with Tukey's post hoc comparison). Black bars indicate class A and B compounds selected for detailed studies. (**FIG. 5B**) Representative confocal images from studies in (**FIG. 5A**). Mitochondria were visualized with MitoTracker Orange. Cell viability was assessed simultaneously with mitochondrial aspect ratio - live cells have green cytoplasm (calcein AM) and dead cells lack calcein staining and have purple nuclei (red ethidium homodimer overlying blue Hoechst). Scale bars are 10 μm. (**FIG. 5C**) Initial dose-response relations of five fusogenic compounds from screening in (**FIG. 5A**). EC_{50} values (indexed to the 100% maximal response elicited by the most effective compound, B1) are shown for the agonists with strong fusion-promoting activity; mean±SEM of 3 independent studies for each compound. (**FIG. 5D**) Competition of the HR1 minipeptide at its MFN2 HR2 binding site by five fusogenic compounds from (**FIG. 5A**). IC_{50} values are shown for agonists with >50% displacement (mean±SEM of 6 independent experiments per compound). Displacement curves for compounds A and B are re-plotted in **FIG. 11C**.

[0043] **FIG. 6A, FIG. 6B, FIG. 6C**, **FIG. 6D** and **FIG. 6E** are a series of line and bar graphs, images, and structures showing compounds A and B synergistically promote mitochondrial fusion by acting upon different mitofusin conformational states and displaying the EC50 values of compounds A and B and a key phosphorylation site in Mfn2. **FIG. 6A** shows A+B synergism. More specifically, that the EC50 values of compounds A and B were each 100-200 nM. Note that when added in equal amounts, compounds A and B synergistically promoted mitochondrial elongation,

with a combined EC50 of ~40 nM and a ~25% greater maximal increase in mitochondrial aspect ratio. **FIG. 6B** is a bar graph showing a negative charge conferred by Ser378 phosphorylation or Asp (D) substitution is essential for mini-peptide fusion promoting activity and shows how a S378D mutation, which mimics phosphorylation of this site, influenced Mfn2 conformation and function similarly to HR1 peptide 374-384 (see e.g., Example 2). **FIG. 6C** is a series of images showing representative confocal micrographs of cells treated with mini-peptides in compound B. **FIG. 6D** and **FIG. 6E** are a series of images showing the structural consequences of Ser378 phosphorylation on the Mfn2 HR1-HR2 interacting face; His 380 rotates out and Leu379 rotates in.

[0044] **FIG. 7A, FIG. 7B** and **FIG. 7C** are a series of structures and graphs showing the evaluation of chimeric small molecule mitofusin agonists. (**FIG. 7A**) Structures of compounds A and B and their chimeras. (**FIG. 7B**) Dose-response of compounds in (A) to promote mitochondrial fusion (increase in aspect ratio) in MFN2-deficient MEFs. Data for compounds A and B and chimera B-A/I in **FIG. 11B** are re-plotted here for comparison. (**FIG. 7C**) Comparison of EC50 values calculated from studies in panel B. p values are from ANOVA with Tukey's test.

[0045] **FIG. 8A** and **FIG. 8B** are a series of immunofluorescence images from cultured mouse neurons. Neurons with the human Charcot Marie Tooth disease mutation, Mfn2 T105M, exhibited increased mitochondrial fragmentation and neuronal pathology compared to control. Note how administration of compounds repaired the defects in mutant neurons (see e.g., Example 2).

[0046] **FIG. 9A, FIG. 9B, FIG. 9C, FIG. 9D, FIG. 9E, FIG. 9F, FIG. 9G and FIG. 9H** are a series of bar graphs and images showing mitofusin agonists correct mitochondrial damage induced by nonfunctioning MFN2 mutants by activating endogenous mitofusins. (**FIG. 9A**) Effects of mitofusin agonists in mitofusin-deficient cells expressing WT or mutant MFN2 (n=3 each). (**FIG. 9B**) Same as (**FIG. 9A**) in $MFN1^{+/+}$, $MFN2^{-/-}$ cells. (**FIG. 9C**) Representative mitochondrial pathology in cultured neonatal mouse neurons expressing MFN2 R94Q and correction by mitofusin agonists. Immunoblot showing MFN2R94Q expression in individual mouse pups is above. Scale bars are 21 mm; expanded views are from white squares. (**FIG. 9D**) Group data for studies in (**FIG. 9C**). (**FIG. 9E**) Results of similar studies in cultured neonatal mouse neurons expressing MFN2 T105M. **FIG. 9F** is a series of sequences

and plots and bar graphs showing the identification of critical amino acids for Mfn antagonist peptido-mimetic design. Top, parent peptide (Ref 11) and depiction of N- and C- terminal fragments. Left, C-terminal (407-418) half-peptide suppresses mitochondrial fusion. Right, Ala substitutions identify critical amino acids in HR1407-418. **FIG. 9G** is a bar graph and a series of chemical compounds showing screening results and structures of mitofusin antagonists. **FIG. 9H** is a series of images showing intravenous mitofusin antagonist decreases brain infarct size after ischemia-reperfusion.

[0047] **FIG. 10** is illustration showing Mfn agonist peptide binding and its displacement by compounds A and B. The schematic demonstrates components of the system, depicting FITC labeled peptide binding to its immobilized target (top) and displacement of the FITC peptide by competing small molecule.

[0048] **FIG. 11A, FIG. 11B, FIG. 11C, FIG. 11D, FIG.11E,** and **FIG. 11F** are a series of images and graphs showing small molecule mimetics of MFN2 HR1 amino acid side chains that interact with HR2 are mitofusin agonists. (**FIG. 11A**) (top) Three dimensional representations of minipeptide conformations driven by Ser378 phosphorylation, and (bottom) their respective small molecule mimetics. (**FIG. 11B**) Dose-dependent mitofusin agonism by small molecule agonists (n=6 each). (**FIG. 11C**) Displacement of minipeptide 374-384 from its HR2 binding site by mitofusin agonists (n=3 each). (**FIG. 11D**) Restoration of MFN2 T105M-impaired mitochondrial fusion in MEFs by mitofusin agonists. (**FIG. 11E**) Selectivity of a class A, but not a class B, mitofusin agonist for Ser^{378}-phosphorylated MFN2. (**FIG. 11F**) Impaired basal function, but normal proportional agonist responsiveness, of MFN2 mutations altering HR1-HR2 interacting amino acids.

[0049] **FIG. 12A, FIG. 12B, FIG. 12C** and **FIG. 12D** are a series of drawings that diagram the working model of Mfn2 conformation and function and Mfn folding/unfolding measured by FRET. **FIG. 8** shows that HR1 and HR2 domain interaction can result in a folded conformation in which tethering to adjacent Mfn proteins is unfavorable. Disruption of HR1 and HR2 domains can result in an unfolded conformation in which tethering is favorable. **FIG. 12A** and **FIG. 12B** are illustrations of change in FRET signaling evoked by Mfn conformation. **FIG. 12D** is a graph of a representative experiment with changes in Δ80-275 Mfn2 FRET signal provoked by Mfn antagonist MP2 and agonist MP1. This novel Forster resonance

energy transfer (FRET) assay screens compounds that induce unfolding of a fluorescently tagged Mfn2 construct. Note that both mini-peptides 1 and 2 influenced the FRET signal, suggesting that they induced Mfn2 conformational changes (see e.g., Example 4).

[0050] **FIG. 13A, FIG. 13B, FIG. 13C, FIG. 13D, FIG. 13E, FIG. 13F, FIG. 13G, FIG. 13H, FIG. 13I** and **FIG. 13J** shows a multi-species alignment of MFN2 amino acid sequence. Black highlighting shows identity with human MFN2 protein. (SEQ ID NOs: 6, and 29-65).

[0051] **FIG. 14A, FIG. 14B** and **FIG. 14C** are a homology plot of MFN2 amino acid sequence by functional domain. Positions of HR1 MP374-384 ("fuse") and its HR2 interacting site ("Binding") are shown on exploded views below.

[0052] **FIG. 15A** and **FIG. 15B** is a series of images and a bar graph showing MFN2 Ser378 charge status determines fusion-promoting activity of HR1 MP374-384. Ser378 substitution analysis of mitochondrial fusion promoted by HR1 MP374-384. Representative confocal images of MitoTracker Green/TMRE (red) stained live cells are on the left; scale bars are 10 μm. Group mean data from **FIG. 2D** are to the right; p values are by ANOVA with Tukey's post hoc comparison.

[0053] **FIG. 16A, FIG. 16B, FIG. 16C, FIG. 16D, FIG. 16E, FIG. 16F** and **FIG. 16G** are a series of NMR spectroscopy images and calculated structures. NMR spectroscopy suggests a structural mechanism for effects of Ser378 phosphorylation on HR1 372-384 minipeptide fusogenic function. (**FIG. 16A, FIG. 16B**) Amide proton regions of 2D NOESY spectra of Ala371 to Arg384 fragment of hMFN2. *left* – unphosphorylated Ser378 peptide; *right* – peptide synthesized with phosphorylated Ser-378. Sequential cross peaks between amide groups indicative of α-helical secondary structure are labeled. (**FIG. 16C, FIG. 16D**) Overlaid ^{15}N-^{1}H heteronuclear single quantum coherence spectra of minipeptide backbone amides (bold highlights on covalent wire-model to the left). Red is Ser378 peptide; green is (p)-Ser378 peptide. # marks the positions of Ser378 and (p)-Ser378. In addition to Ser378, the amide signals for amino acids 379-382 shifted down-field (i.e. to higher values) after phosphorylation, as observed when amides within peptides form or strengthen hydrogen bonds. Here, phosphorylation of Ser378 can induce hydrogen bonding for the amide of Leu379, stabilizing the downstream helix and evoking the observed down-field shifts for amides of His380 and Met381. (**FIG. 16C**) Ensembles of

structures calculated from NMR restraints. Color coding is the same as in (**FIG. 16C**). (**FIG. 16E, FIG. 16F**) PepFold3 modeling of the HR1 minipeptide shows how different backbone structure provoked by Ser378 phosphorylation (see panel B) can alter Leu379 and His 380. * in (**FIG. 16B**) and (**FIG. 16D**) mark amino acids with the greatest changes between Ser378 and (p)-Ser378 peptides.

[0054] **FIG. 17A** and **FIG. 17B** show calculated structures from the modeling of HR1 MP374-384 conformation before (top) and after (bottom) S378 phosphorylation.

[0055] **FIG. 18A, FIG. 18B, FIG. 18C, FIG. 18D, FIG. 18E, FIG. 18F, FIG. 18G** and **FIG. 18H** show mutagenesis analysis of MFN2-function based on Ser378 phosphorylation status and integrity of Met376 and His380 that are spatially regulated by Ser378 phosphorylation. Group data and representative confocal images showing mitochondrial aspect ratio in mitofusin deficient cells (MFN1-/-, MFN2-/- MEFs) infected with adnoviri expressing β-galactosidase (negative control), wild-type (WT) MFN2 (positive control), or different single amino acid MFN2 mutants. Fusogenic function was impaired in pseudo-phosphorylated MFN2 Ser378Asp (S378D) and alanine-substituted MFN2 Met376Ala (M376A) and His380Ala (H380A); non-phosphorylatable MFN2 Ser378Ala (S378A) and MFN2 Val372Ala (V372A, which is not in the HR1-HR2 interacting domain) retained full activity. p values are by ANOVA with Tukey's post hoc comparison. MEFs were stained as described in FIG. 15 legend. Scale bar is 10 μm.

[0056] **FIG. 19A, FIG. 19B, FIG. 19C, FIG. 19D, FIG.19E, FIG. 19F, FIG. 19G, FIG. 19H, FIG. 19I** and **FIG. 19J** are a series of high-resolution tandem mass spectra of peptides from a tryptic digest of PINK1-treated recombinant human MFN2. The spectra of the phosphopeptide with the Ser-378 phosphorylation site (**FIG. 19A, FIG. 19B**), a stable isotope-labeled synthetic phosphopeptide (**FIG. 19C, FIG. 19D**), and the non-phosphorylated peptide (**FIG. 19E**) are shown from a 4-hour in vitro PINK1 phosphorylation experiment. (**FIG. 19F**) and (**FIG. 19G**) are like (**FIG. 19A**) and (**FIG. 19D**) after an overnight period for PINK1 phosphorylation. The m/z values for the assigned ions are highlighted in the adjacent ion tables.

[0057] **FIG. 20A, FIG. 20B, FIG. 20C, FIG. 20D** and **FIG. 20E** are a series of high-resolution mass spectra of PINK1-phosphorylated recombinant human MFN2 demonstrating phosphorylation of Thr111 and Ser442. These spectra were obtained

in the study shown in **FIG. 19D** and E. *m/z* values for assigned fragmentation ions are shown to the right.

[0058] **FIG. 21A, FIG. 21B, FIG. 21C, FIG. 21D** and **FIG. 21E** are a series of high-resolution tandem mass spectra of peptides from tryptic digest of GRK-treated recombinant human MFN2. (**FIG. 21A**) Representative non-matching spectrum from the elution window of the Ser-378 phosphopeptide. (**FIG. 21B)** Matching spectrum for the non-phosphorylated peptide from the GRK tryptic digest. The m/z values for the assigned ions are highlighted in the adjacent ion tables. (**FIG. 21C**) Retention time/m/z coordinates of tandem spectra that were analyzed by targeted LC-MS for phosphorylation of the Ser-378 containing peptide. The seven tandem spectra that were acquired at retention times between 82-83 min at m/z = 446.542 showed no evidence of phosphorylation.

[0059] **FIG. 22** is a series of representative live-cell confocal images and a bar graph from studies described in FIG. 2H. Mitochondria of MFN1-/-, MFN2-/- MEFs infected with adenoviri expressing MFN2 mutants with or without adeno-PINK1 kinase were co-stained with MitoTracker Green (green) and TMRE (red); nuclei are stained blue with Hoechst. Scale bars are 10 μm. Quantitative group mean data to the right are reproduced from **FIG. 2H** for comparison.

[0060] **FIG. 23** is a series of images and a bar graph showing effects of MFN2 mutations that prevent or mimic Ser378 phosphorylation on mitochondrial fusion measured as content exchange. (left) Representative live cell confocal images showing mitochondrial fusion (red/green mixing) 3 hours after PEG treatment of MFN1-/-, MFN2-/- MEFs expressing MFN2 Ser378 mutants. Scale bar is 21 μm. N=3 independent studies; p values are by ANOVA with Tukey's post hoc comparison.

[0061] **FIG. 24A** and **FIG. 24B** show functional screening for fusogenic activity of mitofusin agonist pharmacophores. (A) Mitochondrial fusogenicity measured as aspect ratio of MFN2 null MEFs after overnight treatment with 1 mM indicated library compound. Chemical details, structures, and commercial sources of these compounds are in TABLE 4. Mock = DMSO vehicle control. Horizontal dotted line indicates baseline value. Cells treated with 5 mM mitofusin agonist peptide HR1 367-384 (positive control) had aspect ratios of ~6. Inset: correlation of rank order for initial model fit vs actual fusogenicity (r=0.214). Red dots are compounds A10 and B1 that ranked 4th and 2nd for fusogenicity, but 22nd and 31st, respectively, for fit to

the original pharmacophore model. (**FIG. 24B**) Cytotoxicity measured by live-dead assay. Compounds are ranked by fusogenicity as in A. Means±SEM of 3 independent experiments examining ~30 cells per experiment.

[0062] **FIG. 25A, FIG. 25B,** and **FIG. 25C** shows functional validation and dose-response relations of candidate fusogenic small molecules. (**FIG. 25A**) Chemical structures of 4 top candidate fusogenic compounds from initial screening (see e.g., **FIG. 24**). (**FIG. 25B**) Dose relations with representative images of vehicle and 1 mM treated Mfn2 null MEFs for each of the compounds, only 3 of which were true positives. Cells are stained with Mitotracker orange, calcein AM (green; alive) and ethidium homodimer (red nucleus; dead). There are no dead cells. EC_{50} values are provided for true positives; D9 showed no true fusogenic activity. Scale bars are 10 microns. Dose-response curves are means±SEM of 3 independent experiments. (**FIG. 25C**) Schematic depiction of pharmacophore model fit for the 3 true positive fusogenic compounds.

[0063] **FIG. 26A, FIG. 26B, FIG. 26C** and **FIG. 26D** are a graph and image showing the synergistic effects of a class A and class B mitofusin agonist. Mitochondrial elongation (increase in aspect ratio) in MFN2-deficient MEFs stimulated by equimolar concentrations of mitofusin agonists A and B. Dose-response curve on the left is from 6 independent experiments. Peak aspect ratio achieved with A+B is ~25% greater than with either agonist alone (compare to SF10C). Representative live-cell confocal images are on right. Scale bar is 10 mm.

[0064] **FIG. 27A, FIG. 27B** and **FIG. 27C** are a series of graphs and an image showing the functional evaluation of structurally diverse mitofusin agonists. (**FIG. 27A**) Mitochondrial elongation stimulated by mitofusin agonists A and B or chimera B-A/I in cells having different MFN expression profiles. White bars are vehicle (DMSO) treated, black bars are 1 μM agonist overnight; * = $p<0.05$ vs vehicle (t-test). (**FIG. 27B**) Effects of cpds A and B or chimera B-A/I (1μM) on dynamin-mediated endocytosis of Alexa-Fluor 594 Dextran. Dynasore is a dynamin inhibitor. (**FIG. 27C**) Cell viability assessed after overnight exposure to indicated concentrations of mitofusin agonist (n=4). Test compounds were not fully soluble at concentrations greater than 50 μM. p values are by ANOVA with Tukey's test.

[0065] **FIG. 28A, FIG. 28B, FIG. 28C, FIG. 28D, FIG. 28E, FIG. 28F** and **FIG. 28G** are a series of graphs and images showing mitofusin agonists restore

axonal mitochondrial trafficking suppressed by CMT2A mutant MFN2 T105M. (**FIG. 28A- FIG. 28C**) Chimera B-A/I effects on mitochondrial mobility (**FIG. 28A**), function (**FIG. 28B**), and morphology (**FIG. 28C**) in cultured CMT2A MFN2 T105M mouse neurons. (**FIG. 28D**) Kymograph of mitochondrial trafficking in a Ctrl mouse sciatic nerve. (**FIG. 28E**) Serial kymographs of mitochondria in a MFN2 T105M mouse sciatic nerve before and after chimera B-A/I. (**FIG. 28F**) Quantitative data for sciatic nerve mitochondrial motility studies. (**FIG. 28G**) Size of motile and static mitochondria in Ctrl and B-A/I-treated (60 minutes) sciatic nerves. Data information: Mean, standard deviation, and P-values calculated using two-tailed t-test are shown. MitoSOX n=4, TMRM n=6, Mito Aspect ratio n=4.

[0066] **FIG. 29A FIG. 29B** and **FIG. 29C** shows *in vitro* mouse mitochondrial mobility in Ctrl neuron, MFN2 T105M neuron, and MFN2 T105M neuron treated with compounds A+B (24 hours).

[0067] **FIG. 30** is a series of images showing mitofusin agonist chimera B-A/I reverses mitochondrial abnormalities induced by CMT2A mutant MFN2 T105M in cultured mouse neurons. Representative confocal images of living mouse neurons expressing MitoGFP and stained with TMRE and Hoescht from experiments reported in **FIG. 28B** and **FIG. 28C**. Scale bars are 21 μm; expanded views are from white squares. MFN2 T105M was induced by addition of adeno-Cre.

[0068] **FIG. 31** shows mitochondrial mobility in a neuronal axon of a control mouse sciatic nerve. Blue arrows represent the mitochondrial transport in the nerve.

[0069] **FIG. 32A** and **FIG. 32B** shows mitochondrial mobility in axons of a MFN2 T105M mouse sciatic nerve before and at serial 15 minute periods after application of chimera B-A/I. Blue arrows represent the mitochondrial transport in the nerve.

[0070] **FIG. 33** shows the synthetic route for preparation of Chimera B-A/I (compound 5).

[0071] **FIG. 34A** and **FIG. 34B** show RP-HPLC and HRMS of newly synthesized chimera B-A/I. (**FIG. 34A**) HPLC spectrum of chimera B-A/I. From top to bottom: UV Absorbance at 215nm; UV Absorbance at 254 nm; complete ionization mass selective detector (MSD) spectrum; evaporative light scattering detection spectrum. Chimera B-A/I was 99.99% pure. (**FIG. 34B**) HRMS chromatogram of compound B-A/I ($C_{21}H_{29}N_5OS$) shows exact mass: $[M + H]^+$: 400.2.

[0072] **FIG. 35A** and **FIG. 35B** show the proton and carbon-13 NMR of newly synthesized chimera B-A/l. (**FIG. 35A**) Full ^{1}H NMR spectrum (400 MHz) of compound B-A/l (DMSO-d_6 solvent) and expanded view of region δ 0.0 – 4.0 PPM. (**FIG. 35B**) ^{13}C NMR spectrum (126 MHz) of compound B-A/l ($CDCl_3$ solvent).

[0073] **FIG. 36** shows the synthetic route for preparation of chimera B-A/s (compound 3).

[0074] **FIG. 37A** and **FIG. 37B** show RP-HPLC and HRMS of newly synthesized chimera B-A/s. (**FIG. 37A**) HPLC spectrum of compound B-A/s. From top to bottom: UV Absorbance at 215nm; UV Absorbance at 254 nm; complete ionization MSD spectrum; evaporative light scattering detection spectrum. Chimera B-A/s was 99.99% pure. (**FIG. 37B**) HRMS chromatogram of compound B-A/s (C21H28N4OS) shows exact mass found: $[M + H]^+$: 385.2.

[0075] **FIG. 38A** and **FIG. 38B** show the proton and carbon-13 NMR of newly synthesized chimera B-A/s. (**FIG. 38A**) Full ^{1}H NMR spectrum (500 MHz) of compound B-A/s (DMSO-d_6 solvent) and expanded view of region δ0.5 – 4.8 PPM. (**FIG. 38B**) ^{13}C NMR spectrum (126 MHz) of compound B-A/s (DMSO-d_6 solvent) and expanded view of region δ 5 – 60 PPM.

[0076] **FIG. 39** shows the synthetic route for preparation of chimera A-B/l (compound 5).

[0077] **FIG. 40A** and **FIG. 40B** show RP-HPLC and HRMS of newly synthesized chimera A-B/l. (**FIG. 40A**) HPLC spectrum of newly synthesized chimera A-B/l. From top to bottom: UV Absorbance at 215nm; UV Absorbance at 254nm; complete ionization MSD spectrum; evaporative light scattering detection spectrum. Chimera A-B/l was 97.56% pure. (**FIG. 40B**) HRMS chromatogram of compound A-B/l (C18H21N3O2S2) shows exact mass found: $[M + H]^+$: 376.0.

[0078] **FIG. 41A** and **FIG. 41B** show Proton and carbon-13 NMR of newly synthesized chimera A-B/l. (**FIG. 41A**) Full ^{1}H NMR spectrum (400 MHz) of newly synthesized chimera A-B/l (DMSO-d_6 solvent) and expanded view of region δ 2.0 – 4.1 PPM. (**FIG. 41**b) ^{13}C NMR spectrum (126 MHz) of chimera A-B/l (DMSO solvent).

[0079] **FIG. 42** is a schematic showing the synthetic route for preparation of chimera A-B/s (compound 3).

[0080] **FIG. 43A** and **FIG. 43B** show RP-HPLC and HRMS of newly synthesized chimera A-B/s. (**FIG. 43A**) HPLC spectrum of compound A-B/s. From top to bottom: UV Absorbance at 215 nm; UV Absorbance at 254 nm; complete ionization MSD spectrum; evaporative light scattering detection spectrum. Chimera A-B/s was 98.76% pure. (**FIG. 43B**) HRMS chromatogram of chimera A-B/s (C18H20N2O2S2) shows exact mass found: $[M + H]^+$: 361.2.

[0081] **FIG. 44A** and **FIG. 44B** show the proton and carbon-13 NMR spectra of newly synthesized chimera A-B/s. (**FIG. 44A**) Full ^1H NMR spectrum (400 MHz) of chimera A-B/s (DMSO-d_6 solvent) and expanded view of region δ 5.7 – 8.2 PPM. (**FIG. 44B**) ^{13}C NMR spectrum (126 MHz) of chimera A-B/s (DMSO-d_6 solvent).

[0082] **FIG. 45** shows the initial PK studies of Chimera B-A/l, a.k.a. Regeneurin-S. In vitro pharmacokinetic profiling of Regeneurin-S reveals rapid degradation by liver mcirosomes. Chimera B-A/l from Rocha, et al *Science* 2018 was designated Regeneurin-S. Shown is its chemical structure and results of three independent pharmacokinetic (PK) assays performed months apart.

[0083] **FIG. 46** is a series of structures showing structural considerations for chemical evolution of the lead mitofusin agonist. (top left) Structural model of human Mfn2 HR1 367-384 agonist peptide (ribbon) in context of Mfn2 HR1 domain from which it was derived (space-filling; from Franco *Nature* 2016); side chains of HR1-HR2 interacting amino acids Val372, Met376, and His380 are depicted. (top right) Structure of HR1 367-384 peptidomimetic Regeneurin-S (chimera B-A/l from Rocha *Science* 2018) is shown mimicking function-critical side chains from HR1 367-384. Modeled using Chimera UCSF. (bottom) Functional groups of Regeneurin-S are depicted as conceived for chemical engineering: methylated cyclohexyl corresponding to ring structure of His380; thioether backbone providing proper spacing; phenyl-, cyclopropyl-substituted triazol ring mimicking hydrophobicity of Met376 and Val372.

[0084] **FIG. 47** is a series of structures and a graph showing backbone sulfur modifications or substitutions do not alter Regeneurin mitofusin agonist efficacy or affect its degradation by liver microsomes. The backbone sulfur of the parent thioether was oxidized using hydrogen peroxide to generate the sulfoxide and sulfone, which are potential metabolites (top). The ether and carbon variants and

carbon variant with tetrahydropyran substituted for methylated cyclohexane were synthesized de novo (bottom). Red rectangles show substitutions. T½ is for human liver microsomes, % bound is for human plasma. (All PK studies were not performed on all backbone variants.) Dose-response curves for mitochondrial elongation (bottom left) are similar for all compounds.

[0085] **FIG. 48A** and **FIG. 48B** is a bar graph and a series of structures showing functional screening of commercially available Cpd B triazol ring substitution variants. Top: Rank order of fusogenicity (increase in mitochondrial aspect ratio of Mfn2 null MEFs in response to 1 mM compound overnight) provoked by compounds in Supplemental dataset 1. Red dashed line indicates baseline aspect ratio (DMSO-treated MEFs, negative control); green dashed line shows aspect ratio in response to Cpd B (positive control). Bottom: Triazol ring substitutions of 17 compounds otherwise having the common structure $R_{(B)}$. Cpd B is indicated with red rectangle; the other four fusogenic compounds are indicated with green rectangles. Results of detailed studies of these compounds are in **FIG. 49**.

[0086] **FIG. 49** is a series of structures and a graph showing dose-response and human liver microsomal stability data for fusogenic compounds from **FIG. 22**. EC_{50} values are mean±SEM of 3 independent experiments assessing mitochondrial aspect ratio in Mfn2 null MEFs ; Group data dose-response curves are on the left. $T_{1/2}$ values are from human liver microsome stability assay.

[0087] **FIG. 50** is a series of structures and a graph showing a mitolityn series of mitofusin agonists. The feature that distinguishes Mitolityns from Regeneurins is replacement of the 2-phenyl group on the 2,4,5 triazol ring with ethyl or methyl groups. Mitolityns 1 and 2 are 2-ethyl cyclohexane variants and Mitolityns 3 and 4 are 2-ethyl tetrahydropyran variants; Mitolityns 5 and 6 are like 3 and 4 with 2-methyl rather than 2-ethyl groups off the 2,4,5 triazol ring. Chemical differences from Mitolityn-1 are shown in red rectangles; molecular weights are in parentheses. EC_{50} values are for stimulated increase in mitochondrial aspect ratio in Mfn2 null MEFs (n=3 each, mean±SEM); $T_{1/2}$ values are for human, rat, and mouse liver microsome stability assay, in that order. % bound is for human plasma. Group mitochondrial aspect ratio dose response data are shown at the bottom. Mitolityns-4 and -6 exhibited highest potency in the fusogenicity assay, stability in the liver microsome assay, and low plasma protein binding.

[0088] **FIG. 51A** and **FIG. 51B** shows dose-dependent mitochondrial fusion without cytotoxicity of structurally diverse mitofusin agonists. At the top are depictions of Mitolityn-4 (left) and Regeneurin-C (right) mimicry of function-critical side chains of parent agonist peptide Mfn2 HR1 367-384. At the bottom are dose-response relations for each agonist: circles/solid lines show fusogenic responses (mitochondrial elongation assay); squares/dashed lines show % dead cells assayed using the Live-Dead stain. Mfn2 null MEFs were treated with compounds overnight. Indicated EC_{50} values are mean±SEM, n=3 each.

[0089] **FIG. 52** shows the results of in vitro pharmacokinetic studies of Regeneurin-C, Regeneurin-C/O, and Mitolityn-4 mitofusin agonists.

[0090] **FIG. 53A** and **FIG. 53B** are a series of graphs and corresponding structures showing in vivo pharmacokinetics of Regeneurin-C, Regeneurin C/O and Mitolityn-4. (**FIG. 53A**) Three mice each were administered 1mg/kg agonist IV, IP, or IM. Graphs are mean plasma concentration for each administration route. (**FIG. 53B**) Results for individual mice were administered 1 mg/kg indicated agonist IM.

[0091] **FIG. 54** is a series of structures describing the ongoing chemical modifications and optimizations of Regeneurin C/O.

[0092] **FIG. 55** is a series of structures of the Fusogenin series of Mfn agonists currently being synthesized.

[0093] **FIG. 56A, FIG. 56B** and **FIG. 56C** are a series of graphs describing Regeneurin-C (100 nM overnight) treatment of primary fibroblasts from human patients with genetically diverse neurodegenerative diseases. FCCP treatment shows effects of complete mitochondrial uncoupling. Ctrl are control primary human fibroblasts.

FIG. 57A, FIG. 57B, FIG. 57C and **FIG. 57D** are an illustration, traces, and bar graphs describing the initial phenotyping studies of CMT2A mouse (Mfn2 T105M flox-stop x H9B Cre). (**FIG. 57A**) Schematic depiction of nerve conduction studies; red arrows show positions of stimulating electrodes, blue arrows of sensing electrodes. (**FIG. 57B**) Representative CMAP tracings from normal control (top) and CMT2A Mfn2 T105M (bottom) mice. Posterior tibial tracings control for CMAP sensing, and are no different as expected. Note marked decrease in amplitude of Sciatic nerve tracing in T105M mouse. (**FIG. 57C**) Group data from ongoing CMAP studies; each n is a mouse. CMAP amplitude, but not conduction velocity

(latency/length) is diminished after 20 weeks in CMT2A mice. (**FIG. 57D**) Group data from ongoing Rotarod studies suggest functional decline between 10 and 20 weeks.

[0094] **FIG. 58** is a series of images and a graph showing Regeneurin-C/O corrects CMT2A neuronal mitochondrial dymotility *in vivo*. 10 week old CMT2A MFN2 T105M mice were injected IM with Mfn agonist Regeneurin-C/O 2 mg/kg twice, or vehicle. Sciatic nerve mitochondrial motility was measured 4 hours later. Results for 2 CMT2A mice per group.

[0095] **FIG. 59A, FIG. 59B, FIG. 59C, FIG. 59D,** and **FIG. 59E** show conformationally active mitofusins bind MIRO1 and are essential for MIRO1-Milton complex formation. **FIG. 59A**. MFN2 GTPase-activity assay. Mfn1/Mfn2 null mouse embryonic fibroblasts (MEFs) were transduced with indicated MFN2 adenoviri, mitochondria isolated, and GTPase activity assessed using a luminescence assay. Each point is an independent experiment (n=4). Error bars show mean ± s.e.m.; p values by ANOVA (NS=non-significant). Immunoblot at top shows MFN2 expression. VDAC1 is mitochondrial protein loading control. **FIG. 59B**. MFN2-MIRO1 co-immunoprecipitation assay. Fibroblasts were transfected with Flag-tagged WT or Met376Ala MFN2 and myc-MIRO1; immunoprecipitated (IP) with anti-Flag; and immunoblotted (IB). Blot to right is input cell homogenates. **FIG. 59C**. Mitochondrial aspect ratio (length/width) in vehicle (DMSO) and mitofusin agonist Regeneurin S-treated (100 nM, 24 hours) Mfn1/Mfn2 null MEFs expressing wild-type (WT) or mutant MFN2. Decreased aspect ratio reflects impaired mitochondrial fusion. Each point is the average value measured of ~20 mitochondria from a single cell; total numbers of cells assayed per treatment group in 4 or 5 independent experiments are shown below the horizontal axis. Error bars are mean ± s.d.; p values are from 2-way ANOVA (NS=non-significant). **FIG. 59D**. MFN2-MIRO1 and MFN2-CAST co-immunoprecipitation. Regeneurin (Regen) S did not change MIRO1 binding to WT or Met376Ala MFN2. **FIG. 59E**. MIRO1-Milton co-immunoprecipitation as a function of mitofusin activation with Regeneurin S. On left are results in wild-type MEFs; on right in Mfn1/Mfn2 double knockout (DKO) MEFs. Regen S increased MIRO1-Milton complexing, but Mfn2 was not part of the complex. Absence of Regeneurin effect in Mfn DKO MEFs (right) indicates Mfn regulation of MIRO-Milton interactions.

[0096] **FIG. 60A, FIG. 60B, FIG. 60C, FIG. 60D, FIG. 60E** and **FIG. 60F** show mitofusin activation reverses mitochondrial defects in amyotrophic lateral

sclerosis, Huntington disease, and CMT2A patient fibroblasts. Mitochondrial dysmorphology (**FIG. 60A**) or depolarization (**FIG. 60B**), and cellular autophagy (**FIG. 60C**) in primary fibroblasts from genetically diverse Charcot-Marie-Tooth disease type 2A (CMT2A), Parkinson's disease (PD), Alzheimer's disease, Huntington disease (HD), amyotrophic lateral sclerosis (ALS), and control (CTRL) patients. (Results by individual patient genotype are in **FIG. 69-FIG. 74**). Each point is the average value measured of ~15 mitochondria from a single cell; total numbers of cells assayed per treatment group in 4 or 5 independent experiments are shown below the horizontal axis. Error bars are mean ± s.d.; p values are from 2-way ANOVA. **FIG. 60D-FIG. 60F**. Confocal micrographs (representative of >40 cells/line) showing reversal of mitochondrial fragmentation and depolarization by Regeneurin C (100 nM, 24 h) in CMT2A MFN2 T105M (e) and ALS SOD1 I113T (**FIG. 60F**) patient fibroblasts; CTRL cells (**FIG. 60D**) are shown for comparison. Scale bars, 10 μm. Representative confocal micrographs for all individual patient genotypes are in **FIG. 69-FIG. 74**.

[0097] **FIG. 61A, FIG. 61B, FIG. 61C, FIG. 61D, FIG. 61E** and **FIG. 61F** show mitofusin activation promotes mitochondrial trafficking and neuron growth in vitro. **FIG. 61A**. Confocal micrographs (representative of >90 neurons/condition) of β-III tubulin (green), DAPI (blue) co-stained adult mouse DRG neurons expressing mitochondrial targeted RFP (red) 48 hours after dissociation axotomy; left is DMSO treatment and right is mitofusin agonist Regeneurin C (Regen) treatment. Scale bars, 44 μm; insets show enlarged axon termini. To the right are quantitative analyses of DRG axon regrowth after Regeneurin or DMSO treatment for 12, 24 or 48 hours. Treatment was randomized, and both the imager and analyst were blinded. Each dot is average result from one β-III-tubulin positive neuron; numbers of neurons are indicated below p values, which are from 2-way ANOVA. Error bars are mean ± s.d. Complete time course data and Sholl analysis for Regeneurin and mitofusin agonist peptide and their vehicles are in **FIG. 75**. **FIG. 61B**. Histogram of maximum axon length in DRG neurons 48 hours after dissociation axotomy as a function of treatment with Regeneurin (100 nM, red) or peptide mitofusin agonist HR1 374-384 (1 μM, blue), or their vehicles (dashed lines). **FIG. 61C**. Effect of Regeneurin C on mitochondrial localization to axon termini in regrowing adult mouse DRG neurons. Each dot is average result from one β-III-tubulin positive neuron; numbers of neurons

are indicated below p values, which are from t-test. Error bars are mean ± s.d. **FIG. 61D**. Regeneurin effects on mitochondrial density and aspect ratio in axons of normal DRG neurons 48 hours after dissociation axotomy. Each dot is average result from one β-III-tubulin positive neuron; numbers of neurons are indicated below p values, which are from t-test. Representative (of >30 neurons) confocal images showing axons and their mitochondria are to the right; scale bars, 44 and 10 μm for lower and higher power images, respectively. Error bars are mean ± s.d. **FIG. 61E**. Mitochondrial studies of CMT (MFN2 T105M) mouse DRGs grown in vehicle- (DMSO), forskolin (Forsk)- or Regeneurin-treated CMT mouse adult DRG neurons 48 hours after plating. Representative of >20 neurons from 3 individual DRG preparations; scale bars, 44 μm. Quantitative data are to the right. Each dot represents results from a single adult DRG neuron; n values are below the horizontal axes. P values are from ANOVA. Error bars are mean ± s.d. **FIG. 61F** Relationship between axon regrowth (green confocal images on top) and mitochondrial motility (red kymographs on bottom) in vehicle, forskolin (Forsk)-, or Regeneurin-treated CMT (MFN2 T105M) mouse adult DRG neurons. Scale bars, 263 μm. Quantitative data are to the right. Each dot represents results from a single adult DRG neuron; n values are below the horizontal axes. P values are from ANOVA. Error bars are mean ± s.d.

[0098] **FIG. 62A, FIG. 62B, FIG. 62C, FIG. 62D, FIG. 62E, FIG. 62F** and **FIG. 62G** show mitofusin agonists promote regeneration of injured neuronal axons *in vitro* and *in vivo*. **FIG. 62A** Confocal images (representative of 6 independent preparations per group) of embryonic mouse cortical neurons cultured in microgroove chambers; in each image cell bodies are to the left, horizontal microgrooves containing axons in the middle, and axon termini to the right (labeled in first panel). After 12 days in vitro (DIV) axon termini were removed by suction (aspiration axotomy; second panel). Vehicle (DMSO) or Regeneurin C (100 nM) were added after axotomy, and axon regeneration measured three days thereafter (panels 3 and 4, respectively). **FIG. 62B** Post axotomy axon regrowth (terminal axon area/microgroove channel). Each dot represents a single axon. Numbers of axons are indicated below p values, which are from t-test. Error bars are mean ± s.d. **FIG. 62C** Representative live cell confocal images of axonal mitochondria pre- (top) and 1 hour post (middle and bottom) aspiration axotomy. Squares show areas enlarged to

the right. **FIG. 62D** Quantitative group data for mitochondrial aspect ratio (left) and polarization status (right). Each dot represents aggregate data of 10-20 mitochondria from a single axon; numbers of axons are below X-axis. Error bars are mean ± s.d. (ANOVA). **FIG. 62E** (top) Design of in vivo sciatic nerve (n.) crush injury study; (bottom) quantitative group tibialis anterior compound muscle action potential (CMAP) amplitude data 3 and 7 days after sciatic n. crush injury. Each point represents one mouse; lines show individual progression from 3 to 7 days post sciatic n. crush injury. Error bars are mean ± s.d.; p values are from Student t-test; NS = non-significant. **FIG. 62F** Representative (of five mice per group) tibialis anterior CMAP tracings 3 and 7 days after sciatic nerve crush injury; "uninjured" tracing is from contralateral leg of same mouse. **FIG. 62G** Immunohistological detection of neuronal regeneration marked by Superior Cervical Ganglion 10 (SCG10; red) in mouse sciatic nerves. * indicates area of sciatic nerve crush injury.

[0099] **FIG. 63A, FIG. 63B** and **FIG. 63C** show mitofusin agonist Regeneurin S corrects dysfunction of MFN2 Met376Ala (M376A), but not MFN2 Arg94Gln (R94Q) or Lys109Ala (K109A). **FIG. 63A**, **FIG. 63B**. Mitochondrial morphology (a, duplicated from Figure 1c for comparison) and polarization status (**FIG. 63B**) in vehicle (DMSO) and mitofusin agonist Regeneurin S-treated (100 nM, 24 hours) Mfn1/Mfn2 null MEFs expressing the MFN2 mutants in (**FIG. 63C**). Mitochondrial depolarization reflects loss of bioenergetic function that characteristically accompanies fusion defects. Each point is the average value measured of ~20 mitochondria from a single cell from 4 or 5 independent experiments are shown below the horizontal axis. Error bars are mean ± s.d.; p values are from 2-way ANOVA. **FIG. 63C**. Confocal micrographs (representative of 20-90 cells/group) of MitoTracker Green, Tetramethylrhodamine, ethyl ester (TMRE; red) stained Mfn1/Mfn2 double-deficient MEFs transduced with adenoviri expressing wild-type (WT) or MFN2 mutants as indicated; Adeno β-gal is negative control. Images are representative of data in **FIG. 59C** and panels a and b. Mitochondrial fragmentation and depolarization were improved by Regeneurin S in cells expressing conformationally impaired MFN2 Met376Ala, but not GTPase defective MFN2 Arg94Gln or Lys109Ala. Scale bars, 10 μm. Regeneurin S vehicle is DMSO (1:1000).

[00100] **FIG. 64A, FIG. 64B, FIG. 64C** and **FIG. 65D** show different effects on mitochondrial fitness of functionally diverse MFN2 mutants expressed in normal

MEFs. **FIG. 64A**. Immunoblot analysis of MFN2 after viral vector-mediated expression of human MFN2 (MFN2) or indicated mutants in control C57BL/6J MEFs. β–gal (adeno β-galactosidase) is negative control; anti-β-actin is protein loading control. **FIG. 64B**. Mitochondrial length (aspect ratio: length/width) assessed by MitoTracker Green staining of MEFs 48 hours after viral-mediated expression. **FIG. 64C**. Mitochondrial depolarization (loss of the normal inner mitochondrial membrane electrochemical potential) assessed as loss of TMRE fluorescence. All 3 MFN2 loss-of-function mutants induced mitochondrial fragmentation (decreased mitochondrial aspect ratio), revealing dominant inhibition of mitochondrial fusion. However, only the 2 GTPase-defective mutants (MFN2 Arg94Gln and Lys109Ala) provoked mitochondrial depolarization. Each point represents the mean of 15-20 mitochondria measured in a single cell; cell numbers are indicated on graphs for each treatment group. Each experiment was performed 5 independent times. Error bars indicate mean ± s.d.; p values are from ANOVA. **FIG. 64D**. Confocal micrographs (representative of >100 cells/group) of MitoTracker Green/TMRE (red) stained wild-type MEFs transduced with adenoviri expressing wild-type (WT) or MFN2 mutants as indicated. Blue Hoechst stains nuclei. Scale bars, 10 μm.

[00101] **FIG. 65A, FIG. 65B** and **FIG. 65C** show Regeneurin S activates endogenous Mfn1 to overcome dominant inhibition of mitochondrial fusion by all MFN2 mutants. **FIG. 65A**. Mitochondrial morphology (top) and polarization status (bottom) in vehicle (DMSO) or Regeneurin C treated (100 nM, 24 hours) Mfn2 null MEFs virally transduced with WT MFN2 or indicated MFN2 mutants; Mfn2 gene ablation does not reduce expression of endogenous Mfn1 (**FIG. 81**). Each point is the average value from 15-20 mitochondria in a single cell; total numbers of cells assayed per treatment group in 4 or 5 independent experiments are shown below the horizontal axis. Error bars are mean ± s.d.; p values are from 2-way ANOVA. **FIG. 65B**. Confocal micrographs (representative of >30 cells/group) of MitoTracker Green/TMRE (red) stained Mfn2 null wild-type MEFs transduced with adenoviri expressing wild-type (WT) or mutant MFN2 as indicated. Blue Hoechst stains nuclei. Scale bars, 10 μm. Comparison of these results with those from identical studies performed in Mfn1/Mfn2 double deficient MEFs (see **FIG. 59C** and **FIG. 64**) demonstrates that endogenous Mfn1can be a substrate for mitofusin agonists to

surmount mitochondrial abnormalities provoked by either GTPase-defective or conformational shift-impaired MFN2 mutants.

[00102] **FIG. 66A, FIG. 66B,** and **FIG. 66C** show Regeneurin S reverses mitochondrial abnormalities produced by MFN2 mutants in mouse neurons. **FIG. 66A**. Immunoblot analysis of MFN2 after viral vector-mediated expression of human MFN2 (MFN2) or indicated mutants in perinatal mouse hippocampal neurons. β–gal is negative control; anti-β-actin shows protein loading. **FIG. 66B**. Mitochondrial aspect ratio (top) and depolarization (bottom) assessed as in **FIG.65**. Each point is the average value from 15-20 mitochondria in a single cell; total numbers of cells assayed per treatment group in 4 or 5 independent experiments are shown below the horizontal axis. Error bars are mean ± s.d.; p values are from 2-way ANOVA. **FIG. 66C**. Confocal micrographs (representative of >70 neurons/group) corresponding to results in (b). Scale bars, 22 μm. Regeneurin S benefits are similar in neurons and Mfn2-null MEFs (**FIG. 65**), reflecting in both models overpowering of MFN2 mutant effects through activation of normal endogenous mitofusins.

[00103] **FIG. 67A** and **FIG. 67B** shows structures and fusogenicities of mitofusin agonists Regeneurin S and Regeneurin C. Regeneurin S (left) is identical to “chimera B-A/I” in reference 6. Regeneurin C (right) is the carbon backbone variant, which was synthesized to eliminate the possibility of thioether oxidation to sulfoxide and sulfone in cells or tissues; the sulfur (S) and relevant carbon (C) in the two Regeneurin structures are indicated by arrows. Because the backbone functions as a spacer to position the small molecule functional groups mimicking amino acid side chains of Val372, Met376 and His380 within the prototype MFN2 HR1 367-384 mitofusin agonist peptide (top structures), substitution of C for S in the backbone did not affect fusogenic potency (left vertical axes and closed circles) or lack of cytotoxicity (right vertical axes and closed squares) of dose-response curves shown below structures (n=5 for Regeneurin S and n=3 for Regeneurin C). Fusogenecity EC50 values (concentration that provokes a half-maximal response) are 10±4 nM for Regeneurin S (n=5) and 5±1 nM for Regeneurin C (n=3).

[00104] **FIG. 68A, FIG. 68B,** and **FIG. 68C** show Mitofusin activation reverses mitochondrial defects in CMT2A MFN2 Thr105Met (T105M), Arg274Trp (R274W) and His361Tyr (H361Y) patient fibroblasts. **FIG. 68A**. Mitochondrial dysmorphology (left), depolarization (center), and cellular autophagy (right) in

genetically diverse CMT2A patient primary fibroblasts. Each point is the average value measured of ~15 mitochondria from a single cell; total numbers of cells assayed per treatment group in 4 or 5 independent experiments are shown above. Error bars are mean ± s.d.; p values are from unpaired t-tests. **FIG. 68B**. Confocal micrographs of MitoTracker Green, TMRE, Hoechst triple-stained patient fibroblasts (representative of >40 cells/line) showing reversal of mitochondrial fragmentation and depolarization by Regeneurin C (100 nM, 24 h). **FIG. 68C**. Confocal micrographs of LC3-green fluorescent protein (GFP), Hoechst double-stained patient fibroblasts showing reduction of autophagy assessed as LC3-GFP dots per cell. Scale bars, 10 μm. DMSO (1:1000) is the vehicle for Regeneurin C.

[00105] **FIG. 69A, FIG. 69B,** and **FIG. 69C** show Mitofusin activation can improve mitochondrial fragmentation and depolarization in Parkinson's disease LRRK2 Gly2019Ser (G2019S), PARK2 Arg275Trp (R275W) and PINK1 Ile368Asn (I368N) patient fibroblasts. **FIG. 69A**. Mitochondrial dysmorphology (left), depolarization (center), and cellular autophagy (right) in genetically diverse Parkinson's disease patient primary fibroblasts. Each point is the average value measured of ~15 mitochondria from a single cell; total numbers of cells assayed per treatment group in 4 or 5 independent experiments are shown above. Error bars are mean ± s.d.; p values are from unpaired t-tests; NS = non-significant. **FIG. 69B**. Confocal micrographs of MitoTracker Green, TMRE, Hoechst triple-stained patient fibroblasts (representative of >40 cells/line) showing effects of Regeneurin C (100 nM, 24 h) on mitochondrial length and polarization status. **FIG. 69C**. Confocal micrographs of LC3-GFP, Hoescht double-stained patient fibroblasts (representative of >40 cells/line) showing normal levels of autophagy assessed as LC3-GFP punctae (fluorescent green dots) per cell (see **FIG.60C** for comparison with CTRL), and no effect of Regeneurin C. Scale bars, 10 μm. DMSO (1:1000) is the vehicle for Regeneurin C.

[00106] **FIG. 70A, FIG. 70B,** and **FIG. 70C** show Mitofusin activation has no effect on mitochondria from Alzheimer's disease PSEN1 Met146Ile (M146I), Glu184Asp (E184D), and Pro264Leu (P264L) patient fibroblasts. **FIG. 70A**. Mitochondrial dysmorphology (left), depolarization (center), and cellular autophagy (right) in genetically diverse Alzheimer's disease patient primary fibroblasts. Each point is the average value measured of ~15 mitochondria from a single cell; total

numbers of cells assayed per treatment group in 4 or 5 independent experiments are shown above. Error bars are mean ± s.d.; p values are from unpaired t-tests; NS = non-significant. **FIG. 70B**. Confocal micrographs of MitoTracker Green, TMRE, Hoechst triple-stained patient fibroblasts (representative of >40 cells/line) showing effects of Regeneurin C (100 nM, 24 h) on mitochondrial length and polarization status. **FIG. 70C**. Confocal micrographs of LC3-GFP, Hoechst double-stained patient fibroblasts (representative of >40 cells/line) showing normal levels of autophagy assessed as LC3-GFP punctae (fluorescent green dots) per cell (see **FIG. 60C** for comparison with CTRL), and no effect of Regeneurin C. Scale bars, 10 μm. DMSO (1:1000) is the vehicle for Regeneurin C.

[00107] **FIG. 71A, FIG. 71B,** and **FIG. 71C** show Mitofusin activation improves mitochondria from Huntington disease patient fibroblasts with HTT CAG repeat numbers of 40 (CAG#40), 57 (CAG#57), and 66 (CAG#66). **FIG. 71A**. Mitochondrial dysmorphology (left), depolarization (center), and cellular autophagy (right) in genetically diverse Huntington disease patient primary fibroblasts. Each point is the average value measured of ~15 mitochondria from a single cell; total numbers of cells assayed per treatment group in 4 or 5 independent experiments are shown above. Error bars are mean ± s.d.; p values are from unpaired t-tests. **FIG. 71B**. Confocal micrographs of MitoTracker Green, TMRE, Hoechst triple-stained patient fibroblasts (representative of >40 cells/line) showing improvement in mitochondrial fragmentation and depolarization by Regeneurin C (100 nM, 24 h). **FIG. 71C**. Confocal micrographs of LC3-GFP, Hoechst double-stained patient fibroblasts showing reduction of autophagy assessed as LC3-GFP punctae (fluorescent green dots) per cell. Scale bars, 10 μm. DMSO (1:1000) is the vehicle for Regeneurin C.

[00108] **FIG. 72A, FIG. 72B,** and **FIG. 72C** show Mitofusin activation reverses mitochondrial defects in amyotrophic lateral sclerosis SOD1 Leu38Val (L38V), Ile113Thr (I113T), and Leu144Pro (L144P) patient fibroblasts. **FIG. 72A**. Mitochondrial dysmorphology (left), depolarization (center), and cellular autophagy (right) in genetically diverse amyotrophic lateral sclerosis patient primary fibroblasts. Each point is the average value measured of ~15 mitochondria from a single cell; total numbers of cells assayed per treatment group in 4 or 5 independent experiments are shown above. Error bars are mean ± s.d.; p values are from

unpaired t-tests. **FIG. 72B**. Confocal micrographs of MitoTracker Green, TMRE, Hoechst triple-stained patient fibroblasts (representative of >40 cells/line) showing reversal of mitochondrial fragmentation and depolarization by Regeneurin C (100 nM, 24 h). **FIG. 72C**. Confocal micrographs of LC3-GFP, Hoechst double-stained patient fibroblasts showing reversal of increased autophagy assessed as LC3-GFP punctae (fluorescent green dots) per cell. Scale bars, 10 μm. DMSO (1:1000) is the vehicle for Regeneurin C.

[00109] **FIG. 73** shows Mitofusin activation has little effect on mitochondria in normal human primary fibroblasts. Mitochondrial morphology (top), polarization status (center), and cellular autophagy (bottom) in five different lines of normal human primary fibroblasts used as negative controls (CTRL) for comparison to fibroblasts from neurological disease patients. Each point on the graphs is the average value measured of ~15 mitochondria from a single cell; total numbers of cells assayed per treatment group in 4 or 5 independent experiments are shown above. Error bars are mean ± s.d.; p values are from unpaired t-tests; NS = non-significant. On the left are confocal micrographs of MitoTracker Green, TMRE, Hoechst triple-stained normal fibroblasts (top, representative of >40 cells/line) and LC3-GFP, Hoechst double-stained normal fibroblasts (bottom, representative of >40 cells/line) treated with Regeneurin C (100 nM) or vehicle (DMSO, 1:1000) for 24 hours.

[00110] **FIG. 74** shows the peptide and small molecule peptidomimetic mitofusin agonists accelerate axon regrowth in cultured adult mouse DRG neurons. Representative low power images of >50 cells per treatment group in 4 independent experiments (left) and quantitative group data of individual cell axon intersections (right) for the studies reported and shown at higher magnification in **FIG. 61A, FIG. 61B**: Regeneurin C (100 nM) results are above; agonist peptide HR1 374-384 (1 μM) results are below. Each point in the graphs is the number of axonal intersections computationally identified by blinded Sholl analysis of an individual β-III tubulin-positive cultured mouse dorsal root ganglion neuron. Treatment was randomized, and both the imager (AF) and analyst (BK) were blinded. Scale bars are 200 micrometers. Total number of neurons examined per treatment group is shown below the horizontal axes. Error bars are mean ± s.d.; p values are from unpaired t-tests; NS = non-significant.

[00111] **FIG. 75A, FIG. 75B,** and **FIG. 75C** show Mitofusin agonists do not affect DRG neuronal survival in vitro. **FIG. 75A**. Representative images (of >24 neurons/treatment group, 2 independent experiments) of cell viability studies in adult mouse DRG neurons treated with mitofusin agonist peptide or small molecule Regeneurin C or their respective vehicles. Quantitative group data are in panels **FIG. 75B** (Regeneurin C) and c (agonist peptide). Numbers of neurons evaluated for each group are shown on each graph. Error bars show mean ± s.d.; NS = non-significant (unpaired t-test).

[00112] **FIG. 76A, FIG. 76B, FIG. 76C, FIG. 76D, FIG. 76E, FIG. 76F** and **FIG. 76G** show structure-function relations of Mitolityn series of mitofusin agonists. **FIG. 76A**. Structures of Mitolityns 1-6. **FIG. 76B**. Dose-response curves for Mitolityn series of mitofusin agonists; maximal fusogenicity (increase in mitochondrial aspect ratio) was defined as that promoted by 1 μM Regeneurin C (see Extended Data Fig. 5). **FIG. 76C**. EC50 values for Mitolityns 1-6. Inactive is defined as less provoking less than a half-maximal fusogenic response at 1 μM concentration. **FIG. 76D**. Representative confocal micrographs (of 10 cells per experiment in number of experiments indicated in panel c) for cells treated 48 hours with 1 μM of Mitolityns as indicated. **FIG. 76E**. Schematic depiction of how Mitolityn-4 structure mimics side chains of function-critical Val372, Met376 and His380 within the prototype MFN2 HR1 367-384 mitofusin agonist peptide. **FIG. 76F**. Dose-response curve for Mitolityn-4 showing results of individual experiments; compare with **FIG. 63** for same data for Regeneurins S and C. **FIG. 76G**. Mitolityn-4 stimulation of axonal outgrowth in normal mouse DRGs. Based on these studies Mitolityn-4 (referred to as Mitolityn in the manuscript text) was selected for further pharmacokinetic evaluation.

[00113] **FIG. 77** shows comparative pharmacokinetic properties of Regeneurin S, Regeneurin C, and Mitolityn-4. The protoype mitofusin agonist, Regeneurin S (Chimera B-A/I from reference 6), exhibited plasma protein binding that was too high, and liver microsome stability that was too low, for in vivo application. Substitution of the backbone sulfur of Regeneurin S with carbon in Regeneurin C, the lead molecule in current in vitro biological studies, made little difference in these factors. Replacing the phenyl group on the triazol ring with an ethyl group and substituting tetrahydropyran for the methylated cyclohexane ring on

the other side of the molecule, as in Mitolityn-4, reduced plasma protein binding and stabilized the molecule in liver microsomes. ND = not determined

[00114] **FIG. 78** shows kinetics of Mitolityn-4 release from a biocompatible protein gel matrix. Results of three independent experiments of Mitolityn-4 elution from Matrigel matrix. Drug concentrations were determined by LC-ESI/MS/MS. Linear regressions for each experiment are shown. Average rate of elution of Mitolityn-4 (125 μg/200 μl Matrigel) into 500 μl water was 0.213±0.02 ng/min. Inset: standard curve.

[00115] **FIG. 79A, FIG. 79B, FIG. 79C** and **FIG. 79D** show a theoretical model for MFN2-MIRO-Milton interactions that promote mitochondrial trafficking. **FIG. 79A**. A mitochondrion in its resting state is shown with inactive (closed conformation) MFN2 and MIRO1 at the outer mitochondrial membrane; Milton is in the cytosol. **FIG. 79B**. Transitioning of MFN2 to is open conformation promotes its binding to MIRO1 on mitochondria, which modifies MIRO1 in as-yet unknown ways to enable its binding to Milton. **FIG. 79C**. Milton-MIRO1 complexing either requires or provokes MFN2 separation; MFN2 is not part of a stable MIRO1-Milton complex. **FIG. 79D**. Milton couples mitochondria to microtubules via its binding of mitochondrial MIRO1 and Dynein or Kinesin molecular motors, thus evoking mitochondrial trafficking.

[00116] **FIG. 80A** and **FIG. 80B** show Immunoblot analysis of MFN expression profiles in MEFs used for current studies. **FIG. 80A**. Mfn1 immunoreactivity (top), with GAPDH loading control below. **FIG. 80B**. Mfn2 immunoreactivity (top) with GAPDH loading control below. Representative of 2 independent experiments. DKO: Mfn1/Mfn2 double knockout.

[00117] **FIG. 81** shows the synthetic route for preparation of mitofusin agonist Regeneurin S.

[00118] **FIG. 82** shows the HPLC spectrum of compound Regeneurin S. From top to bottom: UV Absorbance at 220nm; UV Absorbance at 254nm; MS chromatogram. Regeneurin S was 97.6% pure.

[00119] **FIG. 83** shows High resolution mass spectroscopy (HRMS) chromatogram of Regeneurin S (C21H29N5OS) shows exact mass found: [M + H]+: 400.2

[00120] **FIG. 84** shows ^{1}H NMR spectrum (500MHz) of Regeneurin S (CDCl3 solvent).

[00121] **FIG. 85** shows ^{13}C NMR spectrum (126MHz) of Regeneurin S (CDCl3 solvent).

[00122] **FIG. 86** shows the synthetic route for preparation of mitofusin agonist Regeneurin C.

[00123] **FIG. 87** shows HPLC spectrum of compound Regeneurin C. From top to bottom: UV Absorbance at 220nm; UV Absorbance at 254nm; MS chromatogram. Regeneurin C was 98.9% pure.

[00124] **FIG. 88** shows HRMS chromatogram of Regeneurin C (C22H31N5O) shows exact mass found: [M + H]+: 382.2.

[00125] **FIG. 89** shows ^{1}H NMR spectrum (500MHz) of Regeneurin C (CDCl3 solvent).

[00126] **FIG. 90** shows ^{13}C NMR spectrum (126MHz) of Regeneurin C (CDCl3 solvent).

[00127] **FIG. 91** shows the general synthetic route for preparation of Mitolityns1-4.

[00128] **FIG. 92** shows HPLC spectrum of compound Mitolityn-1. From top to bottom: UV Absorbance at 220nm; UV Absorbance at 254nm; MS chromatogram. Mitolityn-1 was 93.5% pure.

[00129] **FIG. 93** shows HRMS chromatogram of Mitolityn-1 (C18H31N5O) shows exact mass found: [M + H]+: 334.2.

[00130] **FIG. 94** shows ^{1}H NMR spectrum (400MHz) of Mitolityn-1 (CDCl3 solvent).

[00131] **FIG. 95** shows ^{13}C NMR spectrum (101MHz) of Mitolityn-1 (CDCl3 solvent).

[00132] **FIG. 96** shows HPLC spectrum of compound Mitolityn-2. From top to bottom: UV Absorbance at 220nm; UV Absorbance at 254nm; MS chromatogram. Mitolityn-2 was 98.0% pure.

[00133] **FIG. 97** shows HRMS chromatogram of Mitolityn-2 (C17H29N5O) shows exact mass found: [M + H]+: 320.1.

[00134] **FIG. 98** shows ^{1}H NMR spectrum (400MHz) of Mitolityn-2 (CDCl3 solvent).

[00135] **FIG. 99** shows ^{13}C NMR spectrum (101MHz) of *Mitolityn-2* ($CDCl_3$ solvent).

[00136] **FIG. 100** shows HPLC spectrum of compound Mitolityn-3. From top to bottom: UV Absorbance at 220nm; UV Absorbance at 254nm; MS chromatogram. Mitolityn-3 was 88.9% pure.

[00137] **FIG. 101A, FIG. 101B and FIG. 101C** show HRMS chromatogram of Mitolityn-3 (C17H29N5O2) shows exact mass found: [M + H]+: 336.3.

[00138] **FIG. 102** shows ^{1}H NMR spectrum (400MHz) of *Mitolityn-3* ($CDCl_3$ solvent).

[00139] **FIG. 103** shows ^{13}C NMR spectrum (101MHz) of *Mitolityn-3* ($CDCl_3$ solvent).

[00140] **FIG. 104** shows HPLC spectrum of compound *Mitolityn-4*. From top to bottom: UV Absorbance at 220nm; UV Absorbance at 254nm; MS chromatogram. *Mitolityn-4* was 99.9% pure.

[00141] **FIG. 105** shows HRMS chromatogram of *Mitolityn-4* (C16H27N5O2) shows exact mass found: [M + H]+: 322.3.

[00142] **FIG. 106** shows ^{1}H NMR spectrum (400MHz) of *Mitolityn-4* ($CDCl_3$ solvent).

[00143] **FIG. 107** shows ^{13}C NMR spectrum (101MHz) of *Mitolityn-4* ($CDCl_3$ solvent).

[00144] **FIG. 108** shows the synthetic route for preparation of Mitolityns 5 and 6.

[00145] **FIG. 109** shows HPLC spectrum of compound Mitolityn-5. From top to bottom: UV Absorbance at 220nm; UV Absorbance at 254nm; MS chromatogram. Mitolityn-5 was 94.8% pure.

[00146] **FIG. 110** shows HRMS chromatogram of Mitolityn-5 (C16H27N5O2) shows exact mass found: [M + H]+: 322.2.

[00147] **FIG. 111** shows ^{1}H NMR spectrum (400MHz) of *Mitolityn-5* ($CDCl_3$ solvent).

[00148] **FIG. 112** shows ^{13}C NMR spectrum (101MHz) of *Mitolityn-5* ($CDCl_3$ solvent).

[00149] **FIG. 113** shows HPLC spectrum of compound Mitolityn-6. From top to bottom: UV Absorbance at 220nm; UV Absorbance at 254nm; MS chromatogram. Mitolityn-6 was 66.1% pure.

[00150] **FIG. 114** shows HRMS chromatogram of Mitolityn-6 (C15H25N5O2) shows exact mass found: [M + H]+: 308.2.

[00151] **FIG. 115** shows ^{1}H NMR spectrum (400MHz) of *Mitolityn-6* ($CDCl_3$ solvent).

[00152] **FIG. 116** shows ^{13}C NMR spectrum (101MHz) of *Mitolityn-6* ($CDCl_3$ solvent).

[00153] **FIG. 117** shows characteristics and sourcing of primary human fibroblast lines derived from patients with genetically and mechanistically diverse neurodegenerative diseases.

DETAILED DESCRIPTION

[00154] The present disclosure is based, at least in part, on the discovery that modeling mini peptides can provide small molecule regulators of mitochondrial fusion for use in treating mitochondrial associated diseases, disorders, and conditions. As shown herein, the present disclosure provides new compositions, uses, and techniques for regulating mitochondrial function, including mitochondrial tracking and fusion. These compositions and methods can be useful to correct cell and organ dysfunction caused by primary abnormalities in mitochondrial fission, fusion and subcellular motility/distribution. In particular, the compositions and methods can be useful to enhance mitochondrial trafficking facilitating regeneration of axons and nerves in CNS and PNS related injuries and traumas.

[00155] As described herein, novel small molecules were designed that incorporated functional features (e.g., potency, specificity) of two mitofusin agonist peptidomimetic compounds identified from a functional screen (Cpds A and B) which were functionally synergistic because they acted on different phosphorylated forms of MFN (see e.g., Example 2).

[00156] As described herein, the discovery that “super-activating” / “turbocharging” the endogenous normal mitofusins to overwhelm dominant inhibition by mutant mitofusins constitutes a novel approach to treating diseases caused by loss of function MFN2 mutations. Not only was (1) a way to pharmacologically

stimulate mitofusin activity (e.g., fusion and trafficking) discovered, but (2) a therapeutic approach was also designed that bypasses effects of the mutant Mfn2 in CMT2A. This makes the approach applicable no matter the nature of a patient's individual mutation. As such, this approach is better than "personalized medicine"; this approach can be used to treat any individual with any mitofusin mutation.

[00157] Conventional wisdom is that unopposed mitochondrial fission (resulting in small mitochondrial size) is primarily responsible for disease (e.g., as in Charcot Marie Tooth Disease). But the present disclosure provides for the surprising discovery that, mitochondrial transport, not mitochondria size, is a more important causative factor in disease state and progression. As described herein, it was discovered that mitochondrial trafficking (e.g., the ability for mitochondria to get from point A to point B) is responsible (see e.g., Example 5). Because the compositions discovered herein are useful to enhance mitochondrial trafficking has been, it was discovered that the mitofusin modulatory agents described herein can be used to treat PNS or CNS injuries or traumas.

[00158] The present disclosure shows that pharmacological disruption of intramolecular restraints in MFN2 enhances mitochondrial fusion and trafficking in CMT2A neurons. Mitofusins (MFNs) promote fusion-mediated mitochondrial content exchange and subcellular trafficking. Damaging Mfn2 gene mutations cause neurodegenerative Charcot Marie Tooth Disease type 2A (CMT2A). Here it has been shown that Mfn2 activity is determined by Met376 and His380 interactions with Asp725 and Leu727 and controlled by PINK1 kinase-mediated phosphorylation of adjacent Mfn2 Ser378. Also shown here, are small molecule mimics of the peptide-peptide interface disrupted this interaction, *allosterically activating Mfn2* and *promoting mitochondrial fusion*. These first-in-class mitofusin agonists overcame dominant mitochondrial defects provoked in cultured neurons by CMT2A mutants Mfn2 Arg94Gln and Thr105Met, as evidenced by improved mitochondrial dysmotility, fragmentation, depolarization, and clumping. Mitofusin agonists normalized axonal mitochondrial trafficking within sciatic nerves of Mfn2 Thr105Met mice, promising a therapeutic approach for CMT2A and other untreatable diseases of impaired neuronal mitochondrial dynamism or trafficking.

[0100] As described herein (see e.g., Example 5), based on molecular modeling and a detailed structural and functional interrogation of MFN2-derived

minipeptides encompassing Met^{376}, Ser^{378}, and His^{380} small molecule mitofusin agonists were developed that reversed mitochondrial dysmorphometry and normalized impaired mobility evoked by 2 CMT2A *MFN2* mutants. CMT2A is the prototypical clinical disorder of defective mitochondrial fusion, but impaired mitochondrial trafficking may play as great a role as mitochondrial fragmentation in CMT2A axonal degeneration. Individuals with CMT2A express one mutant MFN2 allele in combination with one normal MFN2 allele and harbor two normal MFN1 alleles. As such, it has been shown herein that it is possible that a therapeutic substrate for agonists to "supercharge" normal mitofusins and overcome dominant inhibition by MFN2 mutants. As shown herein, *in vivo* mitochondrial dysmotility (provoked by CMT2A mutants), normalized by mitofusin agonists, mechanistically links abnormal mitochondrial trafficking in CMT2A to MFN2 dysfunction. Mitofusin agonists show clinical promise not only for diseases primarily caused by loss-of-function MFN2 mutations, but as adjunctive therapy for other neurodegenerative conditions wherein mitochondrial damage is contributory, and in millions of otherwise normal individuals who suffer from accidental or iatrogenic traumatic nerve damage.

MITOFUSIN MODULATING AGENT

[0101] The present disclosure provides for small molecule mimics of a Mfn2 peptide-peptide interface. As described herein, a composition for the treatment of a mitochondria-associated disease, disorder, or condition, can comprise a mitofusin modulating agent, such as a peptide mimetic (e.g., a small-molecule peptide mimetic). A peptide mimetic can be a chemical peptide mimetic. For example, the peptide mimetic can mimic a mitofusin peptide.

[0102] As described herein, chemical peptido-mimetics were identified, and second generation small molecules were designed, based on structural modeling of functionally-critical amino acid side chains of mitofusin (Mfn)-derived mini-peptides (mini-peptides described in Franco et al. Nature 2016). These peptide mimetic compounds activate mitochondrial fusion by directing Mfn1 and Mfn2 to different conformational states. It is believed that these are the first small molecules to target Mfn1 or Mfn2. Specific combinations of small molecules that activate mitochondrial trafficking and mitochondrial fusion, and their use to correct mitochondrial and cellular dysfunction, are described herein.

[0103] As described herein, mitofusin modulating agents (e.g., mitofusin agonists) can reverse mitochondrial defects. For example, mitofusin modulating agents can also have mitochondria transport activity. As another example, a mitofusin modulating agent can modulate or enhance the transport (e.g., trafficking, mobility, or movement) of mitochondria, in for example, a nerve. Example 5 shows that mitofusin agonists restore axonal mitochondrial trafficking (see e.g., **FIG. 28**). Also described herein, mitofusin agonists enhance mitochondrial elongation or mitochondrial elongation aspect ratio. Examples further show, pharmacological disruption of intramolecular restraints in Mfn2 by mitofusin modulating agents promotes mitochondrial fusion and trafficking in neurons.

[0104] As described herein, the mitofusin modulating agents can increase mitochondrial trafficking without affecting or substantially affecting mitochondrial fusion or fission.

Mitofusin Mini Peptide

[0105] As described herein, a peptide mimetic can be a mitofusin mini-peptide as described in US Provisional Patent Application US 62/397,110 (incorporated herein by reference) filed September 20, 2016 and Franco et al. Nature 2016.

Mfn Agonist (Fusion-Promoting) Peptido-Mimetic

[0106] As described herein, a peptide mimetic can be a Mfn agonist (fusion-promoting) peptido-mimetic that competes with endogenous HR1-HR2 binding.

[0107] The Mfn agonist was designed based on the discovery that Mfn1 and Mfn2 share a common domain structure and structural homology with human Mfn1 and *Arabidopsis thaliana* dynamin-related protein. As described herein, Mfn1 and Mfn2 share a common domain structure that was modeled with I-TASSER and structural homology with bacterial dynamin-like protein, human Mfn1 and *Arabidopsis thaliana* dynamin-related protein (see e.g., **FIG. 1**). The model shows how the first heptad repeat domain (HR1) interacts in an anti-parallel manner with the carboxyl terminal second heptad repeat (HR2) domain to restrain it and prevent its extension into the cytosol, which is currently believed to be necessary for mitochondrial tethering and fusion (see e.g., Example 1).

[0108] As described herein, an Mfn agonist can inhibit or block HR1-HR2 binding or interaction. For example, Met376, Ser378, His380, or Met 381 amino acids were discovered to be necessary for the HR1-HR2 interaction. Amino acids implicated in HR1-HR2 binding or interactions were identified by first defining a minimal HR1-derived mini-peptide that competes with endogenous HR1-HR2 binding (see e.g., **FIG. 2A-FIG. 2B**), followed by functional analyses of a complete series of alanine substituted peptides (see e.g., **FIG. 2C**). Based on these results chemical peptido-mimetics were derived that, by mimicking the 3-dimensional spatial and charge characteristics of these critical amino acid side chains, have similar modulatory activity on mitochondrial fusion as the N-terminal mini-peptide (see e.g., Example 1).

Novel Regeneurin agonists (see Example 6, TABLE 8) are described below.

Compound ID	IUPAC Name	Structure	M.W. (g/mol)	Formula
Regeneurin-C	1-(3-(5-cyclopropyl-4-phenyl-4H-1,2,4-triazol-3-yl)propyl)-3-(2-methylcyclohexyl)urea	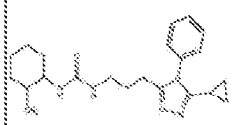	381.52	C22H31N5O
Regeneurin-O	1-(2-((5-cyclopropyl-4-phenyl-4H-1,2,4-triazol-3-yl)oxy)ethyl)-3-(2-methylcyclohexyl)urea	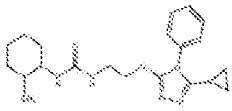	383.49	C21H29N5O2
Regeneurin-C/O	1-(3-(5-cyclopropyl-4-phenyl-4H-1,2,4-triazol-3-yl)propyl)-3-(tetrahydro-2H-pyran-4-yl)urea	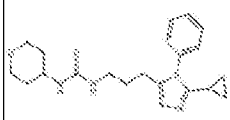	369.47	C20H27N5O2

Regeneurin-SO	1-(2-((5-cyclopropyl-4-phenyl-4H-1,2,4-triazol-3-yl)sulfinyl)ethyl)-3-(2-methylcyclohexyl)urea	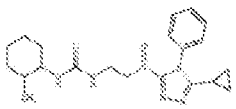	415.55	C21H29N5O2S
Regeneurin-SO_2	1-(2-((5-cyclopropyl-4-phenyl-4H-1,2,4-triazol-3-yl)sulfonyl)ethyl)-3-(2-methylcyclohexyl)urea	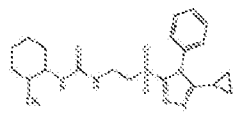	431.56	C21H29N5O3S

Novel Mitolityn agonists (see Example 6, TABLE 9) are described below.

Compound ID	IUPAC Name	Structure	M.W. (g/mol)	Formula
Mitolityn-1	1-(3-(5-cyclopropyl-4-ethyl-4H-1,2,4-triazol-3-yl)propyl)-3-(2-methylcyclohexyl)urea	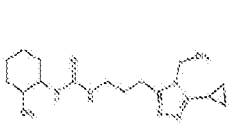	333.47	C18H31N5O
Mitolityn-2	1-cyclohexyl-3-(3-(5-cyclopropyl)-4-ethyl-4H-1,2,4-triazol-3-yl)propyl)urea	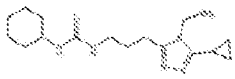	319.45	C17H29N5O
Mitolityn-3	1-(3-(5-cyclopropyl-4-ethyl-4H-1,2,4-triazol-3-yl)propyl)-3-(3-methyltetrahydro-2H-pyran-4-yl)urea	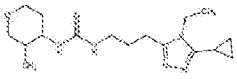	335.44	C17H29N5O2

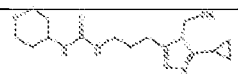

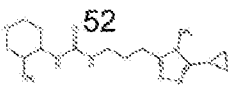

Mitolityn-4	1-(3-(5-cyclopropyl-4-ethyl-4H-1,2,4-triazol-3-yl)propyl)-3-(tetrahydro-2H-pyran-4-yl)urea		321.42	C16H27N5O2
Mitolityn-5 (Renamed after Fusogenin-4a)	1-(3-(5-cyclopropyl-4-methyl-4H-1,2,4-triazol-3-yl)propyl)-3-(3-methyltetrahydro-2H-pyran-4-yl)urea		321.43	C16H27N5O2
Mitolityn-6 (Renamed after Fusogenin-3a)	1-(3-(5-cyclopropyl-4-methyl-4H-1,2,4-triazol-3-yl)propyl)-3-(tetrahydro-2H-pyran-4-yl)urea	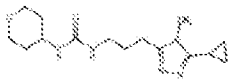	307.4	C15H25N5O2

Novel Fusogenin agonists (see Example 6, TABLE 10) are described below.

Compound ID	IUPAC Name	Structure	M.W. (g/mol)	Formula
Fusogenin-1	1-(3-(4-methyl-5-phenyl-4H-1,2,4-triazol-3-yl)propyl)-3-(2-methylcyclohexyl)urea	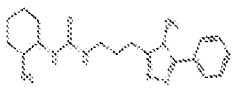	355.49	C20H29N5O
Fusogenin-3	1-(3-(4-methyl-5-phenyl-4H-1,2,4-triazol-3-yl)propyl)-3-(tetrahydro-2H-pyran-4-yl)urea	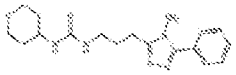	343.43	C18H25N5O2
Fusogenin-4	1-(3-(4-methyl-5-phenyl-4H-1,2,4-triazol-3-yl)propyl)-3-(3-methyltetrahydro-2H-pyran-4-yl)urea	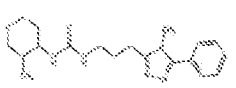	357.46	C19H27N5O2

Mitofusin Modulating Agents: Small Molecules to Target Mfn1 and/or Mfn2

[0109] The small molecule Mfn regulators as described herein are allosteric agonists. An agonist can be a substance that fully activates the receptor that it binds to, and an antagonist can be a substance that binds to a receptor but does not activate and can block the activity of other agonists.

[0110] Examples of mitofusin modulating agents are described herein (see e.g., Example 2). Mitofusin modulating agents can be, of the formula:

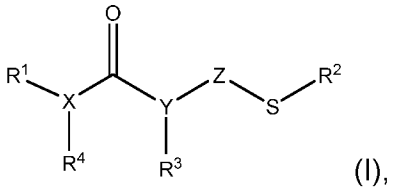

(I),

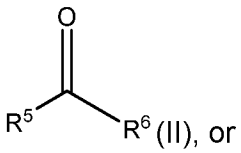

(II), or

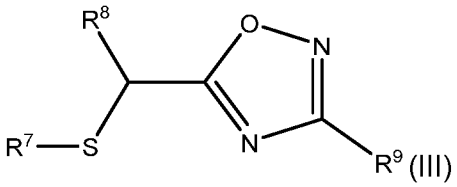

(III)

or a pharmaceutically acceptable salt, tautomer, or stereoisomer thereof wherein,

R^1 is selected from the group consisting of C_{1-8} alkyl, C_{1-8} alkyl substituted with S, S, thiophene, C_{3-8} cycloalkyl, C_{3-8} heteroaryl, C_{3-8} heterocyclyl, thiophene, and thiophene carboxamide;

R^2 is selected from the group consisting of C_{3-8} cycloalkyl, C_{3-8} heteroaryl, C_{3-8} heterocyclyl, imidazole, thiophene, thiophene carboxamide, and triazole;

R^3 is absent or selected from the group consisting of hydrogen (H) and C_{1-8} alkyl;

R^4 is absent or selected form the group consisting of hydrogen (H) and C_{1-8} alkyl;

R^5 is selected from the group consisting of C_{1-8} alkyl, C_{1-8} alkyl substituted with S, S, thiophene, C_{3-8} cycloalkyl, C_{3-8} heteroaryl, C_{3-8} heterocyclyl, thiophene, thiophene carboxamide, and triazole;

R^6 is selected from the group consisting of bicyclononanone, pyrrole,

benzimidizole, pyrrole substituted pyrrole, and substituted benzimidizole;

R^7 is selected from the group consisting of C_{1-8} alkyl, pyrrole, pyrrole substituted pyrrole, benzimidizole, and substituted benzimidizole;

R^8 is selected from the group consisting of hydrogen (H);

R^9 is selected from the group consisting of C_{1-8} alkyl; pyrrole, substituted pyrrole, pyrrole substituted pyrrole, benzimidizole, and substituted benzimidizole;

X is selected from the group consisting of O, C, and N;

Y is selected from the group consisting of O, C, and N; and

Z is a linker group selected from the group consisting of a bond or C_{1-6} alkyl; and

optionally, R^1 and R^2 form a cyclic group, R^1 and R^4 form a cyclic group, R^2 and R^3 form a cyclic group, R^4 and R^3 form a cyclic group; or R^8 and R^7 form a cyclic group,

wherein,

the bicyclononanone optionally comprises one or more N atoms.

[0111] Optionally, the compound of formula (I), (II), or (III) is not a compound of TABLE 4, TABLE 5, TABLE 7, or the commercially sourced compositions in TABLE 1 or TABLE 2.

[0112] Furthermore, R^1, R^2, R^3, R^4, R^5, R^6, R^7, R^8, or R^9 can be optionally substituted by one or more of acetamide, C_{1-8} alkoxy, amino, azo, Br, C_{1-8} alkyl, carbonyl, carboxyl, Cl, cyano, C_{3-8} cycloalkyl, C_{3-8} heteroaryl, C_{3-8} heterocyclyl, hydroxyl, F, halo, indole, N, nitrile, O, phenyl, S, sulfoxide, sulfur dioxide, or thiophene and optionally further substituted with acetamide, alkoxy, amino, azo, Br, C_{1-8} alkyl, carbonyl, carboxyl, Cl, cyano, C_{3-8} cycloalkyl, C_{3-8} heteroaryl, C_{3-8} heterocyclyl, hydroxyl, F, halo, indole, N, nitrile, O, phenyl, S, sulfoxide, sulfur dioxide, or thiophene and the alkyl, cycloalkyl, heteroaryl, heterocyclyl, indole, or phenyl is optionally further substituted with one or more selected from the group consisting of acetamide, alkoxy, amino, azo, Br, C_{1-8} alkyl, carbonyl, carboxyl, Cl, cyano, C_{3-8} cycloalkyl, C_{3-8} heteroaryl, C_{3-8} heterocyclyl, hydroxyl, F, halo, indole, N, nitrile, O, phenyl, S, sulfoxide, or thiophene.

[0113] The R^1, R^2, R^3, R^4, R^5, R^6, R^7, R^8, or R^9 groups can be optionally substituted or further substituted with one or more groups independently selected from the group consisting of hydroxyl; C_{1-10} alkyl hydroxyl; amine; C_{1-10} carboxylic

acid; C_{1-10} carboxyl; straight chain or branched C_{1-10} alkyl, optionally containing unsaturation; a C_{2-8} cycloalkyl optionally containing unsaturation or one oxygen or nitrogen atom; straight chain or branched C_{1-10} alkyl amine; heterocyclyl; heterocyclic amine; and aryl comprising a phenyl; heteroaryl containing from 1 to 4 N, O, or S atoms; unsubstituted phenyl ring; substituted phenyl ring; unsubstituted heterocyclyl; and substituted heterocyclyl, wherein the unsubstituted phenyl ring or substituted phenyl ring can be optionally substituted with one or more groups independently selected from the group consisting of hydroxyl; C_{1-10} alkyl hydroxyl; amine; C_{1-10} carboxylic acid; C_{1-10} carboxyl; straight chain or branched C_{1-10} alkyl, optionally containing unsaturation; straight chain or branched C_{1-10} alkyl amine, optionally containing unsaturation; a C_{2-10}cycloalkyl optionally containing unsaturation or one oxygen or nitrogen atom; straight chain or branched C_{1-10} alkyl amine; heterocyclyl; heterocyclic amine; aryl comprising a phenyl; and heteroaryl containing from 1 to 4 N, O, or S atoms; and the unsubstituted heterocyclyl or substituted heterocyclyl can be optionally substituted with one or more groups independently selected from the group consisting of hydroxyl; C_{1-10} alkyl hydroxyl; amine; C_{1-10} carboxylic acid; C_{1-10} carboxyl; straight chain or branched C_{1-10} alkyl, optionally containing unsaturation; straight chain or branched C_{1-10} alkyl amine, optionally containing unsaturation; a C_{2-8} cycloalkyl optionally containing unsaturation or one oxygen or nitrogen atom; heterocyclyl; straight chain or branched C_{1-10} alkyl amine; heterocyclic amine; and aryl comprising a phenyl; and heteroaryl containing from 1 to 4 N, O, or S atoms. Any of the above can be further optionally substituted.

[0114] In some embodiments, R^1, R^2, R^3, R^4, R^5, R^6, R^7, R^8, or R^9 are optionally substituted by one or more of: acetamide, alkoxy, amino, azo, Br, C_{1-8} alkyl, carbonyl, carboxyl, Cl, cyano, C_{3-8} cycloalkyl, C_{3-8} heteroaryl, C_{3-8} heterocyclyl, hydroxyl, F, halo, indole, N, nitrile, O, phenyl, S, sulfoxide, sulfur dioxide, or thiophene; and optionally further substituted with one or more acetamide, alkoxy, amino, azo, Br, C_{1-8} alkyl, carbonyl, carboxyl, Cl, cyano, C_{3-8} cycloalkyl, C_{3-8} heteroaryl, C_{3-8} heterocyclyl, hydroxyl, F, halo, indole, N, nitrile, O, phenyl, S, sulfoxide, sulfur dioxide, or thiophene; wherein the alkyl, cycloalkyl, heteroaryl, heterocyclyl, indole, or phenyl, is optionally further substituted with one or more of acetamide, alkoxy, amino, azo, Br, C_{1-8} alkyl, carbonyl, carboxyl, Cl, cyano, C_{3-8}

cycloalkyl, C_{3-8} heteroaryl, C_{3-8} heterocyclyl, hydroxyl, F, halo, indole, N, nitrile, O, phenyl, S, sulfoxide, sulfur dioxide, or thiophene.

[0115] In some embodiments, mitofusin modulating agent or agonists can be selected from the compounds below or the R^1, R^2, R^3, R^4, or R^5 groups or X or Y comprised in the below compounds can be selected independently and placed into formula (I), (II), or (III) (see e.g., TABLE 7, 70 commercially available compounds):

% long compare to B	1 - Position	Structure	Name
202	1 - F9	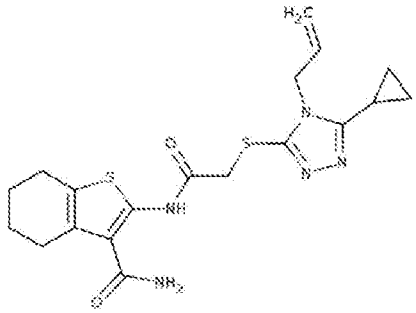	2-(2-{[5-cyclopropyl-4-(prop-2-en-1-yl)-4H-1,2,4-triazol-3-yl]sulfanyl}acetamido)-4,5,6,7-tetrahydro-1-benzothiophene-3-carboxamide
141	1 - G1	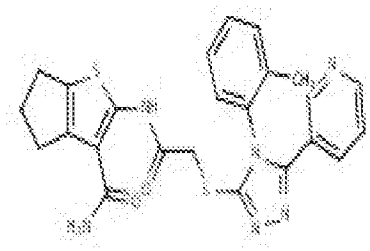	2-(2-{[4-(2-methylphenyl)-5-(pyridin-3-yl)-4H-1,2,4-triazol-3-yl]sulfanyl}acetamido)-4H,5H,6H-cyclopenta[b]thiophene-3-carboxamide
128	1 - D2	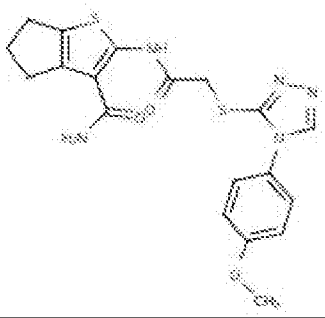	2-(2-{[4-(4-methoxyphenyl)-4H-1,2,4-triazol-3-yl]sulfanyl}acetamido)-4H,5H,6H-cyclopenta[b]thiophene-3-carboxamide
114	D08	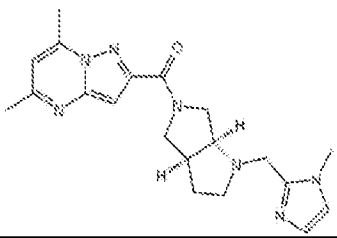	2-{[(3aS,6aS)-5-{5,7-dimethylpyrazolo[1,5-a]pyrimidine-2-carbonyl}-octahydropyrrolo[3,4-b]pyrrol-1-yl]methyl}-1-methyl-1H-imidazole

107	1 - B1	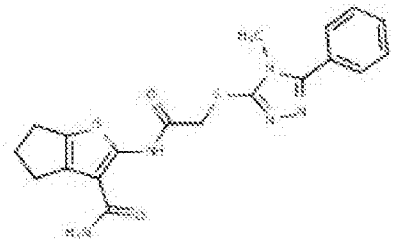	2-{2-[(4-methyl-5-phenyl-4H-1,2,4-triazol-3-yl)sulfanyl]acetamido}-4H,5H,6H-cyclopenta[b]thiophene-3-carboxamide
105	1 - D4	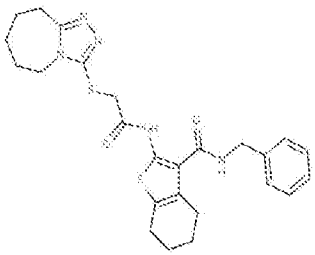	N-benzyl-2-(2-{5H,6H,7H,8H,9H-[1,2,4]triazolo[4,3-a]azepin-3-ylsulfanyl}acetamido)-4,5,6,7-tetrahydro-1-benzothiophene-3-carboxamide
100	B01	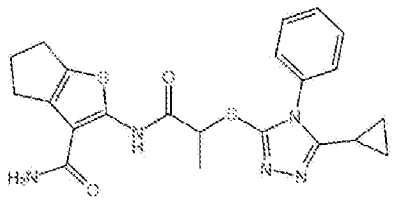	2-{2-[(5-cyclopropyl-4-phenyl-4H-1,2,4-triazol-3-yl)sulfanyl]propanamido}-4H,5H,6H-cyclopenta[b]thiophene-3-carboxamide
99	1 - G11	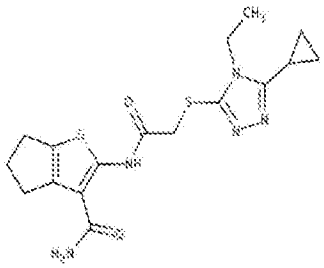	2-{2-[(5-cyclopropyl-4-ethyl-4H-1,2,4-triazol-3-yl)sulfanyl]acetamido}-4H,5H,6H-cyclopenta[b]thiophene-3-carboxamide

92	1 - D7	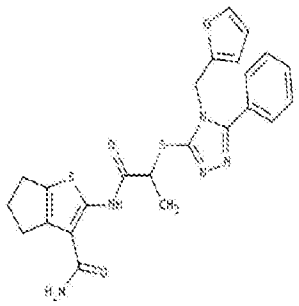	2-[2-({4-[(furan-2-yl)methyl]-5-phenyl-4H-1,2,4-triazol-3-yl}sulfanyl)propanamido]-4H,5H,6H-cyclopenta[b]thiophene-3-carboxamide
90	1 - B3	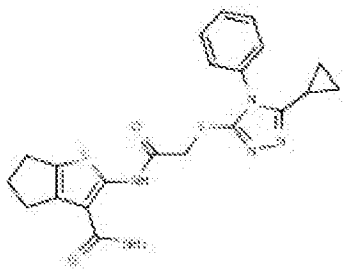	2-{2-[(5-cyclopropyl-4-phenyl-4H-1,2,4-triazol-3-yl)sulfanyl]acetamido}-4H,5H,6H-cyclopenta[b]thiophene-3-carboxamide
75	**A4**	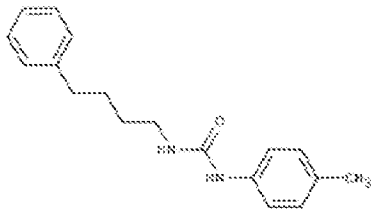	3-(4-methylphenyl)-1-(4-phenylbutyl)urea
73	D09	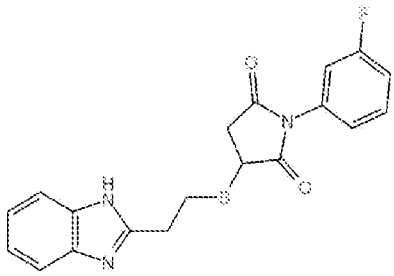	3-{[2-(1H-1,3-benzodiazol-2-yl)ethyl]sulfanyl}-1-(3-fluorophenyl)pyrrolidine-2,5-dione

71	A10	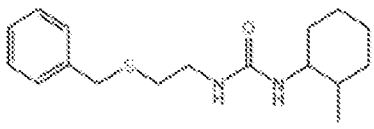	1-[2-(benzylsulfanyl)ethyl]-3-(2-methylcyclohexyl)urea
68	1 - B6	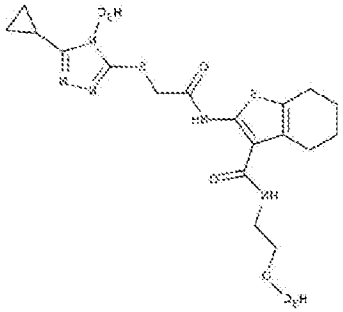	2-{2-[(5-cyclopropyl-4-methyl-4H-1,2,4-triazol-3-yl)sulfanyl]acetamido}-N-(2-methoxyethyl)-4,5,6,7-tetrahydro-1-benzothiophene-3-carboxamide
64	B07	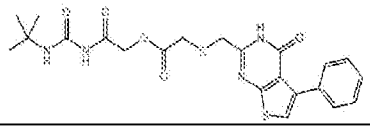	2-[(tert-butylcarbamoyl)amino]-2-oxoethyl 2-[({4-oxo-5-phenyl-3H,4H-thieno[2,3-d]pyrimidin-2-yl}methyl)sulfanyl]acetate
59	**pA**	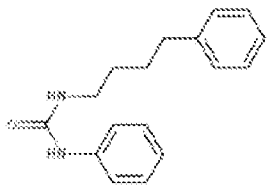	3-phenyl-1-(4-phenylbutyl)urea

55	A09	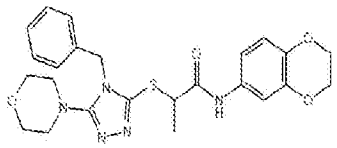	2-{[4-benzyl-5-(morpholin-4-yl)-4H-1,2,4-triazol-3-yl]sulfanyl}-N-(2,3-dihydro-1,4-benzodioxin-6-yl)propanamide
47	A08	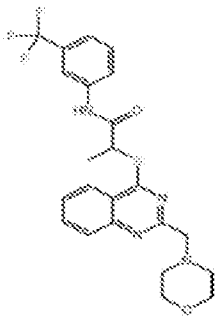	2-({2-[(morpholin-4-yl)methyl]quinazolin-4-yl}sulfanyl)-N-[3-(trifluoromethyl)phenyl]propanamide
47	1 - A8	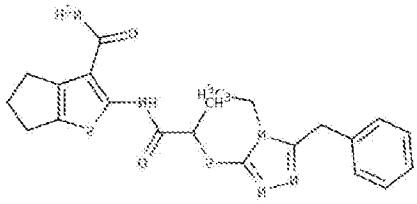	2-{2-[(5-benzyl-4-ethyl-4H-1,2,4-triazol-3-yl)sulfanyl]propanamido}-4H,5H,6H-cyclopenta[b]thiophene-3-carboxamide
45	1 - A10	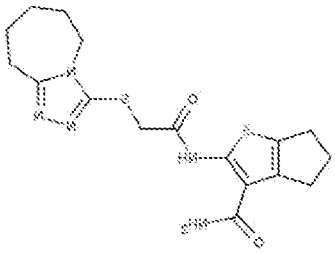	2-(2-{5H,6H,7H,8H,9H-[1,2,4]triazolo[4,3-a]azepin-3-ylsulfanyl}acetamido)-4H,5H,6H-cyclopenta[b]thiophene-3-carboxamide

41	1 - B7	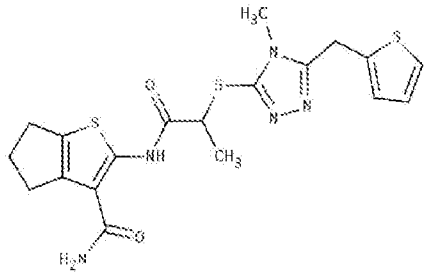	2-[2-({4-methyl-5-[(thiophen-2-yl)methyl]-4H-1,2,4-triazol-3-yl}sulfanyl)propanamido]-4H,5H,6H-cyclopenta[b]thiophene-3-carboxamide
39	1 - C10	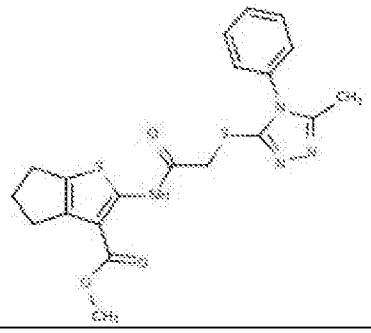	methyl 2-{2-[(5-methyl-4-phenyl-4H-1,2,4-triazol-3-yl)sulfanyl]acetamido}-4H,5H,6H-cyclopenta[b]thiophene-3-carboxylate
39	B03	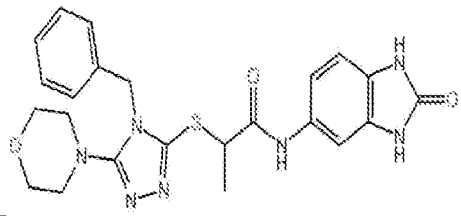	2-{[4-benzyl-5-(morpholin-4-yl)-4H-1,2,4-triazol-3-yl]sulfanyl}-N-(2-oxo-2,3-dihydro-1H-1,3-benzodiazol-5-yl)propanamide
38	1 - E1	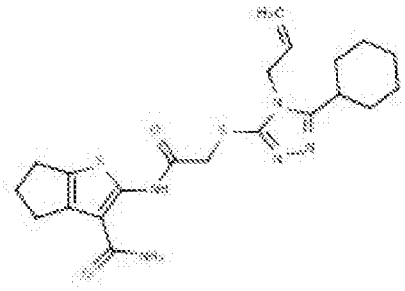	2-(2-{[5-cyclohexyl-4-(prop-2-en-1-yl)-4H-1,2,4-triazol-3-yl]sulfanyl}acetamido)-4H,5H,6H-cyclopenta[b]thiophene-3-carboxamide

36	B09	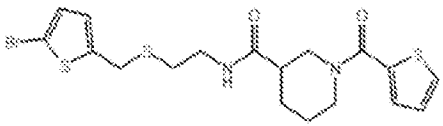	N-(2-{[(5-bromothiophen-2-yl)methyl]sulfanyl}ethyl)-1-(thiophene-2-carbonyl)piperidine-3-carboxamide
35	1 - C8	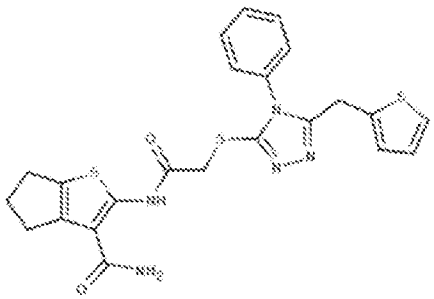	2-[2-({4-phenyl-5-[(thiophen-2-yl)methyl]-4H-1,2,4-triazol-3-yl}sulfanyl)acetamido]-4H,5H,6H-cyclopenta[b]thiophene-3-carboxamide
32	**A3**	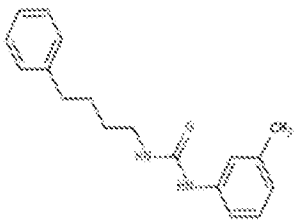	3-(3-methylphenyl)-1-(4-phenylbutyl)urea
31	A12	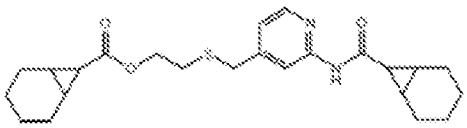	2-{[(2-{bicyclo[4.1.0]heptane-7-amido}pyridin-4-yl)methyl]sulfanyl}ethyl bicyclo[4.1.0]heptane-7-carboxylate

30	1 - F6	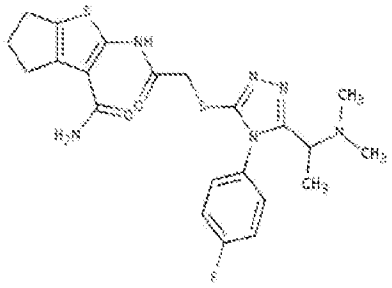	2-[2-({5-[1-(dimethylamino)ethyl]-4-(4-fluorophenyl)-4H-1,2,4-triazol-3-yl}sulfanyl)acetamido]-4H,5H,6H-cyclopenta[b]thiophene-3-carboxamide
29	1 - F10	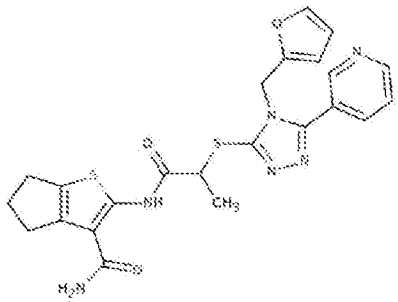	2-[2-({4-[(furan-2-yl)methyl]-5-(pyridin-3-yl)-4H-1,2,4-triazol-3-yl}sulfanyl)propanamido]-4H,5H,6H-cyclopenta[b]thiophene-3-carboxamide
29	C07	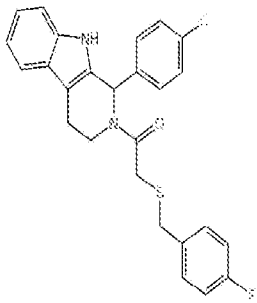	1-[1-(4-chlorophenyl)-1H,2H,3H,4H,9H-pyrido[3,4-b]indol-2-yl]-2-{[(4-fluorophenyl)methyl]sulfanyl}ethan-1-one
29	1 - H9		1-[2-(benzylsulfanyl)ethyl]-3-cyclopentylurea

26	2 - A1 (also B5 on screen 2)	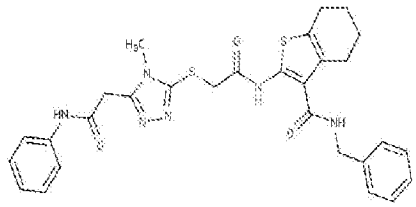	N-benzyl-2-[2-({4-methyl-5-[(phenylcarbamoyl)methyl]-4H-1,2,4-triazol-3-yl}sulfanyl)acetamido]-4,5,6,7-tetrahydro-1-benzothiophene-3-carboxamide
26	B12	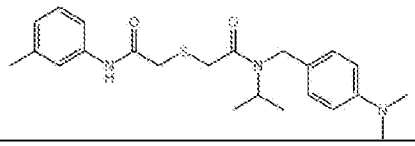	N-{[4-(dimethylamino)phenyl]methyl}-2-({[(3-methylphenyl)carbamoyl]methyl}sulfanyl)-N-(propan-2-yl)acetamide
24	D04	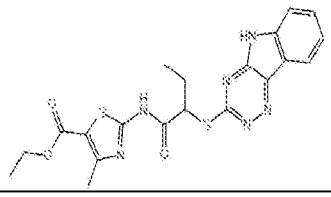	ethyl 4-methyl-2-(2-{5H-[1,2,4]triazino[5,6-b]indol-3-ylsulfanyl}butanamido)-1,3-thiazole-5-carboxylate
23	1 - D1	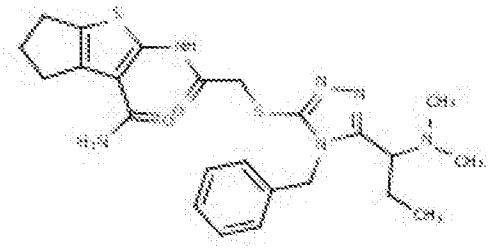	2-[2-({4-benzyl-5-[1-(dimethylamino)propyl]-4H-1,2,4-triazol-3-yl}sulfanyl)acetamido]-4H,5H,6H-cyclopenta[b]thiophene-3-carboxamide

23	1 - H5	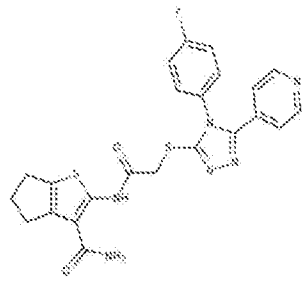	2-(2-{[4-(4-fluorophenyl)-5-(pyridin-4-yl)-4H-1,2,4-triazol-3-yl]sulfanyl}acetamido)-4H,5H,6H-cyclopenta[b]thiophene-3-carboxamide
23	B11	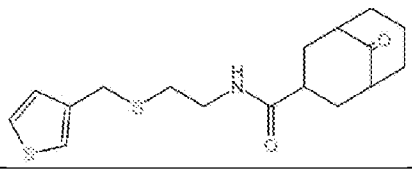	9-oxo-N-(2-{[(thiophen-3-yl)methyl]sulfanyl}ethyl)bicyclo[3.3.1]nonane-3-carboxamide
23	1 - C6	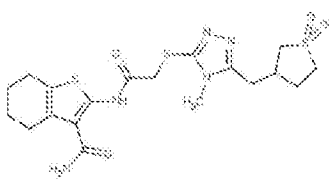	2-[2-({5-[(1,1-dioxo-1λ⁶-thiolan-3-yl)methyl]-4-methyl-4H-1,2,4-triazol-3-yl}sulfanyl)acetamido]-4,5,6,7-tetrahydro-1-benzothiophene-3-carboxamide
22	1 - F4	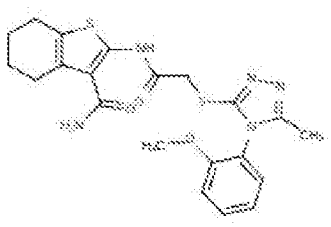	2-(2-{[4-(2-methoxyphenyl)-5-methyl-4H-1,2,4-triazol-3-yl]sulfanyl}acetamido)-4,5,6,7-tetrahydro-1-benzothiophene-3-carboxamide

21	1 - F1	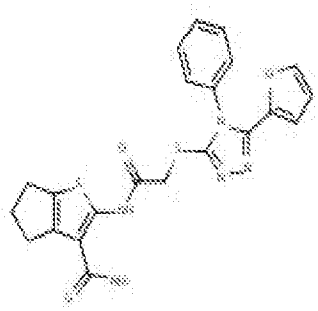	2-(2-{[5-(furan-2-yl)-4-phenyl-4H-1,2,4-triazol-3-yl]sulfanyl}acetamido)-4H,5H,6H-cyclopenta[b]thiophene-3-carboxamide
21	1 - E10	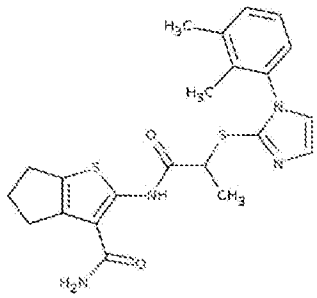	2-(2-{[1-(2,3-dimethylphenyl)-1H-imidazol-2-yl]sulfanyl}propanamido)-4H,5H,6H-cyclopenta[b]thiophene-3-carboxamide
20	1 - G2	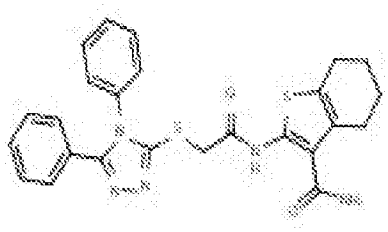	2-{2-[(diphenyl-4H-1,2,4-triazol-3-yl)sulfanyl]acetamido}-4,5,6,7-tetrahydro-1-benzothiophene-3-carboxamide
20	1 - B8	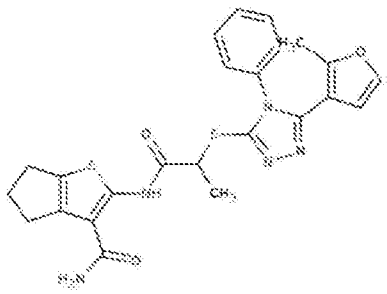	2-(2-{[5-(2-methylfuran-3-yl)-4-phenyl-4H-1,2,4-triazol-3-yl]sulfanyl}propanamido)-4H,5H,6H-cyclopenta[b]thiophene-3-carboxamide

19	1 - C1	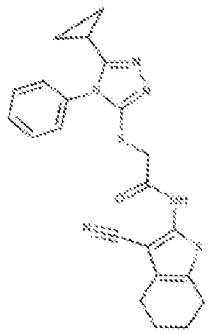	N-(3-cyano-4,5,6,7-tetrahydro-1-benzothiophen-2-yl)-2-[(5-cyclopropyl-4-phenyl-4H-1,2,4-triazol-3-yl)sulfanyl]acetamide
18	1 - D12	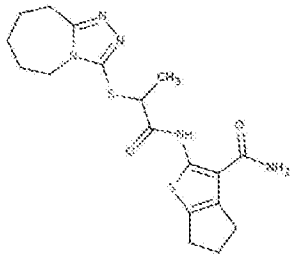	2-(2-{5H,6H,7H,8H,9H-[1,2,4]triazolo[4,3-a]azepin-3-ylsulfanyl}propanamido)-4H,5H,6H-cyclopenta[b]thiophene-3-carboxamide
18	1 - B9	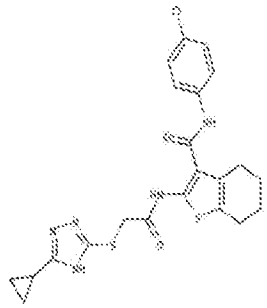	N-(4-chlorophenyl)-2-{2-[(5-cyclopropyl-4H-1,2,4-triazol-3-yl)sulfanyl]acetamido}-4,5,6,7-tetrahydro-1-benzothiophene-3-carboxamide
17	1 - E4	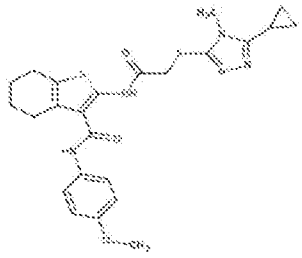	2-{2-[(5-cyclopropyl-4-methyl-4H-1,2,4-triazol-3-yl)sulfanyl]acetamido}-N-(4-methoxyphenyl)-4,5,6,7-tetrahydro-1-benzothiophene-3-carboxamide

17	1 - E2	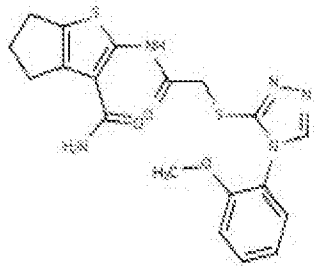	2-(2-{[4-(2-methoxyphenyl)-4H-1,2,4-triazol-3-yl]sulfanyl}acetamido)-4H,5H,6H-cyclopenta[b]thiophene-3-carboxamide
17	1 - D10	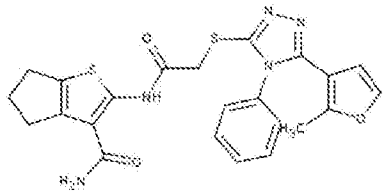	2-(2-{[5-(2-methylfuran-3-yl)-4-phenyl-4H-1,2,4-triazol-3-yl]sulfanyl}acetamido)-4H,5H,6H-cyclopenta[b]thiophene-3-carboxamide
16	C01	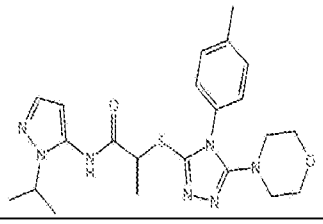	2-{[4-(4-methylphenyl)-5-(morpholin-4-yl)-4H-1,2,4-triazol-3-yl]sulfanyl}-N-[1-(propan-2-yl)-1H-pyrazol-5-yl]propanamide
15	B05	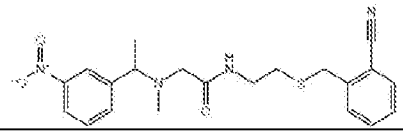	N-(2-{[(2-cyanophenyl)methyl]sulfanyl}ethyl)-2-{methyl[1-(3-nitrophenyl)ethyl]amino}acetamide

15	1 - H11	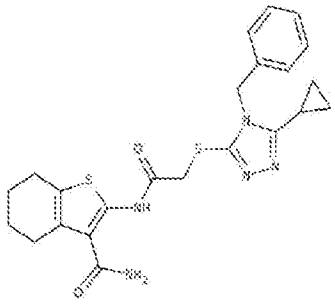	2-{2-[(4-benzyl-5-cyclopropyl-4H-1,2,4-triazol-3-yl)sulfanyl]acetamido}-4,5,6,7-tetrahydro-1-benzothiophene-3-carboxamide
14	1 - G8	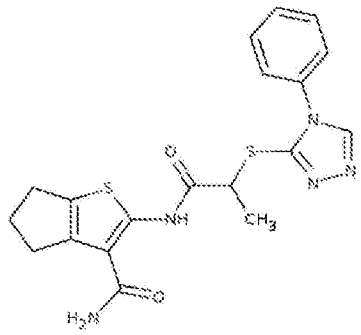	2-{2-[(4-phenyl-4H-1,2,4-triazol-3-yl)sulfanyl]propanamido}-4H,5H,6H-cyclopenta[b]thiophene-3-carboxamide
14	A07	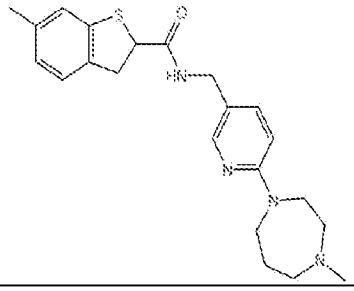	6-methyl-N-{[6-(4-methyl-1,4-diazepan-1-yl)pyridin-3-yl]methyl}-2,3-dihydro-1-benzothiophene-2-carboxamide
14	C02	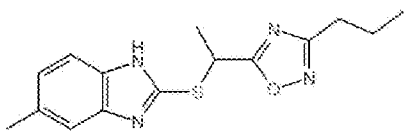	5-methyl-2-{[1-(3-propyl-1,2,4-oxadiazol-5-yl)ethyl]sulfanyl}-1H-1,3-benzodiazole

13	1 - C12	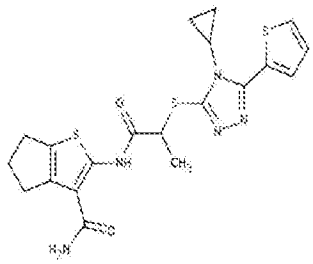	2-(2-{[4-cyclopropyl-5-(thiophen-2-yl)-4H-1,2,4-triazol-3-yl]sulfanyl}propanamido)-4H,5H,6H-cyclopenta[b]thiophene-3-carboxamide
13	1 - F11	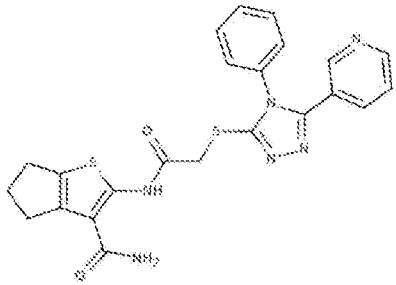	2-(2-{[4-phenyl-5-(pyridin-3-yl)-4H-1,2,4-triazol-3-yl]sulfanyl}acetamido)-4H,5H,6H-cyclopenta[b]thiophene-3-carboxamide
13	D02	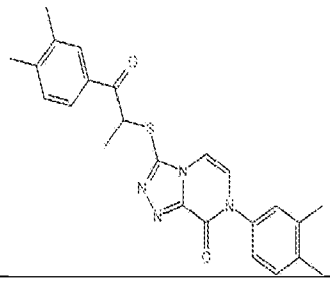	7-(3,4-dimethylphenyl)-3-{[1-(3,4-dimethylphenyl)-1-oxopropan-2-yl]sulfanyl}-7H,8H-[1,2,4]triazolo[4,3-a]pyrazin-8-one
13	1 - F3	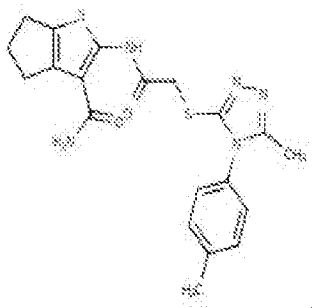	2-(2-{[5-methyl-4-(4-methylphenyl)-4H-1,2,4-triazol-3-yl]sulfanyl}acetamido)-4H,5H,6H-cyclopenta[b]thiophene-3-carboxamide

12	**B2**	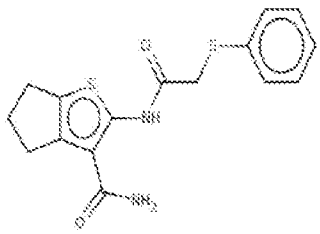	2-[2-(phenylsulfanyl)acetamido]-4H,5H,6H-cyclopenta[b]thiophene-3-carboxamide
12	1 - C5	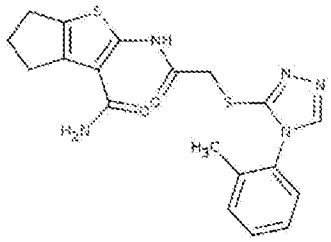	2-(2-{[4-(2-methylphenyl)-4H-1,2,4-triazol-3-yl]sulfanyl}acetamido)-4H,5H,6H-cyclopenta[b]thiophene-3-carboxamide
12	B08	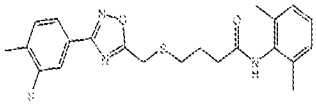	N-(2,6-dimethylphenyl)-4-({[3-(3-fluoro-4-methylphenyl)-1,2,4-oxadiazol-5-yl]methyl}sulfanyl)butanamide
11	1 - A1	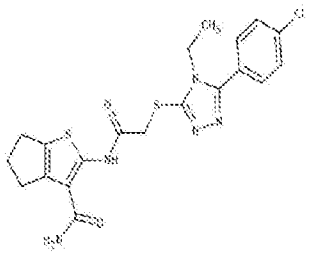	2-(2-{[5-(4-chlorophenyl)-4-ethyl-4H-1,2,4-triazol-3-yl]sulfanyl}acetamido)-4H,5H,6H-cyclopenta[b]thiophene-3-carboxamide

11	E02	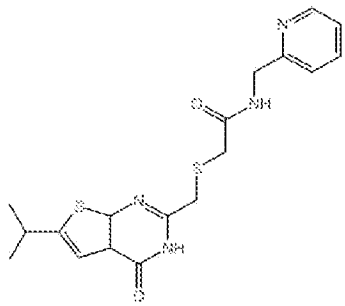	2-({[4-oxo-6-(propan-2-yl)-3H,4H,4aH,7aH-thieno[2,3-d]pyrimidin-2-yl]methyl}sulfanyl)-N-[(pyridin-2-yl)methyl]acetamide
11	1 - E3	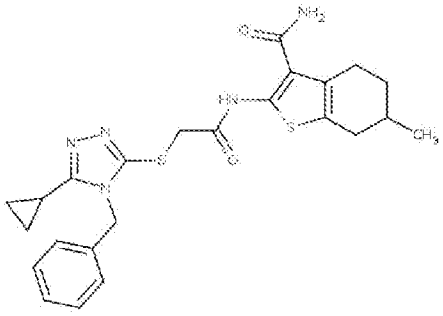	2-{2-[(4-benzyl-5-cyclopropyl-4H-1,2,4-triazol-3-yl)sulfanyl]acetamido}-6-methyl-4,5,6,7-tetrahydro-1-benzothiophene-3-carboxamide
10	1 - E6	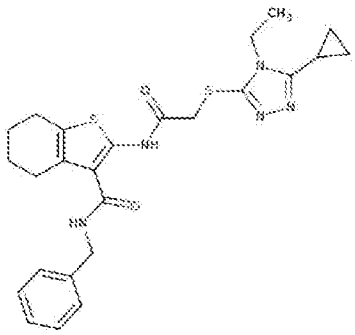	N-benzyl-2-{2-[(5-cyclopropyl-4-ethyl-4H-1,2,4-triazol-3-yl)sulfanyl]acetamido}-4,5,6,7-tetrahydro-1-benzothiophene-3-carboxamide
10	1 - H3	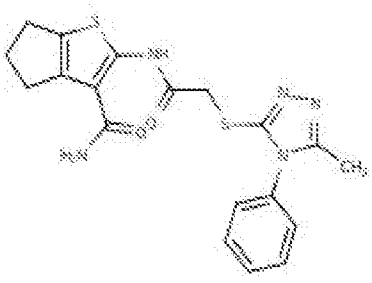	2-{2-[(5-methyl-4-phenyl-4H-1,2,4-triazol-3-yl)sulfanyl]acetamido}-4H,5H,6H-cyclopenta[b]thiophene-3-carboxamide

10	1 - D6	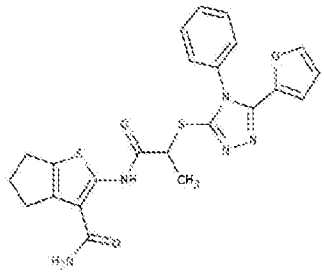	2-(2-{[5-(furan-2-yl)-4-phenyl-4H-1,2,4-triazol-3-yl]sulfanyl}propanamido)-4H,5H,6H-cyclopenta[b]thiophene-3-carboxamide
10	1 - B4	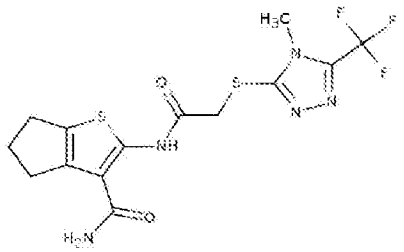	2-(2-{[4-methyl-5-(trifluoromethyl)-4H-1,2,4-triazol-3-yl]sulfanyl}acetamido)-4H,5H,6H-cyclopenta[b]thiophene-3-carboxamide
10	C03	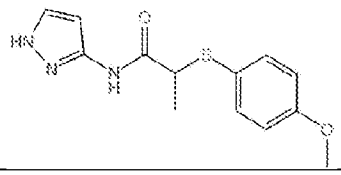	2-[(4-methoxyphenyl)sulfanyl]-N-(1H-pyrazol-3-yl)propanamide
9	1 - E7	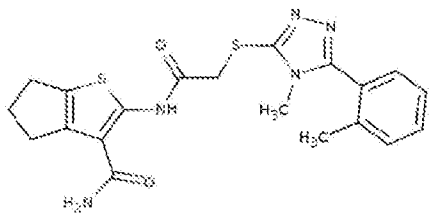	2-(2-{[4-methyl-5-(2-methylphenyl)-4H-1,2,4-triazol-3-yl]sulfanyl}acetamido)-4H,5H,6H-cyclopenta[b]thiophene-3-carboxamide

9	1 - G6	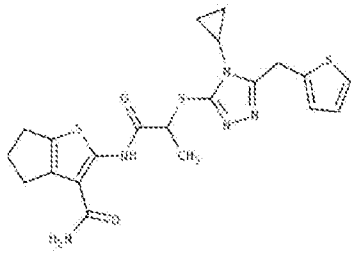	2-[2-({4-cyclopropyl-5-[(thiophen-2-yl)methyl]-4H-1,2,4-triazol-3-yl}sulfanyl)propanamido]-4H,5H,6H-cyclopenta[b]thiophene-3-carboxamide
9	B04	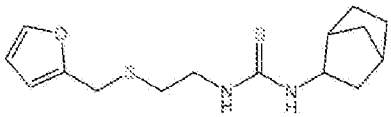	1-{bicyclo[2.2.1]heptan-2-yl}-3-(2-{[(furan-2-yl)methyl]sulfanyl}ethyl)thiourea
9	D01	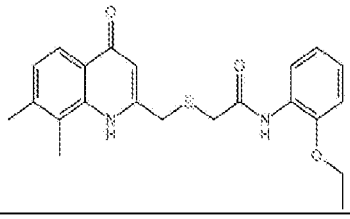	2-{[(7,8-dimethyl-4-oxo-1,4-dihydroquinolin-2-yl)methyl]sulfanyl}-N-(2-ethoxyphenyl)acetamide
8	1 - H6	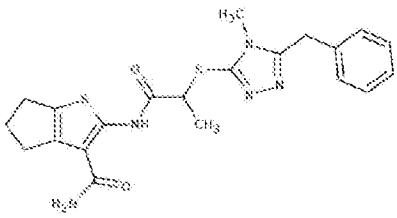	2-{2-[(5-benzyl-4-methyl-4H-1,2,4-triazol-3-yl)sulfanyl]propanamido}-4H,5H,6H-cyclopenta[b]thiophene-3-carboxamide

7	1 - G5	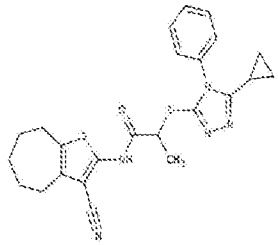	N-{3-cyano-4H,5H,6H,7H,8H-cyclohepta[b]thiophen-2-yl}-2-[(5-cyclopropyl-4-phenyl-4H-1,2,4-triazol-3-yl)sulfanyl]propanamide
7	**A5**	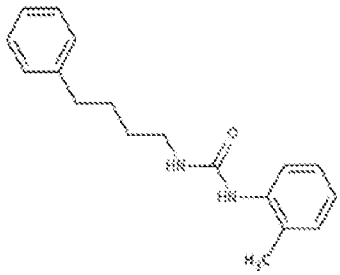	3-(2-methylphenyl)-1-(4-phenylbutyl)urea
6	**pB**	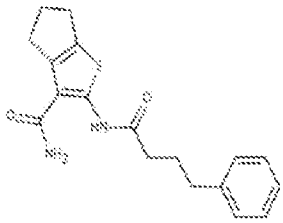	2-(4-phenylbutanamido)-4H,5H,6H-cyclopenta[b]thiophene-3-carboxamide
6	B10	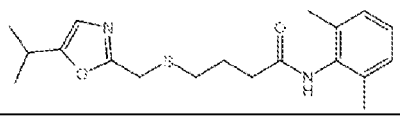	N-(2,6-dimethylphenyl)-4-({[5-(propan-2-yl)-1,3-oxazol-2-yl]methyl}sulfanyl)butanamide

6	1 - H7	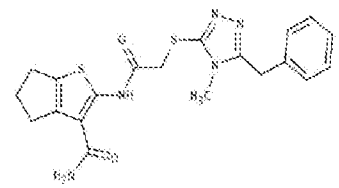	2-{2-[(5-benzyl-4-methyl-4H-1,2,4-triazol-3-yl)sulfanyl]acetamido}-4H,5H,6H-cyclopenta[b]thiophene-3-carboxamide
6	1 - A11	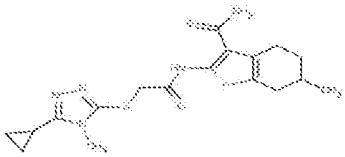	2-{2-[(5-cyclopropyl-4-methyl-4H-1,2,4-triazol-3-yl)sulfanyl]acetamido}-6-methyl-4,5,6,7-tetrahydro-1-benzothiophene-3-carboxamide
6	1 - D11	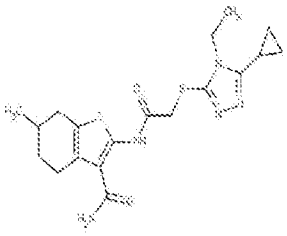	2-{2-[(5-cyclopropyl-4-ethyl-4H-1,2,4-triazol-3-yl)sulfanyl]acetamido}-6-methyl-4,5,6,7-tetrahydro-1-benzothiophene-3-carboxamide
6	1 - B10	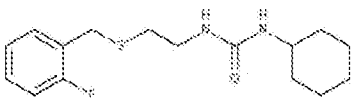	1-cyclohexyl-3-(2-{[(2-fluorophenyl)methyl]sulfanyl}ethyl)urea

5	1 - D9	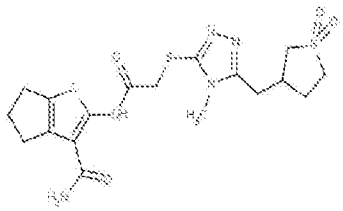	2-[2-({5-[(1,1-dioxo-1λ⁶-thiolan-3-yl)methyl]-4-methyl-4H-1,2,4-triazol-3-yl}sulfanyl)acetamido]-4H,5H,6H-cyclopenta[b]thiophene-3-carboxamide
5	1 - E8	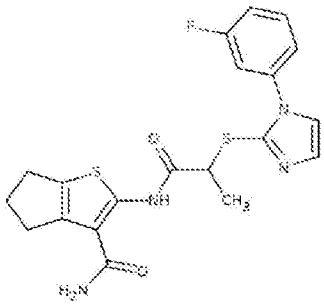	2-(2-{[1-(3-fluorophenyl)-1H-imidazol-2-yl]sulfanyl}propanamido)-4H,5H,6H-cyclopenta[b]thiophene-3-carboxamide
4	1 - G3	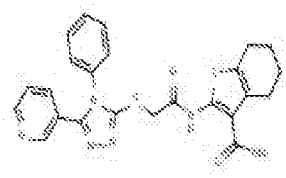	2-(2-{[4-phenyl-5-(pyridin-3-yl)-4H-1,2,4-triazol-3-yl]sulfanyl}acetamido)-4,5,6,7-tetrahydro-1-benzothiophene-3-carboxamide
4	2 - A2	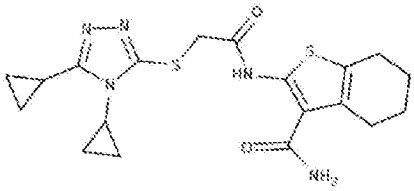	2-{2-[(dicyclopropyl-4H-1,2,4-triazol-3-yl)sulfanyl]acetamido}-4,5,6,7-tetrahydro-1-benzothiophene-3-carboxamide

4	**B4**	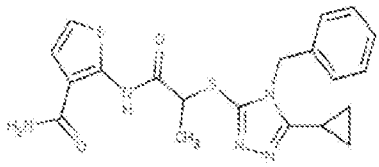	2-{2-[(4-benzyl-5-cyclopropyl-4H-1,2,4-triazol-3-yl)sulfanyl]propanamido}thiophene-3-carboxamide
4	D05	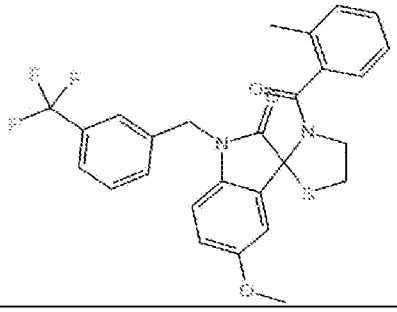	5-methoxy-3'-(2-methylbenzoyl)-1-{[3-(trifluoromethyl)phenyl]methyl}-1,2-dihydrospiro[indole-3,2'-[1,3]thiazolidine]-2-one
4	A11	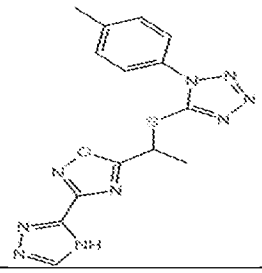	1-(4-methylphenyl)-5-({1-[3-(4H-1,2,4-triazol-3-yl)-1,2,4-oxadiazol-5-yl]ethyl}sulfanyl)-1H-1,2,3,4-tetrazole
4	E07	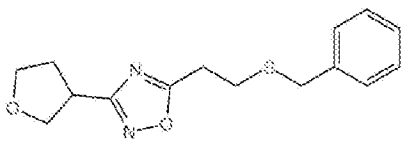	5-[2-(benzylsulfanyl)ethyl]-3-(oxolan-3-yl)-1,2,4-oxadiazole

3	1 - G7	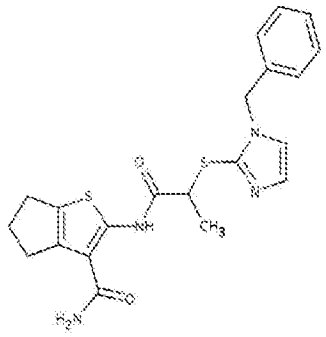	2-{2-[(1-benzyl-1H-imidazol-2-yl)sulfanyl]propanamido}-4H,5H,6H-cyclopenta[b]thiophene-3-carboxamide
3	2 - A4	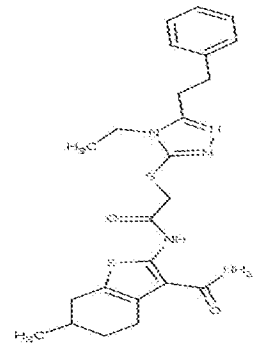	2-(2-{[4-ethyl-5-(2-phenylethyl)-4H-1,2,4-triazol-3-yl]sulfanyl}acetamido)-6-methyl-4,5,6,7-tetrahydro-1-benzothiophene-3-carboxamide
2	2 - A5	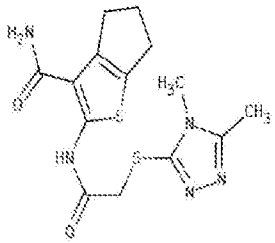	2-{2-[(dimethyl-4H-1,2,4-triazol-3-yl)sulfanyl]acetamido}-4H,5H,6H-cyclopenta[b]thiophene-3-carboxamide
2	1 - A4	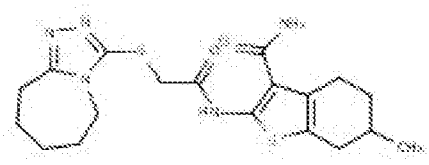	6-methyl-2-(2-{5H,6H,7H,8H,9H-[1,2,4]triazolo[4,3-a]azepin-3-ylsulfanyl}acetamido)-4,5,6,7-tetrahydro-1-benzothiophene-3-carboxamide

2	1 - F8	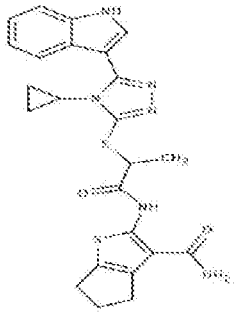	2-(2-{[4-cyclopropyl-5-(1H-indol-3-yl)-4H-1,2,4-triazol-3-yl]sulfanyl}propanamido)-4H,5H,6H-cyclopenta[b]thiophene-3-carboxamide
2	1 - D5	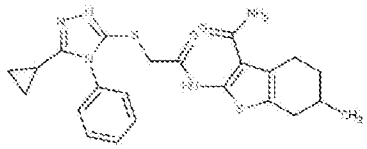	2-{2-[(5-cyclopropyl-4-phenyl-4H-1,2,4-triazol-3-yl)sulfanyl]acetamido}-6-methyl-4,5,6,7-tetrahydro-1-benzothiophene-3-carboxamide
1	1 - D3	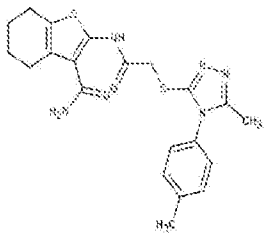	2-(2-{[5-methyl-4-(4-methylphenyl)-4H-1,2,4-triazol-3-yl]sulfanyl}acetamido)-4,5,6,7-tetrahydro-1-benzothiophene-3-carboxamide
1	E05	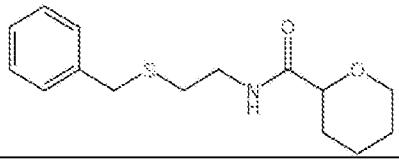	N-[2-(benzylsulfanyl)ethyl]oxane-2-carboxamide

1	E04	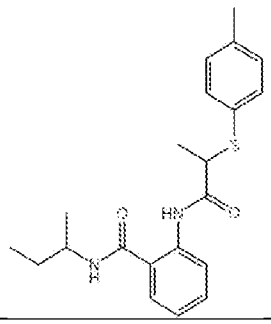	N-(butan-2-yl)-2-{2-[(4-methylphenyl)sulfanyl]propanamido}benzamide
1	1 - C11	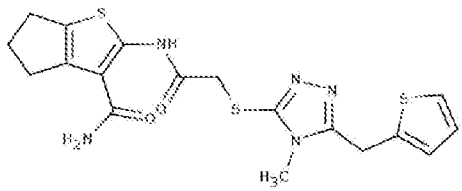	2-[2-({4-methyl-5-[(thiophen-2-yl)methyl]-4H-1,2,4-triazol-3-yl}sulfanyl)acetamido]-4H,5H,6H-cyclopenta[b]thiophene-3-carboxamide
0	1 - H2	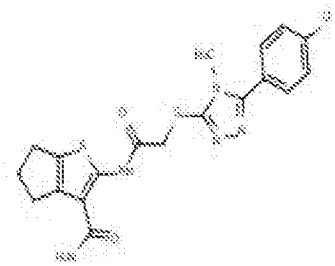	2-(2-{[5-(4-chlorophenyl)-4-methyl-4H-1,2,4-triazol-3-yl]sulfanyl}acetamido)-4H,5H,6H-cyclopenta[b]thiophene-3-carboxamide
0	1 - E9	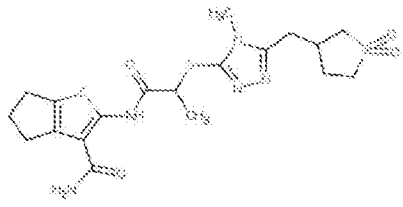	2-[2-({5-[(1,1-dioxo-1λ⁶-thiolan-3-yl)methyl]-4-methyl-4H-1,2,4-triazol-3-yl}sulfanyl)propanamido]-4H,5H,6H-cyclopenta[b]thiophene-3-carboxamide

0	C10	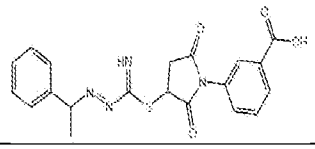	3-(2,5-dioxo-3-{[(E)-N-[(1-phenylethyl)imino]carbamimidoyl]sulfanyl}pyrrolidin-1-yl)benzoic acid
-1	C04	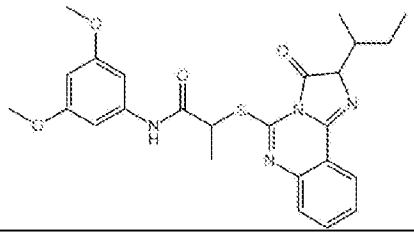	2-{[2-(butan-2-yl)-3-oxo-2H,3H-imidazo[1,2-c]quinazolin-5-yl]sulfanyl}-N-(3,5-dimethoxyphenyl)propanamide
-1	1 - D8	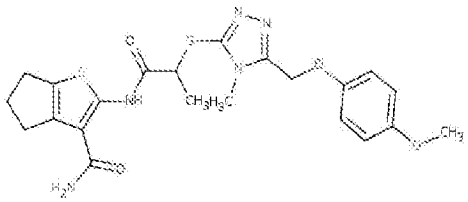	2-[2-({5-[(4-methoxyphenoxy)methyl]-4-methyl-4H-1,2,4-triazol-3-yl}sulfanyl)propanamido]-4H,5H,6H-cyclopenta[b]thiophene-3-carboxamide
-1	1 - B12	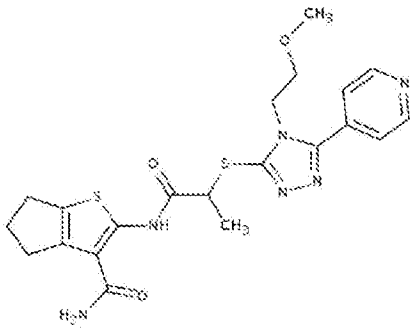	2-(2-{[4-(2-methoxyethyl)-5-(pyridin-4-yl)-4H-1,2,4-triazol-3-yl]sulfanyl}propanamido)-4H,5H,6H-cyclopenta[b]thiophene-3-carboxamide

-2	A05	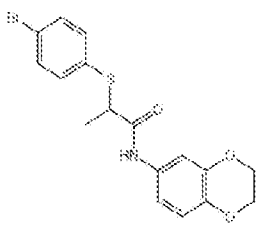	2-[(4-bromophenyl)sulfanyl]-N-(2,3-dihydro-1,4-benzodioxin-6-yl)propanamide
-3	**B3**	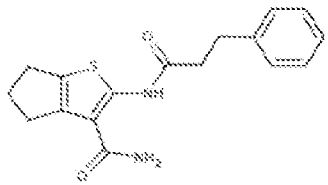	2-(3-phenylpropanamido)-4H,5H,6H-cyclopenta[b]thiophene-3-carboxamide
-3	1 - H1	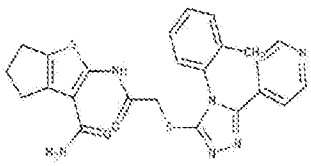	2-(2-{[4-(2-methylphenyl)-5-(pyridin-4-yl)-4H-1,2,4-triazol-3-yl]sulfanyl}acetamido)-4H,5H,6H-cyclopenta[b]thiophene-3-carboxamide
-3	1 - G10	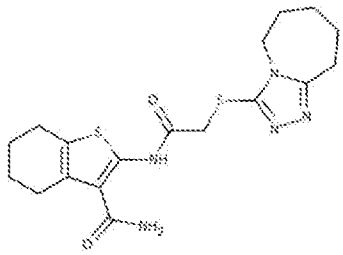	2-(2-{5H,6H,7H,8H,9H-[1,2,4]triazolo[4,3-a]azepin-3-ylsulfanyl}acetamido)-4,5,6,7-tetrahydro-1-benzothiophene-3-carboxamide

-3	1 - C9	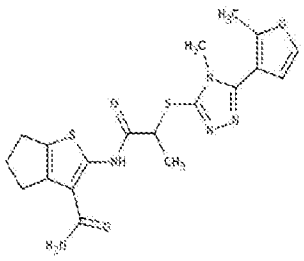	2-(2-{[4-methyl-5-(2-methylfuran-3-yl)-4H-1,2,4-triazol-3-yl]sulfanyl}propanamido)-4H,5H,6H-cyclopenta[b]thiophene-3-carboxamide
-3	E06	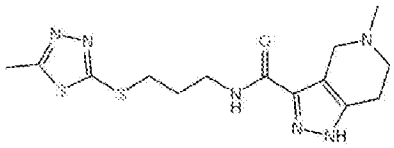	5-methyl-N-{3-[(5-methyl-1,3,4-thiadiazol-2-yl)sulfanyl]propyl}-1H,4H,5H,6H,7H-pyrazolo[4,3-c]pyridine-3-carboxamide
-3	1 - E12	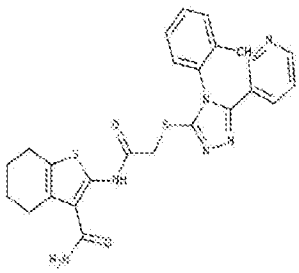	2-(2-{[4-(2-methylphenyl)-5-(pyridin-3-yl)-4H-1,2,4-triazol-3-yl]sulfanyl}acetamido)-4,5,6,7-tetrahydro-1-benzothiophene-3-carboxamide
-3	1 - E5	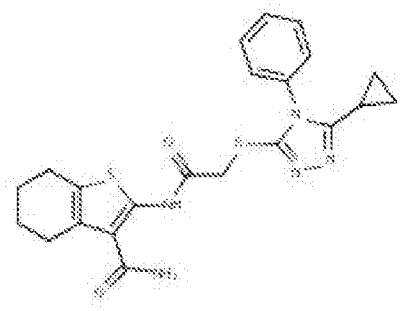	2-{2-[(5-cyclopropyl-4-phenyl-4H-1,2,4-triazol-3-yl)sulfanyl]acetamido}-4,5,6,7-tetrahydro-1-benzothiophene-3-carboxamide

-4	A2	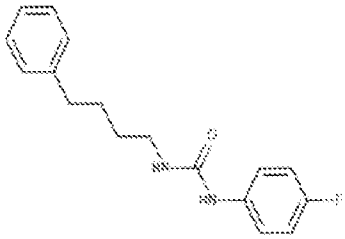	3-(4-fluorophenyl)-1-(4-phenylbutyl)urea
-4	D12	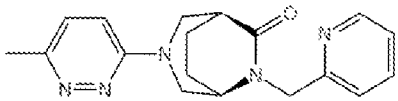	(1S,5R)-3-(6-methylpyridazin-3-yl)-6-[(pyridin-2-yl)methyl]-3,6-diazabicyclo[3.2.2]nonan-7-one
-4	C11	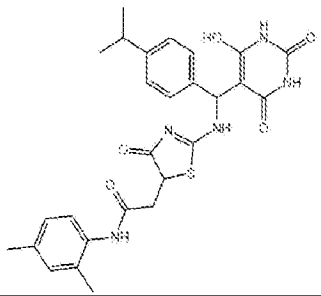	N-(2,4-dimethylphenyl)-2-(2-{[(6-hydroxy-2,4-dioxo-1,2,3,4-tetrahydropyrimidin-5-yl)[4-(propan-2-yl)phenyl]methyl]amino}-4-oxo-4,5-dihydro-1,3-thiazol-5-yl)acetamide
-4	1 - H8	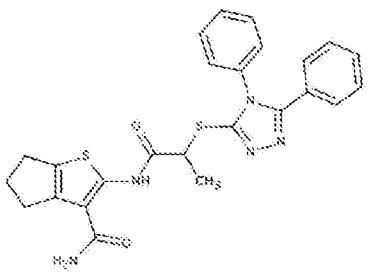	2-{2-[(diphenyl-4H-1,2,4-triazol-3-yl)sulfanyl]propanamido}-4H,5H,6H-cyclopenta[b]thiophene-3-carboxamide

-5	C09	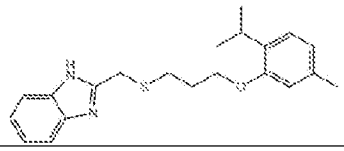	2-[({3-[5-methyl-2-(propan-2-yl)phenoxy]propyl}sulfanyl)methyl]-1H-1,3-benzodiazole
-6	1 - A5	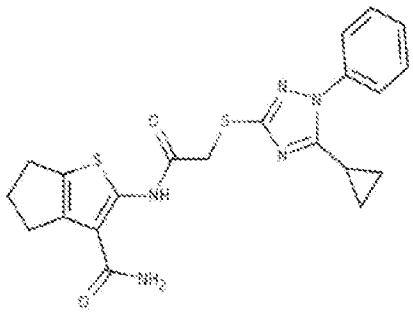	2-{2-[(5-cyclopropyl-1-phenyl-1H-1,2,4-triazol-3-yl)sulfanyl]acetamido}-4H,5H,6H-cyclopenta[b]thiophene-3-carboxamide
-6	D07	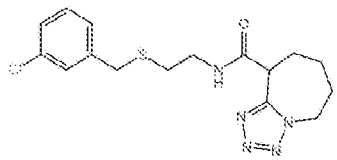	N-(2-{[(3-chlorophenyl)methyl]sulfanyl}ethyl)-5H,6H,7H,8H,9H-[1,2,3,4]tetrazolo[1,5-a]azepine-9-carboxamide
-7	1 - F5	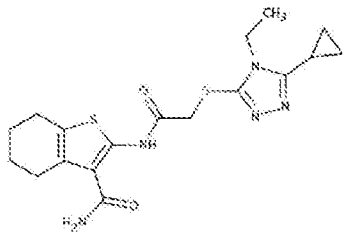	2-{2-[(5-cyclopropyl-4-ethyl-4H-1,2,4-triazol-3-yl)sulfanyl]acetamido}-4,5,6,7-tetrahydro-1-benzothiophene-3-carboxamide

-7	D10	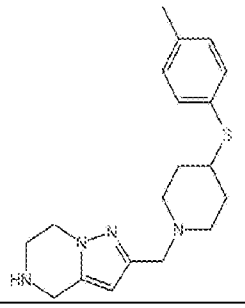	4-[(4-methylphenyl)sulfanyl]-1-({4H,5H,6H,7H-pyrazolo[1,5-a]pyrazin-2-yl}methyl)piperidine
-8	C06	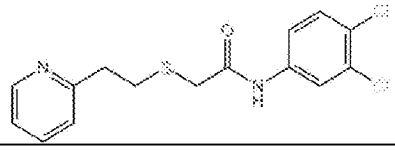	N-(3,4-dichlorophenyl)-2-{[2-(pyridin-2-yl)ethyl]sulfanyl}acetamide
-8	D11	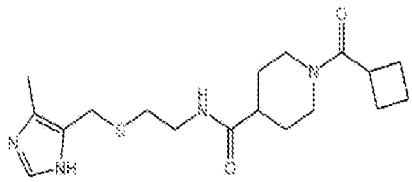	1-cyclobutanecarbonyl-N-(2-{[(4-methyl-1H-imidazol-5-yl)methyl]sulfanyl}ethyl)piperidine-4-carboxamide
-8	1 - A12	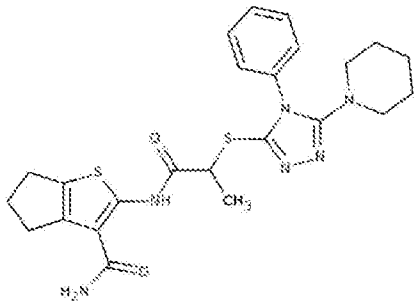	2-(2-{[4-phenyl-5-(piperidin-1-yl)-4H-1,2,4-triazol-3-yl]sulfanyl}propanamido)-4H,5H,6H-cyclopenta[b]thiophene-3-carboxamide

-9	1 - C3	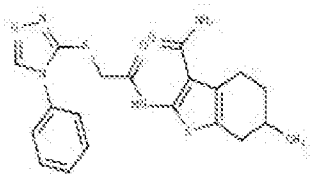	6-methyl-2-{2-[(4-phenyl-4H-1,2,4-triazol-3-yl)sulfanyl]acetamido}-4,5,6,7-tetrahydro-1-benzothiophene-3-carboxamide
-9	1 - C7	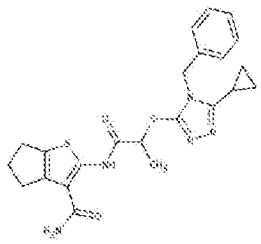	2-{2-[(4-benzyl-5-cyclopropyl-4H-1,2,4-triazol-3-yl)sulfanyl]propanamido}-4H,5H,6H-cyclopenta[b]thiophene-3-carboxamide
-10	1 - F2	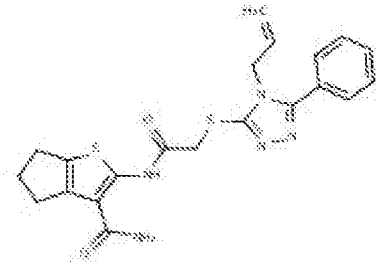	2-(2-{[5-phenyl-4-(prop-2-en-1-yl)-4H-1,2,4-triazol-3-yl]sulfanyl}acetamido)-4H,5H,6H-cyclopenta[b]thiophene-3-carboxamide
-10	1 - A3	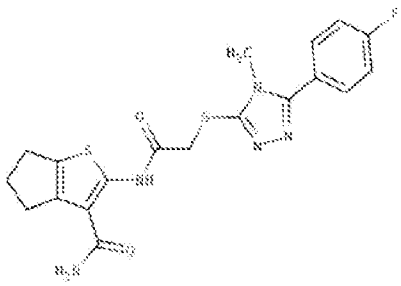	2-(2-{[5-(4-fluorophenyl)-4-methyl-4H-1,2,4-triazol-3-yl]sulfanyl}acetamido)-4H,5H,6H-cyclopenta[b]thiophene-3-carboxamide

-10	E03	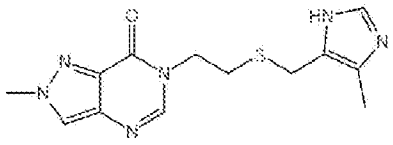	2-methyl-6-(2-{[(4-methyl-1H-imidazol-5-yl)methyl]sulfanyl}ethyl)-2H,6H,7H-pyrazolo[4,3-d]pyrimidin-7-one
-11	1 - B2	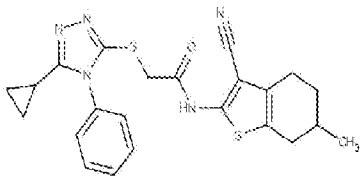	N-(3-cyano-6-methyl-4,5,6,7-tetrahydro-1-benzothiophen-2-yl)-2-[(5-cyclopropyl-4-phenyl-4H-1,2,4-triazol-3-yl)sulfanyl]acetamide
-12	1 - B11	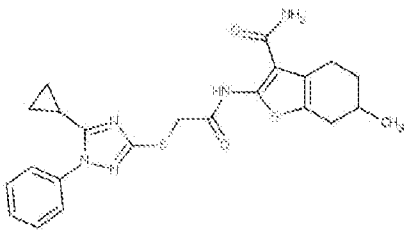	2-{2-[(5-cyclopropyl-1-phenyl-1H-1,2,4-triazol-3-yl)sulfanyl]acetamido}-6-methyl-4,5,6,7-tetrahydro-1-benzothiophene-3-carboxamide
-13	1 - C4	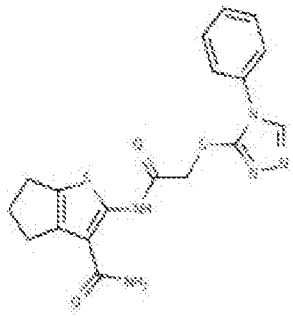	2-{2-[(4-phenyl-4H-1,2,4-triazol-3-yl)sulfanyl]acetamido}-4H,5H,6H-cyclopenta[b]thiophene-3-carboxamide

-14	A01	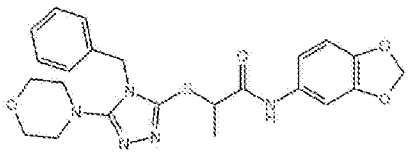	N-(2H-1,3-benzodioxol-5-yl)-2-{[4-benzyl-5-(morpholin-4-yl)-4H-1,2,4-triazol-3-yl]sulfanyl}propanamide
-17	D03	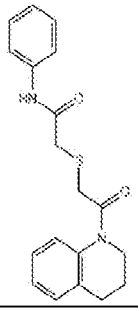	2-{[2-oxo-2-(1,2,3,4-tetrahydroquinolin-1-yl)ethyl]sulfanyl}-N-phenylacetamide
-18	1 - C2	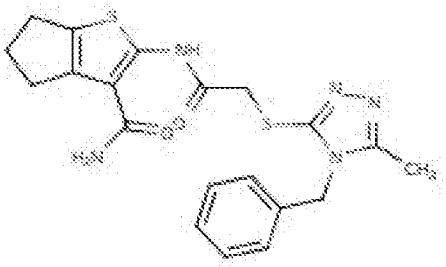	2-{2-[(4-benzyl-5-methyl-4H-1,2,4-triazol-3-yl)sulfanyl]acetamido}-4H,5H,6H-cyclopenta[b]thiophene-3-carboxamide
-23	1 - A2	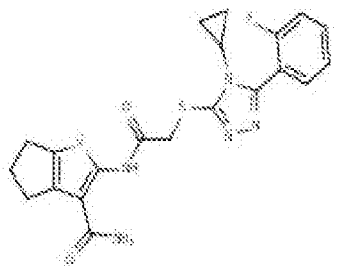	2-(2-{[4-cyclopropyl-5-(2-fluorophenyl)-4H-1,2,4-triazol-3-yl]sulfanyl}acetamido)-4H,5H,6H-cyclopenta[b]thiophene-3-carboxamide

-24	1 - A7	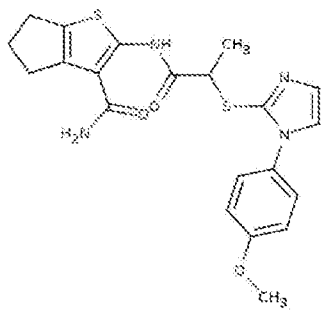	2-(2-{[1-(4-methoxyphenyl)-1H-imidazol-2-yl]sulfanyl}propanamido)-4H,5H,6H-cyclopenta[b]thiophene-3-carboxamide
-26	1 - F7	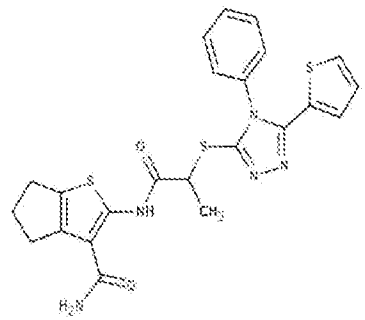	2-(2-{[4-phenyl-5-(thiophen-2-yl)-4H-1,2,4-triazol-3-yl]sulfanyl}propanamido)-4H,5H,6H-cyclopenta[b]thiophene-3-carboxamide
-31	1 - A6	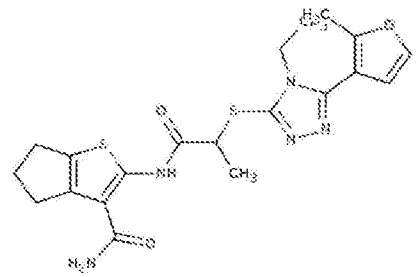	2-(2-{[4-ethyl-5-(2-methylfuran-3-yl)-4H-1,2,4-triazol-3-yl]sulfanyl}propanamido)-4H,5H,6H-cyclopenta[b]thiophene-3-carboxamide
-31	1 - B5	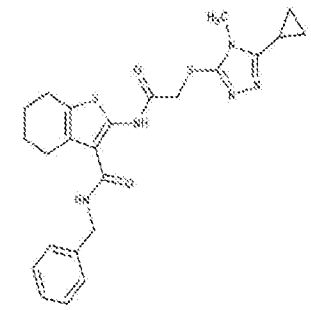	N-benzyl-2-{2-[(5-cyclopropyl-4-methyl-4H-1,2,4-triazol-3-yl)sulfanyl]acetamido}-4,5,6,7-tetrahydro-1-benzothiophene-3-carboxamide

[0116] In some embodiments, the mitofusin modulating agent can comprise a methylated cyclohexy, a backbone, and a substituted triazole ring (see e.g., **FIG. 46**).

In some embodiments, the mitofusin modulating agent can comprise one of the following compounds:

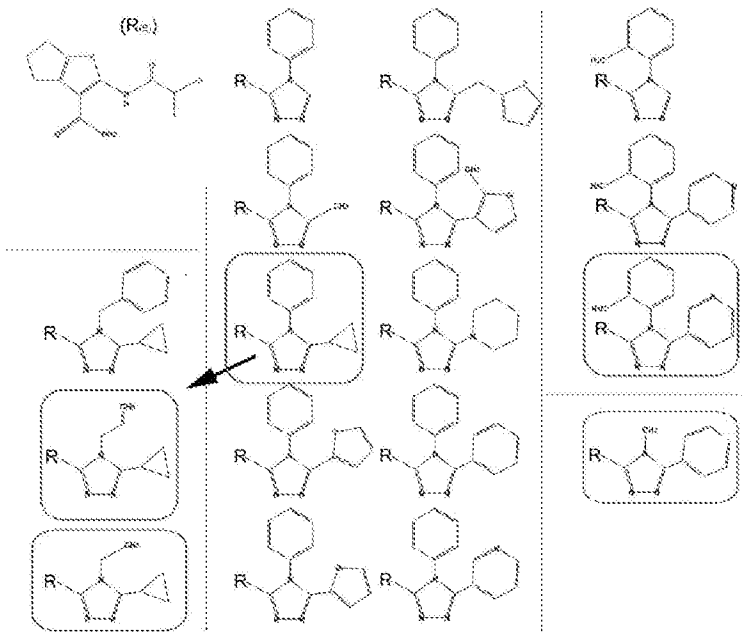

(see e.g., **FIG. 48**).

[0117] The term “imine” or “imino”, as used herein, unless otherwise indicated, includes a functional group or chemical compound containing a carbon-nitrogen double bond. The expression “imino compound”, as used herein, unless otherwise indicated, refers to a compound that includes an “imine” or an “imino” group as defined herein. The “imine” or “imino” group can be optionally substituted.

[0118] The term “hydroxyl”, as used herein, unless otherwise indicated, includes -OH. The “hydroxyl” can be optionally substituted.

[0119] The terms “halogen” and “halo”, as used herein, unless otherwise indicated, include a chlorine, chloro, Cl; fluorine, fluoro, F; bromine, bromo, Br; or iodine, iodo, or I.

[0120] The term “acetamide”, as used herein, is an organic compound with the formula CH_3CONH_2. The “acetamide” can be optionally substituted.

[0121] The term “aryl”, as used herein, unless otherwise indicated, include a carbocyclic aromatic group. Examples of aryl groups include, but are not limited to, phenyl, benzyl, naphthyl, or anthracenyl. The “aryl” can be optionally substituted.

[0122] The terms “amine” and “amino”, as used herein, unless otherwise indicated, include a functional group that contains a nitrogen atom with a lone pair of electrons and wherein one or more hydrogen atoms have been replaced by a

substituent such as, but not limited to, an alkyl group or an aryl group. The “amine” or “amino” group can be optionally substituted.

[0123] The term “alkyl”, as used herein, unless otherwise indicated, includes saturated monovalent hydrocarbon radicals having straight or branched moieties, such as but not limited to, methyl, ethyl, propyl, butyl, pentyl, hexyl, octyl groups, etc. Representative straight-chain lower alkyl groups include, but are not limited to, -methyl, -ethyl, -n-propyl, -n-butyl, -n-pentyl, -n-hexyl, -n-heptyl and -n-octyl; while branched lower alkyl groups include, but are not limited to, -isopropyl, -sec-butyl, -isobutyl, -tert-butyl, -isopentyl, 2-methylbutyl, 2-methylpentyl, 3-methylpentyl, 2,2-dimethylbutyl, 2,3-dimethylbutyl, 2,2-dimethylpentyl, 2,3-dimethylpentyl, 3,3-dimethylpentyl, 2,3,4-trimethylpentyl, 3-methylhexyl, 2,2-dimethylhexyl, 2,4-dimethylhexyl, 2,5-dimethylhexyl, 3,5-dimethylhexyl, 2,4-dimethylpentyl, 2-methylheptyl, 3-methylheptyl, unsaturated C_{1-8} alkyls include, but are not limited to, -vinyl, -allyl, -1-butenyl, -2-butenyl, -isobutylenyl, -1-pentenyl, -2-pentenyl, -3-methyl-1-butenyl, -2-methyl-2-butenyl, -2,3-dimethyl-2-butenyl, 1-hexyl, 2-hexyl, 3-hexyl, -acetylenyl, -propynyl, -1-butynyl, -2-butynyl, -1-pentynyl, -2-pentynyl, or -3-methyl-1 butynyl. An alkyl can be saturated, partially saturated, or unsaturated. The “alkyl” can be optionally substituted.

[0124] The term “carboxyl”, as used herein, unless otherwise indicated, includes a functional group consisting of a carbon atom double bonded to an oxygen atom and single bonded to a hydroxyl group (-COOH). The “carboxyl” can be optionally substituted.

[0125] The term “alkenyl”, as used herein, unless otherwise indicated, includes alkyl moieties having at least one carbon-carbon double bond wherein alkyl is as defined above and including E and Z isomers of said alkenyl moiety. An alkenyl can be partially saturated or unsaturated. The “alkenyl” can be optionally substituted.

[0126] The term “alkynyl”, as used herein, unless otherwise indicated, includes alkyl moieties having at least one carbon-carbon triple bond wherein alkyl is as defined above. An alkynyl can be partially saturated or unsaturated. The “alkynyl” can be optionally substituted.

[0127] The term “acyl”, as used herein, unless otherwise indicated, includes a functional group derived from an aliphatic carboxylic acid, by removal of the hydroxyl (–OH) group. The “acyl” can be optionally substituted.

[0128] The term “alkoxyl”, as used herein, unless otherwise indicated, includes O-alkyl groups wherein alkyl is as defined above and O represents oxygen. Representative alkoxyl groups include, but are not limited to, -O-methyl, -O-ethyl, -O-n-propyl, -O-n-butyl, -O-n-pentyl, -O-n-hexyl, -O-n-heptyl, -O-n-octyl, -O-isopropyl, -O-sec-butyl, -O-isobutyl, -O-tert-butyl, -O-isopentyl, -O-2-methylbutyl, -O-2-methylpentyl, -O-3-methylpentyl, -O-2,2-dimethylbutyl, -O-2,3-dimethylbutyl, -O-2,2-dimethylpentyl, -O-2,3-dimethylpentyl, -O-3,3-dimethylpentyl, -O-2,3,4-trimethylpentyl, -O-3-methylhexyl, -O-2,2-dimethylhexyl, -O-2,4-dimethylhexyl, -O-2,5-dimethylhexyl, -O-3,5-dimethylhexyl, -O-2,4dimethylpentyl, -O-2-methylheptyl, -O-3-methylheptyl, -O-vinyl, -O-allyl, -O-1-butenyl, -O-2-butenyl, -O-isobutylenyl, -O-1-pentenyl, -O-2-pentenyl, -O-3-methyl-1-butenyl, -O-2-methyl-2-butenyl, -O-2,3-dimethyl-2-butenyl, -O-1-hexyl, -O-2-hexyl, -O-3-hexyl, -O-acetylenyl, -O-propynyl, -O-1-butynyl, -O-2-butynyl, -O-1-pentynyl, -O-2-pentynyl, -O-3-methyl-1-butynyl, -O-cyclopropyl, -O-cyclobutyl, -O-cyclopentyl, -O-cyclohexyl, -O-cycloheptyl, -O-cyclooctyl, -O-cyclononyl, -O-cyclodecyl, -O-CH_2-cyclopropyl, -O-CH_2-cyclobutyl, -O-CH_2-cyclopentyl, -O-CH_2-cyclohexyl, -O-CH_2-cycloheptyl, -O-CH_2-cyclooctyl, -O-CH_2-cyclononyl, -O-CH_2-cyclodecyl, -O-$(CH_2)_n$-cyclopropyl, -O-$(CH_2)_n$-cyclobutyl, -O-$(CH_2)_n$-cyclopentyl, -O-$(CH_2)_n$-cyclohexyl, -O-$(CH_2)_n$-cycloheptyl, -O-$(CH_2)_n$-cyclooctyl, -O-$(CH_2)_n$-cyclononyl, or -O-$(CH_2)_n$-cyclodecyl. An alkoxyl can be saturated, partially saturated, or unsaturated. The “alkoxyl” can be optionally substituted. n can be between 1 and 20.

[0129] The term “cycloalkyl”, as used herein, unless otherwise indicated, includes a non-aromatic, saturated, partially saturated, or unsaturated, monocyclic or fused, spiro or unfused bicyclic or tricyclic hydrocarbon referred to herein containing a total of from 3 to 10 carbon atoms. Examples of cycloalkyls include, but are not limited to, C_{3-10} cycloalkyl groups include, but are not limited to, -cyclopropyl, -cyclobutyl, -cyclopentyl, -cyclopentadienyl, -cyclohexyl, -cyclohexenyl, -1,3-cyclohexadienyl, -1,4-cyclohexadienyl, -cycloheptyl, -1,3-cycloheptadienyl, -1,3,5-cycloheptatrienyl, -cyclooctyl, and -cyclooctadienyl. The term “cycloalkyl” also includes -lower alkyl-cycloalkyl, wherein lower alkyl and cycloalkyl are as defined herein. Examples of -lower alkyl-cycloalkyl groups include, but are not limited to, -CH_2-cyclopropyl, -CH_2-cyclobutyl, -CH_2-cyclopentyl, -CH_2-cyclopentadienyl, -CH_2-

cyclohexyl, -CH_2-cycloheptyl, or -CH_2-cyclooctyl. The "cycloalkyl" can be optionally substituted.

[0130] The term "heterocyclyl" (e.g., a "heteroaryl"), as used herein, unless otherwise indicated, includes an aromatic or non-aromatic cycloalkyl in which one to four of the ring carbon atoms are independently replaced with a heteroatom from the group consisting of O, S and N. Representative examples of a heterocycle include, but are not limited to, benzofuranyl, benzothiophene, indolyl, benzopyrazolyl, coumarinyl, isoquinolinyl, pyrrolyl, pyrrolidinyl, thiophenyl, furanyl, thiazolyl, imidazolyl, pyrazolyl, triazolyl, quinolinyl, pyrimidinyl, pyridinyl, pyridonyl, pyrazinyl, pyridazinyl, isothiazolyl, isoxazolyl, (1,4)-dioxane, (1,3)-dioxolane, 4,5-dihydro-1H-imidazolyl, or tetrazolyl. Heterocycles can be substituted or unsubstituted. Heterocycles can also be bonded at any ring atom (i.e., at any carbon atom or heteroatom of the heterocyclic ring). A heterocyclic can be saturated, partially saturated, or unsaturated. The "heterocyclic" can be optionally substituted.

[0131] The term "indole", as used herein, is an aromatic heterocyclic organic compound with formula C_8H_7N. It has a bicyclic structure, consisting of a six-membered benzene ring fused to a five-membered nitrogen-containing pyrrole ring. The "indole" can be optionally substituted.

[0132] The term "cyano", as used herein, unless otherwise indicated, includes a -CN group. The "cyano" can be optionally substituted.

[0133] The term "alcohol", as used herein, unless otherwise indicated, includes a compound in which the hydroxyl functional group (-OH) is bound to a carbon atom. In particular, this carbon center should be saturated, having single bonds to three other atoms. The "alcohol" can be optionally substituted.

[0134] The term "solvate" is intended to mean a solvate form of a specified compound that retains the effectiveness of such compound. Examples of solvates include compounds of the invention in combination with, for example: water, isopropanol, ethanol, methanol, dimethylsulfoxide (DMSO), ethyl acetate, acetic acid, or ethanolamine.

[0135] The term "mmol", as used herein, is intended to mean millimole. The term "equiv", as used herein, is intended to mean equivalent. The term "mL", as used herein, is intended to mean milliliter. The term "g", as used herein, is intended to mean gram. The term "kg", as used herein, is intended to mean kilogram. The

term “μg”, as used herein, is intended to mean micrograms. The term “h”, as used herein, is intended to mean hour. The term “min”, as used herein, is intended to mean minute. The term “M”, as used herein, is intended to mean molar. The term "μL", as used herein, is intended to mean microliter. The term “μM”, as used herein, is intended to mean micromolar. The term “nM”, as used herein, is intended to mean nanomolar. The term “N”, as used herein, is intended to mean normal. The term “amu”, as used herein, is intended to mean atomic mass unit. The term “°C”, as used herein, is intended to mean degree Celsius. The term “wt/wt”, as used herein, is intended to mean weight/weight. The term “v/v”, as used herein, is intended to mean volume/volume. The term “MS”, as used herein, is intended to mean mass spectroscopy. The term “HPLC”, as used herein, is intended to mean high performance liquid chromatograph. The term “RT”, as used herein, is intended to mean room temperature. The term "e.g.", as used herein, is intended to mean example. The term “N/A”, as used herein, is intended to mean not tested.

[0136] As used herein, the expression “pharmaceutically acceptable salt” refers to pharmaceutically acceptable organic or inorganic salts of a compound of the invention. Preferred salts include, but are not limited, to sulfate, citrate, acetate, oxalate, chloride, bromide, iodide, nitrate, bisulfate, phosphate, acid phosphate, isonicotinate, lactate, salicylate, acid citrate, tartrate, oleate, tannate, pantothenate, bitartrate, ascorbate, succinate, maleate, gentisinate, fumarate, gluconate, glucaronate, saccharate, formate, benzoate, glutamate, methanesulfonate, ethanesulfonate, benzenesulfonate, p-toluenesulfonate, or pamoate (i.e., 1,1'-methylene-bis-(2-hydroxy-3-naphthoate)) salts. A pharmaceutically acceptable salt may involve the inclusion of another molecule such as an acetate ion, a succinate ion or other counterion. The counterion may be any organic or inorganic moiety that stabilizes the charge on the parent compound. Furthermore, a pharmaceutically acceptable salt may have more than one charged atom in its structure. Instances where multiple charged atoms are part of the pharmaceutically acceptable salt can have multiple counterions. Hence, a pharmaceutically acceptable salt can have one or more charged atoms and/or one or more counterion. As used herein, the expression “pharmaceutically acceptable solvate” refers to an association of one or more solvent molecules and a compound of the invention. Examples of solvents that form pharmaceutically acceptable solvates include, but are not limited to, water,

isopropanol, ethanol, methanol, DMSO, ethyl acetate, acetic acid, and ethanolamine. As used herein, the expression “pharmaceutically acceptable hydrate” refers to a compound of the invention, or a salt thereof, that further includes a stoichiometric or non-stoichiometric amount of water bound by non-covalent intermolecular forces.

MFN1 OR MFN2

[0137] Mitochondria generate ATP that fuels neuronal activity. Mitochondria must fuse in order to exchange genomes and promote mutual repair. The initial stages of mitochondrial fusion proceed through the physiochemical actions of two closely related dynamin family GTPases, mitofusins (Mfn) 1 and 2. The obligatory first step leading to mitochondrial fusion is molecular tethering of two mitochondria via homo- or hetero-oligomerization (in trans) of extended Mfn1 or Mfn2 carboxyl termini. Subsequently, GTP binding to and hydrolysis by Mfn1 or Mfn2 promotes irreversible physical fusion of the organellar outer membranes.

[0138] Mitofusins (Mfn) belong to a class of highly conserved GTPases which are located on the outer membrane of mitochondria in mammals, flies, the worm and budding yeast. Each of Mfn1 and Mfn2, the mitofusins present in mammals, are anchored to the outer membrane by two transmembrane domains such that their N-terminus and C-terminus are exposed to the cytoplasm. Mitofusins on different organelles undergo transdimerization through anti-parallel binding of their extended carboxy terminal α-helical domains to form mitochondria-mitochondria tethers – the obligate initial step in mitochondrial fusion (Koshiba et al., 2004, Science, 305:858-861). Conventional wisdom is that mitofusins exist constitutively in this "active" extended molecular conformation which supports mitochondrial tethering, although other possible conformations and the likelihood of functionally relevant molecular plasticity have not been rigorously tested. The components involved in mitochondrial tethering involve intermolecular and possibly intramolecular interactions of particular Mfn1 and Mfn2 domains. These interactions were further studied and exploited in the design and testing of compositions which affect the interactions and the resultant mitochondrial function.

[0139] Mfn1 and Mfn2 share a common domain structure. The amino terminal GTPase domain is followed by a coiled-coiled heptad repeat region (HR1), two adjacent small transmembrane domains, and a carboxyl terminal coiled heptad

repeat region (HR2). Amino acid conservation between Mfn1 and Mfn2 varies by domain, being most highly conserved in the GTPase, transmembrane, and HR2 domains. HR2 domains extending from Mfn1 molecules located on different mitochondria can bind to each other, forming inter-molecular HR2-HR2 interactions that link the molecules and tether the organelles (Koshiba et al. ibid). HR2 can also bind to HR1 (Huang et al., 2011, PLoS One, 6:e20655), although there has been no determination of whether this is an inter- or intra-molecular interaction.

[0140] The crystal structure of bacterial dynamin-like protein (OLP) (Low and Lowe, 2006, Nature, 444:766-769; Protein Data Bank (PDB) ID No. 2J69) was used to model Mfn2 structure. The domain sequences of the OLP and Mfn2 proteins were aligned. The alignment and modeling of Mfn2 based on the OLP structure provided a template for the expansion and refining of the identities of HR2 amino acids that mediate inter-molecular HR2-HR2 tethering (Koshiba et al., 2004, Science, 305:858-861). This analysis led to the novel conception that these same amino acids mediate inter-molecular antiparallel binding of HR2 to HR2 (see e.g., **FIG. 2A**) and intra-molecular antiparallel binding of HR2 to HR1.

[0141] The amino acid sequence of human Mfn1 is SEQ ID NO:5. The amino acid sequence of human MFN2 is SEQ ID NO: 6. The amino acid sequence of human MFN2 is SEQ ID NO: 29. The amino acid sequence of human MFN2 is SEQ ID NO: 30. The amino acid sequence of chimpanzee MFN2 is SEQ ID NO: 31. The amino acid sequence of gorilla MFN2 is SEQ ID NO: 32. The amino acid sequence of monkey MFN2 is SEQ ID NO: 33. The amino acid sequence of macaque MFN2 is SEQ ID NO: 34. The amino acid sequence of marmoset MFN2 is SEQ ID NO: 35. The amino acid sequence of bushbaby MFN2 is SEQ ID NO: 36. The amino acid sequence of lemur MFN2 is SEQ ID NO: 37. The amino acid sequence of gibbon MFN2 is SEQ ID NO: 38. The amino acid sequence of elephant MFN2 is SEQ ID NO: 39. The amino acid sequence of armadillo MFN2 is SEQ ID NO: 40. The amino acid sequence of cat MFN2 is SEQ ID NO: 41. The amino acid sequence of dog MFN2 is SEQ ID NO: 42. The amino acid sequence of ferret MFN2 is SEQ ID NO: 43. The amino acid sequence of boar MFN2 is SEQ ID NO: 44. The amino acid sequence of dolphin MFN2 is SEQ ID NO: 45. The amino acid sequence of sheep MFN2 is SEQ ID NO: 46. The amino acid sequence of squirrel MFN2 is SEQ ID NO: 47. The amino acid sequence of guinea pig MFN2 is SEQ ID NO: 48. The amino

acid sequence of rat MFN2 is SEQ ID NO: 49. The amino acid sequence of mouse MFN2 is SEQ ID NO: 50. The amino acid sequence of horse MFN2 is SEQ ID NO: 51. The amino acid sequence of opossum MFN2 is SEQ ID NO: 52. The amino acid sequence of collrd flyctchr MFN2 is SEQ ID NO: 53. The amino acid sequence of human MFN2 is SEQ ID NO: 54. The amino acid sequence of zebra finch MFN2 is SEQ ID NO: 55. The amino acid sequence of chicken MFN2 is SEQ ID NO: 56. The amino acid sequence of human MFN2 is SEQ ID NO: 57. The amino acid sequence of turkey MFN2 is SEQ ID NO: 58. The amino acid sequence of turtle MFN2 is SEQ ID NO: 59. The amino acid sequence of pufferfish MFN2 is SEQ ID NO: 60. The amino acid sequence of tilapia MFN2 is SEQ ID NO: 61. The amino acid sequence of stickleback MFN2 is SEQ ID NO: 62. The amino acid sequence of cod MFN2 is SEQ ID NO: 63. The amino acid sequence of platyfish MFN2 is SEQ ID NO: 64. The amino acid sequence of amazon molly MFN2 is SEQ ID NO: 65. The amino acid sequence of spotted gar MFN2 is SEQ ID NO: 66. The amino acid sequence of cave fish MFN2 is SEQ ID NO: 67. The amino acid sequence of zebrafish MFN2 is SEQ ID NO: 68. The amino acid sequence of coelacanth MFN2 is SEQ ID NO: 69. The amino acid sequence of frog MFN2 is SEQ ID NO: 70.

MITOCHONDRIA-ASSOCIATED DISEASES, DISORDERS, OR CONDITIONS

[0142] The present disclosure provides for compositions and methods of treatment for treating mitochondria-related diseases, disorders, or conditions such as diseases or disorders associated with mitofusin 1 (Mfn1) and/or mitofusin 2 (Mfn2) and mitochondrial dysfunction. A mitochondria-associated disease, disorder, or condition can be a disease associated with mitochondrial dysfunction, fragmentation, or fusion or associated with dysfunction in Mfn1 or Mfn2 unfolding. Mitochondria dysfunction can be caused by mutations or can be caused by injury in the central nervous system (CNS) or peripheral nervous system (PNS).

[0143] Furthermore, the conditions associated with the tethering of mitochondria and ER can be cell death during reoxygenation after tissue ischemia in brain or heart infarcts (i.e., thrombotic stroke and myocardial infarction). During re-oxygenation after tissue ischemia (the therapeutic goal of clinical percutaneous mechanical or thrombolytic vascular reperfusion) in brain or heart infarcts (i.e., thrombotic stroke and myocardial infarction), mitochondrial uptake of calcium

released from ER paradoxically stimulates cell death and provokes infarct extension9, 10. Preventing infarct extension is a major therapeutic goal in western countries, and could be accomplished by temporarily breaking the tethers between mitochondria and ER. Because there are currently no pharmacological Mfn antagonists this therapeutic approach has never been attempted.

[0144] Mitochondria transit within cells and undergo fusion to exchange genomes and promote mutual repair. Mitochondrial fusion and subcellular trafficking are mediated in part by mitofusins (Mfn) 1 and 2. Genetic mutations in Mfn2 that suppress mitochondrial fusion and motility cause Charcot Marie Tooth Disease 2A (CMT2A), the most common heritable axonal neuropathy. Mitochondrial fragmentation, dysfunction, and dysmotility are also central features of other genetic neurodegenerative syndromes, such as amyotrophic lateral sclerosis, Huntington's disease, Parkinson's disease, and Alzheimer's disease. Because no therapeutics exist that directly enhance mitochondrial fusion or trafficking, these diseases are unrelenting and irreversible.

[0145] As described herein, mitochondria-related diseases, disorders, or conditions can be any disease disorder or condition that is related to mitochondrial dysfunction. Mitochondrial dysfunction is implicated in chronic degenerative neurological conditions such as Alzheimer's, Parkinson's, and Huntington's diseases. For example, the genetic neurodegenerative condition, Charcot Marie Tooth Disease (type 2A) (CMT) or Hereditary motor and sensory neuropathy, is caused by multiple loss-of-function mutations of Mfn2. The underlying mechanism that causes this debilitating neuropathy is impaired mitochondrial fusion. Currently, because there are no pharmacological Mfn agonists, there is no treatment for CMT.

[0146] Mitochondria-associated diseases, disorders, or conditions can be Alzheimer's disease, Parkinson's disease, Huntington's disease, Charcot Marie Tooth Disease (type 2A) (CMT), hereditary motor and sensory neuropathy, autism, autosomal dominant optic atrophy (ADOA), muscular dystrophy, Lou Gehrig's disease, cancer, mitochondrial myopathy, Diabetes mellitus and deafness (DAD), Leber's hereditary optic neuropathy (LHON), Leigh syndrome, subacute sclerosing encephalopathy, Neuropathy, ataxia, retinitis pigmentosa, and ptosis (NARP), Myoneurogenic gastrointestinal encephalopathy (MNGIE), Myoclonic Epilepsy with Ragged Red Fibers (MERRF), Mitochondrial myopathy, encephalomyopathy, lactic

acidosis, stroke-like symptoms (MELAS), mtDNA depletion, mitochondrial neurogastrointestinal encephalomyopathy (MNGIE), Dysautonomic Mitochondrial Myopathy, Mitochondrial Channelopathy, or pyruvate dehydrogenase complex deficiency (PDCD/PDH).

[0147] Symptoms that can be treated with the methods as described herein can include poor growth, loss of muscle coordination, muscle weakness, visual problems, hearing problems, learning disabilities, heart disease, liver disease, kidney disease, gastrointestinal disorders, respiratory disorders, neurological problems, autonomic dysfunction, and dementia.

Neurodegenerative Disease

[0148] As described herein, mitofusin agonists (e.g., chimera B-A/l) rapidly reverse mitochondrial dysmotility in sciatic nerve axons of a mouse model of Charcot Marie Tooth disease. Because impaired mitochondrial fusion, fitness, and/or trafficking also contribute to neuronal degeneration in various neurodegenerative diseases (e.g., in Charcot Marie Tooth disease (CMT2A), Huntington's disease, Parkinson's disease, and Alzheimer's disease, and especially in Amyotrophic Lateral Sclerosis (ALS)), the present disclosure provides for compositions (e.g., mitofusin agonists) and methods to treat such neurodegenerative diseases, disorders, or conditions.

[0149] For example, a neurodegenerative disease, disorder or condition can be a disease of impaired neuronal mitochondrial dynamism or trafficking, such as a hereditary motor and sensory neuropathy (HMSN) (e.g., Charcot Marie Tooth (CMT) disease), CMT1 (a dominantly inherited, hypertrophic, predominantly demyelinating form), CMT2 (a dominantly inherited predominantly axonal form), Dejerine-Sottas (severe form with onset in infancy), CMTX (inherited in an X-linked manner), CMT4 (includes the various demyelinating autosomal recessive forms of Charcot-Marie-Tooth disease), hereditary sensory and autonomic neuropathy type IE, hereditary sensory and autonomic neuropathy type II, hereditary sensory and autonomic neuropathy type V, HMSN types 1A and 1B (e.g., dominantly inherited hypertrophic demyelinating neuropathies), HMSN type 2 (e.g., dominantly inherited neuronal neuropathies), HMSN type 3 (e.g., hypertrophic neuropathy of infancy [Dejerine-Sottas]), HMSN type 4 (e.g., hypertrophic neuropathy [Refsum] associated

with phytanic acid excess), HMSN type 5 (associated with spastic paraplegia), or HMSN type 6 (e.g., with optic atrophy).

[0150] As another example, a neurodegenerative disease, disorder or condition can be Alzheimer's disease, amyotrophic lateral sclerosis (ALS), Alexander disease, Alpers' disease, Alpers-Huttenlocher syndrome, alpha-methylacyl-CoA racemase deficiency, Andermann syndrome, Arts syndrome, ataxia neuropathy spectrum, ataxia (E.g., with oculomotor apraxia, autosomal dominant cerebellar ataxia, deafness, and narcolepsy), autosomal recessive spastic ataxia of Charlevoix-Saguenay, Batten disease, beta-propeller protein-associated neurodegeneration, Cerebro-Oculo-Facio-Skeletal Syndrome (COFS), Corticobasal Degeneration, CLN1 disease, CLN10 disease, CLN2 disease, CLN3 disease, CLN4 disease, CLN6 disease,CLN7 disease, CLN8 disease, cognitive dysfunction, congenital insensitivity to pain with anhidrosis, dementia, familial encephalopathy with neuroserpin inclusion bodies, familial British dementia, familial Danish dementia, fatty acid hydroxylase-associated neurodegeneration, Gerstmann-Straussler-Scheinker Disease, GM2-gangliosidosis (e.g., AB variant), HMSN type 7 (e.g., with retinitis pigmentosa), Huntington's disease, infantile neuroaxonal dystrophy, infantile-onset ascending hereditary spastic paralysis, Huntington’s disease (HD), infantile-onset spinocerebellar ataxia, juvenile primary lateral sclerosis, Kennedy's disease, Kuru, Leigh's Disease, Marinesco-Sjögren syndrome, Mild Cognitive Impairment (MCI), mitochondrial membrane protein-associated neurodegeneration, Motor neuron disease, Monomelic Amyotrophy, Motor neuron diseases (MND), Multiple System Atrophy, Multiple System Atrophy with Orthostatic Hypotension (Shy-Drager Syndrome), multiple sclerosis, multiple system atrophy, neurodegeneration in Down’s syndrome (NDS), neurodegeneration of aging, Neurodegeneration with brain iron accumulation, neuromyelitis optica, pantothenate kinase-associated neurodegeneration, Opsoclonus Myoclonus, prion disease, Progressive Multifocal Leukoencephalopathy, Parkinson's disease (PD), PD-related disorders, polycystic lipomembranous osteodysplasia with sclerosing leukoencephalopathy, prion disease, progressive external ophthalmoplegia, riboflavin transporter deficiency neuronopathy, Sandhoff disease, Spinal muscular atrophy (SMA), Spinocerebellar ataxia (SCA), Striatonigral degeneration, Transmissible Spongiform Encephalopathies (prion diseases), or Wallerian-like degeneration.

Charcot Marie Tooth (CMT) Disease.

[0151] Charcot Marie Tooth (CMT) disease is an example of a non-curable and currently untreatable neurodegenerative disease, disorder, or condition, which can be characterized by mutations of Mfn2 and/or axonal neuropathy. As described herein, it was discovered that mitochondrial transport, not the conventional wisdom that mitochondria size, is implicated in CMT disease progression. It is shown here that the ability of mitochondria to get from point A to point B is the cause of progression. CMT is a progressive disease, caused by mutation in Mfn2, and characterized by neuronal neuropathy. The disease affects the legs at 8 to 10 years of age, then upper limbs, muscle wasting, skeletal deformities, and results in being wheelchair bound. The present disclosure provides for the discovery that the progression of CMT was not due to small mitochondria size but the length of mitochondrial travel. As such, this disclosure provides for the evaluation of mitochondrial trafficking as a route of therapy in the first mouse model of disease. It was discovered that the mitochondria in the legs do not move, but in the arm, there is mitochondria movement. As such, it was discovered that Mfn2 pays a role in mitochondria trafficking. Data showed that administration of a mitofusin modulating agent allowed for the mitochondria to move in a mouse model where mitochondria were not previously moving, which is applicable in *any neuropathy* (e.g., Huntington's disease, amyotrophic lateral sclerosis (ALS) or ALS-like sclerosis, Alzheimer's disease).

Neurological Disease

[0152] As described herein, mitofusin agonists (e.g., chimera B-A/l) rapidly reverses mitochondrial dysmotility in sciatic nerve axons of a mouse model of Charcot Marie Tooth disease. It is currently believed that impaired mitochondrial trafficking also contribute to neuronal degeneration in various neurological diseases (e.g., in Huntington's, Parkinson's, and Alzheimer's diseases, and especially in Amyotrophic Lateral Sclerosis (ALS)). As such, the present disclosure provides for methods and compositions to treat neurological diseases, disorders, or conditions. For example, a neurological disease, disorder, or condition can be Abulia; Agraphia; Alcoholism; Alexia; Alien hand syndrome; Allan–Herndon–Dudley syndrome; Alternating hemiplegia of childhood; Alzheimer's disease; Amaurosis fugax; Amnesia; Amyotrophic lateral sclerosis (ALS); Aneurysm; Angelman syndrome;

Anosognosia; Aphasia; Apraxia; Arachnoiditis; Arnold–Chiari malformation; Asomatognosia; Asperger syndrome; Ataxia; Attention deficit hyperactivity disorder; ATR-16 syndrome; Auditory processing disorder; Autism spectrum; Behcets disease; Bipolar disorder; Bell's palsy; Brachial plexus injury; Brain damage; Brain injury; Brain tumor; Brody myopathy; Canavan disease; Capgras delusion; Carpal tunnel syndrome; Causalgia; Central pain syndrome; Central pontine myelinolysis; Centronuclear myopathy; Cephalic disorder; Cerebral aneurysm; Cerebral arteriosclerosis; Cerebral atrophy; Cerebral autosomal dominant arteriopathy with subcortical infarcts and leukoencephalopathy (CADASIL); Cerebral dysgenesis–neuropathy–ichthyosis–keratoderma syndrome (CEDNIK syndrome); Cerebral gigantism; Cerebral palsy; Cerebral vasculitis; Cervical spinal stenosis; Charcot–Marie–Tooth disease; Chiari malformation; Chorea; Chronic fatigue syndrome; Chronic inflammatory demyelinating polyneuropathy (CIDP); Chronic pain; Cockayne syndrome; Coffin–Lowry syndrome; Coma; Complex regional pain syndrome; Compression neuropathy; Congenital facial diplegia; Corticobasal degeneration; Cranial arteritis; Craniosynostosis; Creutzfeldt–Jakob disease; Cumulative trauma disorders; Cushing's syndrome; Cyclothymic disorder; Cyclic Vomiting Syndrome (CVS); Cytomegalic inclusion body disease (CIBD); Cytomegalovirus Infection; Dandy–Walker syndrome; Dawson disease; De Morsier's syndrome; Dejerine–Klumpke palsy; Dejerine–Sottas disease; Delayed sleep phase syndrome; Dementia; Dermatomyositis; Developmental coordination disorder; Diabetic neuropathy; Diffuse sclerosis; Diplopia; Disorders of consciousness; Down syndrome; Dravet syndrome; Duchenne muscular dystrophy; Dysarthria; Dysautonomia; Dyscalculia; Dysgraphia; Dyskinesia; Dyslexia; Dystonia; Empty sella syndrome; Encephalitis; Encephalocele; Encephalotrigeminal angiomatosis; Encopresis; Enuresis; Epilepsy; Epilepsy-intellectual disability in females; Erb's palsy; Erythromelalgia; Essential tremor; Exploding head syndrome; Fabry's disease; Fahr's syndrome; Fainting; Familial spastic paralysis; Febrile seizures; Fisher syndrome; Friedreich's ataxia; Fibromyalgia; Foville's syndrome; Fetal alcohol syndrome; Fragile X syndrome; Fragile X-associated tremor/ataxia syndrome (FXTAS); Gaucher's disease; Generalized epilepsy with febrile seizures plus; Gerstmann's syndrome; Giant cell arteritis; Giant cell inclusion disease; Globoid Cell Leukodystrophy; Gray matter heterotopia; Guillain–Barré syndrome; Generalized anxiety disorder; HTLV-1

associated myelopathy; Hallervorden–Spatz syndrome; Head injury; Headache; Hemifacial Spasm; Hereditary Spastic Paraplegia; Heredopathia atactica polyneuritiformis; Herpes zoster oticus; Herpes zoster; Hirayama syndrome; Hirschsprung's disease; Holmes–Adie syndrome; Holoprosencephaly; Huntington's disease; Hydranencephaly; Hydrocephalus; Hypercortisolism; Hypoxia; Immune-Mediated encephalomyelitis; Inclusion body myositis; Incontinentia pigmenti; Infantile Refsum disease; Infantile spasms; Inflammatory myopathy; Intracranial cyst; Intracranial hypertension; Isodicentric 15; Joubert syndrome; Karak syndrome; Kearns–Sayre syndrome; Kinsbourne syndrome; Kleine–Levin syndrome; Klippel Feil syndrome; Krabbe disease; Kufor–Rakeb syndrome; Lafora disease; Lambert–Eaton myasthenic syndrome; Landau–Kleffner syndrome; Lateral medullary (Wallenberg) syndrome; Learning disabilities; Leigh's disease; Lennox–Gastaut syndrome; Lesch–Nyhan syndrome; Leukodystrophy; Leukoencephalopathy with vanishing white matter; Lewy body dementia; Lissencephaly; Locked-in syndrome; Lou Gehrig's disease (amyotrophic lateral sclerosis (ALS)); Lumbar disc disease; Lumbar spinal stenosis; Lyme disease - Neurological Sequelae; Machado–Joseph disease (Spinocerebellar ataxia type 3); Macrencephaly; Macropsia; Mal de debarquement; Megalencephalic leukoencephalopathy with subcortical cysts; Megalencephaly; Melkersson–Rosenthal syndrome; Menieres disease; Meningitis; Menkes disease; Metachromatic leukodystrophy; Microcephaly; Micropsia; Migraine; Miller Fisher syndrome; Mini-stroke (transient ischemic attack); Misophonia; Mitochondrial myopathy; Mobius syndrome; Monomelic amyotrophy; Morvan syndrome; Motor Neurone Disease - see amyotrophic lateral sclerosis; Motor skills disorder; Moyamoya disease; Mucopolysaccharidoses; Multi-infarct dementia; Multifocal motor neuropathy; Multiple sclerosis; Multiple system atrophy; Muscular dystrophy; Myalgic encephalomyelitis; Myasthenia gravis; Myelinoclastic diffuse sclerosis; Myoclonic Encephalopathy of infants; Myoclonus; Myopathy; Myotubular myopathy; Myotonia congenita; Narcolepsy; Neuro-Behçet's disease; Neurofibromatosis; Neuroleptic malignant syndrome; Neurological manifestations of AIDS; Neurological sequelae of lupus; Neuromyotonia; Neuronal ceroid lipofuscinosis; Neuronal migration disorders; Neuropathy; Neurosis; Niemann–Pick disease; Non-24-hour sleep–wake disorder; Nonverbal learning disorder; O'Sullivan-McLeod syndrome; Occipital Neuralgia; Occult Spinal Dysraphism Sequence;

Ohtahara syndrome; Olivopontocerebellar atrophy; Opsoclonus myoclonus syndrome; Optic neuritis; Orthostatic Hypotension; Otosclerosis; Overuse syndrome; Palinopsia; Paresthesia; Parkinson's disease; Paramyotonia congenita; Paraneoplastic diseases; Paroxysmal attacks; Parry–Romberg syndrome; PANDAS; Pelizaeus–Merzbacher disease; Periodic paralyses; Peripheral neuropathy; Pervasive developmental disorders; Phantom limb / Phantom pain; Photic sneeze reflex; Phytanic acid storage disease; Pick's disease; Pinched nerve; Pituitary tumors; PMG; Polyneuropathy; Polio; Polymicrogyria; Polymyositis; Porencephaly; Post-polio syndrome; Postherpetic neuralgia (PHN); Postural hypotension; Prader–Willi syndrome; Primary lateral sclerosis; Prion diseases; Progressive hemifacial atrophy; Progressive multifocal leukoencephalopathy; Progressive supranuclear palsy; Prosopagnosia; Pseudotumor cerebri; Quadrantanopia; Quadriplegia; Rabies; Radiculopathy; Ramsay Hunt syndrome type I; Ramsay Hunt syndrome type II; Ramsay Hunt syndrome type III - see Ramsay-Hunt syndrome; Rasmussen encephalitis; Reflex neurovascular dystrophy; Refsum disease; REM sleep behavior disorder; Repetitive stress injury; Restless legs syndrome; Retrovirus-associated myelopathy; Rett syndrome; Reye's syndrome; Rhythmic Movement Disorder; Romberg syndrome; Saint Vitus dance; Sandhoff disease; Schilder's disease (two distinct conditions); Schizencephaly; Sensory processing disorder; Septo-optic dysplasia; Shaken baby syndrome; Shingles; Shy–Drager syndrome; Sjögren's syndrome; Sleep apnea; Sleeping sickness; Snatiation; Sotos syndrome; Spasticity; Spina bifida; Spinal cord injury; Spinal cord tumors; Spinal muscular atrophy; Spinal and bulbar muscular atrophy; Spinocerebellar ataxia; Split-brain; Steele-Richardson-Olszewski syndrome; Stiff-person syndrome; Stroke; Sturge–Weber syndrome; Stuttering; Subacute sclerosing panencephalitis; Subcortical arteriosclerotic encephalopathy; Superficial siderosis; Sydenham's chorea; Syncope; Synesthesia; Syringomyelia; Tarsal tunnel syndrome; Tardive dyskinesia; Tardive dysphrenia; Tarlov cyst; Tay–Sachs disease; Temporal arteritis; Temporal lobe epilepsy; Tetanus; Tethered spinal cord syndrome; Thomsen disease; Thoracic outlet syndrome; Tic Douloureux; Todd's paralysis; Tourette syndrome; Toxic encephalopathy; Transient ischemic attack; Transmissible spongiform encephalopathies; Transverse myelitis; Traumatic brain injury; Tremor; Trichotillomania; Trigeminal neuralgia; Tropical spastic paraparesis;

Trypanosomiasis; Tuberous sclerosis; 22q13 deletion syndrome; Unverricht–Lundborg disease; Vestibular schwannoma (Acoustic neuroma); Von Hippel–Lindau disease (VHL); Viliuisk Encephalomyelitis (VE); Wallenberg's syndrome; West syndrome; Whiplash; Williams syndrome; Wilson's disease; Y-Linked Hearing Impairment; or Zellweger syndrome.

CNS or PNS Injury or Trauma

[0153] Injury in the central nervous system (CNS) or peripheral nervous system (PNS) (e.g., trauma to the CNS or PNS, crush injury, spinal cord injury (SCI), traumatic brain injury, stroke, optic nerve injury, or related conditions that involve axonal disconnection) can be treated with the compositions and methods as described herein. The central nervous system (CNS) includes the brain and the spinal cord and the peripheral nervous system (PNS) is composed of cranial, spinal, and autonomic nerves that connect to the CNS.

[0154] Damage to the nervous system, caused by mechanical, thermal, chemical, or ischemic factors, can impair various nervous system functions such as memory, cognition, language, and voluntary movement. Most often, this is through crush or transection of nerve tracts. This results in the interruption of communication between nerve cell bodies and their targets. Other types of injuries can include disruption of the interrelations between neurons and their supporting cells or the destruction of the blood–brain barrier. Of all the types of injury, those to the CNS are among the most likely to result in death or permanent disability.

[0155] As described herein, mitofusin agonists (e.g., chimera B-A/l) rapidly reverses mitochondrial dysmotility in sciatic nerve axons of mice with CMT disease. Moreover, accumulating evidence suggests that impaired mitochondrial delivery to sites of injury of crushed (as opposed to severed) nerves is a central determinant of failure to regenerate/repair these injured nerves. For this reason, it is believed that enhancing mitochondrial trafficking with the mitofusin modulatory agents (e.g., mitofusin agonists) will enhance regeneration/repair of contused nerves, as in vehicular and sports injuries. Further testing of the crush-injury regeneration hypothesis will be further developed with the small molecule mitofusin agonists for evaluation of their in vivo effectiveness. As such, the present disclosure provides for compositions and methods to treat an injury such as a crush injury.

[0156] Because crush injury to skeletal muscle is an important cause of morbidity in car accidents, natural disaster, and battlefield settings, a treatment for nerve (e.g., sciatic nerve, median nerve) or muscle crush injury is needed.

[0157] As disclosed herein, mitochondria motility was implicated in neuropathy. It is believed that mitochondrial motility is also implicated in nerve injuries, especially in nerves that have not severed, such as a crush injury. After an accident or crush injury, nerves will regenerate or die. The small molecule mitofusin modulatory agents, as described herein, can increase mitochondiral trafficking, enabling the nerve to regenerate after a crush injury.

MOLECULAR ENGINEERING

[0158] The following definitions and methods are provided to better define the present invention and to guide those of ordinary skill in the art in the practice of the present invention. Unless otherwise noted, terms are to be understood according to conventional usage by those of ordinary skill in the relevant art.

[0159] The terms "heterologous DNA sequence", "exogenous DNA segment" or "heterologous nucleic acid," as used herein, each refer to a sequence that originates from a source foreign to the particular host cell or, if from the same source, is modified from its original form. Thus, a heterologous gene in a host cell includes a gene that is endogenous to the particular host cell but has been modified through, for example, the use of DNA shuffling. The terms also include non-naturally occurring multiple copies of a naturally occurring DNA sequence. Thus, the terms refer to a DNA segment that is foreign or heterologous to the cell, or homologous to the cell but in a position within the host cell nucleic acid in which the element is not ordinarily found. Exogenous DNA segments are expressed to yield exogenous polypeptides. A "homologous" DNA sequence is a DNA sequence that is naturally associated with a host cell into which it is introduced.

[0160] Expression vector, expression construct, plasmid, or recombinant DNA construct is generally understood to refer to a nucleic acid that has been generated via human intervention, including by recombinant means or direct chemical synthesis, with a series of specified nucleic acid elements that permit transcription or translation of a particular nucleic acid in, for example, a host cell. The expression vector can be part of a plasmid, virus, or nucleic acid fragment. Typically,

the expression vector can include a nucleic acid to be transcribed operably linked to a promoter.

[0161] A “promoter” is generally understood as a nucleic acid control sequence that directs transcription of a nucleic acid. An inducible promoter is generally understood as a promoter that mediates transcription of an operably linked gene in response to a particular stimulus. A promoter can include necessary nucleic acid sequences near the start site of transcription, such as, in the case of a polymerase II type promoter, a TATA element. A promoter can optionally include distal enhancer or repressor elements, which can be located as much as several thousand base pairs from the start site of transcription.

[0162] A "transcribable nucleic acid molecule" as used herein refers to any nucleic acid molecule capable of being transcribed into a RNA molecule. Methods are known for introducing constructs into a cell in such a manner that the transcribable nucleic acid molecule is transcribed into a functional mRNA molecule that is translated and therefore expressed as a protein product. Constructs may also be constructed to be capable of expressing antisense RNA molecules, in order to inhibit translation of a specific RNA molecule of interest. For the practice of the present disclosure, conventional compositions and methods for preparing and using constructs and host cells are well known to one skilled in the art (see e.g., Sambrook and Russel (2006) Condensed Protocols from Molecular Cloning: A Laboratory Manual, Cold Spring Harbor Laboratory Press, ISBN-10: 0879697717; Ausubel et al. (2002) Short Protocols in Molecular Biology, 5th ed., Current Protocols, ISBN-10: 0471250929; Sambrook and Russel (2001) Molecular Cloning: A Laboratory Manual, 3d ed., Cold Spring Harbor Laboratory Press, ISBN-10: 0879695773; Elhai, J. and Wolk, C. P. 1988. Methods in Enzymology 167, 747-754).

[0163] The “transcription start site” or "initiation site" is the position surrounding the first nucleotide that is part of the transcribed sequence, which is also defined as position +1. With respect to this site all other sequences of the gene and its controlling regions can be numbered. Downstream sequences (i.e., further protein encoding sequences in the 3' direction) can be denominated positive, while upstream sequences (mostly of the controlling regions in the 5' direction) are denominated negative.

[0164] A nucleic acid sequence or amino acid sequence (e.g., DNA, RNA, a genetic sequence, polynucleotide, oligonucleotide, primer, protein, polypeptide, peptide) can have about 80%; about 81%; about 82%; about 83%; about 84%; about 85%; about 86%; about 87%; about 88%; about 89%; about 90%; about 91%; about 92%; about 93%; about 94%; about 95%; about 96%; about 97%; about 98%; or about 99% sequence identity to a reference sequence or a naturally occurring sequence or contain at least one substitution modification to the reference sequence or naturally occurring sequence. Recitation of each of these discrete values is understood to include ranges between each value.

[0165] A nucleic acid sequence or an amino acid sequence can be operably linked to a heterologous promoter.

[0166] "Operably-linked" or "functionally linked" refers preferably to the association of nucleic acid sequences on a single nucleic acid fragment so that the function of one is affected by the other. For example, a regulatory DNA sequence is said to be "operably linked to" or "associated with" a DNA sequence that codes for an RNA or a polypeptide if the two sequences are situated such that the regulatory DNA sequence affects expression of the coding DNA sequence (i.e., that the coding sequence or functional RNA is under the transcriptional control of the promoter). Coding sequences can be operably-linked to regulatory sequences in sense or antisense orientation. The two nucleic acid molecules may be part of a single contiguous nucleic acid molecule and may be adjacent. For example, a promoter is operably linked to a gene of interest if the promoter regulates or mediates transcription of the gene of interest in a cell.

[0167] A "construct" is generally understood as any recombinant nucleic acid molecule such as a plasmid, cosmid, virus, autonomously replicating nucleic acid molecule, phage, or linear or circular single-stranded or double-stranded DNA or RNA nucleic acid molecule, derived from any source, capable of genomic integration or autonomous replication, comprising a nucleic acid molecule where one or more nucleic acid molecule has been operably linked.

[0168] A constructs of the present disclosure can contain a promoter operably linked to a transcribable nucleic acid molecule operably linked to a 3' transcription termination nucleic acid molecule. In addition, constructs can include but are not limited to additional regulatory nucleic acid molecules from, e.g., the 3'-

untranslated region (3' UTR). Constructs can include but are not limited to the 5' untranslated regions (5' UTR) of an mRNA nucleic acid molecule which can play an important role in translation initiation and can also be a genetic component in an expression construct. These additional upstream and downstream regulatory nucleic acid molecules may be derived from a source that is native or heterologous with respect to the other elements present on the promoter construct.

[0169] The term "transformation" refers to the transfer of a nucleic acid fragment into the genome of a host cell, resulting in genetically stable inheritance. Host cells containing the transformed nucleic acid fragments are referred to as "transgenic" cells, and organisms comprising transgenic cells are referred to as "transgenic organisms".

[0170] "Transformed," "transgenic," and "recombinant" refer to a host cell or organism such as a bacterium, cyanobacterium, animal or a plant into which a heterologous nucleic acid molecule has been introduced. The nucleic acid molecule can be stably integrated into the genome as generally known in the art and disclosed (Sambrook 1989; Innis 1995; Gelfand 1995; Innis & Gelfand 1999). Known methods of PCR include, but are not limited to, methods using paired primers, nested primers, single specific primers, degenerate primers, gene-specific primers, vector-specific primers, partially mismatched primers, and the like. The term "untransformed" refers to normal cells that have not been through the transformation process.

[0171] "Wild-type" refers to a virus or organism found in nature without any known mutation.

[0172] Design, generation, and testing of the variant nucleotides, and their encoded polypeptides, having the above required percent identities and retaining a required activity of the expressed protein is within the skill of the art. For example, directed evolution and rapid isolation of mutants can be according to methods described in references including, but not limited to, Link et al. (2007) Nature Reviews 5(9), 680-688; Sanger et al. (1991) Gene 97(1), 119-123; Ghadessy et al. (2001) Proc Natl Acad Sci USA 98(8) 4552-4557. Thus, one skilled in the art could generate a large number of nucleotide and/or polypeptide variants having, for example, at least 95-99% identity to the reference sequence described herein and screen such for desired phenotypes according to methods routine in the art.

[0173] Nucleotide and/or amino acid sequence identity percent (%) is understood as the percentage of nucleotide or amino acid residues that are identical with nucleotide or amino acid residues in a candidate sequence in comparison to a reference sequence when the two sequences are aligned. To determine percent identity, sequences are aligned and if necessary, gaps are introduced to achieve the maximum percent sequence identity. Sequence alignment procedures to determine percent identity are well known to those of skill in the art. Often publicly available computer software such as BLAST, BLAST2, ALIGN2 or Megalign (DNASTAR) software is used to align sequences. Those skilled in the art can determine appropriate parameters for measuring alignment, including any algorithms needed to achieve maximal alignment over the full-length of the sequences being compared. When sequences are aligned, the percent sequence identity of a given sequence A to, with, or against a given sequence B (which can alternatively be phrased as a given sequence A that has or comprises a certain percent sequence identity to, with, or against a given sequence B) can be calculated as: percent sequence identity = X/Y100, where X is the number of residues scored as identical matches by the sequence alignment program's or algorithm's alignment of A and B and Y is the total number of residues in B. If the length of sequence A is not equal to the length of sequence B, the percent sequence identity of A to B will not equal the percent sequence identity of B to A.

[0174] Generally, conservative substitutions can be made at any position so long as the required activity is retained. So-called conservative exchanges can be carried out in which the amino acid which is replaced has a similar property as the original amino acid, for example the exchange of Glu by Asp, Gln by Asn, Val by Ile, Leu by Ile, and Ser by Thr. For example, amino acids with similar properties can be Aliphatic amino acids (e.g., Glycine, Alanine, Valine, Leucine, Isoleucine); Hydroxyl or sulfur/selenium-containing amino acids (e.g., Serine, Cysteine, Selenocysteine, Threonine, Methionine); Cyclic amino acids (e.g., Proline); Aromatic amino acids (e.g., Phenylalanine, Tyrosine, Tryptophan); Basic amino acids (e.g., Histidine, Lysine, Arginine); or Acidic and their Amide (e.g., Aspartate, Glutamate, Asparagine, Glutamine). Deletion is the replacement of an amino acid by a direct bond. Positions for deletions include the termini of a polypeptide and linkages between individual protein domains. Insertions are introductions of amino acids into the polypeptide

chain, a direct bond formally being replaced by one or more amino acids. Amino acid sequence can be modulated with the help of art-known computer simulation programs that can produce a polypeptide with, for example, improved activity or altered regulation. On the basis of this artificially generated polypeptide sequences, a corresponding nucleic acid molecule coding for such a modulated polypeptide can be synthesized in-vitro using the specific codon-usage of the desired host cell.

[0175] "Highly stringent hybridization conditions" are defined as hybridization at 65 °C in a 6 X SSC buffer (*i.e.,* 0.9 M sodium chloride and 0.09 M sodium citrate). Given these conditions, a determination can be made as to whether a given set of sequences will hybridize by calculating the melting temperature (T_m) of a DNA duplex between the two sequences. If a particular duplex has a melting temperature lower than 65°C in the salt conditions of a 6 X SSC, then the two sequences will not hybridize. On the other hand, if the melting temperature is above 65 °C in the same salt conditions, then the sequences will hybridize. In general, the melting temperature for any hybridized DNA:DNA sequence can be determined using the following formula: $T_m = 81.5\ °C + 16.6(\log_{10}[Na^+]) + 0.41(\text{fraction G/C content}) - 0.63(\%\ \text{formamide}) - (600/l)$. Furthermore, the T_m of a DNA:DNA hybrid is decreased by 1-1.5°C for every 1% decrease in nucleotide identity (see e.g., Sambrook and Russel, 2006).

[0176] Host cells can be transformed using a variety of standard techniques known to the art (*see*, *e.g.*, Sambrook and Russel (2006) Condensed Protocols from Molecular Cloning: A Laboratory Manual, Cold Spring Harbor Laboratory Press, ISBN-10: 0879697717; Ausubel et al. (2002) Short Protocols in Molecular Biology, 5th ed., Current Protocols, ISBN-10: 0471250929; Sambrook and Russel (2001) Molecular Cloning: A Laboratory Manual, 3d ed., Cold Spring Harbor Laboratory Press, ISBN-10: 0879695773; Elhai, J. and Wolk, C. P. 1988. Methods in Enzymology 167, 747-754). Such techniques include, but are not limited to, viral infection, calcium phosphate transfection, liposome-mediated transfection, microprojectile-mediated delivery, receptor-mediated uptake, cell fusion, electroporation, and the like. The transfected cells can be selected and propagated to provide recombinant host cells that comprise the expression vector stably integrated in the host cell genome.

[0177] Exemplary nucleic acids which may be introduced to a host cell include, for example, DNA sequences or genes from another species, or even genes or sequences which originate with or are present in the same species, but are incorporated into recipient cells by genetic engineering methods. The term "exogenous" is also intended to refer to genes that are not normally present in the cell being transformed, or perhaps simply not present in the form, structure, *etc.*, as found in the transforming DNA segment or gene, or genes which are normally present and that one desires to express in a manner that differs from the natural expression pattern, *e.g.*, to over-express. Thus, the term "exogenous" gene or DNA is intended to refer to any gene or DNA segment that is introduced into a recipient cell, regardless of whether a similar gene may already be present in such a cell. The type of DNA included in the exogenous DNA can include DNA which is already present in the cell, DNA from another individual of the same type of organism, DNA from a different organism, or a DNA generated externally, such as a DNA sequence containing an antisense message of a gene, or a DNA sequence encoding a synthetic or modified version of a gene.

[0178] Host strains developed according to the approaches described herein can be evaluated by a number of means known in the art (*see e.g.*, Studier (2005) Protein Expr Purif. 41(1), 207–234; Gellissen, ed. (2005) Production of Recombinant Proteins: Novel Microbial and Eukaryotic Expression Systems, Wiley-VCH, ISBN-10: 3527310363; Baneyx (2004) Protein Expression Technologies, Taylor & Francis, ISBN-10: 0954523253).

[0179] Methods of down-regulation or silencing genes are known in the art. For example, expressed protein activity can be down-regulated or eliminated using antisense oligonucleotides, protein aptamers, nucleotide aptamers, and RNA interference (RNAi) (e.g., small interfering RNAs (siRNA), short hairpin RNA (shRNA), and micro RNAs (miRNA) (see e.g., Fanning and Symonds (2006) Handb Exp Pharmacol. 173, 289-303G, describing hammerhead ribozymes and small hairpin RNA; Helene, C., et al. (1992) Ann. N.Y. Acad. Sci. 660, 27-36; Maher (1992) Bioassays 14(12): 807-15, describing targeting deoxyribonucleotide sequences; Lee et al. (2006) Curr Opin Chem Biol. 10, 1-8, describing aptamers; Reynolds et al. (2004) Nature Biotechnology 22(3), 326 – 330, describing RNAi; Pushparaj and Melendez (2006) Clinical and Experimental Pharmacology and Physiology 33(5-6),

504-510, describing RNAi; Dillon et al. (2005) Annual Review of Physiology 67, 147-173, describing RNAi; Dykxhoorn and Lieberman (2005) Annual Review of Medicine 56, 401-423, describing RNAi). RNAi molecules are commercially available from a variety of sources (*e.g.*, Ambion, TX; Sigma Aldrich, MO; Invitrogen). Several siRNA molecule design programs using a variety of algorithms are known to the art (*see e.g.*, Cenix algorithm, Ambion; BLOCK-iT™ RNAi Designer, Invitrogen; siRNA Whitehead Institute Design Tools, Bioinofrmatics & Research Computing). Traits influential in defining optimal siRNA sequences include G/C content at the termini of the siRNAs, Tm of specific internal domains of the siRNA, siRNA length, position of the target sequence within the CDS (coding region), and nucleotide content of the 3' overhangs.

FORMULATION

[0180] The agents and compositions described herein can be formulated by any conventional manner using one or more pharmaceutically acceptable carriers or excipients as described in, for example, Remington's Pharmaceutical Sciences (A.R. Gennaro, Ed.), 21st edition, ISBN: 0781746736 (2005), incorporated herein by reference in its entirety. Such formulations will contain a therapeutically effective amount of a biologically active agent described herein, which can be in purified form, together with a suitable amount of carrier so as to provide the form for proper administration to the subject.

[0181] The term "formulation" refers to preparing a drug in a form suitable for administration to a subject, such as a human. Thus, a "formulation" can include pharmaceutically acceptable excipients, including diluents or carriers.

[0182] The term "pharmaceutically acceptable" as used herein can describe substances or components that do not cause unacceptable losses of pharmacological activity or unacceptable adverse side effects. Examples of pharmaceutically acceptable ingredients can be those having monographs in United States Pharmacopeia (USP 29) and National Formulary (NF 24), United States Pharmacopeial Convention, Inc, Rockville, Maryland, 2005 ("USP/NF"), or a more recent edition, and the components listed in the continuously updated Inactive Ingredient Search online database of the FDA. Other useful components that are not described in the USP/NF, etc. may also be used.

[0183] The term “pharmaceutically acceptable excipient,” as used herein, can include any and all solvents, dispersion media, coatings, antibacterial and antifungal agents, isotonic, or absorption delaying agents. The use of such media and agents for pharmaceutical active substances is well known in the art (see generally Remington’s Pharmaceutical Sciences (A.R. Gennaro, Ed.), 21st edition, ISBN: 0781746736 (2005)). Except insofar as any conventional media or agent is incompatible with an active ingredient, its use in the therapeutic compositions is contemplated. Supplementary active ingredients can also be incorporated into the compositions.

[0184] A "stable" formulation or composition can refer to a composition having sufficient stability to allow storage at a convenient temperature, such as between about 0 ºC and about 60 ºC, for a commercially reasonable period of time, such as at least about one day, at least about one week, at least about one month, at least about three months, at least about six months, at least about one year, or at least about two years.

[0185] The formulation should suit the mode of administration. The agents of use with the current disclosure can be formulated by known methods for administration to a subject using several routes which include, but are not limited to, parenteral, pulmonary, oral, topical, intradermal, intramuscular, intraperitoneal, intravenous, subcutaneous, intranasal, epidural, ophthalmic, buccal, and rectal. The individual agents may also be administered in combination with one or more additional agents or together with other biologically active or biologically inert agents. Such biologically active or inert agents may be in fluid or mechanical communication with the agent(s) or attached to the agent(s) by ionic, covalent, Van der Waals, hydrophobic, hydrophilic or other physical forces.

[0186] Controlled-release (or sustained-release) preparations may be formulated to extend the activity of the agent(s) and reduce dosage frequency. Controlled-release preparations can also be used to affect the time of onset of action or other characteristics, such as blood levels of the agent, and consequently affect the occurrence of side effects. Controlled-release preparations may be designed to initially release an amount of an agent(s) that produces the desired therapeutic effect, and gradually and continually release other amounts of the agent to maintain the level of therapeutic effect over an extended period of time. In order to maintain a

near-constant level of an agent in the body, the agent can be released from the dosage form at a rate that will replace the amount of agent being metabolized or excreted from the body. The controlled-release of an agent may be stimulated by various inducers, *e.g.*, change in pH, change in temperature, enzymes, water, or other physiological conditions or molecules.

[0187] Agents or compositions described herein can also be used in combination with other therapeutic modalities, as described further below. Thus, in addition to the therapies described herein, one may also provide to the subject other therapies known to be efficacious for treatment of the disease, disorder, or condition.

THERAPEUTIC METHODS

[0188] Also provided is a process of treating a mitochondria-associated disease, disorder, or condition in a subject in need administration of a therapeutically effective amount of mitofusin modulating agent, so as to prevent or treat a mitochondria-associated disease, disorder, or condition.

[0189] For example, the compositions and methods described herein can be used as a primary therapy for Charcot Marie Tooth, or adjunctive therapy for Huntington's, Parkinson's, and Alzheimer's diseases or ALS to reverse or retard progression.

[0190] As another example, the compositions and methods described herein can be used for the treatment of a physical injury. For example, as a primary therapy for any contusive injury involving the spine or peripheral nerves (perhaps even the brain, i.e. concussion), such as motor vehicle or sports injuries. This therapy can help restore normal motor function by augmenting regeneration and repair of injured neurons.

[0191] Methods described herein are generally performed on a subject in need thereof. A subject in need of the therapeutic methods described herein can be a subject having, diagnosed with, suspected of having, or at risk for developing a mitochondria-associated disease, disorder, or condition. A determination of the need for treatment will typically be assessed by a history and physical exam consistent with the disease or condition at issue. Diagnosis of the various conditions treatable by the methods described herein is within the skill of the art. The subject can be an animal subject, including a mammal, such as horses, cows, dogs, cats, sheep, pigs,

mice, rats, monkeys, hamsters, guinea pigs, and chickens, and humans. For example, the subject can be a human subject.

[0192] Generally, a safe and effective amount of a mitofusin modulating agent is, for example, that amount that would cause the desired therapeutic effect in a subject while minimizing undesired side effects. In various embodiments, an effective amount of a mitofusin modulating agent described herein can substantially inhibit mitochondria-associated disease, disorder, or condition, slow the progress of mitochondria-associated disease, disorder, or condition, or limit the development of mitochondria-associated disease, disorder, or condition. For example, a desired therapeutic effect can be a delay in peripheral neuropathy (e.g., over the course of three years) compared to placebo assessed by slower increase in modified composite CMT neuropathy score. As another example, a desired therapeutic effect can be reversal or absence of progression of peripheral neuropathy compared to placebo, as indicated by lower or stable modified composite CMT neuropathy score. As yet another example, a desired therapeutic effect can be reversal or absence of progression of dysregulated motor function or increased regeneration and repair of injured neurons.

[0193] According to the methods described herein, administration can be parenteral, pulmonary, oral, topical, intradermal, intramuscular, intraperitoneal, intravenous, subcutaneous, intranasal, epidural, ophthalmic, buccal, or rectal administration.

[0194] When used in the treatments described herein, a therapeutically effective amount of a mitofusin modulating agent can be employed in pure form or, where such forms exist, in pharmaceutically acceptable salt form and with or without a pharmaceutically acceptable excipient. For example, the compounds of the present disclosure can be administered, at a reasonable benefit/risk ratio applicable to any medical treatment, in a sufficient amount to treat, prevent, or slow the progression of mitochondria-associated disease, disorder, or condition.

[0195] The amount of a composition described herein that can be combined with a pharmaceutically acceptable carrier to produce a single dosage form will vary depending upon the host treated and the particular mode of administration. It will be appreciated by those skilled in the art that the unit content of agent contained in an individual dose of each dosage form need not in itself

constitute a therapeutically effective amount, as the necessary therapeutically effective amount could be reached by administration of a number of individual doses.

[0196] Toxicity and therapeutic efficacy of compositions described herein can be determined by standard pharmaceutical procedures in cell cultures or experimental animals for determining the LD_{50} (the dose lethal to 50% of the population) and the ED_{50}, (the dose therapeutically effective in 50% of the population). The dose ratio between toxic and therapeutic effects is the therapeutic index that can be expressed as the ratio LD_{50}/ED_{50}, where larger therapeutic indices are generally understood in the art to be optimal.

[0197] The specific therapeutically effective dose level for any particular subject will depend upon a variety of factors including the disorder being treated and the severity of the disorder; activity of the specific compound employed; the specific composition employed; the age, body weight, general health, sex and diet of the subject; the time of administration; the route of administration; the rate of excretion of the composition employed; the duration of the treatment; drugs used in combination or coincidental with the specific compound employed; and like factors well known in the medical arts (*see e.g.*, Koda-Kimble et al. (2004) Applied Therapeutics: The Clinical Use of Drugs, Lippincott Williams & Wilkins, ISBN 0781748453; Winter (2003) Basic Clinical Pharmacokinetics, 4th ed., Lippincott Williams & Wilkins, ISBN 0781741475; Sharqel (2004) Applied Biopharmaceutics & Pharmacokinetics, McGraw-Hill/Appleton & Lange, ISBN 0071375503). For example, it is well within the skill of the art to start doses of the composition at levels lower than those required to achieve the desired therapeutic effect and to gradually increase the dosage until the desired effect is achieved. If desired, the effective daily dose may be divided into multiple doses for purposes of administration. Consequently, single dose compositions may contain such amounts or submultiples thereof to make up the daily dose. It will be understood, however, that the total daily usage of the compounds and compositions of the present disclosure will be decided by an attending physician within the scope of sound medical judgment.

[0198] Again, each of the states, diseases, disorders, and conditions, described herein, as well as others, can benefit from compositions and methods described herein. Generally, treating a state, disease, disorder, or condition includes preventing or delaying the appearance of clinical symptoms in a mammal that may

be afflicted with or predisposed to the state, disease, disorder, or condition but does not yet experience or display clinical or subclinical symptoms thereof. Treating can also include inhibiting the state, disease, disorder, or condition, *e.g.*, arresting or reducing the development of the disease or at least one clinical or subclinical symptom thereof. Furthermore, treating can include relieving the disease, *e.g.*, causing regression of the state, disease, disorder, or condition or at least one of its clinical or subclinical symptoms. A benefit to a subject to be treated can be either statistically significant or at least perceptible to the subject or to a physician.

[0199] Administration of a mitofusin modulating agent can occur as a single event or over a time course of treatment. For example, a mitofusin modulating agent can be administered daily, weekly, bi-weekly, or monthly. For treatment of acute conditions, the time course of treatment will usually be at least several days. Certain conditions could extend treatment from several days to several weeks. For example, treatment could extend over one week, two weeks, or three weeks. For more chronic conditions, treatment could extend from several weeks to several months or even a year or more.

[0200] Treatment in accord with the methods described herein can be performed prior to, concurrent with, or after conventional treatment modalities for treating, preventing, or slowing the progression of mitochondria-associated disease, disorder, or condition.

[0201] A mitofusin modulating agent can be administered simultaneously or sequentially with another agent, such as an antibiotic, an anti-inflammatory, or another agent. For example, a mitofusin modulating agent can be administered simultaneously with another agent, such as an antibiotic or an anti-inflammatory. Simultaneous administration can occur through administration of separate compositions, each containing one or more of a mitofusin modulating agent, an antibiotic, an anti-inflammatory, or another agent. Simultaneous administration can occur through administration of one composition containing two or more of mitofusin modulating agent, an antibiotic, an anti-inflammatory, or another agent. A mitofusin modulating agent can be administered sequentially with an antibiotic, an anti-inflammatory, or another agent. For example, a mitofusin modulating agent can be administered before or after administration of an antibiotic, an anti-inflammatory, or another agent.

ADMINISTRATION

[0202] Agents and compositions described herein can be administered according to methods described herein in a variety of means known to the art. The agents and composition can be used therapeutically either as exogenous materials or as endogenous materials. Exogenous agents are those produced or manufactured outside of the body and administered to the body. Endogenous agents are those produced or manufactured inside the body by some type of device (biologic or other) for delivery within or to other organs in the body.

[0203] As discussed above, administration can be parenteral, pulmonary, oral, topical, transdermal (e.g., a transdermal patch) intradermal, intramuscular, intraperitoneal, intravenous, subcutaneous, intranasal, epidural, ophthalmic, buccal, or rectal administration.

[0204] Agents and compositions described herein can be administered in a variety of methods well known in the arts. Administration can include, for example, methods involving oral ingestion, direct injection (*e.g.*, systemic or stereotactic), implantation of cells engineered to secrete the factor of interest, drug-releasing biomaterials, polymer matrices, gels, permeable membranes, osmotic systems, multilayer coatings, microparticles, implantable matrix devices, mini-osmotic pumps, implantable pumps, injectable gels and hydrogels, liposomes, micelles (*e.g.*, up to 30 μm), nanospheres (*e.g.*, less than 1 μm), microspheres (*e.g.*, 1-100 μm), reservoir devices, a combination of any of the above, or other suitable delivery vehicles to provide the desired release profile in varying proportions. Other methods of controlled-release delivery of agents or compositions will be known to the skilled artisan and are within the scope of the present disclosure.

[0205] Delivery systems may include, for example, an infusion pump which may be used to administer the agent or composition in a manner similar to that used for delivering insulin or chemotherapy to specific organs or tumors. Typically, using such a system, an agent or composition can be administered in combination with a biodegradable, biocompatible polymeric implant that releases the agent over a controlled period of time at a selected site. Examples of polymeric materials include polyanhydrides, polyorthoesters, polyglycolic acid, polylactic acid, polyethylene vinyl acetate, and copolymers and combinations thereof. In addition, a controlled release

system can be placed in proximity of a therapeutic target, thus requiring only a fraction of a systemic dosage.

[0206] Agents can be encapsulated and administered in a variety of carrier delivery systems. Examples of carrier delivery systems include microspheres, hydrogels, polymeric implants, smart polymeric carriers, and liposomes (*see generally*, Uchegbu and Schatzlein, eds. (2006) Polymers in Drug Delivery, CRC, ISBN-10: 0849325331). Carrier-based systems for molecular or biomolecular agent delivery can: provide for intracellular delivery; tailor biomolecule/agent release rates; increase the proportion of biomolecule that reaches its site of action; improve the transport of the drug to its site of action; allow colocalized deposition with other agents or excipients; improve the stability of the agent *in vivo*; prolong the residence time of the agent at its site of action by reducing clearance; decrease the nonspecific delivery of the agent to nontarget tissues; decrease irritation caused by the agent; decrease toxicity due to high initial doses of the agent; alter the immunogenicity of the agent; decrease dosage frequency, improve taste of the product; or improve shelf life of the product.

SCREENING

[0207] Also provided are methods for screening (see e.g., Example 2, Example 3). As described herein, a FRET method for screening and evaluating small molecular regulators of mitochondrial tethering and fusion is provided. Also provided herein is a binding assay for screening and evaluating small molecular regulators of mitochondrial tethering and fusion.

[0208] The term "FRET" as used herein refers to fluorescence resonance energy transfer between molecules. In FRET methods, one fluorophore is able to act as an energy donor and the other of which is an energy acceptor molecule. These are sometimes known as a reporter molecule and a quencher molecule respectively. The donor molecule is excited with a specific wavelength of light for which it will normally exhibit a fluorescence emission wavelength. The acceptor molecule is also excited at this wavelength such that it can accept the emission energy of the donor molecule by a variety of distance-dependent energy transfer mechanisms. Generally the acceptor molecule accepts the emission energy of the donor molecule when they are in close proximity (e.g., on the same, or a neighboring molecule). See for

example U.S. Pat. Nos. 5,707,804, 5,728,528, 5,853,992, and 5,869,255 (for a description of FRET dyes), T Mergny et al., (1994) Nucleic Acid Res. 22:920-928, and Wolf et al., (1988) Proc. Natl. Acad. Sci. USA 85:8790-8794 (for general descriptions and methods for FRET), each of which is hereby incorporated by reference in its entirety.

[0209] With the modulating compounds and peptides available which have been shown to activate mitochondrial fusion, assays can be designed and performed to screen candidate agents or molecules for specific compositions which can activate mitochondrial fusion. For example, identification of small molecule activators provides an alternate modulating composition which may be more efficient to synthesize and use. Candidate agents encompass numerous chemical classes, typically synthetic, semi-synthetic, or naturally- occurring inorganic or organic molecules. Candidate agents include those found in large libraries of synthetic or natural compounds. Alternatively, libraries of natural compounds in the form of bacterial, fungal, plant and animal extracts are available from commercial resources or are readily producible. In some embodiments, small molecule activators of mitochondrial fusion identified through these screening assays can become promising therapeutic agents for treating diseases or disorders associated with defects in mitochondrial fusion.

[0210] One screening assay can use the HR1 peptide or variant which has been shown to increase mitochondrial aspect ratio. In this assay, the Mfn2 protein or a fragment of the Mfn2 protein which contains the HR2 domain is immobilized to a solid substrate such as nitrocellulose or to the well surface of a high throughput screen plate or array substrate. The immobilized protein or fragment is then incubated with the HR1 peptide or variant in a solution conducive to protein-protein interactions. The HR1 peptide is conjugated to a detectable label such as FITC or other fluorescent dye, generating a signal in each well or array position. Detectable labels are well-known in the art and include isotope, colorimetric, fluorescent, photochromic and electrochemical labels. A candidate agent is assessed for its ability to compete with the HR1 peptide for binding to the solid phase-bound Mfn2 protein or HR2 domain. An agent which can compete with the HR1 peptide for binding to Mfn2 protein or HR2 will reduce or eliminate the signal from the label. A candidate agent able compete with the

HR1peptide is an agent which can activate mitochondrial aspect ratio and/or mitochondrial fusion.

[0211] In some embodiments, a method for identifying an agent or compound able to bind to the Mfn2 protein is provided. In these embodiments, the compound competes with the HR1peptide for binding to Mfn2 or to a fragment of Mfn2 comprising the HR2 domain. A test compound is identified as active it if decreases the binding of the peptide, i.e., its effect on the extent of binding is above a threshold level. More specifically, if the decrease in binding of the labeled HR1 peptide to the solid phase bound Mfn2 protein or HR2 domain is a several-fold different between the control and experimental samples, the compound would be considered as having binding activity. Typically, a 2-fold or 4-fold threshold difference in binding between the test and control samples is sought. In some embodiments, this agent increases the mitochondrial aspect ratio when incubated in a cell.

[0212] In some embodiments, an alternative assay is provided to identify a composition able to activate intermolecular binding of the HR2 domains of two Mfn proteins. In this assay, a first population of Mfn2 proteins is labeled with an acceptor fluorophore on its HR2 arm and a second population of Mfn2 proteins is labeled with a donor fluorophore on its HR2 arm. Use of fluorophore donors and complementary acceptor molecules for FRET analysis is well known (see, e.g., Jager et al., 2005, Protein Sci, 14:2059-2068; Jager et al, 2006, Protein Sci, 15:640-646). Accordingly, as described above, when an HR2 arm is liberated from the configuration in which it is interacting with the HR1 domain within the core of the Mfn protein, the free HR2 arm is able to interact with the free HR2 arm of a second Mfn2 to facilitate mitochondrial tethering and subsequent fusion. It follows that provided herein is an assay to screen a population of agents or compounds for those that facilitate mitochondrial tethering and subsequent fusion wherein the population of candidate compounds is added to an array, wherein each well or position in the array contains a test reaction mix which comprises a first population of Mfn2 proteins labeled at or near the HR2 arm with a donor fluorophore and a second population of Mfn2 proteins labeled at or near the HR2 arm with a acceptor fluorophore. The fluorescence is measured in each test reaction mix and compared with a negative control reaction mix containing no HR2-binding peptide and a

positive control reaction mix which contains an HR2-binding peptide and no candidate compound. A fluorescence signal which is greater in a test reaction mix containing a candidate compound is identified the candidate compound as an activator of mitochondrial fusion.

[0213] In a third screening assay, interaction between the HR1 and HR2 domains of a single Mfn2 protein is assessed. For example, a single Mfn2 protein is labeled with a single FRET donor and acceptor pair, wherein the donor is positioned at or near the HR1 domain and the acceptor is positioned at or near the HR2 domain, or vice versa. Incubation of a peptide which inhibits mitochondrial fusion (decreases mitochondrial aspect ratio) (e.g., the 367-384Gly peptide or variant thereof) will cause the HR2 arm to extend, removing the quenching action of the FRET pair, resulting in fluorescence signal. Accordingly, a library of candidate modulating molecules can be screened by mixing each with the Mfn2 protein labeled with a FRET donor acceptor pair. Any candidate molecule which increases fluorescence of the labeled Mfn2 protein by at least 50%, 60%, 70% compared to the labeled Mfn2 protein in the absence of a candidate molecule will be identified as an activator of mitochondrial fusion.

[0214] The subject methods find use in the screening of a variety of different candidate molecules (*e.g.*, potentially therapeutic candidate molecules). Candidate substances for screening according to the methods described herein include, but are not limited to, fractions of tissues or cells, nucleic acids, polypeptides, siRNAs, antisense molecules, aptamers, ribozymes, triple helix compounds, antibodies, and small (*e.g.*, less than about 2000 mw, or less than about 1000 mw, or less than about 800 mw) organic molecules or inorganic molecules including but not limited to salts or metals.

[0215] Candidate molecules encompass numerous chemical classes, for example, organic molecules, such as small organic compounds having a molecular weight of more than 50 and less than about 2,500 Daltons. Candidate molecules can comprise functional groups necessary for structural interaction with proteins, particularly hydrogen bonding, and typically include at least an amine, carbonyl, hydroxyl or carboxyl group, and usually at least two of the functional chemical groups. The candidate molecules can comprise cyclical carbon or heterocyclic

structures and/or aromatic or polyaromatic structures substituted with one or more of the above functional groups.

[0216] A candidate molecule can be a compound in a library database of compounds. One of skill in the art will be generally familiar with, for example, numerous databases for commercially available compounds for screening (*see e.g.*, ZINC database, UCSF, with 2.7 million compounds over 12 distinct subsets of molecules; Irwin and Shoichet (2005) J Chem Inf Model 45, 177-182). One of skill in the art will also be familiar with a variety of search engines to identify commercial sources or desirable compounds and classes of compounds for further testing (*see e.g.*, ZINC database; eMolecules.com; and electronic libraries of commercial compounds provided by vendors, for example: ChemBridge, Princeton BioMolecular, Ambinter SARL, Enamine, ASDI, Life Chemicals etc.).

[0217] Candidate molecules for screening according to the methods described herein include both lead-like compounds and drug-like compounds. A lead-like compound is generally understood to have a relatively smaller scaffold-like structure (e.g., molecular weight of about 150 to about 350 kD) with relatively fewer features (e.g., less than about 3 hydrogen donors and/or less than about 6 hydrogen acceptors; hydrophobicity character xlogP of about -2 to about 4) (see e.g., Angewante (1999) Chemie Int. ed. Engl. 24, 3943-3948). In contrast, a drug-like compound is generally understood to have a relatively larger scaffold (e.g., molecular weight of about 150 to about 500 kD) with relatively more numerous features (e.g., less than about 10 hydrogen acceptors and/or less than about 8 rotatable bonds; hydrophobicity character xlogP of less than about 5) (see e.g., Lipinski (2000) J. Pharm. Tox. Methods 44, 235-249). Initial screening can be performed with lead-like compounds.

[0218] When designing a lead from spatial orientation data, it can be useful to understand that certain molecular structures are characterized as being “drug-like”. Such characterization can be based on a set of empirically recognized qualities derived by comparing similarities across the breadth of known drugs within the pharmacopoeia. While it is not required for drugs to meet all, or even any, of these characterizations, it is far more likely for a drug candidate to meet with clinical successful if it is drug-like.

[0219] Several of these “drug-like” characteristics have been summarized into the four rules of Lipinski (generally known as the “rules of fives” because of the prevalence of the number 5 among them). While these rules generally relate to oral absorption and are used to predict bioavailability of compound during lead optimization, they can serve as effective guidelines for constructing a lead molecule during rational drug design efforts such as may be accomplished by using the methods of the present disclosure.

[0220] The four “rules of five” state that a candidate drug-like compound should have at least three of the following characteristics: (i) a weight less than 500 Daltons; (ii) a log of P less than 5; (iii) no more than 5 hydrogen bond donors (expressed as the sum of OH and NH groups); and (iv) no more than 10 hydrogen bond acceptors (the sum of N and O atoms). Also, drug-like molecules typically have a span (breadth) of between about 8Å to about 15Å.

[0221] Fragment-based lead discovery (FBLD) also known as fragment-based drug discovery (FBDD) is a method that can be used for finding lead compounds as part of the drug discovery process. It is based on identifying small chemical fragments, which may bind only weakly to the biological target, and then growing them or combining them to produce a lead with a higher affinity. FBLD can be compared with high-throughput screening (HTS). In HTS, libraries with up to millions of compounds, with molecular weights of around 500 Da, are screened, and nanomolar binding affinities are sought. In contrast, in the early phase of FBLD, libraries with a few thousand compounds with molecular weights of around 200 Da may be screened, and millimolar affinities can be considered useful.

[0222] In analogy to the rule of five, it has been proposed that ideal fragments could follow the 'rule of three' (molecular weight < 300, ClogP < 3, the number of hydrogen bond donors and acceptors each should be < 3 and the number of rotatable bonds should be < 3). Since the fragments have relatively low affinity for their targets, they should have high water solubility so that they can be screened at higher concentrations.

[0223] In fragment-based drug discovery, the low binding affinities of the fragments can pose significant challenges for screening. Many biophysical techniques have been applied to address this issue. In particular, ligand-observe nuclear magnetic resonance (NMR) methods such as water-ligand observed via

gradient spectroscopy (waterLOGSY), saturation transfer difference spectroscopy (STD-NMR), 19F NMR spectroscopy and inter-ligand Overhauser effect (ILOE) spectroscopy, protein-observe NMR methods such as 1H-15N heteronuclear single quantum coherence (HSQC) that utilizes isotopically-labelled proteins, surface plasmon resonance (SPR) and isothermal titration calorimetry (ITC) are routinely-used for ligand screening and for the quantification of fragment binding affinity to the target protein.

[0224] Once a fragment (or a combination of fragments) have been identified, protein X-ray crystallography can be used to obtain structural models of the protein-fragment(s) complexes. Such information can then be used to guide organic synthesis for high-affinity protein ligands and enzyme inhibitors.

[0225] Advantages of screening low molecular weight fragment based libraries over traditional higher molecular weight chemical libraries can include:

(i) More hydrophilic hits in which hydrogen bonding is more likely to contribute to affinity (enthalpically driven binding). It is generally much easier to increase affinity by adding hydrophobic groups (entropically driven binding), starting with a hydrophilic ligand increases the chances that the final optimized ligand will not be too hydrophobic (log P < 5).

(ii) Higher ligand efficiency so that the final optimized ligand will more likely be relatively low in molecular weight (MW < 500).

(iii) Since two to three fragments in theory can be combined to form an optimized ligand, screening a fragment library of N compounds is equivalent to screening N2 - N3 compounds in a traditional library.

[0226] Fragments can be less likely to contain sterically blocking groups that interfere with an otherwise favorable ligand-protein interaction, increasing the combinatorial advantage of a fragment library even further.

KITS

[0227] Also provided are kits. Such kits can include an agent or composition described herein and, in certain embodiments, instructions for administration. Such kits can facilitate performance of the methods described herein. When supplied as a kit, the different components of the composition can be packaged in separate containers and admixed immediately before use. Components

include, but are not limited to Mfn1, Mfn2, antagonist target peptides, agonist target peptides, or mitofusin modulating agents. Such packaging of the components separately can, if desired, be presented in a pack or dispenser device which may contain one or more unit dosage forms containing the composition. The pack may, for example, comprise metal or plastic foil such as a blister pack. Such packaging of the components separately can also, in certain instances, permit long-term storage without losing activity of the components.

[0228] Kits may also include reagents in separate containers such as, for example, sterile water or saline to be added to a lyophilized active component packaged separately. For example, sealed glass ampules may contain a lyophilized component and in a separate ampule, sterile water, sterile saline or sterile each of which has been packaged under a neutral non-reacting gas, such as nitrogen. Ampules may consist of any suitable material, such as glass, organic polymers, such as polycarbonate, polystyrene, ceramic, metal or any other material typically employed to hold reagents. Other examples of suitable containers include bottles that may be fabricated from similar substances as ampules, and envelopes that may consist of foil-lined interiors, such as aluminum or an alloy. Other containers include test tubes, vials, flasks, bottles, syringes, and the like. Containers may have a sterile access port, such as a bottle having a stopper that can be pierced by a hypodermic injection needle. Other containers may have two compartments that are separated by a readily removable membrane that upon removal permits the components to mix. Removable membranes may be glass, plastic, rubber, and the like.

[0229] In certain embodiments, kits can be supplied with instructional materials. Instructions may be printed on paper or other substrate, and/or may be supplied as an electronic-readable medium, such as a floppy disc, mini-CD-ROM, CD-ROM, DVD-ROM, Zip disc, videotape, audio tape, and the like. Detailed instructions may not be physically associated with the kit; instead, a user may be directed to an Internet web site specified by the manufacturer or distributor of the kit.

[0230] Compositions and methods described herein utilizing molecular biology protocols can be according to a variety of standard techniques known to the art (*see*, *e.g.*, Sambrook and Russel (2006) Condensed Protocols from Molecular Cloning: A Laboratory Manual, Cold Spring Harbor Laboratory Press, ISBN-10: 0879697717; Ausubel et al. (2002) Short Protocols in Molecular Biology, 5th ed.,

Current Protocols, ISBN-10: 0471250929; Sambrook and Russel (2001) Molecular Cloning: A Laboratory Manual, 3d ed., Cold Spring Harbor Laboratory Press, ISBN-10: 0879695773; Elhai, J. and Wolk, C. P. 1988. Methods in Enzymology 167, 747-754; Studier (2005) Protein Expr Purif. 41(1), 207–234; Gellissen, ed. (2005) Production of Recombinant Proteins: Novel Microbial and Eukaryotic Expression Systems, Wiley-VCH, ISBN-10: 3527310363; Baneyx (2004) Protein Expression Technologies, Taylor & Francis, ISBN-10: 0954523253).

[0231] Definitions and methods described herein are provided to better define the present disclosure and to guide those of ordinary skill in the art in the practice of the present disclosure. Unless otherwise noted, terms are to be understood according to conventional usage by those of ordinary skill in the relevant art.

[0232] In some embodiments, numbers expressing quantities of ingredients, properties such as molecular weight, reaction conditions, and so forth, used to describe and claim certain embodiments of the present disclosure are to be understood as being modified in some instances by the term “about.” In some embodiments, the term “about” is used to indicate that a value includes the standard deviation of the mean for the device or method being employed to determine the value. In some embodiments, the numerical parameters set forth in the written description and attached claims are approximations that can vary depending upon the desired properties sought to be obtained by a particular embodiment. In some embodiments, the numerical parameters should be construed in light of the number of reported significant digits and by applying ordinary rounding techniques. Notwithstanding that the numerical ranges and parameters setting forth the broad scope of some embodiments of the present disclosure are approximations, the numerical values set forth in the specific examples are reported as precisely as practicable. The numerical values presented in some embodiments of the present disclosure may contain certain errors necessarily resulting from the standard deviation found in their respective testing measurements. The recitation of ranges of values herein is merely intended to serve as a shorthand method of referring individually to each separate value falling within the range. Unless otherwise indicated herein, each individual value is incorporated into the specification as if it were individually recited herein.

[0233] In some embodiments, the terms “a” and “an” and “the” and similar references used in the context of describing a particular embodiment (especially in the context of certain of the following claims) can be construed to cover both the singular and the plural, unless specifically noted otherwise. In some embodiments, the term “or” as used herein, including the claims, is used to mean “and/or” unless explicitly indicated to refer to alternatives only or the alternatives are mutually exclusive.

[0234] The terms “comprise,” “have” and “include” are open-ended linking verbs. Any forms or tenses of one or more of these verbs, such as “comprises,” “comprising,” “has,” “having,” “includes” and “including,” are also open-ended. For example, any method that “comprises,” “has” or “includes” one or more steps is not limited to possessing only those one or more steps and can also cover other unlisted steps. Similarly, any composition or device that “comprises,” “has” or “includes” one or more features is not limited to possessing only those one or more features and can cover other unlisted features.

[0235] All methods described herein can be performed in any suitable order unless otherwise indicated herein or otherwise clearly contradicted by context. The use of any and all examples, or exemplary language (*e.g.* “such as”) provided with respect to certain embodiments herein is intended merely to better illuminate the present disclosure and does not pose a limitation on the scope of the present disclosure otherwise claimed. No language in the specification should be construed as indicating any non-claimed element essential to the practice of the present disclosure.

[0236] Groupings of alternative elements or embodiments of the present disclosure disclosed herein are not to be construed as limitations. Each group member can be referred to and claimed individually or in any combination with other members of the group or other elements found herein. One or more members of a group can be included in, or deleted from, a group for reasons of convenience or patentability. When any such inclusion or deletion occurs, the specification is herein deemed to contain the group as modified thus fulfilling the written description of all Markush groups used in the appended claims.

[0237] Citation of a reference herein shall not be construed as an admission that such is prior art to the present disclosure.

[0238] Having described the present disclosure in detail, it will be apparent that modifications, variations, and equivalent embodiments are possible without departing the scope of the present disclosure defined in the appended claims. Furthermore, it should be appreciated that all examples in the present disclosure are provided as non-limiting examples.

EXAMPLES

[0239] The following non-limiting examples are provided to further illustrate the present disclosure. It should be appreciated by those of skill in the art that the techniques disclosed in the examples that follow represent approaches the inventors have found function well in the practice of the present disclosure, and thus can be considered to constitute examples of modes for its practice. However, those of skill in the art should, in light of the present disclosure, appreciate that many changes can be made in the specific embodiments that are disclosed and still obtain a like or similar result without departing from the spirit and scope of the present disclosure.

EXAMPLE 1: IDENTIFICATION OF AMINO ACID RESIDUES IN THE HR1 MFN1 AND MFN2 DOMAIN THAT INFLUENCE CONFORMATION

[0240] The following example shows that Mfn1 and Mfn2 conformation is influenced by a plurality of amino acid residues in the HR1 domain.

[0241] Mitochondria generate ATP that fuels neuronal activity. Mitochondrial dysfunction is implicated in chronic degenerative neurological conditions such as Alzheimer's, Parkinson's, and Huntington's diseases. Mitochondria fuse in order to exchange genomes and promote mutual repair. The initial stages of mitochondrial fusion proceed through the physiochemical actions of two closely related dynamin family GTPases, mitofusins (Mfn) 1 and 2. The obligatory first step leading to mitochondrial fusion is molecular tethering of two mitochondria via homo- or hetero-oligomerization (in trans) of extended Mfn1 or Mfn2 carboxyl termini. Subsequently, GTP binding to and hydrolysis by Mfn1 or Mfn2 promotes irreversible physical fusion of the organellar outer membranes. The genetic neurodegenerative condition, Charcot Marie Tooth Disease (type 2A) (CMT) or Hereditary motor and sensory neuropathy, is caused by multiple loss-of-function mutations of Mfn2. The underlying mechanism that causes this debilitating

neuropathy is impaired mitochondrial fusion. Currently, because there are no pharmacological Mfn agonists, there is no treatment for CMT.

[0242] Mfn1 and Mfn2 share a common domain structure, which was modeled using I-TASSER and structural homology with bacterial dynamin-like protein, human Mfn1 and *Arabidopsis thaliana* dynamin-related protein (see e.g., **FIG. 1**, top panel). The model shows how the first heptad repeat domain (HR1) interacts in an anti-parallel manner with the carboxyl terminal second heptad repeat (HR2) domain to restrain it and prevent its extension into the cytosol, which can be necessary for mitochondrial tethering and fusion (see e.g., **FIG. 1**, top panel). The amino acids necessary for the HR1-HR2 interaction were identified as Met376, Ser378, His380, and Met 381 by first defining a minimal HR1-derived peptide that competes with endogenous HR1-HR2 binding (see e.g., **FIG. 2A-FIG. 2B**) and followed by functional analyses of a complete series of alanine substituted peptides (see e.g., **FIG. 2C**). Based on these results, chemical peptido-mimetics could also mimic the 3-dimensional spatial and charge characteristics of these critical amino acid side chains and would have similar modulatory activity on mitochondrial fusion as the N-terminal mini-peptide (see e.g., Example 2).

EXAMPLE 2: PEPTIDO-MIMETIC COMPOUNDS INFLUENCE MFN1 AND MFN2 CONFORMATIONS

[0243] The following example describes peptide-mimetic compounds that influence conformations of Mfn1 and Mfn2.

Mfn Agonist (Fusion-Promoting) Peptido-Mimetics

[0244] Forty-four candidate compounds were screened, 2 of which (1-[2-(benzylsulfanyl)ethyl]-3-(2-methylcyclohexyl)urea, designated compound A, and 2-{2-[(5-cyclopropyl-4-phenyl-4H-1,2,4-triazol-3yl)sulfanyl] propanamido}-4H,5H,6H-cyclopenta[b]thiophene-3-carboxamide, designated compound B) induced mitochondrial elongation. Detailed analyses of compounds A and B were performed after purification by silica gel chromatography and structural validation by high performance liquid chromatography (HPLC) and mass spectroscopy (see e.g., **FIG. 3**). A cultured murine embryonic fibroblast assay system was used in which mitochondrial elongation (an increase in aspect ratio) reflects enhanced mitochondrial fusion. Mitochondrial elongation evoked by compounds A and B (see

e.g., **FIG. 4A**) was similar in cells expressing only Mfn2 (Mfn1 null) or only Mfn1 (Mfn2 null), but did not occur in the absence of both of their mitofusin targets (Mfn1/Mfn2 double null; see e.g., **FIG. 4B**).

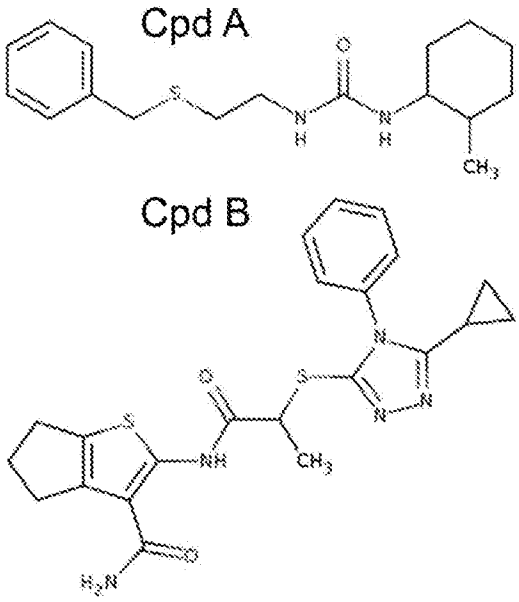

[0245] Structure-activity relationships were interrogated to expand the pool of Mfn agonist compounds and to identify chemical analogs with differing potencies for *in vitro* and *in vivo* comparative efficacy studies of CMT (see e.g., **FIG. 5**). Substitutions were evaluated for the cyclopenta[b]thiophene-3-carboxamide (green), sulfanyl-propanamido (purple), and 5-cyclopropyl-4-phenyl-4H-1,2,4-triazol-3-yl (red) moieties of Compound B. These derivatives are described in detail in TABLE 1 and TABLE 2.

TABLE 1. Mitofusin agonist peptido-mimetics

1-[2-(benzylsulfanyl)ethyl]-3-(2-methylcyclohexyl)urea	MolPort-005-680-744	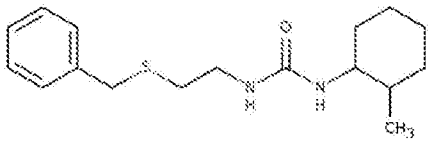
3-{2-[(5-cyclopropyl-4-phenyl-4H-1,2,4-triazol-3-yl)sulfanyl]ethyl}-1-(2-methylcyclohexyl)urea	novel	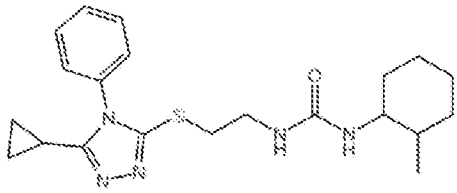
2-[(5-cyclopropyl-4-phenyl-4H-1,2,4-triazol-3-yl)sulfanyl]-N-(2-methylcyclohexyl)propanamide	novel	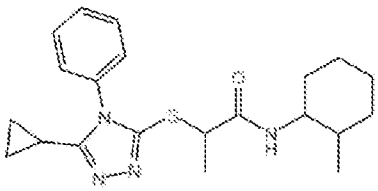
2-({[2-(benzylsulfanyl)ethyl]carbamoyl}amino)-4H,5H,6H-cyclopenta[b]thiophene-3-carboxamide	novel	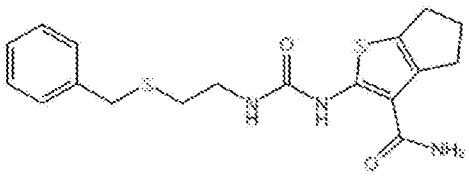
2-[2-(benzylsulfanyl)propanamido]-4H,5H,6Hcyclopenta[b]thiophene-3-carboxamide	novel	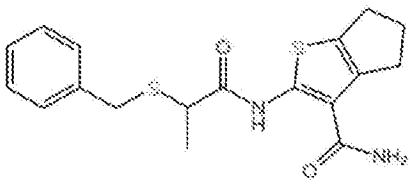

2-{2-[(5-cyclopropyl-4-phenyl-4H-1,2,4-triazol-3-yl)sulfanyl]propanamido}-4H,5H,6H-cyclopenta[b]thiophene-3-carboxamide	MolPort-004-201-234	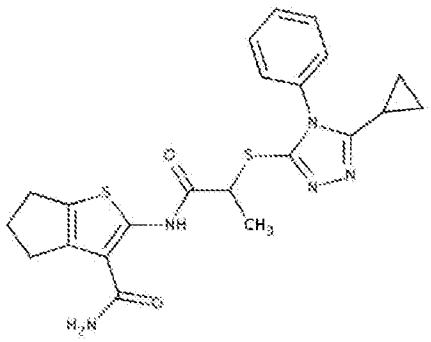
2-{2-[(5-cyclopropyl-4-phenyl-4H-1,2,4-triazol-3-yl)sulfanyl]acetamido}-4H,5H,6H-cyclopenta[b]thiophene-3-carboxamide	MolPort-004-059-486	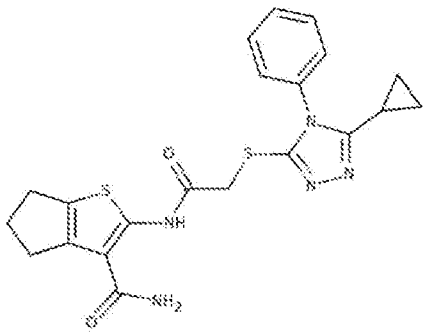
2-(2-{[4-cyclopropyl-5-(1H-indol-3-yl)-4H-1,2,4-triazol-3-yl]sulfanyl}propanamido)-4H,5H,6H-cyclopenta[b]thiophene-3-carboxamide	MolPort-004-214-844	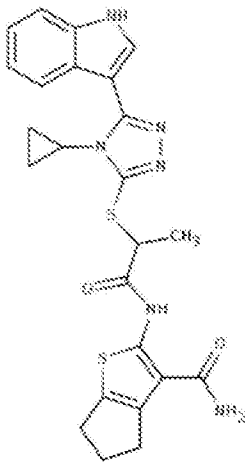

2-{2-[(diphenyl-4H-1,2,4-triazol-3-yl)sulfanyl]propanamido}-4H,5H,6H-cyclopenta[b]thiophene-3-carboxamide	MolPort-005-522-531	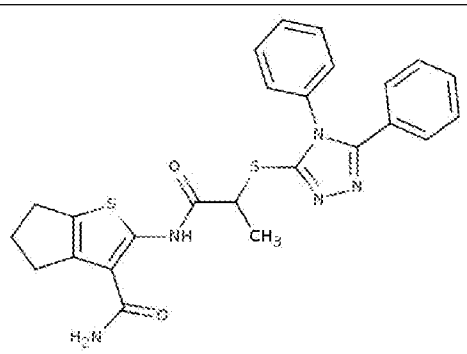
N-(4-chlorophenyl)-2-{2-[(5-cyclopropyl-4H-1,2,4-triazol-3-yl)sulfanyl]acetamido}-4,5,6,7-tetrahydro-1-benzothiophene-3-carboxamide	MolPort-005-784-050	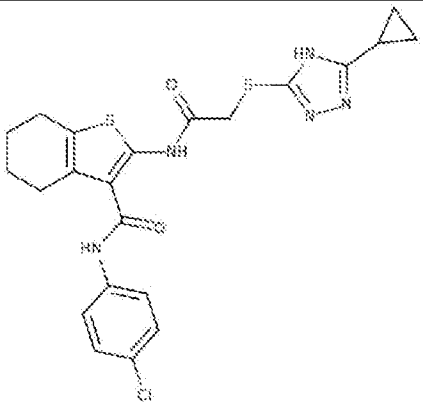
N-benzyl-2-{2-[(5-cyclopropyl-4-ethyl-4H-1,2,4-triazol-3-yl)sulfanyl]acetamido}-4,5,6,7-tetrahydro-1-benzothiophene-3-carboxamide	MolPort-005-803-773	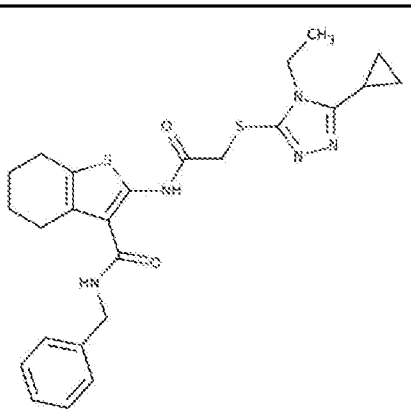
2-{2-[(5-cyclopropyl-4-ethyl-4H-1,2,4-triazol-3-yl)sulfanyl]acetamido}-4H,5H,6H-cyclopenta[b]thiophene-3-carboxamide	MolPort-009-869-122	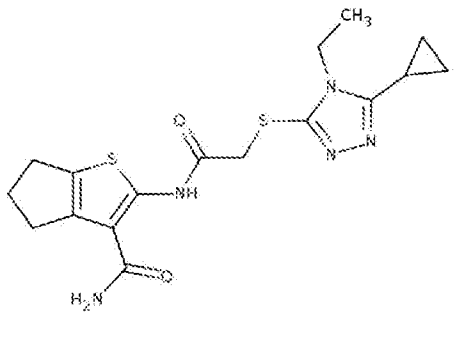

N-benzyl-2-[2-({4-methyl-5-[(phenylcarbamoyl)methyl]-4H-1,2,4-triazol-3-yl}sulfanyl)acetamido]-4,5,6,7-tetrahydro-1-benzothiophene-3-carboxamide	MolPort-002-272-952	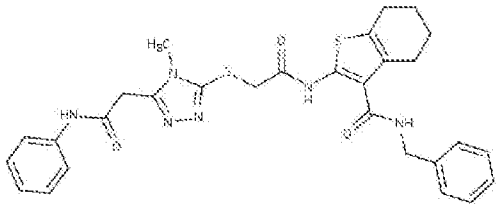
2-{[(3aS,6aS)-5-{5,7-dimethylpyrazolo[1,5-a]pyrimidine-2-carbonyl}-octahydropyrrolo[3,4-b]pyrrol-1-yl]methyl}-1-methyl-1H-imidazole	MolPort-023-329-196	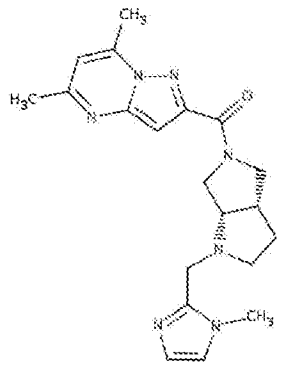

TABLE 2 (continuation of TABLE 1). Mitofusin agonist lower potency compounds

2-{2-[(4-benzyl-5-cyclopropyl-4H-1,2,4-triazol-3-yl)sulfanyl]propanamido}-4H,5H,6H-cyclopenta[b]thiophene-3-carboxamide	MolPort-004-201-235	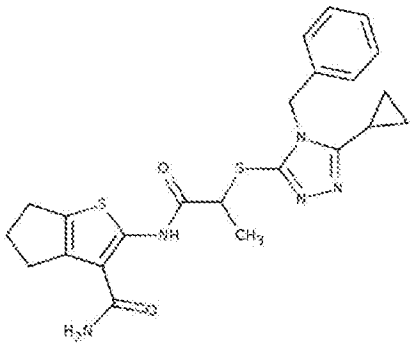
2-{2-[(4-phenyl-4H-1,2,4-triazol-3-yl)sulfanyl]propanamido}-4H,5H,6H-cyclopenta[b]thiophene-3-carboxamide	MolPort-005-522-674	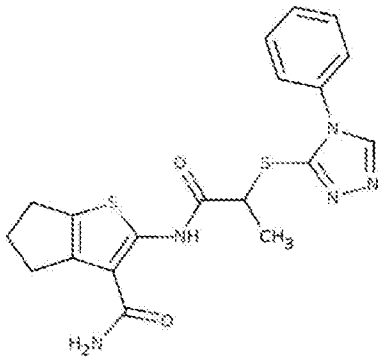

[0246] EC50 values for mitochondrial elongation by compounds A and B were 100-200 nM, which is comparable to the prototype mini-peptide (Franco et al 2016 Nature 540: 74-79). When added in equal amounts, compounds A and B synergistically promoted mitochondrial elongation, with a combined EC50 of ~40 nM and a ~25% greater maximal increase in mitochondrial aspect ratio ($P<0.05$ vs each compound alone; see e.g., **FIG. 6A**).

[0247] The mechanism for compound synergy was determined to be preferential binding of A and B to different phosphorylated forms of Mfn1 and Mfn2 (see e.g., **FIG. 6B, FIG. 6C**): When Ser378 is replaced by non-phosphorylatable alanine (A), cysteine (C), asparagine (N), or glycine (G) mini-peptide activity is abrogated because alternate salt-bridge formation provokes α-helix destabilization of replacement of His380 by Leu379 and the HR1-HR2 interface (see e.g., **FIG. 6D**). Because compound B is hydrophobic (phenyl) at one end and polar (carboxamide) at the other it mimics side chains presented by Val372/Met376/His381 (see e.g., **FIG. 1**, top panel). By contrast, compound A is hydrophobic (phenyl and cyclohexyl) at both ends, which mimics the side chains presented to the Mfn2 hydrophobic core after the conformational shift to Val372/Met376/Leu379.

[0248] Partial unwinding of the HR1 alpha helix and shifting of Met 380 for His381 at the HR1-HR2 interacting interface is controlled by the phosphorylation status of Ser378 (see e.g., **FIG. 6B**). Thus, synergistic effects of compounds A and B are likely the consequence of their preferential binding to different phosphorylated forms of Mfn1 and Mfn2.

[0249] The efficacy and synergy of the prototype Mfn agonist peptido-mimetics (small molecule mitochondrial fusion activators) were enhanced and their specificity modified by engineering novel chimeric compounds combining optimal features of the parental molecules (see e.g., **FIG. 7**, TABLE 1, TABLE 2). The ability of these compounds to repair mitochondrial fragmentation and neuronal pathology conditionally expressing a human Charcot Marie Tooth disease mutation, Mfn2 T105M, was demonstrated (see e.g., **FIG. 8, FIG. 9).**

EXAMPLE 3: HR1-HR2 COMPETITION BINDING ASSAY FOR SCREENING AND EVALUATING MFN PEPTIDO-MIMETIC TARGETING AND BINDING AFFINITY

[0250] The following example describes a HR1-HR2 competition binding assay for screening and evaluating Mfn peptido-mimetic targeting and binding affinity.

[0251] The Mfn-derived fusion-promoting and -inhibiting mini-peptides (simulated to obtain the chemical Mfn agonists in TABLE 1 and TABLE 2) were modified from amino acid heptad repeats (HR) in the HR1 domain and predicted to interact with their counterparts in the carboxyl terminus HR2 domain within the Mfn stalk region (see e.g., **FIG. 1,** top panel). A high-throughput binding assay was designed whereby the target HR2 peptide sequences, modified to include amino terminal 6 x His tags and Gly linkers, were bonded to Ni-chelate resin (20 µg/ml) and used as immobilized "receptor" for amino-FITC-tagged Mfn2 374-384 (agonist ligand) in which the Ser analogous to Ser378 was replaced with Asp to confer the negative charge essential for activity. For antagonist studies the ligand was amino-FITC-tagged Mfn2 406-418. The FITC peptide ligands are suspended at 1 mM in 30% DMSO, 70% water (to minimize spontaneous aggregation) and diluted into binding buffer (de-ionized water) to a final concentration of 25 µM in the presence or absence of competing compound. Dose-dependent loss of resin-bound FITC signal (485 nm excitation/ 538 nm emission) measured in a 96 well spectrofluorometer represents binding of compound to its HR2 target (see e.g., **FIG. 10, FIG. 11**). Either the ligand peptide or the receptor peptide can be modified to represent mutations, variations, or posttranslational modifications of Mfn2. Target peptide-bound resin pre-incubated with FITC ligand in column form can be used for high throughput screening by monitoring FITC in the eluate.

[0252] Amino acid sequences for Mfn agonist peptido-mimetic binding assay components:

SEQ ID NO: 1: (NH3) HHHHHH-GGGG-AAMNKKIEVLDSLQSKAKLLRNKA-GG (COOH) (receptor)

SEQ ID NO: 2: (NH3) FITC-GGGG-AVRGIMDDLHMAAR-GG (COOH) (amino FITC labeled ligand)

Amino acid sequences for Mfn antagonist peptido-mimetic binding assay:

SEQ ID NO: 3: (NH3) HHHHHH-GGGG-LHAFTGSLEQQVQHSCNSG-GG

(COOH) (receptor)

SEQ ID NO: 4: (NH3) FITC-GGGG-KQLELLAQDYKLRIKQ-GG (COOH) (amino FITC labeled ligand)

[0253] The system can be modified to contain the respective Mfn1 sequences if specific interrogation of both Mfn isoforms is desired.

EXAMPLE 4: A FRET ASSAY FOR SCREENING AND EVALUATING MFN PEPTIDO-MIMETIC EFFECTS ON MFN CONFORMATION

[0254] The following examples describe a FRET assay for screening and evaluating Mfn peptido-mimetic effects on Mfn conformation.

[0255] The small molecules described herein enhance mitochondrial fusion by destabilizing the folded conformation of Mfn1 or Mfn2, thus promoting extension of HR2 carboxyl termini that mediate mitochondrial tethering by interacting in trans with similarly extended carboxyl termini of Mfn1 or Mfn2 on neighboring mitochondria (see e.g., **FIG. 12A**). The Forster resonance energy transfer (FRET) assay was designed to screen for and evaluate candidate agents of any chemical class, or molecules with specific alternate compositions, including large libraries of synthetic or natural compounds.

[0256] The mechanism by which Mfn2 HR1 mini-peptides regulate Mfn1 and Mfn2 activity is by directing Mfns into either an unfolded active or folded inactive conformation, as demonstrated by a change in FRET signal of Mfn2 labeled with amino-terminal mCerulean and carboxyl terminal mVenus. This FRET system was limited by low transfection efficiency as a plasmid, an unacceptably poor signal to noise ratio, and the confounding influences of Mfn GTPase activity.

[0257] These problems were solved by re-engineering the Mfn2 FRET probe after deleting the GTPase domain (Δ80-275) (which is dispensable to Mfn folding/unfolding) and cloning it into an adenoviral vector for high efficiency expression. Briefly, mCerulean1 and mVenus were cloned onto the 5' and 3' ends of a hMfn2 cDNA from which the entire GTPase domain (amino acids 80-275) was deleted (see e.g., **FIG. 12C**, top). Removal of the GTPase domain eliminates the need for adding GTPase inhibitors such as GTPγS in the assay and increases the FRET signal to noise ratio. The sequence-confirmed construct was sub-cloned into an adenoviral vector for expression in murine embryonic fibroblasts having different

mitofusin expression profiles (wild-type, Mfn1 null, Mfn2 null, Mfn1/Mfn2 double null) or other cell types. Forty-eight hours after adenoviral transduction cells were pre-treated with the anti-fusion mini-peptide MP2 to increase FRET (1 μM, 1 hour; see e.g., **FIG. 12C**). Cells were then exposed to screening compound(s) for 1 hour in a 96 well format fluorescence plate reader or on the stage of a confocal microscope. FRET was analyzed as follows: mCerulean was excited at 436 nm with emission at 480 nm. mVenus was excited at 500 nm with emission at 535 nm. FRET was imaged with excitation at 436 nm and emission at 535 nm. Data are represented as FRET signal/ mCerulean signal. Increased FRET reflects folded Mfn2; loss of FRET reflects Mfn2 unfolding that favors mitochondrial tethering and fusion.

[0258] The adeno-Mfn2 FRET Δ80-275 is expressed at near 100% efficiency at 50 MOI in cultured murine embryonic fibroblasts (the cell of choice for functional screening of Mfn activity), and exhibits 5-fold greater signal/noise that the original Mfn2 FRET probe. This system is useful in 96 or 384 well formats for high-throughput screening of Mfn agonists (extinguishing of HR1 398-418 induced FRET) and antagonists (stimulation of baseline FRET or reversal of HR1 374-384 FRET suppression; see e.g., **FIG. 12**).

EXAMPLE 5: RATIONALLY DESIGNED MITOFUSIN AGONISTS REVERSE IN VITRO AND IN VIVO CMT2A MITOCHONDRIAL DEFECTS

[0259] This example describes the reversal mitochondrial defects in preclinical models of Charcot Marie Tooth disease type 2A with MFN2 agonists and that pharmacological disruption of intramolecular restraints in MFN2 promotes mitochondrial fusion and trafficking in CMT2A neurons.

[0260] Mitofusins (MFNs) promote fusion-mediated mitochondrial content exchange and subcellular trafficking. Mutations in *MFN2* cause neurodegenerative Charcot Marie Tooth Disease type 2A (CMT2A). Here, it has been shown that MFN2 activity is determined by Met^{376} and His^{380} interactions with Asp^{725} and Leu^{727} and controlled by PINK1 kinase-mediated phosphorylation of adjacent MFN2 Ser^{378}.

[0261] Also shown here is that small molecule mimics of the peptide-peptide interface of MFN2 disrupted this interaction, allosterically activating MFN2 and promoting mitochondrial fusion. These first-in-class mitofusin agonists overcame dominant mitochondrial defects provoked in cultured neurons by CMT2A mutants

MFN2 Arg^{94}→Gln^{94} and Thr^{105}→Met^{105}, as demonstrated by amelioration of mitochondrial dysmotility, fragmentation, depolarization, and clumping. A mitofusin agonist normalized axonal mitochondrial trafficking within sciatic nerves of MFN2 Thr^{105}→Met^{105} mice, promising a therapeutic approach for CMT2A and other untreatable diseases of impaired neuronal mitochondrial dynamism and/or trafficking.

[0262] Mitochondria are organelles that generate a rich energy source for cells, which require their continuous subcellular redistribution via mitochondrial trafficking and mutual repair via mitochondrial fusion. Mitochondrial fusion and subcellular trafficking are mediated in part by mitofusin 1 (MFN1) and MFN2. Genetic mutations in *MFN2* that suppress mitochondrial fusion and motility cause Charcot Marie Tooth Disease 2A (CMT2A), the most common heritable axonal neuropathy. Because no therapeutics exist that directly enhance mitochondrial fusion or trafficking, this disease is unrelenting and irreversible.

[0263] Computational modeling based on the closed structure of bacterial dynamin–related protein (BDRP) and the more open structure of optic atrophy-1 suggested that MFN2 can change conformation according to how closely the first and second heptad repeat (HR) domains interact (see e.g., **FIG. 1**). A closed conformation is fusion incompetent, whereas an open conformation favoring mitochondrial fusion can be induced by a competing peptide analogous to amino acids 367 to 384 within the MFN2 HR1 domain. Amino acids controlling these events were identified, first by truncation analysis to define the smallest fusion promoting minipeptide (residues 374 to 384) (see e.g., **FIG. 2A-FIG. 2B**), and then through functional investigation of this minimal peptide by alanine (Ala) scanning. Substitution of Ala for Met^{376}, Ser^{378}, His^{380}, and Met^{381} which are highly conserved across vertebrate species (see e.g., **FIG. 13, FIG. 14**) impaired minipeptide-stimulated mitochondrial fusion, as measured by an increase in the mitochondrial length/width (aspect ratio) (see e.g., **FIG. 2C**). The structural model of human MFN2 in a closed conformation on the basis of homology with BDRP predicted a helical interaction between HR1 and HR2 domains, with alignment of Met^{376} and His^{380} side chains in the HR1 domain with Leu^{727} and Asp725 in the HR2 domain (see e.g., **FIG. 1**). This arrangement suggested that Met^{376} and His^{380} stabilize the MFN2 HR1-HR2 interaction, potentially explaining their critical function as defined by minipeptide Ala

scanning. By contrast, Ser^{378} was modeled as extending from the noninteracting surface of the HR1 α helix (see e.g., **FIG. 1**), implying a different mechanism for its involvement in mitochondrial fusion.

[0264] To address whether Ser^{378} might be phosphorylated, Ser^{378} was substituted (with Ala, Cys, Asn or Gly) in the mini-peptide and it was found that phosphorylation and fusion activity were abrogated. Functionality was restored by substituting Asp to mimic phosphorylated Ser, or by inserting phospho-Ser [(p)Ser] itself (see e.g., **FIG. 2D, FIG. 15**). Moreover, in an *in vitro* binding assay devoid of cellular kinases the Asp^{378}-substituted minipeptide bound to its putative HR2 interacting domain, whereas Ser^{378} and Ala^{378} minipeptides did not (see e.g., **FIG. 2E**). Elimination of minipeptide binding by replacement of HR2 Leu^{724}, Asp^{725}, and Leu^{727} with Ala confirmed the HR1-HR2 interaction model (see e.g., **FIG. 2F**).

[0265] Nuclear magnetic resonance spectrometry of the minipeptides showed low conformational stability with a propensity to form helical structures. Ser^{378} phosphorylation reduced the peptide dynamics most visibly for residues Leu^{379} to Met^{381}, potentially changing amino acid side chains presented to HR2 (see e.g., **FIG. 16, FIG. 17**). Indeed, recombinant MFN2 mutations that replaced Ser^{378} with Asp (mimicking MFN2 Ser^{378} phosphorylation) or substituted Ala for Met^{376} or His^{380} (disrupting the putative HR1-HR2 interaction controlled by Ser^{378} phosphorylation) impaired MFN2-stimulated mitochondrial fusion (see e.g., **FIG. 18**). By contrast, replacing MFN2 Ser^{378} with Ala (to prevent its phosphorylation), or substitution Ala for neighboring Val^{372}, which was not important for HR1-HR2 interactions, did not depress MFN2-mediated fusion (see e.g., **FIG. 18**).

[0266] MFN2 can be phosphorylated by mitochondrial PTEN-induced putative kinase 1 (PINK1). Targeted mass spectrometry demonstrated phosphorylation of MFN2 Ser^{378} as well as MFN2 Thr^{111} and Ser^{442} by PINK1 kinase (see e.g., **FIG. 2G; FIG. 19** and **FIG. 20**; TABLE 3), but not by software-nominated G-protein receptor kinase 2 (see e.g., **FIG. 21**). MFN2 Ser^{378} mutants were expressed with or without PINK1 in MFN1 and MFN2 doubly deficient ($MFN1^{-/-}$, $MFN2^{-/-}$) cells. Fusion-defective mitochondria in these cells were abnormally short at baseline, but forced expression of wild-type (Ser^{378}) MFN2 resulted in elongation from restoration of fusion (see e.g., **FIG. 2H, FIG. 22**). Co-expression of PINK1 with MFN2, or mutational replacement of MFN2 Ser^{378} with Asp (which mimics PINK1-

mediated Ser^{378} phosphorylation) restrained MFN2-stimulated elongation (see e.g., **FIG. 2H, FIG. 22**). By contrast, MFN2 Ala^{378} (which cannot be phosphorylated) promoted mitochondrial fusion resistant to PINK1 suppression (see e.g., **FIG. 2H**, **FIG. 22**). The effects of MFN2 Ser^{378} mutants were recapitulated in assays of fusion-mediated mitochondrial content exchange (see e.g., **FIG. 23**).

TABLE 3. Fragmentation ions from tandem MS of MFN phosphopeptides.

LIMDsLHMAAR[1] (*m/z*=446.543)

ion	*m/z* (Theoretical)	m/z (Observed)	ppm
y_1	**175.119**	**175.120**	**3.7**
y_3	**317.193**	**317.194**	**1.4**
y_4	**448.234**	**448.230**	**-9.0**
y_5	**585.293**	**585.290**	**-3.6**
y_6	**698.377**	**698.380**	**5.0**
y_7-$H_3PO_4^{+2}$	**384.203^{+2}**	**384.203**	**0.7**
y_8-H_3PO_4	**882.425**	**882.427**	**2.3**

LIMDsLHMAAR-[$^{13}C_6$][$^{15}N_4$] (*m/z*=449.880)

ion	*m/z* (Theoretical)	*m/z* (Observed)	ppm
y_1	**185.127**	**185.127**	**0.2**
y_2	**256.164**	**256.163**	**-4.3**
y_3	**327.201**	**327.200**	**-3.1**
y_4	**458.242**	**458.242**	**-0.7**
y_5	**595.301**	**595.300**	**-1.0**
y_6	**708.385**	**708.382**	**-4.6**
y_7-H_3PO_4	**777.406**	**777.404**	**-3.7**
y_8-H_3PO_4	**892.433**	**892.431**	**-2.1**
y_9-H_3PO_4	**1023.474**	**1023.472**	**-1.7**
y_{10}-H_3PO_4	**1136.558**	**1136.549**	**-8.0**

[1] The lower case single amino acid abbreviation indicates the phosphorylated residue.

Identification and *de novo* design of small molecule mitofusin agonists

[0267] A pharmacophore model was generated based on the interactions of HR1 and HR2 domains in the calculated structural model of Mfn2 in the closed conformation. The key features included hydrophobic interactions involving Mfn2

HR1: Val372 and Met376, and aromatic interactions and hydrogen bonding involving Mfn2 HR1 His380. Although the pharmacophore model did not structurally model mitofusin agonist minipeptide HR1 (367-384), it was noted that peptide residues Val6, Met10, and His14 correspond to Mfn2 HR1: Val372, Met376 and His380. A library comprising ~14 million commercially available compounds was prepared *in silico* and evaluated using PHASE to fit these criteria. Top ranked hits were clustered, and filtered based on pharmacological properties using Qikprop. The top 55 (see TABLE 4) commercially available small molecules conforming to the model were selected for functional screening and purchased in 1 mg aliquots. Each compound was dissolved to a stock concentration of 10 mM in DMSO and applied to Mfn2 null MEFs overnight at a final concentration of 1 mM. Eleven of the library members were not soluble in DMSO at the required concentration. The 44 fully soluble compounds were screened in groups of 6 at a time for cytotoxicity (calcein AM/ethidium homodimer staining; ThermoFisher LIVE/DEAD Assay cat #L3224) and fusogenicity (increase in mitochondrial aspect ratio; MitoTracker Orange staining) compared to cells treated overnight with 5 mM of the parent HR1 367-384 mitofusin agonist peptide (positive control) or vehicle (DMSO). Images were acquired by confocal microscopy. Each compound was scored for fusogenicity (see e.g., **FIG. 24A**) and % cell death (see e.g., **FIG. 24B**). Pharmacophore model fit generally correlated with actual fusogenic activity (Pearson correlation coefficient r=0.214; see e.g., **FIG. 24A**, *inset*; TABLE 4).

TABLE 4. Fusogenicity screening results and characteristics of 55 candidate mitofusin agonists (commercially sourced). *Treatment with 1 μM compound.

Goodness of fit Rank	IUPAC Name	Structure	Aspect ratio (MEAN ± SEM)*	Fusogenicity Rank
1	2-{[(3aS,6aS)-5-{5,7-dimethylpyrazolo[1,5-a]pyrimidine-2-carbonyl}-octahydropyrrolo[3,4-b]pyrrol-1-yl]methyl}-1-methyl-1H-imidazole	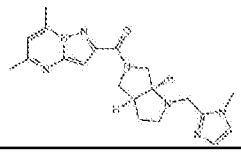	9.0 ± 3.1	1
2	3-{[2-(1H-1,3-benzodiazol-2-yl)ethyl]sulfanyl}-1-(3-fluorophenyl)pyrrolidine-2,5-dione	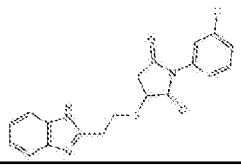	6.9 ± 0.8	3
3	2-[({3-[5-methyl-2-(propan-2-yl)phenoxy]propyl}sulfanyl)methyl]-1H-1,3-benzodiazole	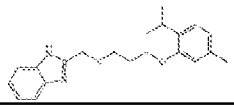	3.0 ± 0.4	37
4	2-[(4-methoxyphenyl)sulfanyl]-N-(1H-pyrazol-3-yl)propanamide	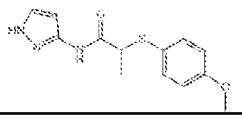	3.8 ± 0.4	22
5	1-[1-(4-chlorophenyl)-1H,2H,3H,4H,9H-pyrido[3,4-b]indol-2-yl]-2-{[(4-fluorophenyl)methyl]sulfanyl}ethan-1-one	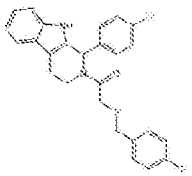	4.7 ± 0.9	11
6	ethyl 4-methyl-2-(2-{5H-[1,2,4]triazino[5,6-b]indol-3-ylsulfanyl}butanamido)-1,3-thiazole-5-carboxylate	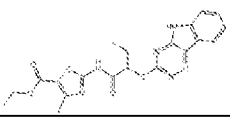	4.5 ± 0.5	13

7	2-({[4-oxo-6-(propan-2-yl)-3H,4H,4aH,7aH-thieno[2,3-d]pyrimidin-2-yl]methyl}sulfanyl)-N-[(pyridin-2-yl)methyl]acetamide	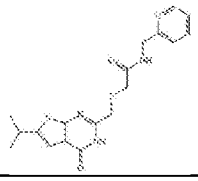	3.8 ± 0.6	21
8	N-(3,4-dichlorophenyl)-2-{[2-(pyridin-2-yl)ethyl]sulfanyl}acetamide	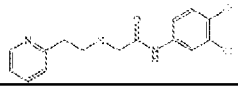	2.8 ± 0.1	41
9	2-methyl-6-(2-{[(4-methyl-1H-imidazol-5-yl)methyl]sulfanyl}ethyl)-2H,6H,7H-pyrazolo[4,3-d]pyrimidin-7-one	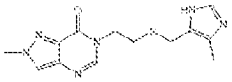	2.8 ± 0.2	42
10	3-acetamido-N-(2-{[(4-methylphenyl)methyl]sulfanyl}ethyl)adamantane-1-carboxamide	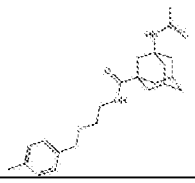	Not obtained	Insoluble
11	N-(2-{[(2-cyanophenyl)methyl]sulfanyl}ethyl)-2-{methyl[1-(3-nitrophenyl)ethyl]amino}acetamide	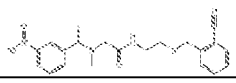	4.0 ± 0.5	16
12	N-(2,6-dimethylphenyl)-4-({[3-(3-fluoro-4-methylphenyl)-1,2,4-oxadiazol-5-yl]methyl}sulfanyl)butanamide	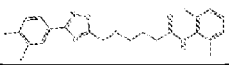	3.9 ± 0.5	20
13	5-methoxy-3'-(2-methylbenzoyl)-1-{[3-(trifluoromethyl)phenyl]methyl}-1,2-dihydrospiro[indole-3,2'-[1,3]thiazolidine]-2-one	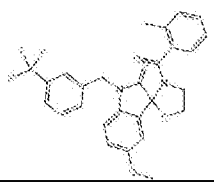	3.5 ± 0.6	26

14	N-(2,6-dimethylphenyl)-4-({[5-(propan-2-yl)-1,3-oxazol-2-yl]methyl}sulfanyl)butanamide	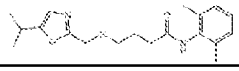	3.5 ± 0.1	25
15	6-methyl-N-{[6-(4-methyl-1,4-diazepan-1-yl)pyridin-3-yl]methyl}-2,3-dihydro-1-benzothiophene-2-carboxamide	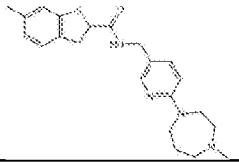	4.0 ± 0.3	18
16	N-(2-{[(5-bromothiophen-2-yl)methyl]sulfanyl}ethyl)-1-(thiophene-2-carbonyl)piperidine-3-carboxamide	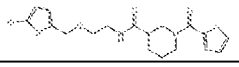	5.1 ± 0.2	9
17	3-{[1-(3,4-dimethylphenyl)-1-oxopropan-2-yl]sulfanyl}-7-phenyl-7H,8H-[1,2,4]triazolo[4,3-a]pyrazin-8-one	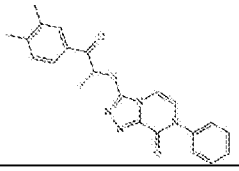	Not obtained	Insoluble
18	1-(4-methylphenyl)-5-({1-[3-(4H-1,2,4-triazol-3-yl)-1,2,4-oxadiazol-5-yl]ethyl}sulfanyl)-1H-1,2,3,4-tetrazole	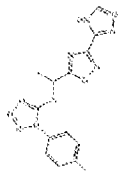	3.4 ± 0.3	27
19	5-methyl-N-{3-[(5-methyl-1,3,4-thiadiazol-2-yl)sulfanyl]propyl}-1H,4H,5H,6H,7H-pyrazolo[4,3-c]pyridine-3-carboxamide	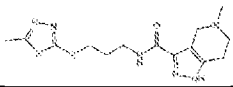	3.1 ± 0.3	34
20	7-(4-bromophenyl)-3-{[1-(3,4-dimethylphenyl)-1-oxopropan-2-yl]sulfanyl}-7H,8H-[1,2,4]triazolo[4,3-a]pyrazin-8-one	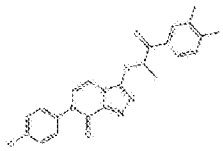	Not obtained	Insoluble

21	N-[2-(benzylsulfanyl)ethyl]oxane-2-carboxamide	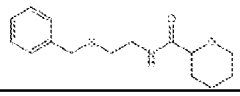	3.3 ± 0.4	30
22	N-(2-{[(4-methylphenyl)methyl]sulfanyl}ethyl)-1-[3-(trifluoromethyl)-[1,2,4]triazolo[4,3-b]pyridazin-6-yl]piperidine-4-carboxamide	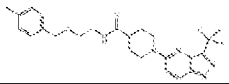	Not obtained	Insoluble
23	1-cyclobutanecarbonyl-N-(2-{[(4-methyl-1H-imidazol-5-yl)methyl]sulfanyl}ethyl)piperidine-4-carboxamide	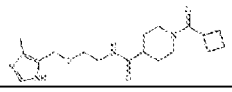	2.9 ± 0.5	40
24	2-{[(2-{bicyclo[4.1.0]heptane-7-amido}pyridin-4-yl)methyl]sulfanyl}ethyl bicyclo[4.1.0]heptane-7-carboxylate	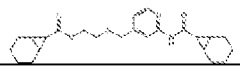	4.8 ± 1.0	10
25	N-(2-{[(3-chlorophenyl)methyl]sulfanyl}ethyl)-5H,6H,7H,8H,9H-[1,2,3,4]tetrazolo[1,5-a]azepine-9-carboxamide	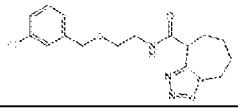	2.9 ± 0.2	38
26	2-{[4-benzyl-5-(morpholin-4-yl)-4H-1,2,4-triazol-3-yl]sulfanyl}-N-(2-oxo-2,3-dihydro-1H-1,3-benzodiazol-5-yl)propanamide	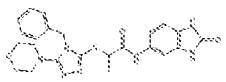	5.2 ± 0.2	8
27	1-[2-(benzylsulfanyl)ethyl]-3-(2-methylcyclohexyl)urea	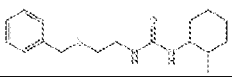	6.8 ± 0.6	4

28	1-{bicyclo[2.2.1]heptan-2-yl}-3-(2-{[(furan-2-yl)methyl]sulfanyl}ethyl)thiourea	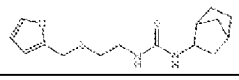	3.7 ± 0.9	23
29	2-{[4-benzyl-5-(morpholin-4-yl)-4H-1,2,4-triazol-3-yl]sulfanyl}-N-(2,3-dihydro-1,4-benzodioxin-6-yl)propanamide	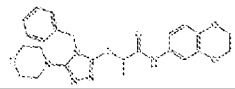	6.0 ± 0.1	6
30	2-({2-[(morpholin-4-yl)methyl]quinazolin-4-yl}sulfanyl)-N-[3-(trifluoromethyl)phenyl]propanamide	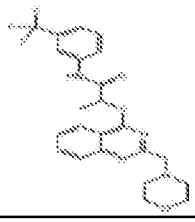	5.6 ± 0.6	7
31	2-{2-[(5-cyclopropyl-4-phenyl-4H-1,2,4-triazol-3-yl)sulfanyl]propanamido}-4H,5H,6H-cyclopenta[b]thiophene-3-carboxamide	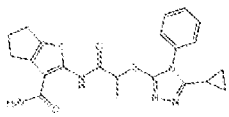	8.3 ± 2.3	2
32	2-{[4-(4-methylphenyl)-5-(morpholin-4-yl)-4H-1,2,4-triazol-3-yl]sulfanyl}-N-[1-(propan-2-yl)-1H-pyrazol-5-yl]propanamide	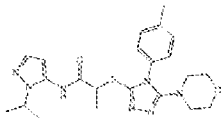	4.1 ± 0.9	15
33	N-[4-(3,4-dihydro-2H-1,5-benzodioxepine-7-sulfonamido)phenyl]-2-[(4-methylphenyl)sulfanyl]propanamide	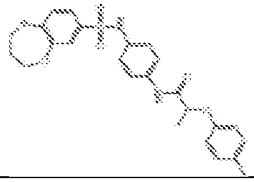	Not obtained	Insoluble
34	5-methyl-2-{[1-(3-propyl-1,2,4-oxadiazol-5-yl)ethyl]sulfanyl}-1H-1,3-benzodiazole	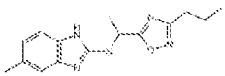	4.0 ± 1.0	17

35	(1S,4S)-2-(4-chloro-2-methoxy-5-methylphenyl)-5-{[1-(pyrimidin-2-yl)-1H-pyrrol-2-yl]methyl}-2,5-diazabicyclo[2.2.1]heptan-3-one	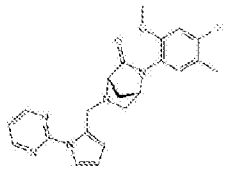	Not obtained	Insoluble
36	1-(7-{3-[(4,6-dimethylpyrimidin-2-yl)sulfanyl]-2-methylpropyl}-3-methyl-2,6-dioxo-2,3,6,7-tetrahydro-1H-purin-8-yl)piperidine-4-carboxamide	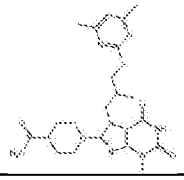	Not obtained	Insoluble
37	2-{[2-(butan-2-yl)-3-oxo-2H,3H-imidazo[1,2-c]quinazolin-5-yl]sulfanyl}-N-(3,5-dimethoxyphenyl)propanamide	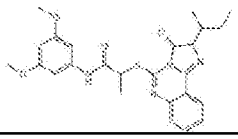	3.2 ± 0.3	32
38	N-(5-methyl-1,2-oxazol-3-yl)-2-{[({4-[(1-phenylethyl)amino]phenyl}carbamoyl)methyl]sulfanyl}propanamide	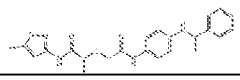	Not obtained	Insoluble
39	N-(butan-2-yl)-2-{2-[(4-methylphenyl)sulfanyl]propanamido}benzamide	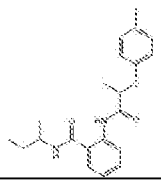	3.3 ± 0.4	29
40	N-ethyl-2-({12-ethyl-5-oxa-1,10,11-triazatricyclo[6.4.0.0^{2,6}]dodeca-2(6),3,7,9,11-pentaen-9-yl}sulfanyl)-N-(3-methylphenyl)butanamide	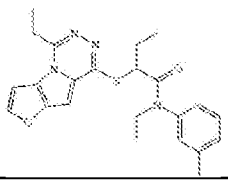	Not obtained	Insoluble
41	5-[2-(benzylsulfanyl)ethyl]-3-(oxolan-3-yl)-1,2,4-oxadiazole	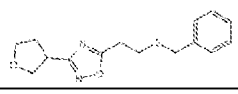	3.4 ± 0.6	28

42	2-[(4-bromophenyl)sulfanyl]-N-(2,3-dihydro-1,4-benzodioxin-6-yl)propanamide	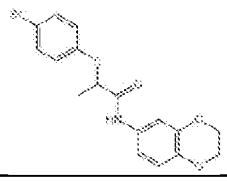	3.2 ± 0.5	33
43	7-(3,4-dimethylphenyl)-3-{[1-(3,4-dimethylphenyl)-1-oxopropan-2-yl]sulfanyl}-7H,8H-[1,2,4]triazolo[4,3-a]pyrazin-8-one	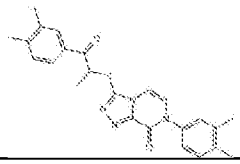	3.9 ± 0.8	19
44	9-oxo-N-(2-{[(thiophen-3-yl)methyl]sulfanyl}ethyl)bicyclo[3.3.1]nonane-3-carboxamide	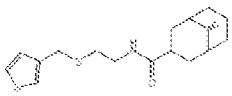	4.4 ± 0.6	14
45	N-(2H-1,3-benzodioxol-5-yl)-2-{[4-benzyl-5-(morpholin-4-yl)-4H-1,2,4-triazol-3-yl]sulfanyl}propanamide	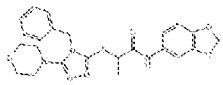	2.5 ± 0.6	43
46	N-(cyclohexylmethyl)-2-({2,8-dicyclopropyl-5,7-dioxo-5H,6H,7H,8H-pyrimido[4,5-d][1,3]diazin-4-yl}sulfanyl)propanamide	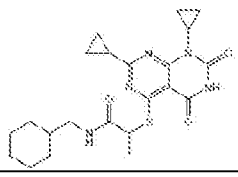	Not obtained	Insoluble
47	N-{[4-(dimethylamino)phenyl]methyl}-2-({[(3-methylphenyl)carbamoyl]methyl}sulfanyl)-N-(propan-2-yl)acetamide	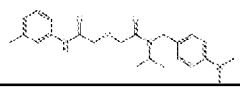	4.6 ± 0.2	12
48	(1S,5R)-3-(6-methylpyridazin-3-yl)-6-[(pyridin-2-yl)methyl]-3,6-diazabicyclo[3.2.2]nonan-7-one		3.0 ± 0.4	36

49	4-[(4-methylphenyl)sulfanyl]-1-({4H,5H,6H,7H-pyrazolo[1,5-a]pyrazin-2-yl}methyl)piperidine	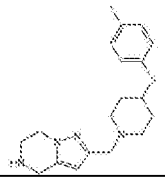	2.9 ± 0.2	39
50	3-(2,5-dioxo-3-{[(E)-N-[(1-phenylethyl)imino]carbamimidoyl]sulfanyl}pyrrolidin-1-yl)benzoic acid	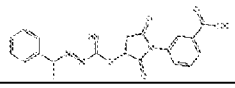	3.3 ± 0.0	31
51	2-{[(7,8-dimethyl-4-oxo-1,4-dihydroquinolin-2-yl)methyl]sulfanyl}-N-(2-ethoxyphenyl)acetamide	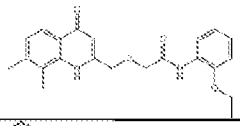	3.7 ± 0.6	24
52	2-{[2-oxo-2-(1,2,3,4-tetrahydroquinolin-1-yl)ethyl]sulfanyl}-N-phenylacetamide		2.4 ± 0.4	44
53	2-[(tert-butylcarbamoyl)amino]-2-oxoethyl 2-[({4-oxo-5-phenyl-3H,4H-thieno[2,3-d]pyrimidin-2-yl}methyl)sulfanyl]acetate	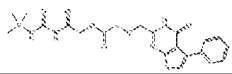	6.5 ± 0.4	5
54	2-({2-[2-(3,5-dimethyl-1H-pyrazol-1-yl)ethyl]-8,9-dimethoxy-[1,2,4]triazolo[1,5-c]quinazolin-5-yl}sulfanyl)-N-(4-fluorophenyl)butanamide	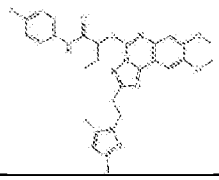	Not obtained	Insoluble
55	N-(2,4-dimethylphenyl)-2-(2-{[(6-hydroxy-2,4-dioxo-1,2,3,4-tetrahydropyrimidin-5-yl)[4-(propan-2-yl)phenyl]methyl]amino}-4-oxo-4,5-dihydro-1,3-thiazol-5-yl)acetamide	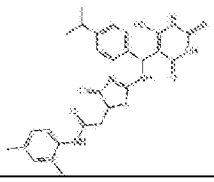	3.1 ± 0.3	35

[0268] Of nine compounds exhibiting apparent fusogenic activity on the initial screen (defined as an increase in mitochondrial aspect ratio to >5 after 24h exposure to 1 mM compound), one (A8) was mildly cytotoxic and therefore did not undergo further evaluation. The remaining eight candidate fusogenic compounds were evaluated in a second series of experiments for their ability to provoke dose-dependent mitochondrial elongation. Fusogenicity of six compounds was confirmed, with EC_{50} values between ~25 nM and 150 nM (see e.g., **FIG. 25**, TABLE 4). Two compounds (D9 and A9) failed validation in the secondary screen.

[0269] The present results defining a minimal fusogenic HR1 peptide (see e.g., **FIG. 2B**), identifying function-critical amino acids within the minipeptide (see e.g., **FIG. 2C**), and defining HR1-HR2 interacting amino acids through binding assays (see e.g., **FIG. 2E** and **FIG. 2F**) suggested that the Mfn2 HR1-HR2 interaction model (see e.g., Example 1) was imperfect, thus providing a likely reason for the poor correlation between *in silico* pharmacophore model fit of compounds B1 and A10 and their actual fusogenicity: Val372 was proven to be functionally dispensable and His380 paired with Asp725 rather than Lys720 as indicated in the original model. Moreover, the present studies revealed that phosphorylation of Ser378 in both the mitofusin agonist peptide and intact Mfn2 protein can change amino acids presented to the HR1-HR2 interface (see e.g., **FIG. 11A**); this key transitional feature was not part of the initial model. Compounds A10 and B1 (which ranked 4^{th} and 2^{nd} in fusogenicity, but 27^{th} and 31^{st} in fit to the pharmacophore model) and their chemosimilars conformed well to an Mfn2 HR1-HR2 interaction model incorporating these biological findings, as depicted in **FIG. 1**. These two compounds were therefore purified (see e.g., **FIG. 3**) and used in subsequent studies.

[0270] The ultimate goal was to design mitofusin agonists having optimal activity profiles. (Here, a “fusogenic compound” is defined as promoting mitochondrial elongation without a clearly defined mechanism, while a “mitofusin agonist” is a fusogenic compound that binds to the Mfn2 HR2 minipeptide target domain, promotes Mfn2 opening, and loses its fusogenic activity when endogenous mitofusin proteins are not present). Molecular modeling of class A and B agonists assumed that the minipeptide a-helix is comprised of 3.6 amino acids per turn with a 1.4 A pitch advance per amino acid, resulting in a distance of ~5.4 A between amino

acids of adjacent turns. Aliphatic backbones assumed a distance between single bonded carbons of 1.54 A. Structures were created or edited using Marvin JS at the MolPort website and available chemical analogs (chemosimilars; TABLE 5) identified using the search function and a similarity parameter of 0.5.

TABLE 5. Characteristics of 12 (6 each) class A and class B mitofusin agonists (commercially sourced).

ID	IUPAC Name	Structure
pA	3-phenyl-1-(4-phenylbutyl)urea	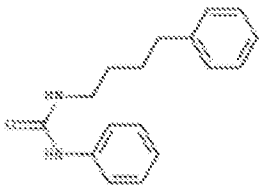
A1	1-[2-(benzylsulfanyl)ethyl]-3-(2-methylcyclohexyl)urea	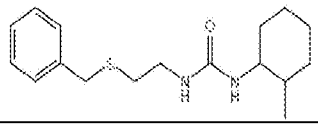
A2	3-(4-fluorophenyl)-1-(4-phenylbutyl)urea	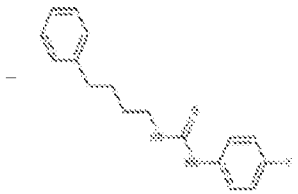
A3	3-(3-methylphenyl)-1-(4-phenylbutyl)urea	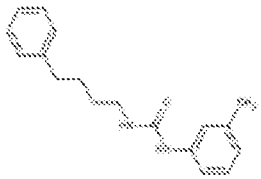
A4	3-(4-methylphenyl)-1-(4-phenylbutyl)urea	
A5	3-(2-methylphenyl)-1-(4-phenylbutyl)urea	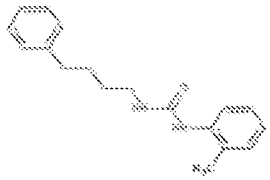

pB	2-(4-phenylbutanamido)-4H,5H,6H-cyclopenta[b]thiophene-3-carboxamide	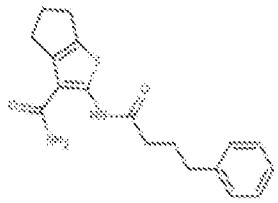
B1	2-{2-[(5-cyclopropyl-4-phenyl-4H-1,2,4-triazol-3-yl)sulfanyl]propanamido}-4H,5H,6H-cyclopenta[b]thiophene-3-carboxamide	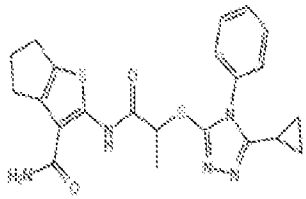
B2	2-[2-(phenylsulfanyl)acetamido]-4H,5H,6H-cyclopenta[b]thiophene-3-carboxamide	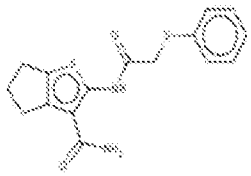
B3	3-acetamido-N-(2-{[(4-methylphenyl)methyl]sulfanyl}ethyl)adamantane-1-carboxamide	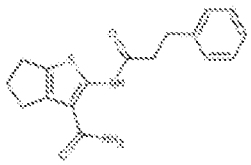
B4	2-{2-[(4-benzyl-5-cyclopropyl-4H-1,2,4-triazol-3-yl)sulfanyl]propanamido}thiophene-3-carboxamide	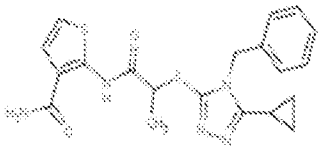
B5	N-benzyl-2-[2-({4-methyl-5-[(phenylcarbamoyl)methyl]-4H-1,2,4-triazol-3-yl}sulfanyl)acetamido]-4,5,6,7-tetrahydro-1-benzothiophene-3-carboxamide	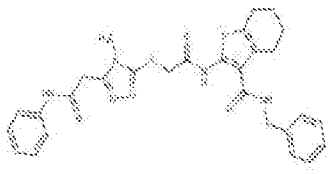

[0271] Fusogenic activity of commercially available small-molecule candidate pharmacophores (TABLE 4), focusing on those having structures that mimicked Ser^{378}-phosphorylated (class A) and -unphosphorylated (class B) minipeptide amino acid side chains were assessed (see e.g., **FIG. 5**, TABLE 5). It was reasoned that simultaneous application of class A and B agonists could

enhance mitofusin by acting on both MFN2 Ser^{378} phosphorylation states. Indeed, lead compounds (Cpd) A and B acted synergistically to promote mitochondrial fusion (see e.g., **FIG. 26**; compare to **FIG. 5C**). Therefore, Cpd A and B functionality were assimilated into a single molecule by creating Cpd A-B chimeras (see e.g., **FIG. 11**, **FIG. 7**, TABLE 6). The novel chimeric compounds incorporated functional features (e.g., potency, specificity) of both Cpds A and B which were functionally synergistic because they acted on different phosphorylated forms of MFN (see e.g., Example 2). Chimera B-A/long (B-A/l) potently stimulated mitochondrial fusion in MFN2-deficient cells (see e.g., **FIG. 11B**), competed for minipeptide binding at the MFN2 HR2 interaction site (see e.g., **FIG. 11C**), and was as effective as the combination of Cpds A+B in reversing mitochondrial dysmorphology provoked by the CMT2A mutant, MFN2 Thr^{105}→Met^{105} (MFN2 T105M) (see e.g., **FIG. 11D**). Fusogenic effects of Cpd A were specific for the Asp^{378} mutant of MFN2 that mimicked Ser^{378}-phosphorylation, whereas Cpd B and chimera B-A/l were non-selective for the phosphomimic Asp^{378} and nonphosphorylatable Ala^{378} mutants (see e.g., **FIG. 11E**). Because they mimic WT MFN2 HR1 sequence and interact with HR2, mitofusin agonists evoked fusion to proportionally similar degrees in mitochondria expressing mutants of HR1 that are fusion deficient (see e.g., **FIG. 11F**; compare to **FIG. 2H** and **FIG. 18**). Small molecule mitofusin agonists required endogenous MFN1 or MFN2 to promote mitochondrial fusion, exhibited no promiscuous activity for structurally related dynamin, and did not compromise cell viability (see e.g., **FIG. 27**). On the basis of fluorescence resonance energy transfer (FRET) analysis of MFN2 labeled at the N and C termini, mitofusin agonists promoted an open MFN2 conformation favoring mitochondrial fusion, with a rank order paralleling that for HR2 binding and mitochondrial fusion (see e.g., **FIG. 11G**; compare to **FIG. 11B** and **FIG. 11C**), supporting allosteric activation.

[0272] Small molecule mitofusin agonists efficacy was shown in CMT2A model of neuronal degeneration**.** In CMT2A, MFN2 mutants produce mitochondrial "fragmentation" (decreased aspect ratio) and loss of normal membrane polarization through dominant inhibition of normal mitofusins. Experiments using $MFN1^{-/-}$, $MFN2^{-/-}$ deficient murine embryonic fibroblasts (MEFs) showed that in the absence of normal mitofusins, small-molecule mitofusin agonists did not improve mitochondria of cells expressing the guanosine triphosphatase (GTPase)–crippled MFN2 Arg^{94}→Gln^{94}

(R94Q) or Lys^{109}→Ala^{109} (K109A) mutant (see e.g., **FIG. 9A**). However, mitofusin agonists corrected mitochondrial dysmorphology and reversed mitochondrial hypopolarization induced by these MFN2 mutants when MFN1 was present ($MFN1^{+/+}$, $MFN2^{-/-}$ MEFs) (see e.g., **FIG. 9B).** Mitofusin agonists also reversed mitochondrial fragmentation and hypopolarization in cultured neurons expressing (in addition to endogenous mitofusins) CMT2A mutants MFN2 R94Q (see e.g., **FIG. 9C**, **FIG. 9D**) or MFN2 T105M (see e.g., **FIG. 9E).** Thus, mitofusin agonists do not restore function of CMT2A MFN2 GTPase domain mutants. Rather, by destabilizing the fusion-permissive open conformation of endogenous MFN1 or MFN2, mitofusin agonists can overcome dominant suppression of mitochondrial fusion by these disease-causing dysfunctional proteins.

[0273] Clinical CMT2A classically affects long nerves innervating the lower and upper limbs. It is unclear how a principal defect in mitochondrial fusion would cause length-dependent neuronal disease. Conversely, disruption of axonal mitochondrial transport would be predicted to preferentially impact cells requiring mitochondrial transport over the greatest physical distance, such as the sciatic nerves originating in the spine and terminating in the foot. MFN2 interacts with Miro/Milton to promote mitochondrial trafficking in neurons, so the effects of mitofusin agonism on murine neuronal mitochondrial trafficking were tested. Chimera B-A/l reversed mitochondrial “clumping” (formation of static mitochondrial aggregates) and restored mitochondrial motility in cultured neurons expressing the CMT2A mutant MFN2 T105M (see e.g., **FIG. 28A**, **FIG. 29**). Mitochondrial hypopolarization and increased autophagy (see e.g., **FIG. 28B**, **FIG. 30**) and mitochondrial dysmorphology (see e.g., **FIG. 28C**, **FIG. 30**) were concomitantly corrected. Thus, a small molecule mitofusin agonist enhanced organelle and cell fitness in CMT2A neurons by promoting mitochondrial fusion and subcellular transport.

[0274] The concept of activating mitofusins to stimulate axonal mitochondrial trafficking was evaluated in sciatic nerves of mice expressing the CMT2A mutant MFN2 T105M *in vivo*. In normal sciatic nerves ~30% of axonal mitochondria exhibited robust bidirectional transport (see e.g., **FIG. 28**, **FIG. 31**). Mitochondria of MFN2 T105M sciatic nerves were severely hypomotile (see e.g., **FIG. 28E**, **FIG. 32**), but application of chimera B-A/l to MFN2 T105M sciatic nerves restored mitochondrial motility to within normal levels (see e.g., **FIG. 28F**, **FIG. 32**).

Mobile mitochondria in WT and B-A/I-treated MFN2 T105M axons were smaller (see e.g., **FIG. 28G**), supporting *in vitro* observations distinguishing between MFN2-mediated mitochondrial dysmotility and defective fusion in CMT2A.

[0275] Improvement in mitochondrial factors in ALS and HD patient-derived fibroblasts treated with B-A/I was shown. Here, B-A/I enhances mitochondrial structural defects, reduces mitochondrial ROS levels, and improves mitochondrial membrane potential in ALS and HD patient-derived fibroblasts and has no effect on fibroblasts from control subjects (see e.g., **FIG. 28**).

[0276] Here, it was found that PINK1 phosphorylation of MFN2 at Ser^{378} can alter the positions of Met^{376} and His^{380} (in the HR1 domain), which normally interact with HR2 domain amino acids to orchestrate MFN2 toggling between conformations that modulate mitochondrial fusion. MFN2 Ser^{378} phosphorylation (by PINK1 or other kinases) regulated the positions of Met^{376} and His^{380} that interact with HR2 amino acids, thus directing MFN2 conformation and governing fusion. These findings establish a mechanistic basis for clinical observations that MFN2 Met^{376} mutations to Ile, Thr, and Val can cause CMT2A.

[0277] Based on molecular modeling and a detailed structural and functional interrogation of MFN2-derived minipeptides encompassing Met^{376}, Ser^{378}, and His^{380} small molecule mitofusin agonists were developed that reversed mitochondrial dysmorphometry and normalized impaired mobility evoked by 2 CMT2A *MFN2* mutants. CMT2A is the prototypical clinical disorder of defective mitochondrial fusion, but impaired mitochondrial trafficking may play as great a role as mitochondrial fragmentation in CMT2A axonal degeneration. Individuals with CMT2A express one mutant MFN2 allele in combination with one normal MFN2 allele and harbor two normal MFN1 alleles. It is therefore possible that a therapeutic substrate for agonists to “supercharge” normal mitofusins and overcome dominant inhibition by MFN2 mutants. The observation that *in vivo* mitochondrial dysmotility provoked by CMT2A mutants can be normalized by mitofusin agonists mechanistically links abnormal mitochondrial trafficking in CMT2A to MFN2 dysfunction. Mitofusin agonists may also have therapeutic potential for neurological conditions other than CMT2A, such as Alzheimer’s, Parkinson’s, and Huntington’s diseases, wherein mitochondrial dysmotility and fragmentation are contributing factors.

Materials and Methods

Cell lines and adenoviral constructs

[0278] Wild-type MEFs were prepared from E10.5 c57/bl6 mouse embryos. SV-40 T antigen-immortalized Mfn1 null (CRL-2992), Mfn2 null (CRL-2993) and Mfn1/Mfn2 double null MEFs (CRL-2994) were purchased from ATCC. MEFs were subcultured in DMEM (4.5g/L glucose) plus 10% fetal bovine serum, 1× nonessential amino acids, 2 mM L-glutamine, 100U/ml penicillin and 100ug/ml streptomycin.

[0279] Human Mfn2 Ser378 was mutated to Ala or Asp by site-directed mutagenesis using the QuikChange Lightning kit (Agilent Technologies Inc.) and primers:

Mfn2-S378D-fw 5'-cgactcatcatggacgacctgcacatggcggc-3' (SEQ ID NO: 7)

Mfn2-S378D-rv 5'-gccgccatgtgcaggtcgtccatgatgagtcg-3' (SEQ ID NO: 8)

Mfn2-S378A-fw 5'-gactcatcatggacgccctgcacatggcg-3' (SEQ ID NO: 9)

Mfn2-S378A-rv 5' –cgccatgtgcagggcgtccatgatgagtc-3' (SEQ ID NO: 10)

[0280] Mfn2 and its mutants were sub-cloned into adenoviral vector Type 5 (dE1/E3) with RGD-fiber modification (Vector Biolabs) using BamHI/XhoI. All constructs were verified by Sanger DNA sequencing. Adeno-viral PINK1 was purchased from Vector Biolabs. Immunoblotting used mouse anti-Mfn2 (Abcam # ab56889, 1: 1000), anti-PINK1 (Sigma #P0076, 1: 500), and beta-actin (Santa Cruz Biotechnology #sc-81178, 1:1000). Protein detection and digital acquisition used peroxidase-conjugated anti mouse secondary antibody (Cell Signaling #7076S, 1:2500) and Western Lightning PLUS ECL substrate (Perkin Elmer 105001EA) on a Li-COR Odyssey instrument.

Peptide studies

[0281] The C-terminal and N-terminal Mfn2 367-384Gly peptides and Ala substituted variants of Mfn2 374-384 were chemically synthesized and introduced into cells using TAT47–57 conjugation (ThermoFisher Scientific). Except when indicated, 1 mM stocks in sterile water were diluted into culture media 1:1000 to achieve a final concentration of 1 μM. Cells were treated overnight.

[0282] For Alanine scanning the following peptides were synthesized:

(NH3) GIADSLHMAARGGYGRKKRRQRRR (COOH) (SEQ ID NO: 11)

(NH3) GIMASLHMAARGGYGRKKRRQRRR (COOH) (SEQ ID NO: 12)

(NH3) GIMDALHMAARGGYGRKKRRQRRR (COOH) (SEQ ID NO: 13)

(NH3) GIMDSAHMAARGGYGRKKRRQRRR (COOH) (SEQ ID NO: 14)

(NH3) GIMDSLAMAARGGYGRKKRRQRRR (COOH) (SEQ ID NO: 15)

[0283] The following peptides were synthesized for Ser378 substitution studies:

(NH3) GIMDSLHAAARGGYGRKKRRQRRR (COOH) (SEQ ID NO: 16)

(NH3) GIMDDLHMAARGGYGRKKRRQRRR (COOH) (SEQ ID NO: 17)

(NH3) GIMDS(p)LHMAARGGYGRKKRRQRRR (COOH) (SEQ ID NO: 18)

(NH3) GIMDGLHMAARGGYGRKKRRQRRR (COOH) (SEQ ID NO: 19)

(NH3) GIMDCLHMAARGGYGRKKRRQRRR (COOH) (SEQ ID NO: 20)

(NH3) GIMDNLHMAARGGYGRKKRRQRRR (COOH) (SEQ ID NO: 21)

Nuclear Magnetic Resonance (NMR) of HR1 peptide structure

[0284] Carboxyl terminal-amidated S378 parent and substituted peptide were synthesized for NMR studies:

Mfn2-371-384 (378S) – AVRGIMD**S**LHMAAR (SEQ ID NO: 22)

Mfn2-371-384 (378S(p)) – AVRGIMD[**S(p)**]LHMAAR (SEQ ID NO: 23)

[0285] Proton 2D NOESY and ^{15}N-^{1}H heteronuclear single quantum coherence overlay spectra of the above peptides were recorded on 600 MHz Bruker Avance III spectrometer equipped with cryoprobe, at 15 °C, pH 6, 50 mM NaCl, with each peptide at 2 mM concentration. Distance restraints were derived from observed NOE interactions between hydrogens within each peptide, and torsion angle restraints (φ and ψ) were derived from the observed chemical shifts (for C, H and N nuclei). The calculations used only experimental data; no theoretical molecular dynamics simulations/refinements were applied.

[0286] The helical structures/propensities in these peptides were not inferred or assumed from any single type of data. “Diagnostic” NOEs, in particular dNN and dab(i, i+3), were present in 200ms and 500ms mixing time H-H NOESY experiments, wherever signals could be resolved. The structural ensemble calculations used only restraints derived from NMR experiments. Distance restraints were derived from observed NOE interactions between hydrogens within each peptide, and torsion angle restraints (f and y) were derived from the observed chemical shifts (for C, H and N nuclei).

[0287] Both ensembles show preponderance of helical conformation between 378-383. These are more regular in phosphopeptide ensemble (see e.g., **FIG. 16C**). Both ensembles show no regular conformation between 371-376, consistent with a lack of observed NOEs and values of chemical shifts characteristic for unstructured sequences. At the current level of precision, there is little difference between two ensembles in positions of side chains for residues 379-383. The almost identical 13C/1H chemical shifts of these methyl groups also suggest the similarity of their positions and local environments. However, the backbone amide (N-H) and Ca signals clearly show differences, beyond the obvious one caused by phosphate esterification of serine. The amide signals shifted down-field (to higher values), a characteristic observed when amides form (or strengthen) hydrogen bonds within peptides. In general, the helical secondary structure is often stabilized by a negatively charged group “capping” the positive N-terminal end of the helix dipole. Here, a phosphorylation of Ser 378 can produce H-bonding for the amide of Leu-379 and the negative phosphate can additionally stabilize the helical turns following 379, providing an explanation for observed down-field shifts (i.e., H-bonding induced) in amides of 380, 381 and 382. MFN2 FRET for conformational studies

[0288] Mfn2 FRET probes contained N-termini-ceruleum and C-termini-mVenus fused to the human (h) mitofusin protein as previously described. FRET analyses were performed either on mitochondria isolated from Mfn1/Mfn2 null MEFs expressing the WT hMfn2 FRET-hMfn2 protein or intact Mfn1/Mfn2 null MEFs expressing WT or mutant Mfn2 FRET proteins (50 MOI). For isolated mitochondria studies 65 µg of organelle protein was used for each reaction in a total volume of 100 µl diluted in 10 mM Tris-MOPS (pH 7.4), 10mM EGTA/Tris, and 200 mM sucrose. 1 µM of mitofusin agonist in DMSO was added simultaneously with 2 µM mitofusin antagonist peptide, incubated in dark at room-temperature for 30 minutes, and FRET signal corrected for Cerulean signal analyzed using a Tecan Safire II multi-mode plate reader in polystyrene 96 well assay plate (Costar 3916). Data acquisition was: FRET – Excitation 433/8 nm, Emission 528/8 nm; Cerulean – Excitation 433/8 nm, Emission – 475/8 nm. Isolated mitochondria of non-infected cells were used to subtract background, and FRET signals were normalized to respective cerulean signals. The % changes in FRET/Cerulean provoked by mitofusin antagonist peptide and reversed by different mitofusin agonist small

molecules were compared to Mfn2-FRET mitochondria treated with water and DMSO, the vehicles for Mfn antagonist peptide and mitofusin agonist, respectively.

[0289] For FRET in intact cells, Mfn1/Mfn2 double null MEFs at 70% confluence were infected with adenoviri expressing FRET-hMfn2, FRET-hMfn2 (S378A) or FRET hMfn2 (S378D) at 50 MOI. Two-days after transduction and 1 hour after application of 1μM Mfn2 antagonist mini-peptide MP2 to promote the closed/inactive Mfn conformation, cells were released from tissue culture substrate with trypsin/EDTA, washed, and transferred to a polystyrene 96 well assay plate (Costar 3916; 20,000 cells/50 ml/well). Fifty-microliters of modified Krebs-Henseleit buffer containing DMSO (vehicle) or 1 μM mitofusin agonist was added with gentle agitation for 10 min at room temperature. FRET and cerulean signals were assayed in a 96-well plate reader (TriStar 2S LB 942, Berthold Technologies) with 1 sec reading times at low sensitivity. Filters combinations are as follows: FRET – Excitation 430/10, Emission 535/25; Cerulean – Excitation 430/10, Emission – 475/20. Signals from non-infected cells were used for background correction. FRET was normalized to the respective cerulean signal for each well.

MFN2 amino terminal FLAG epitope unmasking assay

[0290] HEK293 cells were transfected with wild-type or mutant MFN2 having an amino terminal FLAG epitope tag using Lipofectamine 3000 (Invitrogen) per the manufacturer's instructions. After 48 hours cells mitofusin agonists or DMSO vehicle were added at the indicated concentrations for 1 hour (37°C). Cells were harvested and proteins extracted using Invitrogen cell extraction buffer supplemented with protease and phosphatase inhibitors (Roche). Proteins were quantified using the Bradford assay (Biorad). Two mg aliquots of protein extract were incubated in a final volume of 500 μl with 50μl (bed volume) of ANTI-FLAG M2 Affinity Gel (Sigma) with gentle agitation for 2 hours at 4°C. Beads were washed twice with 1ml of cold PBS buffer and proteins were eluted by adding 100 μl of reducing SDS sample buffer. Samples of input extract and immunoprecipitated proteins were size-separated on SDS-PAGE mini-gels and immunoblotted for MFN2.

HR1 peptide-HR2 target binding assay

[0291] Target HR2 peptide sequence modified to include amino terminal 6 x His tags and Gly linkers, were bonded to Ni-NTA resin (4.4 μg/ml) (Quiagen) and

used as immobilized "receptor" for amino-FITC-tagged Mfn2 374-384 (ligand) in which the Ser analogous to Ser378 was replaced with Asp to confer the negative charge essential for activity. FITC peptide ligands were suspended at 1 mM in 30% DMSO, 70% water (to minimize spontaneous aggregation) and diluted into binding buffer (de-ionized water). For the displacement binding, 2.5 nmol of FITC labeled agonist peptide was used in the presence or absence of different amounts of competing compounds. Resin-bound FITC signal (485 nm excitation/ 538 nm emission) measured in a 96 well spectrofluorometer (Spectramax M5e, Molecular Devices) represented binding to HR2 target. Competition binding isotherms were plotted and IC_{50} values calculated using Prism 7 (GraphPad).

[0292] Sequences for binding assay components are:

(NH3) HHHHHH-GGGG-AAMNKKIEVLDSLQSKAKLLRNKA-GG (COOH) (target) (SEQ ID NO: 24)

(NH3) HHHHHH-GGGG-AAMNKKIEV**AA**S**A**QSKAKLLRNKA-GG (COOH) (target mutant) (SEQ ID NO: 25)

(NH3) FITC-GGGG-AVRGIMD**S**LHMAAR-GG (COOH) (FITC labeled Ser peptide) (SEQ ID NO: 26)

(NH3) FITC-GGGG-AVRGIMD**D**LHMAAR-GG (COOH) (FITC labeled Asp peptide) (SEQ ID NO: 27)

(NH3) FITC-GGGG-AVRGIMD**A**LHMAAR-GG (COOH) (FITC labeled Ala peptide) (SEQ ID NO: 28)

Protein and peptide Modeling

[0293] The hypothetical structures of human Mfn2 were developed using the I-TASSER Suite package. The putative closed conformation is based on structural homology with bacterial dynamin-like protein (PDB: 2J69), human Mfn1 (PDB:5GNS), and *Arabidopsis* thaliana dynamin-related protein (PDB: 3T34). The putative open conformation was based on structural homology with human Opa1, retrieved from the following structures: rat dynamin (PDB: 3ZVR), human dynamin 1-like protein (PDB: 4BEJ), and human myxovirus resistance protein 2 (PDB: 4WHJ). Minipeptide and protein modeling used PEP-FOLD3 (http://bioserv.rpbs.univ-paris-diderot.fr/services/PEP-FOLD3/) and UCSF Chimera, respectively.

Protein alignment and phylogenetic analysis

[0294] Mfn2 orthologous sequences were retrieved from the Ensembl project database. Protein alignments were performed using Clustal Omega.

In vitro PINK1-Mfn2 phosphorylation assay

[0295] *In silico* prediction of kinases that might phosphorylate Mfn2 Ser378 in the peptide sequence AVRLIMD**S**LHMAARE used GPS 3.0 (http://gps.biocuckoo.org). GRK2/bARK1 was the top hit (score of 31.595), and GRK isoforms comprised 5 of the top 7 hits; ROCK kinase (score 15.919) and PKCa (score 11.48) were the other two hits. PINK1 kinase is not represented at this site, and no other sites reported any likely kinases for Mfn2 Ser378.

[0296] *In vitro* phosphorylation of Mfn2 by PINK1 and GRK kinases used a modified published protocol. Briefly, 20 mg of recombinant human Mfn2 (expressed in HEK293 cells; OriGene: TP326143) plus 10-20 mg *Tribolium castaneum* PINK1 (expressed in *E. coli*; Ubiquigent: 66-0043-050) or 10 mg human GRK2 (Invitrogen: PV3361) were combined in kinase buffer (20 mM Hepes pH 7.4, 10 mM DTT, 0.1 mM EGTA, 0.1 mM ATP and 10 mM MgCl2) and the reactions allowed to proceed at 37°C for 4 hours or overnight.

Mass spectrometric analysis of Mfn2 phosphopeptides

[0297] *Preparation of peptides for nano-LC-MS.* The in vitro kinase solution that contained 10 µg of Mfn2 was spiked (10 µL) with a mixture of five carrier proteins (10 µg each). The mixture consisted of human apo-transferrin (Sigma, T4382), bovine α-casein (Sigma, C6780), bovine β-casein (Sigma, C6905), bovine ribonuclease (Sigma, R7884), and bovine albumin (Sigma A7030) in 100 mM Tris buffer, pH 7.6 with 4% SDS and 100 mM DTT. The sample was lyophilized overnight in a VirTis AdVantage Lyophilizer (SP Scientific).

[0298] Peptides were prepared using a modified filter-aided sample preparation method: dried sample was dissolved in 60 µL of Tris buffer, pH 7.6 that contained 4% SDS and 100 mM DTT and denatured by heating (95ºC) for 5 min. The sample was then alkylated with 50 mM iodoacetamide (Sigma, A3221) for 1 h at room temperature in the dark. After the addition of 1 ml of 50 mM ammonium bicarbonate buffer (pH 8.5) containing 8M urea (UA) and vortexing, equal volumes of the samples were transferred to two YM-30 filter units (Millipore, Ref No.

MRCF0R030) and spun for 14 min at 10,000 rcf (Eppendorf, Model No. 5424). Filters were washed with 200 µl of UA and the spin-wash cycle was repeated twice. The sample was then exchanged into digest buffer with the addition of 200 µl of ammonium bicarbonate buffer, pH 8.5 (ABC) and centrifugation (11,000 rcf) for 10 min. After transferring the upper filter unit to a new collection tube, 80 µL of the ABC buffer was added and the sample was digested with trypsin (1 µg) for 4h at 37ºC. The digestion was continued overnight after another addition of trypsin. Filter units were then spun at 11,000 rcf for 10 min with a subsequent filter washing step with 0.5 M NaCl (50 µL) followed by centrifugation (14,000 rcf for 10 min). The digest was then extracted three times with 1 ml of ethyl acetate and acidified with trifluoroacetic acid (TFA) (50%) to a final concentration of 1%. The pH was < 2.0 using pH paper. Solid phase extraction of the peptides was performed using sequential, robotic pipetting with C4 and porous graphite carbon micro-tips (Glygen). The peptides were eluted with 60% acetonitrile in 0.1% TFA and pooled for drying in a Speed-Vac (Thermo Scientific, Model No. Savant DNA 120 concentrator) after adding TFA to 5%. The peptides were dissolved in 20 µL of 1% acetonitrile in water. An aliquot (10%) was removed for quantification using the Pierce Quantitative Fluorometric Peptide Assay kit (Thermo Scientific, Cat. No. 23290). The remaining sample was transferred to an autosampler vial (Sun-Sri, Cat. No. 200046), dried in the SpeedVac and dissolved in 2.7 µL of 0.1%TFA.

[0299] *Nano-LC-MS/MS Analysis of Phosphopeptides* — The samples were loaded (2.5 µL) at a constant pressure of 700 bar at 100% of mobile phase solvent A (0.1%FA) onto a 75 µm i.d. × 50 cm Acclaim® PepMap 100 C18 RSLC column (Thermo-Fisher Scientific) using an EASY nanoLC (Thermo Fisher Scientific). Before sample loading the column was equilibrated with 100% A using 20µL at 700 bar. Peptide chromatography was initiated with A containing 2% B (100% ACN, 0.1%FA) for 5 min, then linear increased to 20% B over 100 min, to 32% B over 20 min, to 95% B over 1 min and held at 95% B for 7 min, at a flow rate of 300 nL/min. The data dependent mode analysis was performed with in the Orbitrap mass analyzer (Thermo-Fisher Scientific Q-Exactive™ Plus Hybrid Quadrupole-Orbitrap™ mass spectrometer) with a scan range of m/z = 375 to 1500 and a mass resolving power set to 70,000. Ten data-dependent high-energy collisional dissociations were performed with a mass resolving power set to 17,500,

a fixed lower value of *m/z* = 100, an isolation width of 2 Da, and a normalized collision energy of 27. The maximum injection time was 60 ms for parent-ion accumulations and 60 ms for product-ion analysis. The parent ions that were selected for MS2 were dynamically excluded for 20 sec. The automatic gain control was set at a target ion value of 1e6 for MS1 scans and 1e5 for MS2 acquisition. Peptide ions with charge states of one or > 8 were excluded for CID acquisition.

[0300] Phosphopeptide data from the PINK kinase reactions were also acquired in targeted mode. The full-scan mass spectra were acquired by the Orbitrap mass analyzer with a scan range of *m/z* = 350 – 2000 and a mass resolving power set to 70,000. The CID spectra were acquired at resolving power of 17,500 with maximum table time of 120 ms. The loop count was set to 4 and the isolation width was 2 Da. The acquisition of CID spectra were triggered by an inclusion list of four *m/z* values for the +2 and +3 charge state of the natural abundance phosphorylated and non-phosphorylated peptide (see e.g., TABLE 3, above, for values). An AGC target value of 3e6 was used for MS scans and 2e5 for MS/MS scans. The unprocessed LC-MS data were analyzed using SKYLINE (version 3.6.9).

[0301] The high-resolution ion chromatograms for the y ion series from the CID phosphopeptide spectra shown in **FIG. 2G** were acquired during the LC-MS analysis of the tryptic digest of human recombinant Mfn2 after phosphorylation with PINK1. The corresponding chromatograms from the synthetic, isotope-labeled phosphopeptide co-eluted with the PINK1 product and all ions were observed with the same proportional intensities in the CID spectra as shown in the adjacent stacked bar charts, confirming the sequence identity and phosphorylated residue location. The expected mass increment of 10 Da from the Arg-[13C6] [15N4] residue was observed for all y ions in the CID spectra of the synthetic phosphopeptide. The spectra from the PINK1 phosphopeptide product and the synthetic phosphopeptide were acquired from the triply charged parent ions at *m/z* = 446.543 and *m/z* = 449.880, respectively. The site of phosphorylation was confirmed from the series of y ions with neutral losses of the phosphate moiety (H_3PO_4) that were observed as y8-H3PO4 (*m/z* = 882.427*),* and y7- H3PO4 +2 (*m/z* = 384.203*).* The same ion series was observed in the CID spectrum of the synthetic peptide with the expected 10 Da mass increment, y8- H_3PO_4 (*m/z* = 892.432*)* and y7- H_3PO_4 (*m/z* = 777.404*).* Using the synthetic phosphorylated and non-phosphorylated peptides, it was determined

that the phosphopeptide consistently eluted 9.5 – 10.5 min later in all LC-MS analyses. All tandem spectra that were acquired from a precursor ion were also analyzed at *m/z* = 446.543 for any evidence of phosphorylation at Ser-378 in replicate PINK1 experiments, GRK phosphorylation experiments, and in a digest of the recombinant Mfn2 protein without added kinase. Phosphopeptides with the Ser-378 site were only observed from the PINK1 phosphorylation experiments.

Dextran uptake assays of dynamin function

[0302] Wild-type MEFs (100,000 cells) were grown on cover slips. When they reached 60% confluency they were washed with serum-free DMEM. Subsequently, cells were incubated in serum-free DMEM containing either 1 μM compound A; B; B/A-L; dynasore (Calbiochem) or DMSO only (vehicle) for 30 min at 37 °C. AF594-labelled 10,000 MW Dextran (Invitrogen) was then added to a final concentration of 0.5 mg/ml and incubated for additional 10 min. at 37 °C. Internalization was stopped by washing three-times with ice-cold PBS. Residual dextran was removed by washing with 0.1 M Na acetate, 0.05 M NaCl for 10 min. Samples were fixed in 4% PFA followed by confocal microscopy analysis.

Confocal live cell studies of mitochondria

[0303] Confocal imaging used a Nikon Ti Confocal microscope equipped with a 60×1.3NA oil immersion objective. All live cells were grown on cover slips loaded onto a chamber (Warner instrument, RC-40LP) in modified Krebs-Henseleit buffer (138 mM NaCl, 3.7 mM KCl, 1.2 mM KH2PO4, 15 mM Glucose, 20 mM HEPES and 1 mM CaCl2) at room temperature.

[0304] Cells were excited with 408 nm (Hoechst), 561 nm (MitoTracker Green and Calcein AM, GFP), or 637 nm (TMRE, MitoTracker Orange, Ethidium homodimer-1, and AF594- Dextran) laser diodes. For mitochondrial elongation studies mitochondrial aspect ratio (long axis/short axis) was calculated using automated edge detection and Image J software. Mitochondrial depolarization was calculated as % of green mitochondria visualized on MitoTracker Green and TMRE merged images, expressed as green/(green + yellow mitochondria) × 100.

Chemical synthesis, purification and analyses of novel small molecule mitofusin agonists

[0305] Four A-B chimeric molecules designed to incorporate different characteristics of Cpds A and B (TABLE 6) were synthesized de novo:

TABLE 6. Characteristics of 4 novel, newly synthesized chimeric class A/B mitofusin agonists (chimeras).

Compound ID	IUPAC Name	Structure	M.W.	Formula	Purity
A-B/s	2-[2-(benzylsulfanyl)propanamido]-4H,5H,6H-cyclopenta[b]thiophene-3-carboxamide	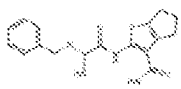	360.4936	C18H20N2O2S2	98.8%
B-A/s	2-[(5-cyclopropyl-4-phenyl-4H-1,2,4-triazol-3-yl)sulfanyl]-N-(2-methylcyclohexyl)propanamide	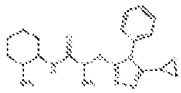	384.53822	C21H28N4OS	99.9%
A-B/l	2-(3-(2-(benzylthio)ethyl)ureido)-5,6-dihydro-4H-cyclopenta[b]thiophene-3-carboxamide	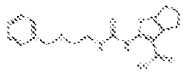	375.50824	C18H21N3O2S2	97.6%
B-A/l	1-(2-((5-cyclopropyl-4-phenyl-4H-1,2,4-triazol-3-yl)thio)ethyl)-3-(2-methylcyclohexyl)urea	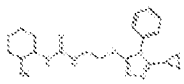	399.55286	C21H29N5OS	99.9%

[0306] Chimera B-A/l – (1-(2-((5-cyclopropyl-4-phenyl-4H-1,2,4-triazol-3-yl)thio)ethyl)-3-(2-methylcyclohexyl)urea) was synthesized by Enamine Ltd as a racemic mixture (see e.g., **FIG. 33**). Step A: 5-Cyclopropyl-4-phenyl-4H-1,2,4-triazole-3-thiol (1) (1 mmol) was dissolved in 1 mL of CH_3OH/H_2O (50:50), then NaOH (1 mmol) was added, stirred for 10 min, and 2-(boc-amino)ethyl bromide (2) (1 mmol) was added at 25 ºC. The reaction was allowed to stir for 3 hours then poured

into 10 mL water. The precipitate was filtered and dried to get a solid. The crude product was dissolved in 10 ml of trifluoroacetic acid (TFA), and heated at 50 ºC for 10 h to remove the solvent and 10ml of water and NaOH (1 mmol) were added. The mixture was stirred at room temperature for 1 h, filtered, and washed with water (50 ml). The residue was purified using reversed phase high-performance liquid chromatography RP-HPLC. Yield: 52 %. Step B: 2-((5-Cyclopropyl-4-phenyl-4H-1,2,4-triazol-3-yl)thio)ethan-1-amine (3) (0.5 mmol) and 1,1′-carbonyldiimidazole (CDI) (1 mmol) were dissolved in 0.6 ml CH_3CN, the mixture was kept at a temperature of 70 ºC for 1 h, and then the 2-methyl-cyclohexylamine (4) (0.5 mmol) was added. The mixture was heated for 2 hours at 70 ºC, then filtered, and evaporated. The residue was purified using RP-HPLC to give the desired product as a white solid; Purity: 99.99% (see e.g., **FIG. 34A**); Yield: 32 %; C21H29N5OS; MW 399.5. Liquid chromatography with high-resolution mass spectrometry using electrospray ionization LC-HRMS (ESI) with expected m/z 399.25 showed exact mass found 400.2 $[M + H]^+$ (see e.g., **FIG. 34B**). Chemical structure was confirmed by proton nuclear magnetic resonance (^{1}H NMR) and carbon-13 nuclear magnetic resonance (^{13}C NMR) (see e.g., **FIG. 35**). ^{1}H NMR (400 MHz, DMSO-*d*6) δ 7.60 (m, 3H), 7.48 (m, 2H), 5.95 (dt, 1H), 5.81 (dd, 1H), 3.26 (q, 2H), 3.07 (t, 2H), 3.00 (m, 1H), 1.62 (m, 4H), 0.99 (m, 10H), 0.81 (d, 2H), 0.75* (d, 1H). ^{13}C NMR (126 MHz, $CDCl_3$) δ 157.45, 156.97, 149.14, 133.14, 129.74, 127.34, 53.83, 48.83, 39.00, 34.12, 33.92, 32.69, 25.39, 25.30, 19.20, 7.15, 5.67.

[0307] Chimera B-A/s (2-((5-cyclopropyl-4-phenyl-4H-1,2,4-triazol-3-yl)thio)-N-(2-methylcyclohexyl)propanamide) was synthesized by Enamine as a racemic mixture (see e.g., **FIG. 36**): 5-Cyclopropyl-4-phenyl-4H-1,2,4-triazole-3-thiol (1) (0.5 mmol) was dissolved in 1 mL of CH_3OH, then KOH (0.5 mmol) was added, stirred for 10 min, and then 2-chloro-N-(2-methylcyclohexyl)propanamide (2) (0.5 mmol), was added at room temperature. The reaction was allowed to stir for 3 hours then poured into 10 mL water. The precipitate was filtered and dried, then was purified using RP-HPLC to give the title compound as a light brown solid; Purity: 99.99% (see e.g., **FIG. 37A**); Yield: 43 %; C21H28N4OS; MW 384.54. LC-HRMS (ESI): expected m/z 384.24, exact mass found 385.2 $[M + H]^+$ (see e.g., **FIG. 37B**). Chemical structure was confirmed by^{1}H NMR and ^{13}C NMR (see e.g., **FIG. 38**): ^{1}H NMR (500 MHz, DMSO-d_6) δ 8.01 (dd, 1H), 7.60 (m, 3H), 7.45 (m, 2H), 4.27 (qd,

1H), 3.14 (qd, 1H), 1.65 (m, 3H), 1.57 (m, 2H), 1.44 (d, 2H), 1.40 (d, 1H), 1.16 (m, 4H), 0.93 (m, 3H), 0.86 (m, 2H), 0.78 (d, 2H), 0.71* (d, 1H). ^{13}C NMR (126 MHz, DMSO-d_6) δ 158.01, 139.15, 129.31, 128.75, 127.18, 54.27, 49.26, 39.36, 38.56, 35.24, 34.61, 34.48, 31.88, 31.83, 25.88, 25.79, 19.70.

[0308] Chimera A-B/l: (2-(3-(2-(benzylthio)ethyl)ureido)-5,6-dihydro-4H-cyclopenta[b]thiophene-3-carboxamide) was synthesized by Enamine Ltd (see e.g., **FIG. 39**). Step A: Under an argon atmosphere, into a reaction vessel of 2-amino-5,6-dihydro-4H-cyclopenta[b]thiophene-3-carboxamide (1) (1.0 mmol), potassium iodide (0.8 mmol), potassium carbonate (1.0 mmol), N,N-dimethylformamide (DMF) 1 mL and 2,2,2-trifluoroethyl chloroformate (2) (1.0 mmol) were added. The reaction vessel was heated to 80 °C, and the mixture was stirred for 12 hours. The reaction vessel was cooled to room temperature, and ethyl acetate 100 mL was added. The organic layer was washed with water (50 mL), saturated brine (50 mL), and dried over sodium sulfate. The sodium sulfate and the solvent were distilled off. Compound 3 was purified using RP-HPLC. Yield: 54%. Step B: To a solution of 2 mmol of a 2,2,2-trifluoroethyl (3-carbamoyl-5,6-dihydro-4H-cyclopenta[b]thiophen-2-yl)carbamate (3) and 2 mmol of an 2-(benzylthio)ethan-1-amine (4) in 2 mL of acetonitrile, 0.2 mmol of 1,8-diazabicyclo[5.4.0]undec-7-ene (DBU) was added. The reaction mixture was heated at 80 °C for 4 h. Then 0.5-2 mL of water was added to the hot reaction mixture. The product precipitated from the solution upon cooling to room temperature then filtered and concentrated in vacuum. The residue was purified using RP-HPLC to give the title compound as a brown solid. Purity: 97.56% (see e.g., **FIG. 40A**); Yield: 51%; C18H21N3O2S2; MW 375.51; LC-HRMS (ESI): expected m/z 375.13, exact mass found 376.0 $[M + H]^+$ (see e.g., **FIG. 40B**); Structure was confirmed by^{1}H NMR and ^{13}C NMR (see e.g., **FIG. 41**): ^{1}H NMR (400 MHz, DMSO-d_6) δ 10.87 (s, 1H), 7.88 (s, 1H), 7.31 (m, 6H), 6.47 (s, 1H), 3.76 (s, 2H), 3.25 (q, 2H), 2.86 (t, 2H), 2.73 (t, 2H), 2.48 (m, 2H), 2.31 (p, 2H). ^{13}C NMR (126 MHz, DMSO-d_6) δ 167.20, 153.47, 151.94, 138.52, 128.88, 128.84, 128.32, 107.82, 34.74, 30.66, 29.30, 28.22, 27.52.

[0309] Chimera A-B/s: (2-(2-(benzylthio)propanamido)-5,6-dihydro-4H-cyclopenta[b]thiophene-3-carboxamide) was synthesized by Enamine Ltd as a racemic mixture (see e.g., **FIG. 42**): Phenylmethanethiol (1) (0.5 mmol) was dissolved in 1 mL of CH_3OH , then ethylbis(propan-2-yl)amine (0.55 mmol) was

added, stirred for 10 min, and then 2-(2-chloropropanamido)-4H,5H,6H-cyclopenta[b]thiophene-3-carboxamide (2) (0.5 mmol) was added. The reaction was allowed to stir at room temperature for 3 hours, and then poured into 10 mL water. The precipitate was filtered and dried, then was purified using RP-HPLC to give the title compound as a yellow solid; Purity: 98.76% (see e.g., **FIG. 43A**); Yield: 37 %; C18H20N2O2S2; MW 360.49; LC-HRMS (ESI): expected m/z 360.12, exact mass found 361.2 [M + H]+ (see e.g., **FIG. 43B**); Structure was confirmed by1H NMR and 13C NMR (see e.g., **FIG. 44**): ^{1}H NMR (500 MHz, DMSO-d_6) δ 12.49 (s, 1H), 7.64 (s, 1H), 7.33 (d, 2H), 7.28 (t, 2H), 7.22 (t, 1H), 6.70 (s, 1H), 3.83 (AB-system, 2H), 3.63 (q, 1H), 2.92 (t, 2H), 2.79 (t, 2H), 2.36 (q, 2H), 1.40 (d, 3H). ^{13}C NMR (126 MHz, DMSO-d_6) δ 168.77, 167.06, 148.07, 139.07, 137.35, 131.71, 128.91, 128.37, 126.99, 111.30, 42.52, 34.88, 29.03, 28.22, 27.68, 17.57.

Purification methods

Preparative HPLC

[0310] Purification was performed using HPLC (H_2O – MeOH; Agilent 1260 Infinity systems equipped with DAD and mass-detectors. Waters Sunfire C18 OBD Prep Column, 100Å, 5 µm, 19 mm X 100 mm with SunFire C18 Prep Guard Cartridge, 100 Å, 10 µm, 19 mm X 10 mm) The material was dissolved in 0.7 mL DMSO. Flow: 30 mL/min. Purity of the obtained fractions was checked via the analytical LCMS. Spectra were recorded for each fraction as it was obtained straight after chromatography in the solution form. The solvent was evaporated in the flow of N_2 at 80°C. On the basis of post-chromatography LCMS analysis fractions were united. Solid fractions were dissolved in 0.5 mL MeOH and transferred into pre-weighted marked vials. Obtained solutions were again evaporated in the flow of N_2 at 80°C. After drying, products were finally characterized by LCMS and ^{1}H NMR and ^{13}C NMR.

Analytical methods

HPLC/HRMS (ESI)

[0311] LC/MS analysis was carried out using Agilent 1100 Series LC/MSD system with DAD\ELSD and Agilent LC\MSD VL (G1956A), SL (G1956B) mass-spectrometer or Agilent 1200 Series LC/MSD system with DAD\ELSD and Agilent LC\MSD SL (G6130A), SL (G6140A) mass-spectrometer. All the LC/MS data were

obtained using positive/negative mode switching. The compounds were separated using a Zorbax SB-C18 1.8 µm 4.6x15mm Rapid Resolution cartridge (PN 821975-932) under a mobile phase (A – acetonitrile, 0.1% formic acid; B – water (0.1% formic acid)). Flow rate: 3ml/min; Gradient 0 min – 100% B; 0.01 min – 100% B; 1.5 min - 0% B; 1.8 min - 0% B; 1.81 min - 100% B; Injection volume 1µl; Ionization mode atmospheric pressure chemical ionization (APCI); Scan range m/z 80-1000.

NMR

^{1}H and ^{13}C NMR spectra were recorded at ambient temperature using Bruker AVANCE DRX 500; Varian UNITYplus 400 spectrometers.

Mouse hippocampal neuron preparation, culture, and live cell imaging

[0312] Neonatal mouse hippocampal neurons were cultured from brains of one day old Mfn2 T105M or non-transgenic sibling mouse pups as described. After 10 days of differentiating culture neurons were infected with Adeno-Cre to induce Mfn2 T105M expression or Adeno-βgal as a control (50 MOI). After an additional 72 hours mitofusin agonists or DMSO vehicle were added. For static confocal imaging neuronal mitochondria were labeled with adenoviral-expressed mitoGFP plus TMRE. Autophagy was measured by LC3 aggregation in neurons infected with adenoviral LC3-GFP. For time-lapse studies of mitochondrial trafficking bi-cistronic Adeno-Cre/GFP marked Cre expression and mitochondria were labeled with adeno-mitoDsRed. Confocal live cell images were acquired with a time-lapse of 1 frame every 90 seconds for 1 hour.

HB9-Cre/Mfn2 T105M mouse creation and sciatic nerve studies

[0313] All mouse procedures were approved by the Institutional Animal Care and Use Committee of Washington University in St. Louis. C57BL/6-Gt(ROSA)26Sortm1(CAG-MFN2*T105M)Dple/J (stock no. 025322 donated by David Pleasure, University of California Davis) and B6.129S1-Mnx1tm4(cre)Tmj/J (here referred to as HB9-Cre; stock no. 006600 donated by Thomas Jessel of Columbia University) were purchased from The Jackson Laboratory. The HB9-Cre driver was bred onto the ROSA26 flox-stop Mfn2 T105 transgene to induce Mfn2 T105M expression in motor neurons. Age- and sex-matched C57/b6 mice or mice carrying the MFN2 T105 flox-stop transgene in the absence of Cre were studied as normal controls.

[0314] Sciatic nerves of 12-18 week old male or female MFN2 T105M mice were removed en bloc with the lumbar spine and axotomy at the tibial nerve, stained with TMEM (200 mM) for 30 minutes in prewarmed Neurobasal Medium without phenol red (Thermo Fisher Scientific) at room temperature, washed, and maintained on the stage of a Nikon A1Rsi Confocal Microscope at 37degrees C for time-lapse confocal studies. Images were acquired with a 40x oil immersion objective at 1 frame every 5 or 10 seconds for sequential 10 minute periods. Mitofusin agonist chimera B-A/l was added after the first 10 minute imaging period (final concentrations of 1 or 5 mM) and nerve axons imaged for another 40 minutes. Because there was no difference in mitochondrial trafficking or response to mitofusin agonist between male and female mice, the data were combined.

Statistical methods

[0315] All data are reported as mean±SEM. Statistical comparisons (two-sided) used one-way ANOVA and Tukey's tests for multiple groups or Student's t-test for paired comparisons. $p<0.05$ was considered significant.

Cell culture.

[0316] HD patient-derived fibroblast cell lines (GM04693 from 33-year-old male patient and GM05539 from 10-year-old male patient) were purchased from Invitrogen. ALS patient-derived fibroblasts (ALS 1: ND29509 from 55-year old male patient having SOD1 mutation; ALS 2: ND30327 having FUS1 mutation) and fibroblasts of control healthy individuals were purchased from Coriell Institute, USA. All fibroblast cultures were maintained in MEM supplemented with 15% (v/v) FBS and 1% (v/v) penicillin/streptomycin at 37°C in 5% CO2-95% air. Galactose media was used, to increase mitochondria-dependent metabolism oxidative phosphorylation. Human fibroblasts were switched to grow for 48 h in DMEM deprived of glucose and containing galactose (4.5 g/l), 1 % FBS, 5 mM sodium pyruvate and 2 mM L-glutamine for the studies.

Immunofluorescence.

[0317] Cells cultured in 8-well chamber slides were washed with cold PBS, fixed in 4% formaldehyde, and permeabilized with 0.1% Triton X-100. After incubation with 2% normal goat serum (to block nonspecific staining), fixed cells were incubated overnight at 4°C with TOM20 antibody (1:500) (Santa Cruz, USA). Cells were washed with PBS and incubated for 60 minutes with FITC-conjugated

goat anti-rabbit IgG (1:500 dilution). The cells were then washed gently with PBS and counterstained with Hoechst 33342 (1:10,000 dilution, Molecular Probes) to visualize nuclei. The coverslips were mounted with Slow-fade anti-fade reagent (Invitrogen), and images were acquired at 60X using an All-in-One Fluorescence Microscope BZ-X700 (Keyence).

Mitochondrial health assays.

[0318] Cells were incubated with tetra-methyl-rhodamine methyl ester (TMRM, 25nM, Invitrogen) in HBSS (Hank's balanced salt solution) for 30 min at 37°C, per the manufacture's protocol, and the fluorescence was analyzed to measure mitochondrial membrane potential. All data were normalized with respect to the fluorescence intensity of control cells. To determine mitochondrial ROS production, cells were treated with 5μM MitoSOX™ Red, a mitochondrial superoxide indicator (Invitrogen) for 20 min at 37°C, according to the manufacturer's protocol, and fluorescence was analyzed using SpectraMax M2e (Molecular devices).

Autophagy assay.

[0319] Activation of autophagy was measured using the autophagy assay kit (Sigma Aldrich) according to the manufacturer's protocol, using SpectraMax M2e (Molecular devices) (λex = 333/λem = 518 nm).

EXAMPLE 6: EVOLUTIONARY DESIGN OF SMALL MOLECULE MITOFUSIN AGONISTS FOR IN VIVO USE

[0320] In vitro pharmacokinetic studies performed on the presently disclosed prototype small molecule mitofusin agonist, Regeneurin-S (S for the backbone sulfur; chimera B-A/I from Example 5), revealed it to be soluble, highly protein bound, stable in plasma, but rapidly degraded by liver microsomes (see e.g., **FIG. 45**). The solubility of 1, 20, and 200 mM solutions of compound in 50 mM phosphate buffer (pH 7.4) was assessed after 24 shaking. Plasma protein binding was measured using equilibrium dialysis; % bound = (1-[free compound in dialysate]/[total compound in retentate]) X 100. Plasma stability of 2 mM compound in clarified freeze-thawed plasma was assessed by LC-MS/MS of supernatants after protein precipitation; 120 min data are reported for studies including 0, 10, 30, 60, and 120 min. Microsome stability of 1 mM compound in liver microsomes (0.5 mg/ml)

after 0, 5, 10, 20, 30, 60 min. incubation was assessed by LC/MS/MS of reaction extracts.

[0321] Regeneurin-S was considered to have three functional domains corresponding to amino acid side chains of the prototype mitofusin agonist minipeptide it was designed to mimic: the methylated cyclohexane group corresponds to Mfn2 His380, the phenyl- and cyclopropyl-substituted triazol ring corresponds to Met376 and Val372, and the thioether backbone provides proper spacing (see Example 5) (see e.g., **FIG. 46**). According to this concept, a step-wise modification was performed of these functional domains to engineer subsequent generations of agonists having different functional and pharmacokinetic properties.

[0322] It was initially posited that oxidation of the backbone sulfur contributed to instability in the liver microsome assay. It was asked: (1) how does oxidation of this sulfur affect function (e.g., Regeneurin-S fusogenic function)? and (2) could replacing the backbone sulfur increase stability in the liver microsome test? Thus, the sulfoxide and sulfone by chemical oxidation of the parent thioether was generated (see e.g., **FIG. 47** top), and the ether and carbon backbone variants were synthesized de novo (see e.g., **FIG. 47** bottom). As illustrated in **FIG. 47**, neither oxidation nor substitution of the backbone sulfur altered fusogenicity, consistent with the backbone acting simply as a spacer to properly position the active terminal groups that mimic amino acid side chains of the prototype agonist peptide. Nor did any of the chemical changes greatly increase molecular stability in the microsome test. However, *Regeneurin-C/O*, having the carbon backbone and with tetrahydropyran substituted for the cyclohexyl group, exhibited enhanced microsomal stability and improved (decreased) plasma protein binding.

[0323] These results showed that the backbone sulfur of Renegeurin-S was neither function-critical, nor the basis for microsomal instability. The results also revealed a solution to microsomal instability evoked by the methylated cyclohexyl group. Recognizing that liver cytochrome P450 enzymes oxidize aromatic rings, such as the phenyl group on the triazol ring of the Regeneurin series of agonists, the structure-function relations of triazol ring group substitutions were next evaluated. In the pharmacophore model, the phenyl, cyclopropyl-substituted triazol ring mimics the hydrophobic side chains of Mfn2 Met376 and Val372 (see e.g., **FIG. 46**). Thus, the mitochondrial fusogenicity of 70 commercially available chemical variants were

compared, 17 of which differed exclusively in their triazol ring substitutions (see e.g., TABLE 7). Five compounds, all of which had a common chemical structure except for triazol ring substitutions, were fusogenic (see e.g., **FIG. 48**); one of these was previously described (designated as "Cpd B" above).

TABLE 7. 70 commercially available compounds evaluated.

ID	IUPAC Name	Structure
Cpd B	2-{2-[(5-cyclopropyl-4-phenyl-4H-1,2,4-triazol-3-yl)sulfanyl]propanamido}-4H,5H,6H-cyclopenta[b]thiophene-3-carboxamide	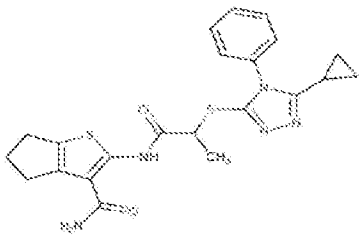
1 - G1	2-(2-{[4-(2-methylphenyl)-5-(pyridin-3-yl)-4H-1,2,4-triazol-3-yl]sulfanyl}acetamido)-4H,5H,6H-cyclopenta[b]thiophene-3-carboxamide	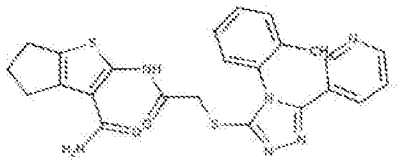
1 - F9	2-(2-{[5-cyclopropyl-4-(prop-2-en-1-yl)-4H-1,2,4-triazol-3-yl]sulfanyl}acetamido)-4,5,6,7-tetrahydro-1-benzothiophene-3-carboxamide	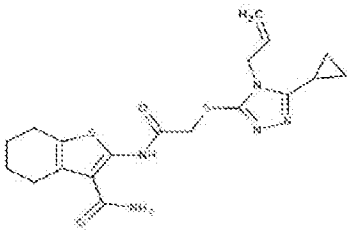
1 - G11	2-{2-[(5-cyclopropyl-4-ethyl-4H-1,2,4-triazol-3-yl)sulfanyl]acetamido}-4H,5H,6H-cyclopenta[b]thiophene-3-carboxamide	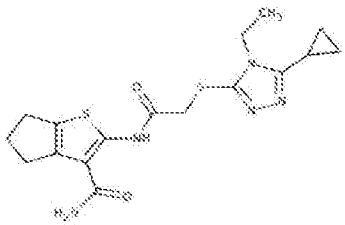
1 - B1	2-{2-[(4-methyl-5-phenyl-4H-1,2,4-triazol-3-yl)sulfanyl]acetamido}-4H,5H,6H-cyclopenta[b]thiophene-3-carboxamide	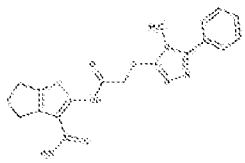

1 - F8	2-(2-{[4-cyclopropyl-5-(1H-indol-3-yl)-4H-1,2,4-triazol-3-yl]sulfanyl}propanamido)-4H,5H,6H-cyclopenta[b]thiophene-3-carboxamide	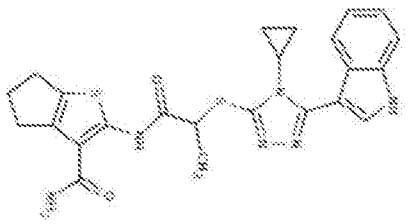
1 - H11	2-{2-[(4-benzyl-5-cyclopropyl-4H-1,2,4-triazol-3-yl)sulfanyl]acetamido}-4,5,6,7-tetrahydro-1-benzothiophene-3-carboxamide	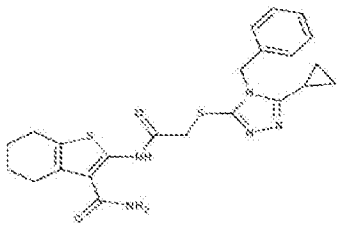
1 - F10	2-[2-({4-[(furan-2-yl)methyl]-5-(pyridin-3-yl)-4H-1,2,4-triazol-3-yl}sulfanyl)propanamido]-4H,5H,6H-cyclopenta[b]thiophene-3-carboxamide	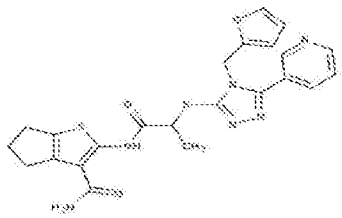
1 - F3	2-(2-{[5-methyl-4-(4-methylphenyl)-4H-1,2,4-triazol-3-yl]sulfanyl}acetamido)-4H,5H,6H-cyclopenta[b]thiophene-3-carboxamide	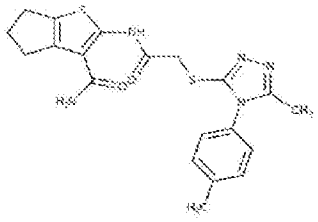
1 - C12	2-(2-{[4-cyclopropyl-5-(thiophen-2-yl)-4H-1,2,4-triazol-3-yl]sulfanyl}propanamido)-4H,5H,6H-cyclopenta[b]thiophene-3-carboxamide	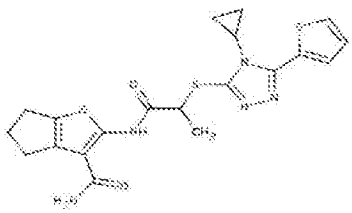
1 - E12	2-(2-{[4-(2-methylphenyl)-5-(pyridin-3-yl)-4H-1,2,4-triazol-3-yl]sulfanyl}acetamido)-4,5,6,7-tetrahydro-1-benzothiophene-3-carboxamide	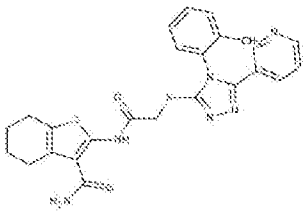

1 - H2	2-(2-{[5-(4-chlorophenyl)-4-methyl-4H-1,2,4-triazol-3-yl]sulfanyl}acetamido)-4H,5H,6H-cyclopenta[b]thiophene-3-carboxamide	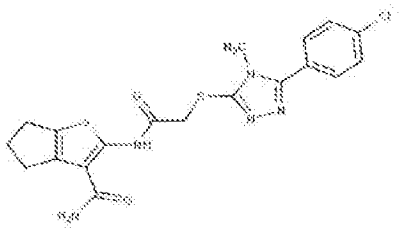
1 - B4	2-(2-{[4-methyl-5-(trifluoromethyl)-4H-1,2,4-triazol-3-yl]sulfanyl}acetamido)-4H,5H,6H-cyclopenta[b]thiophene-3-carboxamide	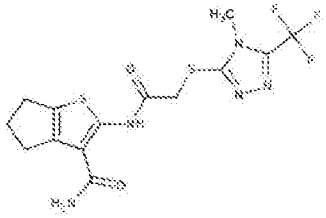
1 - H8	2-{2-[(diphenyl-4H-1,2,4-triazol-3-yl)sulfanyl]propanamido}-4H,5H,6H-cyclopenta[b]thiophene-3-carboxamide	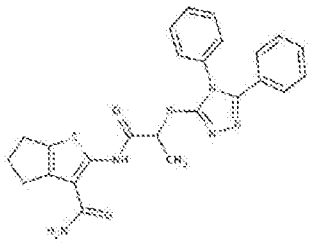
1 - D8	2-[2-({5-[(4-methoxyphenoxy)methyl]-4-methyl-4H-1,2,4-triazol-3-yl}sulfanyl)propanamido]-4H,5H,6H-cyclopenta[b]thiophene-3-carboxamide	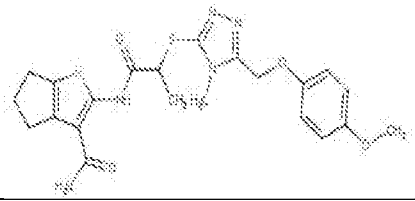
1 - D3	2-(2-{[5-methyl-4-(4-methylphenyl)-4H-1,2,4-triazol-3-yl]sulfanyl}acetamido)-4,5,6,7-tetrahydro-1-benzothiophene-3-carboxamide	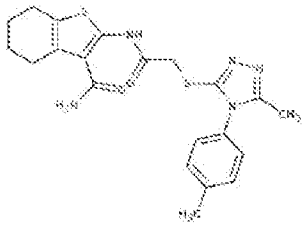
1 - F7	2-(2-{[4-phenyl-5-(thiophen-2-yl)-4H-1,2,4-triazol-3-yl]sulfanyl}propanamido)-4H,5H,6H-cyclopenta[b]thiophene-3-carboxamide	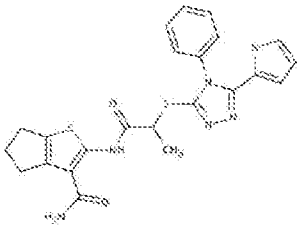

1 - H1	2-(2-{[4-(2-methylphenyl)-5-(pyridin-4-yl)-4H-1,2,4-triazol-3-yl]sulfanyl}acetamido)-4H,5H,6H-cyclopenta[b]thiophene-3-carboxamide	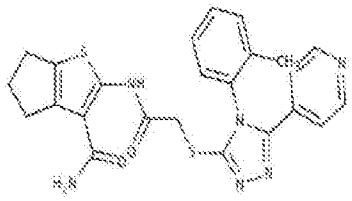
1 - B8	2-(2-{[5-(2-methylfuran-3-yl)-4-phenyl-4H-1,2,4-triazol-3-yl]sulfanyl}propanamido)-4H,5H,6H-cyclopenta[b]thiophene-3-carboxamide	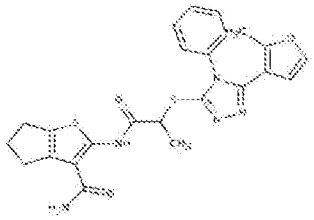
1 - C7	2-{2-[(4-benzyl-5-cyclopropyl-4H-1,2,4-triazol-3-yl)sulfanyl]propanamido}-4H,5H,6H-cyclopenta[b]thiophene-3-carboxamide	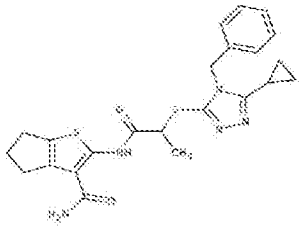
1 - D7	2-[2-({4-[(furan-2-yl)methyl]-5-phenyl-4H-1,2,4-triazol-3-yl}sulfanyl)propanamido]-4H,5H,6H-cyclopenta[b]thiophene-3-carboxamide	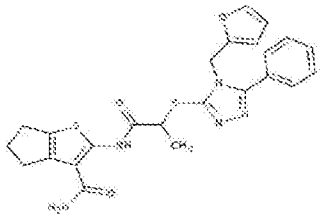
1 - D1	2-[2-({4-benzyl-5-[1-(dimethylamino)propyl]-4H-1,2,4-triazol-3-yl}sulfanyl)acetamido]-4H,5H,6H-cyclopenta[b]thiophene-3-carboxamide	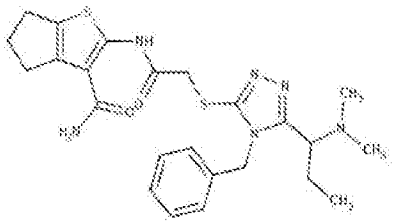
1 - E2	2-(2-{[4-(2-methoxyphenyl)-4H-1,2,4-triazol-3-yl]sulfanyl}acetamido)-4H,5H,6H-cyclopenta[b]thiophene-3-carboxamide	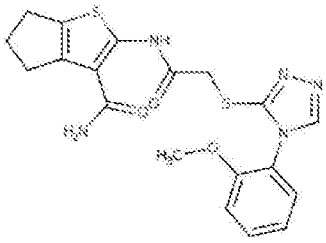

1 - F1	2-(2-{[5-(furan-2-yl)-4-phenyl-4H-1,2,4-triazol-3-yl]sulfanyl}acetamido)-4H,5H,6H-cyclopenta[b]thiophene-3-carboxamide	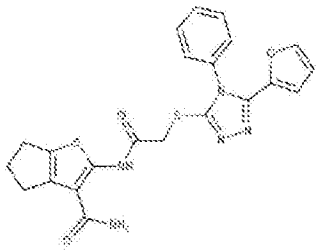
1 - H7	2-{2-[(5-benzyl-4-methyl-4H-1,2,4-triazol-3-yl)sulfanyl]acetamido}-4H,5H,6H-cyclopenta[b]thiophene-3-carboxamide	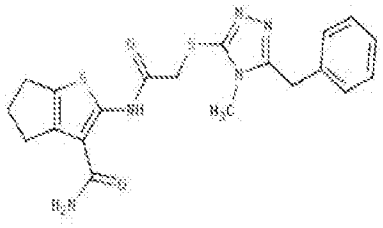
1 - D2	2-(2-{[4-(4-methoxyphenyl)-4H-1,2,4-triazol-3-yl]sulfanyl}acetamido)-4H,5H,6H-cyclopenta[b]thiophene-3-carboxamide	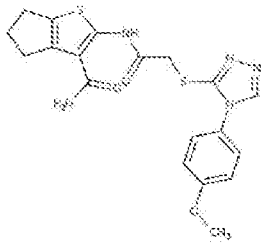
1 - F2	2-(2-{[5-phenyl-4-(prop-2-en-1-yl)-4H-1,2,4-triazol-3-yl]sulfanyl}acetamido)-4H,5H,6H-cyclopenta[b]thiophene-3-carboxamide	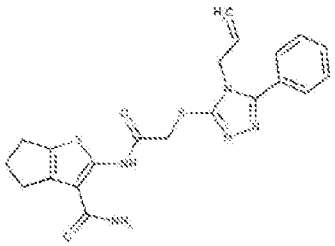
1 - B12	2-(2-{[4-(2-methoxyethyl)-5-(pyridin-4-yl)-4H-1,2,4-triazol-3-yl]sulfanyl}propanamido)-4H,5H,6H-cyclopenta[b]thiophene-3-carboxamide	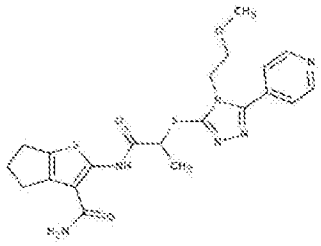
1 - A12	2-(2-{[4-phenyl-5-(piperidin-1-yl)-4H-1,2,4-triazol-3-yl]sulfanyl}propanamido)-4H,5H,6H-cyclopenta[b]thiophene-3-carboxamide	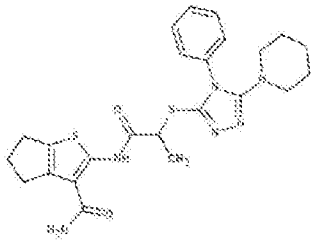

1 - H5	2-(2-{[4-(4-fluorophenyl)-5-(pyridin-4-yl)-4H-1,2,4-triazol-3-yl]sulfanyl}acetamido)-4H,5H,6H-cyclopenta[b]thiophene-3-carboxamide	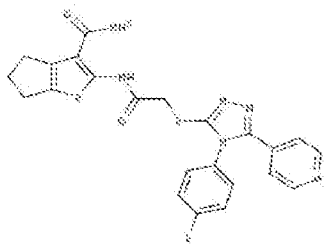
2 - A5	2-{2-[(dimethyl-4H-1,2,4-triazol-3-yl)sulfanyl]acetamido}-4H,5H,6H-cyclopenta[b]thiophene-3-carboxamide	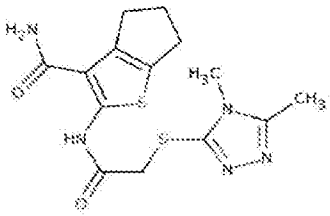
1 - E7	2-(2-{[4-methyl-5-(2-methylphenyl)-4H-1,2,4-triazol-3-yl]sulfanyl}acetamido)-4H,5H,6H-cyclopenta[b]thiophene-3-carboxamide	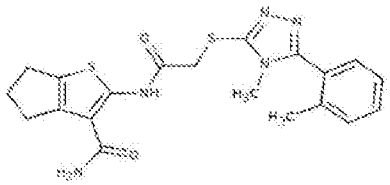
1 - A1	2-(2-{[5-(4-chlorophenyl)-4-ethyl-4H-1,2,4-triazol-3-yl]sulfanyl}acetamido)-4H,5H,6H-cyclopenta[b]thiophene-3-carboxamide	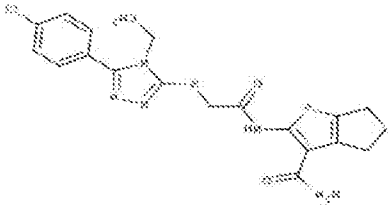
1 - C8	2-[2-({4-phenyl-5-[(thiophen-2-yl)methyl]-4H-1,2,4-triazol-3-yl}sulfanyl)acetamido]-4H,5H,6H-cyclopenta[b]thiophene-3-carboxamide	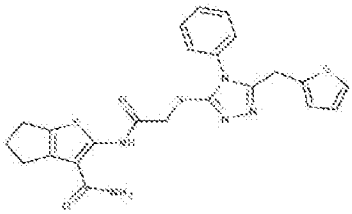
1 - E10	2-(2-{[1-(2,3-dimethylphenyl)-1H-imidazol-2-yl]sulfanyl}propanamido)-4H,5H,6H-cyclopenta[b]thiophene-3-carboxamide	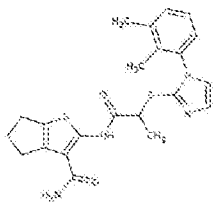

1 - G10	2-(2-{5H,6H,7H,8H,9H-[1,2,4]triazolo[4,3-a]azepin-3-ylsulfanyl}acetamido)-4,5,6,7-tetrahydro-1-benzothiophene-3-carboxamide	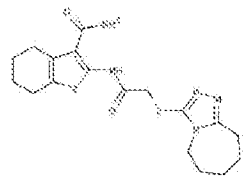
1 - G7	2-{2-[(1-benzyl-1H-imidazol-2-yl)sulfanyl]propanamido}-4H,5H,6H-cyclopenta[b]thiophene-3-carboxamide	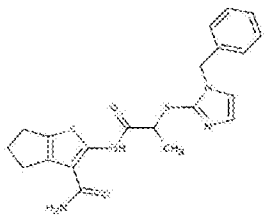
1 - C9	2-(2-{[4-methyl-5-(2-methylfuran-3-yl)-4H-1,2,4-triazol-3-yl]sulfanyl}propanamido)-4H,5H,6H-cyclopenta[b]thiophene-3-carboxamide	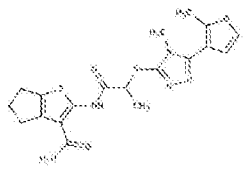
1 - G8	2-{2-[(4-phenyl-4H-1,2,4-triazol-3-yl)sulfanyl]propanamido}-4H,5H,6H-cyclopenta[b]thiophene-3-carboxamide	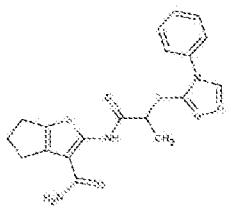
1 - E8	2-(2-{[1-(3-fluorophenyl)-1H-imidazol-2-yl]sulfanyl}propanamido)-4H,5H,6H-cyclopenta[b]thiophene-3-carboxamide	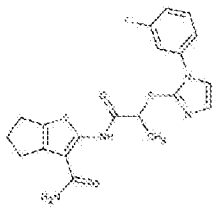
1 - D6	2-(2-{[5-(furan-2-yl)-4-phenyl-4H-1,2,4-triazol-3-yl]sulfanyl}propanamido)-4H,5H,6H-cyclopenta[b]thiophene-3-carboxamide	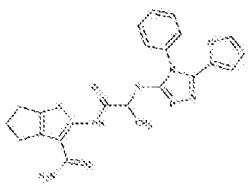

1 - B7	2-[2-({4-methyl-5-[(thiophen-2-yl)methyl]-4H-1,2,4-triazol-3-yl}sulfanyl)propanamido]-4H,5H,6H-cyclopenta[b]thiophene-3-carboxamide	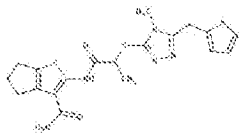
1 - C5	2-(2-{[4-(2-methylphenyl)-4H-1,2,4-triazol-3-yl]sulfanyl}acetamido)-4H,5H,6H-cyclopenta[b]thiophene-3-carboxamide	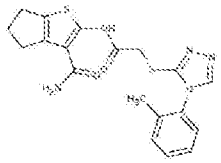
1 - D12	2-(2-{5H,6H,7H,8H,9H-[1,2,4]triazolo[4,3-a]azepin-3-ylsulfanyl}propanamido)-4H,5H,6H-cyclopenta[b]thiophene-3-carboxamide	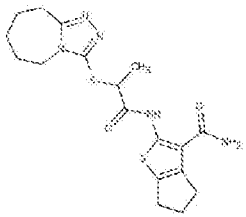
2 - A2	2-{2-[(dicyclopropyl-4H-1,2,4-triazol-3-yl)sulfanyl]acetamido}-4,5,6,7-tetrahydro-1-benzothiophene-3-carboxamide	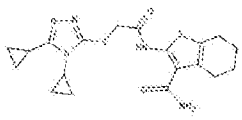
1 - G2	2-{2-[(diphenyl-4H-1,2,4-triazol-3-yl)sulfanyl]acetamido}-4,5,6,7-tetrahydro-1-benzothiophene-3-carboxamide	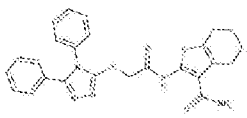
1 - E5	2-{2-[(5-cyclopropyl-4-phenyl-4H-1,2,4-triazol-3-yl)sulfanyl]acetamido}-4,5,6,7-tetrahydro-1-benzothiophene-3-carboxamide	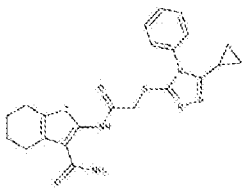

1 - A10	2-(2-{5H,6H,7H,8H,9H-[1,2,4]triazolo[4,3-a]azepin-3-ylsulfanyl}acetamido)-4H,5H,6H-cyclopenta[b]thiophene-3-carboxamide	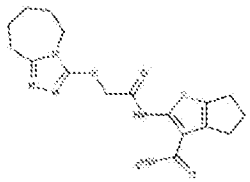
1 - D10	2-(2-{[5-(2-methylfuran-3-yl)-4-phenyl-4H-1,2,4-triazol-3-yl]sulfanyl}acetamido)-4H,5H,6H-cyclopenta[b]thiophene-3-carboxamide	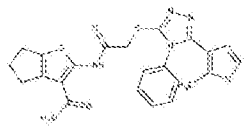
1 - F5	2-{2-[(5-cyclopropyl-4-ethyl-4H-1,2,4-triazol-3-yl)sulfanyl]acetamido}-4,5,6,7-tetrahydro-1-benzothiophene-3-carboxamide	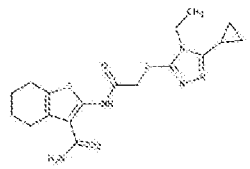
1 - F11	2-(2-{[4-phenyl-5-(pyridin-3-yl)-4H-1,2,4-triazol-3-yl]sulfanyl}acetamido)-4H,5H,6H-cyclopenta[b]thiophene-3-carboxamide	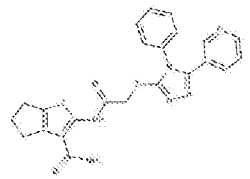
1 - G6	2-[2-({4-cyclopropyl-5-[(thiophen-2-yl)methyl]-4H-1,2,4-triazol-3-yl}sulfanyl)propanamido]-4H,5H,6H-cyclopenta[b]thiophene-3-carboxamide	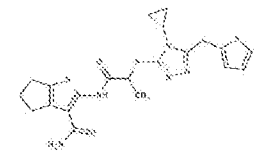
1 - G3	2-(2-{[4-phenyl-5-(pyridin-3-yl)-4H-1,2,4-triazol-3-yl]sulfanyl}acetamido)-4,5,6,7-tetrahydro-1-benzothiophene-3-carboxamide	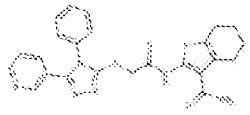

1 - F6	2-[2-({5-[1-(dimethylamino)ethyl]-4-(4-fluorophenyl)-4H-1,2,4-triazol-3-yl}sulfanyl)acetamido]-4H,5H,6H-cyclopenta[b]thiophene-3-carboxamide	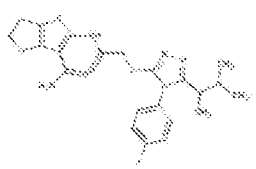
1 - A8	2-{2-[(5-benzyl-4-ethyl-4H-1,2,4-triazol-3-yl)sulfanyl]propanamido}-4H,5H,6H-cyclopenta[b]thiophene-3-carboxamide	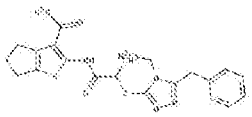
1 - H3	2-{2-[(5-methyl-4-phenyl-4H-1,2,4-triazol-3-yl)sulfanyl]acetamido}-4H,5H,6H-cyclopenta[b]thiophene-3-carboxamide	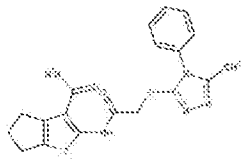
1 - E1	2-(2-{[5-cyclohexyl-4-(prop-2-en-1-yl)-4H-1,2,4-triazol-3-yl]sulfanyl}acetamido)-4H,5H,6H-cyclopenta[b]thiophene-3-carboxamide	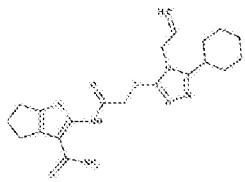
1 - C6	2-[2-({5-[(1,1-dioxo-1λ^6-thiolan-3-yl)methyl]-4-methyl-4H-1,2,4-triazol-3-yl}sulfanyl)acetamido]-4,5,6,7-tetrahydro-1-benzothiophene-3-carboxamide	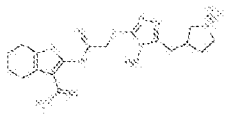
1 - A3	2-(2-{[5-(4-fluorophenyl)-4-methyl-4H-1,2,4-triazol-3-yl]sulfanyl}acetamido)-4H,5H,6H-cyclopenta[b]thiophene-3-carboxamide	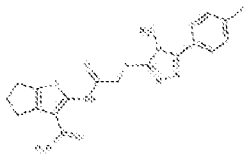

1 - H6	2-{2-[(5-benzyl-4-methyl-4H-1,2,4-triazol-3-yl)sulfanyl]propanamido}-4H,5H,6H-cyclopenta[b]thiophene-3-carboxamide	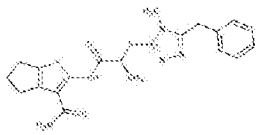
1 - E9	2-[2-({5-[(1,1-dioxo-1λ^6-thiolan-3-yl)methyl]-4-methyl-4H-1,2,4-triazol-3-yl}sulfanyl)propanamido]-4H,5H,6H-cyclopenta[b]thiophene-3-carboxamide	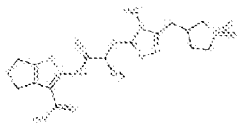
1 - A6	2-(2-{[4-ethyl-5-(2-methylfuran-3-yl)-4H-1,2,4-triazol-3-yl]sulfanyl}propanamido)-4H,5H,6H-cyclopenta[b]thiophene-3-carboxamide	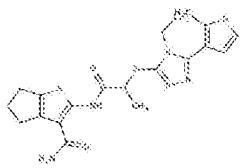
1 - C4	2-{2-[(4-phenyl-4H-1,2,4-triazol-3-yl)sulfanyl]acetamido}-4H,5H,6H-cyclopenta[b]thiophene-3-carboxamide	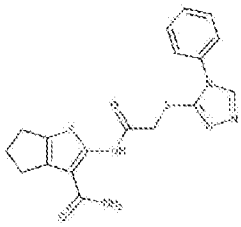
1 - F4	2-(2-{[4-(2-methoxyphenyl)-5-methyl-4H-1,2,4-triazol-3-yl]sulfanyl}acetamido)-4,5,6,7-tetrahydro-1-benzothiophene-3-carboxamide	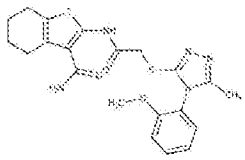
1 - D9	2-[2-({5-[(1,1-dioxo-1λ^6-thiolan-3-yl)methyl]-4-methyl-4H-1,2,4-triazol-3-yl}sulfanyl)acetamido]-4H,5H,6H-cyclopenta[b]thiophene-3-carboxamide	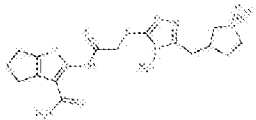

1 - A2	2-(2-{[4-cyclopropyl-5-(2-fluorophenyl)-4H-1,2,4-triazol-3-yl]sulfanyl}acetamido)-4H,5H,6H-cyclopenta[b]thiophene-3-carboxamide	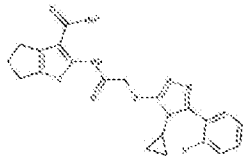
2 - A5	2-{2-[(dimethyl-4H-1,2,4-triazol-3-yl)sulfanyl]acetamido}-4H,5H,6H-cyclopenta[b]thiophene-3-carboxamide	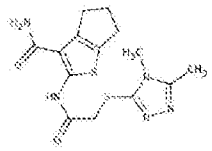
1 - C11	2-[2-({4-methyl-5-[(thiophen-2-yl)methyl]-4H-1,2,4-triazol-3-yl}sulfanyl)acetamido]-4H,5H,6H-cyclopenta[b]thiophene-3-carboxamide	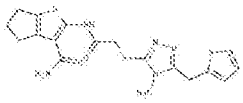
1 - C2	2-{2-[(4-benzyl-5-methyl-4H-1,2,4-triazol-3-yl)sulfanyl]acetamido}-4H,5H,6H-cyclopenta[b]thiophene-3-carboxamide	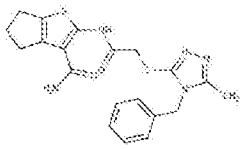
1 - A7	2-(2-{[1-(4-methoxyphenyl)-1H-imidazol-2-yl]sulfanyl}propanamido)-4H,5H,6H-cyclopenta[b]thiophene-3-carboxamide	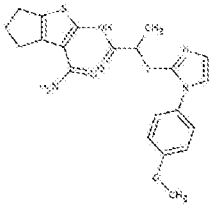

[0324] Two Cpd B chemosimilars, 1-G11 and 1-B1, were more potent and had greater resistance to liver microsomal degradation than their parent, Cpd B (see e.g., **FIG. 49**, TABLE 7). Because compound 1-G11 lacked aromatic groups on the triazol ring, having replaced an ethyl group for the phenyl group in Cpd B, the next series of chemical modifications introduced this configuration; this series of agonists were designated Mitolityns. Mitolityn-1 simply substituted an ethyl group for the

phenyl group of the triazol ring in Regeneurin-C, retaining the rest of its structure (see e.g., FIG. 50).

[0325] Because it was reasoned that the methylated cyclohexane group might also be susceptible to oxidation by liver cytochrome P450, additional modifications were engineered to remove the cyclohexane methyl group (Mitolityn-2), replace the methylated cyclohexane ring with a methylated tetrahydropyran ring (Mitolityn-3), and replace the methylated cyclohexane with an unmethylated tetrahydropyran ring (Mitolityn-4; corresponding to replacing the triazol phenyl group of Regeneurin C/O with an ethyl group. Finally Mitolityn-3 and –4 with methyl rather than ethyl groups on the triazol ring were synthesized (see e.g., FIG. 50). The Mitolityn series of compounds were then assayed for fusogenicity (increase in aspect ratio) and liver microsome stability (see e.g., FIG. 50).

[0326] Neither of the lead compounds in the presently disclosed structurally distinct series of mitofusin agonists, Mitolityn-4 or Regeneurin-C, exhibited cytotoxicity up to drug concentrations of 100 mM, which is more than 4 orders of magnitude greater concentration than their EC50 to stimulate mitochondrial fusion (see e.g., FIG. 51).

[0327] Notwithstanding similar fusogenic efficacies and lack of cytotoxicity, *in vitro* pharmacokinetic studies of the lead compounds revealed marked differences in plasma protein binding, liver microsome stability, and parallel artificial membrane permeability assay (PAMPA) (see e.g., FIG. 52). Like prototypical Regeneurin-S (see e.g., FIG. 2), Regeneurin-C was highly bound to plasma proteins, but rapidly degraded by liver microsomes, showed excellent passive diffusion across a lipid-infused artificial membrane (PAMPA), but was actively transported by P-gp/MDR1. These features suggested that this compound might not be effectively delivered to the central and peripheral nervous systems *in vivo*. Mitolityn-4 exhibited the reciprocal of these features, with low plasma protein binding, stability in the liver microsome assay, no passive diffusion across lipid membrane and therefore no reverse transport by P-gp. These features were also not conducive to central and peripheral nervous system delivery. Regeneurin C/O, however, had intermediate features, being modestly bound to plasma proteins, stable in the liver microsome assay, and exhibiting intermediate passive permeability and P-gp mediated reverse transport.

[0328] Preliminary *in vivo* pharmacokinetic studies revealed that the presently disclosed mitofusin agonists compounds are eliminated from the circulation within 2 hours of IV, IP, or IM administration (see e.g., **FIG. 5**3); IM administration provided the longest plasma half-time and bioavailability. For Regeneurin-C that is ~90% plasma protein bound (see e.g., **FIG. 52**), drug was undetectable 2 hours after IM administration, reflecting virtual absence of free drug. However, for Mitolityn-4 that is only 11.2% plasma protein bound in the mouse (see e.g., **FIG. 52**), total plasma drug concentration 2 hours after IM administration was 7.5 ng/ml, or ~6.66 ng/ml (~20 nM) free drug concentration, which is still several-fold greater than its EC50 of ~3 nM (see e.g., **FIG. 53**). Thus, *in vivo* efficacy for Mitolityn-4 was expected, but not Regeneurin-C, for at least 2 hours after a single IM injection.

[0329] The presently disclosed step-wise chemical evolution from first generation mitofusin agonists, Regeneurin-S (aka chimera B-A/I), Regeneurin-C, and Regeneurin-C/O, to second generation Mitolityns-4 and -6 revealed that the oxygen atom in the tetrahydropyran ring improved in vitro microsomal instability and reduced plasma protein binding relative to the parent 2-methylcyclohexyl group. Moreover, the structure-activity relationships of members of the Regeneurin and Mitolityn series of compounds refined the understanding of how these molecules mimic the prototype mitofusin agonist peptide: the cyclopropyl group extending from the triazol ring of Mitolityn-4 provides a hydrophobic interaction like that of Val372, whereas the tetrahydropyran ring on the opposite end of the molecule mimics both a ringed structure and hydrogen bond acceptor activity of His380.

[0330] Here, the optimization of Regeneurin C/O is shown, enhancing its stability and introducing features that will help it cross the BBB, by modifying it as shown in **FIG. 54**; these methods can be used to further synthesize optimized Regeneurins. Moreover, it is presently thought that substitution of the 3-cyclopropyl group on the 2,4,5 triazol ring with a structurally distinct moiety having similar hydrophobic characteristics should preserve the functional activity of the molecule, retain low plasma protein binding and microsomal stability, but have greater lipophilicity for blood- and nerve-brain barrier permeability. This approach was tested by synthesizing three additional mitofusin agonist candidates having a 3-phenyl replacing the 3-cyclopropyl group in the Mitolityn 2,4,5 triazol ring structure; this new series of Mfn agonists are called Fusogenins (see e.g., **FIG. 55**).

TABLE 8. Novel Regeneurin agonists.

Compound ID	IUPAC Name	Structure	M.W. (g/mol)	Formula
Regeneurin-C	1-(3-(5-cyclopropyl-4-phenyl-4H-1,2,4-triazol-3-yl)propyl)-3-(2-methylcyclohexyl)urea	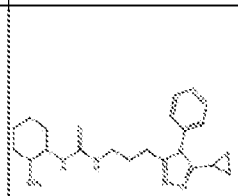	381.52	C22H31N5O
Regeneurin-O	1-(2-((5-cyclopropyl-4-phenyl-4H-1,2,4-triazol-3-yl)oxy)ethyl)-3-(2-methylcyclohexyl)urea	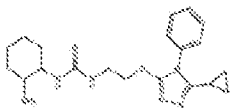	383.49	C21H29N5O2
Regeneurin-C/O	1-(3-(5-cyclopropyl-4-phenyl-4H-1,2,4-triazol-3-yl)propyl)-3-(tetrahydro-2H-pyran-4-yl)urea	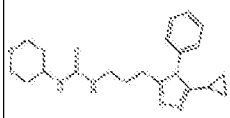	369.47	C20H27N5O2
Regeneurin-SO	1-(2-((5-cyclopropyl-4-phenyl-4H-1,2,4-triazol-3-yl)sulfinyl)ethyl)-3-(2-methylcyclohexyl)urea	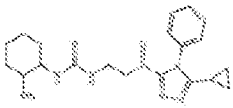	415.55	C21H29N5O2S
Regeneurin-SO_2	1-(2-((5-cyclopropyl-4-phenyl-4H-1,2,4-triazol-3-yl)sulfonyl)ethyl)-3-(2-methylcyclohexyl)urea	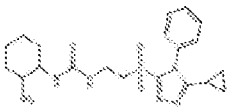	431.56	C21H29N5O3S

TABLE 9. Novel Mitolityn agonists.

Compound ID	IUPAC Name	Structure	M.W. (g/mol)	Formula
Mitolityn-1	1-(3-(5-cyclopropyl-4-ethyl-4H-1,2,4-triazol-3-yl)propyl)-3-(2-methylcyclohexyl)urea	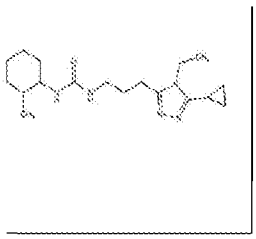	333.47	C18H31N5O
Mitolityn-2	1-cyclohexyl-3-(3-(5-cyclopropyl)-4-ethyl-4H-1,2,4-triazol-3-yl)propyl)urea	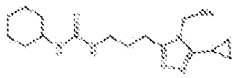	319.45	C17H29N5O
Mitolityn-3	1-(3-(5-cyclopropyl-4-ethyl-4H-1,2,4-triazol-3-yl)propyl)-3-(3-methyltetrahydro-2H-pyran-4-yl)urea	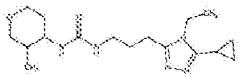	335.44	C17H29N5O2
Mitolityn-4	1-(3-(5-cyclopropyl-4-ethyl-4H-1,2,4-triazol-3-yl)propyl)-3-(tetrahydro-2H-pyran-4-yl)urea	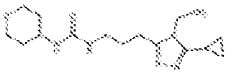	321.42	C16H27N5O2
Mitolityn-5 (Renamed after Fusogenin-4a)	1-(3-(5-cyclopropyl-4-methyl-4H-1,2,4-triazol-3-yl)propyl)-3-(3-methyltetrahydro-2H-pyran-4-yl)urea	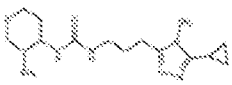	321.43	C16H27N5O2
Mitolityn-6 (Renamed after Fusogenin-3a)	1-(3-(5-cyclopropyl-4-methyl-4H-1,2,4-triazol-3-yl)propyl)-3-(tetrahydro-2H-pyran-4-yl)urea	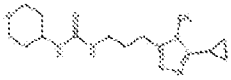	307.4	C15H25N5O2

TABLE 10. Novel Fusogenin agonists.

Compound ID	IUPAC Name	Structure	M.W. (g/mol)	Formula
Fusogenin-1	1-(3-(4-methyl-5-phenyl-4H-1,2,4-triazol-3-yl)propyl)-3-(2-methylcyclohexyl)urea	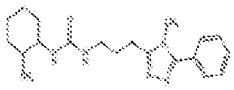	355.49	C20H29N5O
Fusogenin-3	1-(3-(4-methyl-5-phenyl-4H-1,2,4-triazol-3-yl)propyl)-3-(tetrahydro-2H-pyran-4-yl)urea	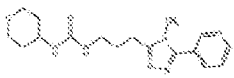	343.43	C18H25N5O2
Fusogenin-4	1-(3-(4-methyl-5-phenyl-4H-1,2,4-triazol-3-yl)propyl)-3-(3-methyltetrahydro-2H-pyran-4-yl)urea	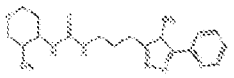	357.46	C19H27N5O2

EXAMPLE 7: PRE-CLINICAL STUDIES EVALUATING THE POTENTIAL EFFICACY OF MITOFUSIN AGONISTS IN CMT2A AND OTHER CHRONIC NEURODEGENERATIVE SYNDROMES

[0331] The following example shows mitofusin agonist effects on mitochondrial pathology in primary fibroblasts from human neurodegenerative disease patients.

[0332] High neuronal metabolic activity makes the neurological system uniquely susceptible to genetic mitochondrial damage. Oxidative stress is frequently invoked as the mechanism linking mitochondrial dysfunction to neurological diseases, but defective mitochondrial transport in long peripheral axons may contribute to neuronal vulnerability. For example, bioenergetic support of neuronal maintenance, repair and regeneration requires mitochondrial redistribution to sites of degeneration. Accordingly, it was examined whether the facilitory effects of the presently disclosed small molecule mitofusin agonist, Regeneurin-C, on mitochondrial trafficking, fusion, and polarization status would improve mitochondria

fitness in primary fibroblasts from human patients with a variety of mutations causing Amyotrophic lateral sclerosis (3 SOD1 gene mutations) Huntington's (HD gene CAG repeat numbers 40, 57, and 66), Parkinson's (Parkin, PINK, and LRRK2 gene mutations), and Alzheimer's diseases (3 PSEN1 gene mutations), as well as CMT2A (3 Mfn2 gene mutations). These studies show evidence that mitofusin agonists markedly enhance or improve mitochondrial function (e.g., trafficking) in ALS and confer a modest benefit in Huntington's disease (see e.g., **FIG. 56**, TABLE 11). FCCP treatment shows effects of complete mitochondrial uncoupling.

TABLE 11. Primary patient-derived fibroblasts used for Regeneurin-C studies

Subject ID	Fibrob ID	Diseases	Gender	Age	Genes	Mutation	Source	P
NDS00108	ND34730	Alzheimer's	M	-	PSEN1	GLU184ASP	NIH	4
NDS00114	ND34732	Alzheimer's	F	-	PSEN1	MET146ILE	NIH	4
NDS00115	ND34733	Alzheimer's	M	-	PSEN1	PRO264LEU	NIH	4
NDS00125	ND29415	ALS	M	51	SOD1	LEU144PRO	NIH	2
NDS00129	ND29523	ALS	M	47	SOD1	LEU38VAL	NIH	2
NDS00211	ND32969	ALS	M	59	SOD1	ILE113THR	NIH	8
NDS00090	ND33382	Huntington's	F	29	HD	CAG:57	NIH	2
NDS00093	ND29970	Huntington's	M	65	HD	CAG:40	NIH	2
NDS00189	ND40536	Huntington's	F	-	HD	CAG: 66	NIH	2
NDS00009	ND33879	Parkinson's	F	68	LRRK2	GLY2019SER	NIH	2
NDS00012	ND29969	Parkinson's	F	61	PARK2	ARG275TRP	NIH	2
NDS00228	ND40066	Parkinson's	M	64	PINK1	ILE368ASN	NIH	6
NDS00035	ND34769	Control	F	68	-	-	NIH	2
NDS00047	ND36320	Control	F	71	-	-	NIH	2
NDS00128	ND29510	Control	F	55	-	-	NIH	2
NDS00085	ND29178	Control	M	66	-	-	NIH	7
NDS00036	ND34770	Control	M	72	-	-	NIH	2
NDS00059	ND38530	Control	M	55	-	-	NIH	5
		CMT2A			MFN2	HIS361TYR	Baloh	
		CMT2A			MFN2	THR105MET	Baloh	
		CMT2A			MFN2	ARG274TRP	Barbara	2

Development of a preclinical mouse model of CMT2A

[0333] Multiple mouse knock-ins of human CMT2A Mfn2 mutations have not developed typical CMT2A neuropathology. High-level transgenic expression of human CMT2A Mfn2 mutants can cause pathology, but the phenotypes are not limited to the neurological system as in human disease. Because a suitable animal model of CMT2A did not exist a mouse was developed having conditional, motor-neuron-specific expression of human Mfn2 T105M (one of the CMT2A mutants used in the presently described in vitro and ex vivo studies (see e.g., Example 5)). Initial studies of these mice indicate that they develop progressive sciatic nerve CMAP

(compound motor action potential) abnormalities (decreased CMAP amplitude) accompanied by impaired neuromuscular function (Rotarod latency) (see e.g., **FIG. 57**). These features are characteristic of the human condition. Moreover, the efficacy of Regeneurin-S was already demonstrated to rapidly correct mitochondrial dysmotility in sciatic nerves of these mice (see e.g., Example 5). It was planned to use this model for *in vivo* assessment of mitofusin agonist efficacy for CMT2A. Standard mouse models for ALS suitable for in vivo efficacy studies are available from Jackson Labs (JAX). A target product profile is shown in TABLE 12, below.

TABLE 12. Preliminary target product profile for mitofusin agonists to treat CMT2A.

Product targets	Minimal acceptable result	Ideal result
Primary indication	Chronic therapy that retards progression of axonal neuropathy in CMT2A	Chronic therapy that reverses axonal neuropathy in CMT2A
Patient population	Children with a new genetic diagnosis of CMT2A and patients of all ages with genetically diagnosed mild to moderate CMT2A	Patients of all ages with mild to moderate genetically diagnosed CMT2A CMT Neuropathy Score <20
Treatment duration	Chronic	Chronic
Delivery mode	IM injection	Transdermal
Dosage form	Prefilled vials	Transdermal patch
Regimen	Once a week	Once a week
Efficacy	Delay in peripheral neuropathy progression over 3 years compared to placebo, assessed by slower increase in modified composite CMT Neuropathy Score*	Reversal or absence of progression of peripheral neuropathy compared to placebo, as indicated by lower or stable modified composite CMT Neuropathy Score*
Risk/side effect	Devoid of local injection effect and clinically meaningful CNS, cardiac or muscular side effects	Devoid of local patch effect and any systemic side effects
Therapeutic modality	Small molecule peptidomimetic	Small molecule peptidomimetic

*Mannil M et al *Neuromuscul Disord* 24:1003-17, 2014

EXAMPLE 8: IN VIVO ADMINISTRATION OF REGENEURIN-C/O REVERSES THE CHARACTERISTIC MITOCHONDRIAL IMMOBILITY IN SCIATIC NERVE AXONS

[0334] The following example describes in vivo administration of Regeneurin-C/O to CMT2A mice (IM, 2 mg/kg) reverses the characteristic mitochondrial immobility in sciatic nerve axons (assessed 4 hours later).

[0335] 10 week old CMT2A MFN2 T105M mice were injected IM with Mfn agonist Regeneurin-C/O 2 mg/kg twice, or vehicle. Sciatic nerve mitochondrial motility was measured 4 hours later. Results described in **FIG. 58** are for 2

CMT2A mice per group. As demonstrated herein, these mitofusin agonists can correct mitochondrial motility.

Example 9: Treatment of Crush Injury

[0336] Crush injury models are well known in the art. Any model for crush injury can be used (see e.g., Dobek et al. Comp Med. 2013 Jun;63(3):227-32; Jager et al., BioMed Research International, Volume 2014 (2014)).

[0337] Administration of the mitofusin modulatory agents can be as described in the preceding examples.

[0338] Although neuronal regeneration is a highly energy-demanding process, axonal mitochondrial transport progressively declines with maturation. Mature neurons typically fail to regenerate after injury. Reduced mitochondrial motility and energy deficits in injured axons are intrinsic mechanisms controlling regrowth in mature neurons (see e.g., Zhou et al. 2016 J. Cell Biol. Facilitation of axon regeneration by enhancing mitochondrial transport and rescuing energy deficits). Axotomy induces acute mitochondrial depolarization and ATP depletion in injured axons. Thus, mature neuron-associated increases in mitochondria-anchoring protein syntaphilin (SNPH) and decreases in mitochondrial transport cause local energy deficits. Enhancing mitochondrial transport via administration of mitofusion modulatory agents is expected to facilitate regenerative capacity by replenishing healthy mitochondria in injured axons, thereby rescuing energy deficits. An in vivo sciatic nerve crush study is expected to show that enhanced mitochondrial transport in accelerates axon regeneration.

[0339] Although mitochondrial transport in axons progressively declines with neuron maturation, axonal injury triggers an acute stress signal that depolarizes local mitochondria, leading to energy deficits near the injured site. Thus, maintaining a local ATP supply via recruiting healthy mitochondria into injured axons is critical to meet the enhanced metabolic requirements during axonal regeneration. Enhancing mitochondrial transport not only helps remove those injury-damaged mitochondria, but also replenishes healthy ones in the injured axons, thus recovering mitochondrial integrity and reversing energy deficits. This cellular process is critical for mature neurons to facilitate their regeneration after injury. Therefore, the study will provide new insights as to how using mitofusin modulatory agents (e.g., peptides, peptide mimetics, agonists) for regeneration. Thus, enhancing mitochondrial transport is one

of the potential new therapeutic strategies to stimulate axon regeneration in the injured CNS and PNS.

Activated mitofusin mobilizes mitochondria in damaged axons to promote nerve regeneration

[0340] Mitochondria generate chemical fuel to sustain neuronal activity. Bioenergetic support of neuronal repair after physical or genetic damage requires active mitochondrial transport through axons to sites of injury or degeneration [1,2]. Impaired mitochondrial trafficking may therefore contribute to the unique susceptibility of neurons to mitochondrial dysfunction and meager neuronal regeneration [3-6]. However, a causal relationship between mitochondrial dysmotility and ineffectual neuron renewal has not been proven, in part because pharmacological agents that promote subcellular mitochondrial transport are lacking. Here, we show that newly described allosteric mitofusin (MFN) agonists stimulate axonal transport of mitochondria and evoke neuronal regrowth after genetic damage or traumatic injury. In addition to stimulating mitochondrial fusion, MFN activation provoked MIRO1-Milton interactions required for mitochondrial transport, enhanced overall mitochondrial and cellular fitness in cells from Charcot Marie Tooth (CMT) type 2A, Huntington disease, and amyotrophic lateral sclerosis (ALS) patients, and strikingly accelerated regrowth of normal or genetically impaired mouse neurons after *in vitro* and *in vivo* traumatic injury. These results mechanistically and therapeutically link mitochondrial fitness and trafficking to neuronal repair and regeneration, uncovering a pivotal regulatory role for mitofusins in mitochondrial hitchhiking aboard the subcellular transport apparatus. Allosteric mitofusin activation shows clinical promise not only for diseases primarily caused by loss-of-function *MFN2* mutations, but as adjunctive therapy for other neurodegenerative conditions wherein mitochondrial damage is contributory, and in millions of otherwise normal individuals who suffer from accidental or iatrogenic traumatic nerve damage.

[0341] Mitochondrial transiting along neuronal axons requires organellar attachment to molecular motors. Thus, mitochondrial MIRO proteins bind to the adaptor protein Milton to anchor organelles to kinesin or dynein on microtubules [7,8]. Although the significance is unclear, MIRO proteins also form complexes with outer mitochondrial membrane mitofusins (MFN) 1 and 2 [3], so designated because they promote mitochondrial fusion [9]. The fusogenic activity of mitofusins depends in part

upon conformational shifts controlled by intra-molecular peptide-peptide interactions [10]. Allosteric MFN activation with competing minipeptides or small molecule peptidomimetics disrupts the critical peptide-peptide interactions that maintain mitofusins in an inactive state, thereby augmenting both mitochondrial fusion and trafficking [6,10].

[0342] We posited that increased mitochondrial motility after allosteric mitofusin activation[6] resulted from enhanced MFN2-MIRO1 interactions. In support of this notion, an MFN2 mutant (MFN2 Met376Ala) with impaired conformational activation, but normal GTPase activity [6] (**FIG. 59A**), bound MIRO1 less effectively than either wild-type MFN2 or the Charcot-Marie-Tooth disease (CMT) GTPase-defective mutant, MFN2 Arg94Gln [11,12] (**FIG. 59A, FIG. 59B)**. Allosteric mitofusin activation with Regeneurin S (identical to Chimera B/A-I[6]) restored defective MFN2 Met376Ala-mediated mitochondrial fusion (**FIG. 59C, FIG. 63-FIG. 65**), but did not correct MFN2 Met376Ala-MIRO1 complex formation (**FIG. 59D**), likely because mitofusins were not stable components of MIRO1-Milton complexes (**FIG. 59E**). However, MIRO1-Milton complex formation both required mitofusins and was enhanced by mitofusin activation with Regeneurin (**FIG. 59E**). Collectively, these findings revealed that allosteric MFN2 activation facilitates, but does directly participate in, MIRO1-Milton-interactions that mediate mitochondrial motility. This mechanism implies that mitofusin agonists have the capacity to stimulate both mitochondrial fusion and trafficking.

[0343] Abnormal mitochondrial fusion and trafficking are hallmarks of genetically diverse neurodegenerative diseases, and mitofusin overexpression in experimental models of CMT2, amyotrophic lateral sclerosis (ALS) [13,14], Alzheimer's disease [15], or Huntington disease [14] can reverse mitochondrial abnormalities. We asked if pharmacological mitofusin activation would restore mitochondrial fitness in neurodegenerative conditions like these not caused by primary MFN2 mutations. Accordingly, we compared mitochondrial structure and polarization status as a function of mitofusin agonist Regeneurin C treatment (**FIG. 66**) in primary human fibroblasts from patients with Parkinson's disease (*PARK2* Arg275Trp, *PINK1* Ile368Asn, and *LRRK2* Gly2019Ser mutations), Huntington disease (HD; *HTT* CAG repeat number of 40, 57, and 66), Alzheimer's disease (*PSEN1* Met146Ile, Glu184Asp, and Pro264Leu mutations), ALS (*SOD1* Leu38Val, Ile113Thr, and

Leu144Pro mutations), and CMT2 (*MFN2* Thr105Met, Arg274Trp, and His361Tyr mutations) (**FIG. 117**). As with mouse cells expressing recombinant human CMT2 MFN2 mutants (**FIG. 63, FIG. 64**), and regardless of specific *MFN2* genotype, pharmacological mitofusin activation reversed mitochondrial fragmentation and depolarization in primary human CMT2 fibroblasts (**FIG. 60A-FIG. 60F**; **FIG. 67**). Mitochondrial dysmorphology was mild and not meaningfully affected by Regeneurin in Parkinson's and Alzheimer's disease fibroblasts (**FIG. 60A-FIG. 60F; FIG. 69 and FIG. 70**) (although mitofusin activation improved mitochondrial depolarization in *PINK1* and *PARK2* mutant Parkinson's disease cells; **FIG. 69**). By contrast, modest mitochondrial dysmorphology and depolarization in Huntington disease cells, and severe mitochondrial fragmentation and loss of polarization in ALS cells, were reversed by mitofusin activation (**FIG. 60A-FIG. 60F; FIG. 71 and FIG. 72**). Increased autophagy, a marker of general cellular dysfunction [16] observed in ALS, Huntington disease and CMT2 fibroblasts, was also reduced by Regeneurin treatment (**FIG. 60C**; **FIG. 68-FIG. 73**).

[0344] The above data support a model wherein multiple potential benefits of mitofusin activation, i.e. enhancing mitochondrial fusion/fitness, reducing autophagy, and promoting mitochondrial trafficking [6,10,17], can negate mitochondrial pathology in genetically and mechanistically heterogenous neurodegenerative diseases. Because mitochondrial fitness and subcellular redistribution are also central to neuronal repair and regeneration after physical injury [1,2,4], we predicted that mitofusin activation would likewise improve post-traumatic neuron regeneration. As anticipated, freshly cultured adult mouse dorsal root ganglion (DRG) neurons in which mitofusins were activated using either a small molecule (Regeneurin) or peptide (TAT-HR1 374-384 [6,10]) mitofusin agonist exhibited accelerated axonal regrowth (**FIG. 61A, FIG. 74 and FIG. 75**) and longer axons (**FIG. 61B**). Mitochondrial localization at axon termini and an increase in the number and aspect ratio of axonal mitochondria in normal (**FIG. 61C, 3d**) and CMT (MFN2 T105M) mouse DRGs (**FIG. 61E**) suggested that mitofusin activation improved mitochondrial transport within regenerating axons. Indeed, Regeneurin treatment stimulated both axonal outgrowth and mitochondrial motility in mitochondrial dynamism-impaired CMT2A DRG neurons (**FIG. 61F**). By contrast, axon outgrowth and reduced mitochondrial fragmentation provoked by forskolin, which mimics neurotropic factor

cAMP signaling and inhibits DRP1, was not associated with improved mitochondrial movement in CMT2A neurons (**FIG. 61E, FIG. 61F**).

[0345] The ability of activated mitofusins to accelerate axon regeneration in normal and diseased mouse neurons, and to improve mitochondrial and cellular fitness in genetically diseased human fibroblasts, suggested concordance of mitochondrial pathologies underlying traumatic and genetic injury. Supporting this notion, aspiration axotomy of normal embryonic mouse cortical axons (**FIG. 62A, FIG. 62B**) provoked mitochondrial abnormalities (**FIG. 62C**) similar to those induced by CMT2 (MFN2 Thr105Met) [6] or ALS (SOD1 Gly93Ala) [18] mutations. Moreover, mitofusin activation with Regeneurin both moderated these abnormalities and stimulated axon regrowth (**FIG. 62A-FIG. 62D**).

[0346] CMT2A and ALS are rare, each having an estimated prevalence of no more than 0.01%. By contrast, 1-3% of all individuals suffering trauma from vehicle accidents, sports injuries, or occupational mishaps will suffer peripheral nerve damage requiring therapeutic intervention [19,20]. To extend our *in vitro* finding that mitofusin activation enhances neuronal regeneration to the *in vivo* context it was necessary to chemically modify Regeneurin to retard hepatocellular degradation and reduce plasma protein binding, thus producing the structurally distinct but equipotent mitofusin agonist, Mitolityn (**FIG. 76 and FIG. 77**Mitolityn was slowly released from a biocompatible protein matrix (**FIG. 78**), providing for extended local release of the mitofusin agonist at the site of nerve injury. In a blinded, placebo-controlled pre-clinical *in vivo* study, Mitolityn gel applied to CMT2A mouse sciatic nerves after standardized crush injury accelerated neuroelectrophysiological recovery (**FIG. 62E, FIG. 62F**) and increased histological evidence of neuronal regrowth (**FIG. 62G)**.

[0347] Our results mechanistically link MFN2 activation, subcellular mitochondrial transport, and neuronal regeneration. Defective mitochondrial trafficking was previously implicated in CMT2[21], but the ability of CMT2 GTPase domain MFN2 mutant proteins to bind MIRO1[3] argued against a causal relationship. Our studies confirm the prior observation, but resolve the paradox by proving it is the ability of MFN2 protein to achieve a favorable conformation, rather than catalytic GTPase activity, that drives MFN2-MIRO1 binding, MIRO-Milton interactions, and mitochondrial transport. The observation that 3 different mitofusin agonists (a peptide and two structurally distinct small molecules) promote neuronal growth supports a

key role for mitofusins in the neuroregenerative process. Because MFN2 was not observed in MIRO1-Milton complexes, we envision that conformationally active MFN2 binding to MIRO1 transiently promotes associations between MIRO1 and Milton without becoming a stable interacting partner (**FIG. 79**).

Peripheral neurons are uniquely handicapped by elongated axonal morphology that entails robust mechanisms for mobilizing healthy mitochondria to, and removing their damaged counterparts from, areas of physical damage or genetic degeneration. It is therefore reasonable that allosteric mitofusin activation, which simultaneously promotes mitochondrial mobilization, enhances mitochondrial fusion, and improves mitochondrial fitness, affords a therapeutic "triple threat" in genetic or traumatic peripheral nerve injury. Indeed, forced MFN1 or MFN2 expression has previously been proposed as a means of restoring fragmented and dysfunctional mitochondria in neurodegenerative disorders, although the underlying rationales largely ignored mitochondrial trafficking [12,13-15,22,23]. However, formidable challenges would have to be overcome before any form of MFN gene therapy could be clinically translated, including assuring proper gene targeting and dosing, and overcoming patient and physician resistance of the inherent limited ability to discontinue or reverse gene therapy via viral vectors. Pharmacological mitofusin activation avoids these shortcomings, thus opening doors to directly correcting mitofusin deficiency in CMT2, to generally supporting mitochondrial function and transport in ALS and Huntington disease, and to promoting neuronal repair and regeneration after traumatic nerve injury.

Methods of Example 9

Mouse lines

[0348] Rosa-STOP-mMFN Thr105Met (T105M) mice (C57BL/6 Gt(ROSA)26 Sortm1 (CAG-MFN2*T105M)Dple/J) from The Jackson Laboratory (Bar Harbor, Maine, USA; Stock No: 025322) were crossed to HB9-Cre mice (B6.129S1-Mnx1tm4(cre)Tmj/J) from The Jackson Laboratory (Stock No: 006600) to generate motor neuron-targeted MFN2 T105M mice as described [6]. SOD1-Gly93Ala (G93A) transgenic mice (B6SJL-Tg(SOD1*G93A)1Gur/J) were obtained from The Jackson Laboratory (Stock No: 002726). All surgical and experimental procedures were approved by the Washington University in St. Louis, School of Medicine Animal Studies Committee; protocol number 20160276.

Cultured cells

[0349] **Normal mouse embryonic fibroblasts (MEFs)** were prepared by enzymatic dissociation from embryonic day 13.5-14.5 C57BL/6J mice (The Jackson Laboratory Cat:# 000664). *Mfn2* null and *Mfn1/Mfn2* double null MEFs and NIH 3T3 fibroblasts were purchase from American Type Culture Collection (ATCC Manassas, Virginia, USA) (CRL-2994, CRL-2993, and CRL-1658 respectively). MEFs were cultured at 37°C, 5% CO2-95% air in Dulbecco's minimal essential medium (DMEM) containing glucose (4.5 g/l) with 10% (v/v) fetal bovine serum (FBS; Gibco, Gaithersburg, Maryland, USA Cat:# 26140-079), 1x nonessential amino-acids (Gibco Cat:# 11130051), 2 mM L-glutamine (Corning, NewYork, USA. Cat:# 34717007), and 1% (v/v) penicillin/streptomycin (Gibco Cat:# 15140-122). All cells were PCR-tested and found to be mycoplasma-free. Mitofusin expression profile of MEFs was validated by immunoblotting (**FIG. 80**).

[0350] **Neonatal mouse cortical neurons** were isolated from individual postnatal day 1 C57BL/6J Gly93Ala mice by papain digestion and mechanical dispersion as described [24]. Briefly, mouse brain cortices were isolated under a dissecting microscope and sliced into 0.5-1 mm thick sections in Leibovitz's L-15 Medium (Gibco Cat:#11415-064) containing BSA (0.23mg/ml, Sigma Cat:#A7030). Papain (1mg/ml, Sigma Cat:#P4762) was added and the tissue digested for 20 min at 37°C. The papain solution was replaced and micropipettes used to triturate the solution until no more tissue was visible. Culture of cortical cells in microfluidic neuron XonaChip chambers and aspiration axotomy methodology is described below.

[0351] **Adult mouse dorsal root ganglion (DRG) neurons** were prepared from 8 week-old C57BL/6J mice as described [25]. Briefly, DRGs were isolated from lumbar roots 1-6 in ice cold Hank's Balanced Salt Solution (HBSS) (Gibco Cat:#14025-076) supplemented with Hepes (pH 7.4) (Gibco Cat:#15630080). Neurons were dissociated by step-wise papain digestion (1mg/ml, Worthington Biochemical, Lakewood, NJ, USA Cat:# LS003126) for 20 min at 37°C and collagenase digestion (14.5 mg/ml, Worthington Biochemical, Lakewood, NJ, USA Cat:# 41J12861) for 20 min at 37°C, followed by trituration through a P1000 pipette tip ~30 times. Dissociated cells were plated on 12-well slide dishes (BD Bioscience, Missisauga, ON, Canada) coated with Poly-d-Lysine (Sigma Aldrich Cat:# P7886) and laminin (Sigma Aldrich Cat:# L2020) and cultured in Gibco Neurobasal-A

medium supplemented with 2% B-27. DRG neurons were distinguished from non-neuronal cells by positive staining with anti-β-III tubulin.

[0352] **Primary human fibroblasts** from CMT2A patients (MFN2 Thr105Met and MFN2 His361Tyr) were from Dr. Robert Baloh (Department of Neurology, Cedars-Sinai Medical Center, Los Angeles, CA USA). Primary human fibroblasts from a CMT2A patient (MFN2 Arg274Trp) [26] were from Dr. Barbara Zablocka (Mossakowski Medical Research Centre, Polish Academy of Sciences, Warsaw, Poland). Primary human Parkinson disease (PARK2 Arg275Trp:ND29969, PINK1 Ile368Asn:ND40066, LRRK2 Gly2019Ser:ND33879), Huntington disease (*HTT* CAG repeat #40:ND29970, #57:ND33392, #66:ND40536), Alzheimer's disease (PSEN1 Met146Ile:ND34732, Glu184Asp:ND34730, Pro264Leu:ND34733), and amyotrophic lateral sclerosis (SOD1 Leu38Val:ND29523, Ile113Thr:ND32969, Leu144Pro:ND29415) patient fibroblasts and primary fibroblasts of control individuals (CTL1:ND34769, CTL2:ND36320, CTL3:ND29510, CTL4:ND29178, CTL5:ND34770) were purchased from the NINDS Human Cell and Data Repository, National Institutes of Health, USA. Human fibroblasts were maintained in DMEM supplemented with 15% (v/v) FBS and 1% (v/v) penicillin/streptomycin at 37°C in 5% CO2-95% air. Prior to live-cell studies fibroblasts were plated on glass coverslips and transitioned to no glucose DMEM (Thermo Fisher Scientific, Waltham, Massachusetts, USA; Catalog No: A1443001) with 4.5g/l galactose (Sigma Aldrich Catalog No: SLBP0699V) substituted for glucose, 1% FBS, 5 mM sodium pyruvate (Thermo Fisher Scientific, Catalog No: 11360-070) and 2mM L-glutamine (Corning, NewYork, USA; Catalog No: 34717007). Patient details and passage numbers of primary fibroblasts used in these studies are reported in **FIG. 117**.

Viral vectors

[0353] Adenoviral (Ad) vectors expressing human FLAG-MFN2 [17], rat Mfn2 Lys109Ala [10] human FLAG-MFN2 Met 376Ala [6], LC3-GFP [6], and lentivirus expressing MFN2 Arg94Gln [21] have been previously described. Ad-FLAG-MFN2 Arg94Gln was generated by PCR mutagenesis of human FLAG-MFN2 using (mutant nucleotide underlined):

MFN2 Arg94Gln forward primer: 5'- gtgaggtgctggctc<u>a</u>gaggcacatgaaagt -3'

MFN2 Arg94Gln reverse primer: 5'- actttcatgtgcctc<u>t</u>gagccagcacctcac -3'

[0354] Sanger sequencing verified correct mutagenesis and absence of unintended sequence variation within the end product. The adenoviral MFN2 Arg94Gln vector was prepared at Vector Biolabs (Malvern, PA, USA).

[0355] Adenoviri expressing β-galactosidase (Ad-CMV-β-Gal; #1080), human Milton1 (Ad-h-TRAK1; #ADV-226338) and human Miro1 (Ad-h-RHOT1; #ADV-221196) were purchased from Vector Biolabs. Adenovirus expressing mitochondrial-targeted green fluorescent protein (Ad-mito-GFP) was purchased from Vigene Biosciences (Rockville, MD, USA). Ad-LC3-GFP was a gift from Dr. Lorrie Kirshenbaum, University of Manitoba, Canada. Live adenovirus titers were determined using the AdEasy Viral Titer Kit (#972500; Agilent Technologies, Cedar Creek, TX, USA). Unless otherwise stated, viral vectors were added to cells at a multiplicity of infection (MOI) of 50.

Antibodies

[0356] Mouse monoclonals anti-mitofusin 2 (ab56889 - 1:1000), anti-VDAC1 (ab14734 - 1:1000), and anti MIRO1 (ab188029 1:1000) were from AbCAM (Cambridge, MA, USA). Monoclonal mouse anti-β-actin (sc-47778 - 1:2000) and anti-mitofusin 1 (sc-50330) were from Santa Cruz Biotechnology (Dallas, TX, USA). Rabbit anti-TRAK1 (Milton) was from Sigma-Aldrich (HPA005853). Rabbit polyclonal anti-GAP 43 (Cat:# AB5200) was from EMD Millipore (Burlington, MA, USA). Rabbit polyclonasl anti-Stathmin-2 (SCGN10; cat # NBP1-49461) was from Novus Biologicals (Littleton, CO, USA) Mouse monoclonal anti-∟-tubulin III (801201- 1:500) was from Biolegend (San Diego, CA, USA). Peroxidase-conjugated anti-mouse IgG (#7076S - 1:1000) was from Cell Signaling (Danvers, MA, USA). Goat anti-rabbit IgG (Spicier reactivity Goat, Host/Isotype Rabbit/IgG; #31460) and Alexa-Fluor 488 Goat anti-mouse IgG were from ThermoFisher (Waltham, MA, USA Cat: #A11029).

Live cell mitochondrial imaging studies

[0357] Live cell studies assessing mitochondrial morphology and polarization status were performed essentially as described [6,10]. MEFs and human fibroblasts were triple-stained with MitoTracker Green (200 nM; Invitrogen, Thermo Fisher Scientific Cat:# M7514) to visualize mitochondria, tetramethylrhodamine ethyl ester (TMRE, 200 nM, Invitrogen Thermo Fisher Scientific Cat:# T-669) that labels mitochondrial with intact polarization of the mitochondrial inner membrane, and Hoechst (10 mg/ml; Invitrogen, Thermo Fisher Scientific Cat:# H3570) that stains

nuclei blue. Mitochondria of cultured neurons were visualized after transduction with ad-mito-GFP 48 hours prior to study and TMRE staining 30 minutes prior to imaging. Autophagy was assessed in primary human fibroblasts after transduction with Ad-LC3-GFP 48 hours prior to visualization.

[0358] Images were acquired at room temperature on a Nikon Ti Confocal microscope using either a 60X1.3 NA oil- immersion objective or 10X0.3 NA dry objective, in Krebs-Henseleit buffer (138 NaCl, 3.7 nM KCL, 1.2 n M KH2PO4, 15 nM Glucose, 20 nM HEPES pH: 7.2-7.5, and 1mM CaCl2) or HBSS for live cell experiments . Laser excitation was 488 nm with emission at 510 nm for MitoTracker Green, Ad-Mito GFP and Ad-LC3 GFP. Laser excitation was 549 nm with emission at 590 nm for TMRE. Laser excitation was 306 nm with emission 405 nm for Hoecsht and DAPI. In some instances, as needed for standardization, the brightness of red, green, or blue layers was adjusted prior to merging; no contrast or other adjustments were made.

Fixed cell imaging of neurons and axonal branching

[0359] Studies of adult mouse DRG axonal outgrowth used a randomized (JA) treatment scheme, and both the investigators performing confocal neuron imaging (AF) and performing Sholl analysis of those images (WK) were blinded as to treatment group. At increasing times after preparation, plating, and treatment with mitofusin agonist small molecule or peptide (or their vehicles) adult mouse DRGs were fixed in 4% paraformaldehyde and 4% sucrose in phosphate-buffered saline (PBS) for 10 min., permeabilized with 0.1% Triton X-100 in PBS for 15 min., and blocked in 10% goat serum (Jackson Immunoresearch, West Grove, PA, USA. Cat:# 005-000121) in PBS. Anti-∟-tubulin III labelling (1:500 in 10% goat serum in PBS) for 30 min at room temperature was followed by staining using Alexa Fluor 488-conjugated goat-anti-mouse secondary antibody 1:1000 for 20 min (1:400 in 10% goat serum and PBS). Vectashield (Vector Laboratories, Burlingame, CA 94010) with DAPI that stains nuclei blue was used to attach cover slips to slides.

[0360] Fixed cell imaging of beta-III tubulin (green) labelled neurons and Ad-mito-RFP labelled mitochondria was acquired at room temperature on a Nikon Ti Confocal microscope system using the 10x objective and excitation at 488 nm/emission 510 nm for Alexa-Flour 488, 579 excitation/599 emission for mito-RFP, and 306 nm excitation/405nm emission for nuclear DAPI. In some instances, as

needed for standardization, the brightness of red, green, or blue layers was adjusted prior to merging; no contrast or other adjustments were made.

[0361] Sholl analyses were preformed using ImageJ as described [27] using an open source Sholl analysis plugin (https://imagej.net/Sholl_Analysis). Briefly, a starting radius was set to encompass the soma of tubulin III-positive DRG neurons. After a scale was set to convert pixel units into microns for the given images a point was placed in the center of the starting radius corresponded to the center of the soma. Next, an ending radius of 40 microns was set, establishing a circle with 40 micron radius. Concentric circles between the starting and ending radii were established at 10 micron increments. The Scholl analysis plugin was initiated and numbers of axon and radii intersections were totaled for all circles to derive intersection number, corresponding to axonal branching. Maximal axon length per cell was determined as the larges radius step size with any intersections. Special attention was given to ensure that there was uniform staining along all parts of the DRG soma and axons so that the plugin was able to accurately assess the number of intersections accurately. Tubulin III-positive cells with no axon/dendrite growth were excluded.

Immunoblot analysis of recombinant MFN2 expression

[0362] Cell lysates for different mitofusin mutants in MEFs were prepared in Cell Extraction Buffer according to manufacturer instructions (Invitrogen, Thermo Fisher Scientific Cat:# FNN0011). To enrich mitochondrial proteins, cells were washed in ice-cold phosphate buffer (PBS) and centrifuged (500 x g at 4C) for 5 min. The whole-cell pellet was disrupted by dounce homogenization in isolation buffer (200 mM sucrose, 1 mM EGTA-Tris and 10 mM Tris-MOPS, pH 7.4) and the homogenate clarified by centrifugation at 800 × *g* for 10 min at 4 degrees C. The supernatant containing cell elements except nuclei and intact cells was recovered and a mitochondria-rich fraction obtained by centrifugation for 10 min at 8,000 × g at 4 degrees C. The mitochondrial pellet was resuspended in NaCl 150 mM, EDTA 1mM, Triton 1%, PMSF 1mM, Tris 50 mM (pH 7.5) for 10 min on ice, and contaminating organelles removed by a final centrifugation at 15,000 x g for 10 min at 4 degrees C. The supernatant, rich in mitochondrial proteins and relatively uncontaminated with reticular or other proteins [28,29], was used for immunoblotting.

[0363] Proteins were quantified by Bradford assay (#5000006, Biorad, Hercules, CA, USA) and size-separated on 10% SDS-PAGE gels (Biorad Cat# 456-1036). After wet transfer to activated 0.45µM Polyvinylidene fluoride (PVDF) membranes (GE- Amersham, Freiburg, Germany Cat# 10600023), blots were blocked with 5% non-fat milk for 30 minutes and incubated with primary antibody overnight at 4˚C. Peroxidase-conjugated secondary antibodies and Chemiluminescence Substrate (Thermo Scientific #32132) were used for signal detection. Quantification of immunoreactive proteins was performed on a LI-COR Odyssey infrared detection system (Lincoln, NE, USA, version 1.0.17).

MFN2-Miro1 co-immunoprecipitation assay

[0364] HEK293 cells (#CRL-1573, ATCC Manassas, Virginia, USA) were subcultured onto 6 wells dishes at a density of 50,000 cells/well; after 2 days cells were at ~70% confluency. Cells were transfected with wild-type FLAG-MFN2 [17], FLAG-MFN2 Arg94Gln, or FLAG-MFN2 Met376Ala [6] plus myc-Miro1 [3] as indicated using Lipofectamine 3000 (Life Technologies, Carlsbad, CA, USA) according to the manufacturer instructions. Briefly, for each well, 2.5µg total plasmid DNA was mixed with 5µl P3000 reagent and 7.5µl Lipofectamine 3000 reagent, incubated for 5 minutes in 250µl serum free OPTI-MEM media (Gibco Cat# 3198506) at room temperature; 250µl was added to each well (total volume = 1.25 ml). Four hours later, 2 ml of DMEM was added to each well, and cells were cultured at 37˚C in 5% CO2/95% air for an additional 48 hours. To test the effect of mitofusin agonist in the MFN2-Miro1 protein interaction, cells were incubated overnight with 0.1µM Regeneurin S. For each experimental condition cells from 3 wells were harvested, pooled, and suspended in 250µl cell extraction buffer (#FNN0011, Life Technologies, Carlsbad, CA, USA) supplemented with phosphatase and protease inhibitors (#04906837001 and #05892791001, Roche, Mannheim, Germany), vortexed, incubated on ice for 30 minutes, and finally clarified by centrifugation at 10,000 x g for 10 minutes at 4˚C). Protein was quantified using a Bradford-based assay.

[0365] Flag-MFN2 –MIRO1 co-immunoprecipitation was performed essentially as described [30]. Briefly, 25µl of anti-FLAG M2 resin (#A-2220, Sigma-Aldrich) was equilibrated in PBS and gently and continuously mixed with the clarified lysate (1mg) in a total volume of 700 µl at 4°C overnight. The resin beads were washed with 1ml PBS and recovered by brief centrifugation (1,000xg at 4˚C for

1min), boiled for 10 minutes in 100µl 2x SDS sample loading buffer containing 50mM dithiothreitol (DTT) to dissociate affinity bound protein complexes, and centrifuged for 10min at 25,000 x g. FLAG-resin bound proteins in the supernatants were size-separated by SDS page electrophoresis on 10% reducing mini-gels (Biorad) and electrically transferred at 4°C overnight for one hour with constant electrical potential of 110V using semi-dry blotting to PVDF membranes. Membranes were immunodecorated with anti-mitofusin 2 (ab56889 - 1:1000) or anti MIRO1 (ab188029 1:1000) and visualized using peroxidase-conjugated anti-mouse IgG (#7076S - 1:2500) from Cell Signaling (Danvers, MA, USA).

Milton-MIRO1 co-immunoprecipitation assay

[0366] Wild-type or Mfn1/Mfn2 double null MEFs were infected with Ad-h-RHOT1 (adenovirus encoding MIRO1) and Ad-h-TRAK1 (adenovirus encoding Milton) for 72 hours. Two hours prior to cell extraction Regeneurin S (1 µM) or vehicle (DMSO) were added. Proteins were extracted and quantified as described above. Milton immunoprecipitation was performed using 50 µl of Protein A agarose (cat # 20333, Thermo Fisher Scientific, Waltham, MA, USA) previously equilibrated in 1ml phosphate-buffered saline, to which was added 600 µg of protein lysate and anti-TRAK1 antibody (HPA005853, Sigma, St. Louis, MO, USA)at 4°C overnight. Agarose beads were washed in PBS and sedimented at 1,000xg at 4°C followed by boiling for 10 minutes in 100µl 2x SDS sample loading buffer containing 50mM dithiothreitol. Immunocomplexes were resolved by SDS-PAGE electrophoresis, transferred to PVDF membranes, and proteins identified by immunoblotting for MIRO1, Milton, MFN2. Equal input protein was verified by GAPDH immunoblotting.

Mitochondrial GTPase activity assay

[0367] *Mfn1/Mfn2* double-null MEFs were transduced with ad-MFN2 (wild-type), lenti-MFN2 Arg94Gln, ad-Mfn2 Lys109Aala, ad-MFN2 Met376Ala, or ad-β-gal (as a negative control) and 72 hours later mitochondria were isolated as described [31]. The GTPase-Glo assay components from Promega (#V7681; Madison, WI, USA) was used to measure intrinsic mitochondrial GTPase activity. Briefly, 100 µg of mitochondria proteins were incubated in GTPase Buffer with 10 µM GTP and 1 mM DTT at room temperature for 90 minutes in 96 well-plates. Following addition of Detection Reagent, luminescence was quantified on a Promega GloMax

Luminometer. Equal expression of wild-type and mutant MFN2 proteins in the Mfn1/Mfn2 null background was demonstrated by immunoblot analysis.

[0368] *In vitro microfluidic studies of cortical neuron axon growth*

[0369] Primary cortical neurons were isolated from embryonic day 18.5 C57bl6 mice essentially as described above and in reference [24]. 200,000 suspended live cells in 20 µl of Earle's Minimal Essential Medium (MEM; #11090-081; Gibco) supplemented with 5% FBS (Gibco #16140-063), 5% horse serum (HS) (Gibco #26050-070), 400µM L-Glutamine (Gibco #25030-149), 50 units/ml each penicillin/streptomycin (Gibco #15070-063) and 0.3% glucose (Sigma G 5767) (5-5 media) were added to microfluidic neuron XonaChips with 450µm microgroove barriers (#XC450; Xona Microfluidics, Temecula, CA, USA) coated with 0.5mg/ml Poly(D)lysine (Sigma #P7280). After 10 minutes, 150µl of 5-5 media supplemented with 0.5µl Insulin-Transferrin-Sodium Selenite (Sigma I 1884) was added to each well and the neurons cultured under standard conditions (37 degrees C, 5%CO_2/95% air). After 24 hours the media was changed to "neuron feeding media" (Neurobasal Media #21103-049; Gibco, Carlsbad, CA, USA), 1x B27 Supplement (#17504-044, Gibco, Carlsbad, CA, USA), 50 units/ml each Penicillin/Streptomycin (#15070-063; Gibco, Carlsbad, CA, USA) and 400µM L-Glutamine (#25030-149; Gibco, Carlsbad, CA, USA). Cells were fed every 2 to 3 days until aspiration axotomy.

[0370] Aspiration axotomy and post-axotomy regrowth analyses were performed as described [27]. Briefly, vacuum aspiration axotomy of DIV (days in vitro) neurons was followed by application of fresh neuron feeding media containing either mitofusin agonist Regeneurin C (100 nM final concentration) or vehicle (Me_2SO, 1:1,000). Cells were fixed in situ; axonal outgrowth and post-axotomy regrowth were analyzed by confocal analysis of β-III tubulin positive cells.

[0371] *In vitro mitochondrial motility studies in live adult mouse DRG neurons*

[0372] DRG neurons from lumbar vertebrae 1-6 were isolated from ~8 week old MFN2 Thr105Met flox-stop transgenic[6], SOD1 Gly93Ala transgenic[18], or normal C57BL/6J mice using papain/collagenase dissociation as described above and in reference 25. Upon plating in 12-well Laminin-coated dishes, MFN2 Thr105Met floxed-stop DRG neurons were infected with Adeno-Cre to induce MFN2 Thr105Met expression. DRG neurons were immediately treated with Regeneurin C

(100 nM), its vehicle Me_2SO_4 (1:1000), or forskolin (5 μM; as a positive control for axonal outgrowth) and infected with Adeno-mitoDsRed2. 48 hours after plating DRGs were co-stained with Calcein AM (0.5uM; Invitrogen, Thermo Fisher Scientific, Waltham, MA, USA Cat:# C3100MP) for 30 minutes at 37℃ to visualize axons. Time-lapse images were acquired at 37℃, 5%CO_2 on a Nikon A1Rsi Confocal Microscope using a 40x oil objective at a frame rate of 5 seconds per frame for a total of 15 minutes (180 total frames). Adeno-mitoDsRed2 was excited at 561 nm and emission monitored at 585nm. Calcein was excited at 488 nm and its emission monitored at 525 nm. Kymographs and quantitative data were generated using an Image-J plug-in as previously described[6].

[0373] *In vivo studies of recovery after sciatic nerve injury*

[0374] **Preparation of Mitolityn-4 matrix for local depo application:** All procedures were performed under sterile conditions. A stock solution of 25 mg/ml Mitolityn-4 in ME_2SO was diluted 1:10 (final concentration 2.5 mg/ml) in 0.9% w/v saline (Winchester Laboratories, Sulzbach-Laufen, Germany) and sterile-filtered (0.22μm PVDF, #SLGV033RS, Millipore, Cork, Ireland). Pre-cooled Matrigel ® solution (#354234; Corning; Corning, NY, USA) was combined with Mitolityn-4 or ME_2SO (vehicle control) at a 3:1 ratio, immediately transferred in 0.2 ml aliquots to 1ml tuberculin syringes (#309659; Becton Dickinson, Franklin Lakes, NJ, USA) and polymerized at room temperature for 1 hour prior to administration.

[0375] **Evaluation of Mitolityn efflux from Matrigel:** For each sample, 125μg of (50μl of 2.5 mg/ml) Mitolityn-4 dissolved in 10% DMSO, 90% saline was mixed with 150μl of ice-cold Matrigel™ Basement Membrane Matrix and polymerized for 1 hour at 37C. The drug/gel-mix was applied to the surface of a 40μm cell strainer, itself placed in reservoirs containing 500μl of H_2O at 37C for incubation times of 5, 10, 20, 20, 120 minutes. This experiment was performed 3 independent times and the samples submitted for mass spectroscopic (MS) analysis of Mitolityn-4 content.

[0376] Prior to MS the samples were diluted 1:100,000 and 2.5 μl of the diluates were analyzed using LC-MS on a ThermoScientific™ Q Exactive™ Plus Hybrid Quadrupole Orbitrap™ mass spectrometer that was linked to an EASY-nLC™ 1000 System that consisted of an autosampler, column and pump (ThermoScientific™). The samples were loaded (2.5 μL) onto a 75 μm i.d. × 50 cm

Acclaim PepMap 100 RP column. The analytes were eluted at a flow rate of 300 nL/min with an acetonitrile (ACN) gradient in aqueous formic acid (FA) (1%) as mobile phase A. After isocratic elution with 2% solvent B (100% ACN, 1% FA) for 1 min the ACN proportion was increased linearly to 20% with solvent B over 15 min, followed by an isocratic wash at 95% B for 18 min. The full-scan mass spectra were acquired over mass-to-charge (m/z) range of 100 to 1500 to a resolution of 70,000 in the orbitrap mass analyzer. The maximum injection time was 60 ms for parent-ion analysis with an automatic gain control target value of 1e6. The instrument files were imported into SKYLINE (version 4.1.1.18179) for signal identification and chromatographic peak integration. A titration curve was generated with 8 concentrations that related MS chromatographic peak areas from the signal at m/z = 322.22 to Mitolityn-4 concentrations. Triplicate LC-MS analyses were performed for each concentration. Linear regression (not forced through zero) analysis was used to calculate the quantity (pg) of Mitolityn-4 in the eluate at each time. Release rate was calculated based on zero order kinetics as the linear best fit line for each individual experiment.

[0377] **Study blinding and randomization:** Evaluation of Mitolityn-4 for nerve regeneration and functional recovery after sciatic nerve crush injury in CMT2A MFN2Thr105Met mice used a randomized treatment scheme. Based on a random number table generated in Microsoft Excel, individual mice were assigned to treatment groups by G.W.D. Mitolityn-4 or vehicle containing syringes were prepared accordingly by X.D. and provided to the mouse surgeon (A.F.), who was blinded as to syringe contents. After the studies were complete, the study was unblinded and outcomes analyzed according to treatment group.

[0378] **In vivo sciatic nerve crush injury** was performed on adult (8-10 week old) male C57BL/6J (The Jackson Laboratory, Bar Harbor, Maine, USA Cat:#000664; for immuunohistology) or MFN2 Thr105Met mice (for neuroelectrophysiology studies). Mice were anesthetized with isofluorane (4-5% induction; 1.5% maintenance). After local anesthesia with subcutaneous lidocaine (1%), the proximal left sciatic nerve was exposed at the upper thigh through a posterior approach, the nerve isolated and supported with a loop of 5-0 nylon suture, and crushed three times at 45, 90, and 135 degrees to the nerve long axis for 15 seconds each using hemostatic forceps. Mitolityn (20 μl of a 1 μM solution) or

vehicle, followed by Matrigel (200 μl total volume) containing either Mitolityn (2mg/kg) or vehicle was applied directly onto the crushed sciatic nerve. The incision was closed in layers using continuous 3-0 nylon sutures. Post-operative analgesia was provided for 48 hours.

[0379] **Neuroelectrophysiologic recording of tibialis compound muscle action potentials** were performed by an operator (A.F.) blinded to treatment group. Mice were anesthetized with isofluorane (4-5% induction and 1.5% to maintenance) and both lower limbs were shaved. Proximal sciatic nerves were stimulated with a needle electrode (Natus, Mundelein, IL, USA Cat:# F-E2-48) using 4 mV pulses of 0.002 ms duration. Ring electrodes (Natus, Mundelein, IL, USA Cat:# 291965) were positioned to record compound tibialis muscle action potentials (CMAP) at the mid forelimb at the belly of the tibialis anterior muscle. Optimal stimulating electrode position was determined that gave the greatest (CMAP) amplitude, and 3-4 independent events were recorded using a Viasys Healthcare Nicolet Biomedical instrument (Middleton, WI, USA Cat:# OL060954) running Viking Quest version 11.2 software. Three or four independent events were acquired for each study and the average data values (amplitude, latency, duration) reported. Studies were performed at 3 and 7 days after surgery. In two mice (one vehicle-treated and one Mitolityn-treated) optimal CMAP tracings could not be obtained. The contralateral non-injured leg was used as control.

[0380] **Sciatic nerve immunohistology** was performed 3d after crush injury using in vivo perfusion fixation of anesthetized mice. Mice were perfused via left ventricular puncture with ice cold phosphate buffered saline (PBS) saline, and perfusion-fixed with ice-cold 4% paraformaldehyde (PFA) in PBS. Sciatic nerves were dissected free intact from spine to ankle, fixed in PFA for 2 additional hours, and transferred to 30% sucrose/PBS overnight at 4 degrees C. The following day nerves were imbedded in optimal cutting temperature (OCT, Tissue-TEK Cat: 4583) medium and maintained thereafter at – 80 degrees C. Immunostaining was performed on 10 μm cryostat sections. Briefly, frozen sections were briefly (5 minutes) brought to room temperature, then re-cooled to-20 degrees C for 30 mins. At room temperature, acetone was applied for 5-10 min followed by washing in PBS for 5 mins, then 0.1 % Triton X-100 in PBS was applied for 15 mins. Tissue antigens were blocked with 10% normal goat serum in PBS for 15 min prior to application of

anti-β-tubulin III and anti-Superior Cervical Ganglion 10 (SCG10), which marks regenerating nerves, 1:200 in 10% goat serum in PBS for 30 min. Antigen visualization used Alexa Fluor 488-conjugated goat-anti-mouse secondary antibody (Life technology, St Peters, MO, USA. Cat:#1611153) for 20 min (1:1000 in 10% goat serum and PBS). Vectashield (Vector Laboratories, Burlingame, CA 94010) with DAPI that stains nuclei blue. Fixed nerve imaging was acquired at room temperature on a Nikon Ti Confocal microscope system using the 20x objective. Red and green images were merged without individual adjustments for all sections. RGB rightness of the representative images (Figure 4g) was increased uniformly for presentation purposes.

[0381] *Functional screening of mitofusin agonist fusogenicity and pharmacokinetic assessment*

[0382] Mfn2-deficient MEFs were seeded on day1 in 6 well plates at a density of $1x10^4$ cells/ml. The next day, 4µl of each dissolved small molecule was added to each well (to achieve a final concentration between 0 and 20µM) and allowed to incubate over night. The solvent used for dissolving the small molecules (DMSO) was used as vehicle (0µM). The next day, mitochondria were stained with MitoTracker Orange (100 nM; M7510; Invitrogen, Carlsbad, CA, USA).

[0383] For viability studies, NIH 3T3 fibroblasts were seeded on day1 in 6 well plates at a density of $2.5x10^4$ cells/ml. The next day, 4µl of each dissolved small molecule was added to each well (to achieve a final concentration between 0 and 100µM) and allowed to incubate over night. The solvent used for dissolving the small molecules (DMSO) was used as vehicle (0µM). As a positive control for cell death, 10µM doxorubicin (D1515, Sigma, St. Louis, MO, USA) was added. The next day, live cells were stained with 0.5µM calcein AM and 1µM ethidium homodimer-1 (L3224; Invitrogen, Carlsbad, CA, USA)

[0384] Images were acquired at room temperature on a Nikon Ti Confocal microscope using a 60X1.3 NA oil- immersion objective in Krebs-Henseleit buffer (138 NaCl, 3.7 nM KCL, 1.2 n M KH2PO4, 15 nM glucose, 20 nM HEPES (pH 7.5) and 1mM CaCl2). Laser excitation was 549 nm with emission at 590 nm for TMRE and ethidium homodimer-1 and excitation at 488 nm with emission at 510 nm for calcein-AM. Images were analyzed using ImageJ [33]. Fusogenecity effect of small molecules was quantified as a means of mitochondrial aspect ratio: the length/width

measurement of each mitochondria. For dose-response and EC50 (dose of compound that provokes a half-maximal response) analyses the maximal fusogenic response was defined as that produced by 1 ㄴM Regeneurin C. EC50 values were calculated for each dose-response study using GraphPad Prism (La Jolla, CA, USA). Three independent experiments were performed for each condition, and ~300 mitochondria were analyzed for each condition.

In vitro pharmacokinetic analyses of mitofusin agonists was performed at WuXi Apptec Co. Ltd. (Shanghai, China).

[0385] **Agonist stability in CD-1 Mouse and Human Plasma.** Pooled frozen plasma was thawed in a water bath at 37℃ prior to experiment. Plasma was centrifuged at 4000 rpm for 5 min and the clots were removed if any. The pH will be adjusted to 7.4 ± 0.1 if required. To prepare the compounds working solution, 1 mM intermediate solution was prepared by diluting 5 µL of the stock solution with 45 µL DMSO; 1 mM intermediate of positive control Propantheline was prepared by diluting 5 µL of the stock solution with 45 µL ultra pure water. One hundred µM dosing solution was prepared by diluting 10 µL of the intermediate solution (1 mM) with 90 µL 45%methanol/H2O. Ninety eight µL of blank plasma was spiked with 2 µL of dosing solution (100 µM) to achieve 2 µM of the final concentration in duplicate and samples were Incubated at 37℃ in a water bath. At each time point (0,10, 30, 60 and 120 min), 400 µL of stop solution was added to precipitate protein and mixed thoroughly. As standard controls 200 ng/mL tolbutamide plus 200 ng/mL labetalol in 50% ACN/MeOH were used. Sample plates were centrifuged at 4,000 rpm for 10 min. An aliquot of supernatant (50 µL) was transferred from each well and mixed with 100 µL ultra pure water. The samples were shacked at 800 rpm for about 10 min before submitting to LC-MS/MS analysis.

[0386] **Agonist solubility in buffer** employed the shake flask method followed by HPLC-UV analysis. Briefly, the test compounds and controls (10 mM in DMSO, 10 µL/well) were added into 50 mM phosphate buffer, pH 7.4 (490 µL/well), and placed in a 96-well plate. Samples were vortexed for 2 minutes followed by a 24 hours incubation period (shaking at 880 rpm) at room temperature. 200 µL of each solubility solution was transferred into a new MultiScreen filter plate and filtered by millipore vacuum manifold. After collection of the filtrates, the test compound concentration was determined using HPLC with UV detection.

[0387] **Binding to human and CD-1 mouse plasma proteins** was measured using equilibrium dialysis. Pooled individual frozen EDTA anticoagulated plasma mouse and human samples were used as test matrix. Warfarin was used as a positive control. The test compounds were spiked into blank matrix at the final concentration of 2 µM. A 150 µL aliquot of matrix sample was added to one side of the chamber in a 96-well equilibrium dialyzer plate (HTD dialysis) and an equal volume of dialysis buffer was added to the other side of the chamber. An aliquot of matrix sample was harvested before the incubation and used as T0 samples for recovery calculation. The incubations were performed in triplicate. The dialyzer plate was placed in a humidified incubator and rotated slowly for 4 hours at 37°C. After incubation, the samples were taken from the matrix side as well as the buffer side. The plasma sample was matched with equal volume of blank buffer; and buffer samples were matched with equal volume of blank plasma. The matrix-matched samples were quenched with stop solution containing internal standard. All samples were analyzed by LC-MS/MS. All test compound concentrations in matrix and buffer samples are expressed as peak area ratios (PAR) of analyte/internal standard.

[0388] **Agonist in vitro stability was measured in human and mouse liver microsomes.** An intermediate solution (100µM of small molecule) was initially prepared in methanol and subsequently used to prepare the working solution. This was achieved by a 10-fold dilution step of the intermediate solution in 100 mM potassium phosphate buffer. Ten µL compound or control working solution was added to all wells of a 96-well plate for the time points (minutes): T0, T5, T10, T20, T30, T60, NCF60, except matrix blank. The microsome solution (680µL/well) (#452117, Corning; Woburn, MA, USA; #R1000, Xenotech; Kansas City, Kansas, USA and #M1000, Xenotech; Kansas City, Kansas, USA) was dispersed to 96-well plate as reservoir according to the plate map. Then, 80 µL/well was added to every plate by ADDA (Apricot Design Dual Arm, Apricot Designs, Inc., Covina, CA, USA), and the mixture of microsome solution and compound were allowed to incubate at 37℃ for about 10 min. Next, 10 µL 100 mM potassium phosphate buffer/well was added to NCF60 and incubated at 37℃ (timer 1H was started). After pre-warming, 90 µL/well of NADPH (#00616, Sigma, Aldrich, St. Louis, Missouri, USA) regenerating system was dispensed to 96-well plate as reservoir according to the plate map. Then 10 µL/well was added to every plate by ADDA to start reaction. To terminate the

reaction, 300 µL/well of stop solution (cold in 4°C, including 100 ng/mL tolbutamide and 100 ng/mL labetalol as internal standards) was used, and sampling plates were shacked for approximately 10 min. The samples were next centrifuged at 4000 rpm for 20 min at 4°C and supernatants were analyzed by LC-MS/MS.

[0389] **Parallel artificial membrane permeability assay (PAMPA).** One hundred and fifty µL of 10 µM small molecule (5% DMSO) solution was added to each well of the donor plate, whose PVDF membrane was pre-coated with 5 µL of 1% brain polar lipid extract (Porcine) /dodecane mixture. Then 300 µL of PBS was added to each well of the PTFE acceptor plate. The donor plate and acceptor plate were combined together and incubated for 4h at room temperature with shaking at 300 rpm. To prepare the T0 sample, 20 µL donor solution was transferred to new well followed by the addition of 250 µL PBS (DF: 13.5) and 130 µL of acetonitrile (ACN) (containing internal standard) as T0 sample. To prepare the acceptor sample: The plate was removed from incubator and 270 µL solution was transferred from each acceptor well and mixed with 130 µL ACN (containing internal standard) as acceptor sample. To prepare the donor sample, 20 µL solution was transferred from each donor well and mixed with 250 µL PBS (DF: 13.5), 130 µL ACN (containing internal standard) as donor sample. The acceptor samples and donor samples were analyzed by LC-MS/MS.

[0390] *Statistical analysis and data reporting*

[0391] Student t-tests were used to compare single treated and untreated groups. One-way analysis of variance (ANOVA) was used for multi-group comparisons. Two-way ANOVA as used to compare drug/peptide responses as a function of different times or different genetic defects. $p<0.05$was considered as significant. Unless otherwise indicated, data are reported as individual cell or mouse values with mean and standard deviation values superimposed. P values for the meaningful comparisons are shown.

***Example 10:* Chemical synthesis, purification and analyses of small molecule mitofusin agonists**

[0392] Synthesis of Regeneurin C and resynthesis of Regeneurin S was performed at Paraza Pharma Inc. (Saint-Laurent, QC, Canada). Because the functional and pharmacokinetic profiles of the two Regeneurins are identical

(Extended Data Figs 5 and 15) in the manuscript text they are referred to simply as "Regeneurin".

[0393] **Regeneurin S** (1-(2-((5-cyclopropyl-4-phenyl-4*H*-1,2,4-triazol-3-yl)thio)ethyl)-3-(2-methylcyclohexyl)urea) was synthesized as a racemic mixture (**FIG. 83)**.

[0394] Preparation of compound 2-(cyclopropanecarbonyl)-*N*-phenylhydrazinecarbothioamide (compound 2): isothiocyanatobenzene 4 (2.39 mL, 20.0 mmol) was added to a dichloromethane (DCM) (30 mL) solution of cyclopropanecarbohydrazide (2.11 g, 20.0 mmol) and the reaction was heated at 85 °C for 18 h in a sealed flask. The product was filtered and rinsed with diethyl ether affording 5 (4.31 g, 92 %) as a white powder. LC-MS: R_T = 1.06 min; MS cal.: 235.31; Mass found: $[M+H]^+$: 236.0.

[0395] Preparation of compound 5-cyclopropyl-4-phenyl-4*H*-1,2,4-triazole-3-thiol (compound 3): A mixture of compound 2 (3.29 g, 14.0 mmol) and 30 mL of a 2 M solution of sodium hydroxide was refluxed for 2 h. Then the solution was neutralized with 10% HCl and the formed precipitate was filtered affording compound 3 (2.85 g, 94 %) as a white powder. LC-MS: R_T = 1.27 min; MS cal.: 217.29; Mass found: $[M+H]^+$: 217.9.

[0396] Preparation of compound *tert*-butyl (2-iodoethyl)carbamate (compound 4): iodine (2.78 g, 10.9 mmol) was added to a DCM (30.4 mL) solution of PPh_3 (2.39 g, 9.12 mmol) and imidazole (621 mg, 9.12 mmol) at r.t. The reaction was stirred for 1 h then *tert*-butyl (2-hydroxyethyl)carbamate (1.44 mL, 9.12 mmol) was added and stirring was continued for 18 h. The resulting mixture was quenched with water (50 mL), washed with a saturated solution of sodium thiosulfate (50 mL), washed with brine, dried over anhydrous Na_2SO_4 and concentrated under reduced pressure. The crude was purified on a silica pad (eluent: 20% EtOAc/Hexanes) affording compound 4 (2.15 g, 87 %) as orange oil.

[0397] Preparation of compound *tert*-butyl (2-((5-cyclopropyl-4-phenyl-4*H*-1,2,4-triazol-3-yl)thio)ethyl)carbamate (compound 5): K_2CO_3 (2.60 g, 18.8 mmol) and compound 4 (1.66 g, 6.12 mmol) were added to a DMF (3.0 mL) solution of compound 3 (1.02 g, 4.71 mmol) and the reaction was stirred at 60 °C for 1 h in a sealed flask. The resulting mixture was partitioned with EtOAc (30 mL) and water (30 mL). The organic layer was washed with water (2 x 30 mL), washed with brine, dried

over anhydrous Na_2SO_4 and concentrated under reduced pressure affording crude compound 5 (1.80 g, 106 %) as a white solid. LC-MS: R_T = 1.53 min; Purity: 95.9%; MS cal.: 361.47; Mass found: $[M\text{-}Boc+H]^+$: 261.0.

[0398] Preparation of compound 1-(2-((5-cyclopropyl-4-phenyl-4*H*-1,2,4-triazol-3-yl)thio)ethyl)-3-(2-methylcyclohexyl)urea (Regeneurin-S): Trifluoroacetic acid (1.82 mL, 23.6 mmol) was added to a DCM (14 mL) solution of compound 5 (1.70 g, 4.71 mmol) and the reaction was stirred for 18 h at r.t. Then a saturated solution of $NaHCO_3$ (40 mL) was added, NaOH (5M) was added to ensure pH < 12. The aqueous layer was extracted with DCM (7 x 50 mL), dried over anhydrous Na_2SO_4 and concentrated under reduced pressure affording the crude deprotected amine (1.24 g, quantitative). LC-MS: R_T = 1.52 min; MS cal.: 260.35; Mass found: $[M+H]^+$: 261.0. A DCM (9.53 mL) solution of compound 6 (663 mg, 4.76 mmol) was added to a DCM (9.53 mL) solution of deprotected amine (1.24 g, 4.76 mmol) and the reaction was stirred for 18 h at r.t. Then water (50 mL) was added; the organic layer was separated, dried over anhydrous Na_2SO_4 and concentrated under reduced pressure. The crude was purified by flash column chromatography (silica 50 g, 5 to 50% MeOH/DCM) affording Regeneurin-S (1.30 g, 68 %) as a white powder. LC-MS: R_T = 1.52 min; Purity: 99.4% (**FIG. 84**); MS cal.: 399.55; Mass found: $[M+H]^+$: 400.2 (**FIG. 85**). Structure was confirmed by ^1H NMR and ^{13}C NMR. ^1H NMR (500 MHz, $CDCl_3$) δ 7.59 – 7.51 (m, 3H), 7.34 – 7.30 (m, 2H), 5.63 (s) and 5.56 (s, 1H), 5.04 (s, 1H), 4.75 (s) and 3.79 (s, 1H), 3.57 (dq, J = 12.7, 6.5 Hz, 2H), 3.29 – 3.09 (m, 2H), 1.98 – 1.02 (m, 12H), 0.98 – 0.90 (m, 4H), 0.85 (d, J = 7.0 Hz, 1H) (**FIG. 86**). ^{13}C NMR (126 MHz, $CDCl_3$) δ 158.4, 158.2, 157.9, 151.2, 151.0, 133.3, 133.3, 130.0, 127.2, 127.2, 55.0, 50.3, 40.7, 40.6, 38.9, 34.7, 34.5, 34.0, 32.8, 32.5, 30.2, 26.0, 25.8, 19.4, 8.10, 6.14 (**FIG. 87**).

[0399] **Regeneurin C** (1-(3-(5-cyclopropyl-4-phenyl-4*H*-1,2,4-triazol-3-yl)propyl)-3-(2-methylcyclohexyl)urea) was synthesized as a racemic mixture (**FIG. 88**).

[0400] Preparation of compound tert-butyl (4-oxo-4-(phenylamino)butyl)carbamate (compound 7): Dicyclohexylcarbodiimide (5.47 g, 26.3 mmol) was added to a DCM (119 mL) solution of 4-((*tert*-butoxycarbonyl)amino)butanoic acid (5.00 g, 23.9 mmol) and the mixture was stirred for 30 min at r.t. (forming a white precipitate). Then aniline (2.42 mL, 26.3 mmol) was

added and the reaction was stirred for 18 h at r.t. The reaction was quenched with water (80 mL), the organic layer was washed with a saturated solution of $NaHCO_3$ (80 mL), washed with brine, dried over anhydrous Na_2SO_4 and concentrated under reduced pressure affording compound 7 (6.60 g, 99 %) as a white solid. LC-MS: R_T = 1.46 min; MS cal.: 278.35; Mass found: $[M\text{-}Boc+H]^+$: 178.7.

[0401] Preparation of compound *tert*-butyl (4-(phenylamino)-4-thioxobutyl)carbamate (compound 8): Lawesson's Reagent (14.5 g, 35.8 mmol) was added to a THF (79.7 mL) solution of (compound 7) (6.65 g, 23.9 mmol) and the reaction was stirred for 3 h at 70 °C in a sealed flask. Then an aqueous solution of NaOH (1M) (100 mL) was added and stirred at r.t. for 30 min. The resulting mixture was extracted with EtOAc (2 x 100 mL), washed with brine, dried over anhydrous Na_2SO_4 and concentrated under reduced pressure affording crude (compound 8) (7.0 g, 99%) as yellow oil. LC-MS: R_T = 1.64 min; MS cal.: 294.41; Mass found: $[M\text{-}H]^+$: 293.1.

[0402] Preparation of compound methyl 4-((tert-butoxycarbonyl)amino)-N-phenylbutanimidothioate (compound 9): iodomethane (2.71 mL, 43.0 mmol) was added to a MeCN (59.7 mL) solution of (compound 8) (7.04 g, 23.9 mmol) and K_2CO_3 (9.25 g, 66.9 mmol) and the reaction was stirred for 3 h at 50 °C. The resulting mixture was concentrated under reduced pressure, dissolved in EtOAc (50 mL), washed with water (3 x 50 mL), washed with brine, dried over anhydrous Na_2SO_4 and concentrated under reduced pressure. The crude was purified by flash column chromatography (silica 220 g, 5 to 50% EtOAc/Hexanes) affording (compound 9) (4.51 g, 61 %) as colorless oil. LC-MS: R_T = 1.80 min; MS cal.: 308.44; Mass found: $[M+H]^+$: 309.0.

[0403] Preparation of compound *tert*-butyl (3-(5-cyclopropyl-4-phenyl-4*H*-1,2,4-triazol-3-yl)propyl)carbamate (compound 10): Cyclopropanecarbohydrazide (882 mg, 8.36 mmol) was added to a DMF (6.97 mL) solution of compound 9 (2.15 g, 6.97 mmol) and the reaction was stirred at 165 °C for 18 h in a 15 mL sealed flask. Then the resulting mixture was partitioned in EtOAc (20 mL) and water (20 mL). The organic layer was washed with water (3 x 20 mL), washed with brine, dried over anhydrous Na_2SO_4 and concentrated under reduced pressure. The crude was purified by flash column chromatography (silica 50 g, 5 to 50% MeOH/DCM)

affording compound 10 (1.70 g, 71 %) as a colorless oil. LC-MS: R_T = 1.43 min; MS cal.: 342.44; Mass found: $[M\text{-Boc+H}]^+$: 243.1.

[0404] Preparation of compound 1-(3-(5-cyclopropyl-4-phenyl-4*H*-1,2,4-triazol-3-yl)propyl)-3-(2-methylcyclohexyl)urea (Regeneurin-C): Trifluoroacetic acid (1.81 mL, 23.4 mmol) was added to a DCM (7.30 mL) solution of compound 10 (1.00 g, 2.92 mmol) and the reaction was stirred at r.t. for 18 h. Then an aquous solution of $NaHCO_3$ (40 mL) was added, NaOH (5M) was added to ensure pH < 12. The aqueous layer was extracted with DCM (7 x 40 mL), dried over anhydrous Na_2SO_4 and concentrated under reduced pressure affording the crude deprotected amine (710 mg, quantitative). LC-MS: R_T = 1.00 min; MS cal.: 242.33; Mass found: $[M+H]^+$: 242.9. A DCM (5.84 mL) solution of compound 6 (406 mg, 2.92 mmol) was added to a DCM (5.84 mL) solution of deprotected amine (708 mg, 2.92 mmol) and the reaction was stirred for 18 h at r.t. Then water (20 mL) was added, the organic layer was separated, dried over anhydrous Na_2SO_4 and concentrated under reduced pressure. The crude was purified by flash column chromatography (silica 50 g, 5 to 50% MeOH/DCM) affording Regeneurin-C (750 mg, 67 %) as a white powder. LC-MS: R_T = 1.43 min; Purity: 98.8% (**FIG. 89)**; MS cal.: 381.51; Mass found: $[M+H]^+$: 382.2 (**FIG. 90**). Structure was confirmed by ^1H NMR and ^{13}C NMR. ^1H NMR (500 MHz, $CDCl_3$) δ 7.59 – 7.51 (m, 3H), 7.28 – 7.26 (m, 1H), 7.26 – 7.25 (m, 1H), 5.67 (s) and 5.61 (s, 1H), 5.07 (d, J = 8.0 Hz) and 4.87 (d, J = 8.9 Hz, 1H), 3.80 (m) and 3.31 – 3.16 (m, 3H), 2.60 (td, J = 7.2, 5.1 Hz, 2H), 1.98 – 1.01 (m, 14H), 0.94 – 0.86 (m, 4H), 0.84 (d, J = 7.0 Hz, 1H) (**FIG. 91**). ^{13}C NMR (126 MHz, $CDCl_3$) δ 158.8, 158.7, 156.5, 154.8, 154.7, 133.7, 133.7, 130.1, 129.9, 127.2, 54.69, 39.5, 39.4, 39.1, 34.7, 34.6, 28.0, 26.0, 25.8, 22.8, 19.4, 7.92, 5.97 (**FIG. 92**).

[0405] *Synthesis of Mitolityns* was performed at WuXi Apptec Co. Ltd. (Hubei, China) The Mitolityn 1-4 synthesis scheme is depicted in **FIG. 93.**

[0406] General procedures; preparation of compound 12: A solution of compound 11 (15.0 g, 81.0 mmol, 13.8 mL) and $NH_2NH_2.H_2O$ (20.3 g, 405 mmol, 19.7 mL) was stirred at 80°C for 5 h. TLC (Petroleum ether: Ethyl acetate = 2 : 1) indicated reactant 1(R_f = 0.30) was consumed completely and one main spot (R_f = 0.00) formed. The reaction mixture was concentrated under reduce pressure to give a residue. Compound 12 (9.00 g, 41.4 mmol, 51.1% yield) was obtained as a white

solid. ^{1}H NMR: 400 MHz ME_2SO -d_6 δ 8.92 (s, 1H), 6.79 (s, 1H), 2.91-2.86 (m, 2H), 2.01-1.98 (t, *J* = 7.6 Hz, 2H), 1.62-1.53 (m, 2H), 1.37 (s, 9H).

[0407] Preparation of compound 14: A solution of K_2CO_3 (26.4 g, 191 mmol) and ethanamine (12.9 g, 287 mmol, 18.8 mL) in DCM (50.0 mL) was added compound 13 (10.0 g, 95.7 mmol, 8.70 mL) and stirred at 15 ~ 20°C for 5 h. TLC (Petroleum ether: Ethyl acetate = 2 : 1) indicated compound 13 (R_f = 0.20) was consumed completely and one main spot (R_f = 0.40) formed. The reaction mixture was added water (100 mL) and extracted with DCM (100 mL * 3). The combined organic layers were dried over Na_2SO_4, filtered and concentrated under reduced pressure to give a residue. ^{1}H NMR showed compound 14 (10.0 g, 88.4 mmol, 92.3% yield) was obtained as a brown solid. ^{1}H NMR: 400 MHz ME2SO-d_6 δ 7.99 (s, 1H), 3.39-2.97 (m, 2H), 1.53-1.50 (m, 1H), 1.03-0.99 (t, *J* = 7.2 Hz, 3H), 0.67-0.59 (m, 4H).

[0408] Preparation of compound 15: Oxalylchloride (4.50 g, 35.5 mmol, 3.10 mL) was added to a solution of compound 14 (4.00 g, 35.4 mmol) and 2,6-LUTIDINE (7.60 g, 70.9 mmol, 8.26 mL) in DCM (160 mL) at 0°C under N_2. The mixture was stirred for 10 min, and compound 12 (6.14 g, 28.3 mmol) was added. The reaction mixture was stirred for 10 min at 5 ~ 10°C. Then the reaction mixture was removed under reduced pressure. The residue was dissolved in $NaHCO_3$ (345 g, 4.11 mol, 160 mL) and refluxed for 0.5 h at 100°C. LC-MS showed compound 12 was consumed completely and desired MS (M + H = 295.4, R_t = 0.720 min) was detected. The reaction mixture was extracted with DCM (100 mL * 3). The combined organic layers were dried over Na_2SO_4, filtered and concentrated under reduced pressure to give a residue. The residue was purified by column chromatography (SiO_2, Ethyl acetate: MeOH = 1 : 0 to 10 : 1). TLC (Ethyl acetate: Methanol = 3 : 1) (R_f = 0.20) was collected. HNMR showed compound 15 (2.20 g, 7.47 mmol, 21.1% yield) was obtained as a brown oil. ^{1}H NMR: 400 MHz $CDCl_3$ δ 5.00 (s, 1H), 4.00-3.95 (m, 2H), 2.26-3.21 (m, 2H), 2.75-2.71 (t, *J* = 7.6 Hz, 2H), 2.07-1.98 (m, 2H), 1.69-1.64 (m, 1H), 1.44 (s, 9H), 1.39-1.35 (t, *J* = 7.2 Hz, 3H), 1.13-1.01 (m, 4H).

[0409] Preparation of compound 16: To a solution of compound 15 (2.00 g, 6.79 mmol) in dioxane (5.00 mL) was added HCl/dioxane (4 M, 17.0 mL) and stirred at 5 ~ 10°C for 12 h. TLC (Ethyl acetate: Methanol = 3 : 1) indicated compound 15

(R_f = 0.20) was consumed completely and one main spot (R_f = 0.00) formed. The reaction mixture was concentrated under reduce pressure to give a residue. The residue was triturated with MTBE (15.0 mL). Then filtered and filter-cake was obtained. HNMR showed compound 16 (1.40 g, crude, HCl) was obtained as a white solid. ^{1}H NMR: 400 MHz ME2SO-d_6 δ 8.39 (s, 1H), 4.31-4.26 (m, 2H), 3.16-3.10 (m, 2H), 2.95-2.91 (m, 2H), 2.36-2.33 (m, 1H), 2.12-2.08 (t, *J* = 7.6 Hz, 2H), 1.40-1.36 (t, *J* = 7.2 Hz, 3H), 1.26-1.19 (m, 4H).

[0410] **Mitolityn-1** (1-(3-(5-cyclopropyl-4-ethyl-4H-1,2,4-triazol-3-yl)propyl)-3-(2-methylcyclohexyl)urea) was synthesized as a racemic mixture (**FIG. 93**). To a solution of compound 1-1 (245 mg, 2.16 mmol, 285 uL) and TEA (625 mg, 6.18 mmol, 860 uL) in DCM (10.0 mL) was added CDI (368 mg, 2.27 mmol) and the reaction mixture was stirred at 5 ~ 10 °C for 3 h. Then compound 6 (400 mg, 1.73 mmol, HCl) was added to the reaction mixture and stirred at 10 ~ 15°C for 2 h. LC-MS showed compound 16 was consumed completely and desired MS (M + H = 344.2, R_t = 1.376 min) was detected. The reaction mixture was concentrated under reduce pressure to remove DCM. The crude product was purified by reversed-phase chromatography (0.1% HCl condition). HNMR, HPLC, LC-MS showed Mitolityn-1 (184.22 mg, 517 μmol, 29.8% yield, 93.5% purity (**FIG. 94**) was obtained as an off-white gum; MS cal.: 333.5; Mass found: $[M+H]^+$: 334.2 (**FIG. 95**). ^{1}H NMR: 400 MHz $CDCl_3$ δ 4.77 (s, 1H), 4.27-4.22 (m, 2H), 6.82 (s, 1H), 3.30-3.27 (t, *J* = 6.4 Hz, 2H),3.16-3.03 (m, 2H), 2.05-2.02 (t, *J* = 6.4 Hz, 2H), 1.90-1.44 (m,10H), 1.28-1.13 (m, 8H), 0.85-0.84(d, *J* = 6.8 Hz, 3H) (**FIG. 96**). ^{13}C NMR: (101MHz, $CDCl_3$) δ 159.58, 159.42, 156.48, 154.12, 55.06, 50.30, 39.77, 38.41, 34.45, 34.08, 30.21, 29.85, 26.68, 26.65, 25.66, 25.57, 23.54, 22.07, 21.11, 21.04, 19.18, 16.23, 14.91, 14.89, 8.17, 4.93 (**FIG. 97**).

[0411] **Mitolityn-2** (1-cyclohexyl-3-(3-(5-cyclopropyl)-4-ethyl-4H-1,2,4-triazol-3-yl)propyl)urea) was synthesized as a racemic mixture (**FIG. 98**). To a solution of compound 1-2 (215 mg, 2.17 mmol, 248 uL) and TEA (626 mg, 6.19 mmol, 861 μL) in DCM (10.0 mL) was added CDI (368 mg, 2.27 mmol) and the reaction mixture was stirred at 5 ~ 10°C for 3 h. Then compound 16 (400 mg, 1.73 mmol, HCl) was added to the reaction mixture and stirred at 10 ~ 15°C for 2 h. LC-MS showed compound 16 was consumed completely and desired MS (M + H = 320.3, R_t = 0.548 min) was detected. The reaction mixture was concentrated under

reduce pressure to remove DCM. The crude product was purified by reversed-phase chromatography (0.1% HCl condition). HNMR, HPLC, LC-MS showed Mitolityn-2 (120.17 mg, 389 umol, 21.3% yield, 98.0% purity (**FIG. 98**) was obtained as a yellow gum; MS cal.: 319.5; Mass found: $[M+H]^+$: 320.1 (**FIG. 99**). ^{1}H NMR: 400 MHz $CDCl_3$ δ 3.95-3.90 (m, 2H), 3.46-3.41 (m, 1H), 3.23-3.20 (t, *J* = 6.4 Hz, 2H), 2.71-2.68 (t, *J* = 7.2 Hz, 2H), 1.95-1.93 (m, 2H), 1.93-1.91 (m, 2H), 1.64-1.60 (m, 3H), 1.55-1.50 (m,2H), 1.33-1.29 (m, 5H), 1.04-0.97(m, 7H) (**FIG. 100**). ^{13}C NMR**:** (101MHz, CDCl3) δ 165.16, 158.47, 155.59, 154.08, 48.76, 39.34, 38.00, 33.91, 27.66, 25.69, 25.09, 22.35, 15.48, 6.64, 5.28 (**FIG. 101**).

[0412] **Mitolityn-3** (1-(3-(5-cyclopropyl-4-ethyl-4H-1,2,4-triazol-3-yl)propyl)-3-(3-methyltetrahydro-2H-pyran-4-yl)urea) was synthesized as a racemic mixture (**FIG. 93**). To a solution of compound 1-3 (249 mg, 2.16 mmol) and TEA (626 mg, 6.19 mmol, 861 uL) in DCM (10.0 mL) was added CDI (368 mg, 2.27 mmol) and the reaction mixture was stirred at 5 ~ 10°C for 3 h. Then compound 16 (400 mg, 1.73 mmol, HCl) was added to the reaction mixture and stirred at 10 ~ 15°C for 2 h. LC-MS showed compound 16 was consumed completely and desired MS (M + H = 336.3, R_t = 0.635 min) was detected. The reaction mixture was concentrated under reduce pressure to remove DCM. The crude product was purified by reversed-phase chromatography (0.1% HCl condition). HNMR, HPLC, LC-MS, showed Mitolityn-3 (272.01 mg, 719 umol, 41.5% yield, 88.9% purity (**FIG. 102**) was obtained as a off-white gum; MS cal.: 335.4; Mass found: $[M+H]^+$: 336.3 (**FIG. 103**). ^{1}H NMR: 400 MHz $CDCl_3$ δ 4.22-4.17 (m, 2H), 3.94-3.91 (m, 1H), 3.86-3.70 (m, 1H), 3.55-3.53 (m, 3H), 3.30-3.27 (m, 2H), 3.02-2.99 (m, 2H), 2.04-1.85 (m, 4H), 1.68-1.64 (m,2H), 1.49-1.46 (m, 3H), 1.21-1.20 (d, *J* = 6.4 Hz, 4H), 0.91-0.83 (d, *J* = 6.4 Hz, 3H) (**FIG. 104**). ^{13}C NMR: (101MHz, CDCl3) δ 159.32, 159.05, 156.36, 154.17, 73.28, 71.01, 67.39, 65.60, 52.32, 47.96, 39.46, 38.57, 38.50, 37.65, 33.82, 33.73, 29.55, 26.90, 21.36, 14.97, 13.68, 11.63, 7.87, 4.96 (**FIG. 105**).

[0413] **Mitolityn-4** 1-(3-(5-cyclopropyl-4-ethyl-4H-1,2,4-triazol-3-yl)propyl)-3-(tetrahydro-2H-pyran-4-yl)urea was synthesized as a racemic mixture (**FIG. 93**). To a solution of compound 1-4 (137 mg, 1.35 mmol) and TEA (392 mg, 3.87 mmol, 539 uL) in DCM (10 mL) was added CDI (230 mg, 1.42 mmol) and the reaction mixture was stirred at 5 ~ 10°C for 3 h. Then compound 16 (250 mg, 1.08 mmol, HCl) was added to the reaction mixture and stirred at 10 ~ 15°C for 2 h. LC-MS showed

compound 16 was consumed completely and desired MS (M + H = 322.3, R_t = 0.603 min) was detected. The reaction mixture was concentrated under reduce pressure to remove DCM. The crude product was purified by reversed-phase chromatography (0.1% HCl condition). HNMR, HPLC, LC-MS showed Mitolityn-4 (165.96 mg, 503 umol, 46.4% yield, 97.4% purity (**FIG. 106**) was obtained as a colourless gum; MS cal.: 321.4; Mass found: $[M+H]^+$: 322.3 (**FIG. 107**). ^{1}H NMR: 400 MHz $CDCl_3$ δ 4.30-4.24 (m, 2H), 4.00-3.97 (m, 2H), 3.74-3.73 (m, 1H), 3.50-3.45 (t, *J* = 4.8 Hz, 2H), 3.37-3.34 (t, *J* = 5.6 Hz, 2H), 3.09-3.06 (t, *J* = 6.8 Hz, 2H), 2.11-2.10 (d, *J* = 6.0 Hz, 2H), 1.91-1.84 (m, 3H), 1.54-1.51 (t, *J* = 7.2 Hz, 5H), 131-1.27 (m, 4H) (**FIG. 108**). ^{13}C NMR: (101MHz, CDCl3) δ 158.24, 155.71, 154.02, 67.07, 46.27, 39.53, 38.04, 33.97, 27.43, 22.49, 15.55, 6.71, 5.35 (**FIG. 109**).

[0414] The Mitolityn 5 and 6 synthesis scheme is depicted in **FIG. 110**. General procedures; preparation of compound 17: A solution of methylamine (2.00 M, 96.0 mL), K_2CO_3 (26.4 g, 191 mmol) and compound 3-1 (10.0 g, 95.7 mmol, 8.70 mL) was stirred at 15 ~ 20°C for 3 h. TLC (Petroleum ether: Ethyl acetate = 2: 1) indicated compound 3-1 (R_f = 0.20) was consumed completely and one main spot (R_f = 0.40) formed. The reaction mixture was added water (100 mL) and extracted with DCM (100 mL * 3). The combined organic layers were dried over Na_2SO_4, filtered and concentrated under reduced pressure to give a residue. HNMR showed compound 17 (7.46 g, 78.7% yield) was obtained as a yellow solid. ^{1}H NMR: 400 MHz ME2SO-d_6 δ 7.93 (s, 1H), 2.59-2.58 (d, *J* = 4.8 Hz, 3H), 1.53-1.47 (m, 1H), 0.66-0.61 (m, 4H)

[0415] Preparation of compound 12: A solution of compound 1 (20.0 g, 108 mmol, 18.4 mL) and $N_2H_4.H_2O$ (27.0 g, 540 mmol, 26.2 mL) was stirred at 80°C for 14 h. TLC (Petroleum ether: Ethyl acetate = 2: 1) indicated compound 11 (R_f = 0.30) was consumed completely and one main spot (R_f = 0.00) formed. The reaction mixture was concentrated under reduce pressure to give a residue. The residue was under lyophilization to give a residue. HNMR showed compound 12 (11.0 g, 46.9% yield) was obtained as a white solid. ^{1}H NMR: EW10761-3-P1A 400 MHz ME2SO-d_6 δ 2.96-2.86 (m, 2H), 2.01 -1.98 (t, *J* = 7.2 Hz, 2H), 1.61-1.53 (m, 2H) , 1.37 (s, 9H).

[0416] was added to a solution of compound 17 (4.00 g, 40.4 mmol) and 2,6-Lutidine (8.65 g, 80.7 mmol, 9.40 mL) in DCM (160 mL) at 0°C under N_2. The mixture was stirred for 10 min, and compound 12 (7.89 g, 36.3 mmol) was added.

The reaction mixture was stirred for 10 min at 5 ~ 10°C. The reaction mixture were added $NaHCO_3$ (346 g, 4.11 mol, 160 mL) and stirred at 80 ~ 85°C for 1 h. LC-MS showed compound 17 was consumed completely and desired MS (M + H = 281.4, R_t = 0.617 min) was detected. The reaction mixture was extracted with DCM (100 mL * 3). The combined organic layers were dried over Na_2SO_4, filtered and concentrated under reduced pressure to give a residue. The crude product was purified by reversed-phase chromatography (0.1% FA condition). HNMR showed compound 18 (4.00 g, 35.4% yield) was obtained as a brown oil. ^{1}H NMR: 400 MHz CDCl3-d_6 δ 5.00 (s, 1H), 3.61 (s, 3H), 3.24-3.19 (m, 2H), 2.83-2.79 (m, 2H), 2.02-1.97 (m, 2H), 1.75-1.73 (m, 1H), 1.44 (s, 9H), 1.14-1.07 (m, 4H).

[0417] Preparation of compound 19: To a solution of compound 18 (3.00 g, 10.7 mmol) in HCl/dioxane (15.0 mL) (4 M) was stirred at 15 ~ 20 °C for 4 h. TLC (Ethyl acetate: Methanol = 3: 1) indicated compound 18 (R_f = 0.5) was consumed completely and one main spot (R_f = 0.05) formed. The reaction mixture was filtered and the filter-cake was obtained. HNMR showed compound 19 (2.00 g, 86.3% yield, HCl) was obtained as a white solid. ^{1}H NMR: 400 MHz ME2SO-d_6 δ 8.37 (s, 2H), 3.78 (s, 3H), 3.08-3.05 (t, *J* = 7.6 Hz, 2H), 2.93-0.88 (m, 2H), 2.30-2.27 (m, 1H), 2.12-2.04 (m, 2H), 1.23-1.21 (d, *J* = 6.8 Hz, 4H).

[0418] **Mitolityn-5** (1-(3-(5-cyclopropyl-4-methyl-4H-1,2,4-triazol-3-yl)propyl)-3-(3-methyltetrahydro-2H-pyran-4-yl)urea) was synthesized as a racemic mixture (**FIG. 111**). To a solution of compound 1-3 (260 mg, 2.26 mmol, 320 uL) and TEA (645 mg, 6.37 mmol, 887 uL) in DCM (10.0 mL) was added CDI (379 mg, 2.34 mmol) and the reaction mixture was stirred at 5 ~ 10°C for 3 h. Then compound 19 (460 mg, 2.12 mmol, HCl) was added to the reaction mixture and stirred at 10 ~ 15°C for 12 h. LC-MS showed compound 19 was consumed completely and desired MS (M + H = 322.4, R_t = 0.209 min) was detected. The reaction mixture was concentrated under reduce pressure to give a residue. The residue was purified by prep-HPLC (column: Xtimate C18 150*25mm*5um; mobile phase: [water (0.05% HCl)-ACN]; B%: 0%-20%, 8min). HNMR, LC-MS showed Mitolityn-5 (162.59 mg, 19.7% yield, 82.6% purity (**FIG. 112**) was obtained as a off-white gum; MS cal.: 321.4; Mass found: $[M+H]^+$: 322.2 (**FIG. 112**). ^{1}H NMR: (400 MHz ME2SO) δ 3.77 (s, 3H), 3.66-3.64 (m, 1H), 3.43-3.42 (d, *J* = 4.4 Hz, 2H), 3.11-3.08 (t, *J* = 6.0 Hz, 2H), 2.28-2.26 (m 1H), 1.85-1.80 (m, 4H), 1.52-1.46(m, 2H), 1.21-1.14 (m, 4H), 0.80-

0.74(m, 4H) (**FIG. 113**). ^{13}C NMR (101MHz, $CDCl_3$) δ 159.52, 157.03, 154.67, 73.08, 70.74, 67.19, 65.22, 53.40, 48.61, 45.89, 38.58, 37.31, 33.74, 31.69, 29.78, 25.87, 21.47, 13.89, 12.12, 8.63, 8.21, 4.96 (**FIG. 114**).

[0419] **Mitolityn-6** 1-(3-(5-cyclopropyl-4-methyl-4H-1,2,4-triazol-3-yl)propyl)-3-(tetrahydro-2H-pyran-4-yl)urea was synthesized as a racemic mixture (**FIG. 115**). To a solution of compound 1-4 (246 mg, 2.43 mmol, 320 uL) and TEA (702 mg, 6.94 mmol, 966 uL) in DCM (10.0 mL) was added CDI (412 mg, 2.54 mmol) and the reaction mixture was stirred at 5 ~ 10°C for 3 h. Then compound 19 (500 mg, 2.31 mmol, HCl) was added to the reaction mixture and stirred at 10 ~ 15°C for 12 h. LC-MS showed compound 19 was consumed completely and desired MS (M + H = 308.4, R_t = 0.234 min) was detected. The reaction mixture was concentrated under reduce pressure to give a residue. The residue was purified by reversed-phase chromatography (0.1% TFA condition). Then the obtained residue used alkaline resin dissociation. HNMR, LC-MS showed Mitolityn-6 (205.53 mg, 28.5% yield, 98.6% purity (**FIG. 116**) was obtained as an off-white gum; MS cal.: 307.4; Mass found: $[M+H]^+$: 308.2 . ^1H NMR: (400 MHz CDCl3) δ 6.55 (s, 1H), 6.16-6.14 (d, *J* = 7.6 Hz, 1H), 3.93-3.80 (m, 3H), 3.57 (s, 3H), 3.47-3.42 (t, *J* = 11.2 Hz, 2H), 3.32-3.27 (m, 2H), 2.74-2.70 (m, 2H), 2.01-1.97 (m, 2H), 1.89-1.86 (d, *J* = 11.6 Hz, 2H), 1.73-1.70 (m, 2H), 1.48-1.45 (m, 2H) , 1.05-1.01(m, 4H). ^{13}C NMR (101MHz, $CDCl_3$) δ 158.40, 157.29, 156.14, 154.49, 66.87, 66.83, 45.94, 45.75, 39.18, 33.85, 33.78, 29.41, 27.31, 22.37, 6.27, 5.14.

Analytical methods

[0420] NMR spectrometry was carried out on a Bruker AVANCE NEO 400MHz with a 5 mm PABBO BB/19F-1H/D Z-GRD probe.

[0421] LC-MS/MS (ESI) was performed using two different systems: 1) SHIMADZU LC-MS-2020 instrument and data analized with LabSolution Version 5.72 software. The HPLC contained a Chromolith@Flash RP-18E 25*2.0 MM column that ran at 50℃ and a PDA (220&254nm) detector. Data was acquired in scan MS Mode (positive mode) and selected with a scan range of m/z = 100-1000. The drying Gas (N2) flow was 15 L/min, the DL Voltage was 120(V) and the Qarray DC Voltage 20(V). 2) Agilent 1200\G6110A instrument and data analized with Agilent ChemStation Rev. B. 04.03[54] software. The HPLC contained a Xbridge C18 2.1*50 mm, 5um column that ran at 40℃ and a DAD（220 nm）/ ELSD detector. Data was

acquired in scan MS Mode (positive mode) and selected with a scan range of m/z = 100-1000. The drying gas (N2) flow was 10 L/min, the capillary voltage was 2500(V), and the drying gas temperature was 350°C and the nebulizer pressure 35 psig.

CLAIMS

What is claimed is:

1. A method of treating a peripheral nervous system (PNS) or central nervous system (CNS) injury comprising:

administering to a subject a therapeutically effective amount of a composition comprising one or more of a mitofusin modulating agent or a pharamaceutically acceptable salt thereof, wherein the mitofusin modulating agent regulates mitochondrial fusion, enhances axonal regeneration, neuronal regeneration, or enhances mitochondrial transport.

2. The method of claim 1, wherein the composition comprises one or more mitofusin modulating agent, wherein the mitofusin modulating agent comprises a mitofusin mini peptide or formula:

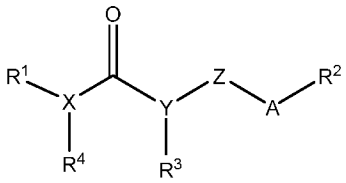

(I);
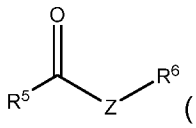

(II); or
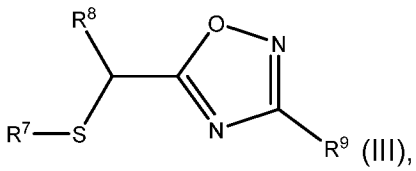

(III),

or a pharmaceutically acceptable salt, tautomer, or stereoisomer thereof wherein,

R^1 is selected from the group consisting of C_{1-8} alkyl, C_{1-8} alkyl substituted with S, S, thiophene, C_{3-8} cycloalkyl, C_{3-8} heteroaryl, C_{3-8} heterocyclyl, thiophene, and thiophene carboxamide;

R^2 is selected from the group consisting of C_{3-8} cycloalkyl, C_{3-8} heteroaryl, C_{3-8} heterocyclyl, imidazole, thiophene, thiophene carboxamide, and triazole;

R^3 is absent or selected from the group consisting of hydrogen (H) and C_{1-8} alkyl;

R^4 is absent or selected form the group consisting of hydrogen (H) and C_{1-8} alkyl;

R^5 is selected from the group consisting of C_{1-8} alkyl, C_{1-8} alkyl substituted with S, S, thiophene, C_{3-8} cycloalkyl, C_{3-8} heteroaryl, C_{3-8} heterocyclyl, thiophene, thiophene carboxamide, and triazole;

R^6 is selected from the group consisting of bicyclononanone, pyrrole, benzimidizole, pyrrole substituted pyrrole, and substituted benzimidizole;

R^7 is selected from the group consisting of C_{1-8} alkyl, pyrrole, pyrrole substituted pyrrole, benzimidizole, and substituted benzimidizole;

R^8 is selected from the group consisting of hydrogen (H);

R^9 is selected from the group consisting of C_{1-8} alkyl, pyrrole, substituted pyrrole, pyrrole substituted pyrrole, benzimidizole, and substituted benzimidizole;

A is selected from the group consisting of a bond, S, C, O, and N;

X is selected from the group consisting of O, C, and N;

Y is selected from the group consisting of O, C, and N; and

Z is a linker group selected from the group consisting of a bond or C_{1-6} alkyl; and

optionally, R^1 and R^2 form a cyclic group, R^1 and R^4 form a cyclic group, R^2 and R^3 form a cyclic group, R^4 and R^3 form a cyclic group; or R^8 and R^7 form a cyclic group,

wherein,

the bicyclononanone optionally comprises one or more N atoms.

3. The method of claim 1, wherein the mitofusin modulating agent is selected from a compound of

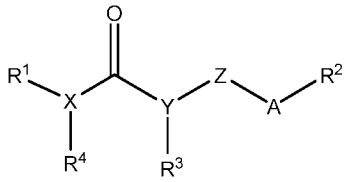

(I), wherein,

R^1 is selected from the group consisting of

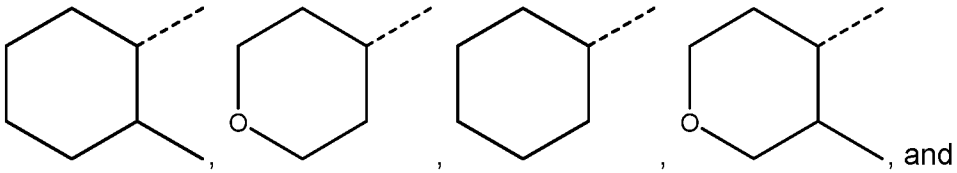

, and

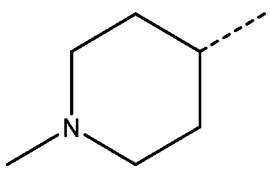

;

R^2 is selected from the group consisting of

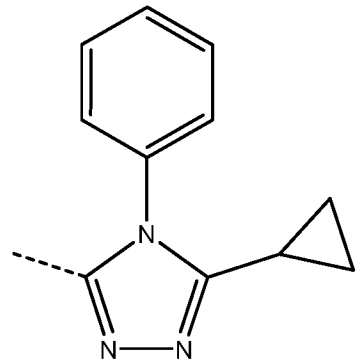
,
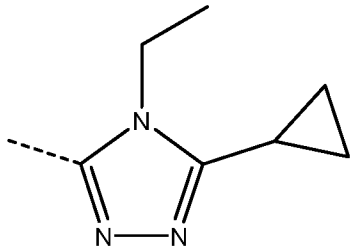
,
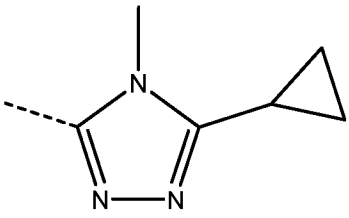
,
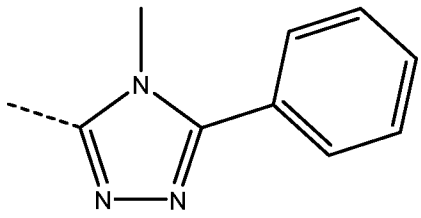
, and
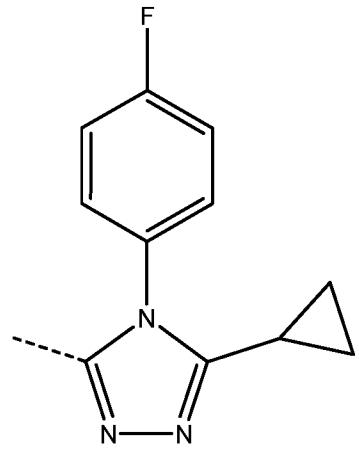
;

R^3 is selected from the group consisting of hydrogen (H) and C_{1-8} alkyl;

R^4 is selected form the group consisting of hydrogen (H) and C_{1-8} alkyl;

A is a bond, S, SO, SO_2, C, or O;

X is N;

Y is N; and

Z is a linker group selected from the group consisting of a bond or C_{1-6} alkyl.

4. The method of claim 3, wherein, R^1, R^2, R^3, or R^4 are optionally substituted by one or more of:

acetamide, C_{1-8} alkoxy, amino, azo, Br, C_{1-8} alkyl, carbonyl, carboxyl, Cl, cyano, C_{3-8} cycloalkyl, C_{3-8} heteroaryl, C_{3-8} heterocyclyl, hydroxyl, F, halo, indole, N, nitrile, O, phenyl, S, sulfoxide, sulfur dioxide, or thiophene; and

optionally further substituted with one or more acetamide, alkoxy, amino, azo, Br, C_{1-8} alkyl, carbonyl, carboxyl, Cl, cyano, C_{3-8} cycloalkyl, C_{3-8} heteroaryl, C_{3-8} heterocyclyl, hydroxyl, F, halo, indole, N, nitrile, O, phenyl, S, sulfoxide, sulfur dioxide, or thiophene;

wherein,

the alkyl, cycloalkyl, heteroaryl, heterocyclyl, indole, or phenyl, is optionally further substituted with one or more selected from the group consisting of acetamide, alkoxy, amino, azo, Br, C_{1-8} alkyl, carbonyl, carboxyl, Cl, cyano, C_{3-8} cycloalkyl, C_{3-8} heteroaryl, C_{3-8} heterocyclyl, hydroxyl, F, halo, indole, N, nitrile, O, phenyl, S, sulfoxide, sulfur dioxide, or thiophene.

5. The method of any one of claims 1 to 3, wherein the compound is selected from the group consisting of:

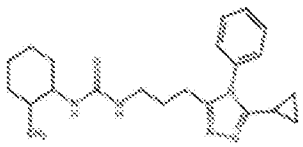

1-(3-(5-cyclopropyl-4-phenyl-4H-1,2,4-triazol-3-yl)propyl)-3-(2-methylcyclohexyl)urea;

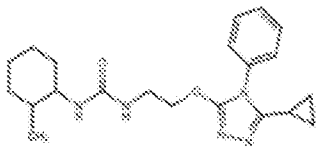

1-(2-((5-cyclopropyl-4-phenyl-4H-1,2,4-triazol-3-yl)oxy)ethyl)-3-(2-methylcyclohexyl)urea;

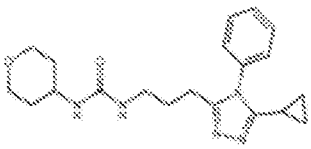

1-(3-(5-cyclopropyl-4-phenyl-4H-1,2,4-triazol-3-yl)propyl)-3-(tetrahydro-2H-pyran-4-yl)urea;

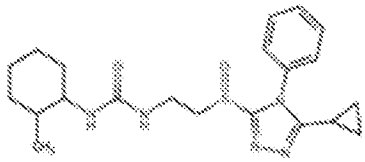

1-(2-((5-cyclopropyl-4-phenyl-4H-1,2,4-triazol-3-yl)sulfinyl)ethyl)-3-(2-methylcyclohexyl)urea;

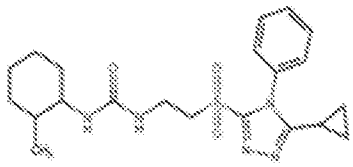

1-(2-((5-cyclopropyl-4-phenyl-4H-1,2,4-triazol-3-yl)sulfonyl)ethyl)-3-(2-methylcyclohexyl)urea;

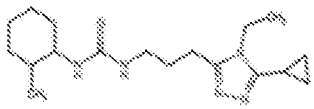

1-(3-(5-cyclopropyl-4-ethyl-4H-1,2,4-triazol-3-yl)propyl)-3-(2-methylcyclohexyl)urea;

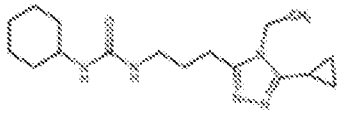

1-cyclohexyl-3-(3-(5-cyclopropyl)-4-ethyl-4H-1,2,4-triazol-3-yl)propyl)urea;

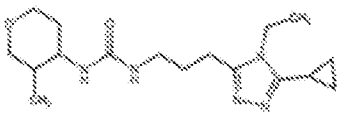

1-(3-(5-cyclopropyl-4-ethyl-4H-1,2,4-triazol-3-yl)propyl)-3-(3-methyltetrahydro-2H-pyran-4-yl)urea;

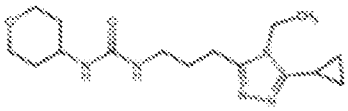

1-(3-(5-cyclopropyl-4-ethyl-4H-1,2,4-triazol-3-yl)propyl)-3-(tetrahydro-2H-pyran-4-yl)urea;

1-(3-(5-cyclopropyl-4-methyl-4H-1,2,4-triazol-3-yl)propyl)-3-(3-methyltetrahydro-2H-pyran-4-yl)urea;

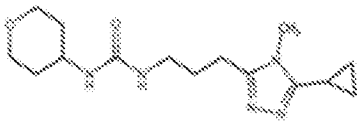

1-(3-(5-cyclopropyl-4-methyl-4H-1,2,4-triazol-3-yl)propyl)-3-(tetrahydro-2H-pyran-4-yl)urea;

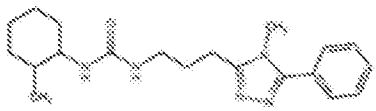

1-(3-(4-methyl-5-phenyl-4H-1,2,4-triazol-3-yl)propyl)-3-(2-methylcyclohexyl)urea;

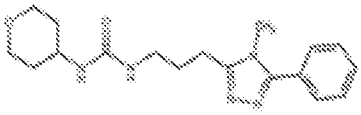

1-(3-(4-methyl-5-phenyl-4H-1,2,4-triazol-3-yl)propyl)-3-(tetrahydro-2H-pyran-4-yl)urea; and

1-(3-(4-methyl-5-phenyl-4H-1,2,4-triazol-3-yl)propyl)-3-(3-methyltetrahydro-2H-pyran-4-yl)urea.

6. The method of any one of claims 1 to 3, wherein the compound is selected from the group consisting of:

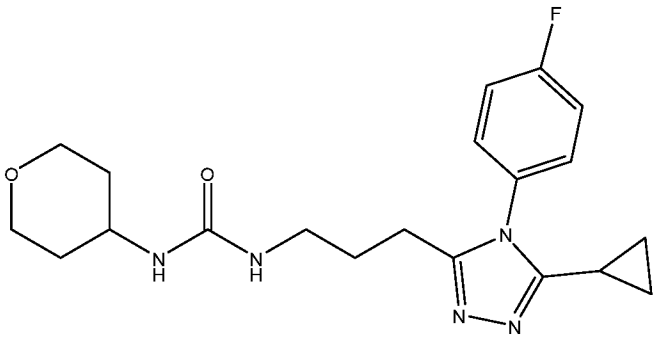

1-(3-(5-cyclopropyl-4-(4-fluorophenyl)-4H-1,2,4-triazol-3-yl)propyl)-3-(tetrahydro-2H-pyran-4-yl)urea;

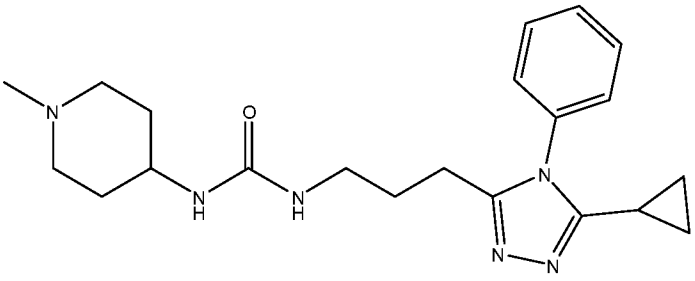

1-(3-(5-cyclopropyl-4-phenyl-4H-1,2,4-triazol-3-yl)propyl)-3-(1-methylpiperidin-4-yl)urea;

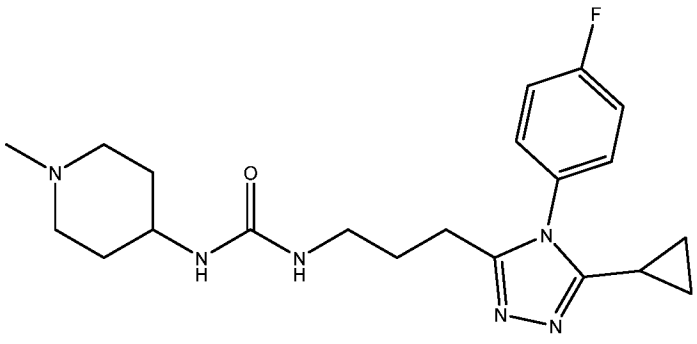

1-(3-(5-cyclopropyl-4-(4-fluorophenyl)-4H-1,2,4-triazol-3-yl)propyl)-3-(1-methylpiperidin-4-yl)urea;

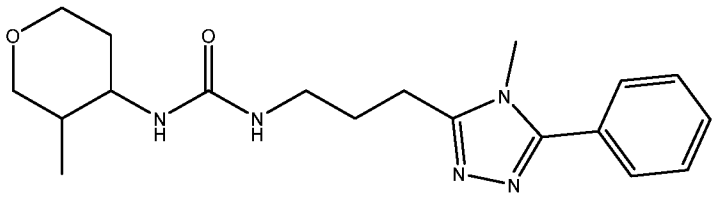

1-(3-(4-methyl-5-phenyl-4H-1,2,4-triazol-3-yl)propyl)-3-(3-methyltetrahydro-2H-pyran-4-yl)urea; and

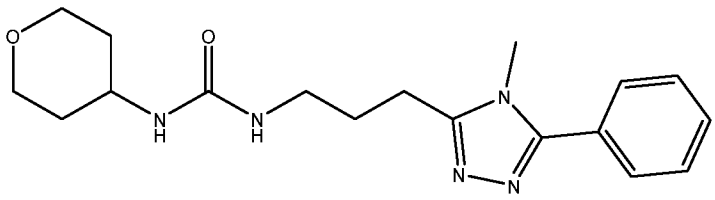

1-(3-(4-methyl-5-phenyl-4H-1,2,4-triazol-3-yl)propyl)-3-(tetrahydro-2H-pyran-4-yl)urea.

7. The method of claim 1, wherein the the PNS or CNS injury is selected from the group consisting of crush injury, spinal cord injury (SCI), traumatic brain injury, stroke, optic nerve injury, and related conditions that involve axonal disconnection.

8. The method of claim 1, wherein the compsotion does not comprise a compound of Table 4.

9. The method of any one of the preceding claims, wherein the mitofusin modulating agent comprises:

a small molecule mimetic of a Mfn2 peptide-peptide interface; or

a mitofusin agonist;

wherein the mitofusin modulating agent

allosterically activates Mfn2 or promotes mitochondrial fusion;

improves mitochondrial dysmotility, mitochondrial fragmentation, mitochondrial depolarization, or mitochondrial clumping;

normalizes or enhances axonal mitochondrial trafficking within nerves of a subject with a Mfn2 mutation;

regulates mitochondrial fusion;

inhibits or blocks HR1-HR2 interaction;

regulates mitochondrial function;

regulates mitochondrial tethering and fusion;

corrects mitochondrial and cellular dysfunction;

repairs defects in neurons with mitochondrial mutations;

inhibits mitochondrial fusion by directing Mfn1 and Mfn2 to different conformational states;

targets Mfn1 or Mfn2;

activates or inhibits mitochondrial tethering or mitochondrial fusion;

activates or inhibits mitochondrial fusion by directing Mfn1 and Mfn2 to different conformational states;

breaks down tethers between mitochondria and ER; or

restores mitochondrial fusion.

10. The method according to any one of the preceding claims comprising a pharmaceutically acceptable excipient.

11. A method of treating a CNS or PNS related injury or trauma in a subject comprising administering to the subject a therapeutically effective amount of a mitofusin modulating agent of any one of claims 2 to 10.

12. The method of claim 11, wherein the subject is diagnosed with or is suspected of having a CNS or PNS related injury or trauma.

13. The method of claim 11, wherein the CNS or PNS related injury or trauma is selected from one or more of the group consisting of: crush injury; spinal cord injury (SCI); traumatic brain injury (TBI); stroke; optic nerve injury; related conditions that involve axonal disconnection or damage; damage to the nervous system,

caused by mechanical, thermal, chemical, or ischemic factors; disruption between neurons and their supporting cells; or destruction of the blood–brain barrier.

14. The method of any one of the preceding claims wherein the mitofusin modulating agent corrects cell and organ dysfunction caused by injury to the CNS or PNS or ischemia-reperfusion injury.

15. The method of any one of the preceding claims wherein the mitofusin modulating agent or mitofusin agonists:

reverses mitochondrial defects;

promotes mitochondria transport activity;

modulates or enhances the transport, trafficking, mobility, or movement of mitochondria (in, optionally, a nerve);

restores or enhances axonal mitochondrial trafficking;

enhances mitochondrial elongation or mitochondrial elongation aspect ratio;

disrupts intramolecular restraints in Mfn2; or

promotes mitochondrial fusion or trafficking in neurons.

16. A method of designing a peptide mimetic comprising:

(i) providing an HR1-derived mini-peptide that competes with endogenous HR1-HR2 binding;

(ii) functionally analyzing a complete series of alanine substituted peptides by structural modeling of functional amino acid side chains of mitofusin (Mfn)-derived mini-peptides, thereby identifying functionally-critical amino acid side chains;

(iii) identifying a chemical structure that mimics the 3-dimensional spatial and charge characteristics of these functional amino acid side chains; and

(iv) designing a peptide mimetic based on the identified chemical structure.

17. A method of screening and evaluating one or more candidate molecules for mitochondrial fusion modulatory activity, the method comprising:

(i) providing a Mfn2 protein receptor comprising a HR2 peptide sequence or a fragment of Mfn2 comprising an HR2 domain;

(ii) immobilizing the receptor on a solid substrate to generate a bound substrate;

(iii) contacting the immobilized receptor to amino-FITC-tagged Mfn2 374-384 (agonist ligand) or amino-FITC-tagged Mfn2 406-418 (antagonist ligand);

(iv) incubating at least one candidate molecule with a combination comprising a labeled peptide and a bound substrate to generate a test assay mixture; and

(v) detecting or measuring a signal present at the location of a bound substrate.

18. The method of any claim 17, wherein an increase in aspect ratio (mitochondrial elongation) indicates increased Mfn-mediated mitochondrial fusion.

19. The method according to claim 17, further comprising identifying a candidate molecule as an activator of mitochondrial fusion when a signal of the test assay mixture present at the location of the bound substrate is less than the signal of a control assay mixture which comprises a labeled peptide and bound substrate in the absence of the at least one candidate molecule.

20. The method of any claim 17, wherein

if the method is screening for an agonist, the receptor comprises SEQ ID NO: 1 and the ligand comprises a FITC labeled SEQ ID NO: 2; or

if the method is screening for an antagonist, the receptor comprises SEQ ID NO 4 and the ligand comprises a FITC labeled SEQ ID NO: 4.

21. The method of any claim 17, wherein a Ser is replaced with Asp, conferring a negative charge essential for activity.

22. A method of screening one or more candidate molecules for mitochondrial fusion modulatory activity comprising:

(i) labeling a first Mfn2 protein with at least 90% sequence identity to SEQ ID NO: 6 or a functional fragment thereof with amino acids 80-275 deleted with an acceptor fluorophore within or near the HR2 domain to generate a first labeled Mfn2

protein, wherein the first Mfn2 protein or functional fragment comprises the HR2 domain (amino acids 681 to 757 of SEQ ID NO: 6);

(ii) labeling a second Mfn2 protein with at least 90% sequence identity to SEQ ID NO: 6 or a functional fragment thereof with amino acids 80-275 deleted with a donor fluorophore to generate a second labeled Mfn2 protein, wherein the first Mfn2 protein or functional fragment comprises the HR2 domain (amino acids 681 to 757 of SEQ ID NO: 6);

(iii) combining the first labeled Mfn2 protein or fragment thereof with the second labeled Mfn2 protein or fragment thereof to generate a control mixture;

(iv) combining the first labeled Mfn2 protein or fragment thereof with the second labeled Mfn2 protein or fragment thereof and at least one candidate molecule to generate a test mixture; and

(v) measuring fluorescence of the test mixture and the fluorescence of the control mixture.

23. The method of claim 22, further comprising comparing the fluorescence of the test mixture with the fluorescence of the control mixture, wherein when the fluorescence of the test mixture is less than the fluorescence of the control mixture, the one or more candidate molecules in the test mixtures is identified as an activator of mitochondrial fusion.

24. A method for screening one or more candidate molecules for mitochondrial fusion modulatory activity, the method comprising:

(i) labeling an Mfn2 protein with at least 90% sequence identity to SEQ ID NO: 6 or a functional fragment thereof with amino acids 80-275 deleted with an acceptor fluorophore within or near the HR1 domain and labeling the Mfn2 protein with a donor fluorophore within or near the HR2 domain to generate a labeled Mfn2 protein;

(ii) combining the labeled Mfn2 protein with one or more candidate molecules to generate a test mixture; and

(iii) measuring the fluorescence of the test mixture and the fluorescence of a control mixture.

25. The method of claim 24, further comprising comparing the fluorescence of the test mixture with the fluorescence of the control mixture, wherein when the fluorescence of the test mixture is less than the fluorescence of the control mixture, the one or more candidate molecules in the test mixtures is identified as an activator of mitochondrial fusion.

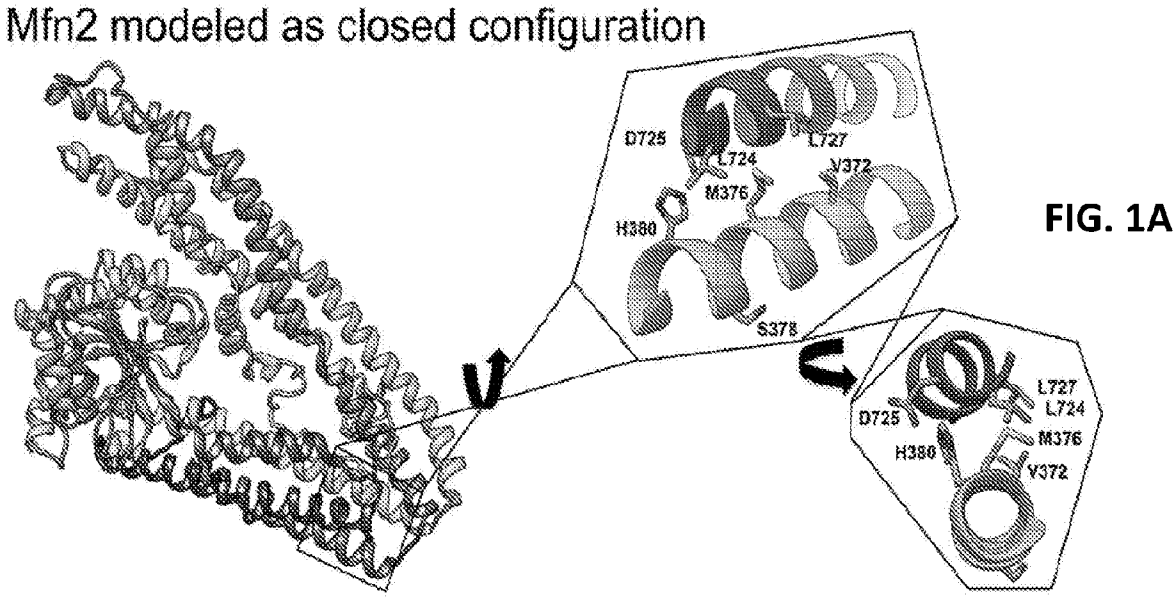
Mfn2 modeled as closed configuration
D725
L727
L724
V372
M376
H380
S378
L727
L724
D725
M376
H380
V372

FIG. 1A

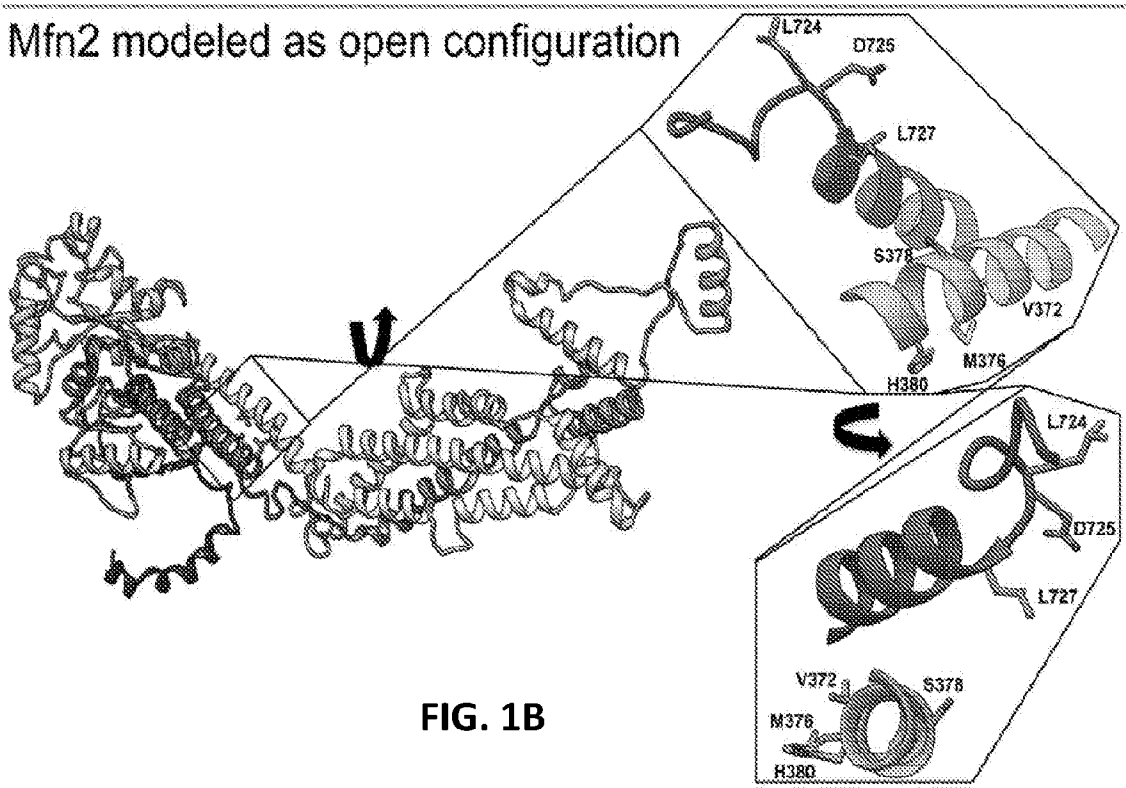
Mfn2 modeled as open configuration
L724
D725
L727
S378
V372
M376
H380
L724
D725
L727
V372
S378
M376
H380

FIG. 1B

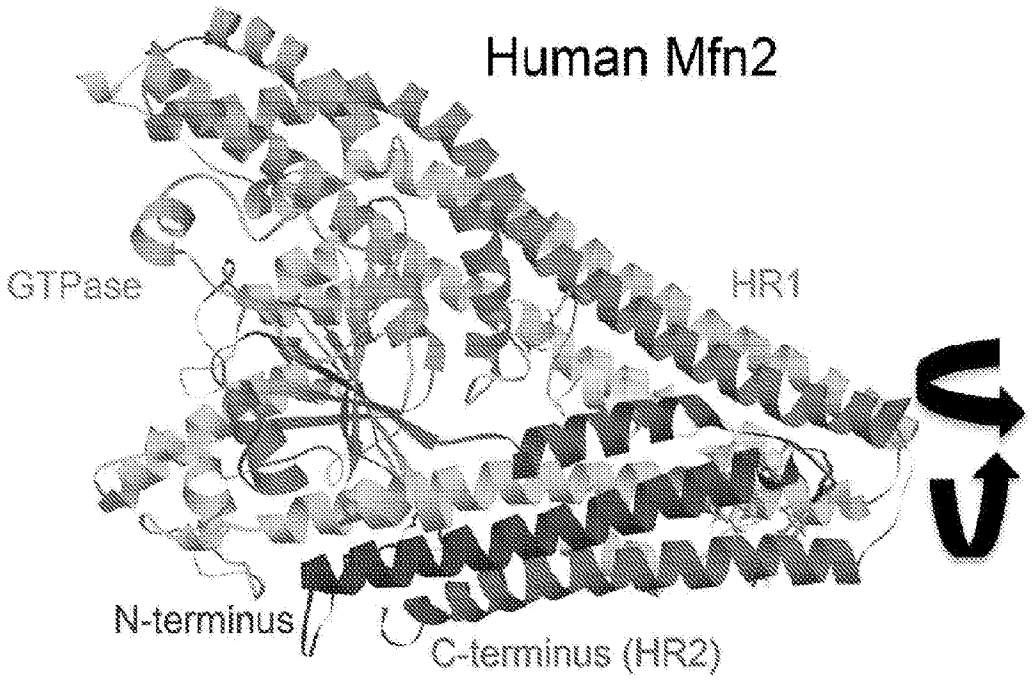
Human Mfn2
GTPase
HR1
N-terminus
C-terminus (HR2)

FIG. 1C

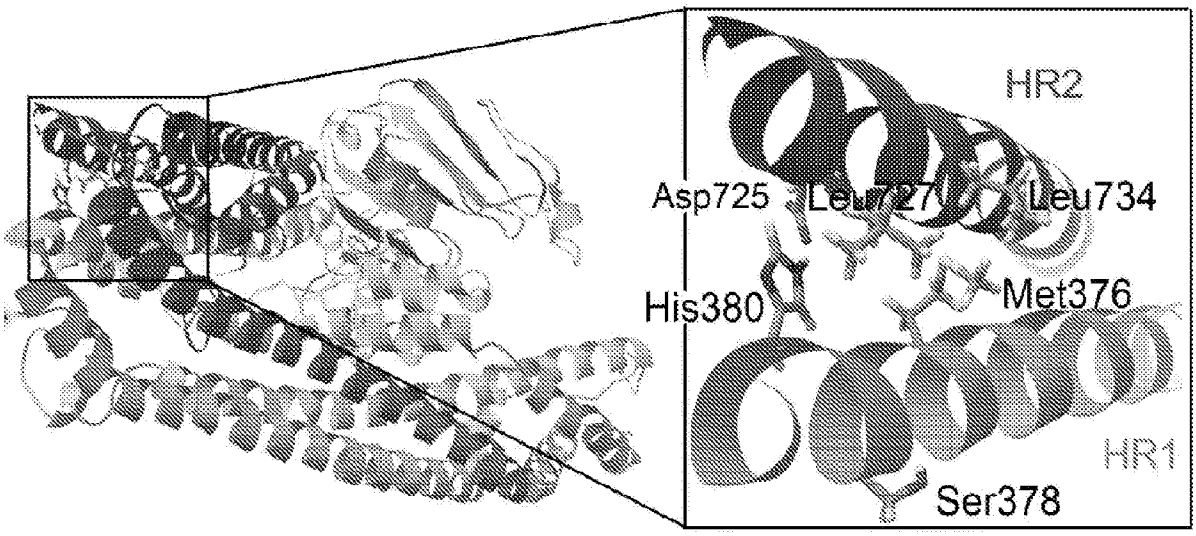
HR2
Asp725
Leu727
Leu734
His380
Met376
HR1
Ser378

FIG. 1D

HR1 367-384

H- + H+H+ HH-HH+HHH- H+HHH+-

hMfn2 HR1 358 N-FEQHTIRAKQIAEAVRLLMDSLHMAARQQ-C 389

FIG. 2A

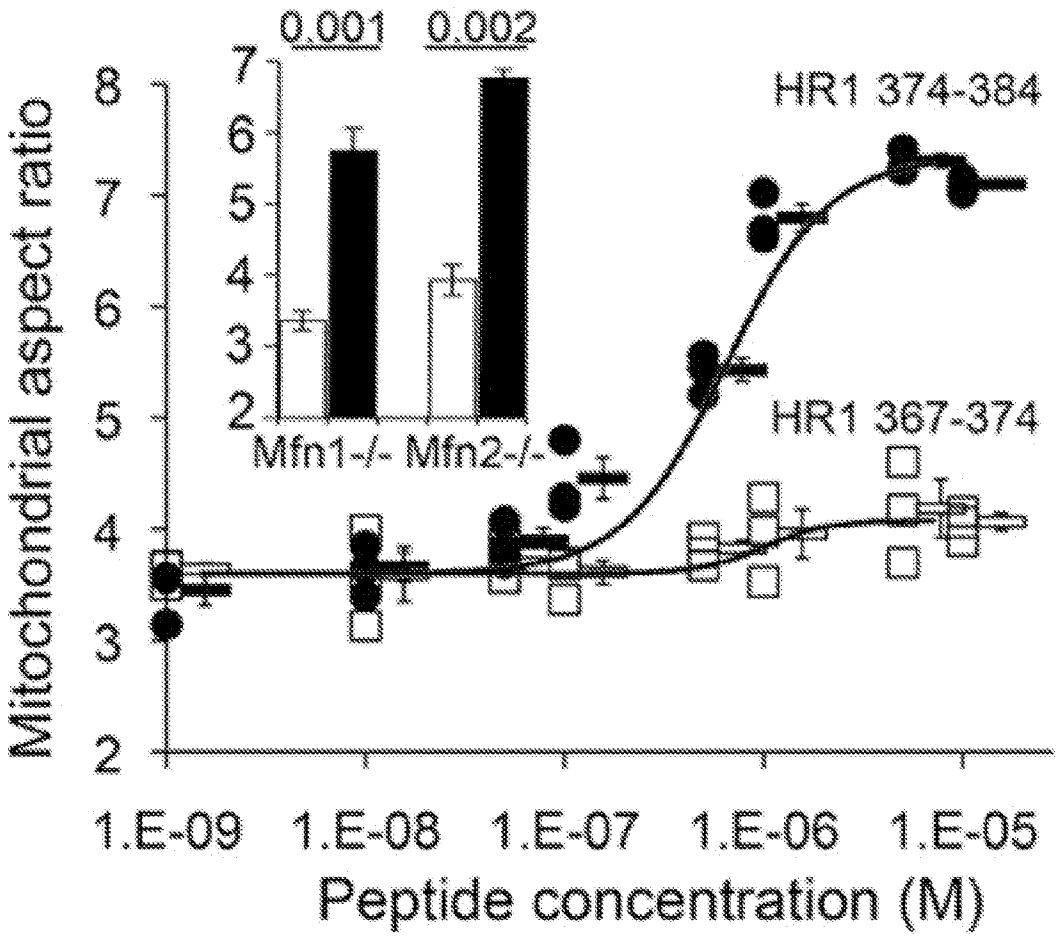

FIG. 2B

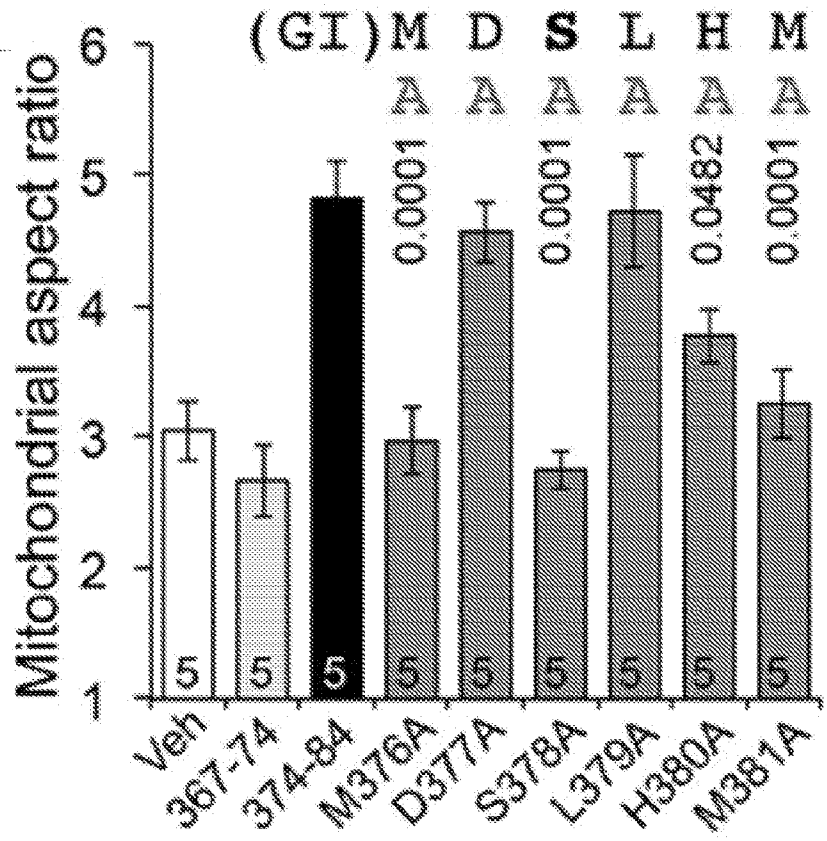
(GI)M D S L H M
A A A A A A
Mitochondrial aspect ratio
1
2
3
4
5
6
0.0001
0.0001
0.0482
0.0001
5
Veh
367-74
374-84
M376A
D377A
S378A
L379A
H380A
M381A

FIG. 2C

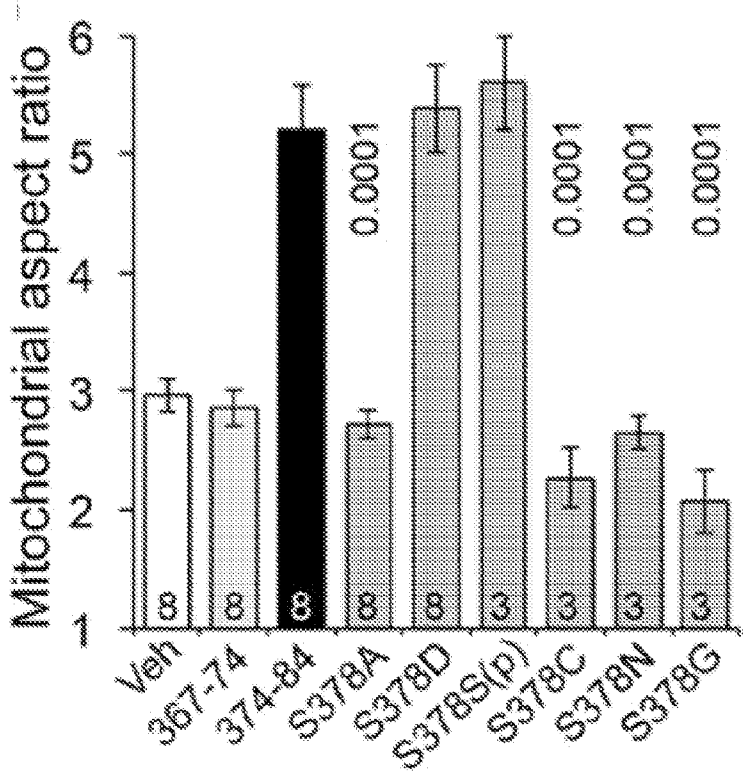
Mitochondrial aspect ratio
1
2
3
4
5
6
0.0001
0.0001
0.0001
0.0001
8
3
Veh
367-74
374-84
S378A
S378D
S378S(p)
S378C
S378N
S378G

FIG. 2D

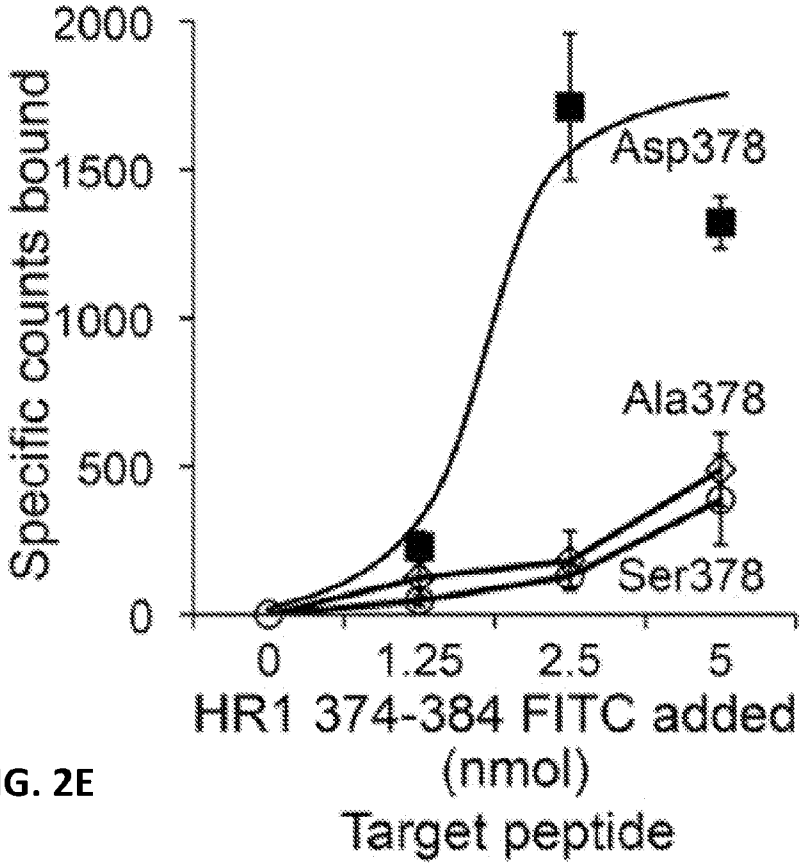
2000
1500
1000
500
0
Specific counts bound
Asp378
Ala378
Ser378
0
1.25
2.5
5
HR1 374-384 FITC added
(nmol)
Target peptide

FIG. 2E

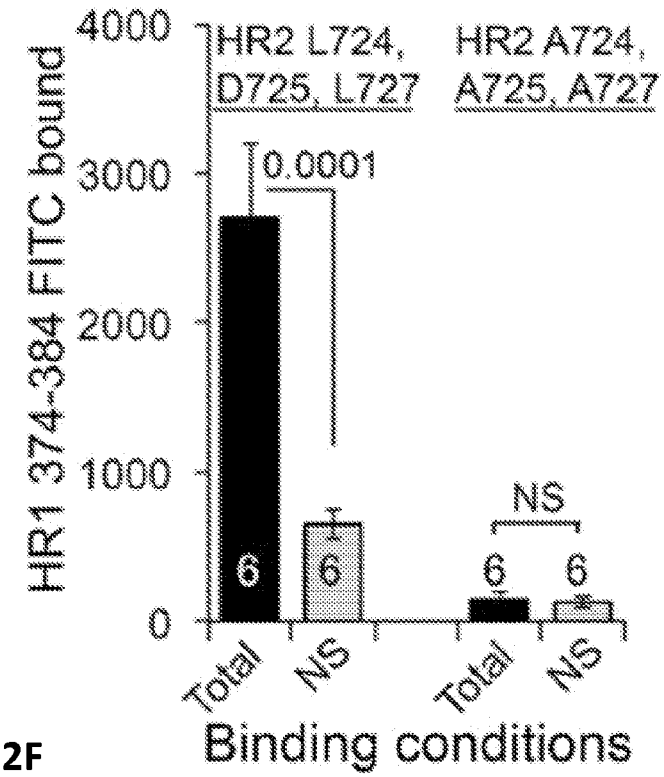
4000
3000
2000
1000
0
HR1 374-384 FITC bound
HR2 L724, D725, L727
HR2 A724, A725, A727
0.0001
NS
6
6
6
6
Total
NS
Total
NS
Binding conditions

FIG. 2F

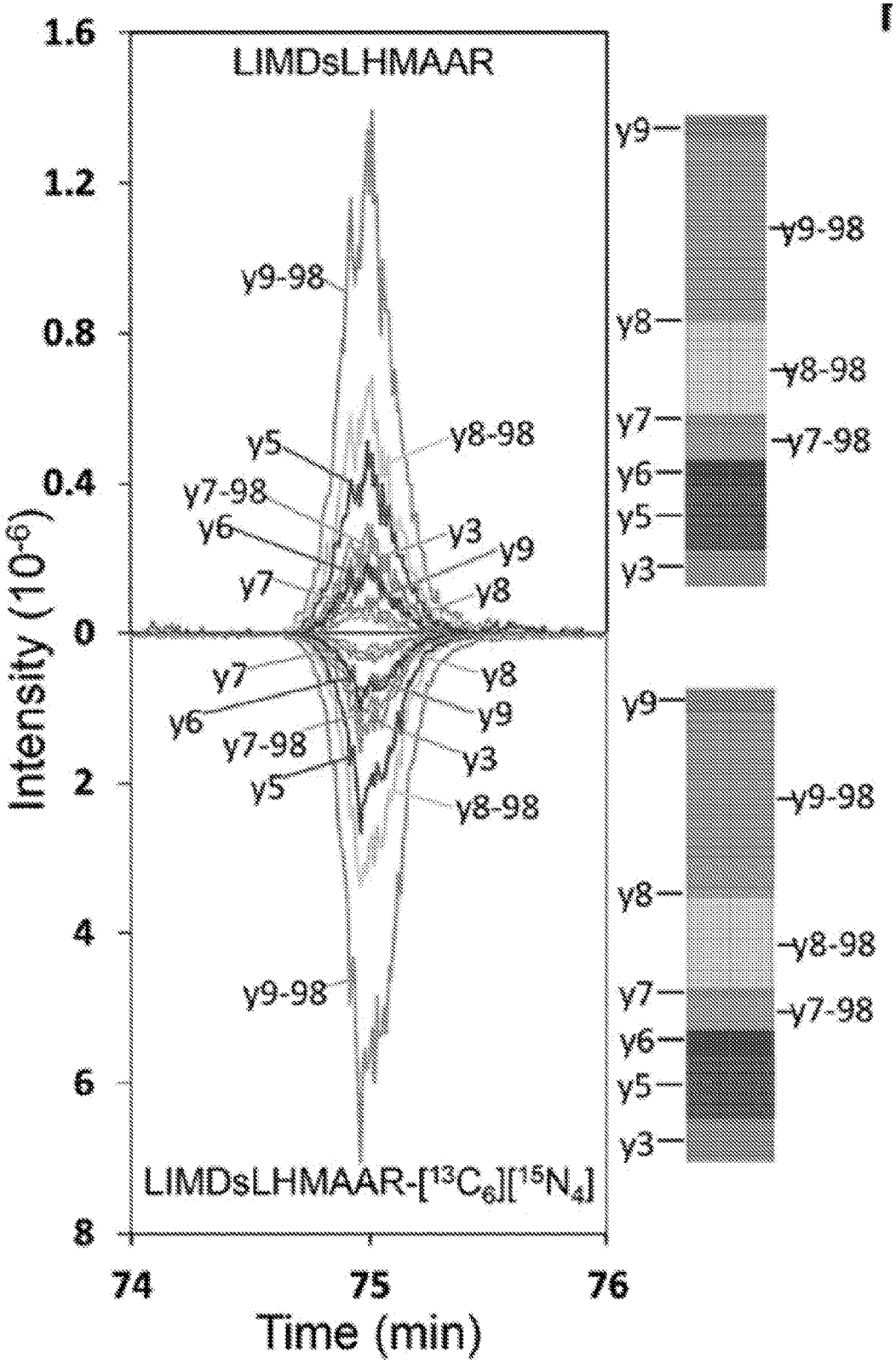
LIMDsLHMAAR
LIMDsLHMAAR-[13C6][15N4]
Intensity (10-6)
Time (min)
1.6
1.2
0.8
0.4
0
2
4
6
8
74
75
76
y9
y9-98
y8
y8-98
y7
y7-98
y6
y5
y3

FIG. 2G

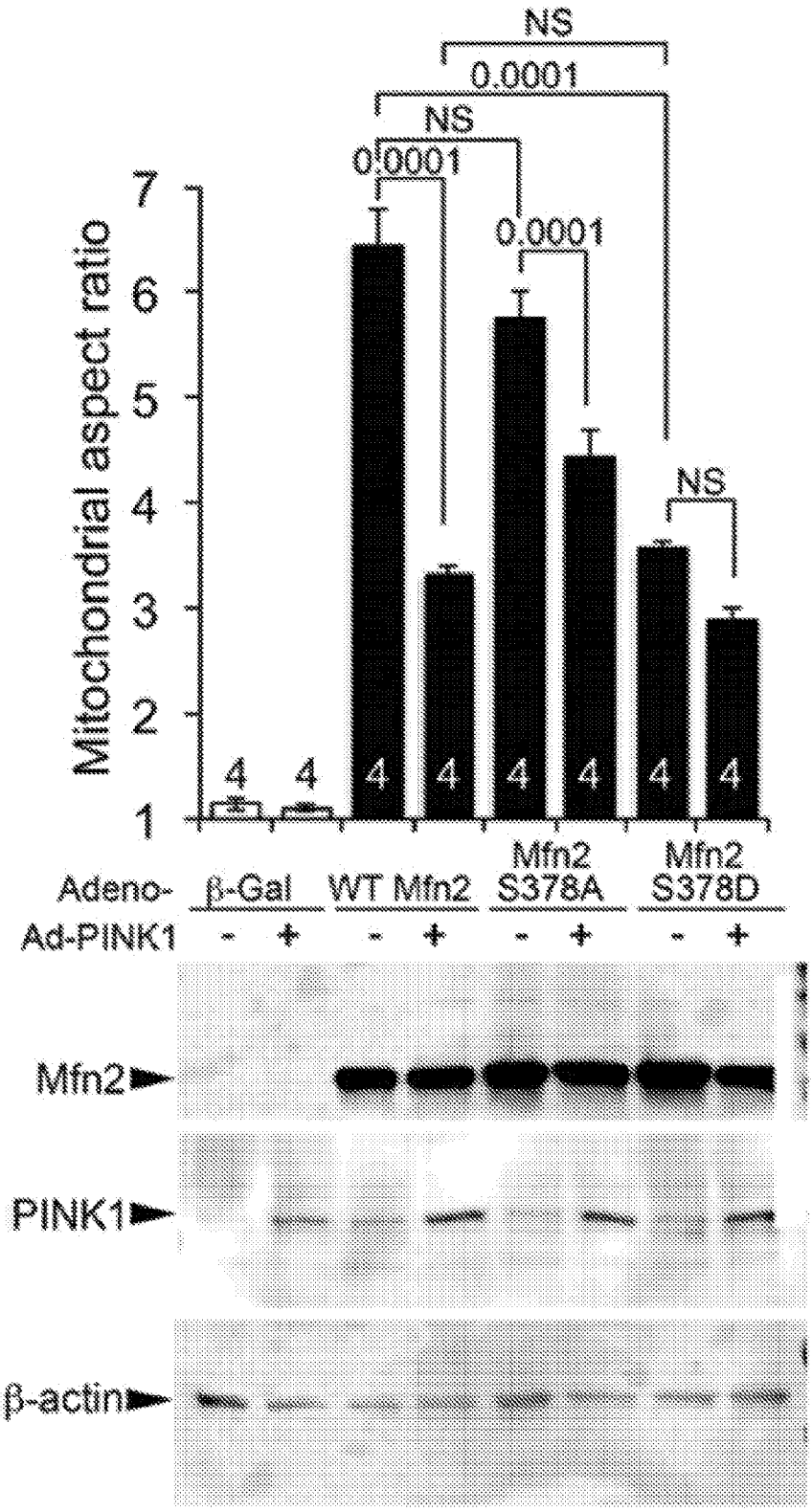
NS
0.0001
NS
0.0001
0.0001
NS
Mitochondrial aspect ratio
7
6
5
4
3
2
1
4 4 4 4 4 4 4 4
Adeno- β-Gal WT Mfn2 Mfn2 S378A Mfn2 S378D
Ad-PINK1 - + - + - + - +
Mfn2
PINK1
β-actin

FIG. 2H

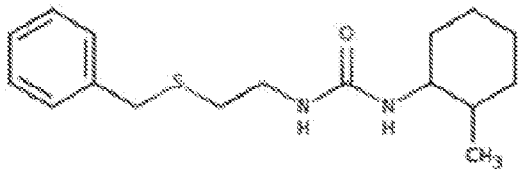

Compound A from vendor

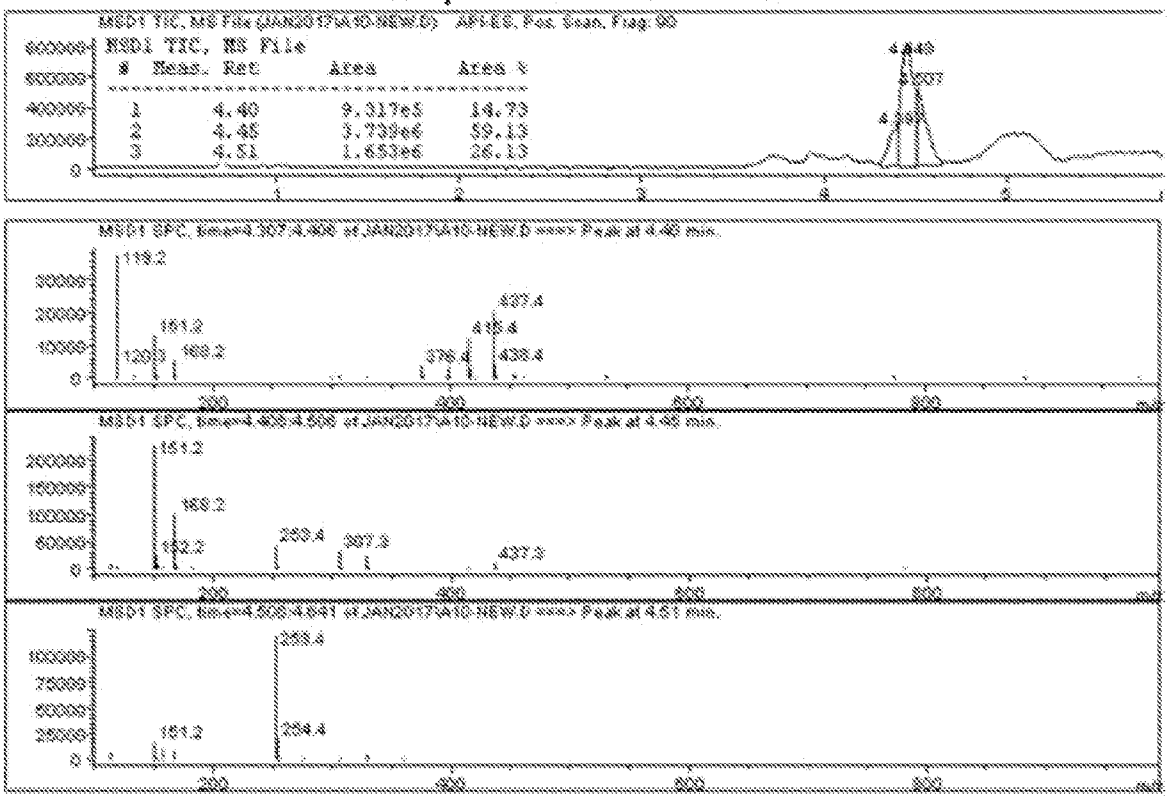

Compound A after purification

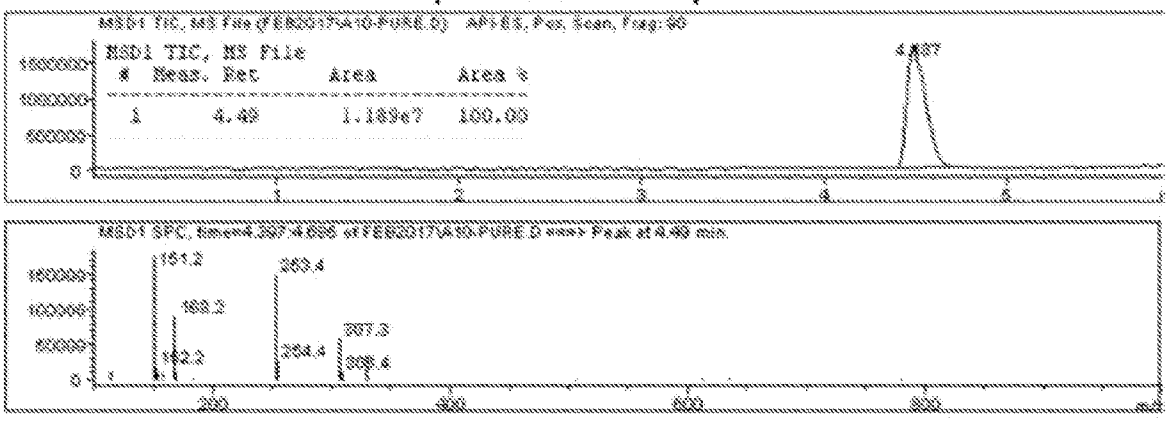

FIG. 3A

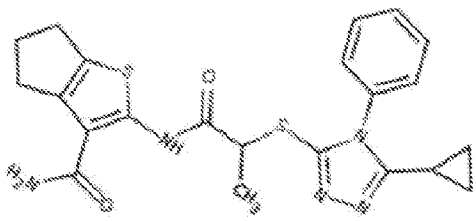

Compound B from vendor

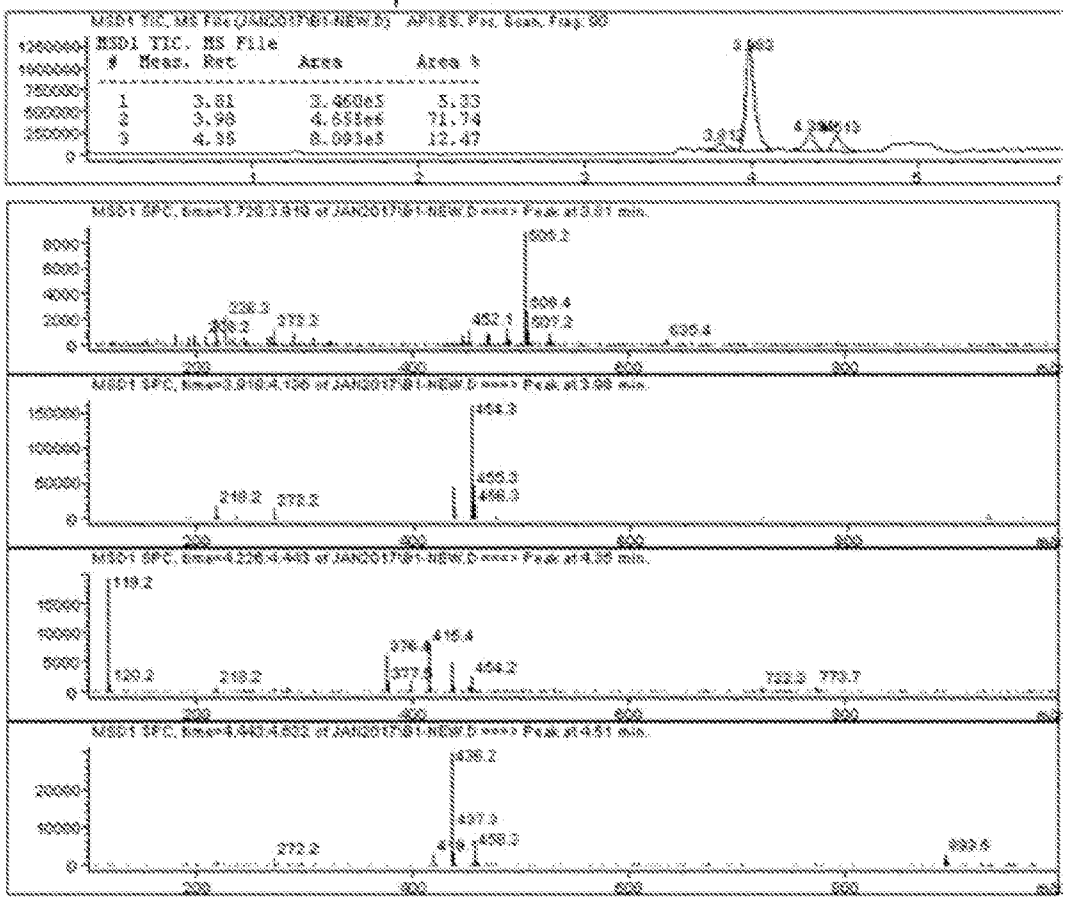

Compound B after purification

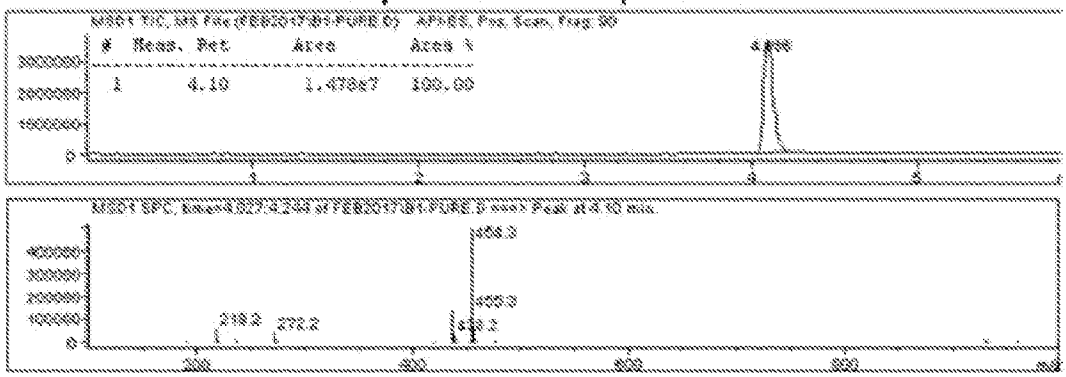

FIG. 3B

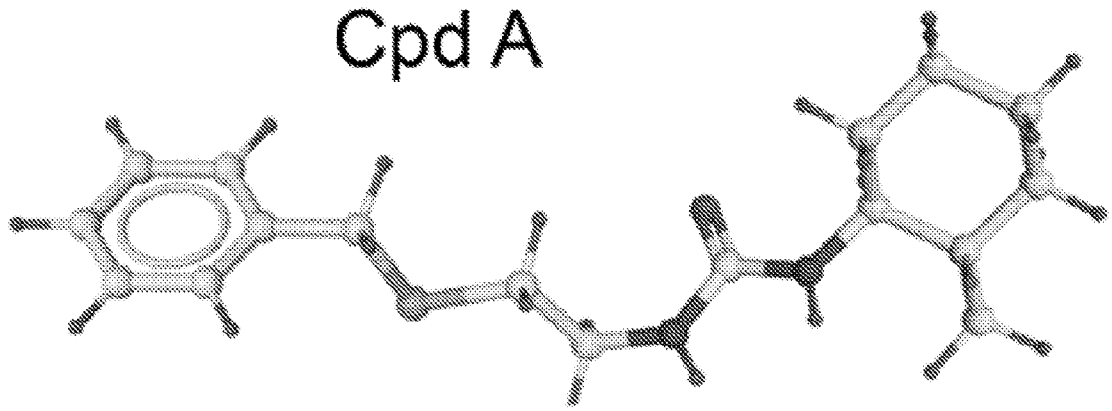

FIG. 4A

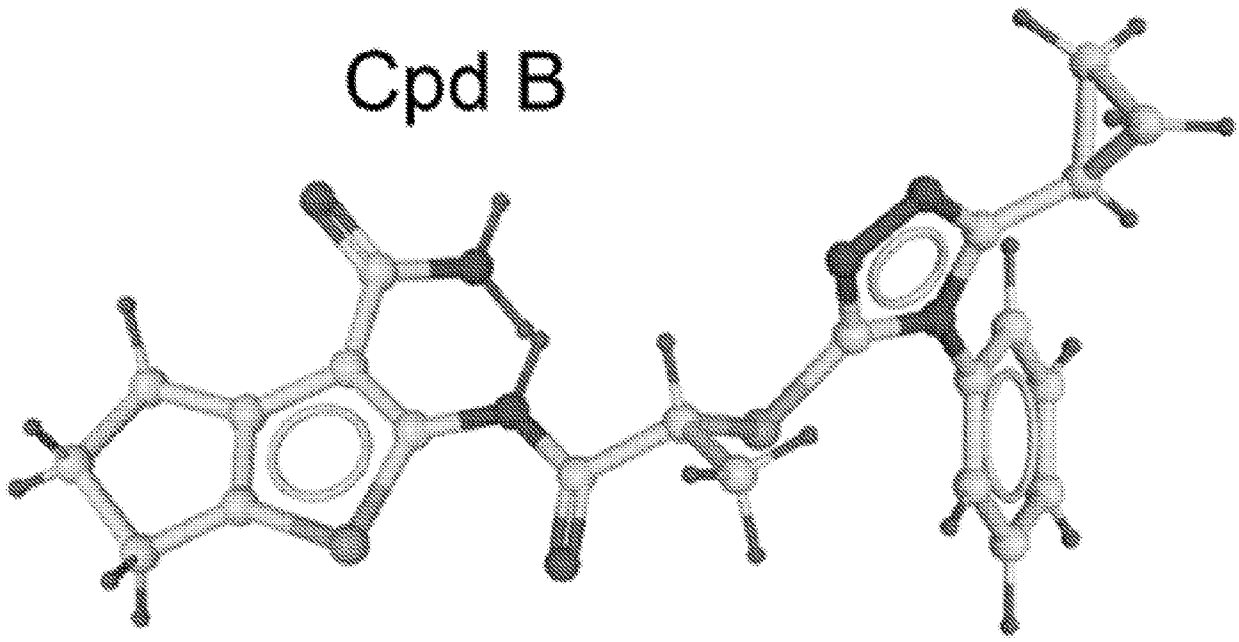

FIG. 4B

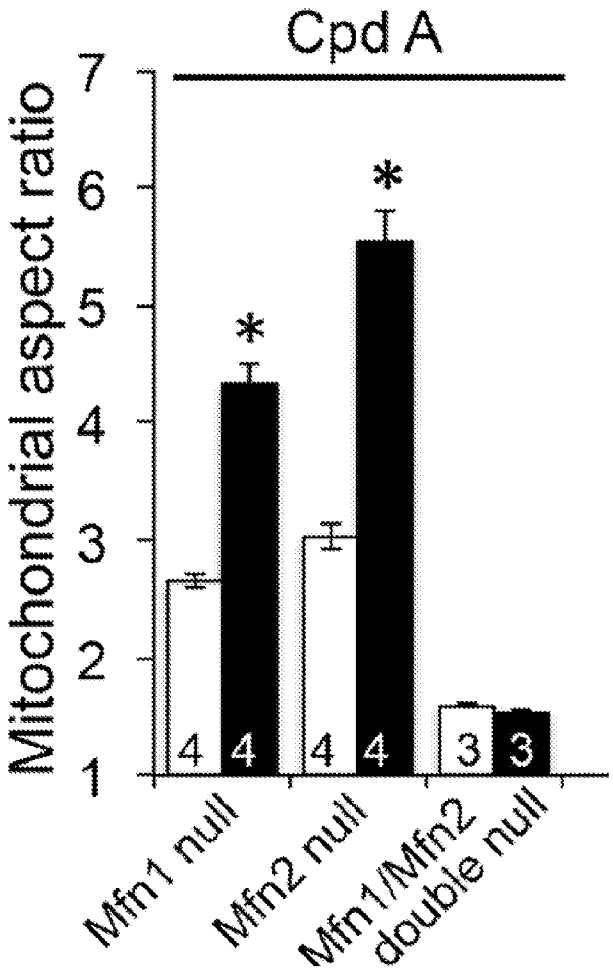
Cpd A
Mitochondrial aspect ratio
1
2
3
4
5
6
7
*
*
4
4
4
4
3
3
Mfn1 null
Mfn2 null
Mfn1/Mfn2 double null

FIG. 4C

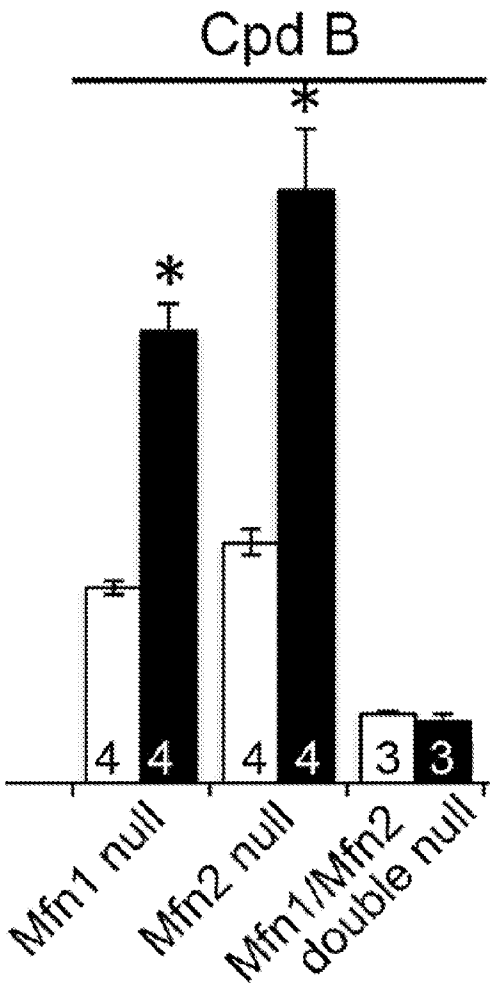
Cpd B
*
*
4
4
4
4
3
3
Mfn1 null
Mfn2 null
Mfn1/Mfn2 double null

FIG. 4D

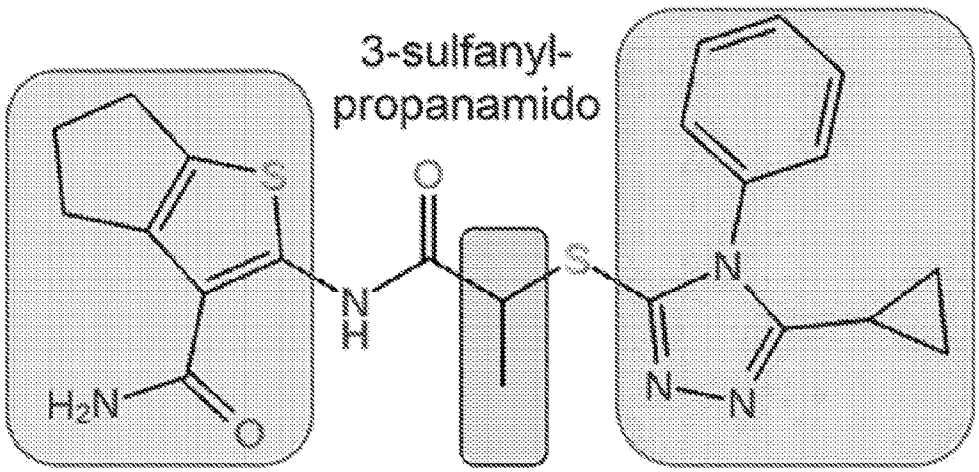
3-sulfanyl-
propanamido
S
O
N
H
S
N
N
N
H2N
O
4H,5H,6H-cyclopenta[b]
thiophene-3-carboxamide
5-cyclopropyl-4-
phenyl-4H-1,2,4-triazole

FIG. 4E

FIG. 4F

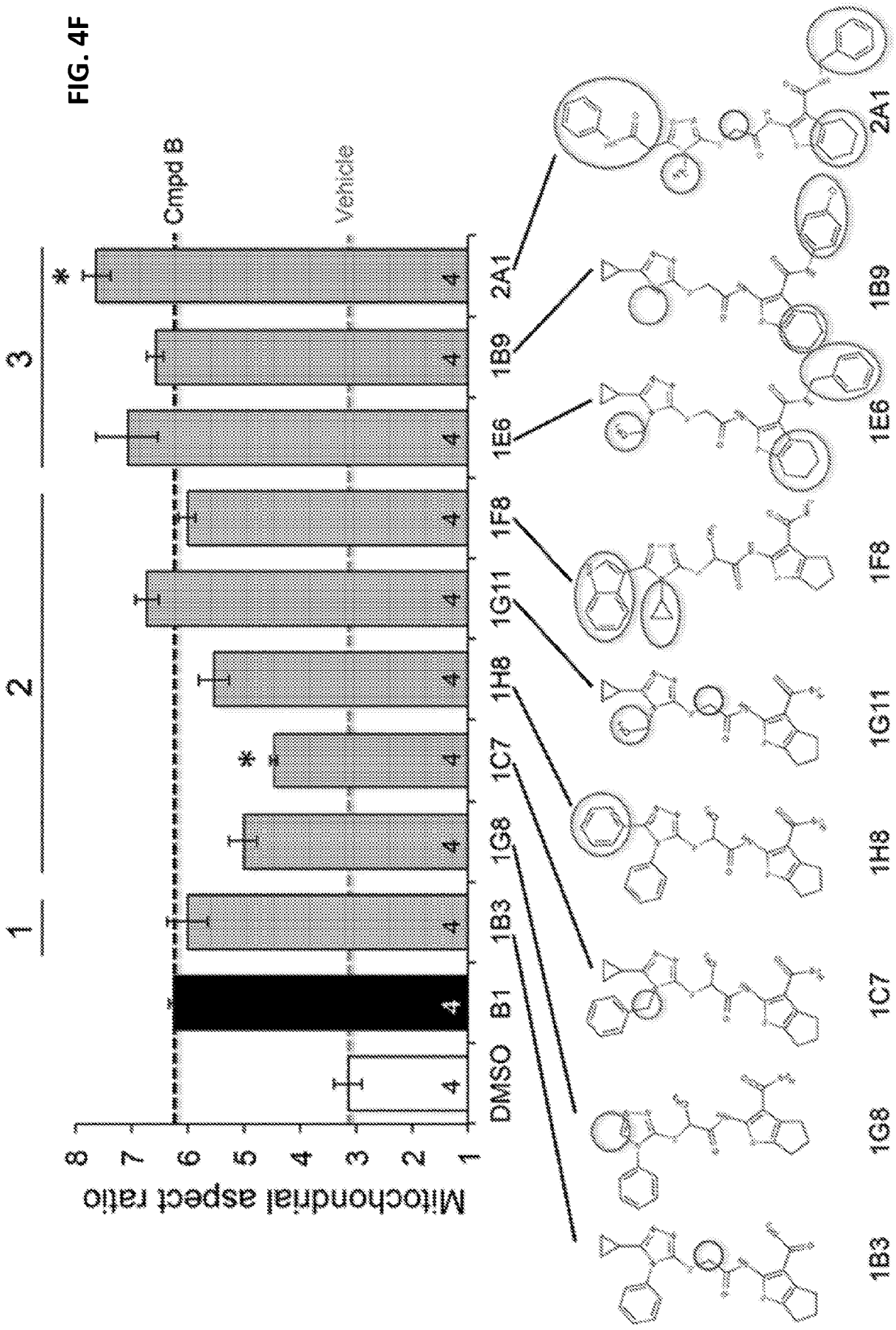
1
2
3
Cmpd B
Vehicle
Mitochondrial aspect ratio
8
7
6
5
4
3
2
1
DMSO
B1
1B3
1G8
1C7
1H8
1G11
1F8
1E6
1B9
2A1
4
*

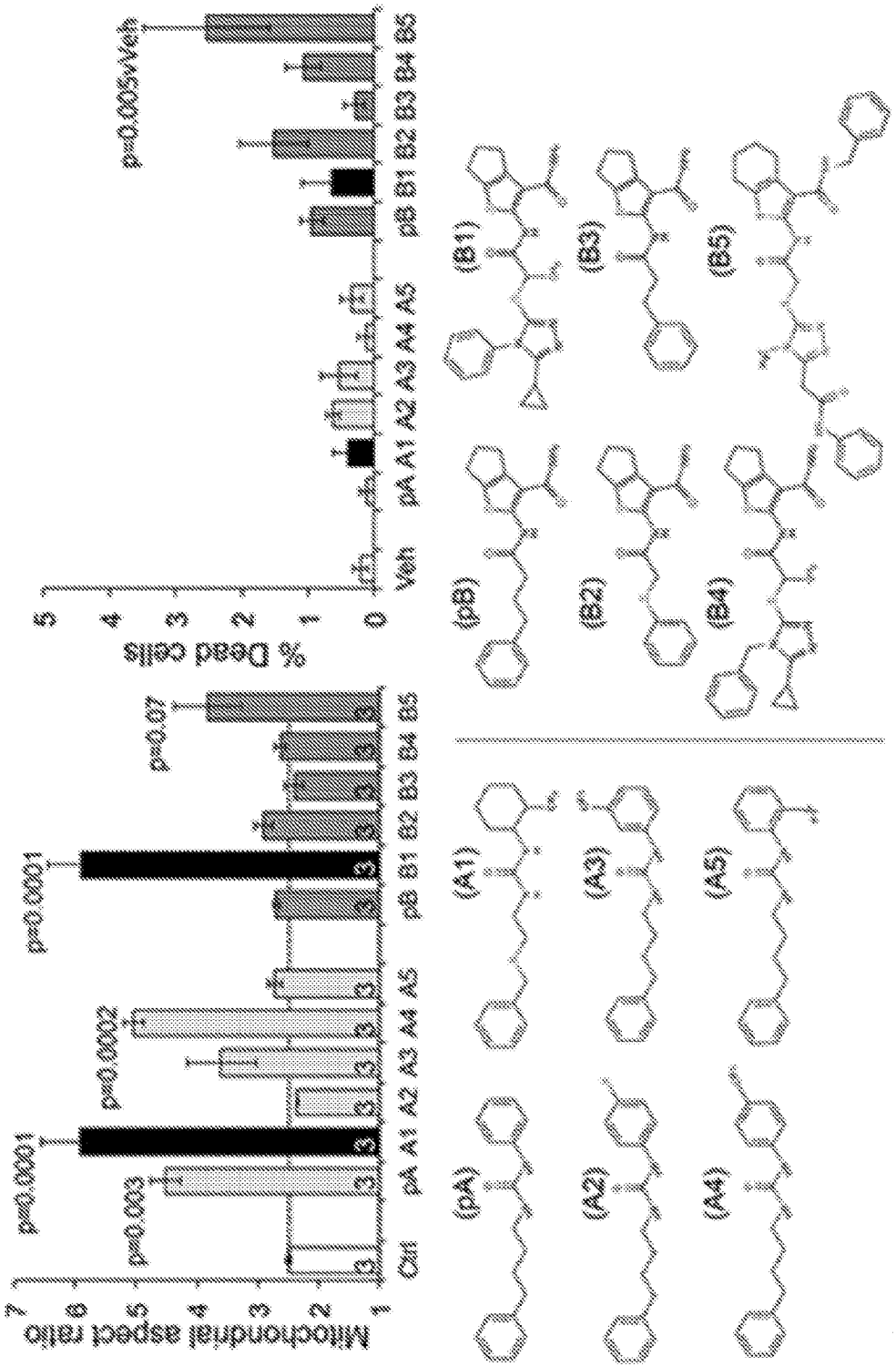
Mitochondrial aspect ratio
Ctrl pA A1 A2 A3 A4 A5 pB B1 B2 B3 B4 B5
p=0.003
p=0.0001
p=0.0002
p=0.0001
p=0.07
% Dead cells
Veh pA A1 A2 A3 A4 A5 pB B1 B2 B3 B4 B5
p=0.005vsVeh
(pA)
(A1)
(A2)
(A3)
(A4)
(A5)
(pB)
(B1)
(B2)
(B3)
(B4)
(B5)

FIG. 5A

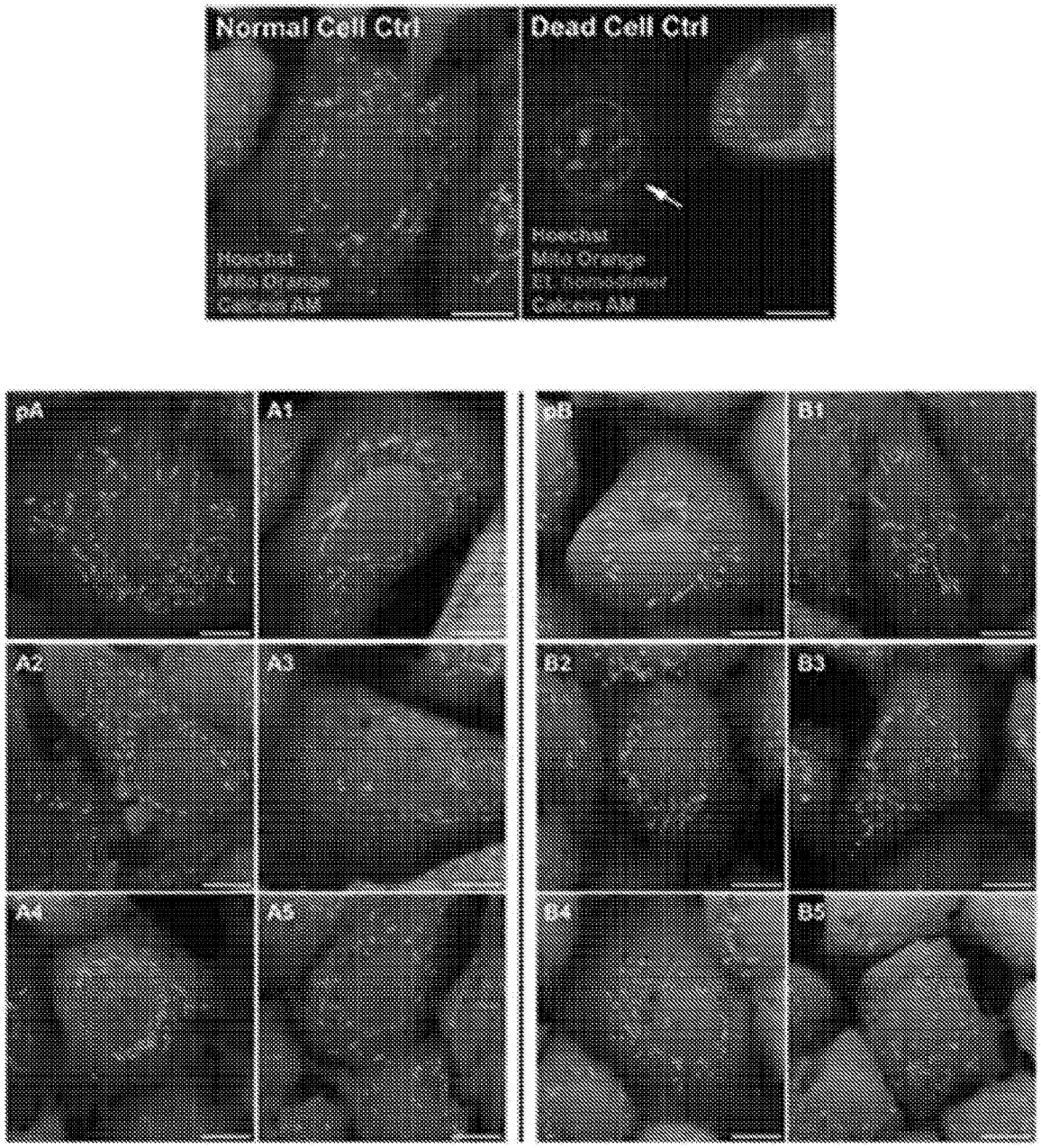
Normal Cell Ctrl
Dead Cell Ctrl
pA
A1
A2
A3
A4
A5
pB
B1
B2
B3
B4
B5

FIG. 5B

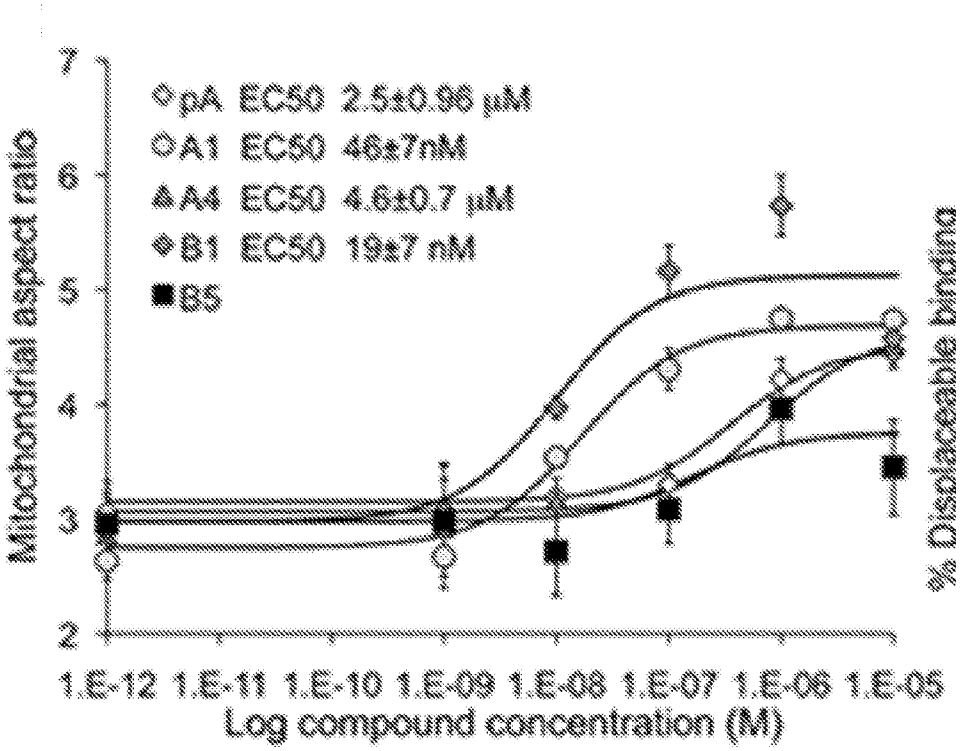
pA EC50 2.5±0.96 μM
A1 EC50 46±7nM
A4 EC50 4.6±0.7 μM
B1 EC50 19±7 nM
B5
Mitochondrial aspect ratio
% Displaceable binding
7
6
5
4
3
2
1.E-12 1.E-11 1.E-10 1.E-09 1.E-08 1.E-07 1.E-06 1.E-05
Log compound concentration (M)

FIG. 5C

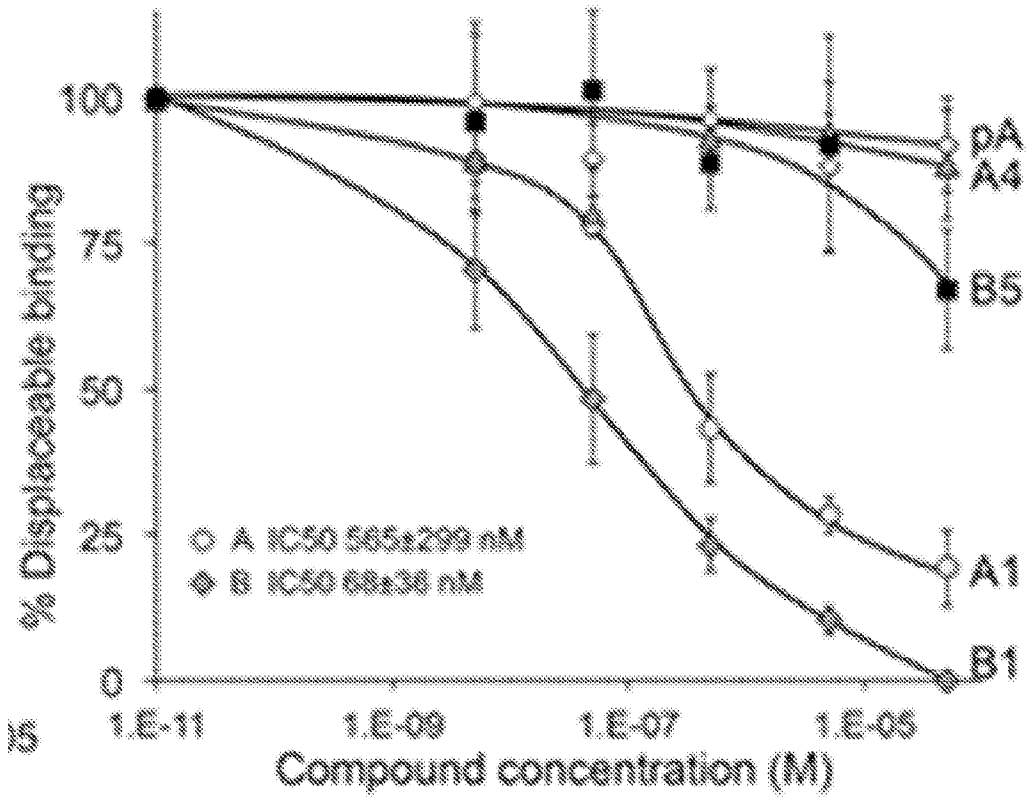
100
75
50
25
0
% Displaceable binding
A IC50 565±299 nM
B IC50 68±36 nM
pA
A4
B5
A1
B1
1.E-11
1.E-09
1.E-07
1.E-05
Compound concentration (M)

FIG. 5D

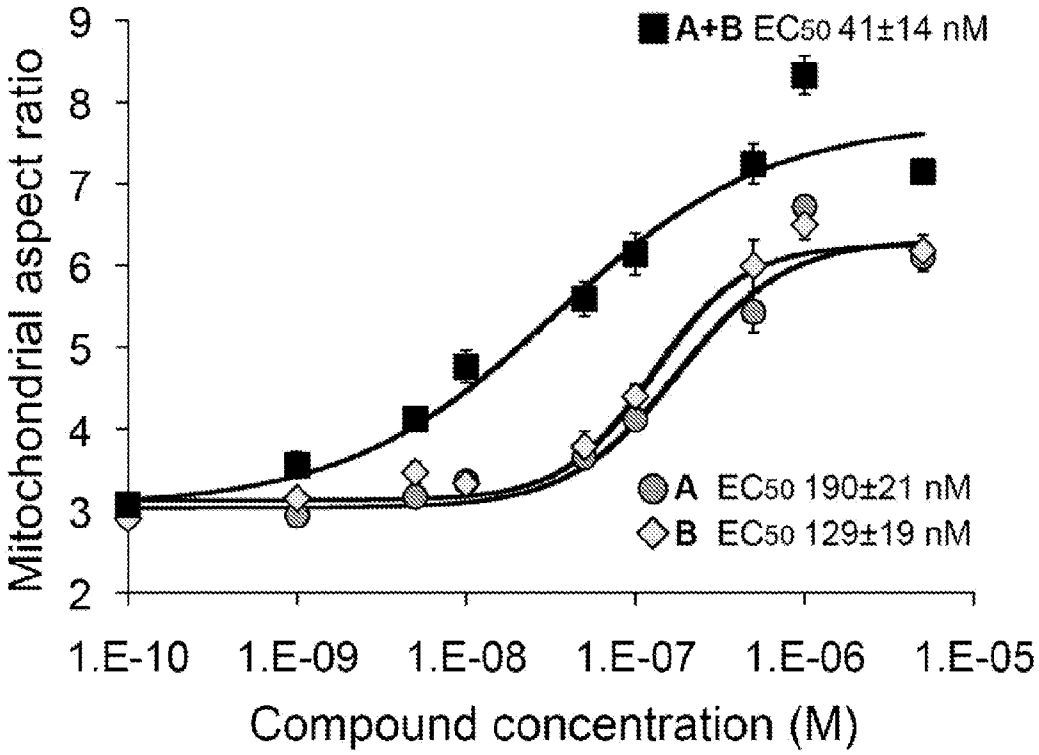
A+B EC50 41±14 nM
A EC50 190±21 nM
B EC50 129±19 nM
Mitochondrial aspect ratio
9
8
7
6
5
4
3
2
1.E-10
1.E-09
1.E-08
1.E-07
1.E-06
1.E-05
Compound concentration (M)

FIG. 6A

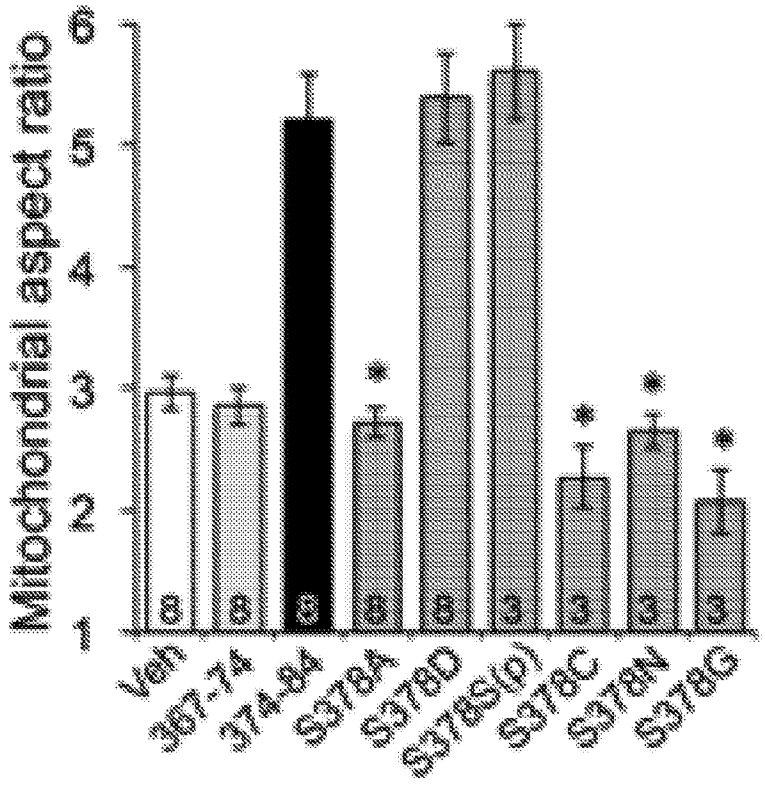
Mitochondrial aspect ratio
6
5
4
3
2
1
8
8
8
8
8
3
3
3
3
Veh
367-74
374-84
S378A
S378D
S378S(p)
S378C
S378N
S378G

FIG. 6B

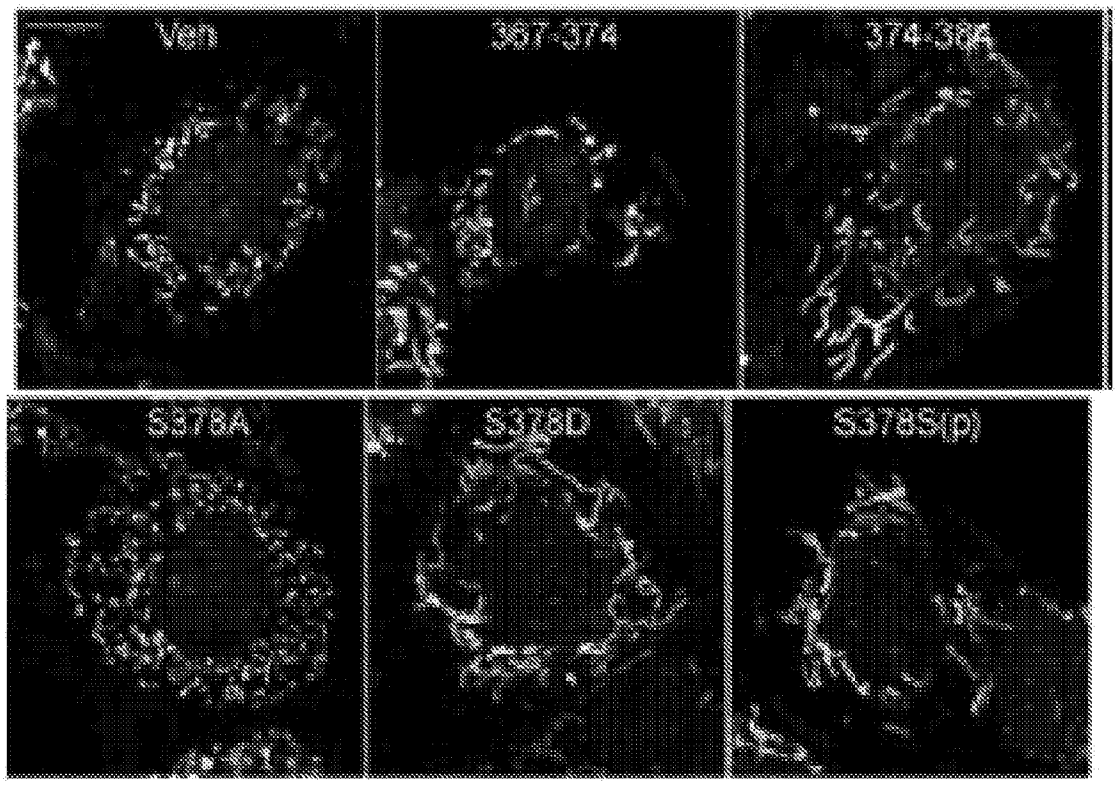

FIG. 6C

FIG. 6D

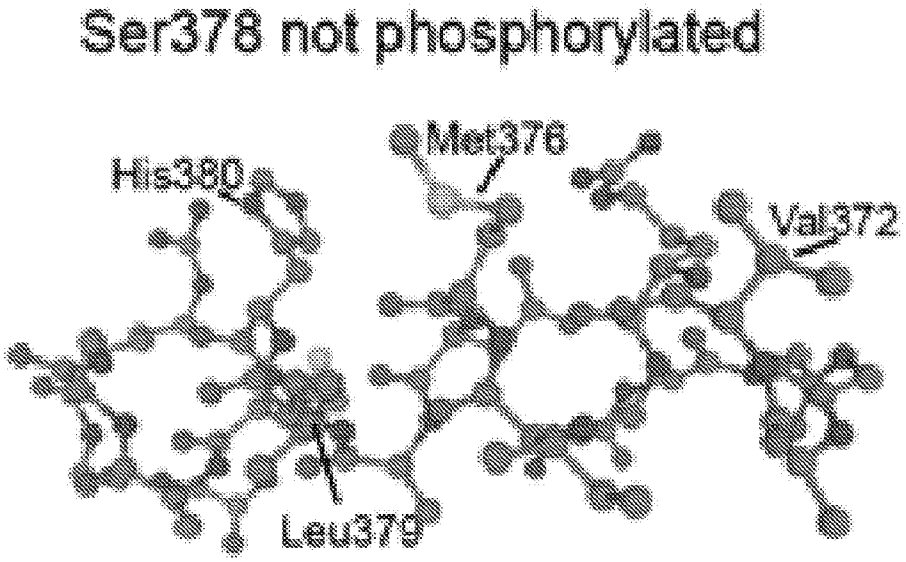
Ser378 not phosphorylated
Met376
His380
Val372
Leu379

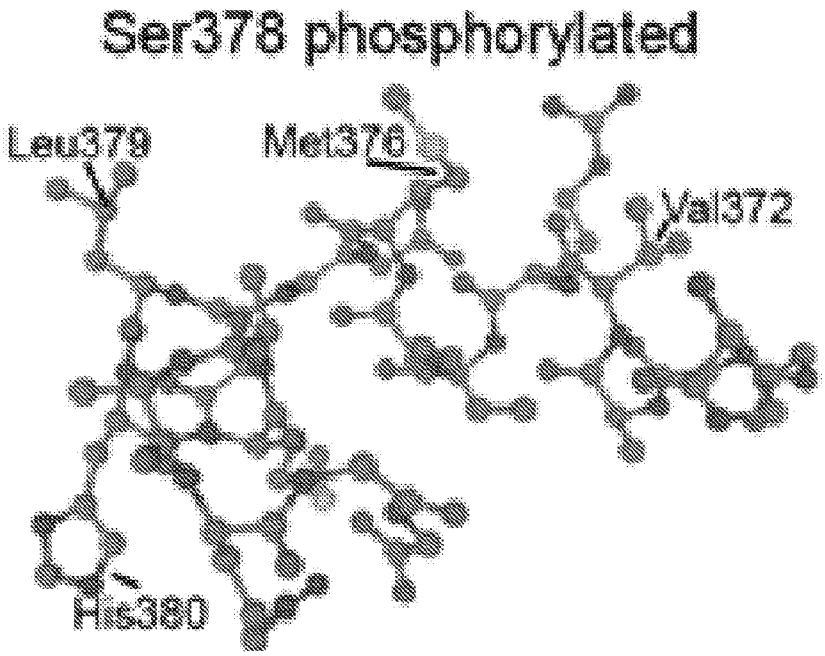
Ser378 phosphorylated
Leu379
Met376
Val372
His380

FIG. 6E

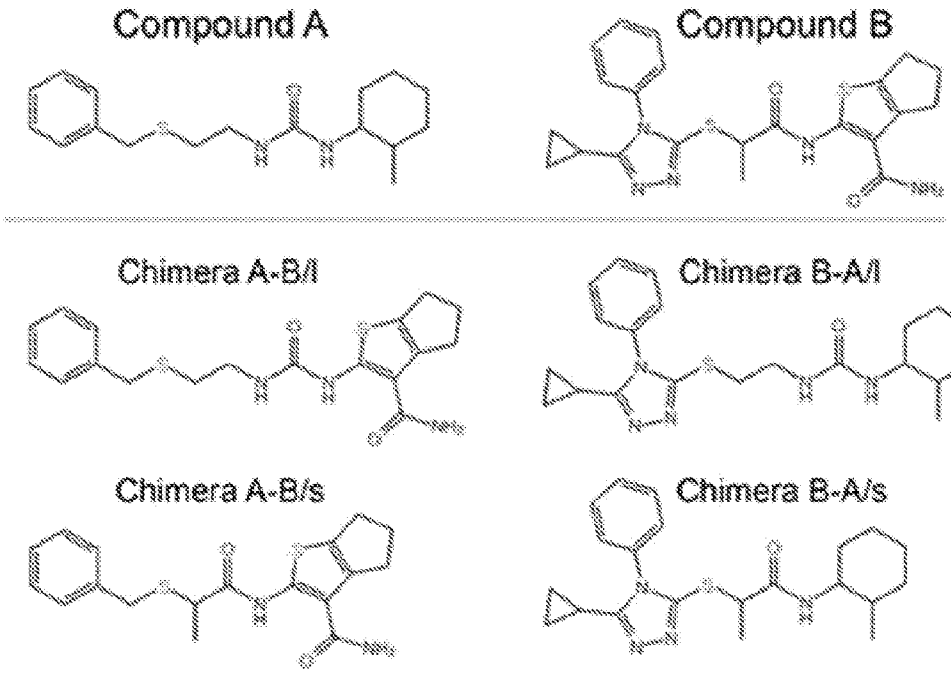
Compound A
Compound B
Chimera A-B/l
Chimera B-A/l
Chimera A-B/s
Chimera B-A/s

FIG. 7A

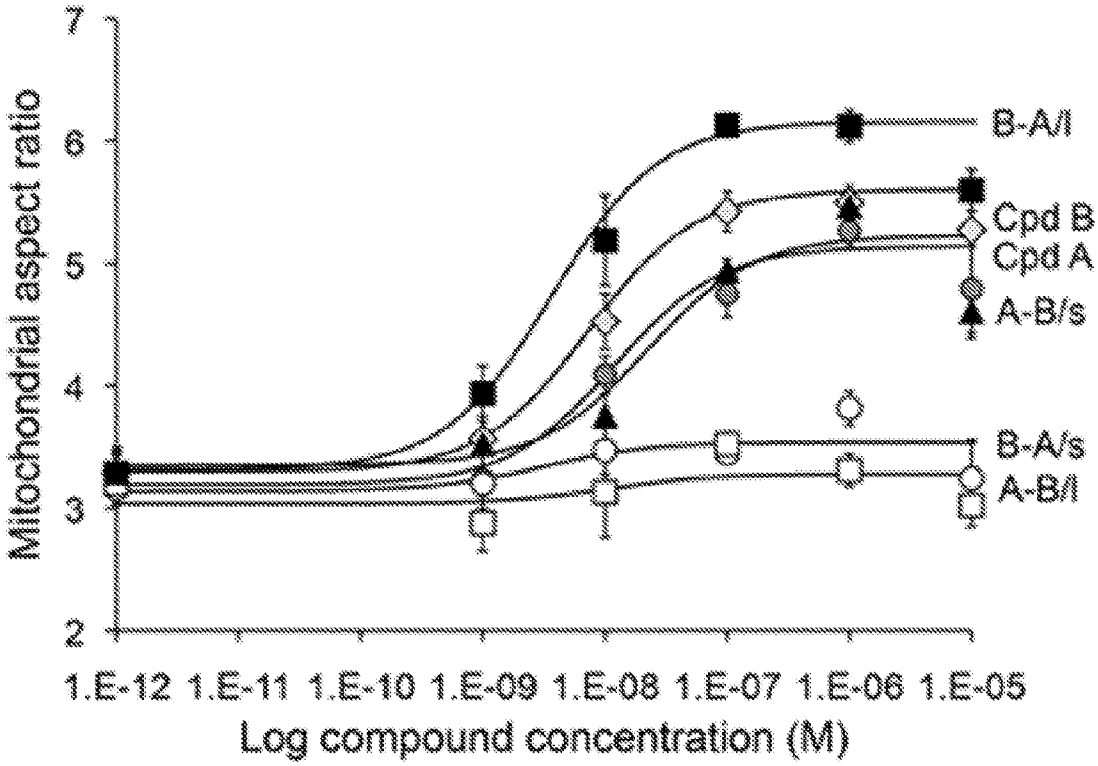
Mitochondrial aspect ratio
7
6
5
4
3
2
B-A/l
Cpd B
Cpd A
A-B/s
B-A/s
A-B/l
1.E-12 1.E-11 1.E-10 1.E-09 1.E-08 1.E-07 1.E-06 1.E-05
Log compound concentration (M)

FIG. 7B

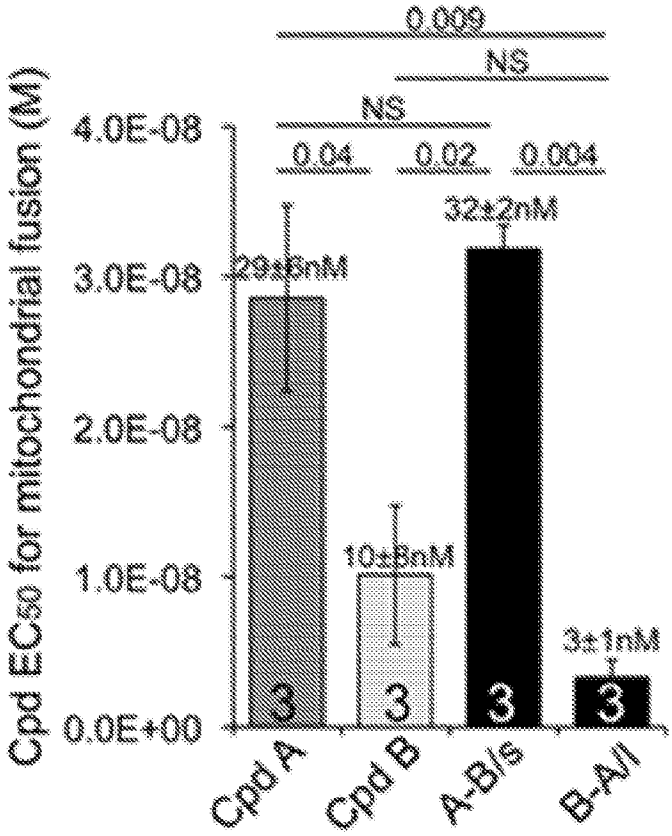
0.009
NS
NS
0.04
0.02
0.004
4.0E-08
3.0E-08
2.0E-08
1.0E-08
0.0E+00
Cpd EC50 for mitochondrial fusion (M)
29±6nM
10±8nM
32±2nM
3±1nM
3
3
3
3
Cpd A
Cpd B
A-B/s
B-A/l

FIG. 7C

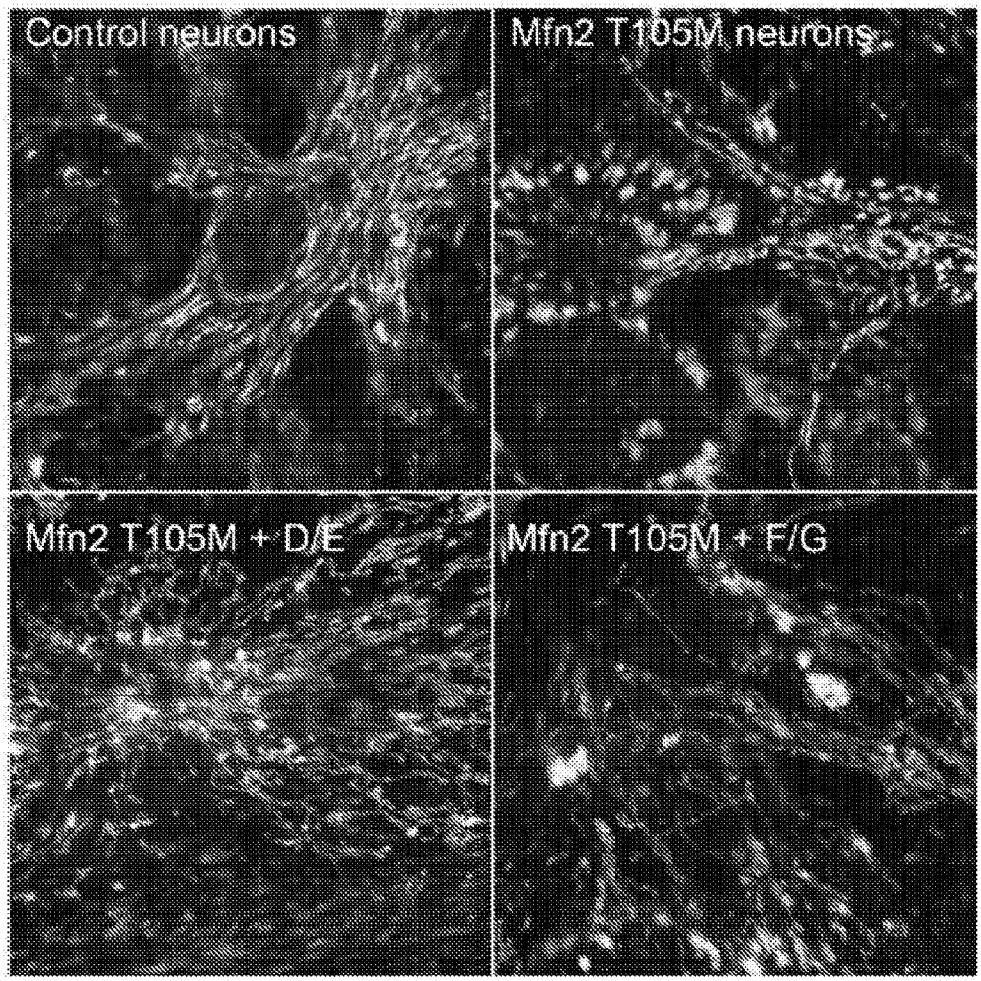
Control neurons
Mfn2 T105M neurons
Mfn2 T105M + D/E
Mfn2 T105M + F/G

FIG. 8A

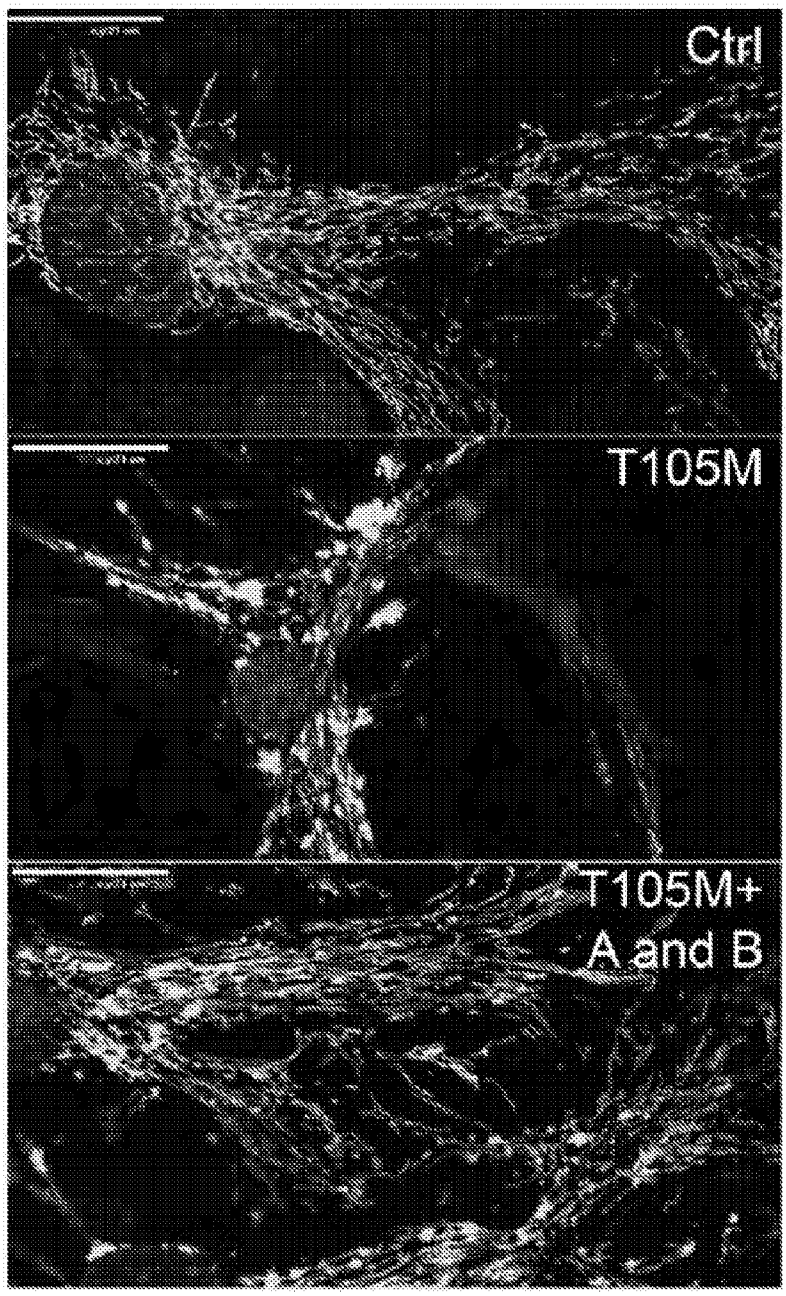

FIG. 8B

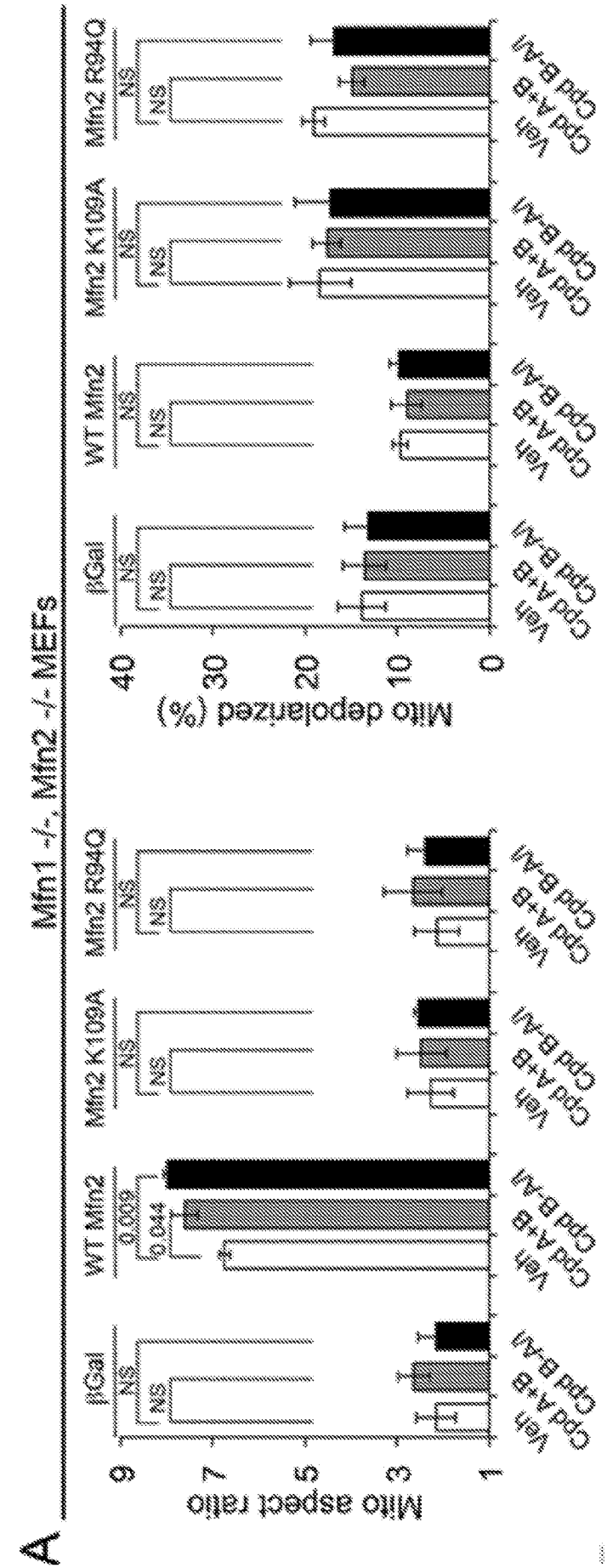
A
Mfn1 -/-, Mfn2 -/- MEFs
Mito aspect ratio
Mito depolarized (%)
βGal
WT Mfn2
Mfn2 K109A
Mfn2 R94Q
NS
0.009
0.044
Veh
Cpd A+B
Cpd B-Aln

FIG. 9A

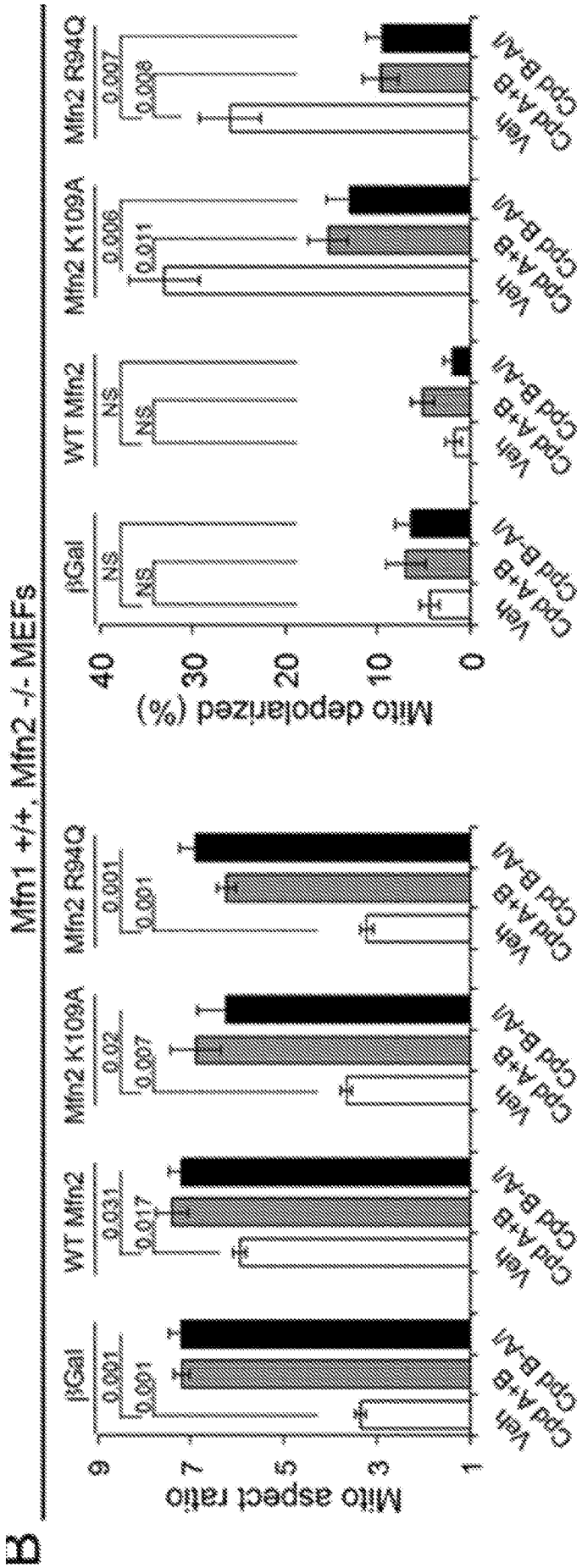
B
Mfn1 +/+, Mfn2 -/- MEFs
Mito aspect ratio
Mito depolarized (%)
jGal
WT Mfn2
Mfn2 K109A
Mfn2 R94Q
Veh
Cpd A+B
Cpd B-Aut
0.001
0.031
0.02
0.001
0.017
0.007
0.001
NS
0.006
0.011
0.007

FIG. 9B

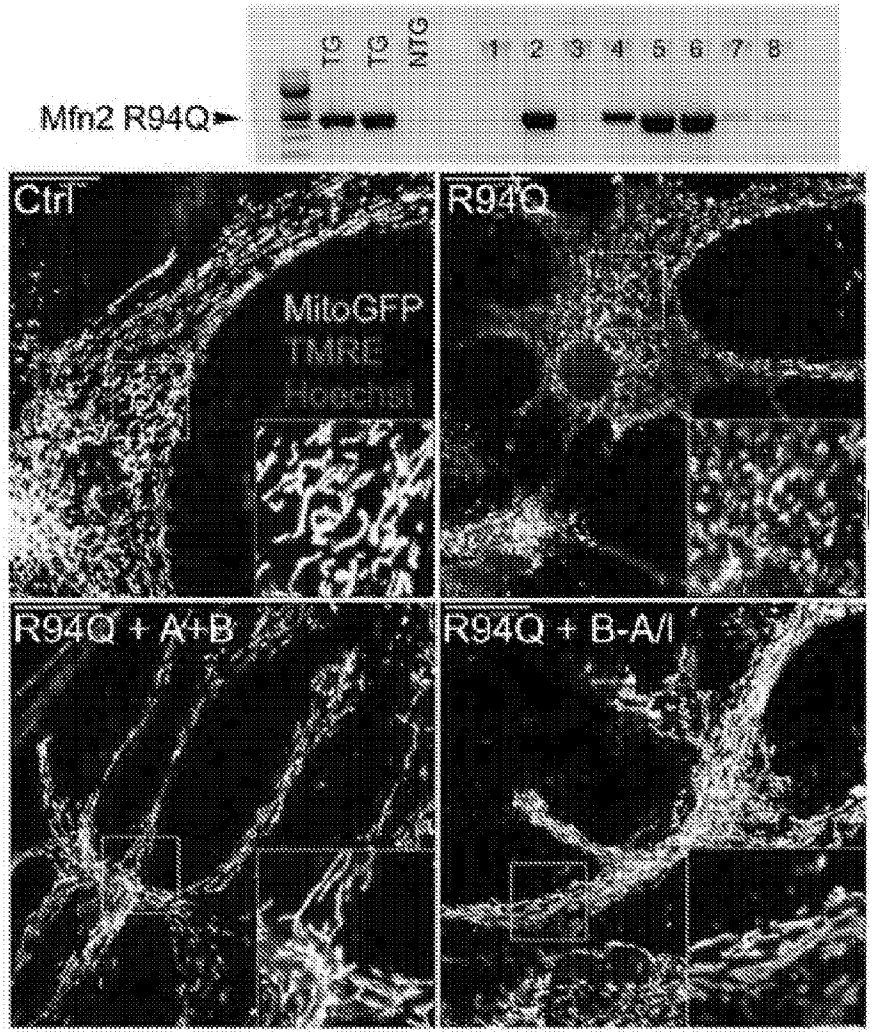
TG
TG
NTG
1
2
3
4
5
6
7
8
Mfn2 R94Q
Ctrl
MitoGFP
TMRE
Hoechst
R94Q
R94Q + A+B
R94Q + B-A/I

FIG. 9C

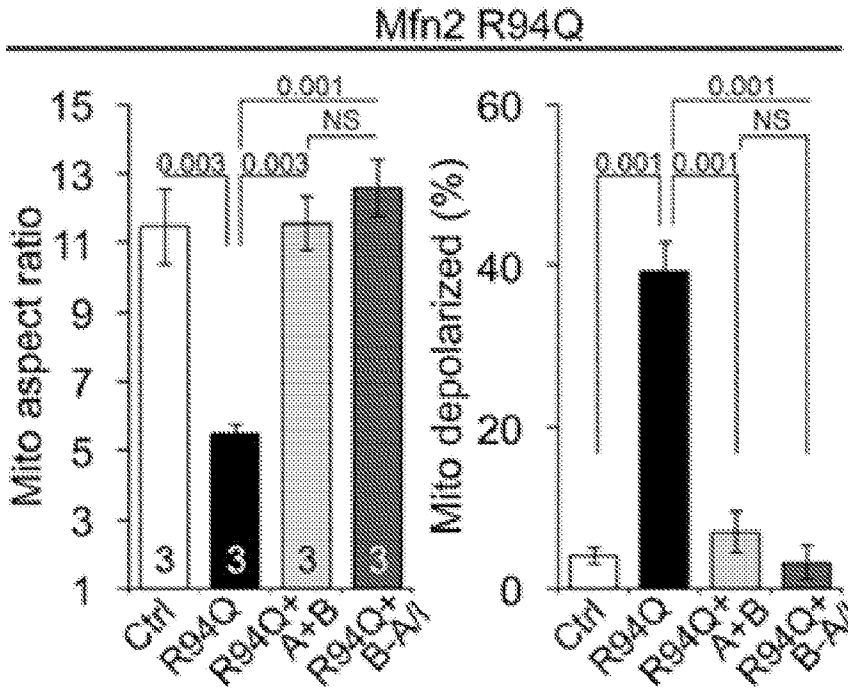
Mfn2 R94Q
Mito aspect ratio
15
13
11
9
7
5
3
1
0.003
0.003
0.001
NS
3
3
3
3
Ctrl
R94Q
R94Q+ A+B
R94Q+ B-A/I
Mito depolarized (%)
60
40
20
0
0.001
0.001
0.001
NS
Ctrl
R94Q
R94Q+ A+B
R94Q+ B-A/I

FIG. 9D

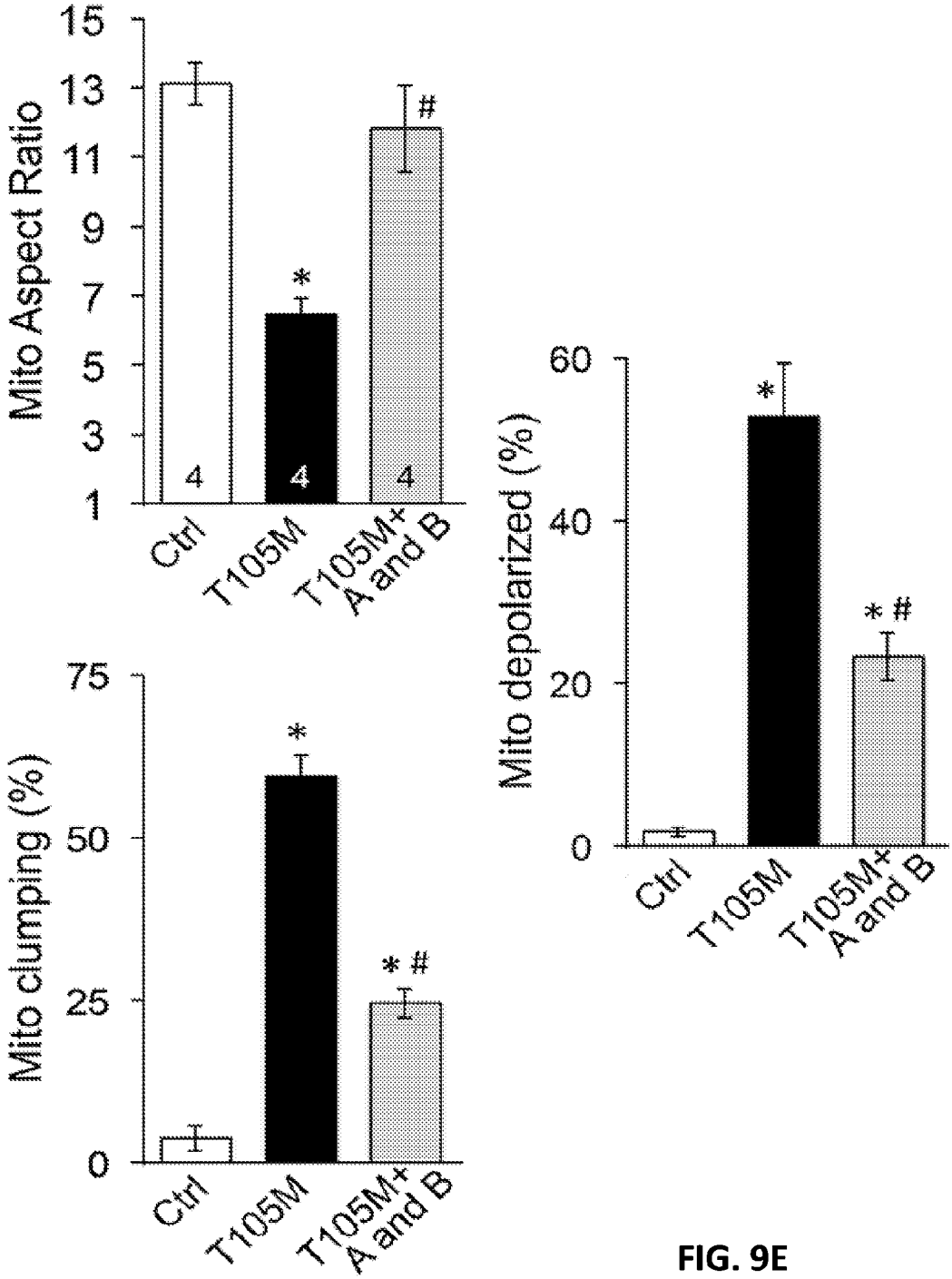
Mito Aspect Ratio
15
13
11
9
7
5
3
1
4
4
4
*
#
Ctrl
T105M
T105M+ A and B
Mito clumping (%)
75
50
25
0
*
* #
Ctrl
T105M
T105M+ A and B
Mito depolarized (%)
60
40
20
0
*
* #
Ctrl
T105M
T105M+ A and B

FIG. 9E

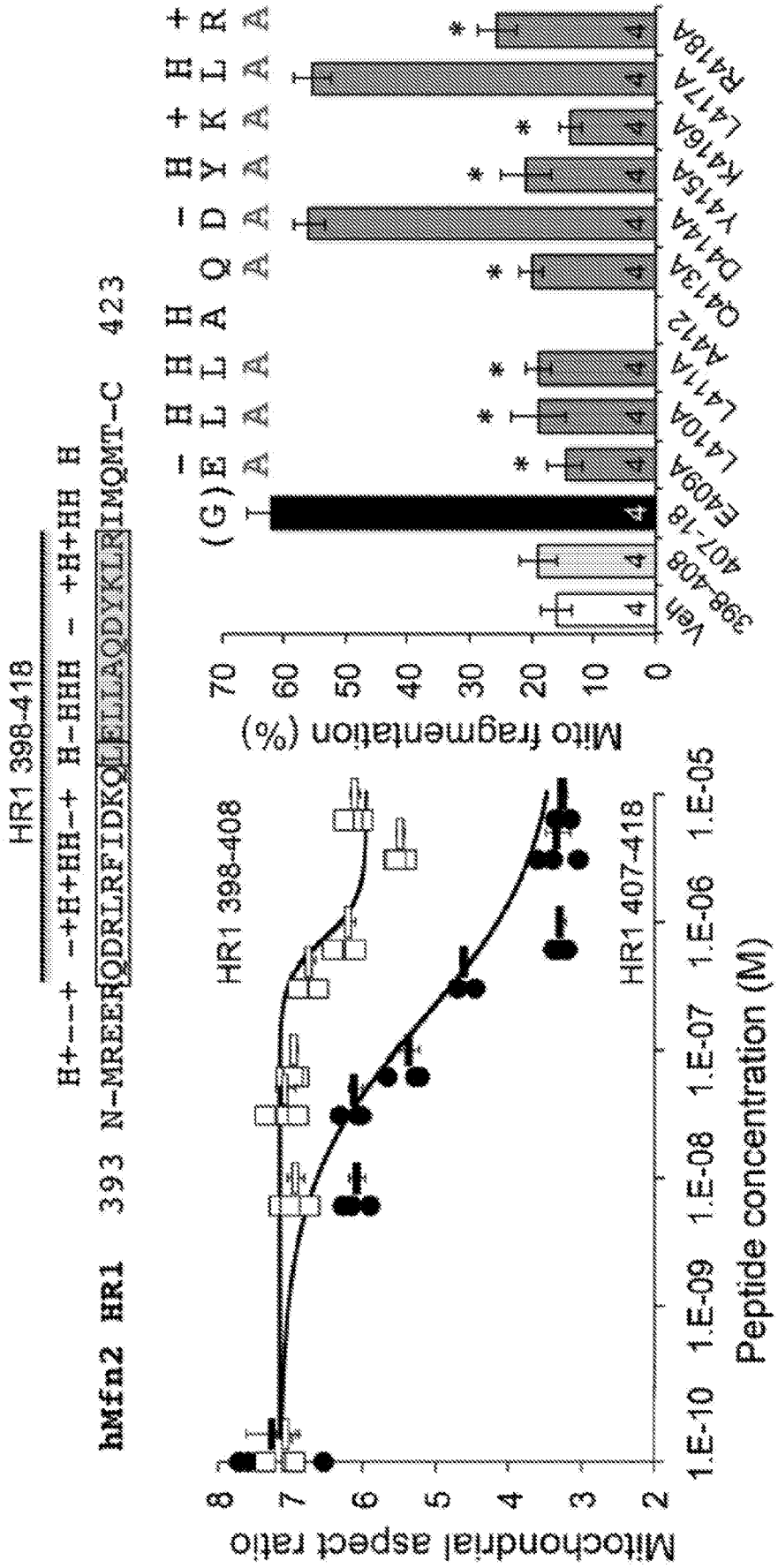
HR1 398-418
hMfn2 HR1 393 N-MREERQDRLRFIDKQLELLAQDYKLRIMQMT-C 423
H+--+ --+H+HH--+ H-HHH - +H+HH H
- H H H H H + H
(G)E L L A Q D Y K L A R
A A A A A A A A A
Mito fragmentation (%)
0 10 20 30 40 50 60 70
Veh
398-408
407-418
E409A
L410A
L411A
A412
Q413A
D414A
Y415A
K416A
L417A
R418A
Mitochondrial aspect ratio
2 3 4 5 6 7 8
HR1 398-408
HR1 407-418
1.E-10 1.E-09 1.E-08 1.E-07 1.E-06 1.E-05
Peptide concentration (M)

FIG. 9F

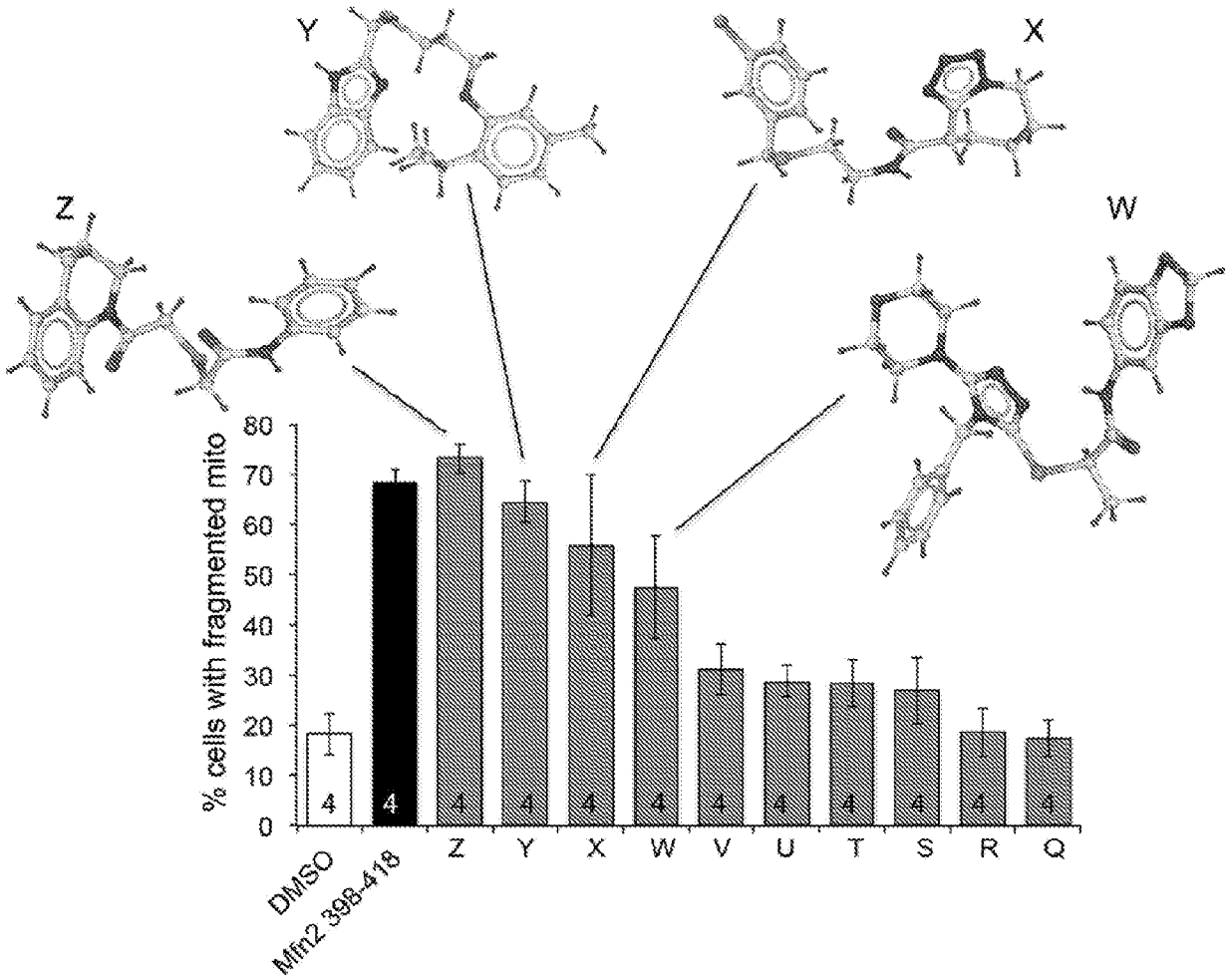
Y
X
Z
W
% cells with fragmented mito
0
10
20
30
40
50
60
70
80
4
DMSO
Mfn2 398-418
Z
Y
X
W
V
U
T
S
R
Q

FIG. 9G

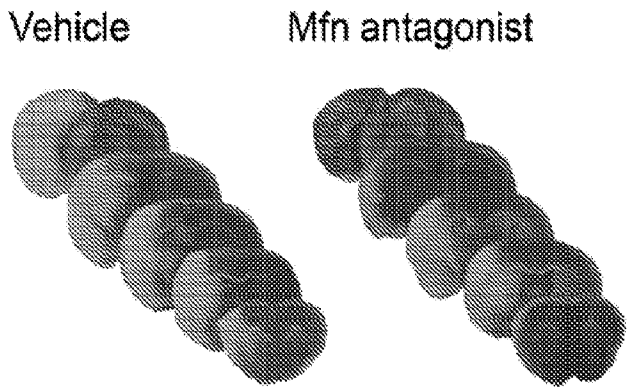
Vehicle
Mfn antagonist

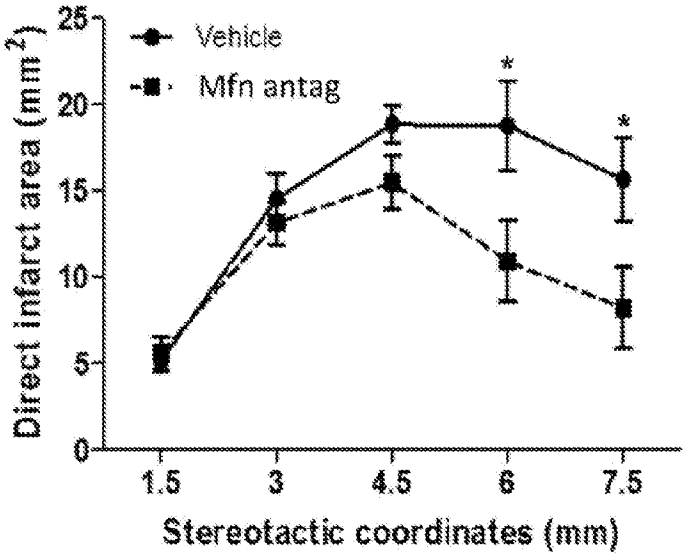
Direct infarct area (mm^2)
25
20
15
10
5
0
Vehicle
Mfn antag
*
*
1.5
3
4.5
6
7.5
Stereotactic coordinates (mm)

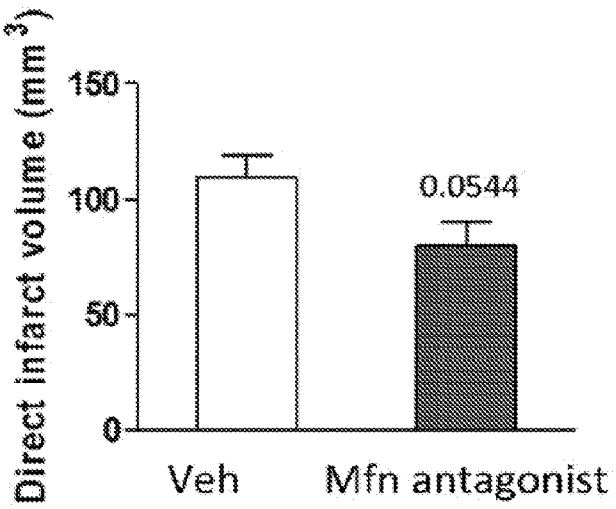
Direct infarct volume (mm^3)
150
100
50
0
0.0544
Veh
Mfn antagonist

FIG. 9H

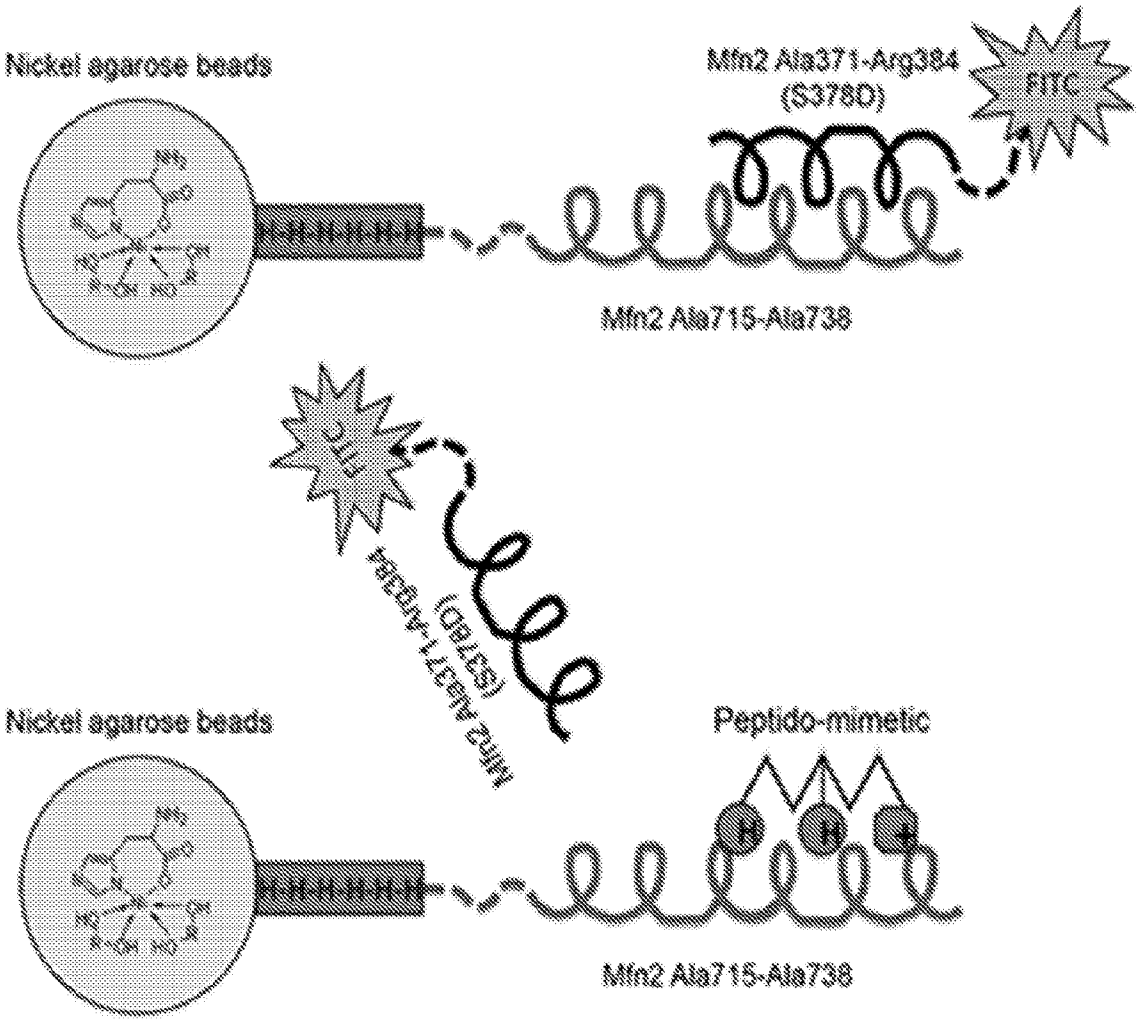
Nickel agarose beads
Mfn2 Ala371-Arg384
(S378D)
FITC
Mfn2 Ala715-Ala738
FITC
Mfn2 Ala371-Arg384
(S378D)
Nickel agarose beads
Peptido-mimetic
Mfn2 Ala715-Ala738

FIG. 10

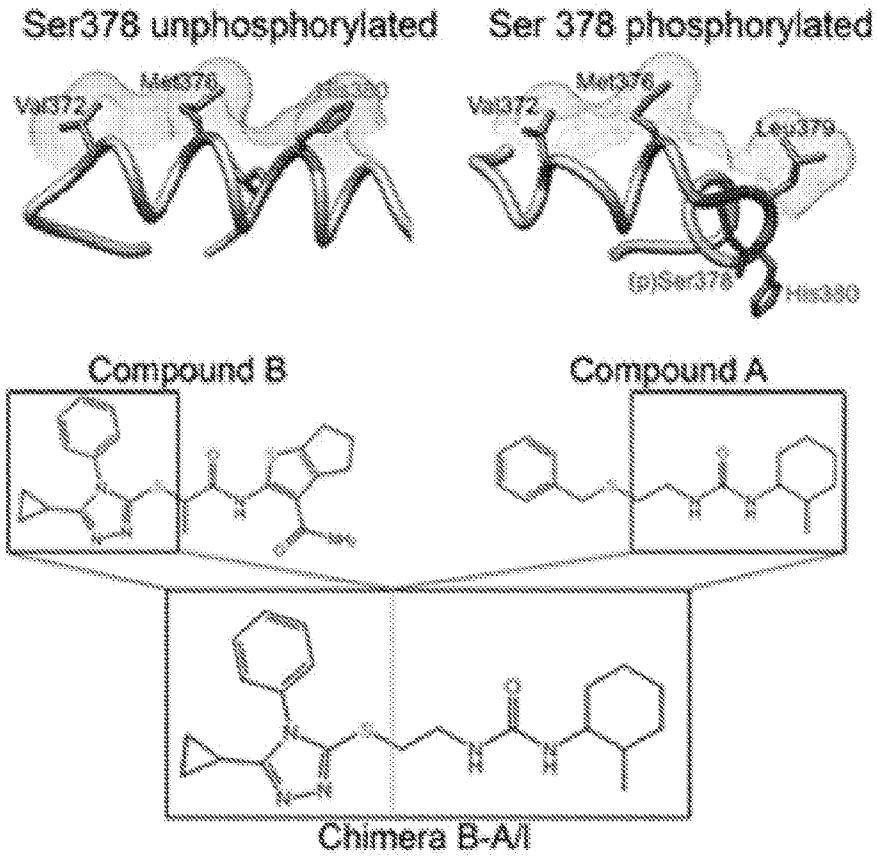

FIG. 11A

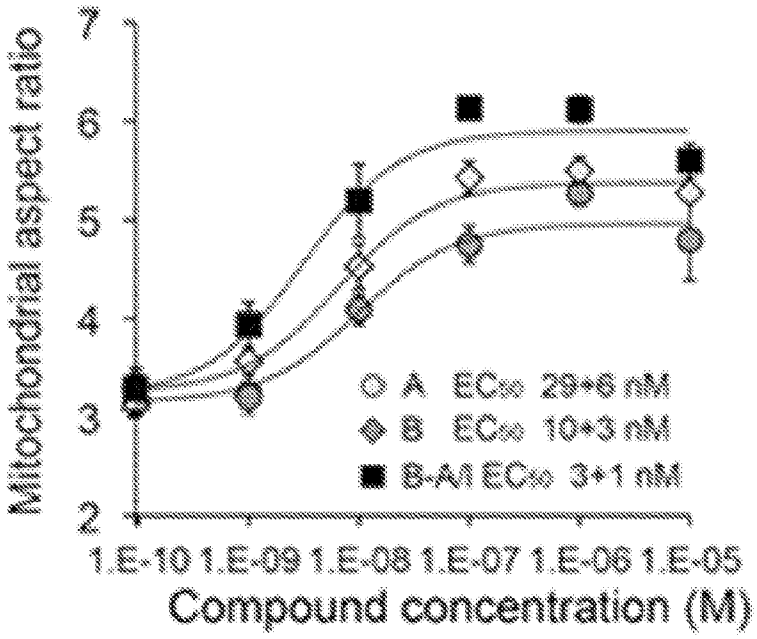

FIG. 11B

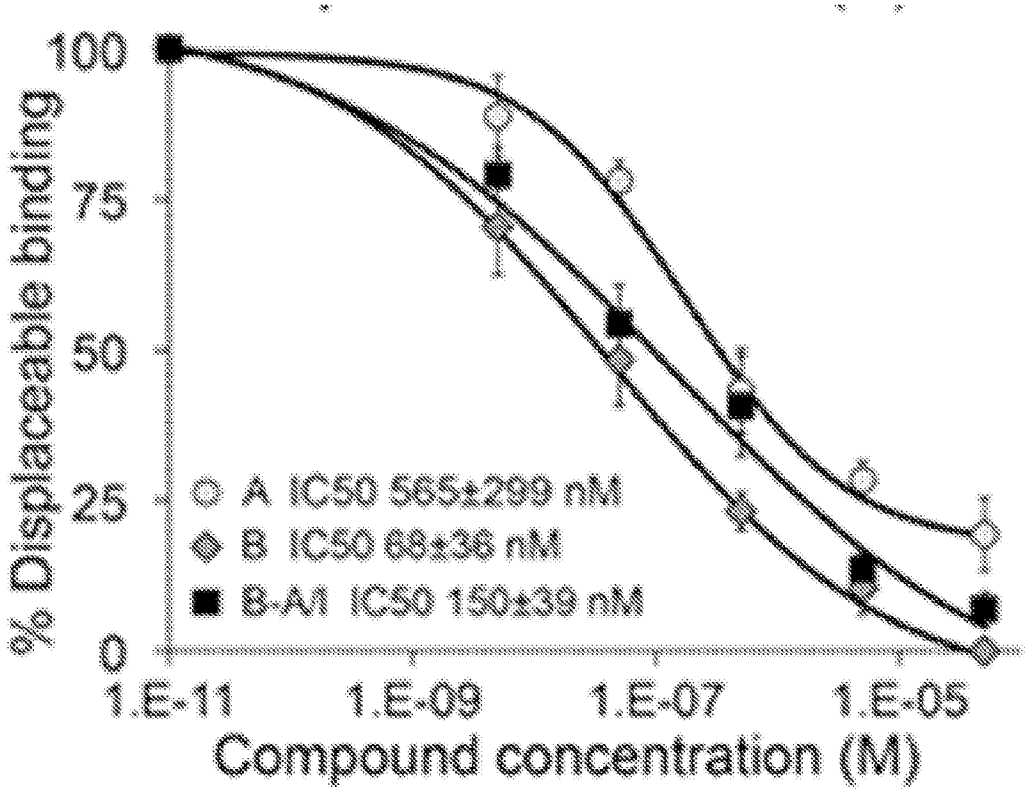

FIG. 11C

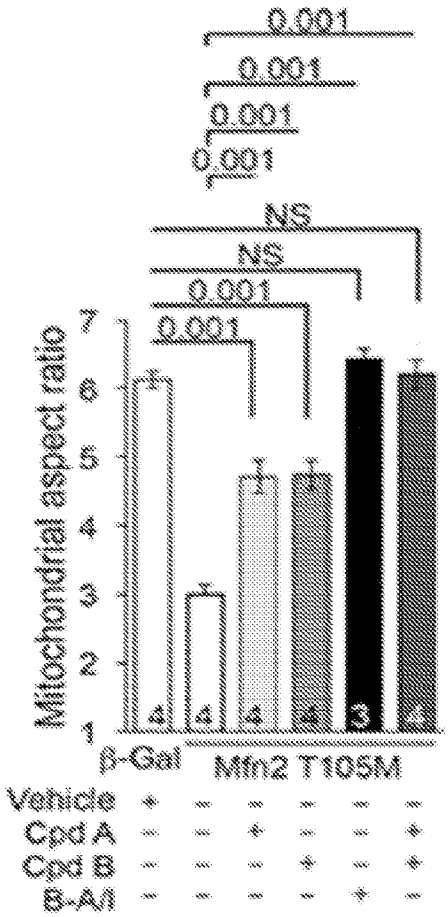

FIG. 11D

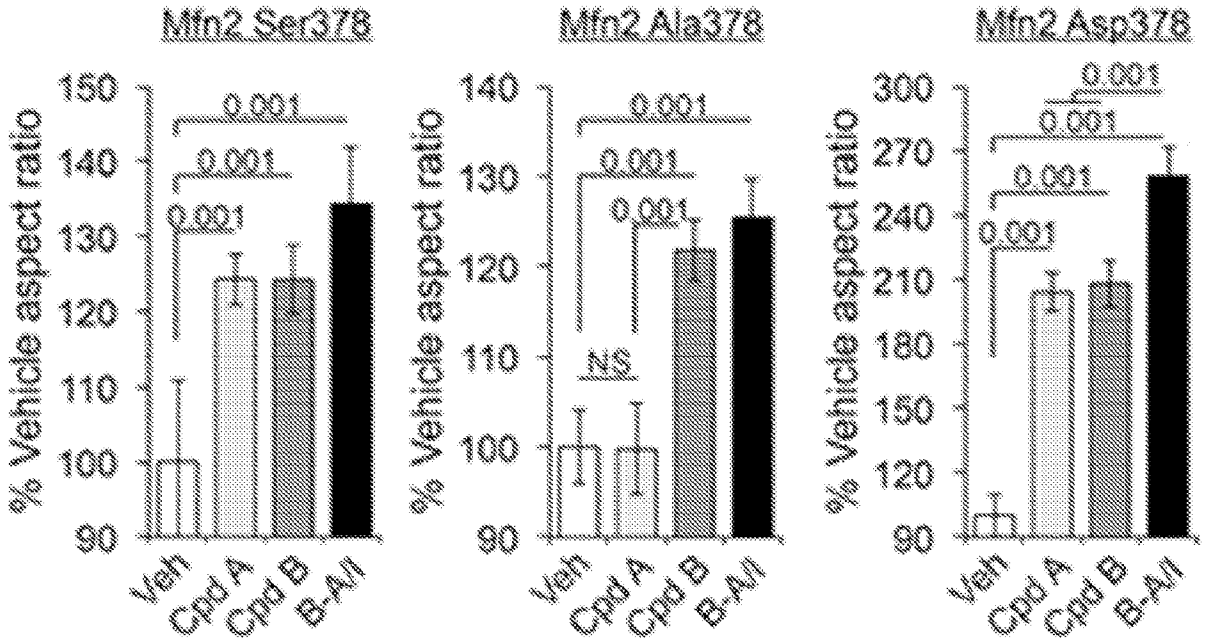

FIG. 11E

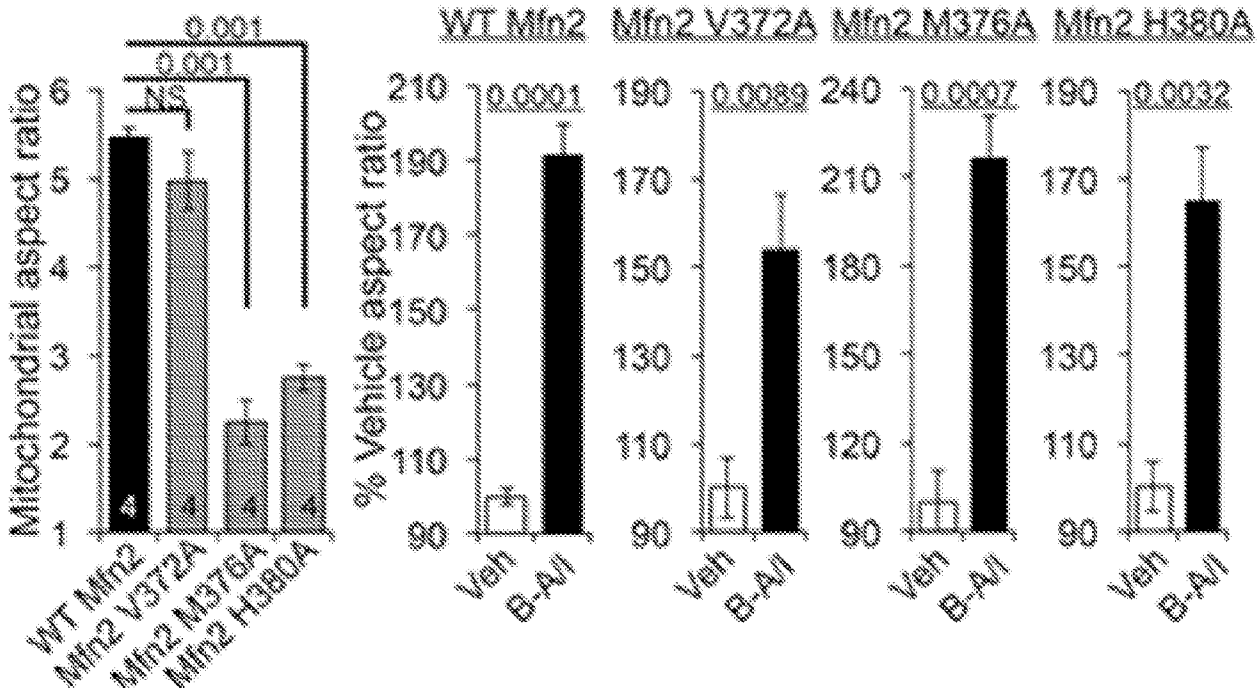

FIG. 11F

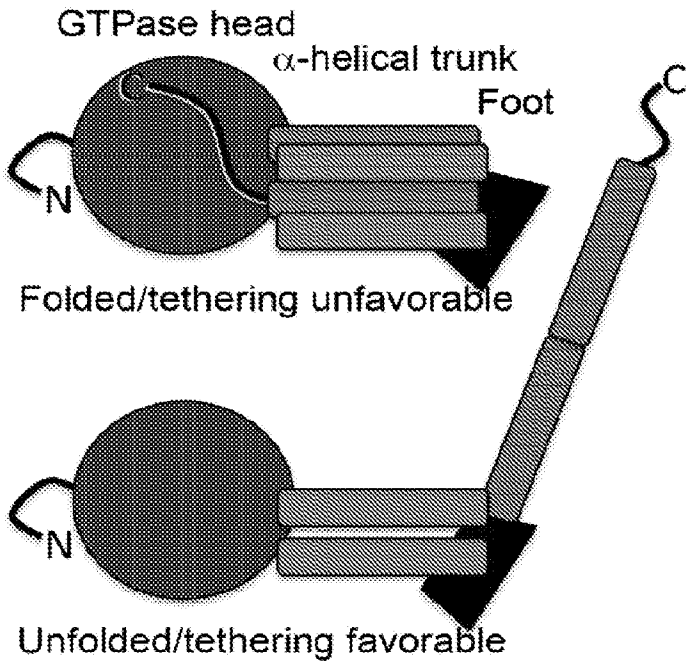
GTPase head
α-helical trunk
Foot
C
N
Folded/tethering unfavorable
N
Unfolded/tethering favorable

FIG. 12A

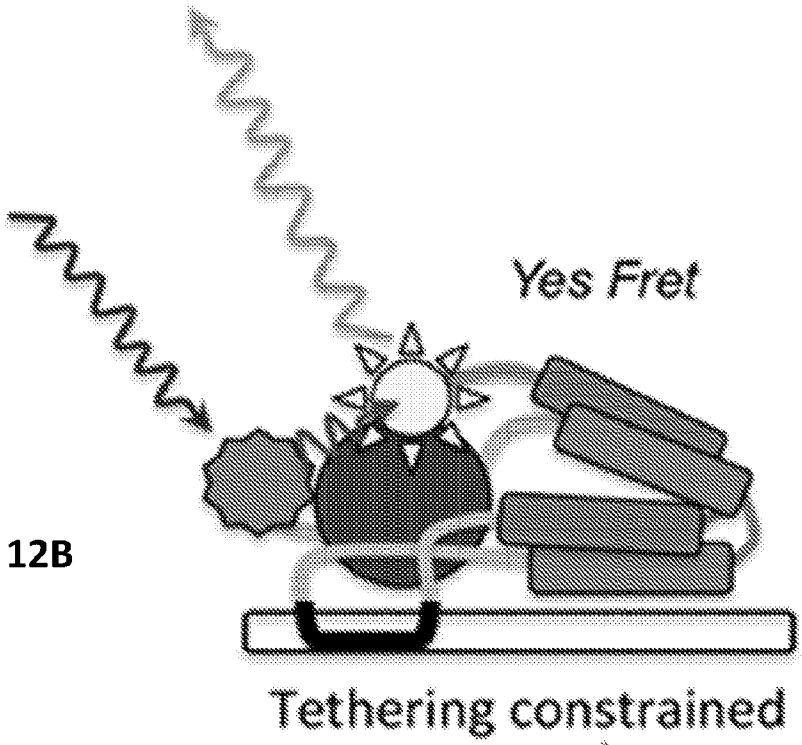

FIG. 12B

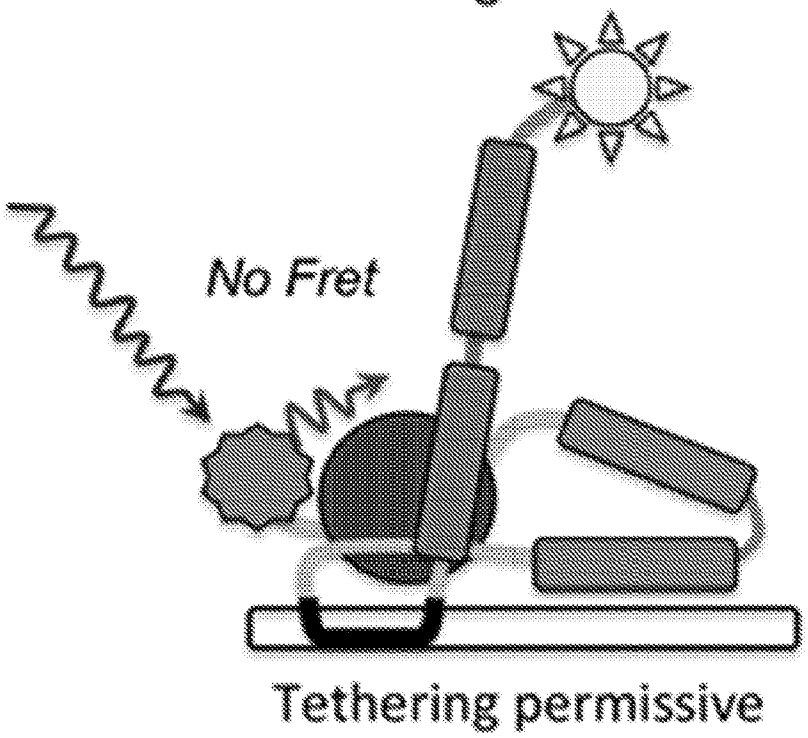

FIG. 12C

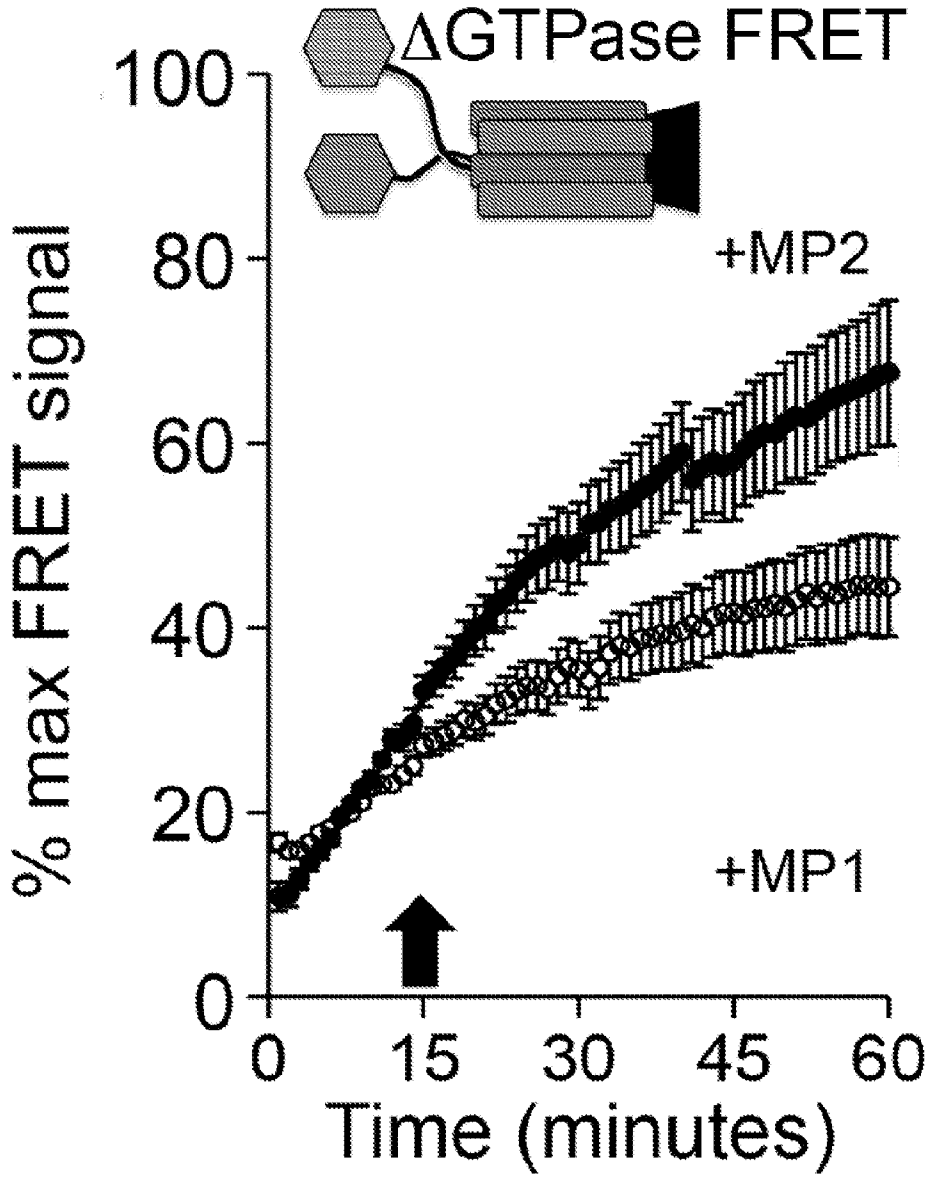
ΔGTPase FRET
+MP2
+MP1
% max FRET signal
100
80
60
40
20
0
0
15
30
45
60
Time (minutes)

FIG. 12D

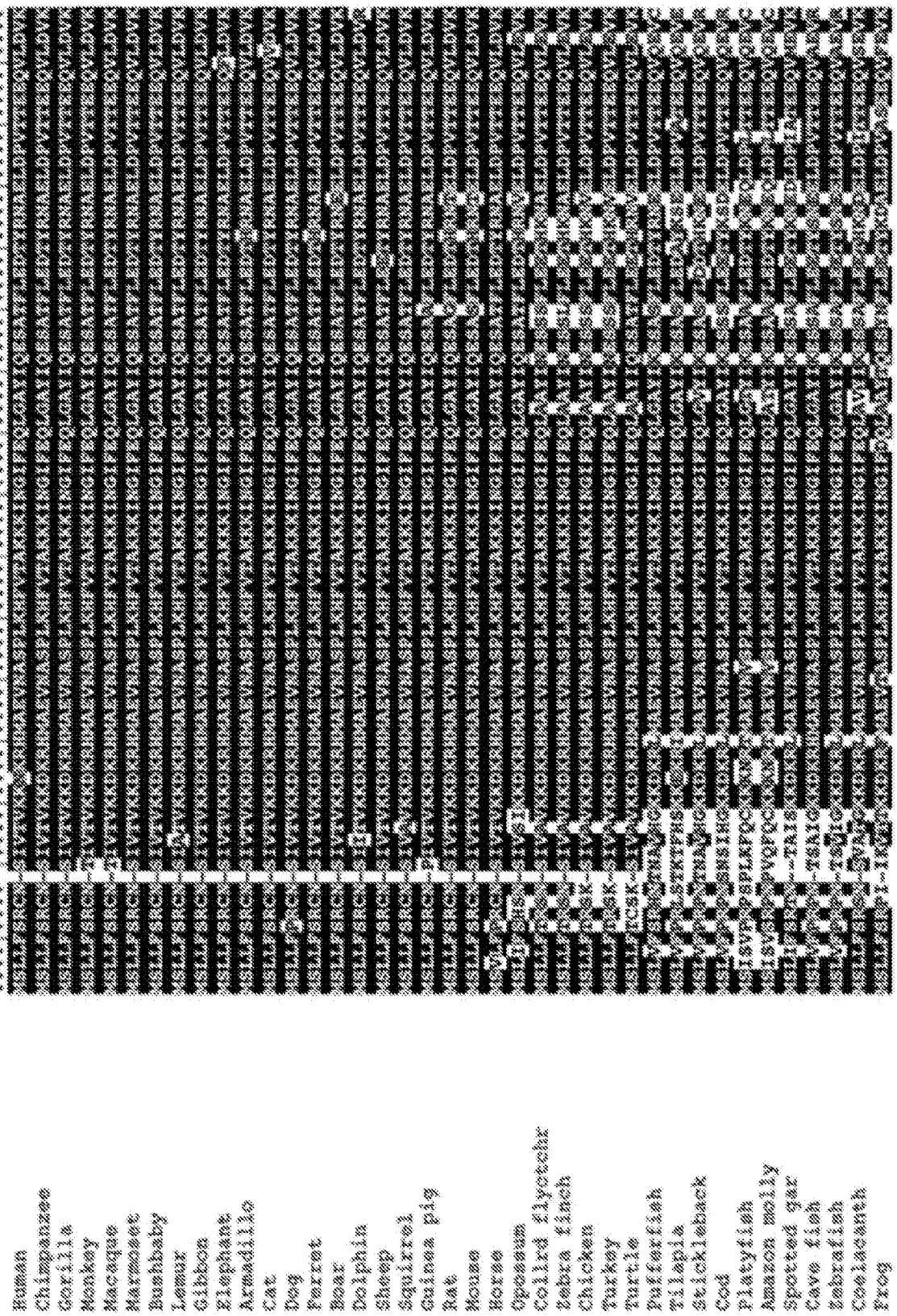
10
20
30
40
50
60
70
Human
Chimpanzee
Gorilla
Monkey
Macaque
Marmoset
Bushbaby
Lemur
Gibbon
Elephant
Armadillo
Cat
Dog
Ferret
Boar
Dolphin
Sheep
Squirrel
Guinea pig
Rat
Mouse
Horse
Opossum
Collrd flycchr
Zebra finch
Chicken
Turkey
Turtle
Pufferfish
Tilapia
stickleback
Cod
Platyfish
Amazon molly
spotted gar
Cave fish
Zebrafish
Coelacanth
Frog

FIG. 13A

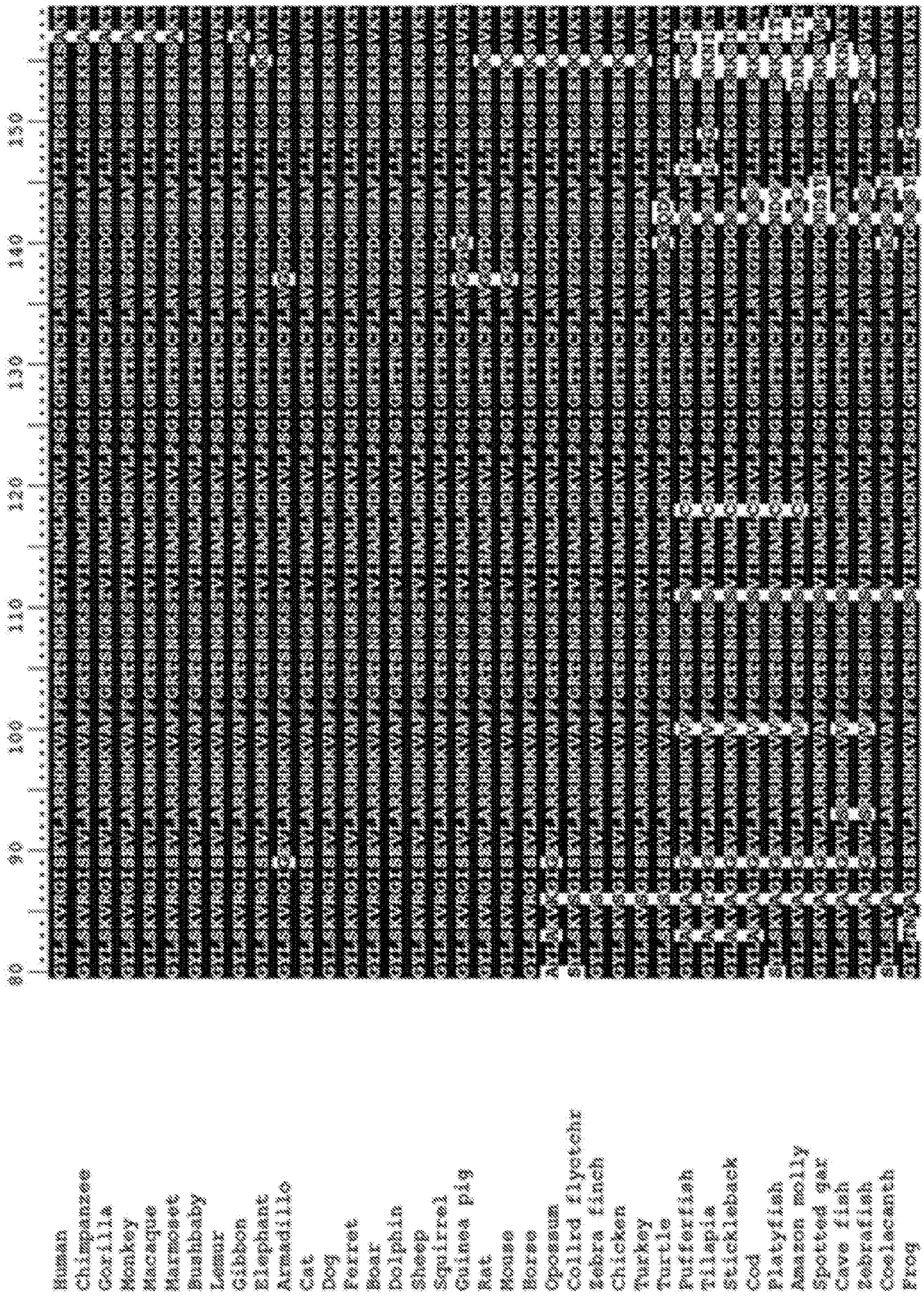
Human
Chimpanzee
Gorilla
Monkey
Macaque
Marmoset
Bushbaby
Lemur
Gibbon
Elephant
Armadillo
Cat
Dog
Ferret
Boar
Dolphin
Sheep
Squirrel
Guinea pig
Rat
Mouse
Horse
Opossum
Collrd flycatchr
Zebra finch
Chicken
Turkey
Turtle
Pufferfish
Tilapia
Stickleback
Cod
Platyfish
Amazon molly
Spotted gar
Cave fish
Zebrafish
Coelacanth
Frog

FIG. 13B

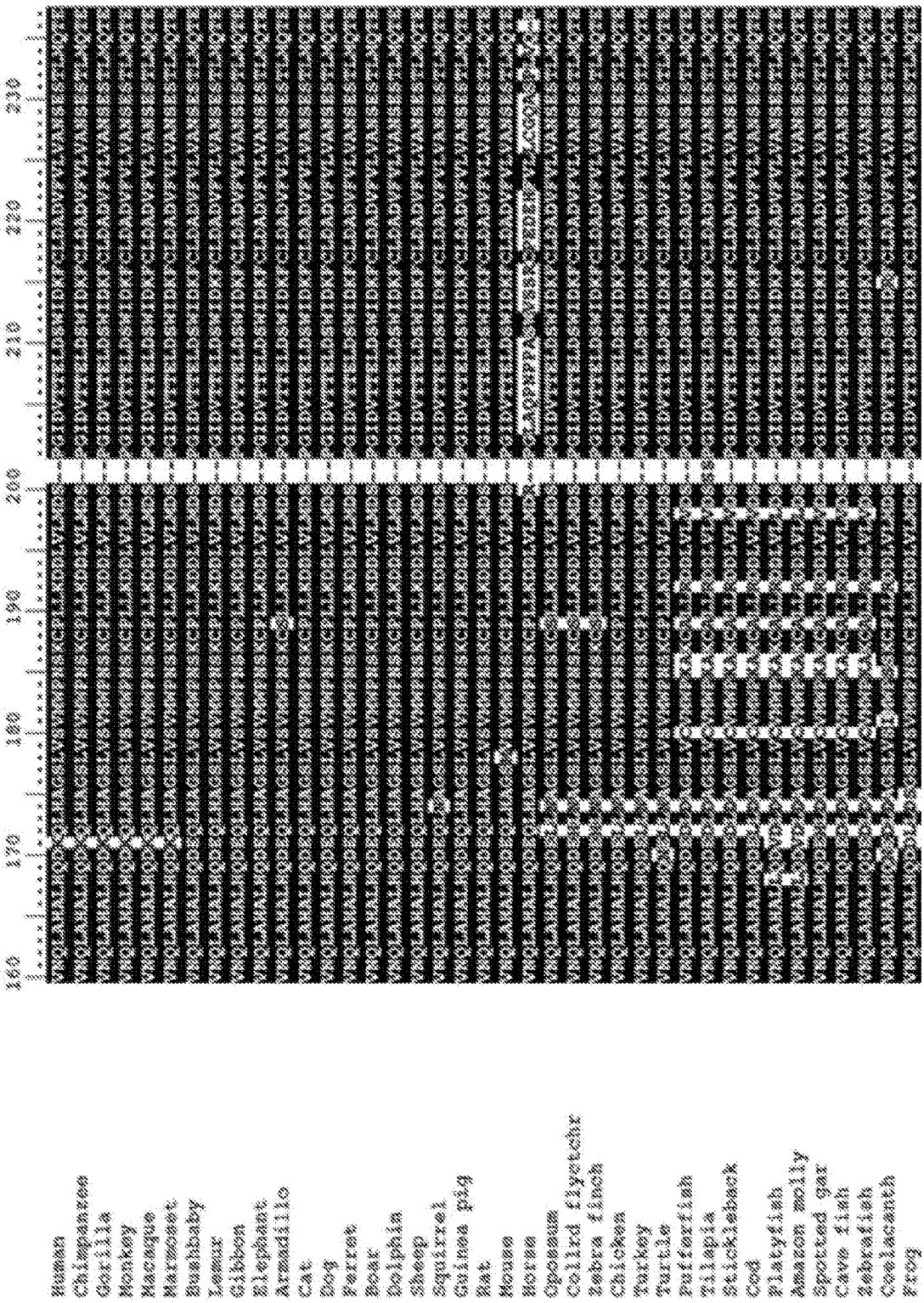
160
170
180
190
200
210
220
230
Human
Chimpanzee
Gorilla
Monkey
Macaque
Marmoset
Bushbaby
Lemur
Gibbon
Elephant
Armadillo
Cat
Dog
Ferret
Bear
Dolphin
Sheep
Squirrel
Guinea pig
Rat
Mouse
Horse
Opossum
Collrd flycatchr
Zebra finch
Chicken
Turkey
Turtle
Pufferfish
Tilapia
Stickleback
Cod
Platyfish
Amazon molly
Spotted gar
Cave fish
Zebrafish
Coelacanth
Frog

FIG. 13C

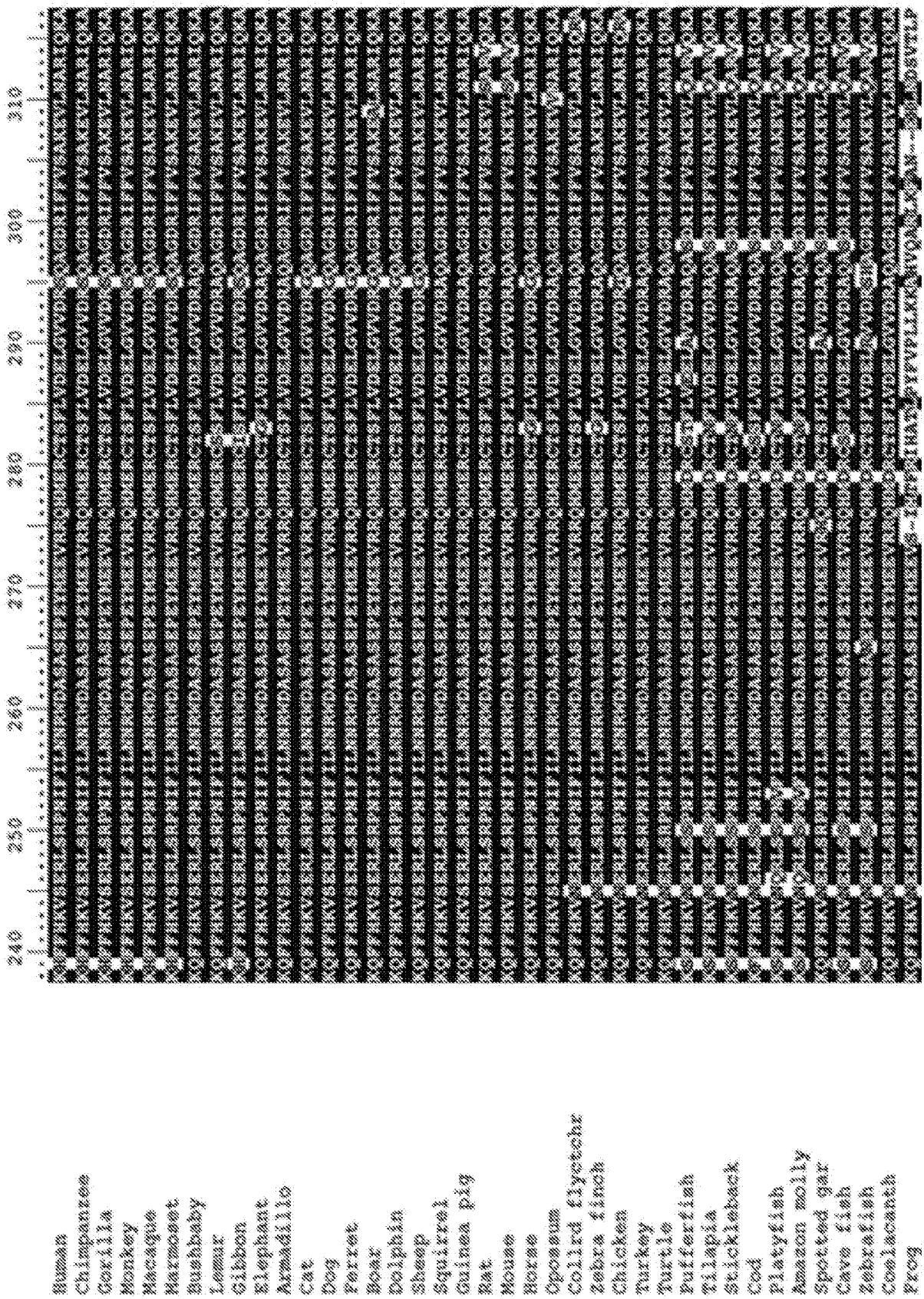
240
250
260
270
280
290
300
310
Human
Chimpanzee
Gorilla
Monkey
Macaque
Marmoset
Bushbaby
Lemur
Gibbon
Elephant
Armadillo
Cat
Dog
Ferret
Boar
Dolphin
Sheep
Squirrel
Guinea pig
Rat
Mouse
Horse
Opossum
Colrd flyctchr
Zebra finch
Chicken
Turkey
Turtle
Pufferfish
Tilapia
Stickleback
Cod
Platyfish
Amazon molly
Spotted gar
Cave fish
Zebrafish
Coelacanth
Frog

FIG. 13D

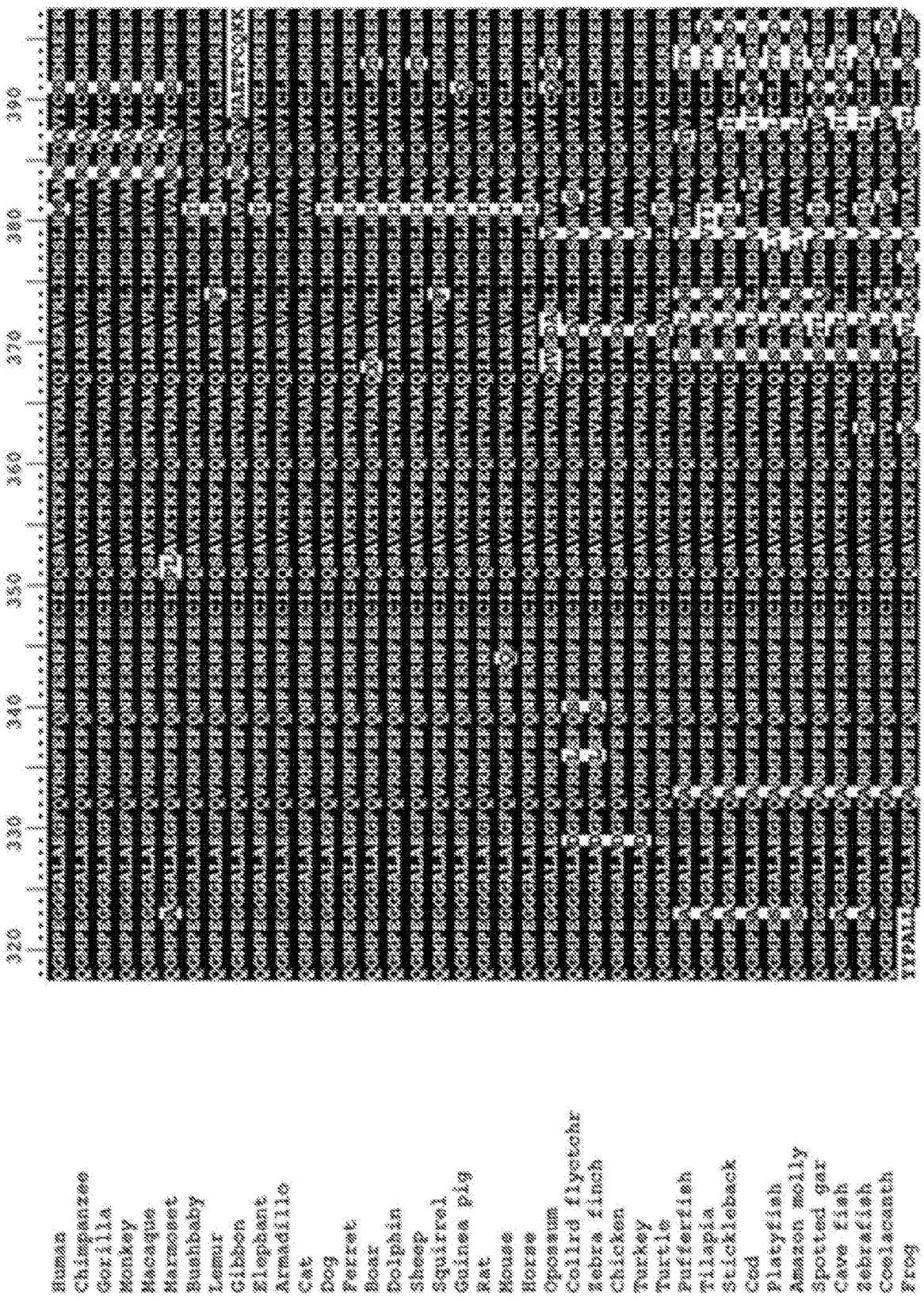
320
330
340
350
360
370
380
390
Human
Chimpanzee
Gorilla
Monkey
Macaque
Marmoset
Bushbaby
Lemur
Gibbon
Elephant
Armadillo
Cat
Dog
Ferret
Boar
Dolphin
Sheep
Squirrel
Guinea pig
Rat
Mouse
Horse
Opossum
Collrd flycatchr
Zebra finch
Chicken
Turkey
Turtle
Tuffedfish
Tilapia
Stickleback
Cod
Platyfish
Amazon molly
Spotted gar
Cave fish
Zebrafish
Coelacanth
Frog

FIG. 13E

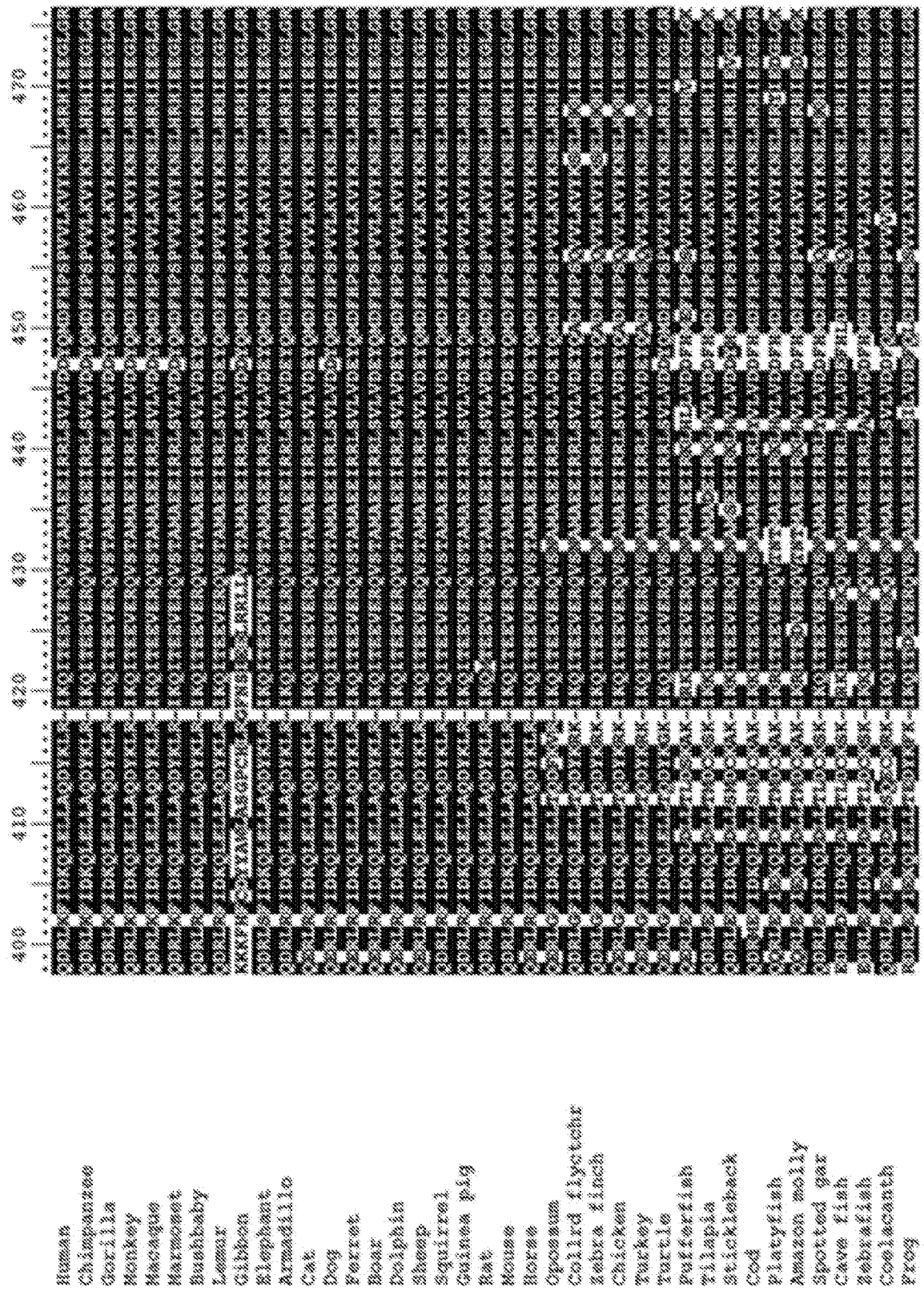
400
410
420
430
440
450
460
470
Human
Chimpanzee
Gorilla
Monkey
Macaque
Marmoset
Bushbaby
Lemur
Gibbon
Elephant
Armadillo
Cat
Dog
Ferret
Boar
Dolphin
Sheep
Squirrel
Guinea pig
Rat
Mouse
Horse
Opossum
Collrd flycatchr
Zebra finch
Chicken
Turkey
Turtle
Pufferfish
Tilapia
Stickleback
Cod
Platyfish
Amazon molly
Spotted gar
Cave fish
Zebrafish
Coelacanth
Frog

FIG. 13F

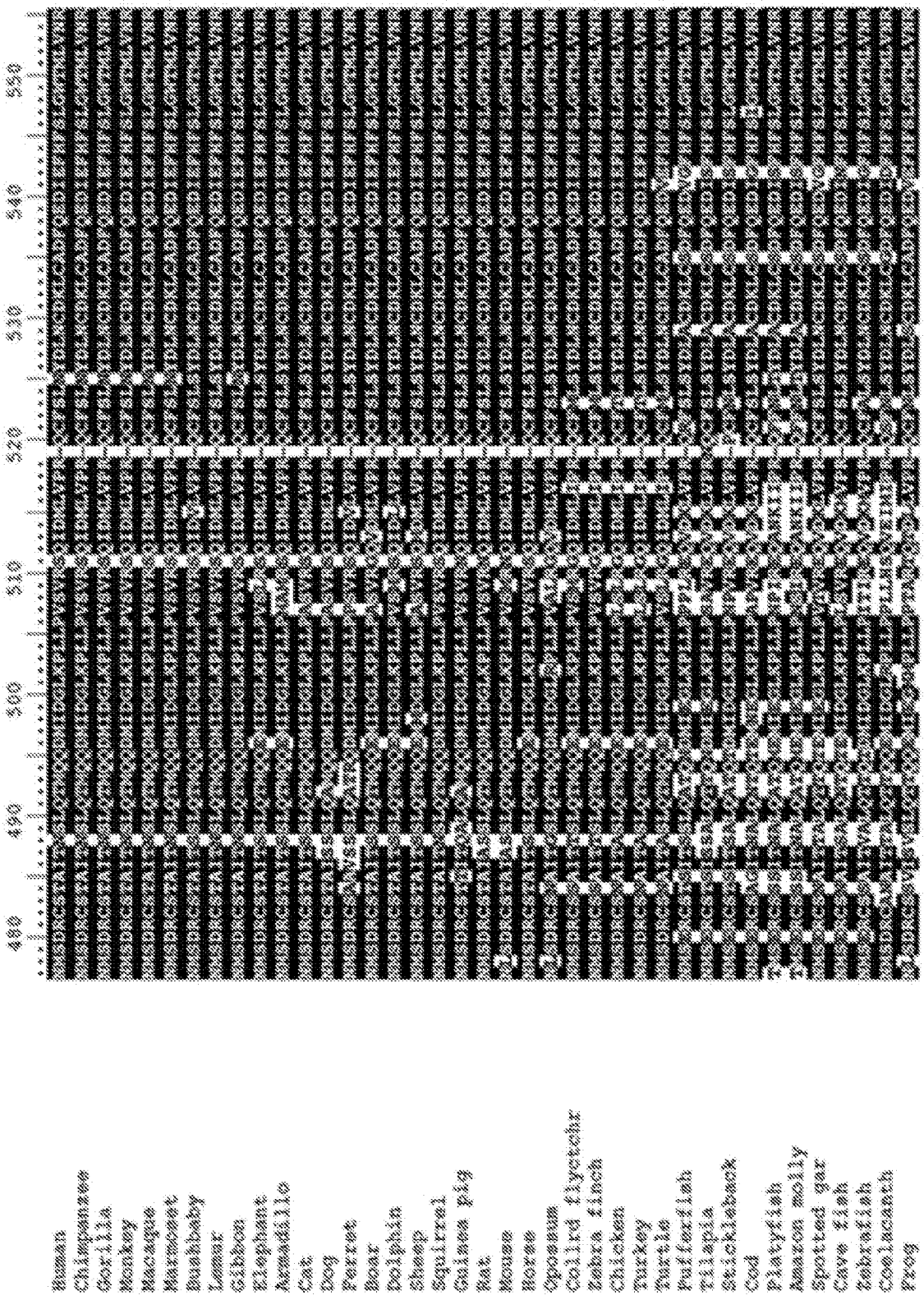
480
490
500
510
520
530
540
550
Human
Chimpanzee
Gorilla
Monkey
Macaque
Marmoset
Bushbaby
Lemur
Gibbon
Elephant
Armadillo
Cat
Dog
Ferret
Boar
Dolphin
Sheep
Squirrel
Guinea pig
Rat
Mouse
Horse
Opossum
Collrd flycatchr
Zebra finch
Chicken
Turkey
Turtle
Pufferfish
Tilapia
Stickleback
Cod
Platyfish
Amazon molly
Spotted gar
Cave fish
Zebrafish
Coelacanth
Frog

FIG. 13G

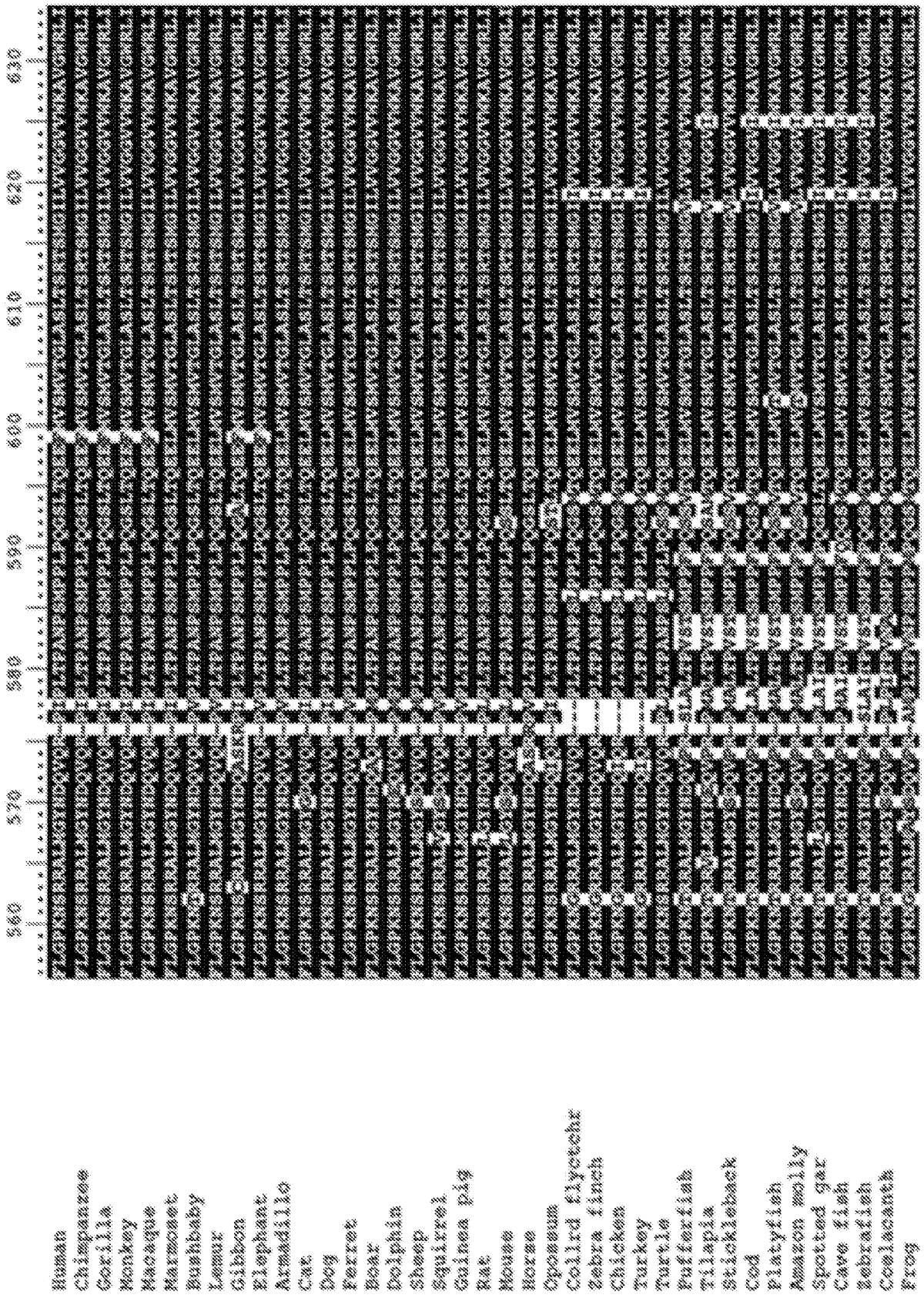
560
570
580
590
600
610
620
630
Human
Chimpanzee
Gorilla
Monkey
Macaque
Marmoset
Bushbaby
Lemur
Gibbon
Elephant
Armadillo
Cat
Dog
Ferret
Bear
Dolphin
Sheep
Squirrel
Guinea pig
Rat
Mouse
Horse
Opossum
Collrd flycatchr
Zebra finch
Chicken
Turkey
Turtle
Pufferfish
Tilapia
Stickleback
Cod
Platyfish
Amazon molly
Spotted gar
Cave fish
Zebrafish
Coelacanth
Frog

FIG. 13H

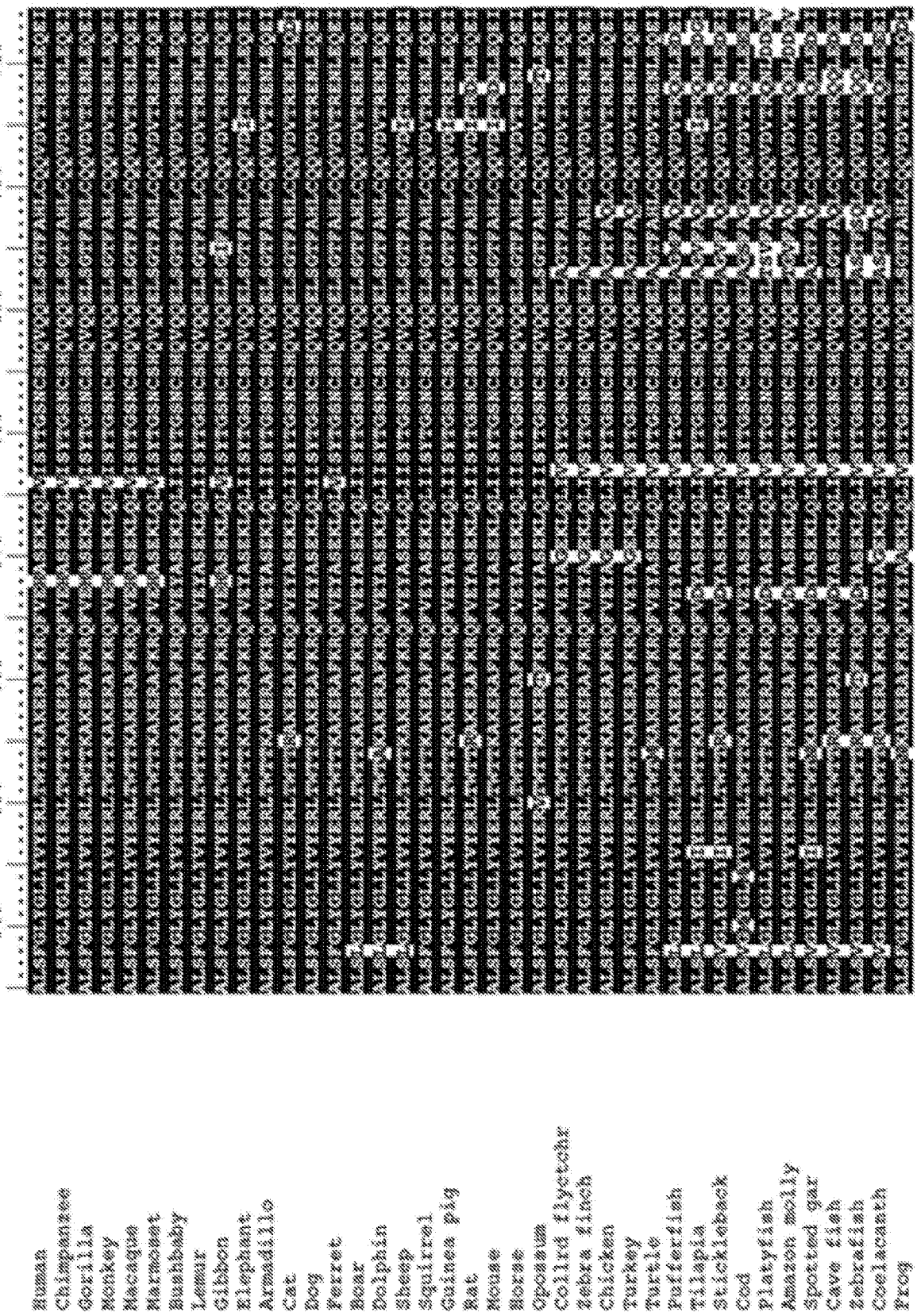
640
650
660
670
680
690
700
710
Human
Chimpanzee
Gorilla
Monkey
Macaque
Marmoset
Bushbaby
Lemur
Gibbon
Elephant
Armadillo
Cat
Dog
Ferret
Bear
Dolphin
Sheep
Squirrel
Guinea pig
Rat
Mouse
Horse
Opossum
Collrd flycatchr
Zebra finch
Chicken
Turkey
Turtle
Pufferfish
Tilapia
Stickleback
Cod
Platyfish
Amazon molly
Spotted gar
Cave fish
Zebrafish
Coelacanth
Frog

FIG. 13I

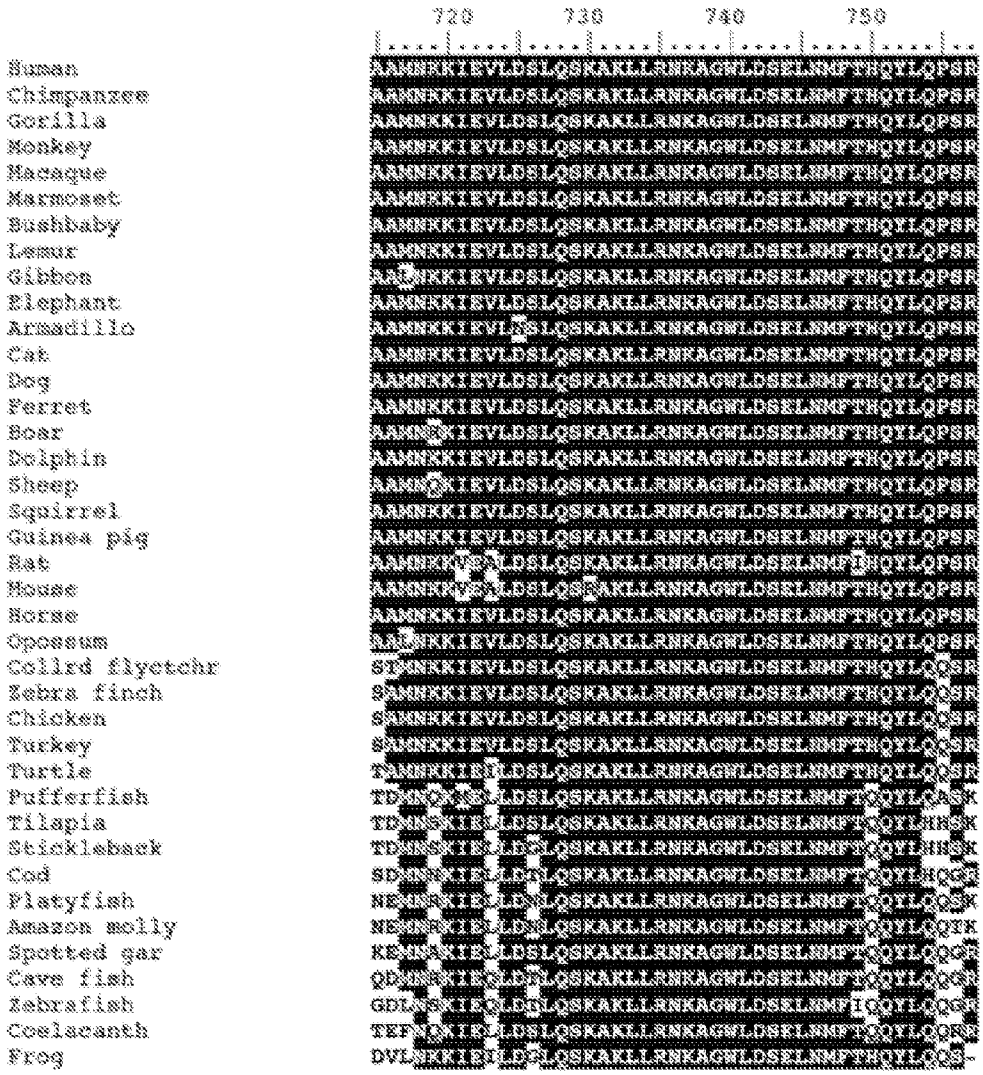
720
730
740
750
Human
Chimpanzee
Gorilla
Monkey
Macaque
Marmoset
Bushbaby
Lemur
Gibbon
Elephant
Armadillo
Cat
Dog
Ferret
Boar
Dolphin
Sheep
Squirrel
Guinea pig
Rat
Mouse
Horse
Opossum
Collrd flycatchr
Zebra finch
Chicken
Turkey
Turtle
Pufferfish
Tilapia
Stickleback
Cod
Platyfish
Amazon molly
Spotted gar
Cave fish
Zebrafish
Coelacanth
Frog

FIG. 13J

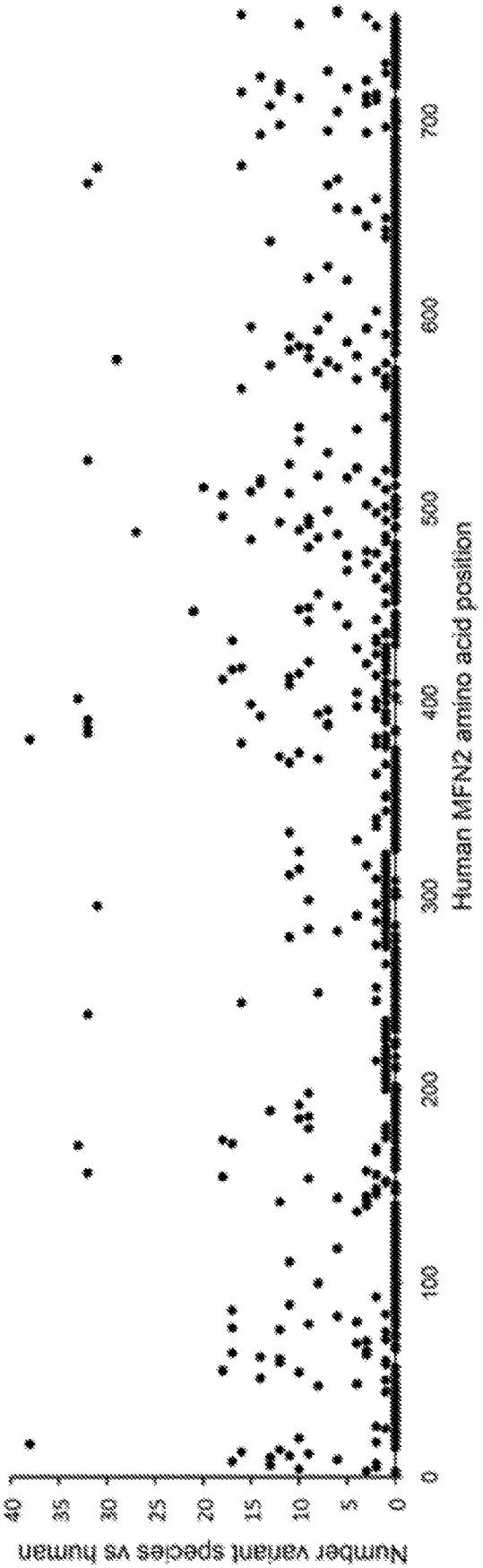
Number variant species vs human
0
5
10
15
20
25
30
35
40
0
100
200
300
400
500
600
700
Human MFN2 amino acid position

FIG. 14A

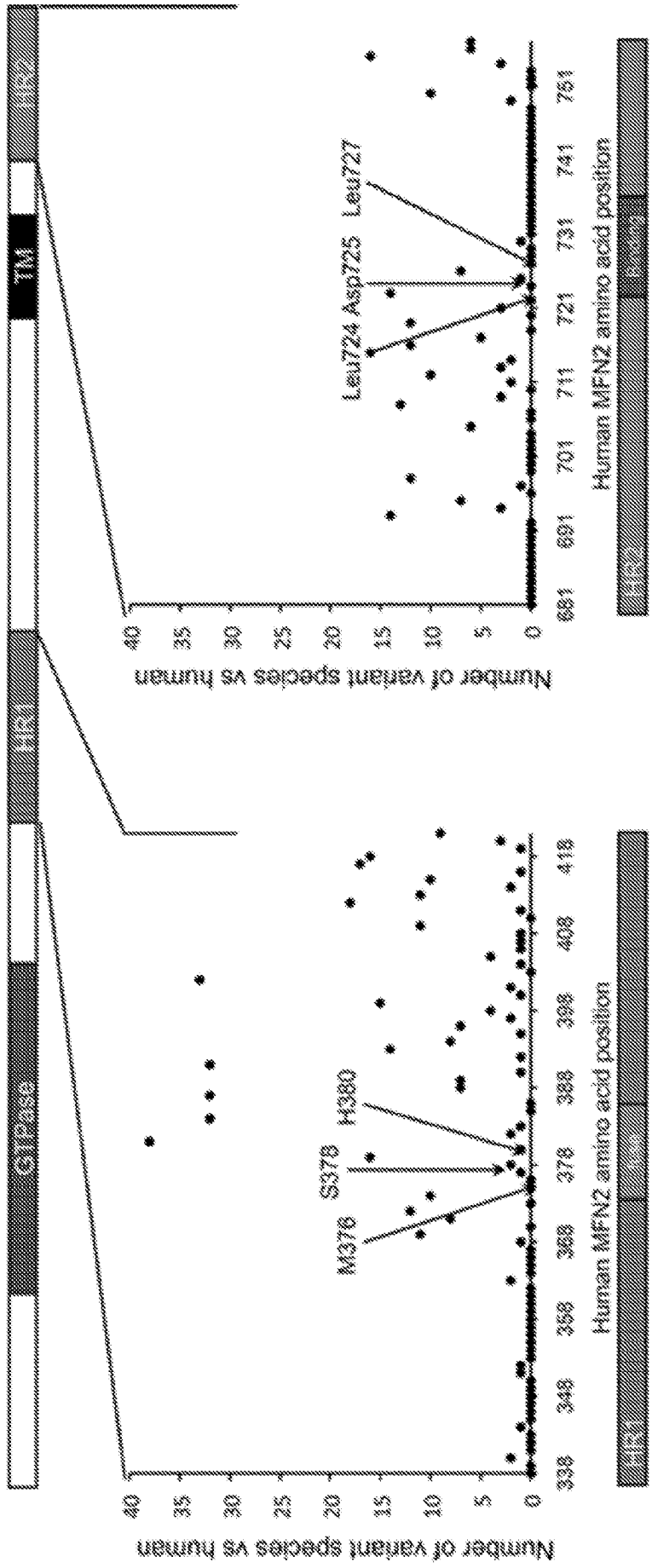

FIG. 14B

FIG. 14C

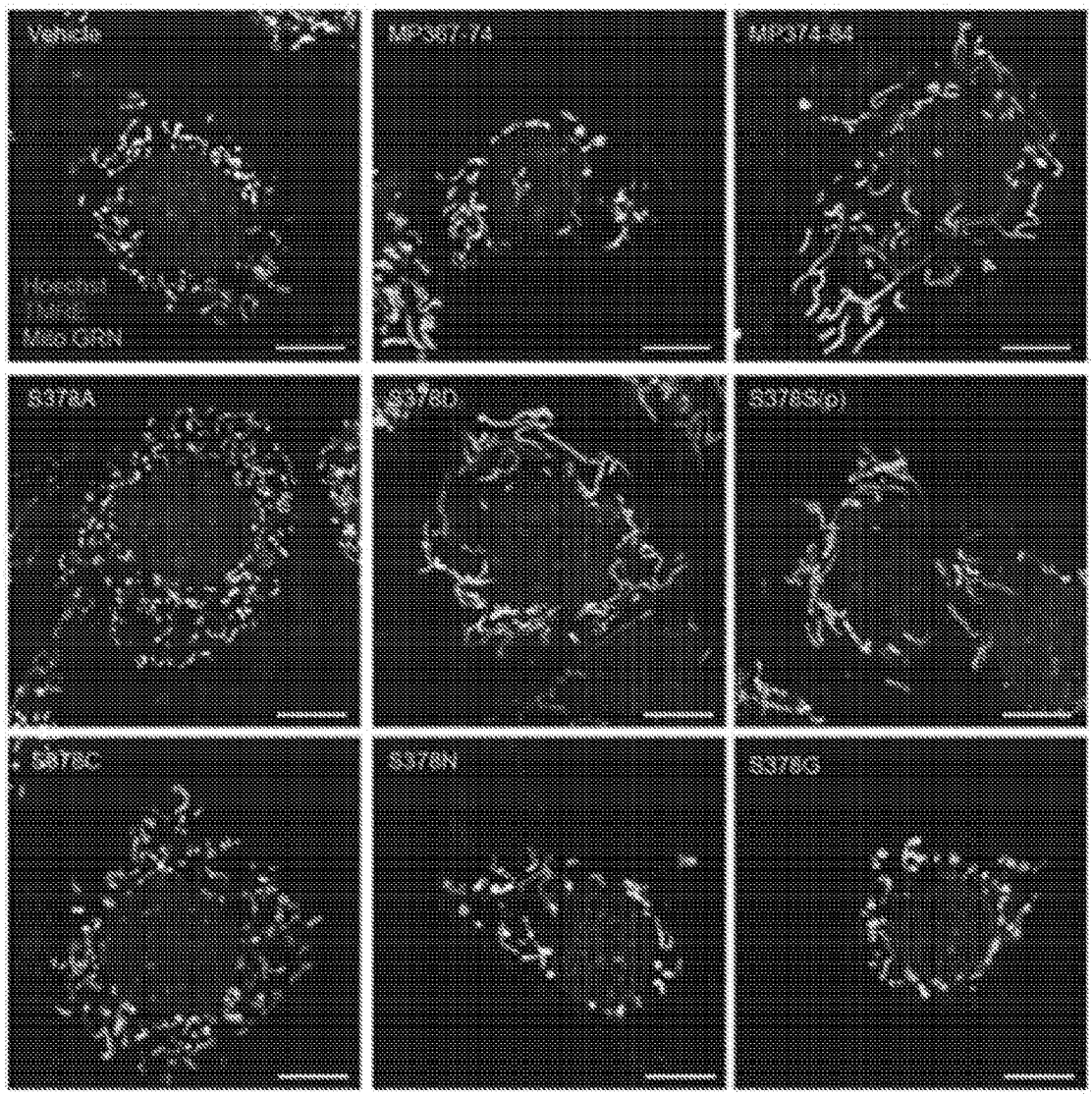
Vehicle
MK-5108
MBS GRN
MP387-74
MP378-93
S378A
S378D
S378S(p)
S378C
S378N
S378G

FIG. 15A

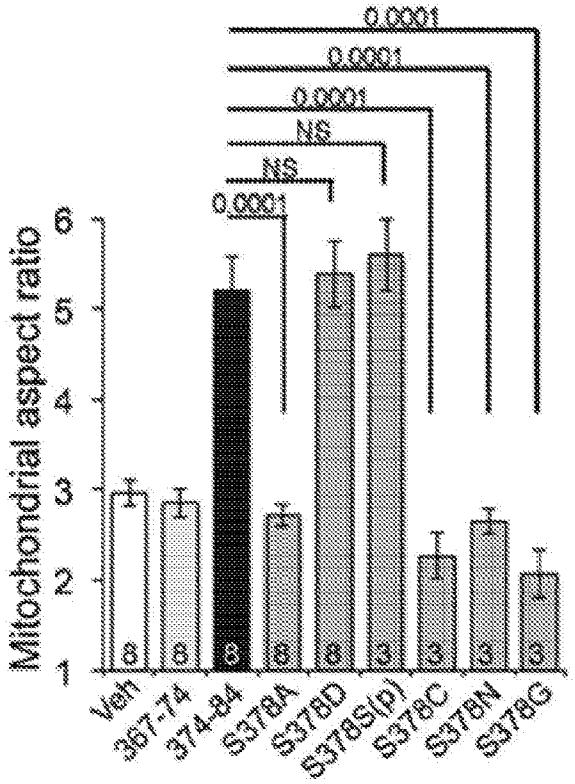
0.0001
0.0001
0.0001
NS
NS
0.0001
Mitochondrial aspect ratio
1
2
3
4
5
6
8
8
8
8
8
3
3
3
3
Veh
367-74
374-84
S378A
S378D
S378S(p)
S378C
S378N
S378G

FIG. 15B

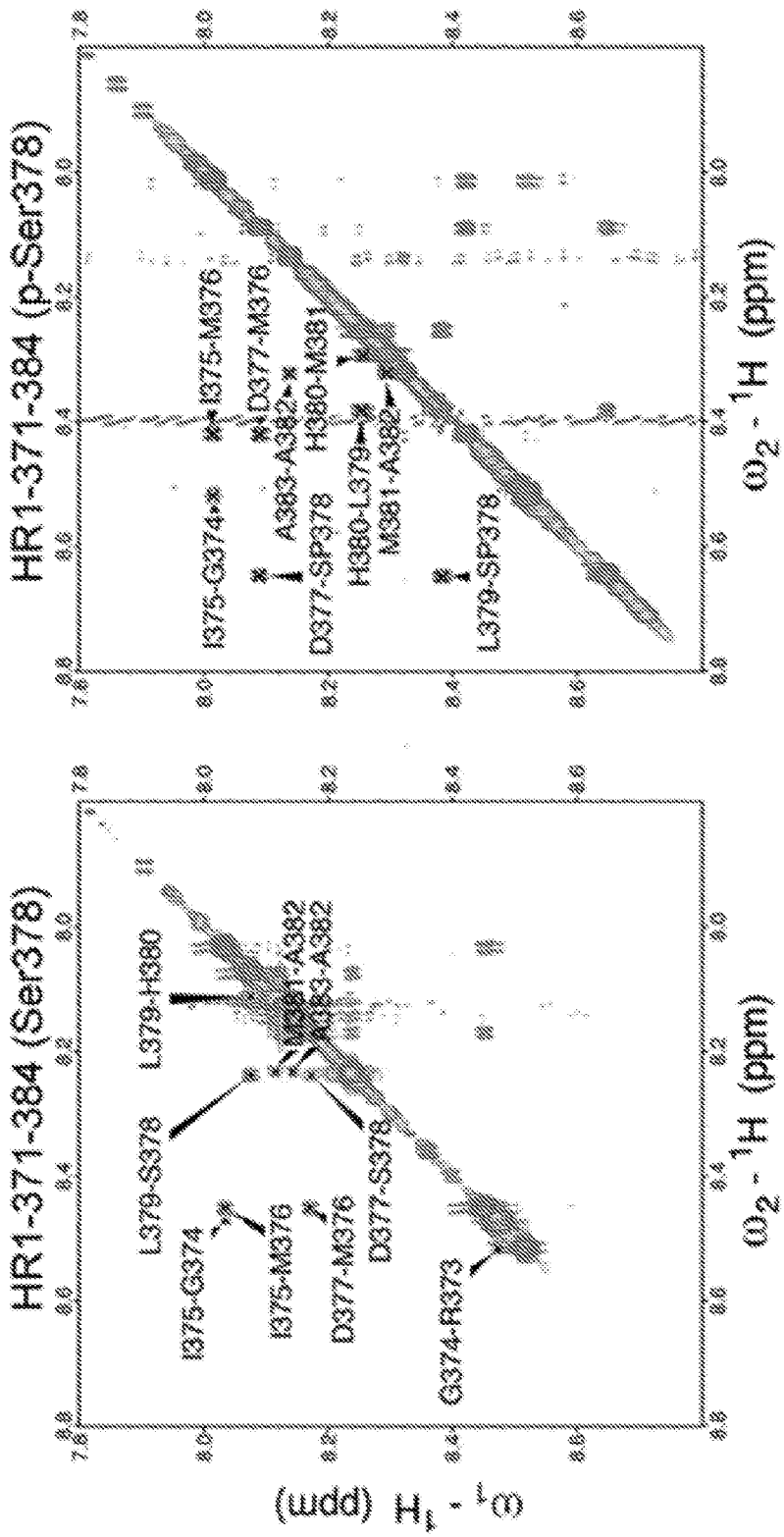

FIG. 16A

FIG. 16B

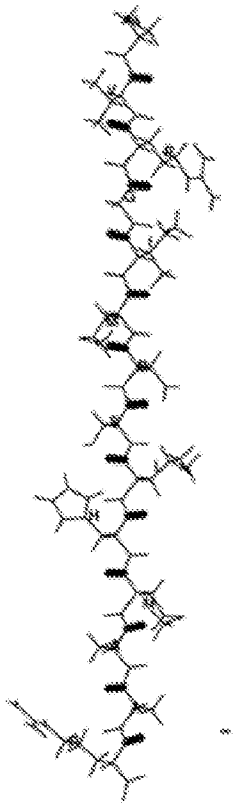

FIG. 16C

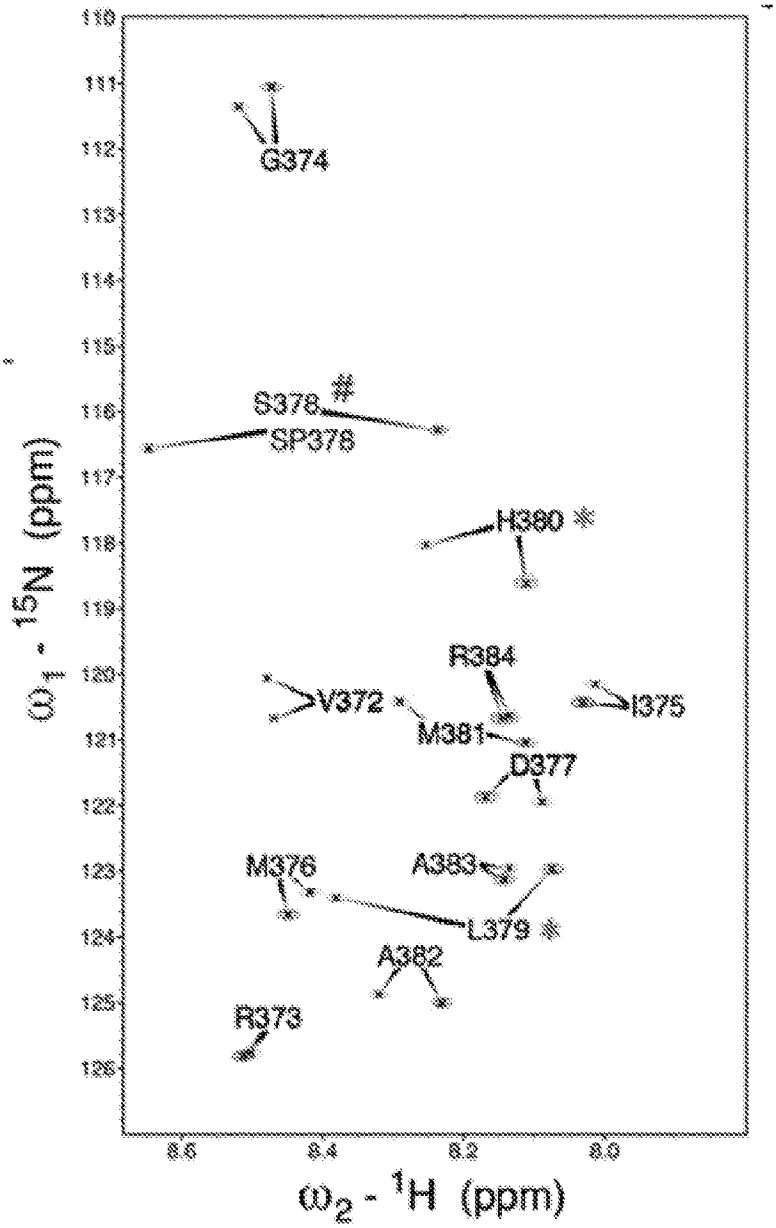

FIG. 16D

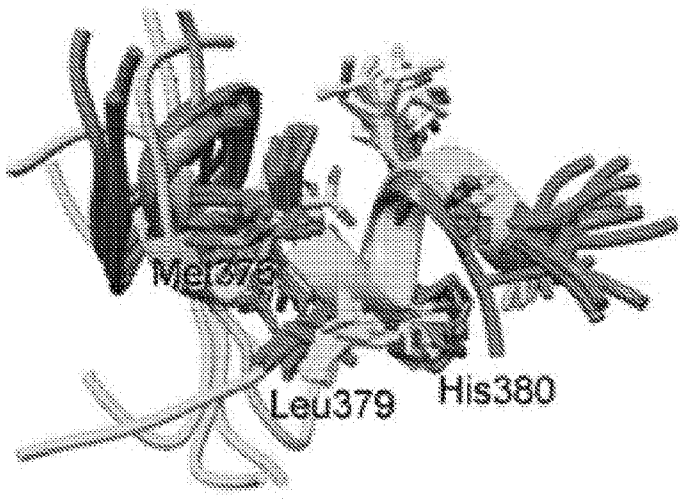

FIG. 16E

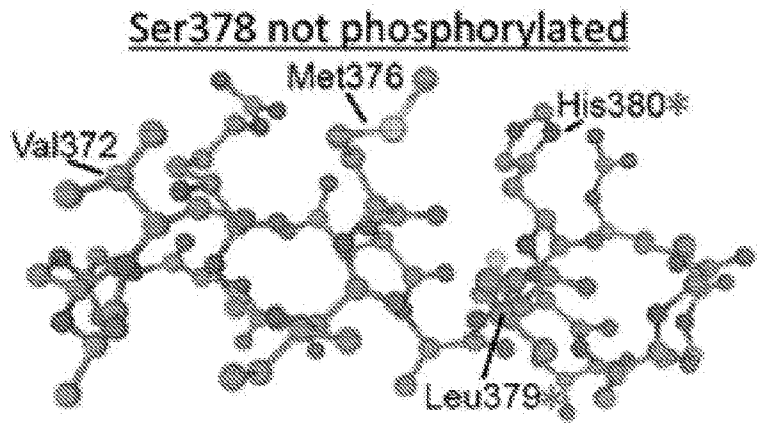

FIG. 16F

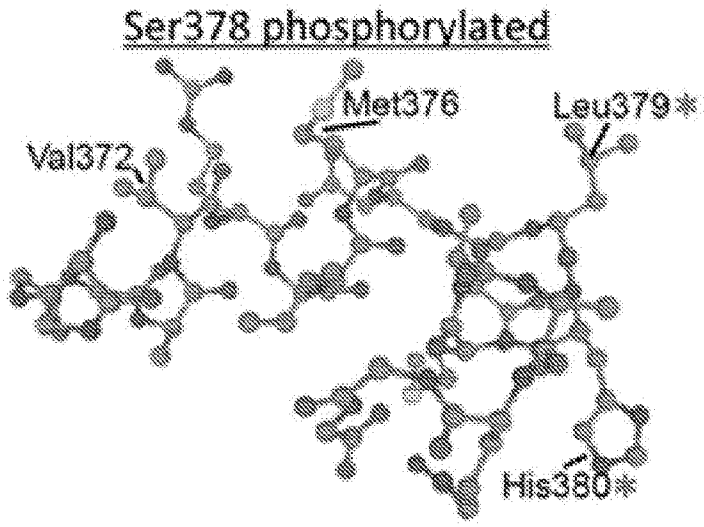

FIG. 16G

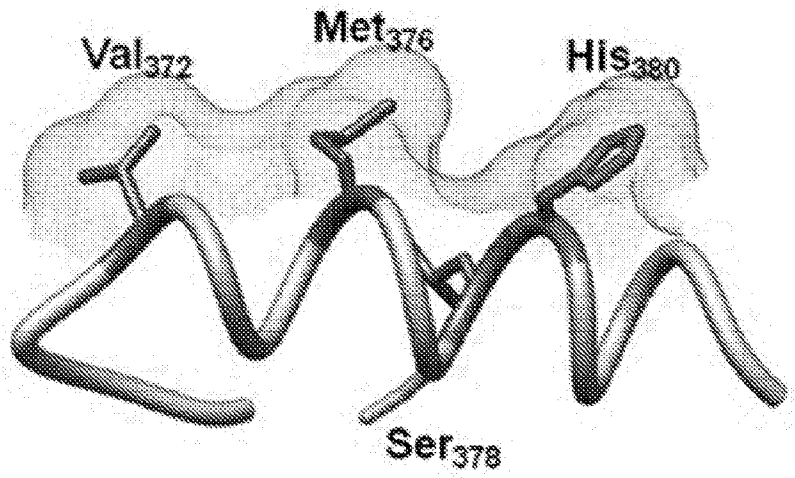

FIG. 17A

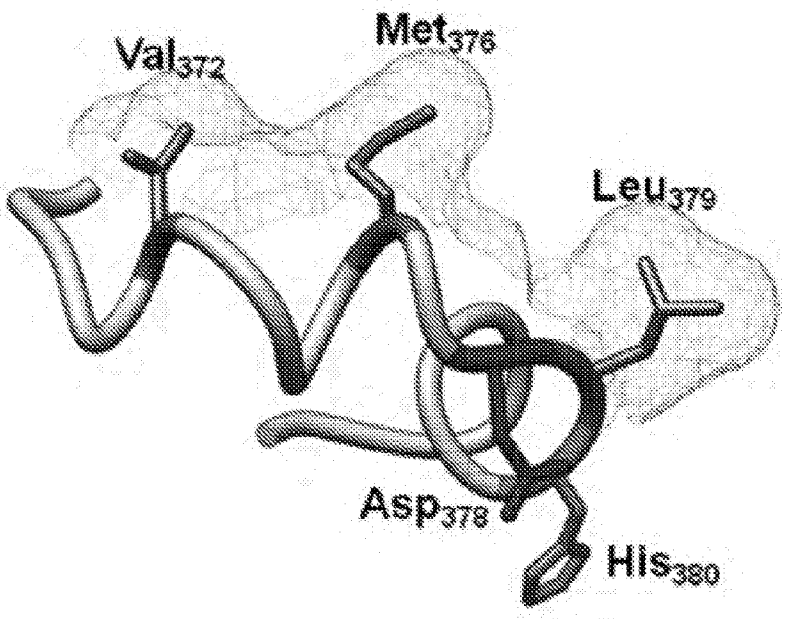

FIG. 17B

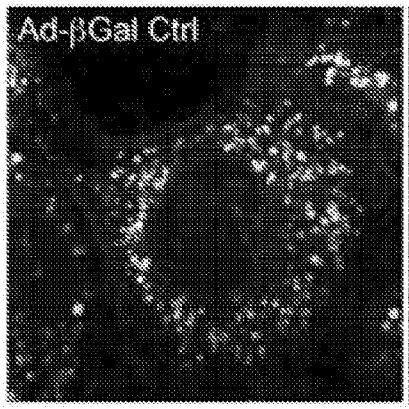

FIG. 18A

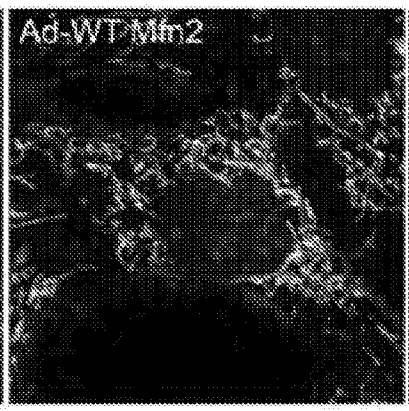

FIG. 18B

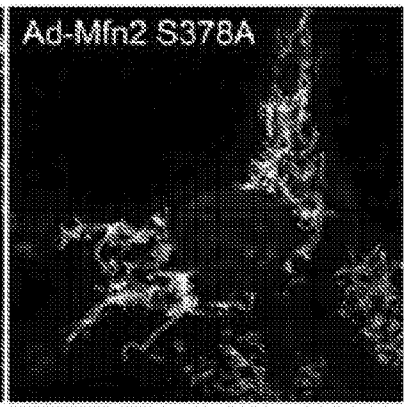

FIG. 18C

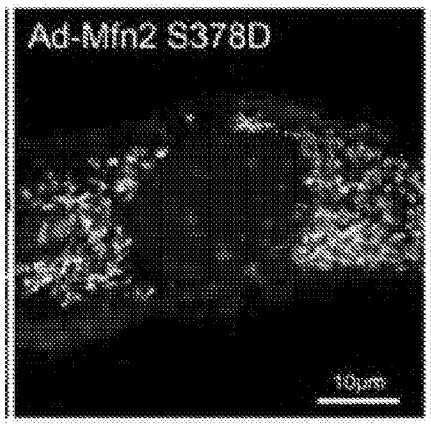

FIG. 18D

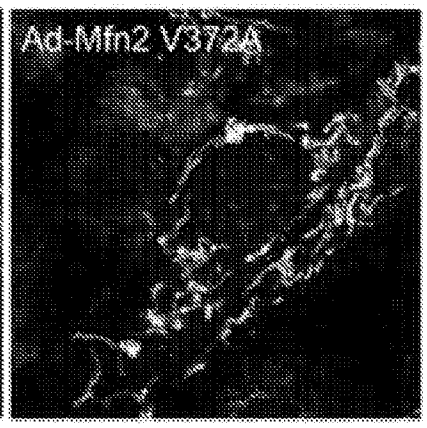

FIG. 18E

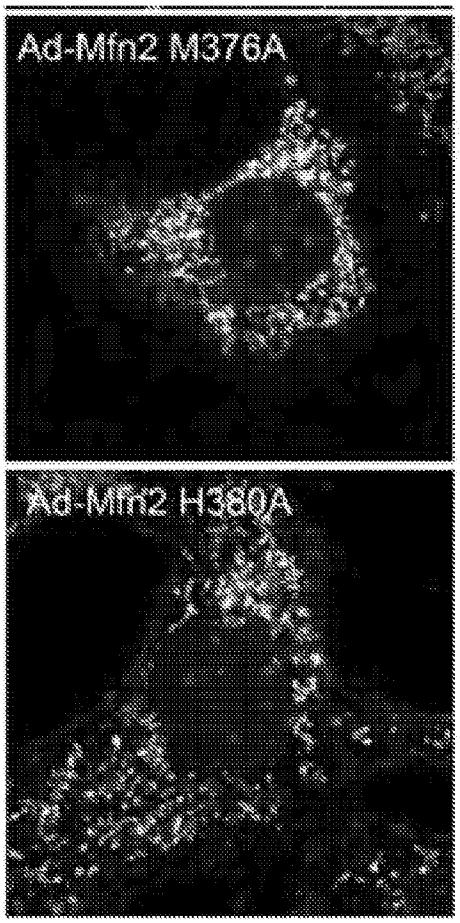

FIG. 18F

FIG. 18G

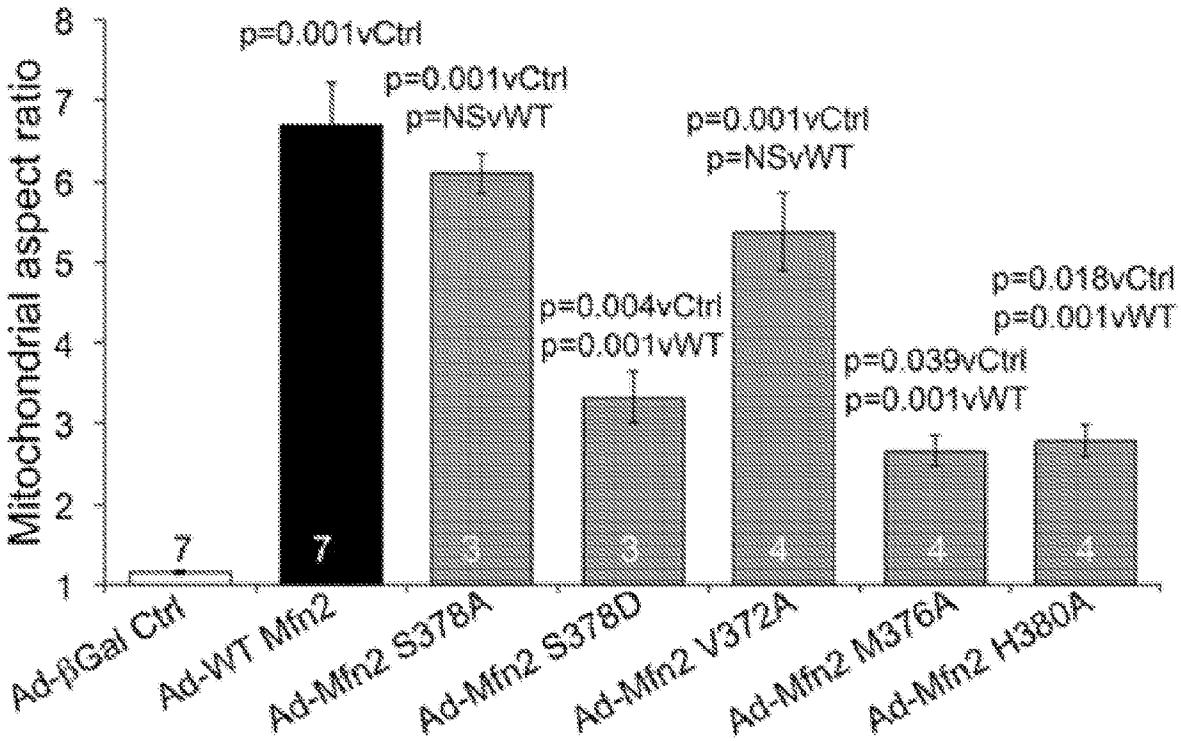

FIG. 18H

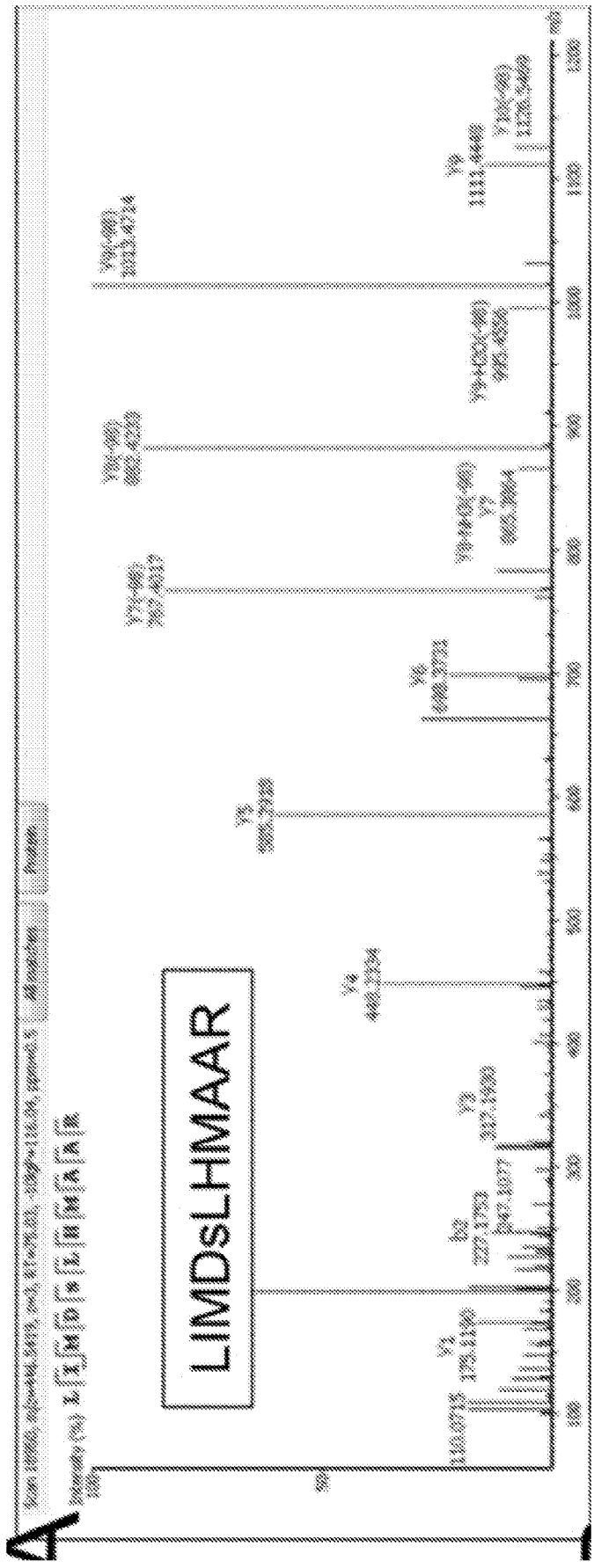

FIG. 19A

#	b	b-H2O	b-NH3	Seq.	i	y	y-H2O	y-NH3	#
1	114.0919	96.0813	97.0649	L	1	1224.5365	1206.5260	1207.4995	10
2	227.1753	209.1654	210.1489	L	1	1111.4440	1093.4019	1094.4154	9
3	358.2164	340.2059	341.1895	M	0	960.4019	942.3914	943.3749	8
4	473.2434	455.2328	456.2164	Q	0	829.3604	811.3499	812.3344	7
5	640.3417	622.3311	623.3147	K(+79.97)	0	714.3331	696.3225	697.3060	6
6	753.3258	735.3152	736.2988	L	0	585.2918	567.2809	568.2656	5
7	890.3947	872.3741	873.3577	H	0	472.2231	454.2126	455.1962	4
8	1021.4252	1003.4146	1004.3982	M	0	335.1642	317.1536	318.1372	3
9	1092.4623	1074.4518	1075.4353	A	0	204.1337	186.1231	187.1067	2
10	1163.4994	1145.4889	1146.4724	A	0	133.0966	115.0860	116.0696	1
11				R	0	72.0813	54.0708	55.0544	0

FIG. 19B

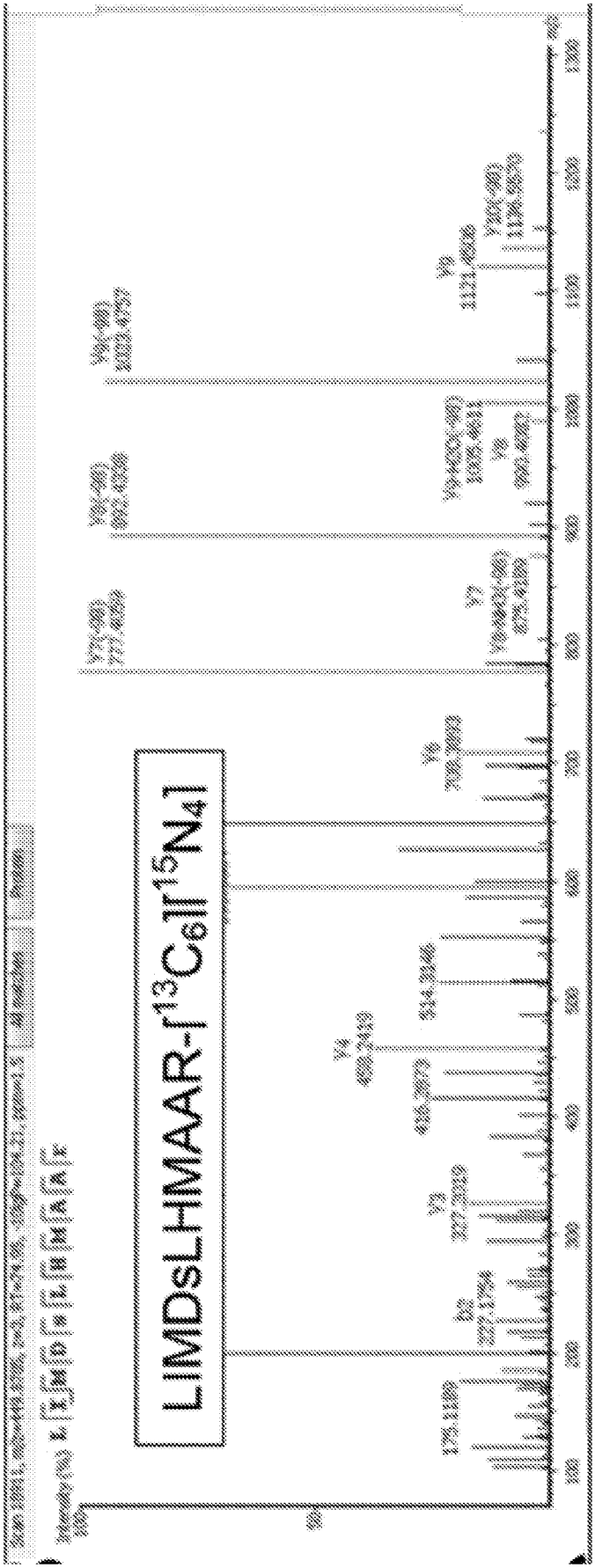

FIG. 19C

#	b	b-H2O	b-NH3	Seq.	i	y	y-H2O	y-NH3	#
1	114.0919	96.0813	97.0649	L	1	1234.6341	1216.5340	1217.5079	11
2	227.1754	209.1654	210.1489	I	1	1121.5501	1103.4402	1104.4237	10
3	358.2164	340.2059	341.1895	M	M	1008.4661	990.4561	991.4396	9
4	473.2434	455.2328	456.2164	D	D	877.4251	859.4146	860.3982	8
5	640.3417	622.3311	623.3147	S+79.97	S+79.97	762.3981	744.3876	745.3712	7
6	753.3258	735.3152	736.2988	L	L	595.3008	577.2903	578.2739	6
7	890.3847	872.3741	873.3577	H	H	482.2168	464.2062	465.1898	5
8	1031.4282	1013.4176	1014.3982	M	M	345.1589	327.1484	328.1320	4
9	1082.4603	1074.4518	1075.4353	A	A	204.1159	186.1054	187.0890	3
10	1163.4994	1145.4889	1146.4724	A	A	73.0749	55.0644	56.0480	2
11				R(+10.01)	R(+10.01)	1.0735	-17.0371	-16.0535	1

FIG. 19D

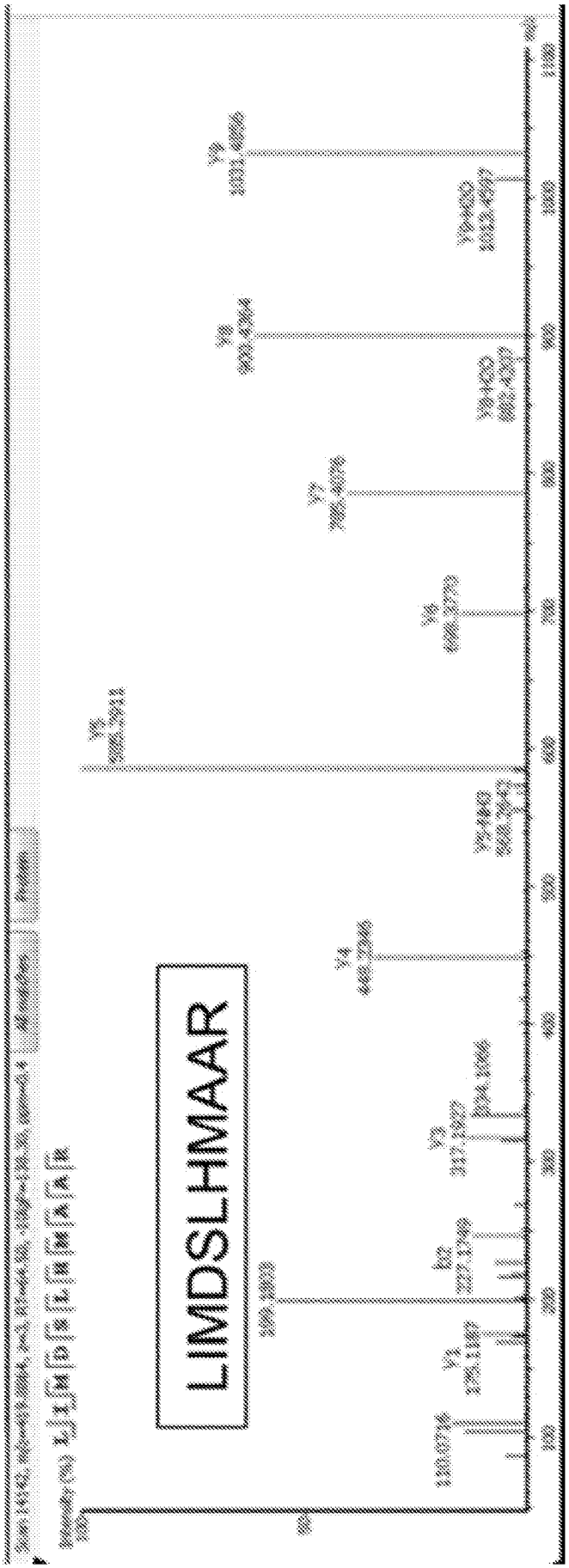

FIG. 19E

#	b	b-H2O	b-NH3	Seq.	y	y-H2O	y-NH3	#
1	114.0913	96.0813	97.0649	L				11
2	227.1749	209.1654	210.1489	I	1144.5602	1126.5497	1127.5332	10
3	358.2164	340.2059	341.1895	M	1031.4806	1013.4697	1014.4491	9
4	473.2434	455.2328	456.2164	D	900.4391	882.4287	883.4086	8
5	560.2754	542.2648	543.2484	S	785.4126	767.3981	768.3844	7
6	673.3594	655.3489	656.3325	L	698.3770	680.3640	681.3496	6
7	810.4184	792.4078	793.3914	H	585.2911	567.2820	568.2643	5
8	941.4609	923.4483	924.4319	M	448.2396	430.2231	431.2067	4
9	1012.4980	994.4854	995.4690	A	317.1967	299.1829	300.1662	3
10	1083.5351	1065.5225	1066.5061	A	246.1642	228.1495	229.1329	2
11				R	175.1187	157.1084	158.0924	1

FIG. 19F

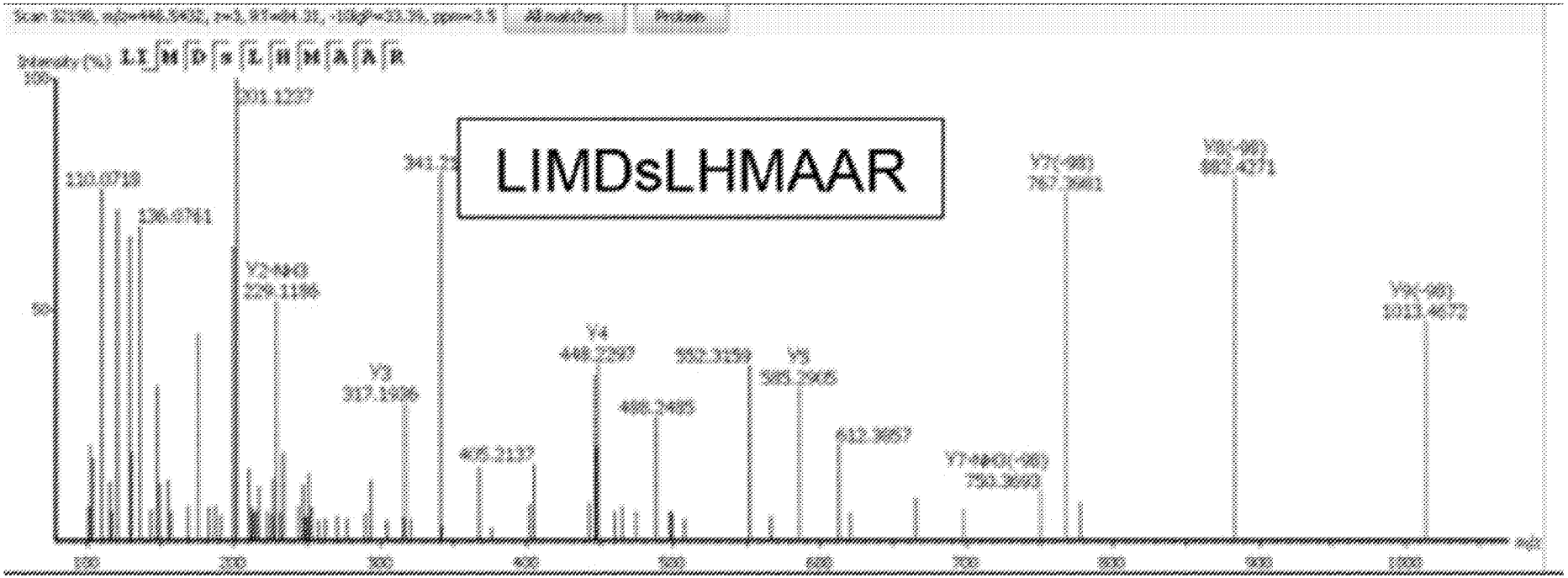

FIG. 19G

FIG. 19H

#	b	b-H2O	b-NH3	Seq.	y	y-H2O	y-NH3	#
1	114.0919	96.0813	97.0649	L				11
2	227.1758	209.1654	210.1489	I	1224.5265	1206.5160	1207.4995	10
3	358.2164	340.2059	341.1895	M	1111.4424	1093.4319	1094.4154	9
4	473.2434	455.2328	456.2164	D	980.4019	962.3914	963.3749	8
5	640.2417	622.2311	623.2147	S(+79.97)	865.3750	847.3644	848.3480	7
6	753.3258	735.3152	736.2988	L	698.3801	680.3695	681.3496	6
7	890.3847	872.3741	873.3577	H	585.2965	567.2859	568.2656	5
8	1021.4252	1003.4146	1004.3982	M	448.2377	430.2231	431.2067	4
9	1092.4623	1074.4518	1075.4353	A	317.1936	299.1826	300.1662	3
10	1163.4994	1145.4889	1146.4724	A	246.1561	228.1455	229.1186	2
11				R	175.1190	157.1084	158.0919	1

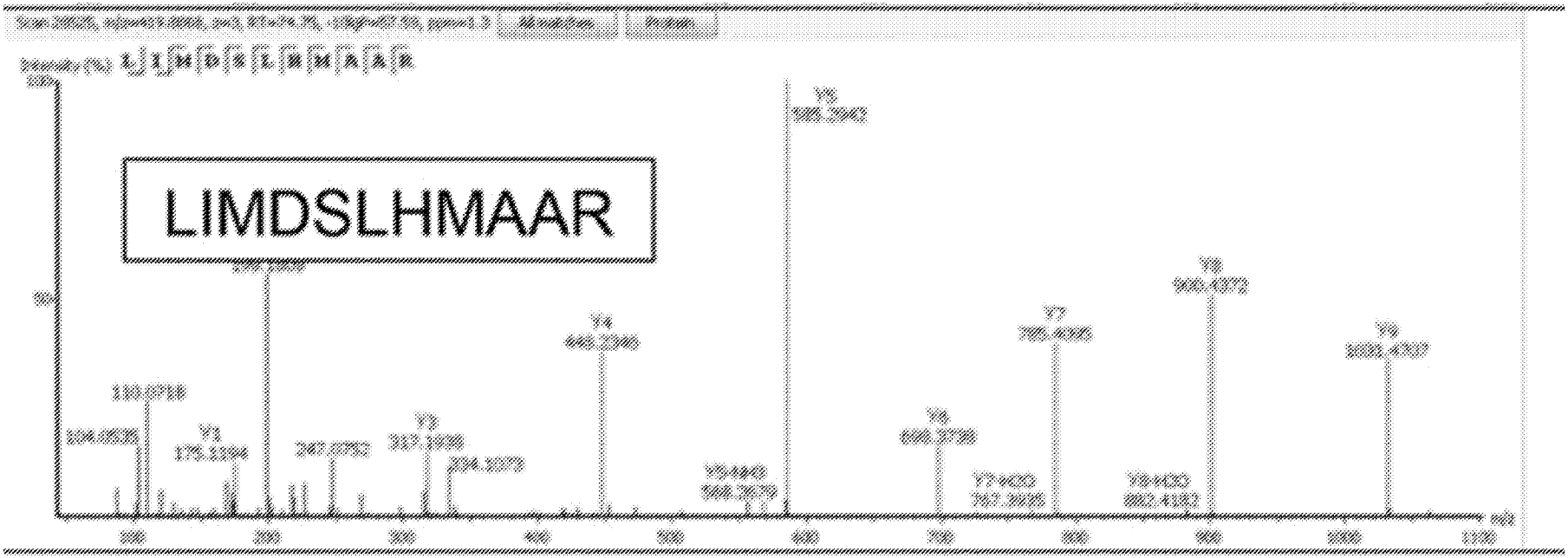

FIG. 19I

FIG. 19J

#	b	b-H2O	b-NH3	Seq	y	y-H2O	y-NH3	#
1	114.0920	96.0813	97.0649	L				11
2	227.1757	209.1654	210.1489	I	1144.5602	1126.5497	1127.5332	10
3	358.2164	340.2059	341.1895	M	1031.4767	1013.4655	1014.4491	9
4	473.2434	455.2328	456.2164	D	900.4372	882.4162	883.4312	8
5	560.2754	542.2648	543.2484	S	785.4095	767.3935	768.3817	7
6	673.3594	655.3489	656.3325	L	698.3778	680.3660	681.3496	6
7	810.4199	792.4078	793.3914	H	585.2942	567.2820	568.2679	5
8	941.4589	923.4483	924.4319	M	448.2346	430.2231	431.2100	4
9	1012.4960	994.4854	995.4690	A	317.1938	299.1826	300.1671	3
10	1083.5331	1065.5226	1066.5061	A	246.1567	228.1455	229.1296	2
11				R	175.1194	157.1102	158.0919	1

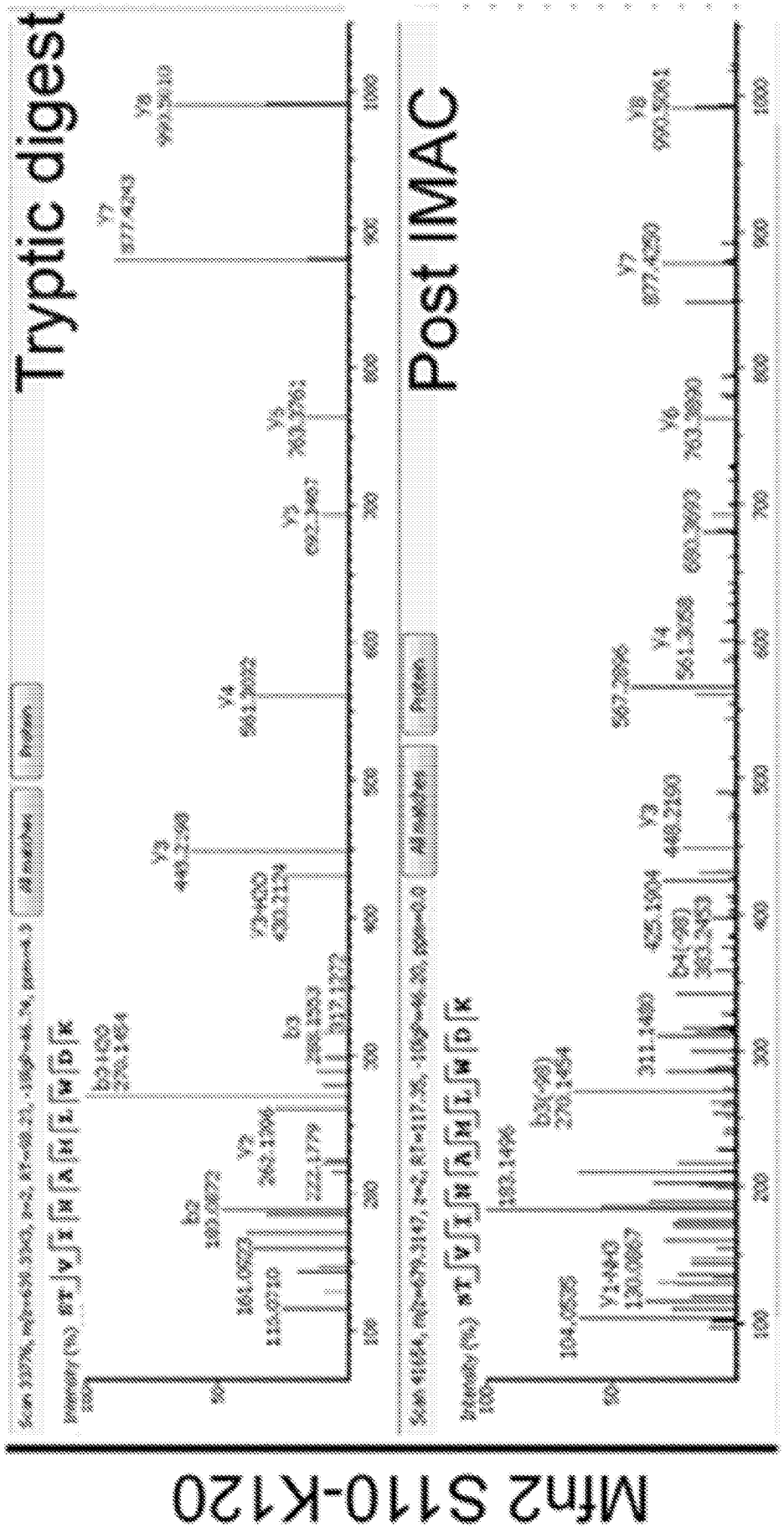

FIG. 20A

#	b	b-H2O	b-NH3	b (2+)	Seq.	y	y-H2O	y-NH3	y (2+)	#
1	88.0399	70.0293	71.0133	44.5169	S					11
2	169.0872	151.0765	152.0605	85.0438	T	1189.6239	1172.6133	1173.5973	595.3119	10
3	288.1553	270.1447	271.1286	144.5780	V	1089.5760	1071.5654	1072.5493	545.2880	9
4	401.2400	383.2294	384.2133	201.1200	T	970.5071	952.4965	953.4807	485.7440	8
5	515.2830	497.2724	498.2563	258.1451	N	857.4224	839.4118	840.3957	429.2118	7
6	686.3301	668.3195	669.3034	293.6690	A	743.3794	725.3688	726.3527	382.1803	6
7	717.3665	699.3559	700.3398	359.1803	M	572.3264	554.3158	555.3146	286.6718	5
8	830.4446	812.4340	813.4179	415.7223	L	501.2900	483.2794	484.2633	251.1356	4
9	1014.5229	996.5124	997.4963	507.7620	W	443.2318	425.2212	426.2051	224.6065	3
10	1131.5629	1113.5524	1114.5363	564.2755	Q	257.1738	239.1632	240.1471	131.5699	2
11					K	147.1128	129.1022	130.0863	74.0604	1

#	b	b-NH3	b-H2O	b (2+)	Seq.	y	y-NH3	y-H2O	y (2+)	#
1	88.0399	71.0133	70.0293	44.5169	S					11
2	169.0872	152.0605	151.0765	85.0438	T	1189.6239	1172.6133	1171.5973	595.3119	10
3	288.1553	271.1286	270.1447	144.5780	V	1089.5760	1072.5493	1071.5654	545.2880	9
4	401.2400	384.2133	383.2294	201.1200	T	970.5071	953.4807	952.4965	485.7440	8
5	515.2830	498.2563	497.2724	258.1451	N	857.4224	840.4111	839.4118	429.2118	7
6	686.3301	669.3034	668.3195	293.6690	A	743.3794	726.3527	725.3688	382.1803	6
7	717.3665	700.3398	699.3559	359.1803	M	572.3264	555.2997	554.3158	286.6718	5
8	830.4446	813.4179	812.4340	415.7223	L	501.2900	484.2633	483.2794	251.1356	4
9	1014.5229	997.4963	996.5124	507.7620	W	443.2318	426.2051	425.2212	224.6065	3
10	1131.5629	1114.5363	1113.5524	564.2755	Q	257.1738	240.1471	239.1632	131.5699	2
11					K	147.1128	130.1022	129.1022	74.0604	1

FIG. 20B

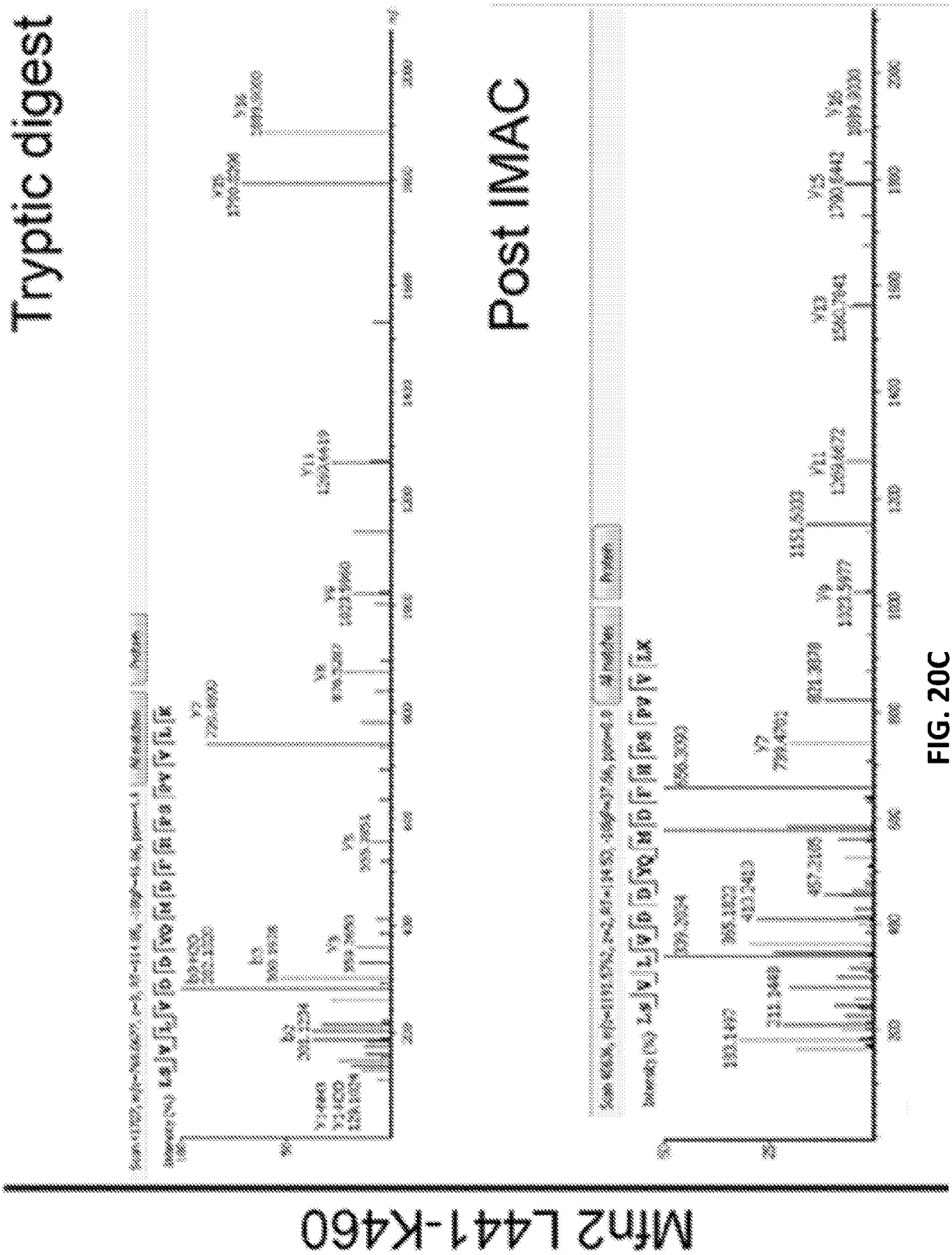

FIG. 20C

#	b	b-H2O	b-NH3	b (2+)	Seq	y	y-H2O	y-NH3	y (2+)	#
1	114.0913	96.0813	97.0649	57.5459	L					20
2	201.1234	183.1125	184.0969	101.0623	S	2189.0947	2171.0842	2172.0676	1095.0474	19
3	300.1919	282.1809	283.1653	150.5862	V	2102.0627	2084.0522	2085.0356	1051.5314	18
4	413.2760	395.2650	396.2494	207.1382	L	2002.9943	1984.9838	1985.9673	1001.9973	17
5	512.3448	494.3342	495.3178	256.6724	V	1889.9099	1871.8997	1872.8832	945.4551	16
6	627.3717	609.3611	610.3447	314.1859	D	1790.8796	1772.8313	1773.8148	895.9209	15
7	742.3987	724.3881	725.3717	371.6993	D	1675.8148	1657.8043	1658.7878	838.4182	14
8	905.4628	887.4514	888.4350	453.2310	Y	1560.7878	1542.7773	1543.7609	780.8901	13
9	1033.5235	1015.5099	1016.4935	517.2603	Q	1397.7245	1379.7140	1380.6975	699.3622	12
10	1164.5610	1146.5505	1147.5341	582.7805	M	1269.6619	1251.6585	1252.6390	635.3330	11
11	1279.5880	1261.5775	1262.5610	640.2940	D	1138.6218	1120.6150	1121.5985	569.8127	10
12	1426.6564	1408.6459	1409.6294	713.8282	F	1023.5948	1005.5880	1006.5715	512.2993	9
13	1563.7153	1545.7048	1546.6884	782.3577	H	876.5267	858.5196	859.5032	438.7651	8
14	1660.7681	1642.7576	1643.7411	830.8842	P	739.4689	721.4606	722.4442	370.2356	7
15	1747.8000	1729.7896	1730.7731	874.4003	S	642.4165	624.4079	625.3915	321.7092	6
16	1844.8529	1826.8424	1827.8259	922.9265	P	555.3851	537.3759	538.3594	278.1932	5
17	1943.9213	1925.9108	1926.8943	972.4608	V	458.3337	440.3231	441.3067	229.6668	4
18	2042.9897	2024.9792	2025.9628	1021.9949	V	359.2653	341.2547	342.2383	180.1326	3
19	2156.0737	2138.0632	2139.0466	1078.5369	L	260.1968	242.1863	243.1698	130.5984	2
20					K	147.1130	129.1024	130.0860	74.0564	1

FIG. 20D

#	b	b-H2O	b-NH3	b (2+)	Seq	y	y-H2O	y-NH3	y (2+)	#
1	114.0913	96.0813	97.0649	57.5459	L					20
2	201.0902	183.0797	184.0632	141.0451	S(+79.97)	2269.0610	2251.0505	2252.0339	1135.0305	19
3	300.1586	282.1481	283.1317	190.5793	V	2102.0627	2084.0522	2085.0356	1051.5314	18
4	413.2427	395.2321	396.2157	247.1214	L	2002.9943	1984.9838	1985.9673	1001.9973	17
5	512.3111	494.3006	495.2841	296.6555	V	1889.9099	1871.8997	1872.8832	945.4640	16
6	707.3383	689.3275	690.3111	354.1693	D	1790.8442	1772.8313	1773.8148	895.9209	15
7	822.3652	804.3544	805.3380	411.6825	D	1675.8172	1657.8043	1658.7878	838.4074	14
8	985.4293	967.4178	968.4014	493.2142	Y	1560.7901	1542.7773	1543.7609	780.8939	13
9	1113.4899	1095.4764	1096.4600	557.2435	Q	1397.7245	1379.7140	1380.6975	699.3622	12
10	1244.5273	1226.5168	1227.5004	622.7637	M	1269.6672	1251.6585	1252.6390	635.3330	11
11	1359.5543	1341.5438	1342.5273	680.2772	D	1138.6270	1120.6150	1121.5985	569.8127	10
12	1506.6227	1488.6122	1489.5957	753.8113	F	1023.5997	1005.5880	1006.5715	512.2993	9
13	1643.6816	1625.6711	1626.6547	822.3408	H	876.5300	858.5196	859.5032	438.7651	8
14	1740.7344	1722.7239	1723.7074	870.8672	P	739.4701	721.4606	722.4442	370.2356	7
15	1827.7665	1809.7560	1810.7396	914.3832	S	642.4165	624.4079	625.3915	321.7092	6
16	1924.8192	1906.8087	1907.7922	962.9096	P	555.3871	537.3759	538.3594	278.1932	5
17	2023.8876	2005.8771	2006.8606	1012.4438	V	458.3337	440.3231	441.3067	229.6668	4
18	2122.9561	2104.9456	2105.9292	1061.9783	V	359.2653	341.2547	342.2383	180.1326	3
19	2236.0400	2218.0295	2219.0129	1118.5200	L	260.1967	242.1863	243.1698	130.5984	2
20					K	147.1128	129.1022	130.0858	74.0564	1

FIG. 20E

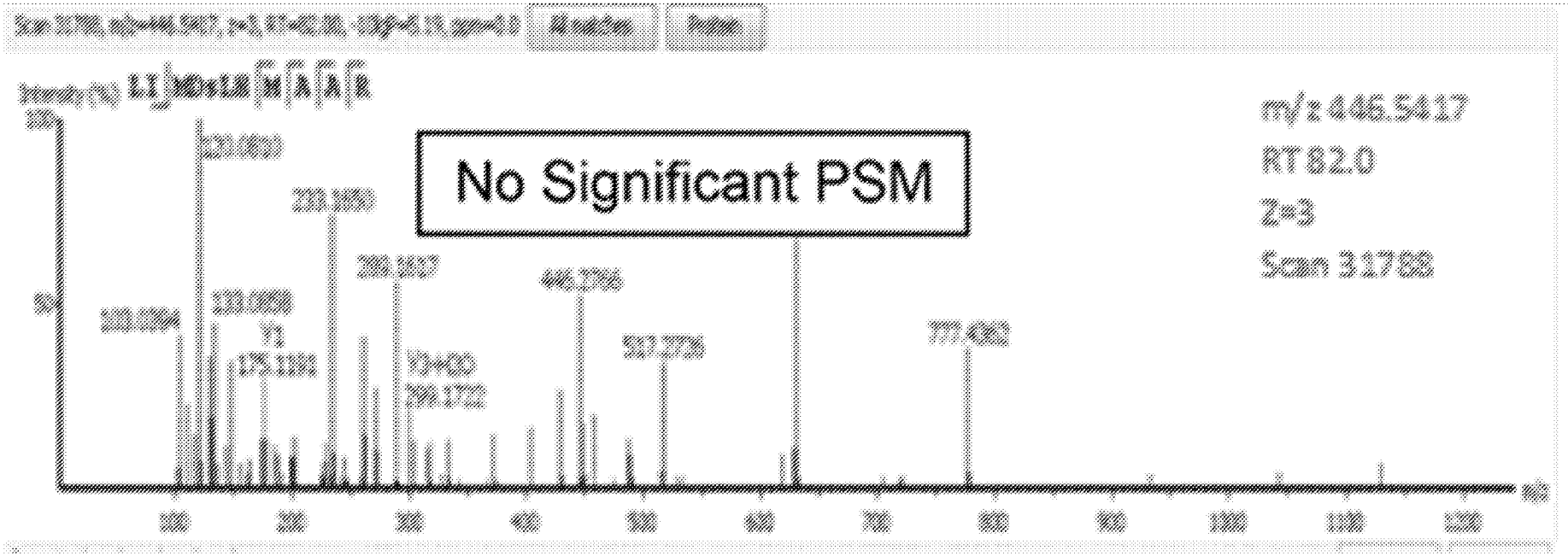

FIG. 21A

FIG. 21B

#	b	b+CO	b+NH3	Seq	y	y+CO	y+NH3
1	114.0913	86.0913	97.0640	L			
2	227.1753	255.1654	210.1469	I	1224.5265	1252.5160	1207.4995
3	358.2164	340.2059	341.1805	H	1111.4424	1083.4319	1094.4154
4	473.2434	455.2329	456.2164	D	980.4013	952.3904	963.3749
5	660.3417	632.3311	643.3147	S(+79.97)	865.3753	837.3644	848.3480
6	763.3858	735.3752	736.3588	L	678.3796	650.3660	661.3496
7	880.3947	872.3741	873.3577	H	585.2925	567.2820	568.2656
8	1321.4752	1003.4146	1004.3982	M	448.2166	430.2231	431.2067
9	1392.4823	1074.4538	1075.4353	A	317.1751	299.1722	300.1662
10	1163.4994	1145.4889	1146.4724	A	246.1581	228.1551	229.1390
11				R	175.1191	157.1084	158.0919

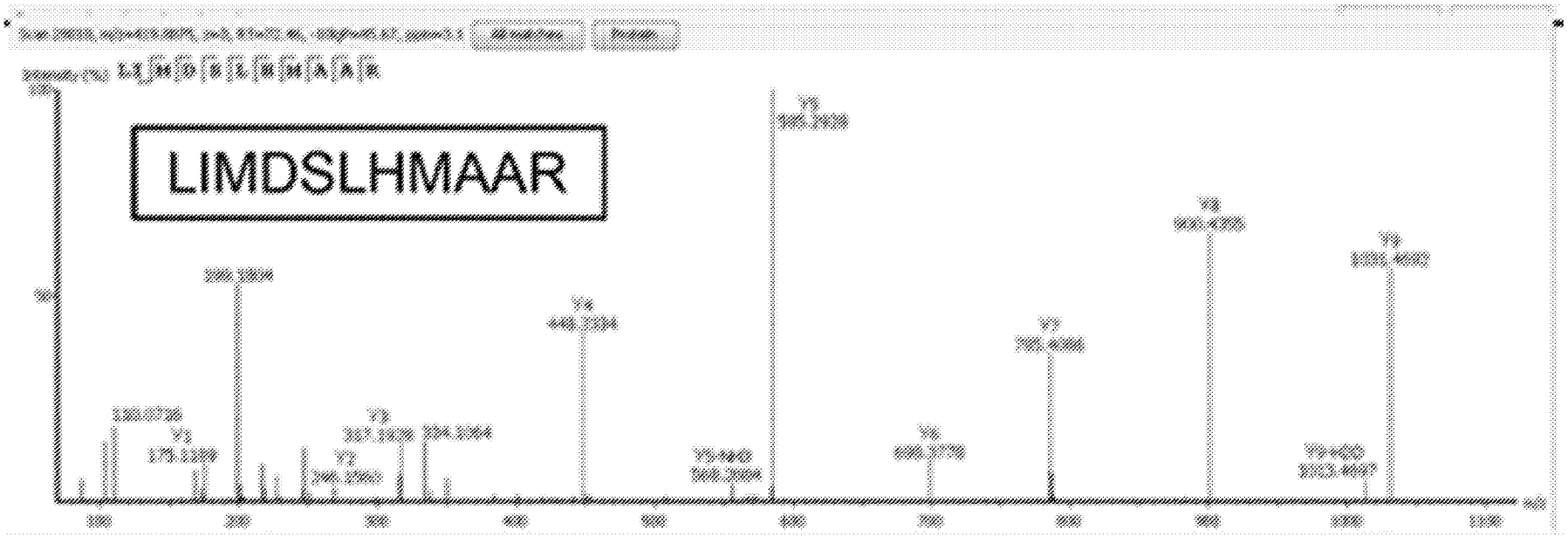

FIG. 21C

FIG. 21D

#	b	b-H2O	b-NH3	Seq.	y	y-H2O	y-NH3	#
1	114.0919	96.0813	97.0649	L				11
2	227.1754	209.1654	210.1489	I	1234.5341	1216.5243	1217.5078	10
3	358.2164	340.2059	341.1895	M	1121.4506	1103.4402	1104.4237	9
4	473.2434	455.2328	456.2164	D	990.4092	972.3996	973.3832	8
5	640.2417	622.2311	623.2147	S(+79.97)	875.3826	857.3727	858.3563	7
6	753.3258	735.3152	736.2988	L	708.3843	690.3743	691.3579	6
7	890.3847	872.3741	873.3577	H	595.3004	577.2903	578.2739	5
8	1021.4252	1003.4146	1004.3982	M	458.2419	440.2320	441.2149	4
9	1092.4623	1074.4518	1075.4353	A	327.3019	309.1909	310.1744	3
10	1163.4994	1145.4889	1146.4724	A	256.1639	238.1401	239.1373	2
11				R(+10.01)	185.1273	167.1035	168.1002	1

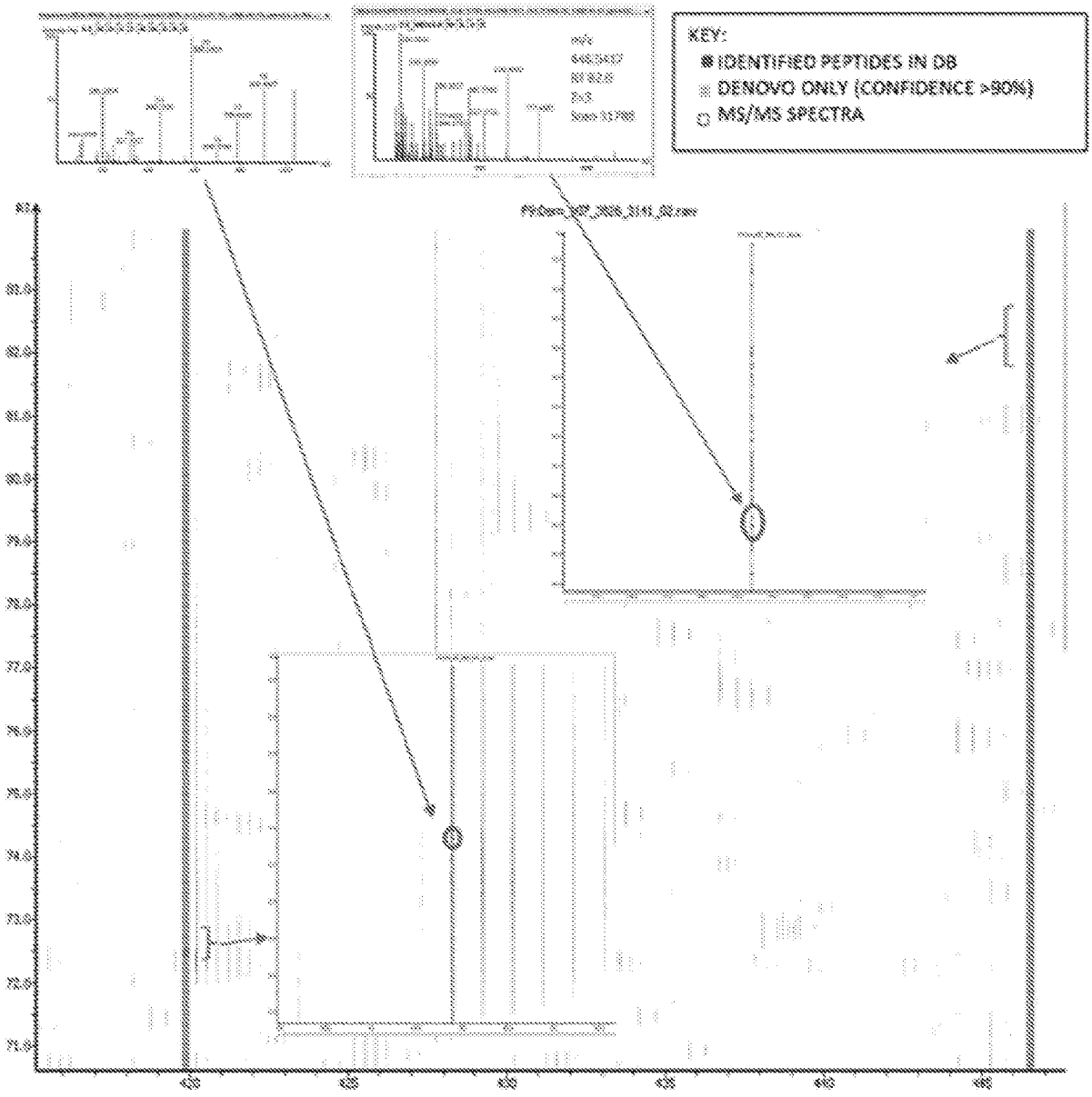
KEY:
IDENTIFIED PEPTIDES IN DB
DENOVO ONLY (CONFIDENCE >80%)
MS/MS SPECTRA

FIG. 21E

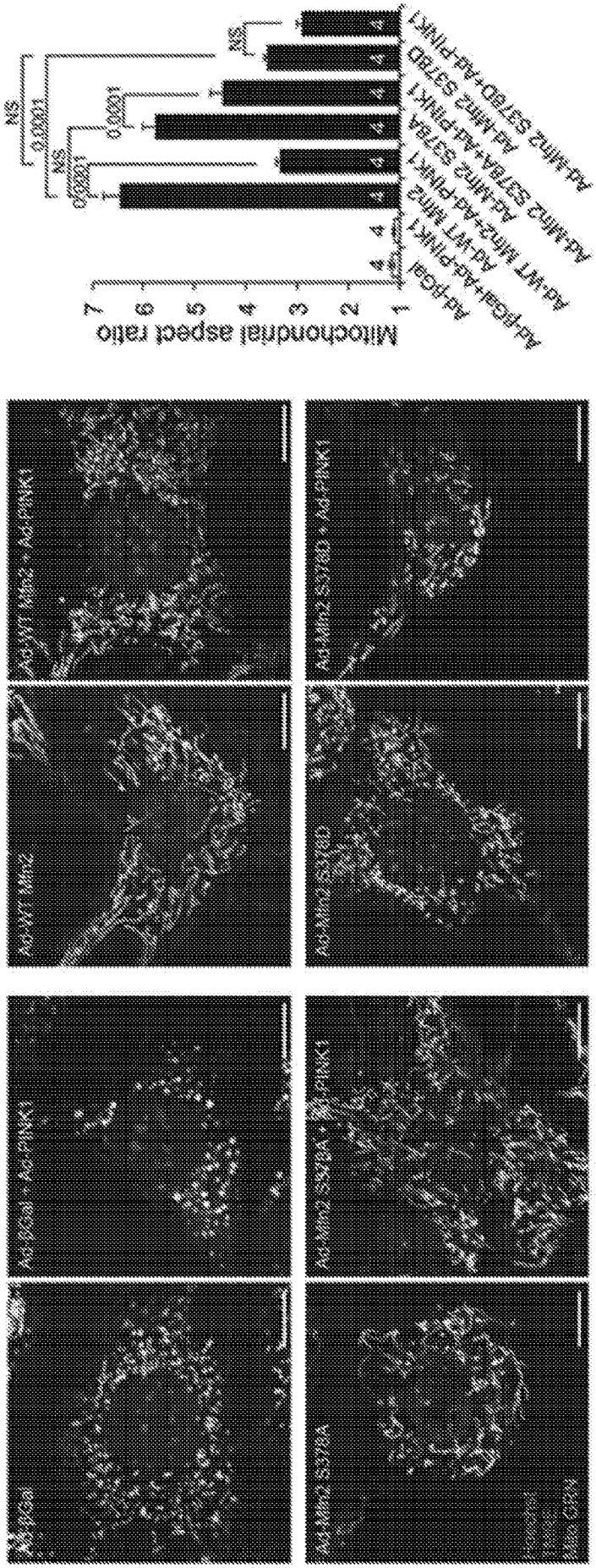
Mitochondrial aspect ratio
Ad-PGam
Ad-PGam+Ad-PINK1
Ad-WT Mtm2
Ad-WT Mtm2+Ad-PINK1
Ad-Mtm2 S373A
Ad-Mtm2 S373A+Ad-PINK1
Ad-Mtm2 S373D
Ad-Mtm2 S373D+Ad-PINK1
NS
0.0001
NS
0.0001
Ad-PGam + Ad-PINK1
Ad-WT Mtm2 + Ad-PINK1
Ad-Mtm2 S373D
Ad-Mtm2 S373D + Ad-PINK1
Ad-PGam
Ad-Mtm2 S373A
Ad-Mtm2 S373A + Ad-PINK1
Ad-WT Mtm2

FIG. 22

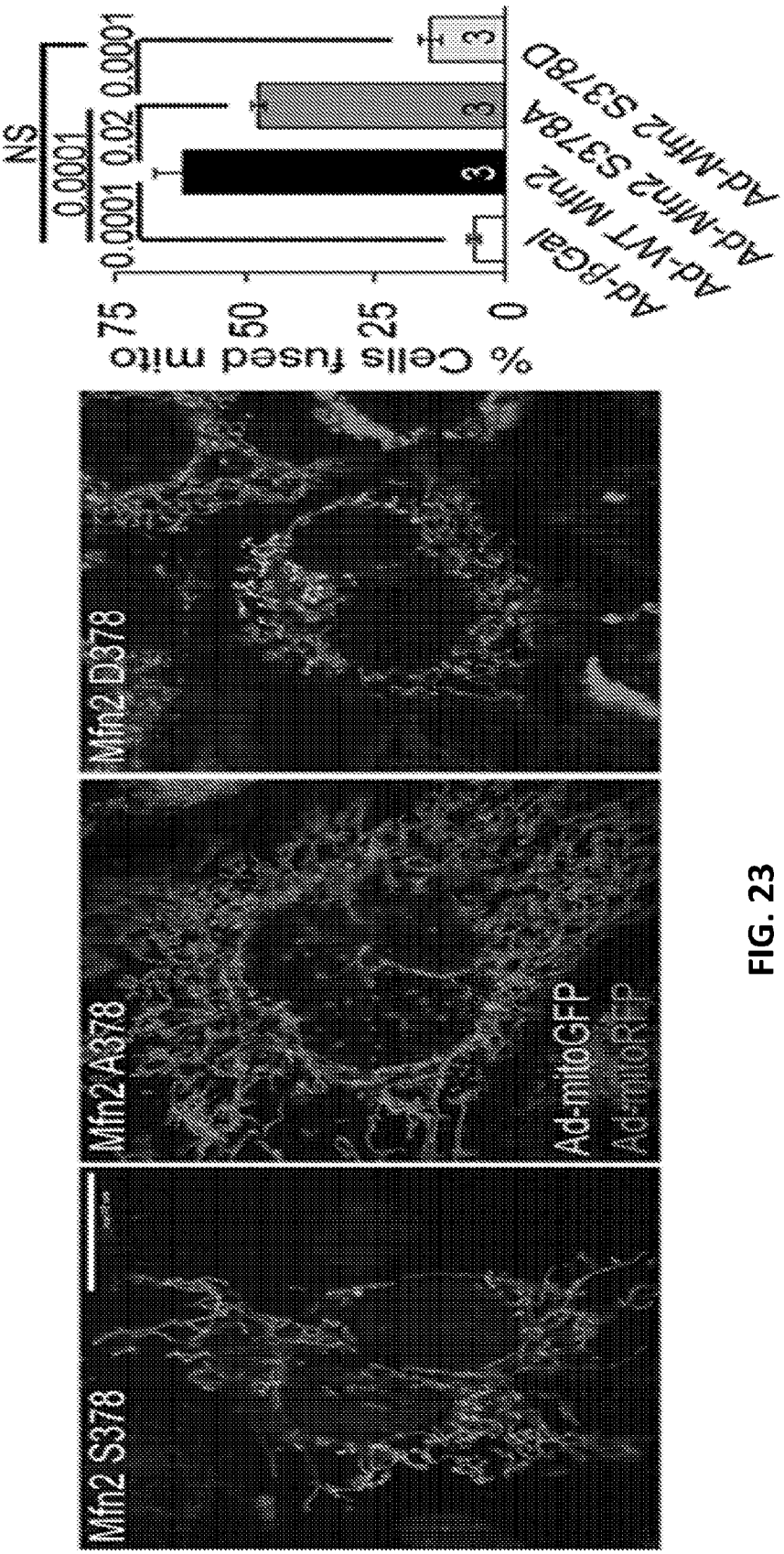
Mfn2 S378
Mfn2 A378
Ad-mitoGFP
Ad-mitoRFP
Mfn2 D378
% Cells fused mito
75
50
25
0
Ad-βGal
Ad-WT Mfn2
Ad-Mfn2 S378A
Ad-Mfn2 S378D
NS
0.0001
0.0001
0.02
0.0001
3
3
3

FIG. 23

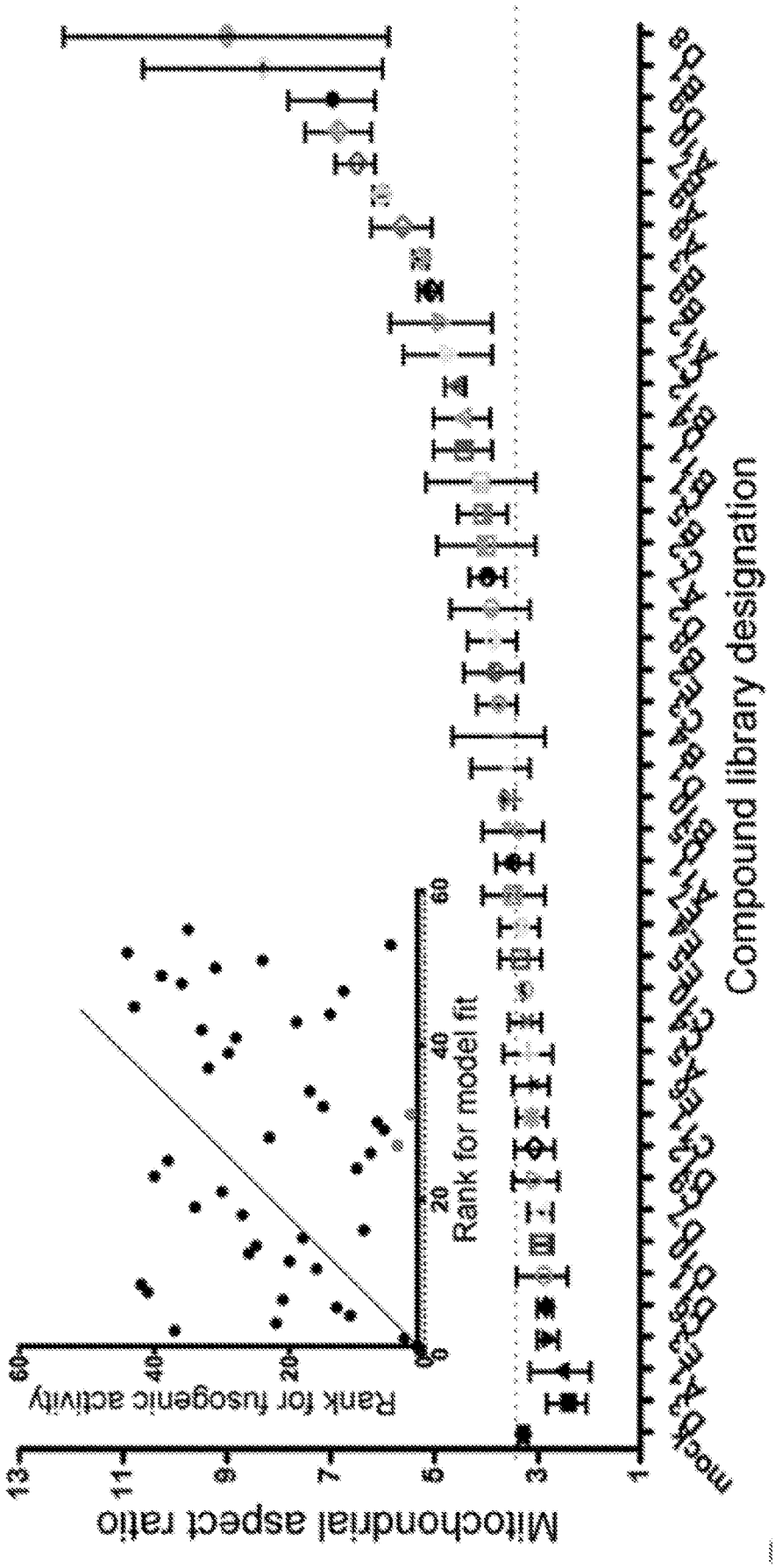
Mitochondrial aspect ratio
13
11
9
7
5
3
1
Rank for fusogenic activity
60
40
20
0
Rank for model fit
60
40
20
0
Compound library designation

FIG. 24A

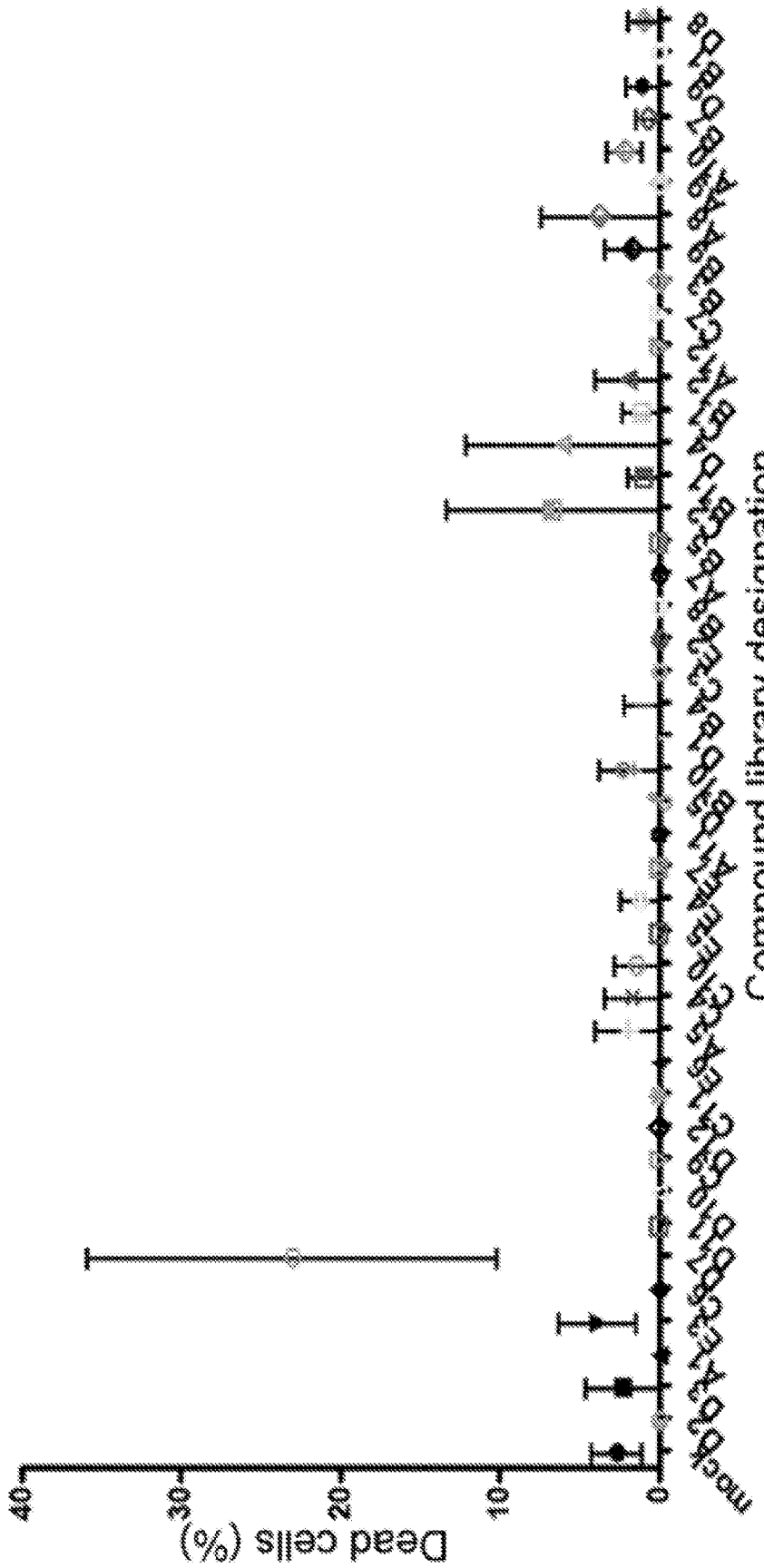

FIG. 24B

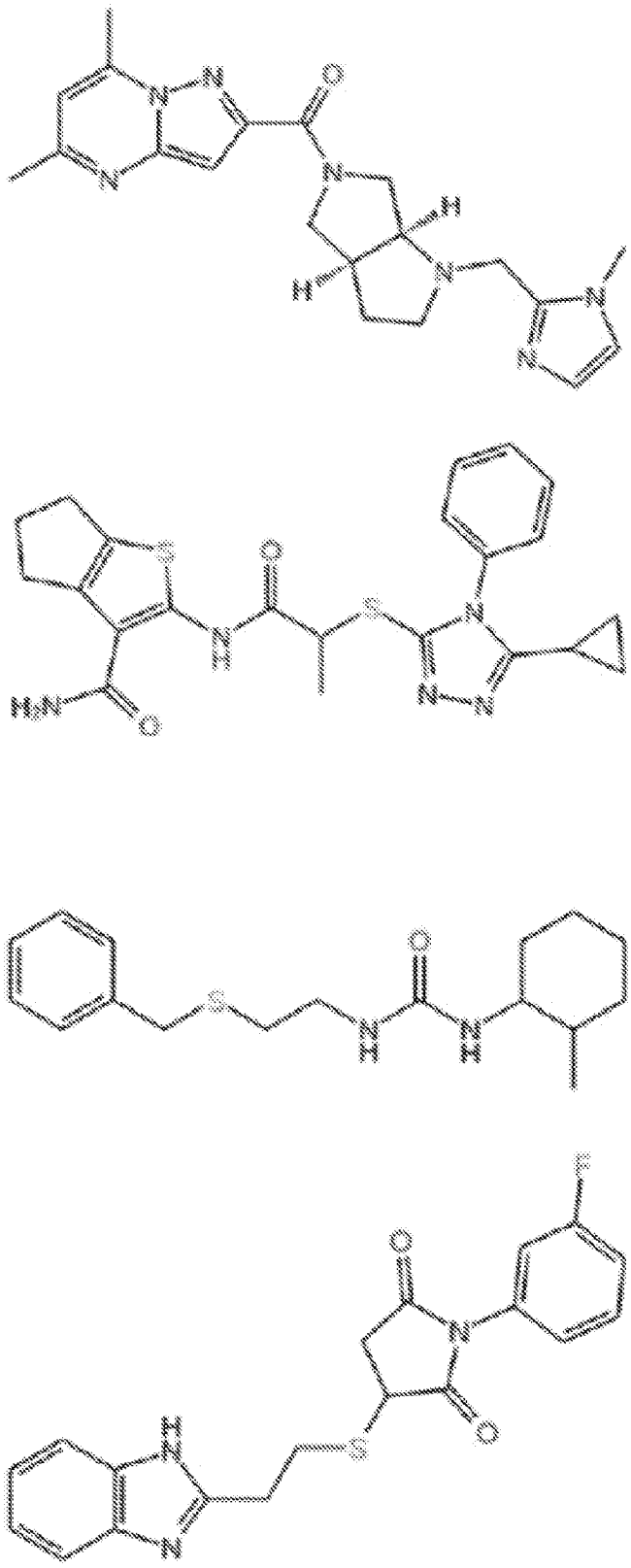

FIG. 25A

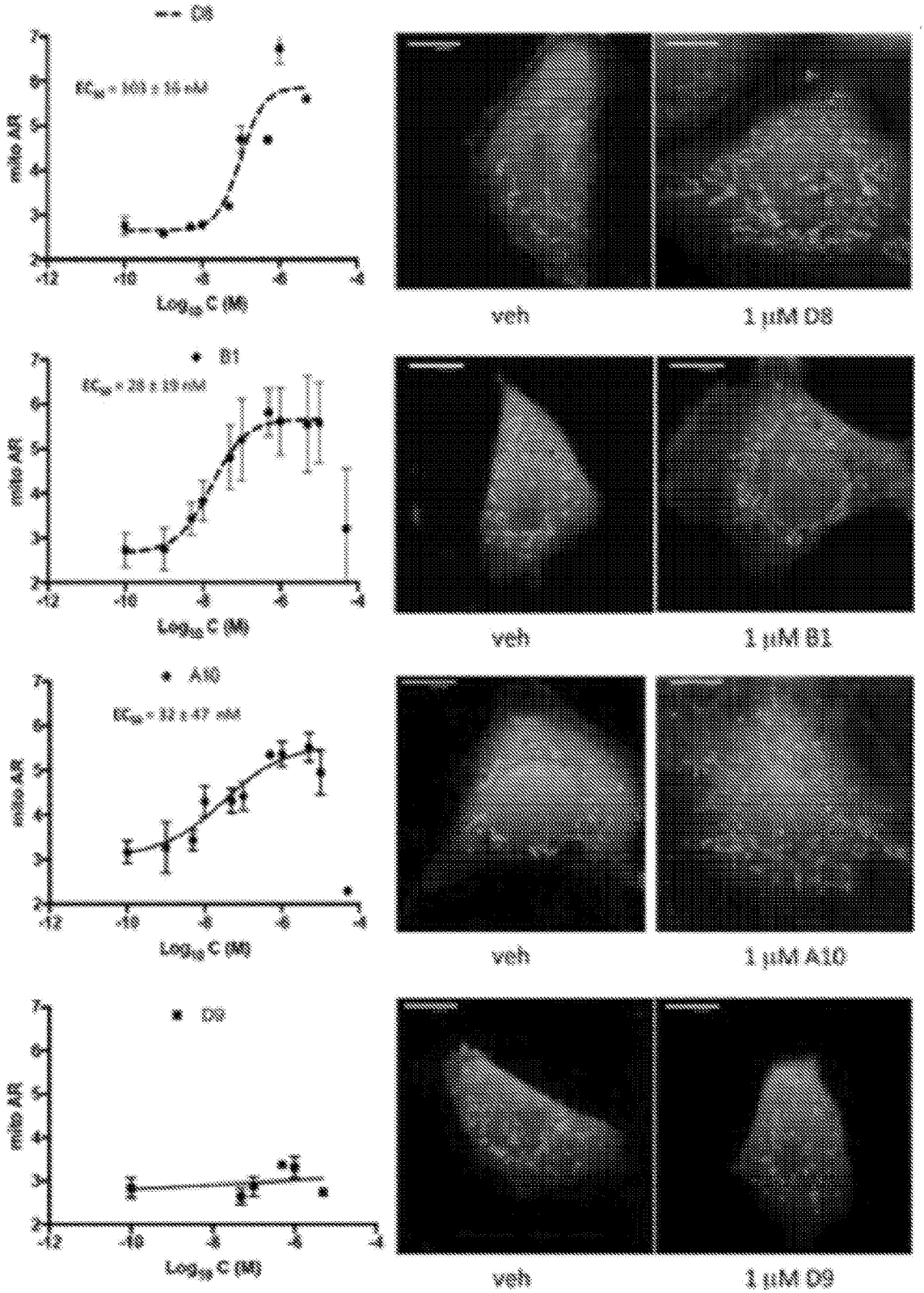

FIG. 25B

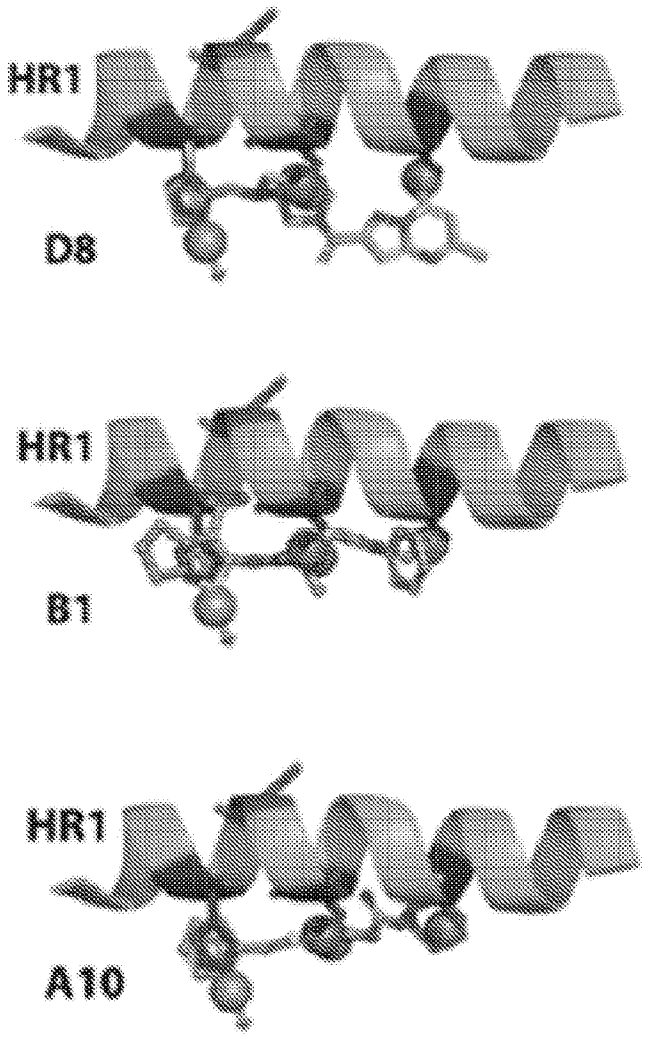

FIG. 25C

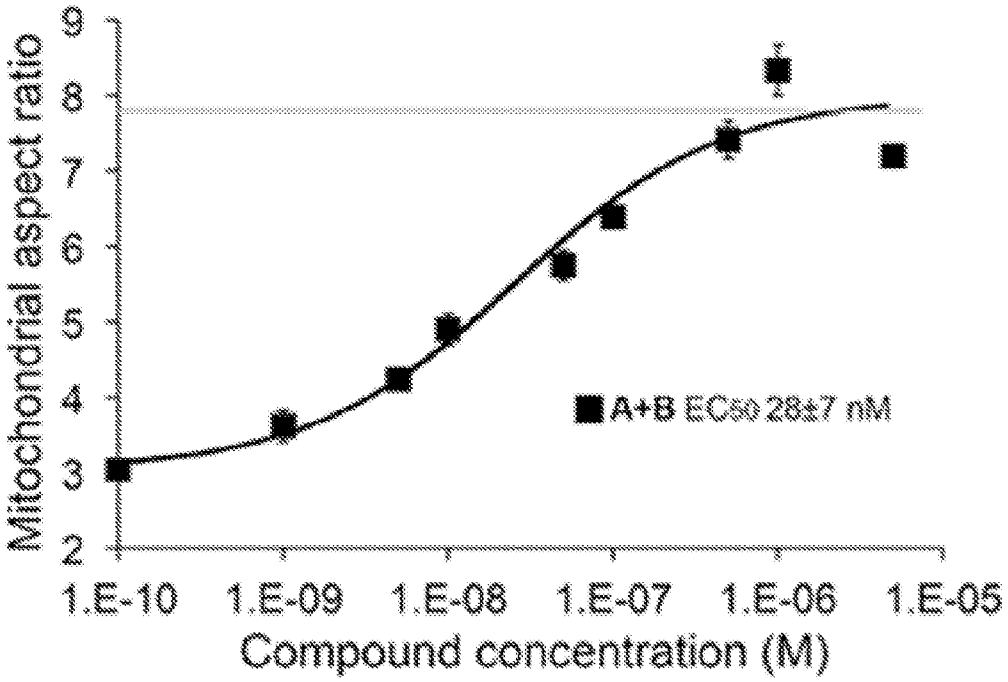

FIG. 26A

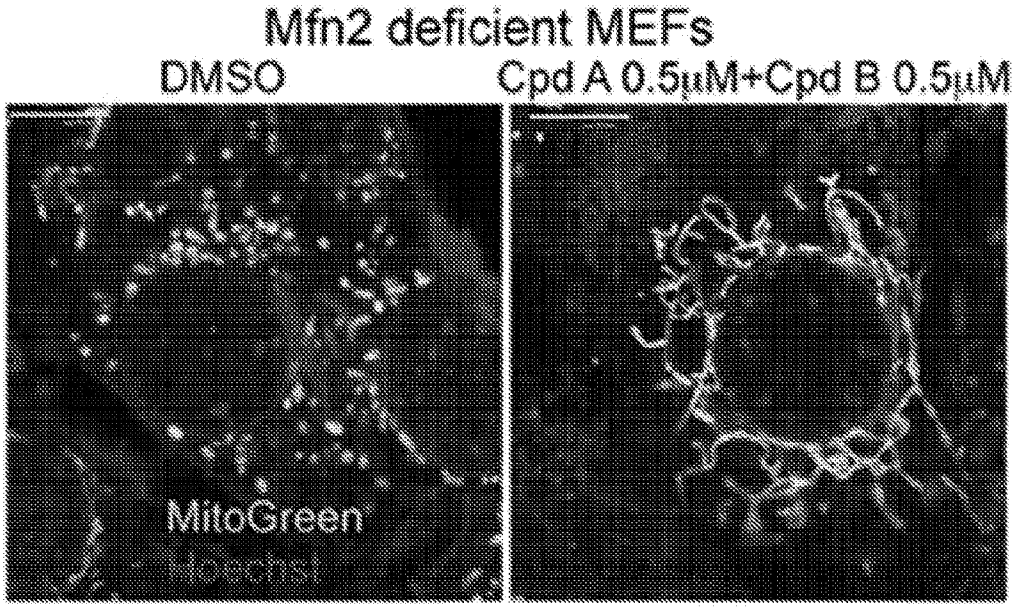

FIG. 26B

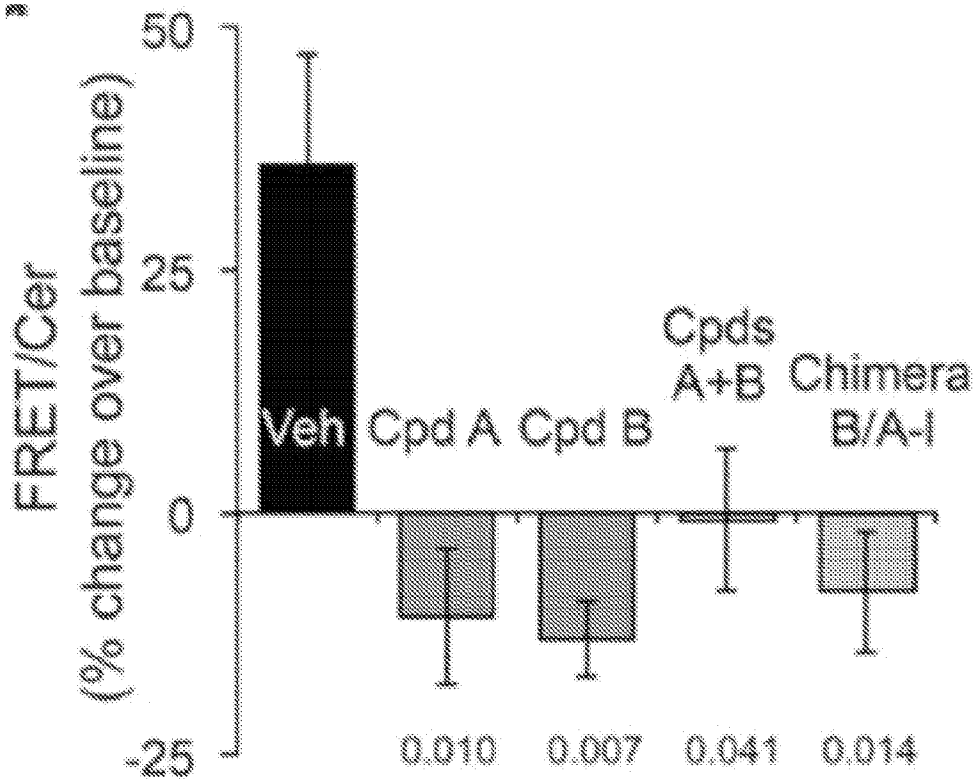

FIG. 26C

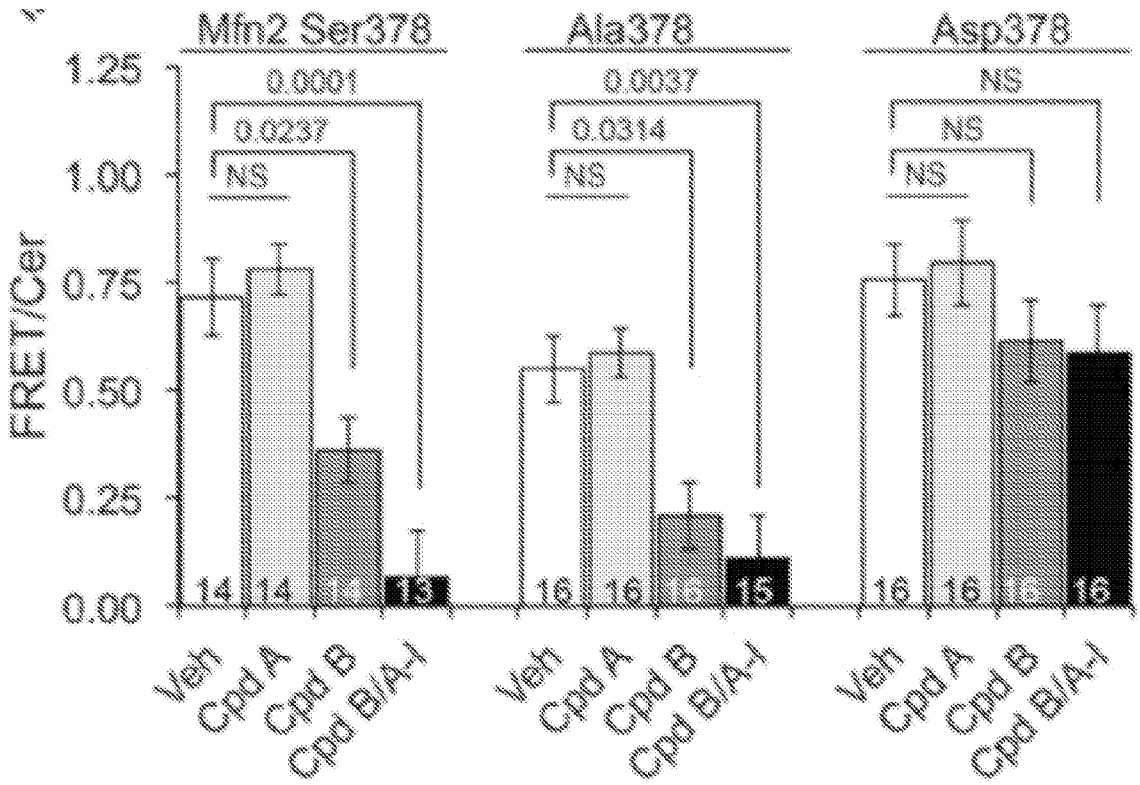

FIG. 26D

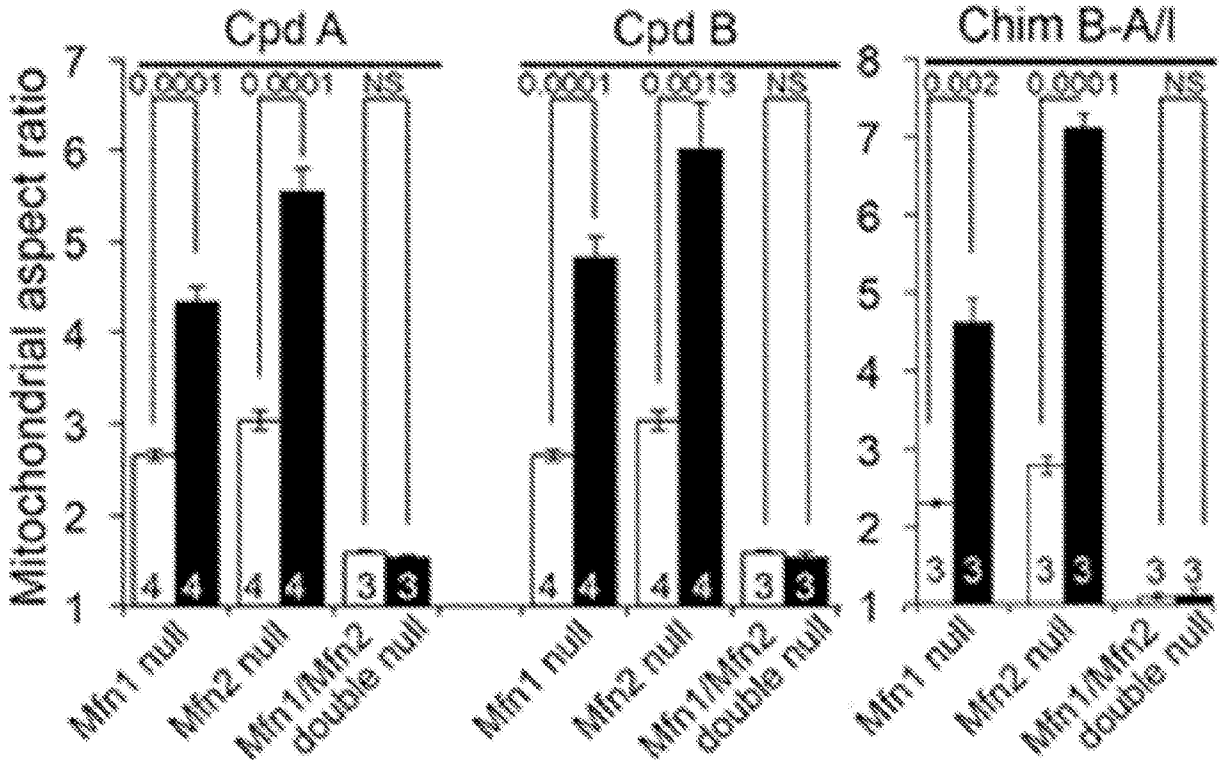

FIG. 27A

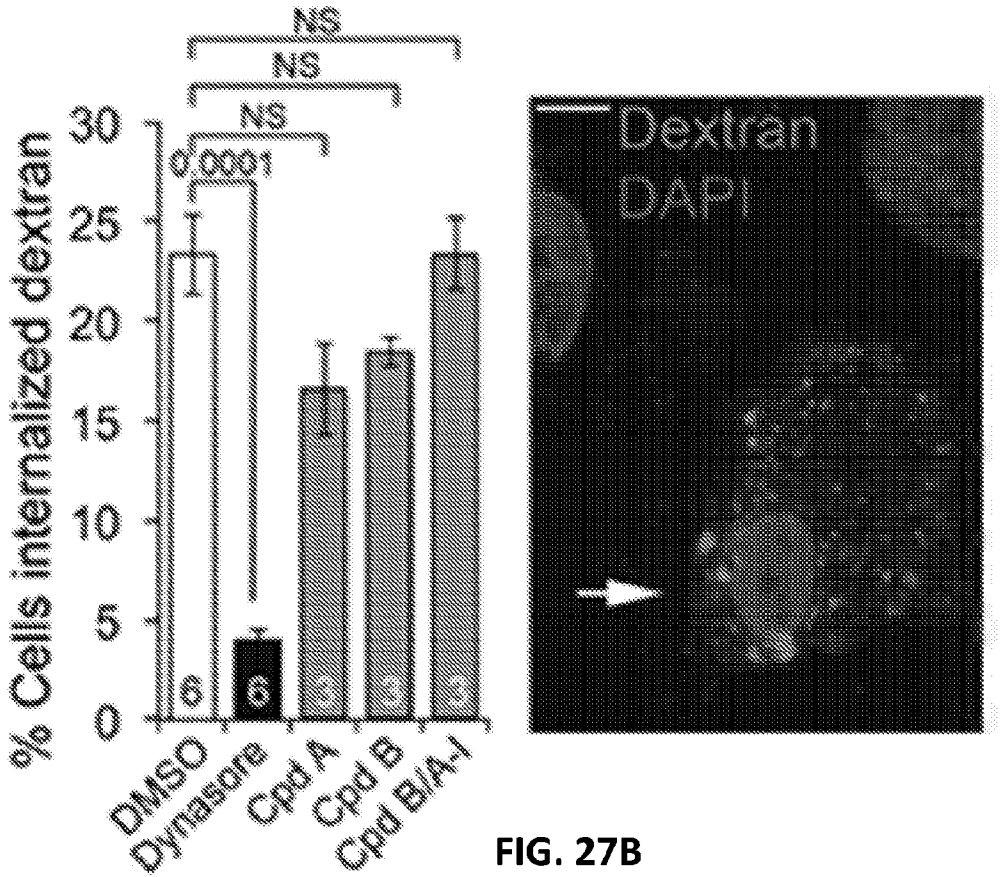

FIG. 27B

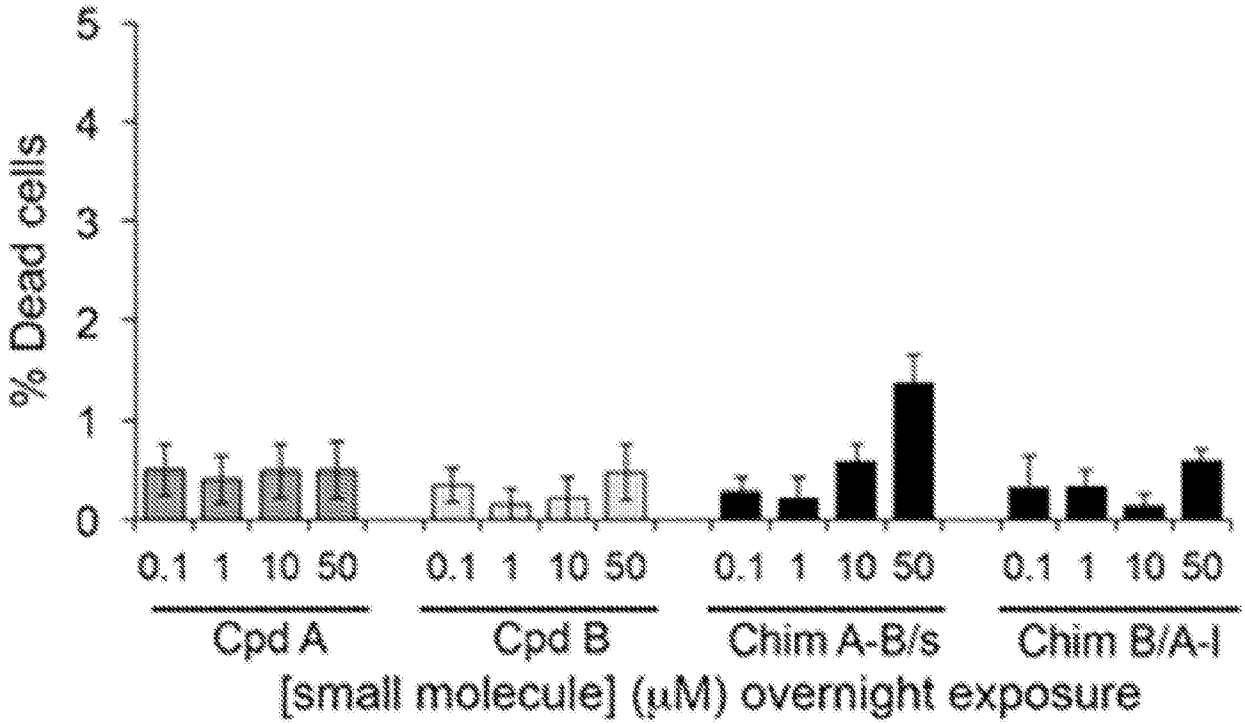

FIG. 27C

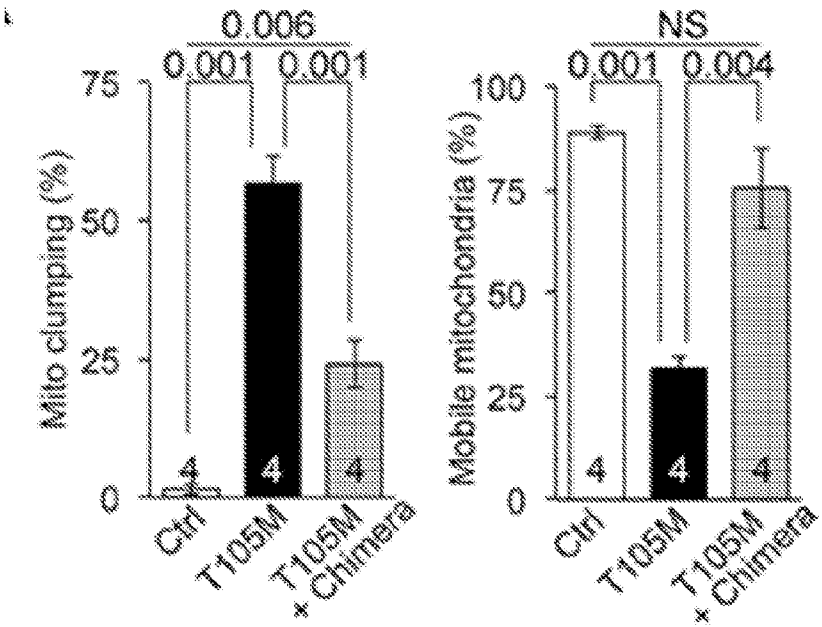

FIG. 28A

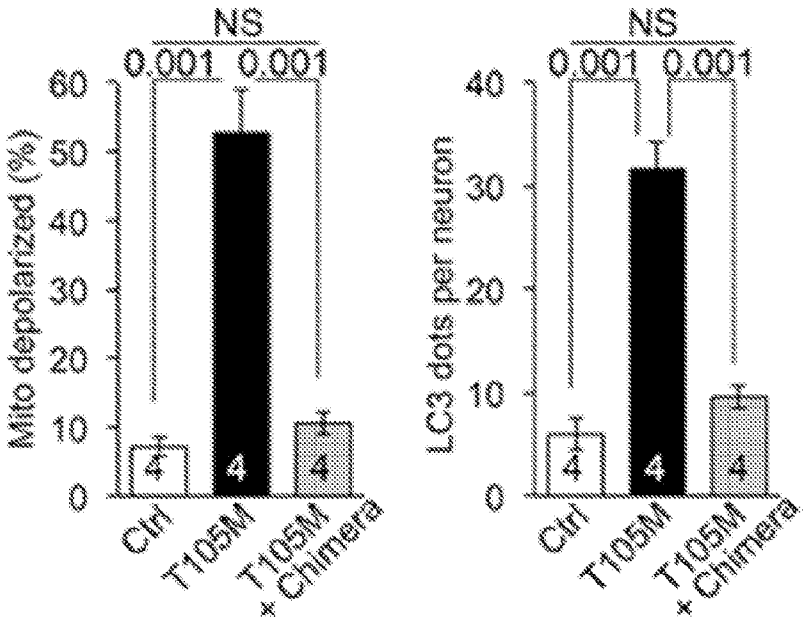

FIG. 28B

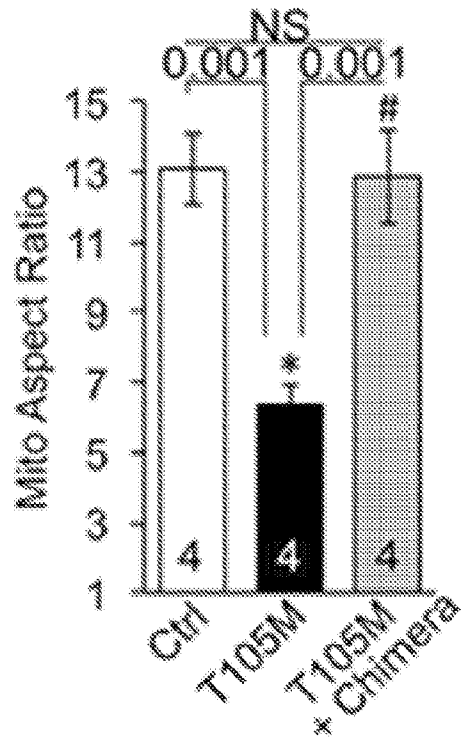

FIG. 28C

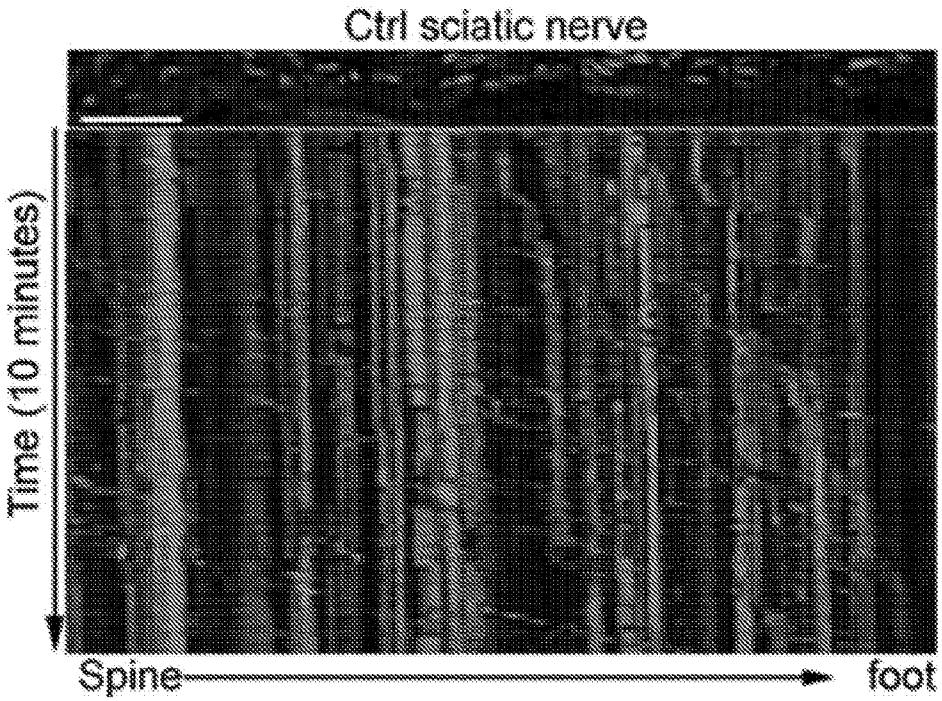

FIG. 28D

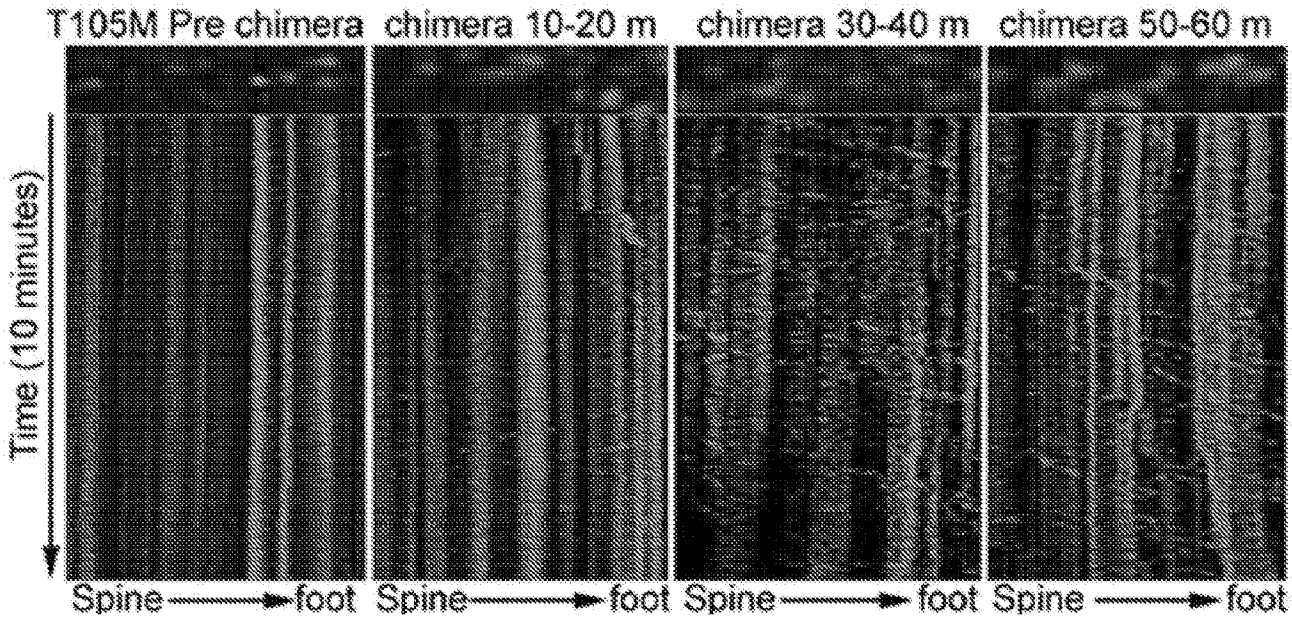

FIG. 28E

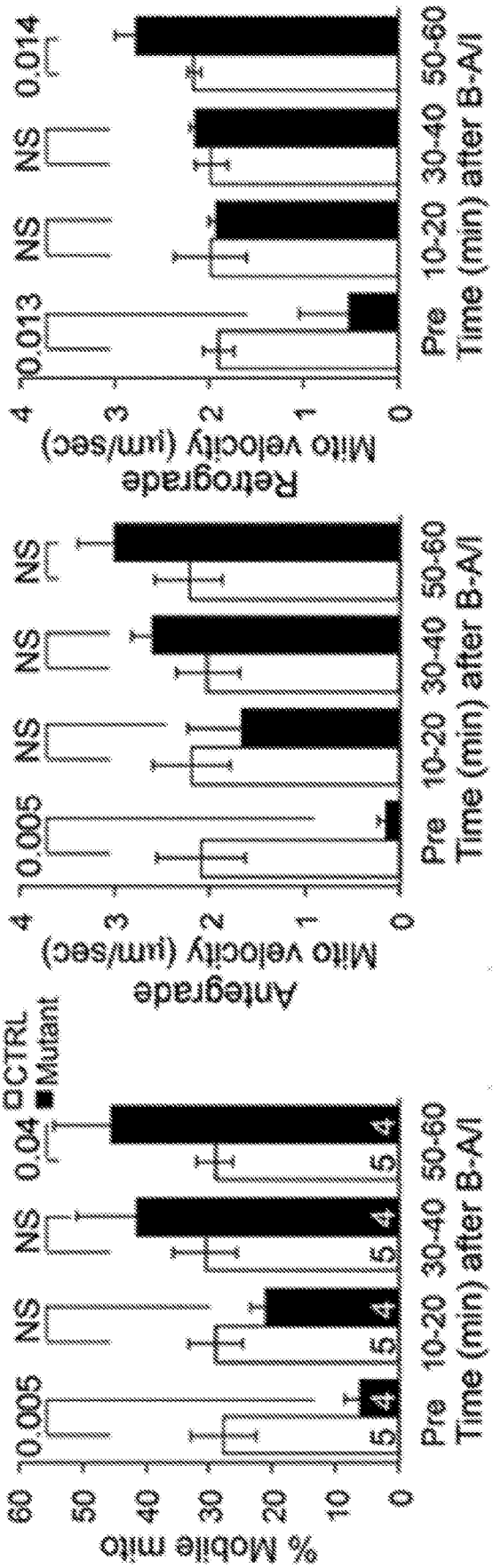
% Mobile mito
60
50
40
30
20
10
0
0.005
NS
NS
0.04
5
4
5
4
5
4
5
4
CTRL
Mutant
Pre
10-20
30-40
50-60
Time (min) after B-AI
Anterograde
Mito velocity (μm/sec)
4
3
2
1
0
0.005
NS
NS
NS
Pre
10-20
30-40
50-60
Time (min) after B-AI
Retrograde
Mito velocity (μm/sec)
4
3
2
1
0
0.013
NS
NS
0.014
Pre
10-20
30-40
50-60
Time (min) after B-AI

FIG. 28F

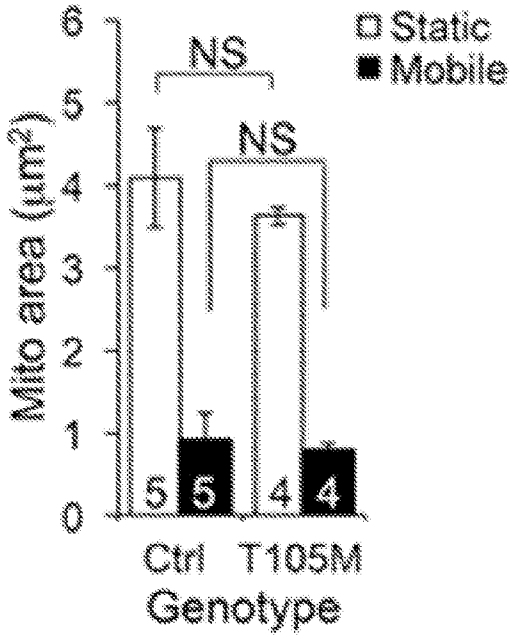
Static
Mobile
NS
NS
Mito area (μm²)
0
1
2
3
4
5
6
5
6
4
4
Ctrl
T105M
Genotype

FIG. 28G

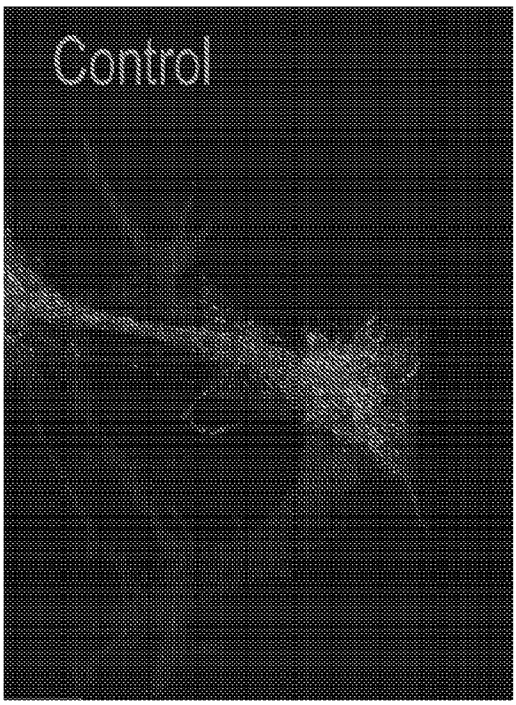

FIG. 29A

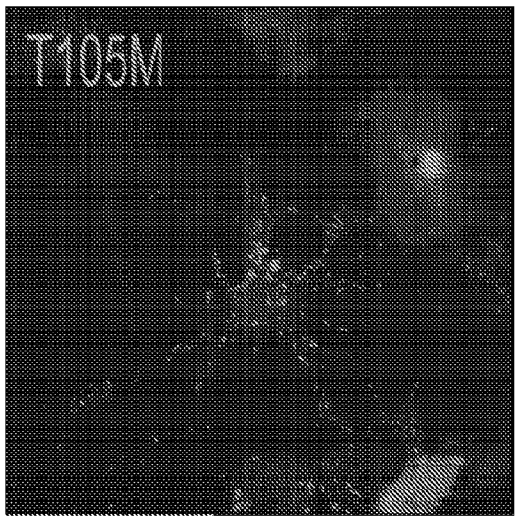

FIG. 29B

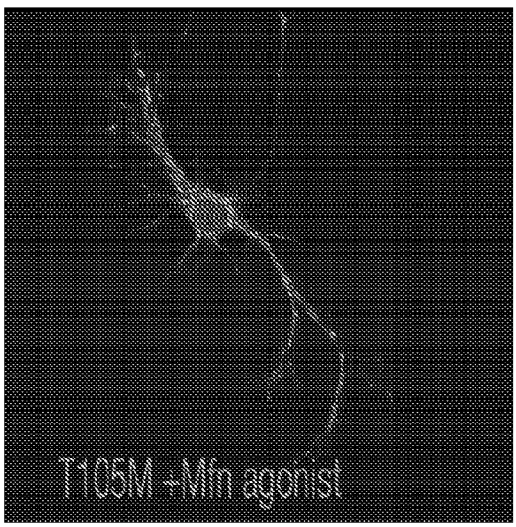

FIG. 29C

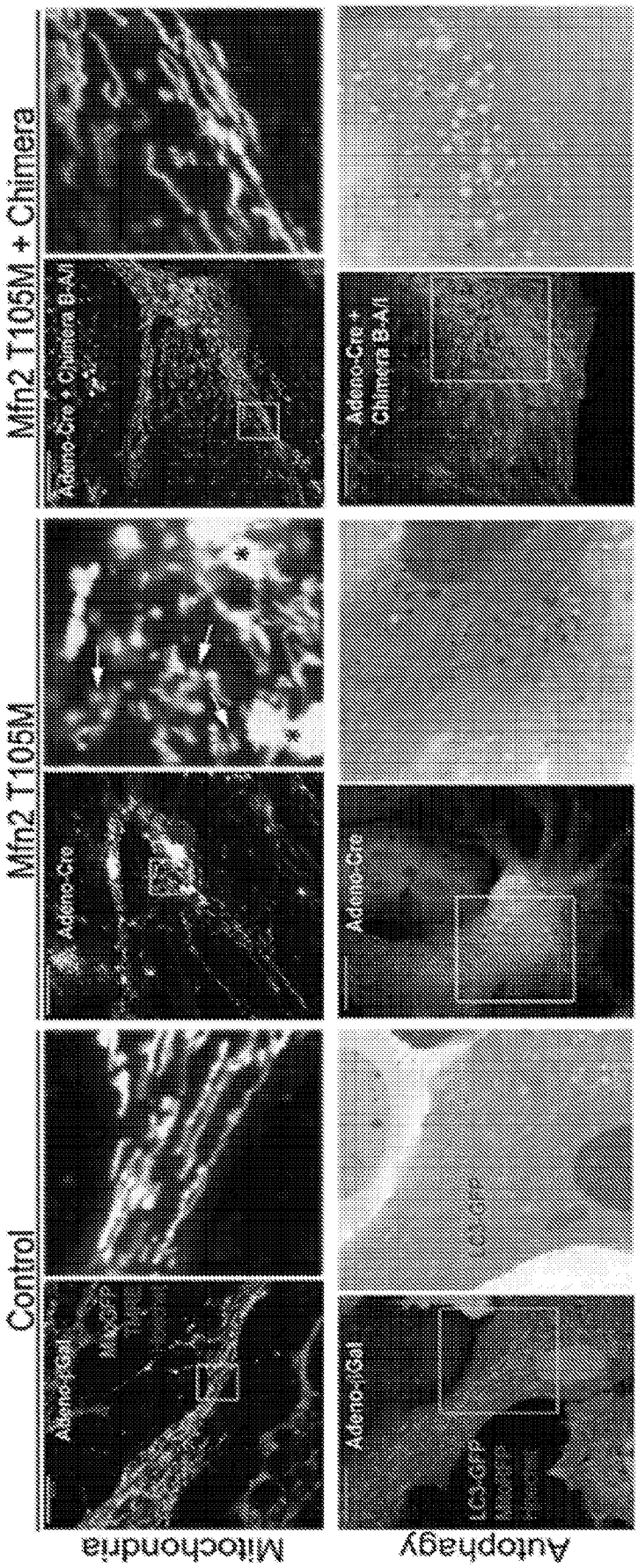
Control
Mfn2 T105M
Mfn2 T105M + Chimera
Mitochondria
Autophagy
Adeno-iCre
Adeno-Cre
Adeno-Cre + Chimera B-A/I
LC3-GFP

FIG. 30

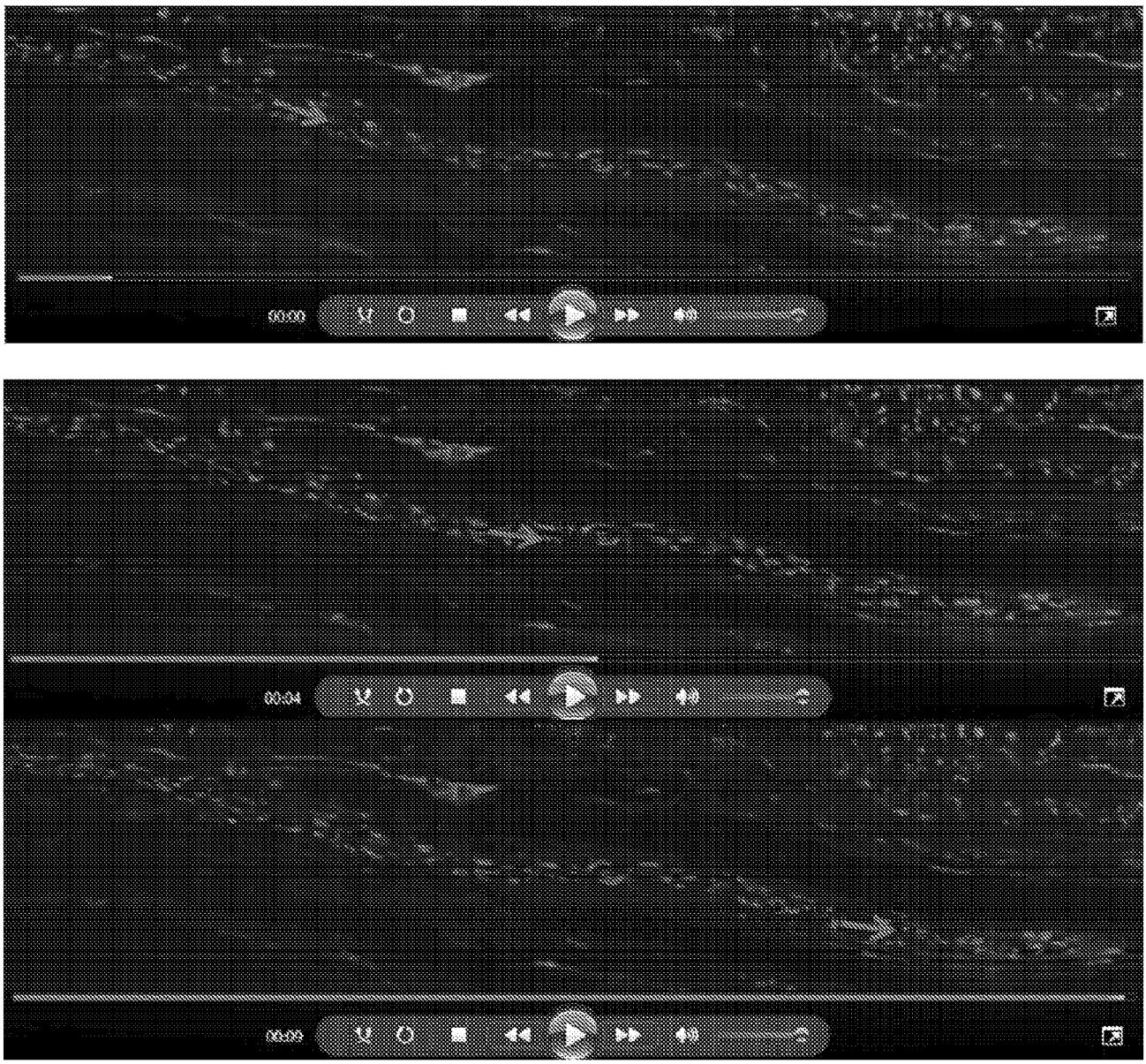

FIG. 31

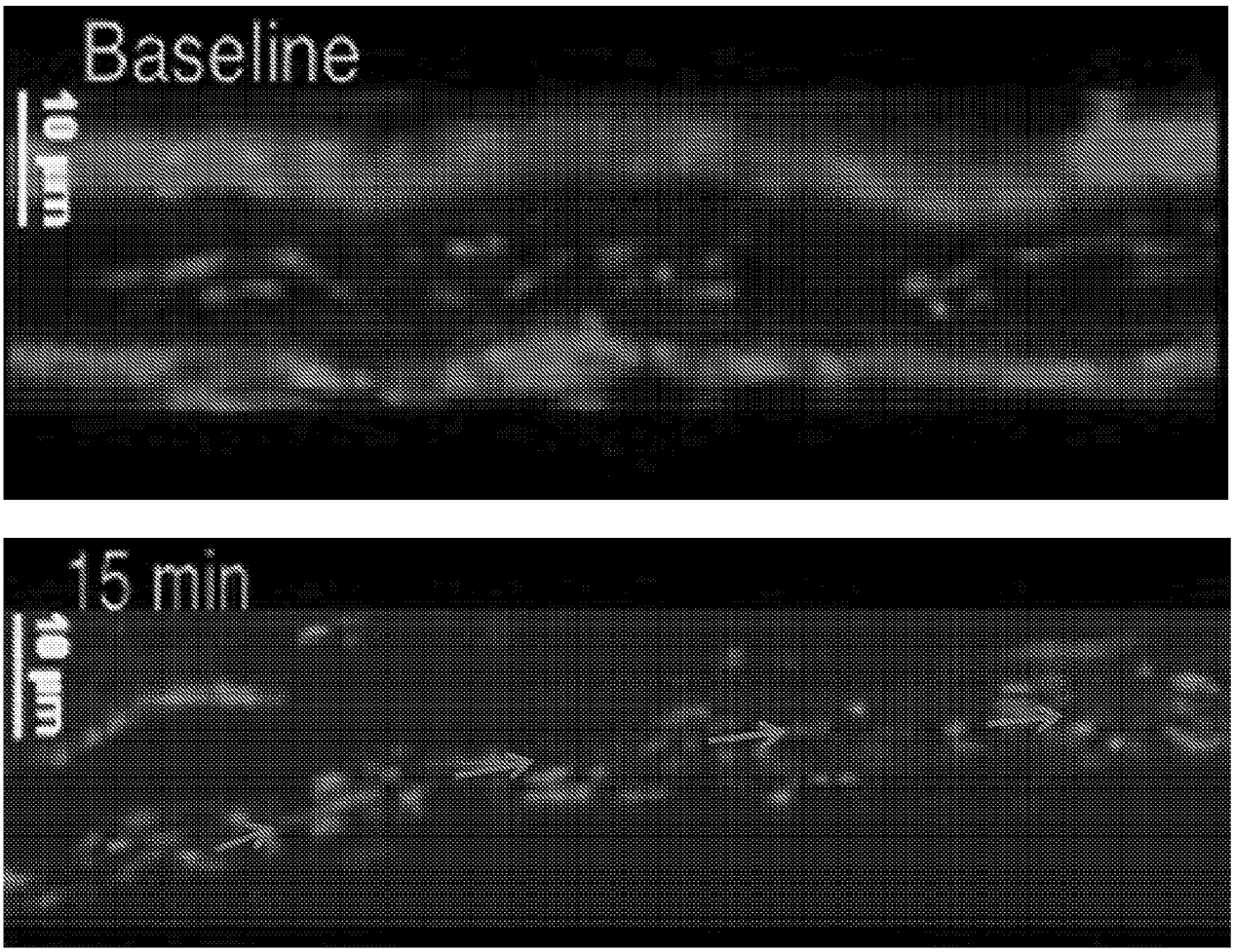

FIG. 32A

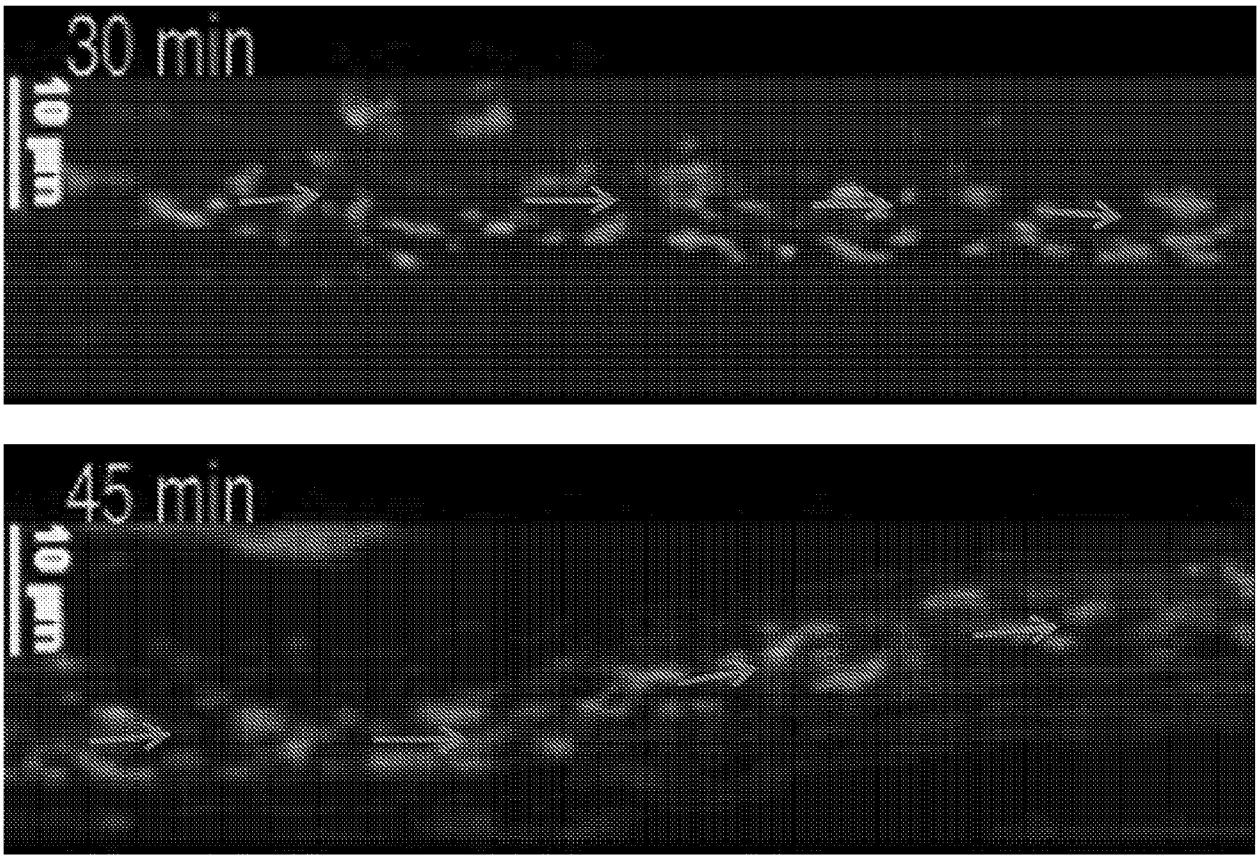

FIG. 32B

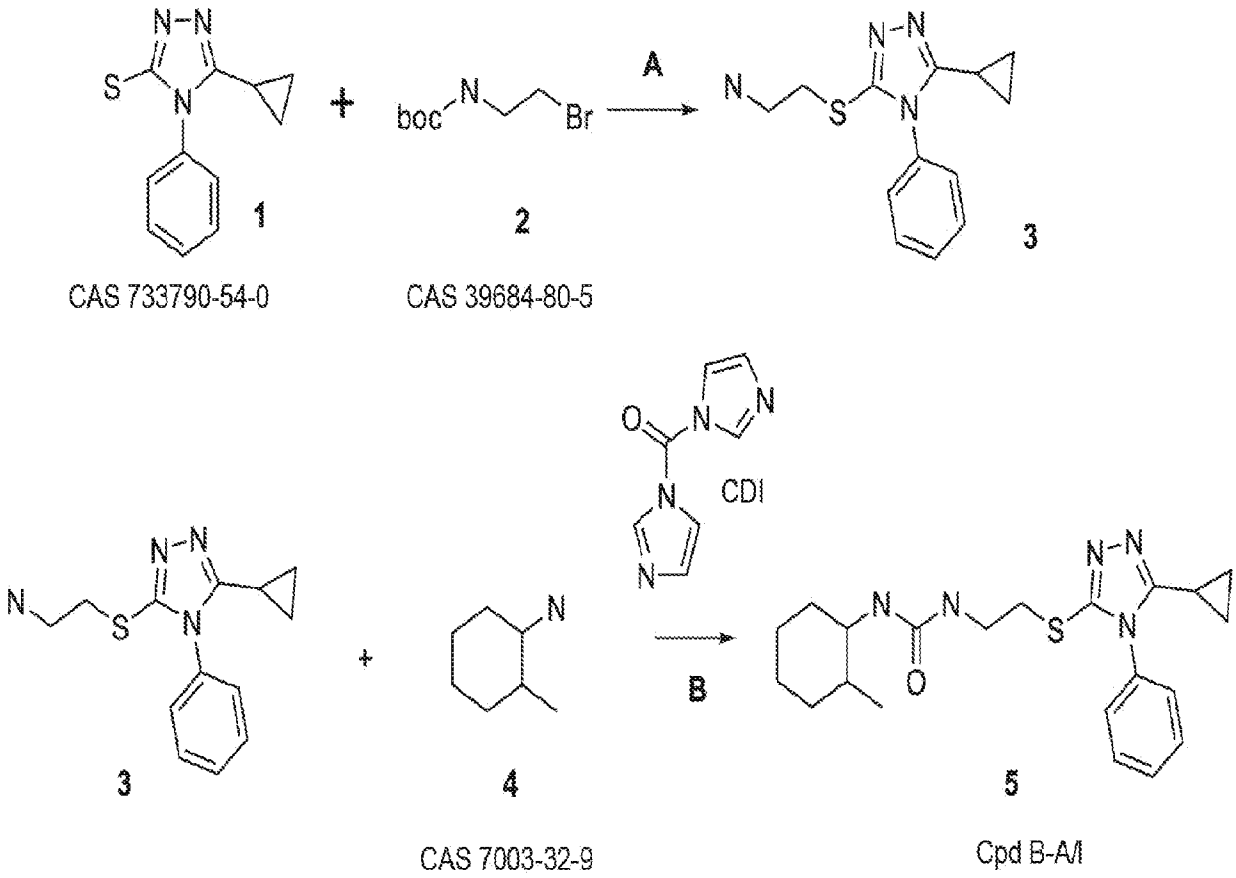
A
1
2
3
CAS 733790-54-0
CAS 39684-80-5
CDI
B
3
4
5
CAS 7003-32-9
Cpd B-A/I

FIG. 33

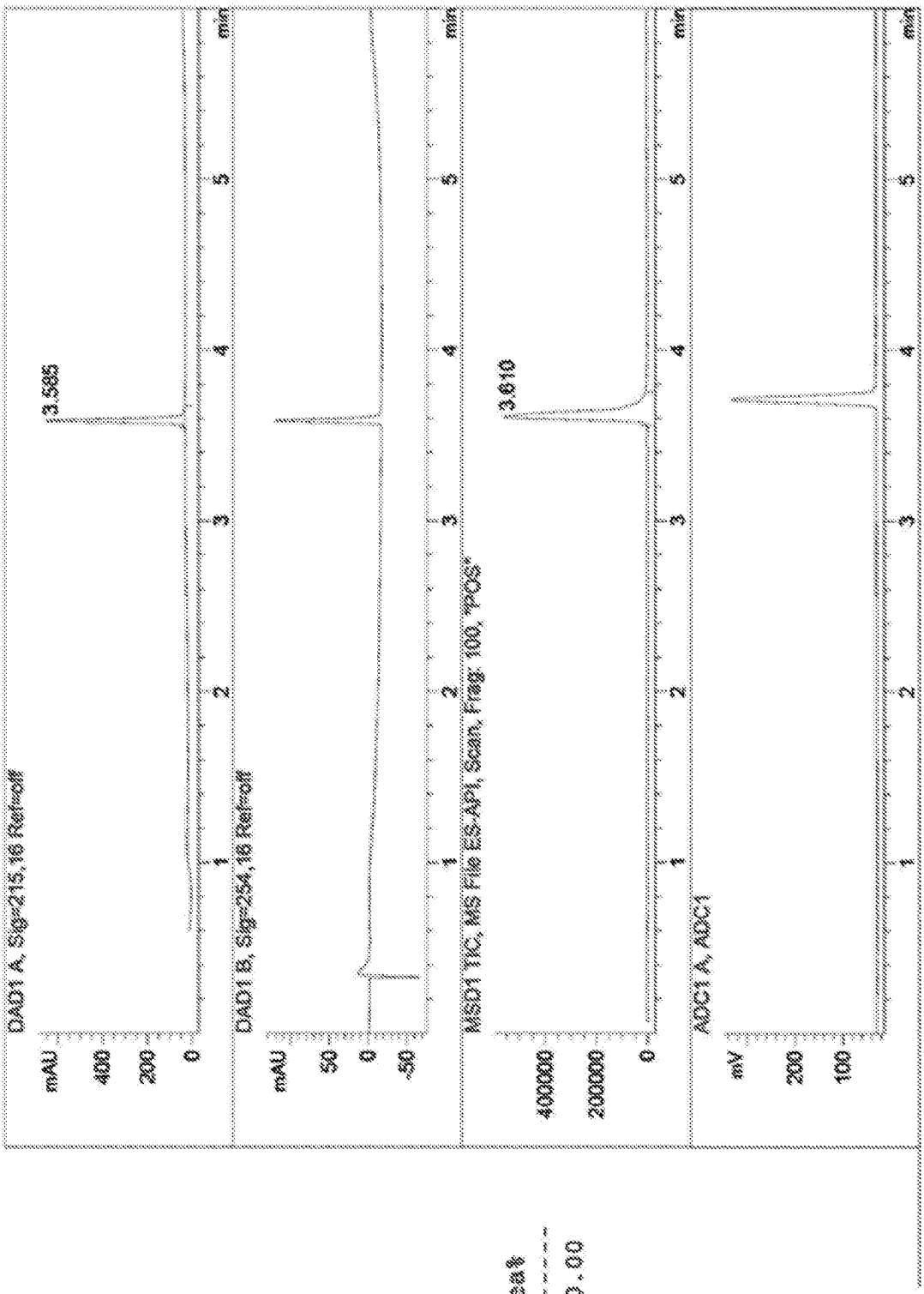

#	Time	Area%
1	3.585	100.00

FIG. 34A

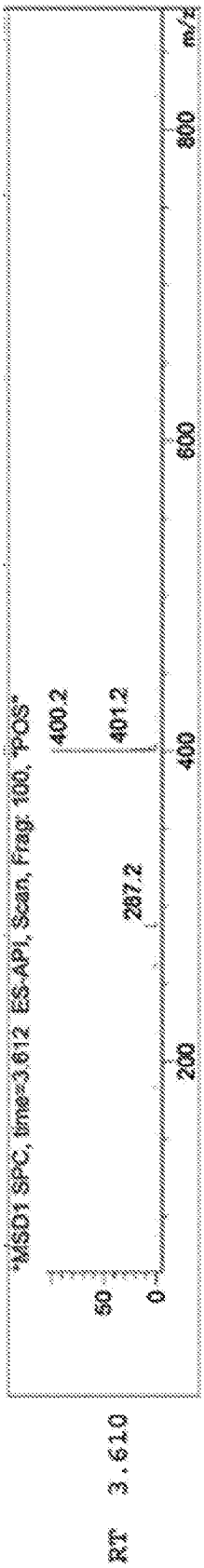
RT 3.610
"MSD1 SPC, time=3.612 ES-API, Scan, Frag: 100, "POS"
400.2
401.2
287.2
m/z
800
600
400
200
60
0

FIG. 34B

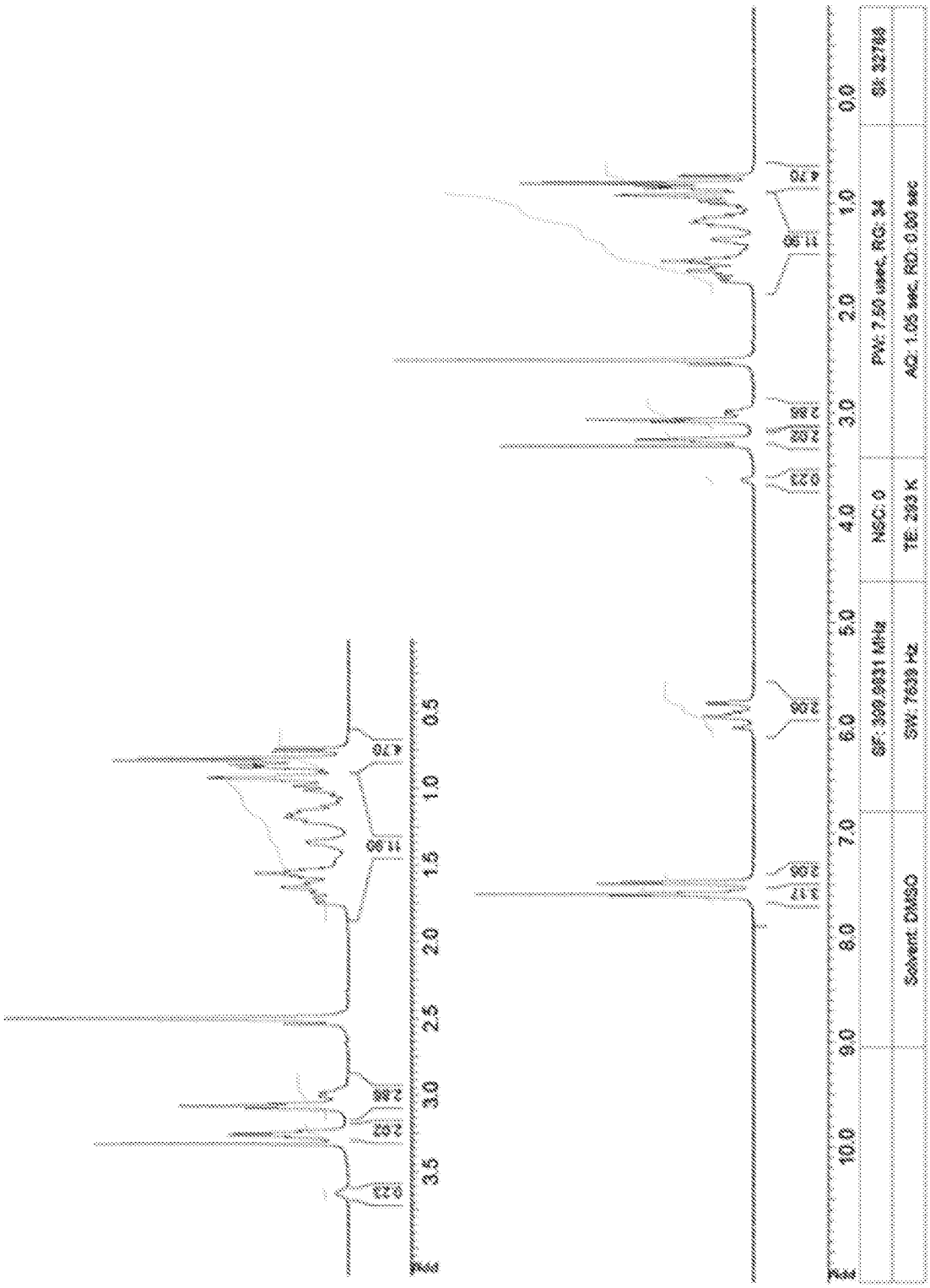
Solvent: DMSO
SW: 7639 Hz
SF: 300.2031 MHz
NSC: 0
TE: 293 K
PW: 7.50 usec, RG: 34
AQ: 1.05 sec, RD: 0.00 sec
SI: 32768

FIG. 35A

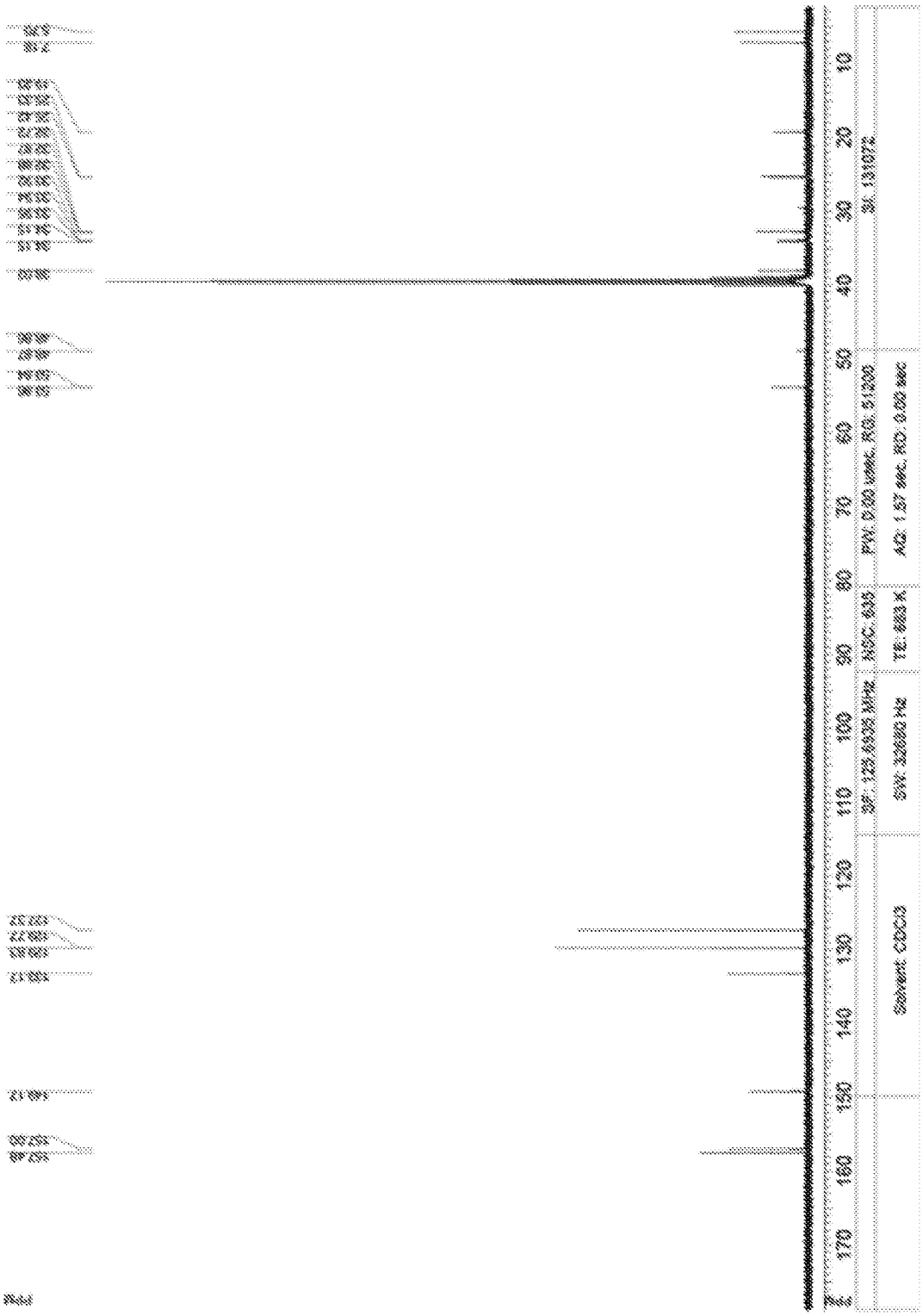
Solvent: CDCl3
SW: 32680 Hz
SF: 125.6936 MHz
NSC: 635
TE: 323 K
PW: 9.00 usec, RG: 512.00
AQ: 1.57 sec, RD: 0.00 sec
SI: 131072

FIG. 35B

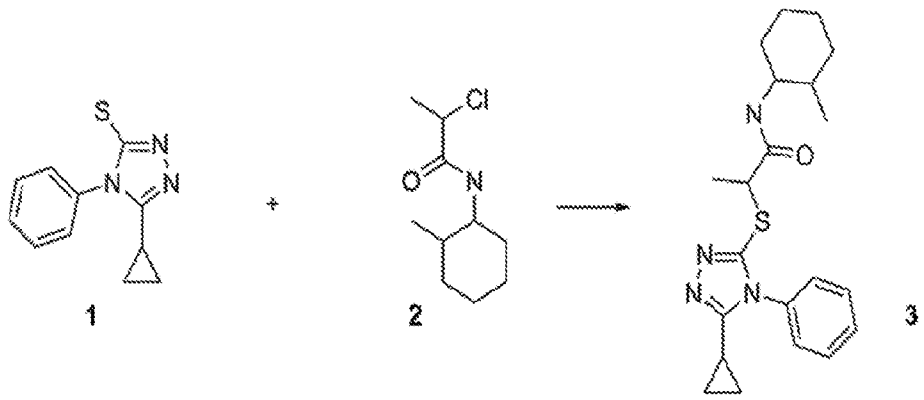

FIG. 36

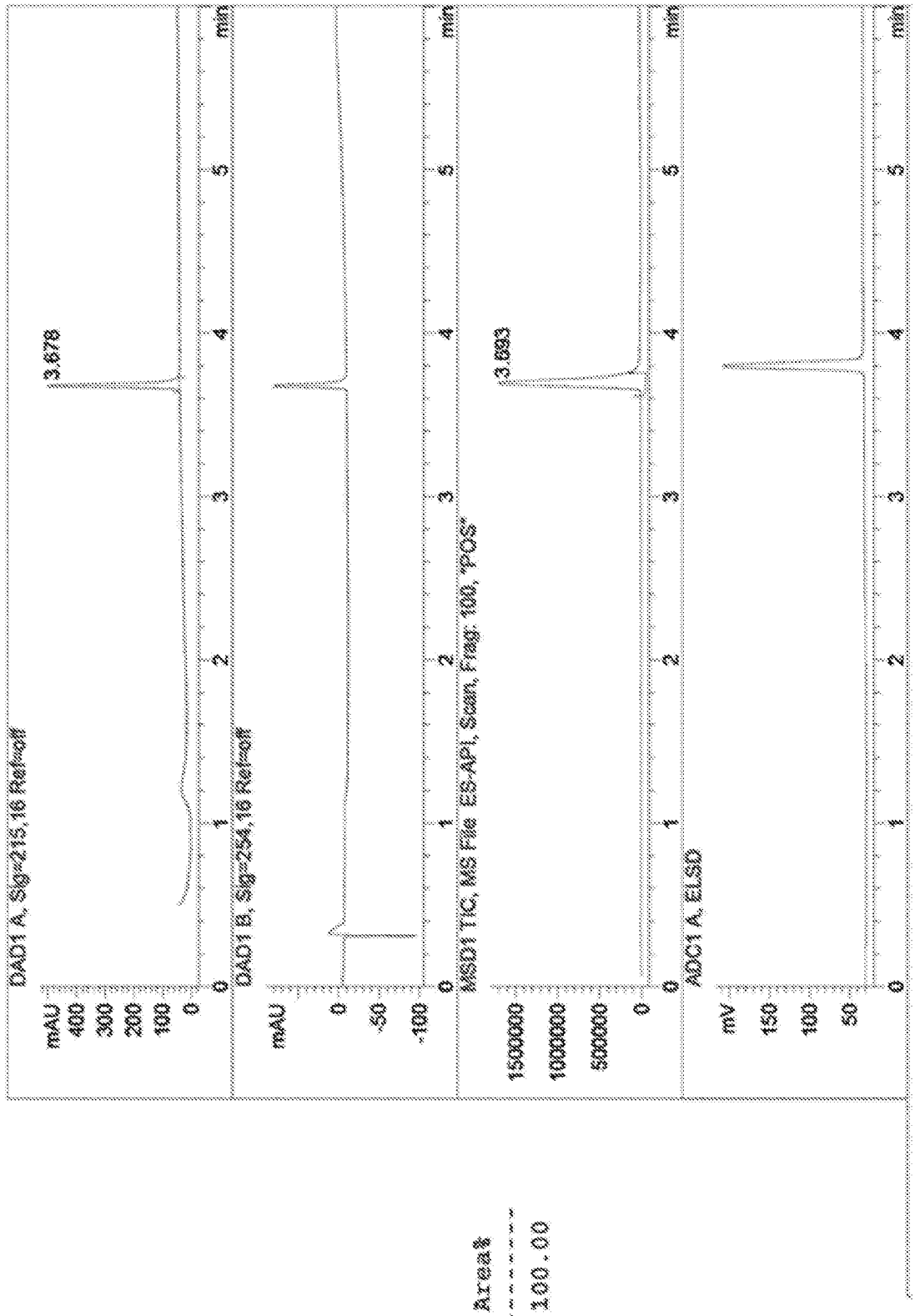

#	Time	Area%
1	3.678	100.00

FIG. 37A

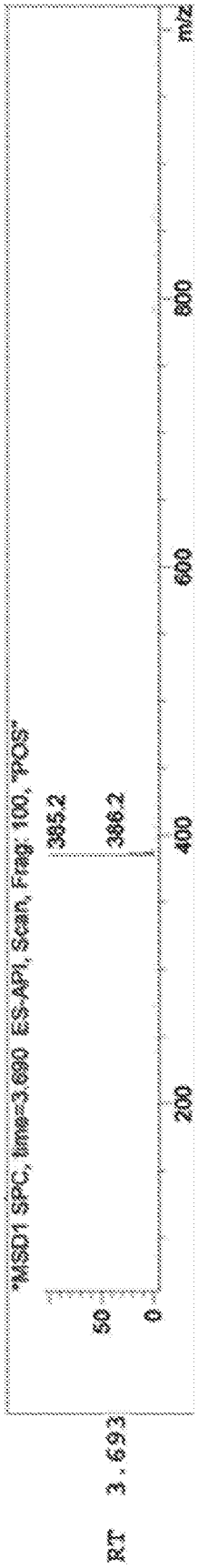
RT
3.693
"MSD1 SPC, time=3.690 ES-API, Scan, Frag=100, "POS"
385.2
386.2
50
0
200
400
600
800
m/z

FIG. 37B

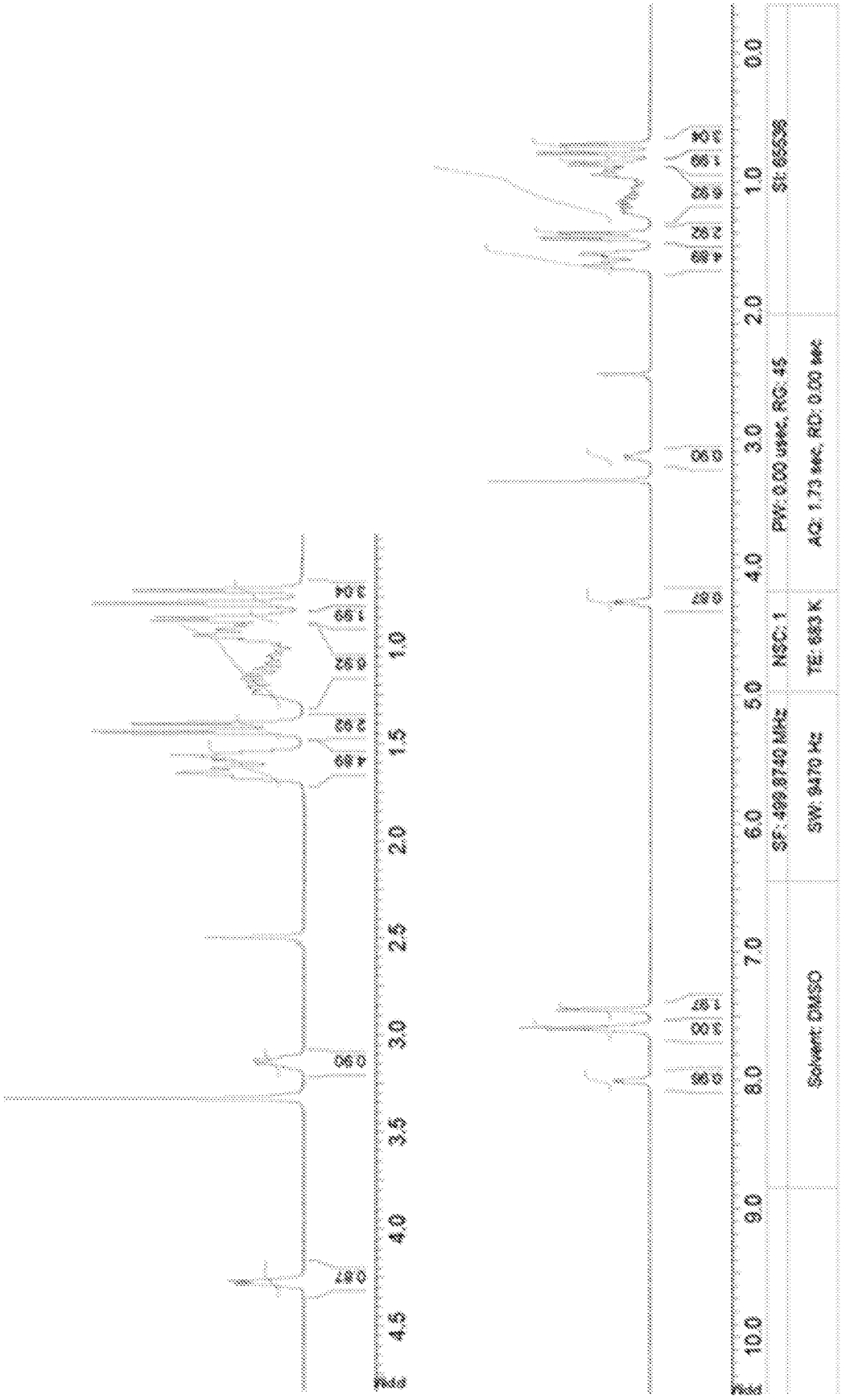
Solvent: DMSO
SW: 9470 Hz
SF: 499.8740 MHz
NSC: 1
TE: 293 K
PW: 9.00 usec, RG: 45
AQ: 1.73 sec, RD: 0.00 sec
SI: 65536

FIG. 38A

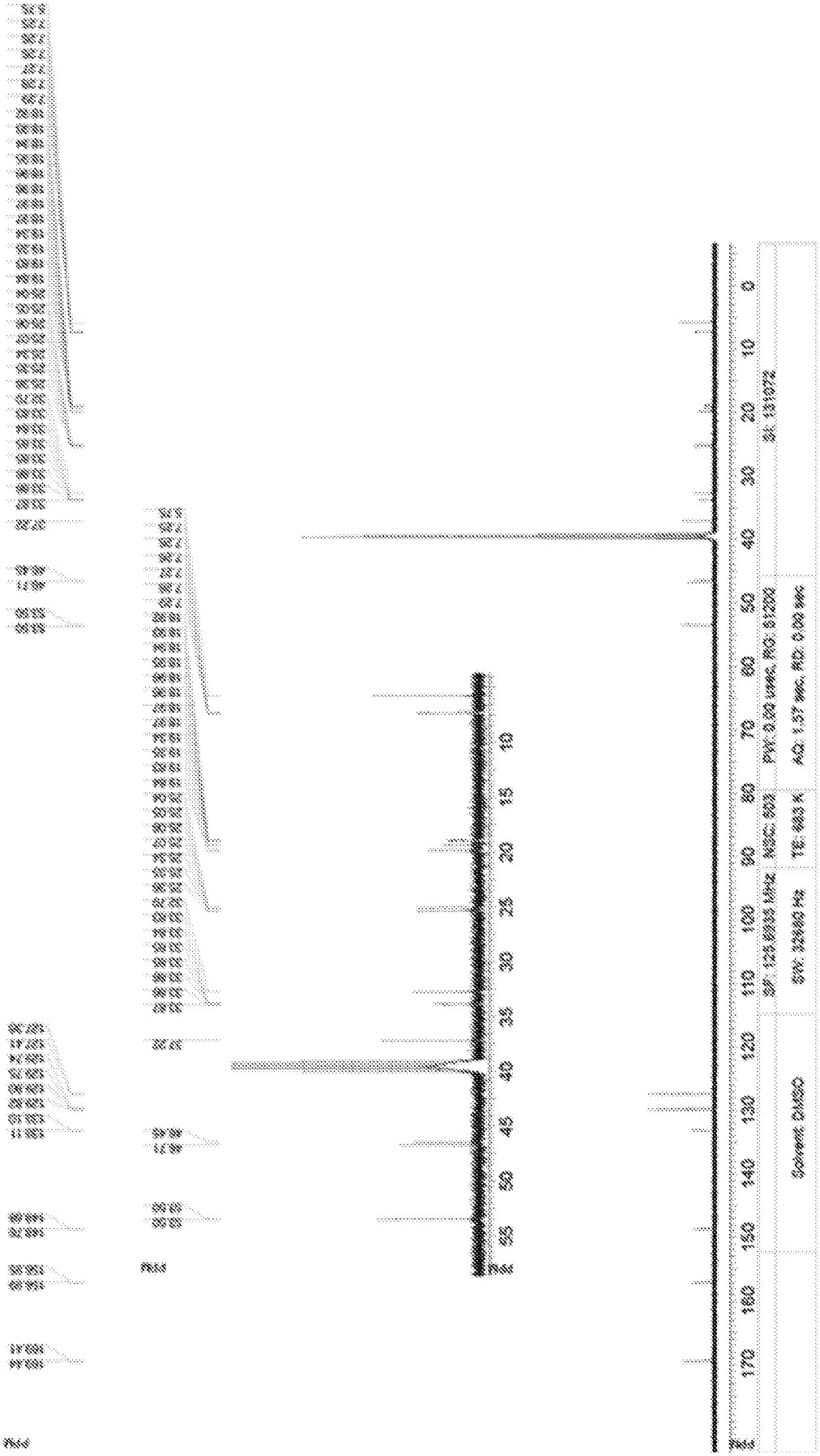
Solvent: DMSO
SW: 32680 Hz
TE: 403 K
NSC: 500
PW: 8.00 usec, RG: 81200
AQ: 1.57 sec, RD: 0.00 sec
SI: 131072

FIG. 38B

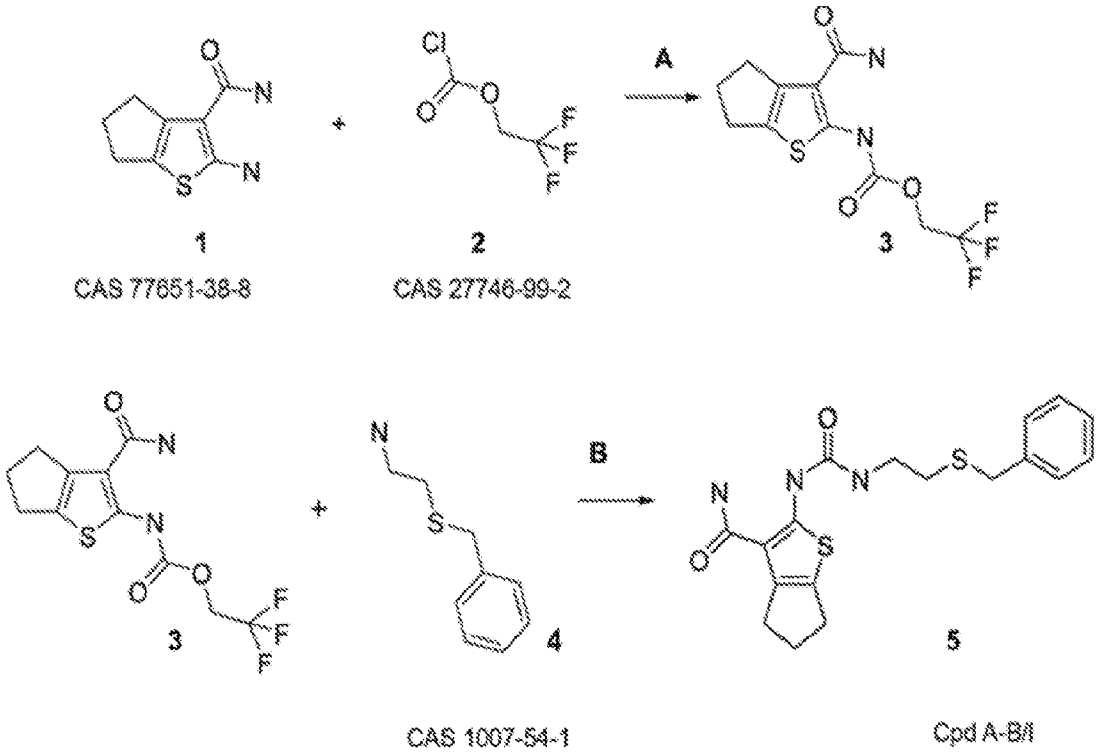

FIG. 39

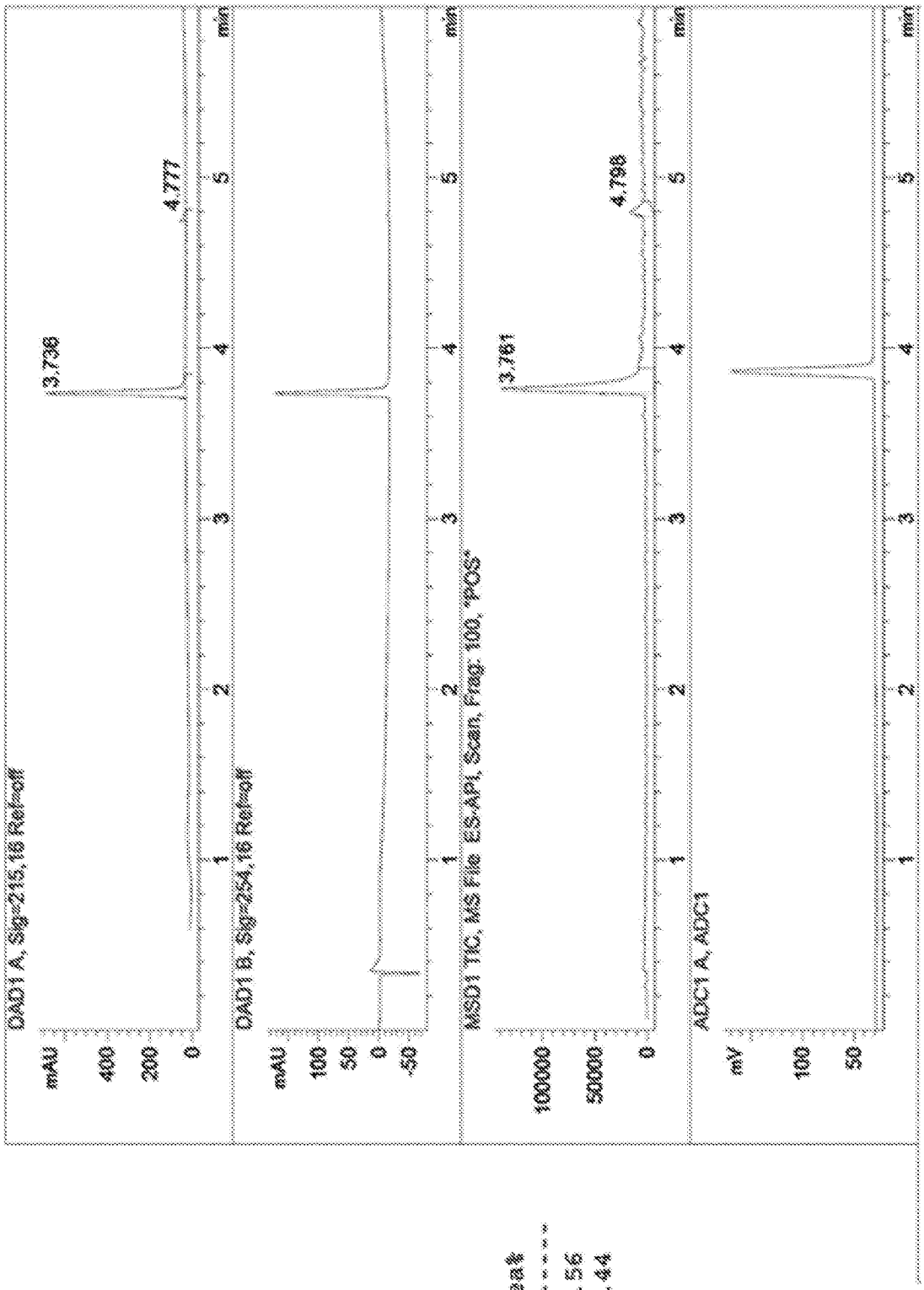

#	Time	Area%
1	3.736	97.56
2	4.777	2.44

FIG. 40A

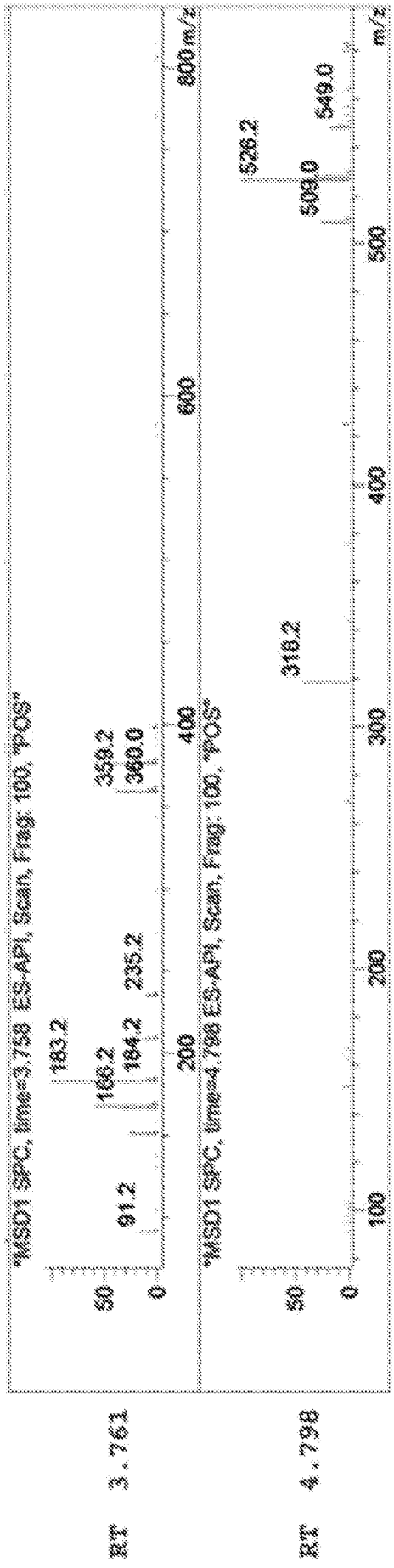
RT 3.761
*MSD1 SPC, time=3.758 ES-API, Scan, Frag: 100, "POS"
91.2
183.2
166.2
184.2
235.2
359.2
340.0
RT 4.798
*MSD1 SPC, time=4.796 ES-API, Scan, Frag: 100, "POS"
318.2
526.2
509.0
549.0
m/z

FIG. 40B

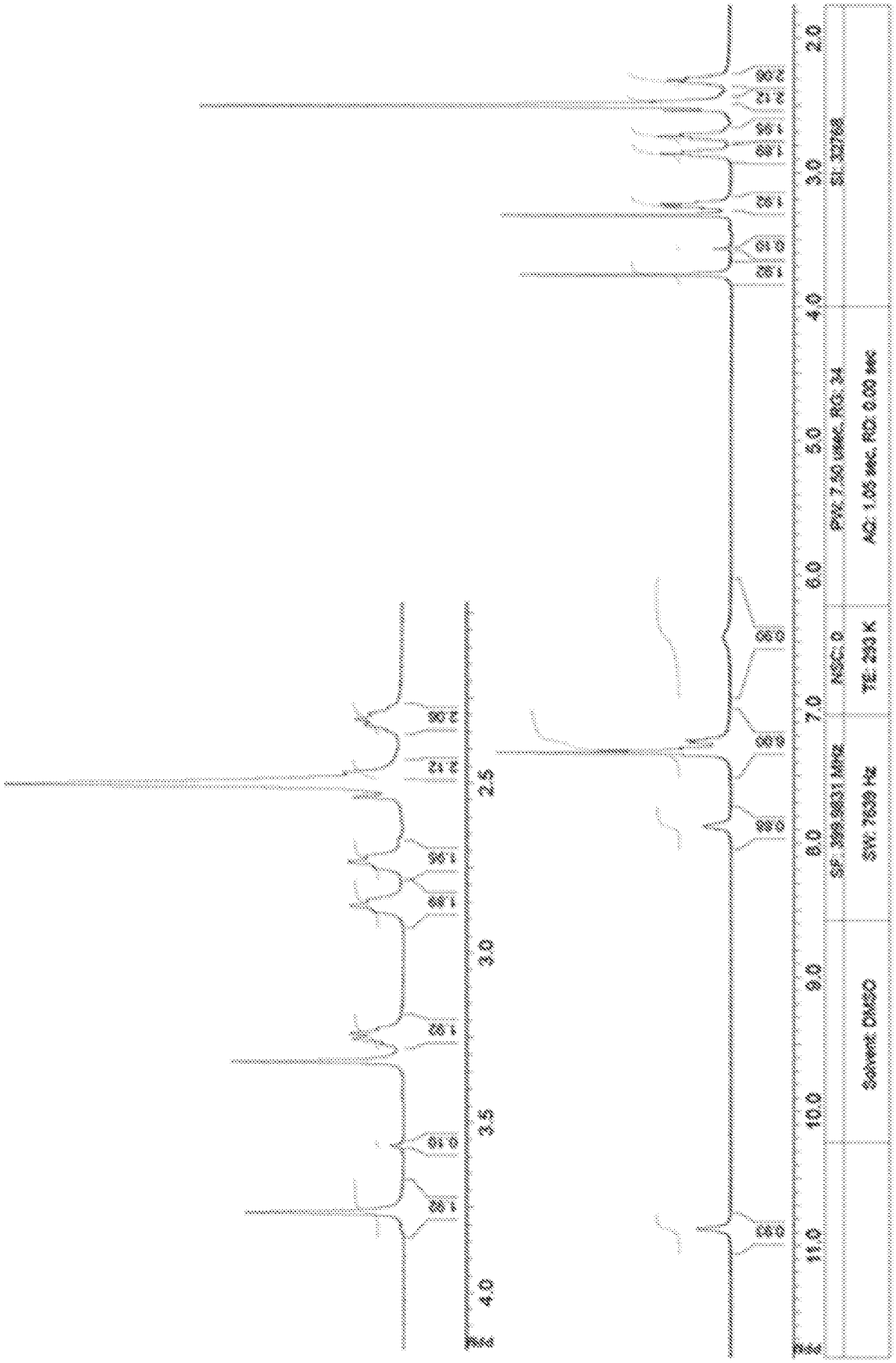
Solvent: DMSO
SW: 7639 Hz
SF: 399.9831 MHz
NOC: 0
TE: 293 K
PW: 7.50 usec, RD: 34
AQ: 1.05 sec, RD: 0.00 sec
SI: 32768
2.0
3.0
4.0
5.0
6.0
7.0
8.0
9.0
10.0
11.0
ppm
4.0
3.5
3.0
2.5

FIG. 41A

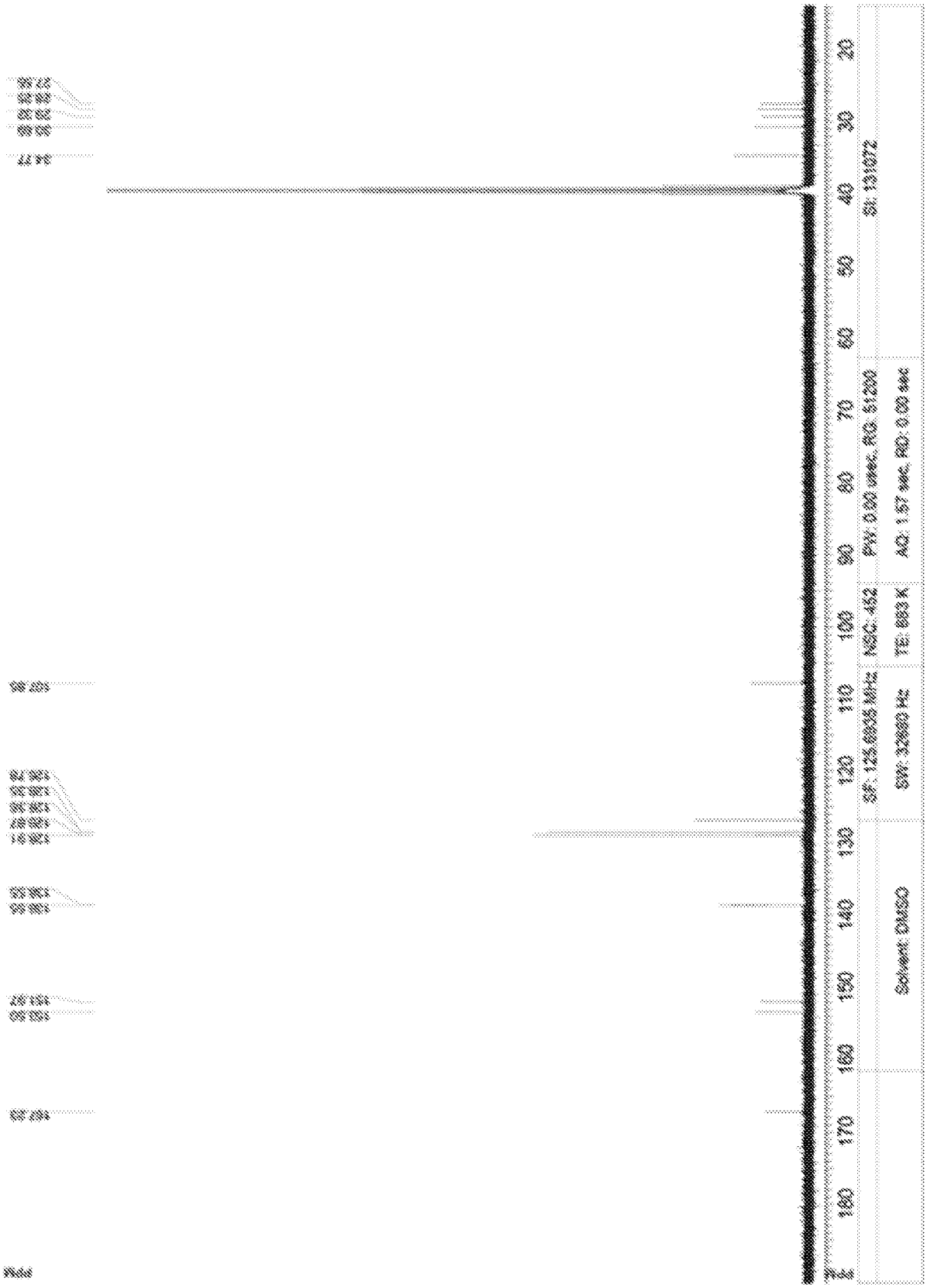
Solvent: DMSO
SF: 125.6835 MHz
SW: 32680 Hz
NSC: 452
TE: 683 K
PW: 0.00 usec, RD: 61200
AQ: 1.67 sec, RD: 0.00 sec
SI: 131072

FIG. 41B

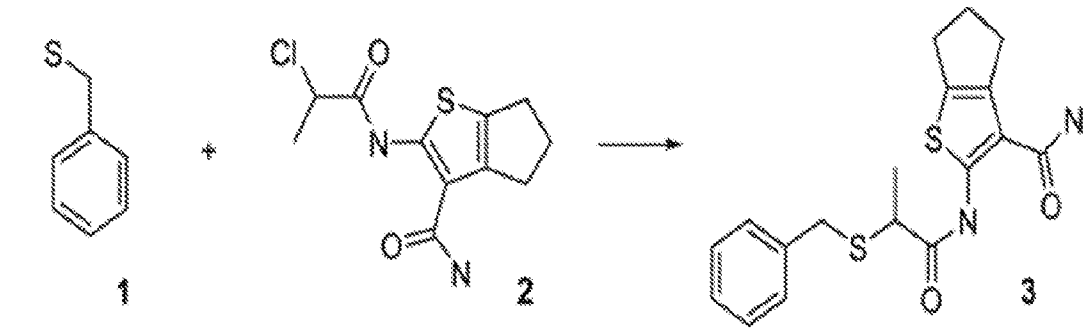

FIG. 42

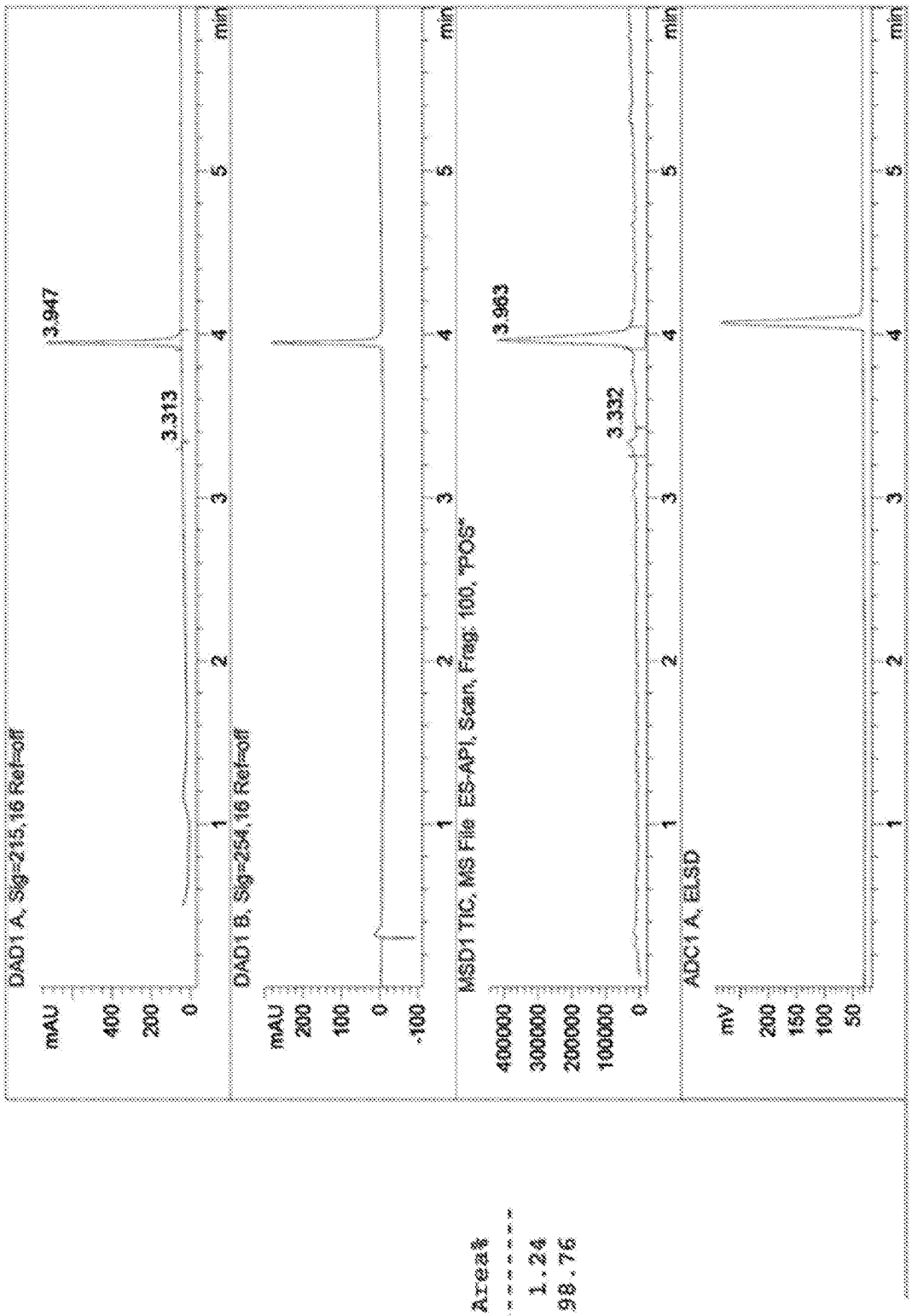

#	Time	Area%
1	3.313	1.24
2	3.947	98.76

FIG. 43A

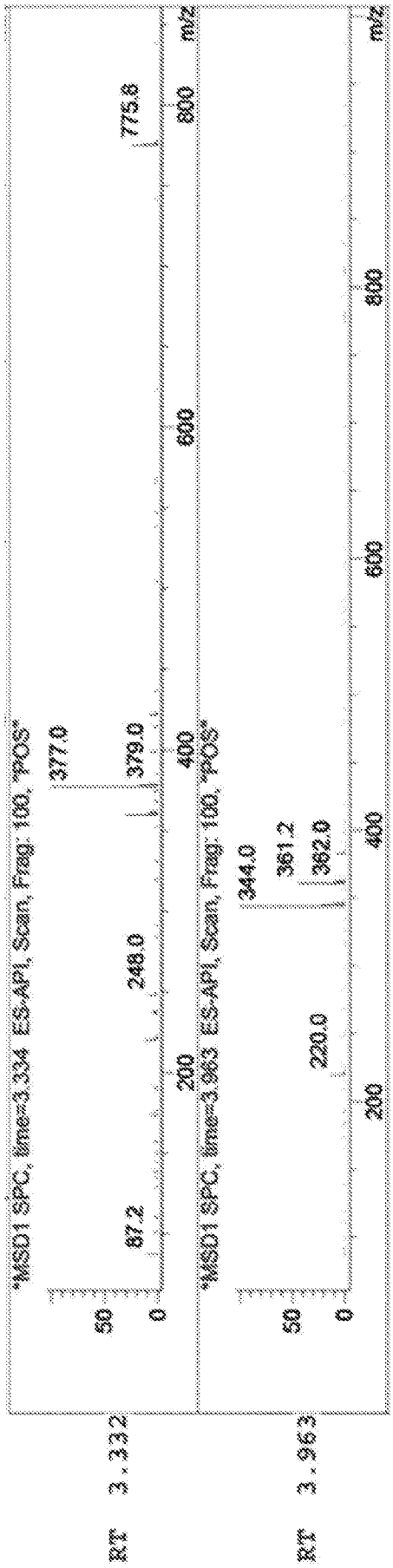
RT 3.332
*MSD1 SPC, time=3.334 ES-API, Scan, Frag: 100, "POS"
87.2
248.0
377.0
379.0
775.8
m/z
RT 3.963
*MSD1 SPC, time=3.963 ES-API, Scan, Frag: 100, "POS"
220.0
244.0
361.2
362.0
m/z

FIG. 43B

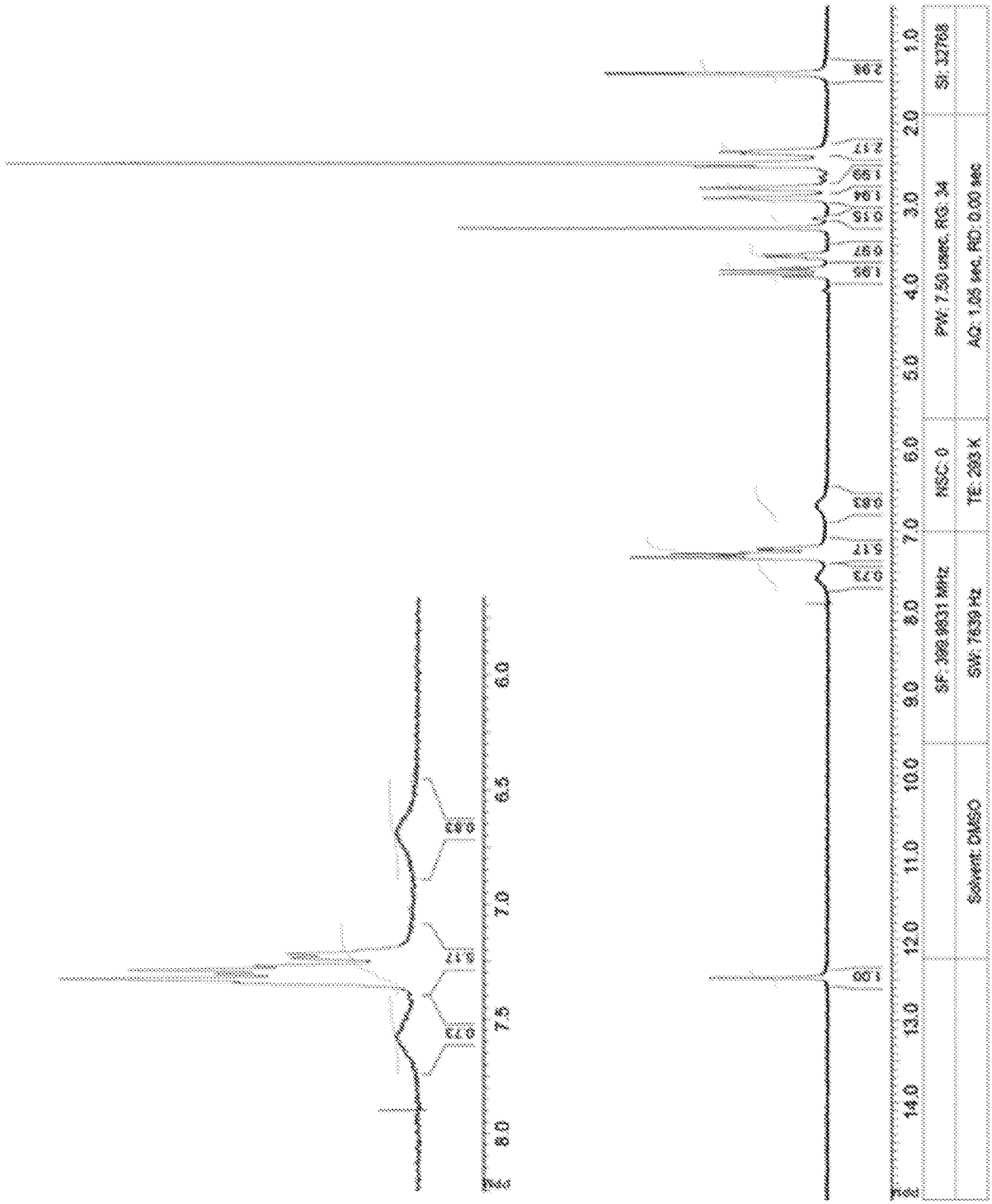
Solvent: DMSO
SF: 399.9831 MHz
SW: 7639 Hz
NSC: 0
TE: 293 K
PW: 7.50 usec, FIG: 34
AQ: 1.05 sec, RD: 0.00 sec
SI: 32768

FIG. 44A

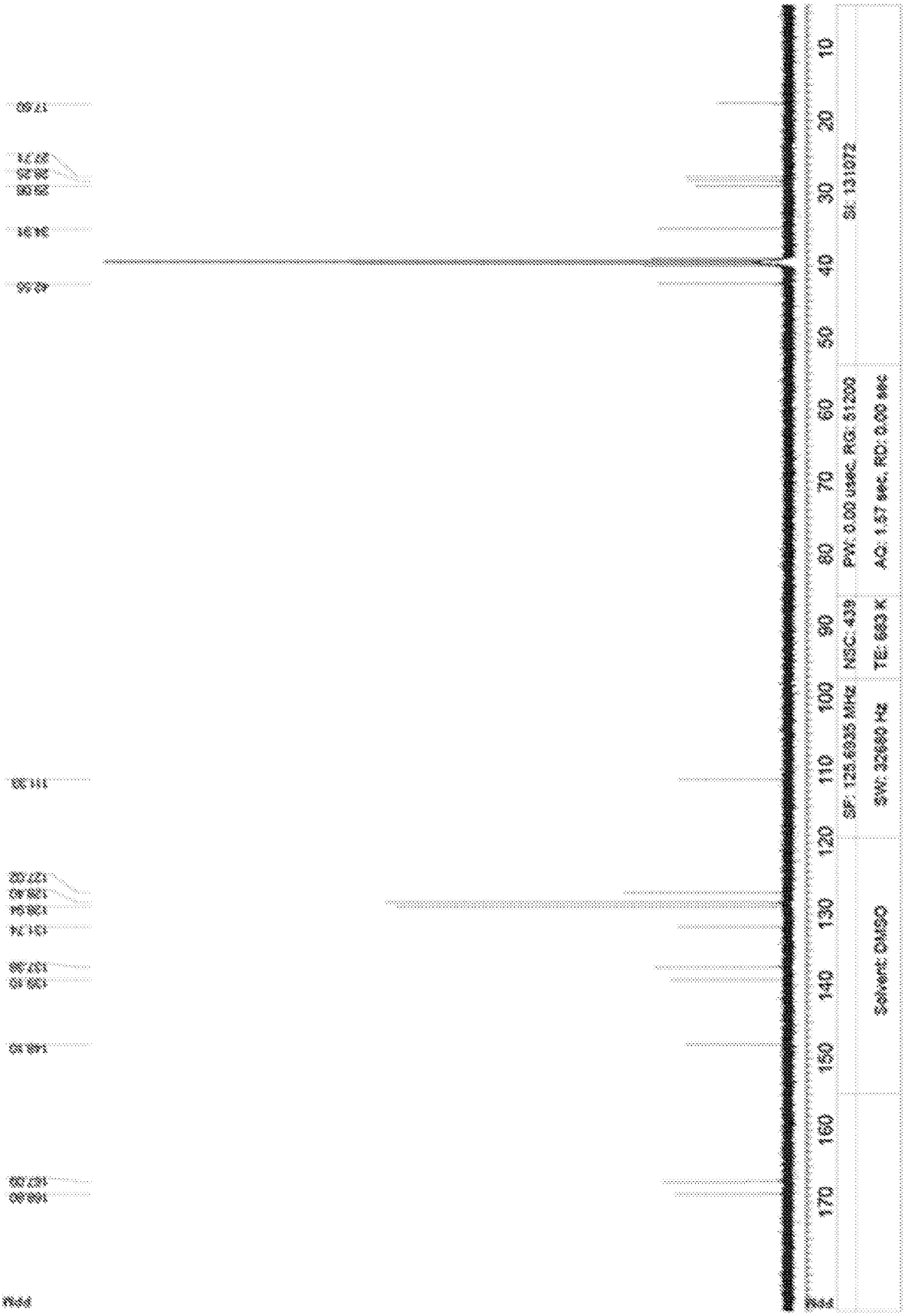
Solvent: DMSO
SF: 125.6835 MHz
SW: 32680 Hz
TE: 603 K
NSC: 439
PW: 8.00 usec, PG: 81200
AQ: 1.57 sec, RD: 0.00 sec
SI: 131072
PPM

FIG. 44B

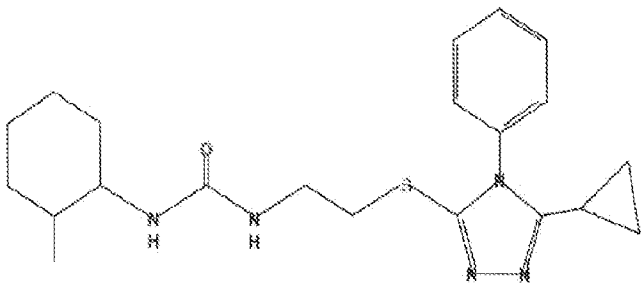

Regeneurin-S/Chimera B-A/I

	Aug-17	Nov-17	Feb-18
Molecular weight	399.6 g/mol		
Solubility	157 μM	67 μM	
Plasma protein binding			
human	97.80%	98.20%	98.8%
CD-1 mouse	93.80%	92.10%	96.2%
Plasma stability [120 min]			
human	78.70%	94.60%	92.1%
mouse	78%	93.00%	96.7%
Microsome stability (T1/2)			
human liver	2.9 min	3.1 min	2.6 min
rat liver			1.9 min
mouse liver	0.8 min	0.7 min	1.2 min

FIG. 45

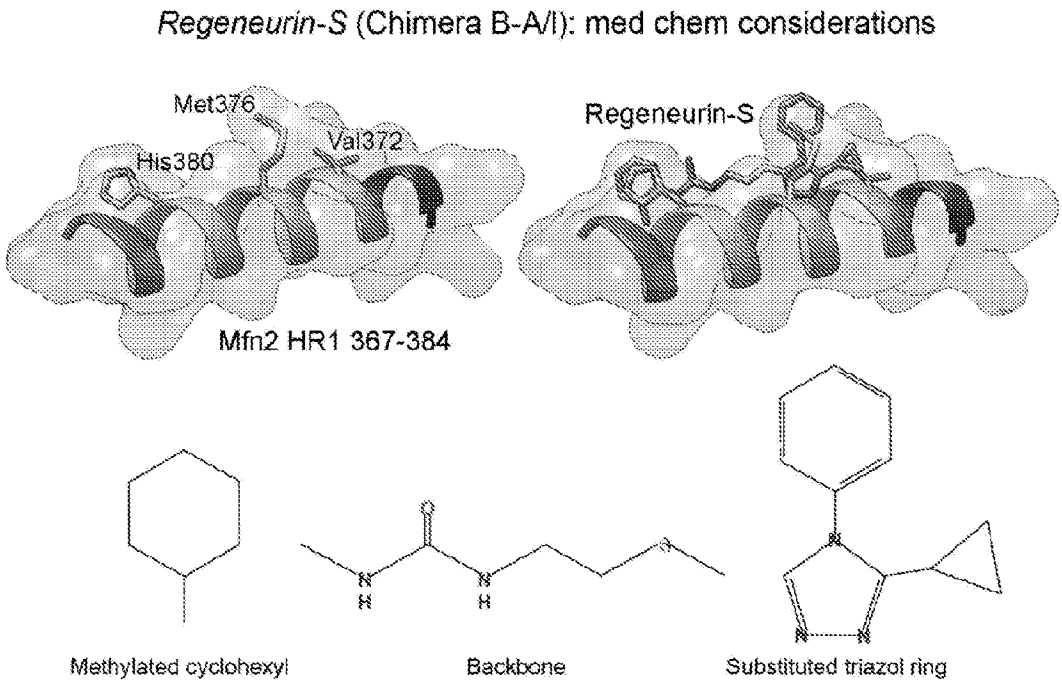
Regeneurin-S (Chimera B-A/I): med chem considerations
Met376
Val372
His380
Mfn2 HR1 367-384
Regeneurin-S
Methylated cyclohexyl
Backbone
Substituted triazol ring

FIG. 46

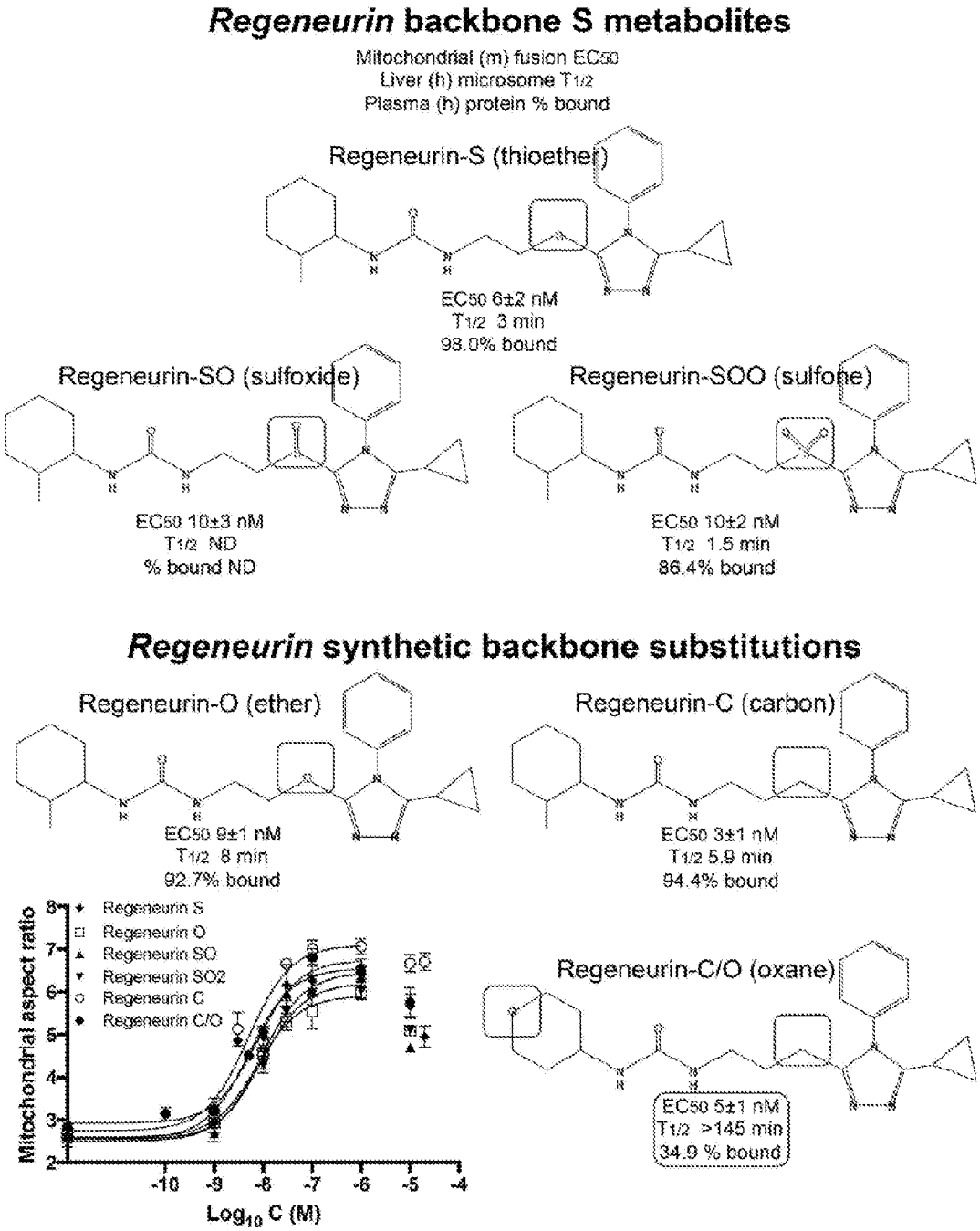
Regeneurin backbone S metabolites
Mitochondrial (m) fusion EC50
Liver (h) microsome T1/2
Plasma (h) protein % bound
Regeneurin-S (thioether)
EC50 6±2 nM
T1/2 3 min
98.0% bound
Regeneurin-SO (sulfoxide)
EC50 10±3 nM
T1/2 ND
% bound ND
Regeneurin-SOO (sulfone)
EC50 10±2 nM
T1/2 1.5 min
86.4% bound
Regeneurin synthetic backbone substitutions
Regeneurin-O (ether)
EC50 9±1 nM
T1/2 8 min
92.7% bound
Regeneurin-C (carbon)
EC50 3±1 nM
T1/2 5.9 min
94.4% bound
Regeneurin S
Regeneurin O
Regeneurin SO
Regeneurin SO2
Regeneurin C
Regeneurin C/O
Mitochondrial aspect ratio
Log10 C (M)
Regeneurin-C/O (oxane)
EC50 5±1 nM
T1/2 >145 min
34.9 % bound

FIG. 47

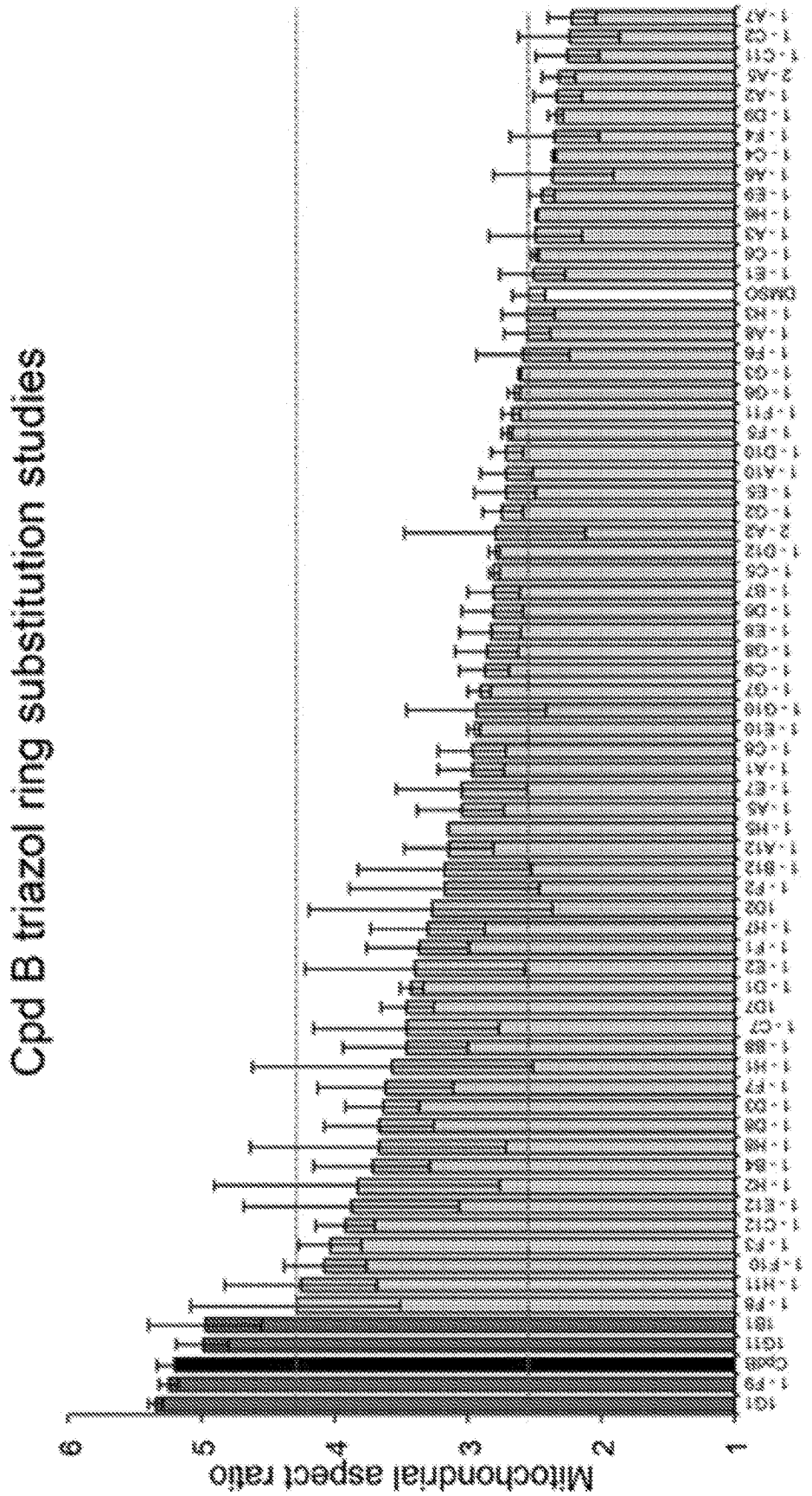
Cpd B triazol ring substitution studies
Mitochondrial aspect ratio
6
5
4
3
2
1

FIG. 48A

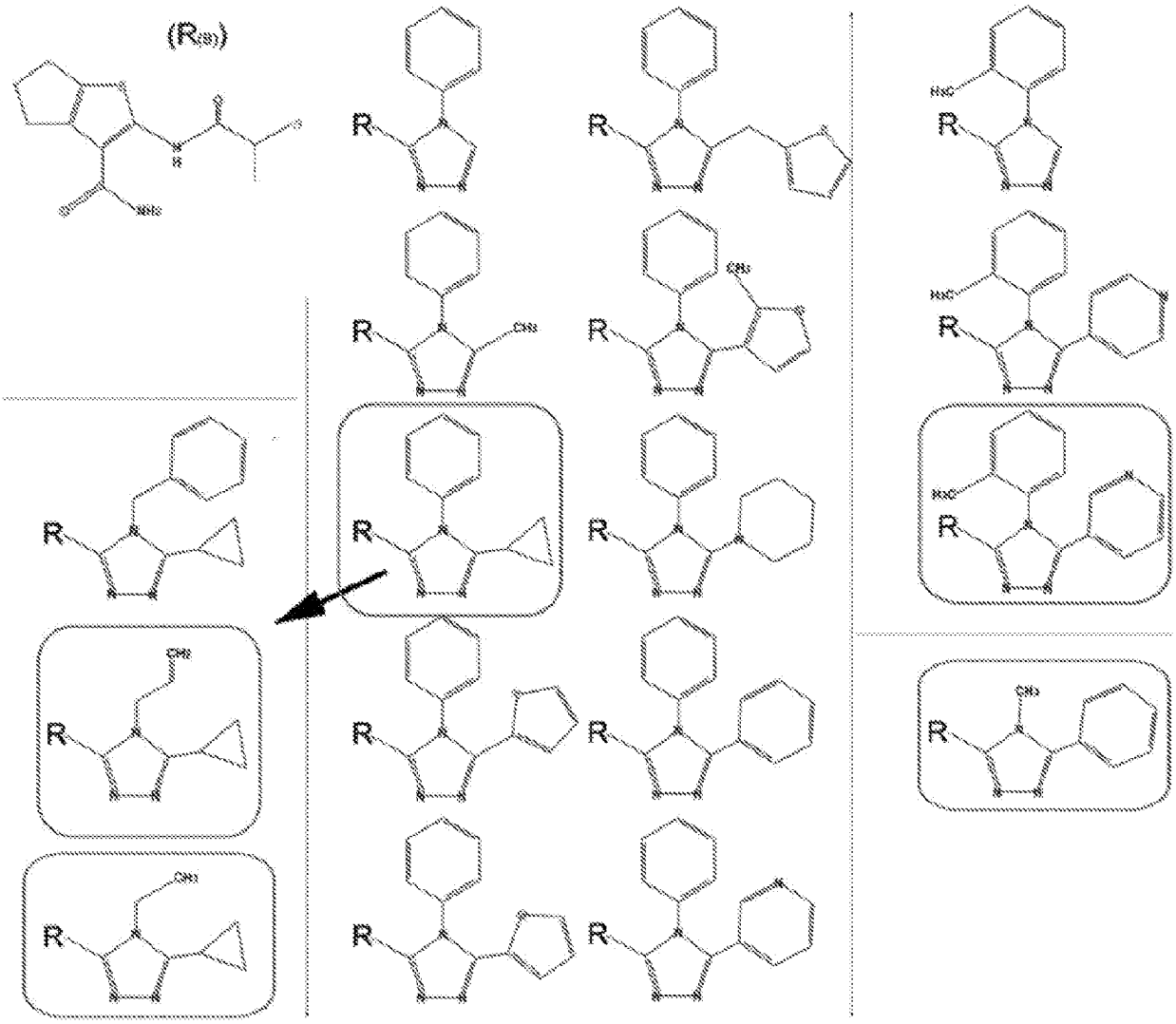

FIG. 48B

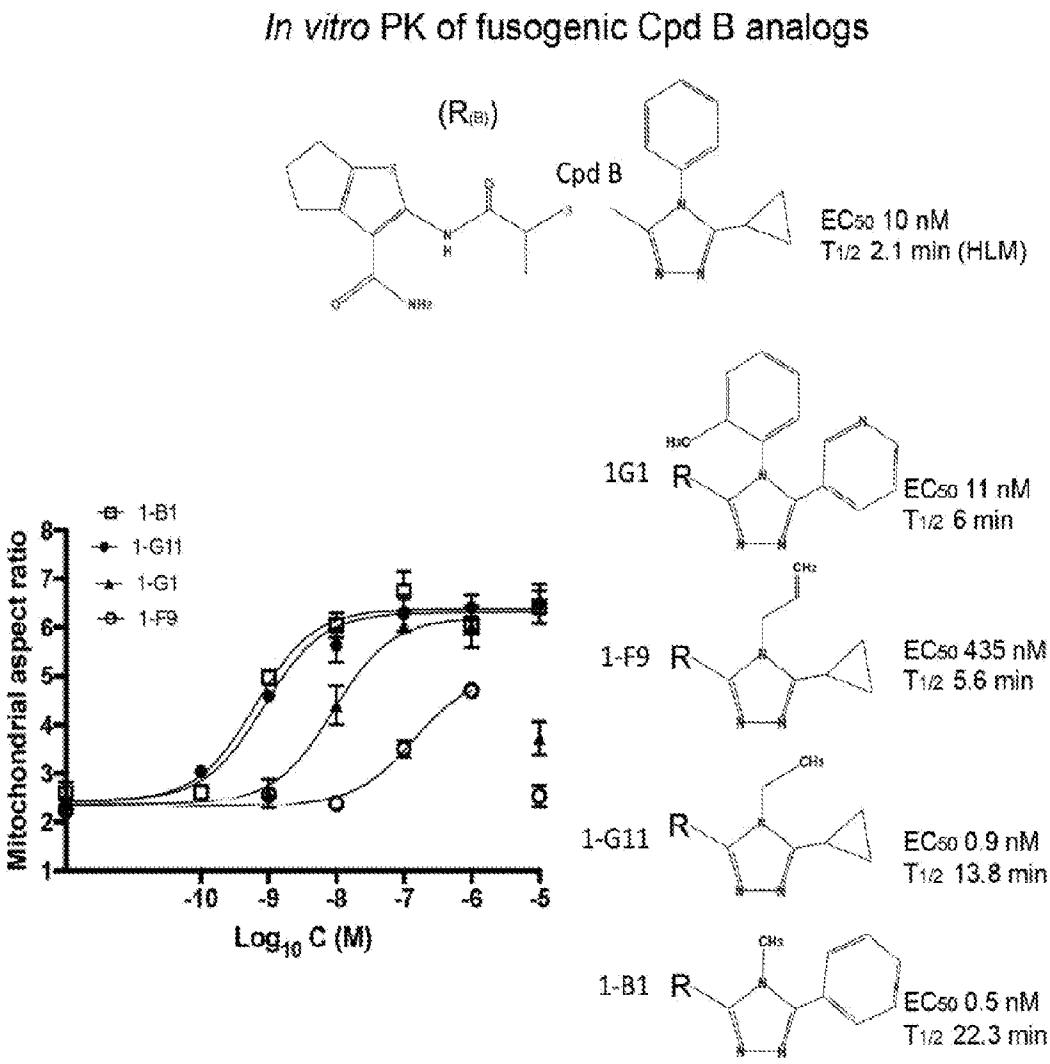
In vitro PK of fusogenic Cpd B analogs
(R(B))
Cpd B
EC50 10 nM
T1/2 2.1 min (HLM)
1G1
EC50 11 nM
T1/2 6 min
1-F9
EC50 435 nM
T1/2 5.6 min
1-G11
EC50 0.9 nM
T1/2 13.8 min
1-B1
EC50 0.5 nM
T1/2 22.3 min
1-B1
1-G11
1-G1
1-F9
Mitochondrial aspect ratio
Log10 C (M)

FIG. 49

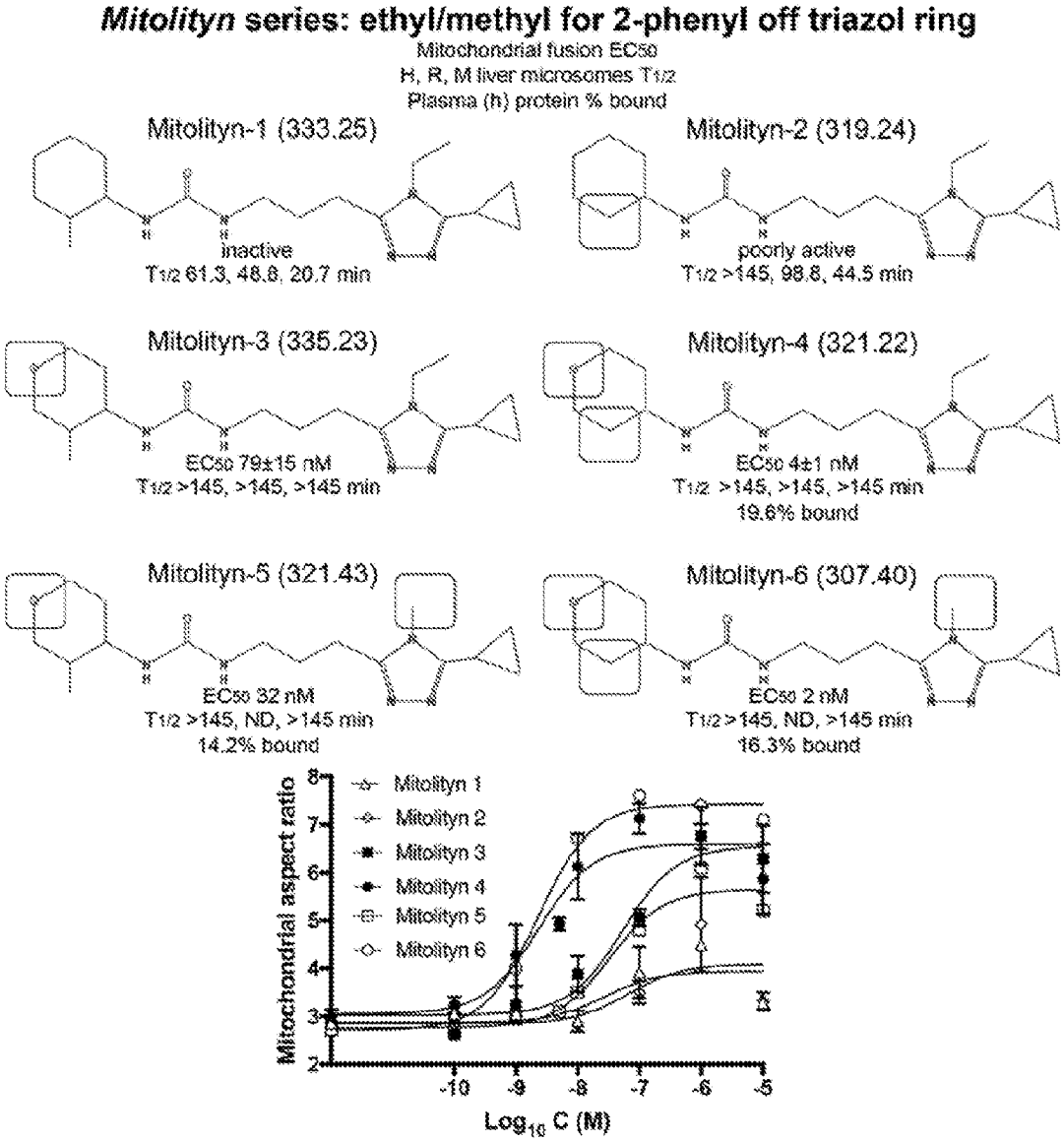
Mitolityn series: ethyl/methyl for 2-phenyl off triazol ring
Mitochondrial fusion EC50
H, R, M liver microsomes T1/2
Plasma (h) protein % bound
Mitolityn-1 (333.25)
inactive
T1/2 61.3, 48.8, 20.7 min
Mitolityn-2 (319.24)
poorly active
T1/2 >145, 98.8, 44.5 min
Mitolityn-3 (335.23)
EC50 79±15 nM
T1/2 >145, >145, >145 min
Mitolityn-4 (321.22)
EC50 4±1 nM
T1/2 >145, >145, >145 min
19.6% bound
Mitolityn-5 (321.43)
EC50 32 nM
T1/2 >145, ND, >145 min
14.2% bound
Mitolityn-6 (307.40)
EC50 2 nM
T1/2 >145, ND, >145 min
16.3% bound
Mitochondrial aspect ratio
Log10 C (M)
Mitolityn 1
Mitolityn 2
Mitolityn 3
Mitolityn 4
Mitolityn 5
Mitolityn 6

FIG. 50

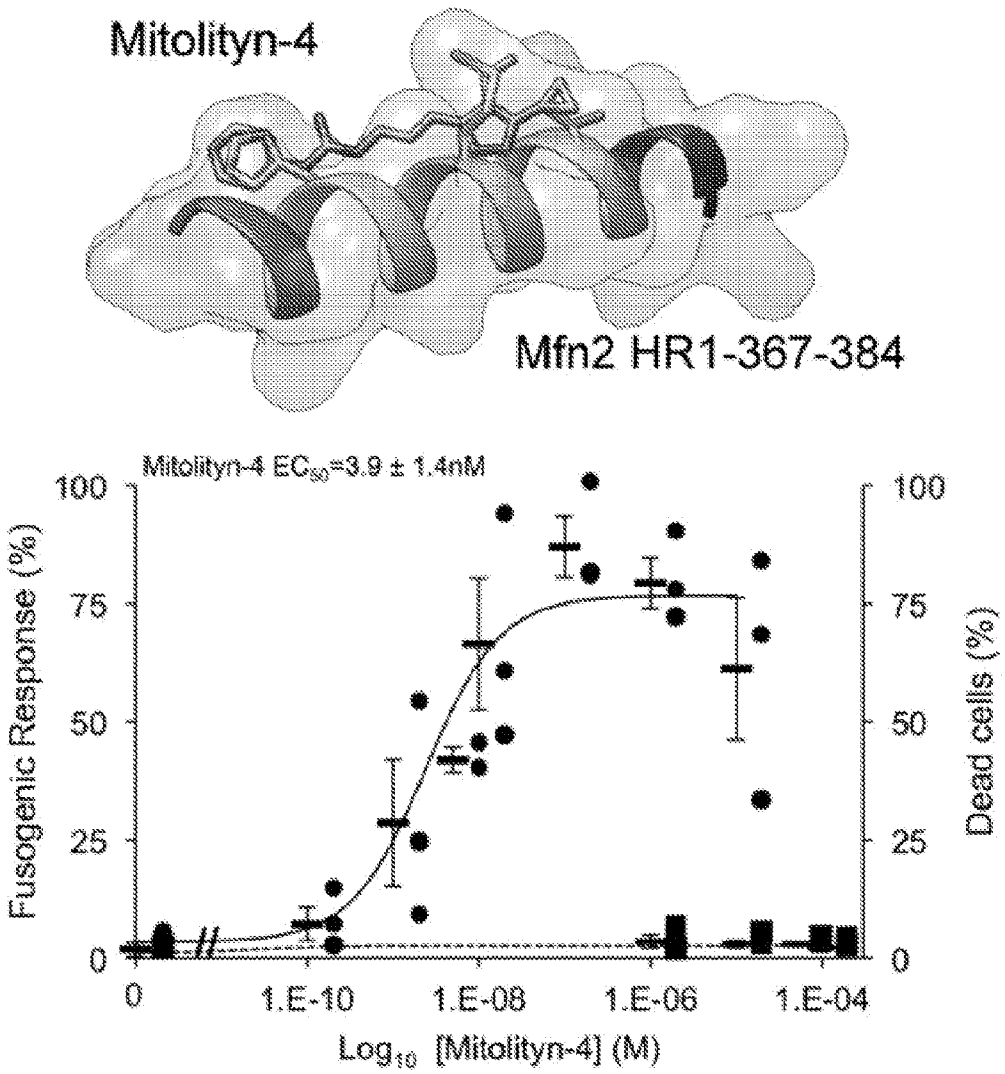
Mitolityn-4
Mfn2 HR1-367-384
Mitolityn-4 EC50=3.9 ± 1.4nM
Fusogenic Response (%)
Dead cells (%)
100
75
50
25
0
1.E-10
1.E-08
1.E-06
1.E-04
Log10 [Mitolityn-4] (M)

FIG. 51A

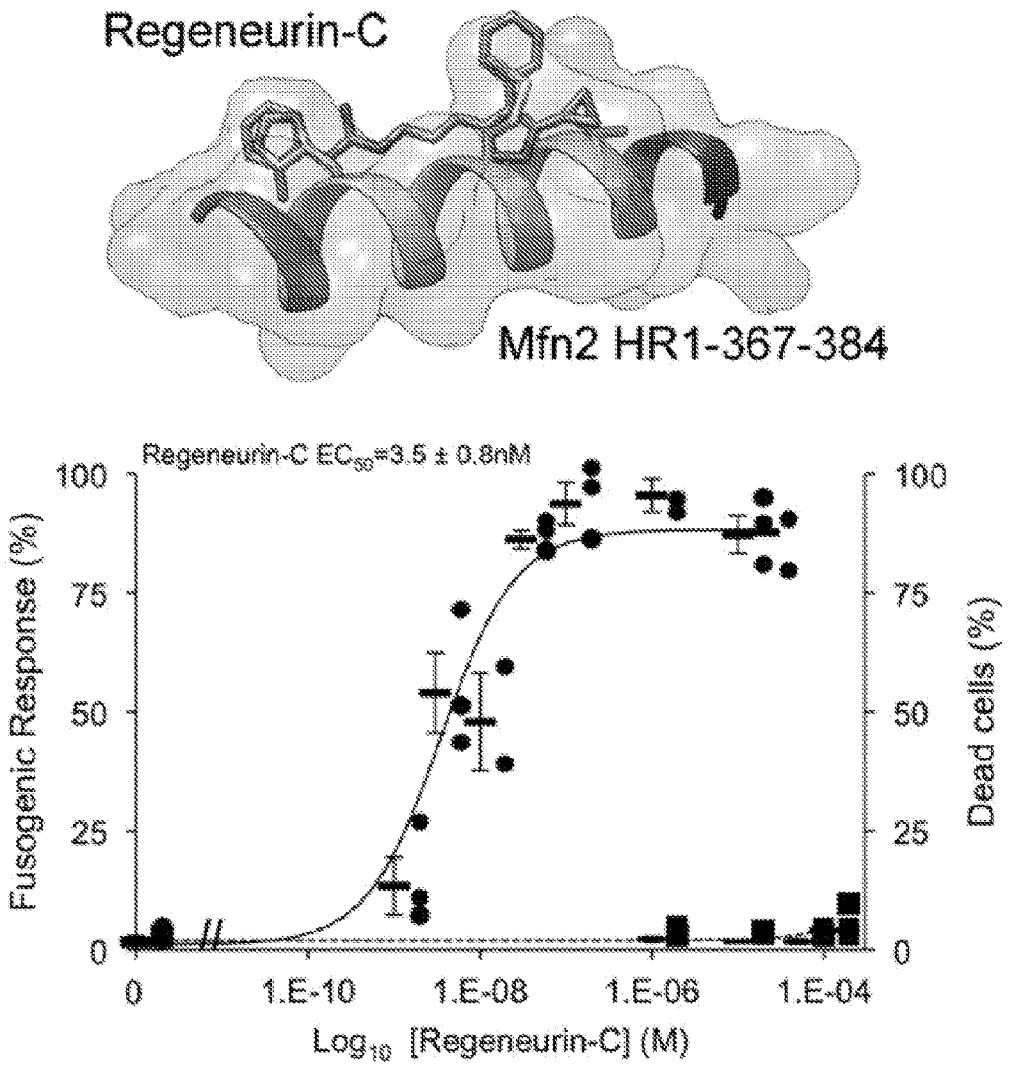
Regeneurin-C
Mfn2 HR1-367-384
Regeneurin-C EC50=3.5 ± 0.8nM
Fusogenic Response (%)
Dead cells (%)
100
75
50
25
0
0
1.E-10
1.E-08
1.E-06
1.E-04
Log10 [Regeneurin-C] (M)

FIG. 51B

Comparative *in vitro* PK of lead Regeneurins and Mitolityn

Regeneurin-C

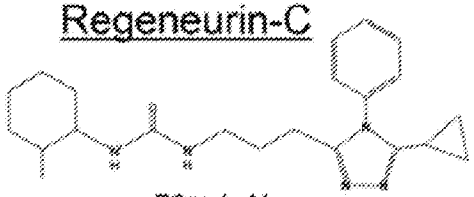

EC50 4 nM

Regeneurin-C

	18 Feb
Molecular weight	381.5 g/mol
Solubility	>200 μM
Plasma protein binding	
human	94.40%
CD-1 mouse	86.80%
Plasma stability [120 min]	
human	95%
mouse	>95%
Microsome stability (T1/2)	
human liver	5.9 min
rat liver	4.5 min
mouse liver	1.6 min
PAMPA (Pe)	21.7 nm/s
MDR Papp (B to A)	
veh	33.4
+GF120918	12.7

Regeneurin-C/O

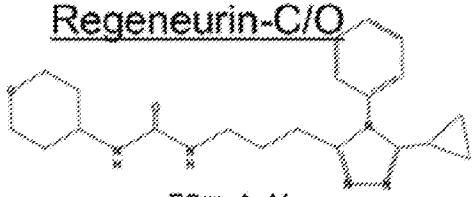

EC50 4 nM

Regeneurin-C/O

	21 Mar
Molecular weight	369.5 g/mol
Solubility	>200 μM
Plasma protein binding	
human	34.90%
CD-1 mouse	16.20%
Plasma stability [120 min]	
human	100%
mouse	82%
Microsome stability (T1/2)	
human liver	>145 min
rat liver	
mouse liver	91.1 min
PAMPA (Pe)	1.03 nm/s
MDR Papp (B to A)	
veh	7.74
+GF120918	1.84

Mitolityn-4

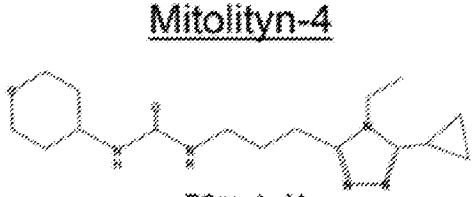

EC50 4 nM

Mitolityn-4

	18 Feb
Molecular weight	321.4 g/mol
Solubility	196.19 μM
Plasma protein binding	
human	19.60%
CD-1 mouse	11.20%
Plasma stability [120 min]	
human	91%
mouse	97%
Microsome stability (T1/2)	
human liver	>145 min
rat liver	>145 min
mouse liver	>145 min
PAMPA (Pe)	0.029 nm/s
MDR Papp (B to A)	
veh	0.65
+GF120918	0.56

FIG. 52

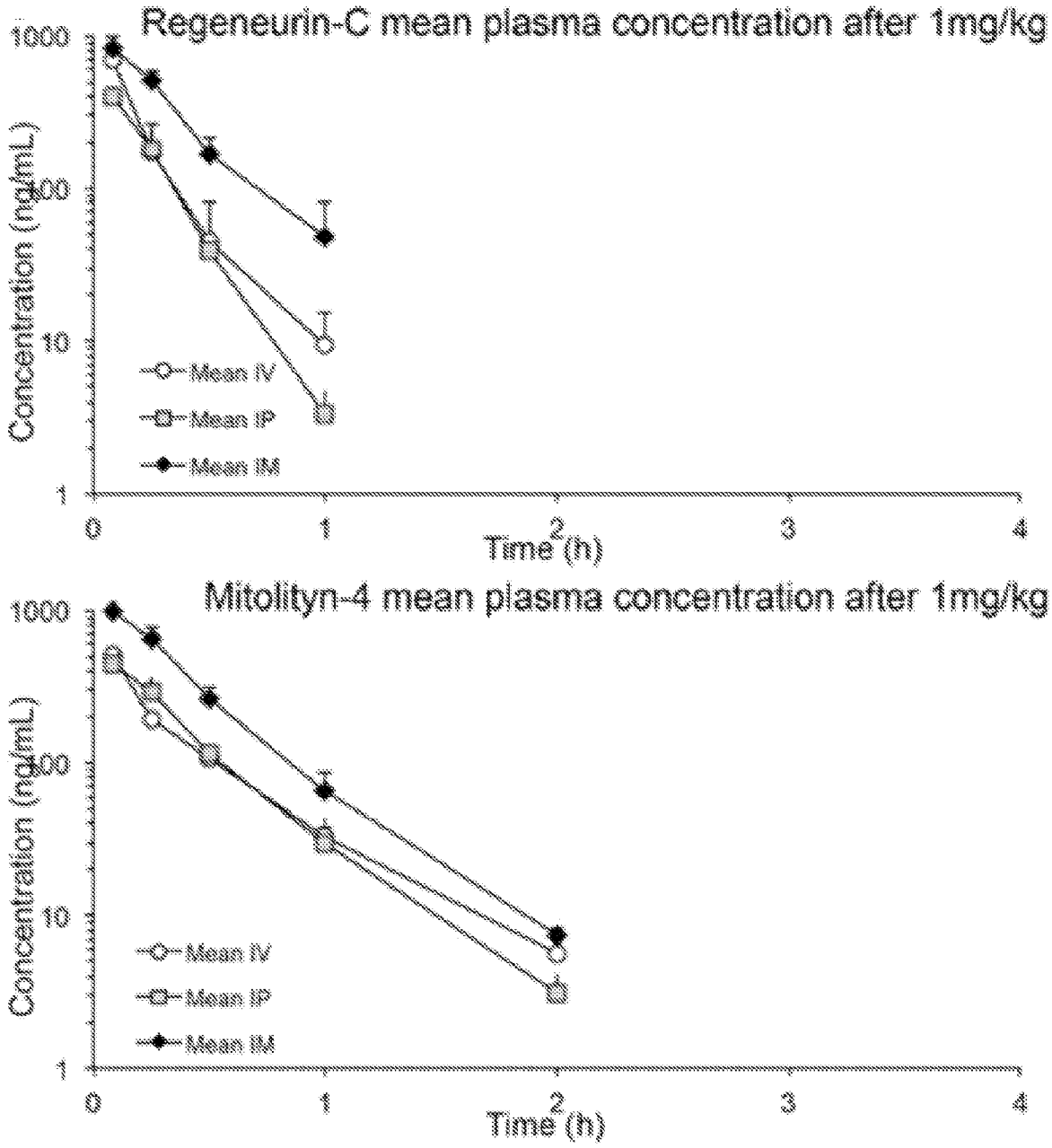
Regeneurin-C mean plasma concentration after 1mg/kg
Concentration (ng/mL)
1000
100
10
1
0
1
2
3
4
Time (h)
Mean IV
Mean IP
Mean IM
Mitolityn-4 mean plasma concentration after 1mg/kg
Concentration (ng/mL)
1000
100
10
1
0
1
2
3
4
Time (h)
Mean IV
Mean IP
Mean IM

FIG. 53A

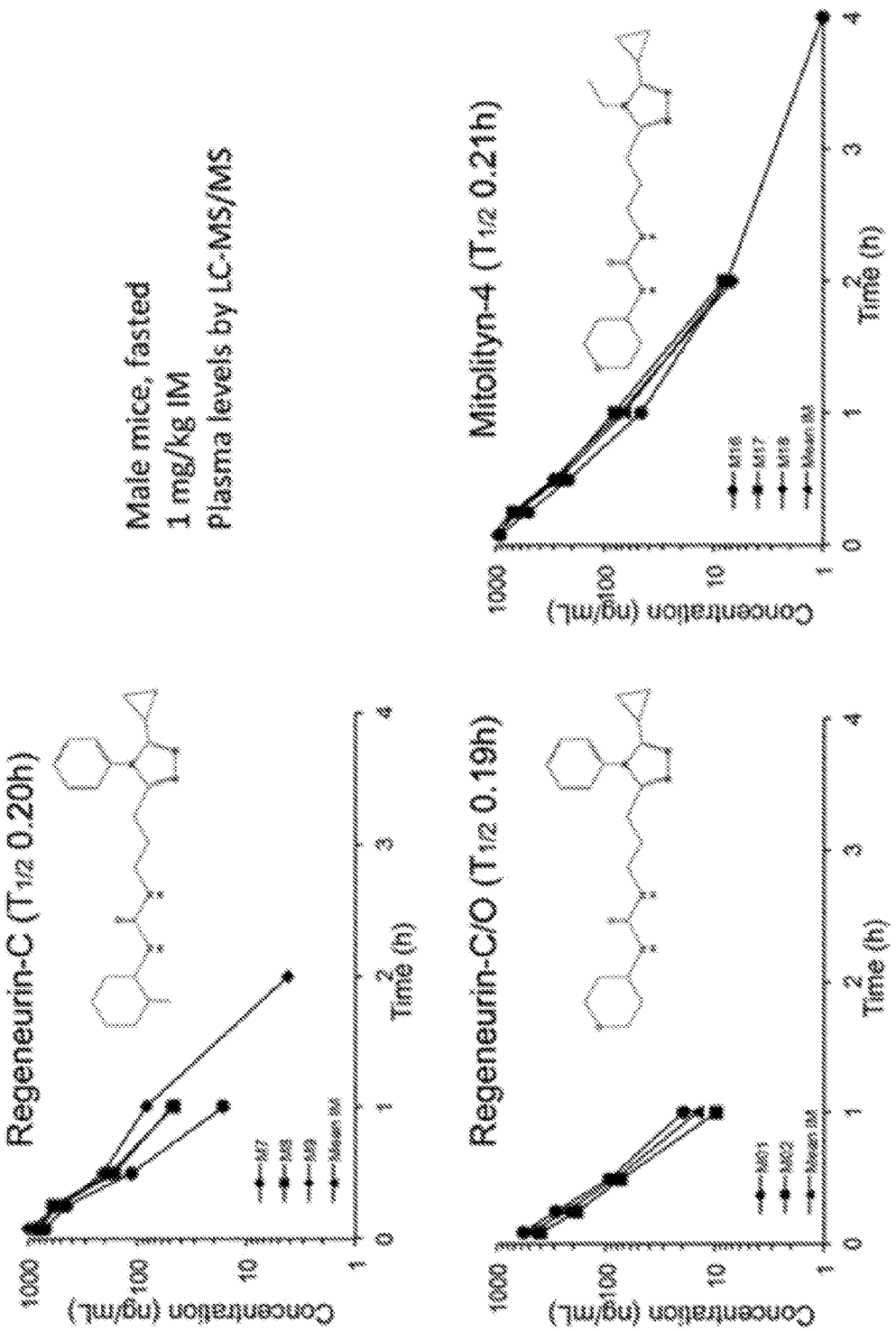
Male mice, fasted
1 mg/kg IM
Plasma levels by LC-MS/MS
Regeneurin-C ($T_{1/2}$ 0.20h)
Regeneurin-C/O ($T_{1/2}$ 0.19h)
Mitolityn-4 ($T_{1/2}$ 0.21h)
Concentration (ng/mL)
Time (h)
1000
100
10
1
0
1
2
3
4
M1
M2
M3
Mean IM
M16
M17
M18
Mean IM

FIG. 53B

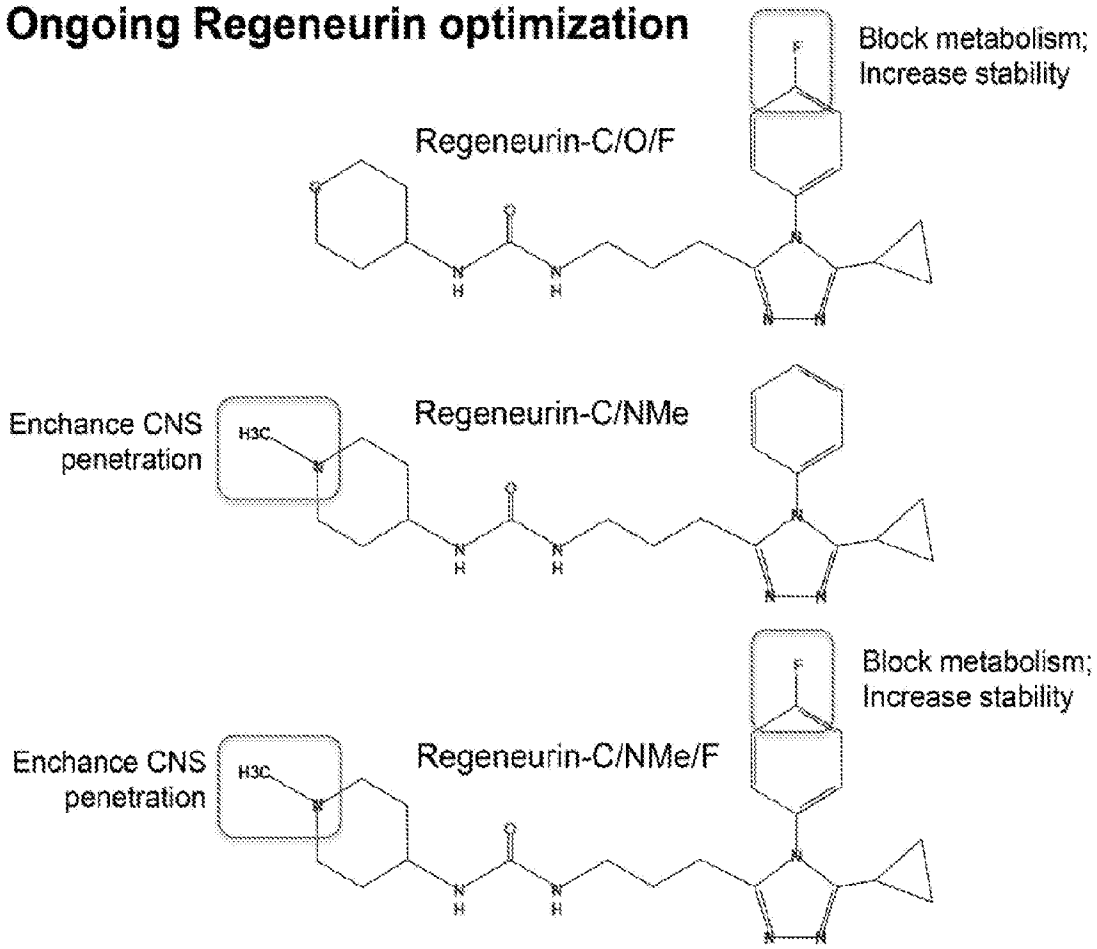
Ongoing Regeneurin optimization
Block metabolism;
Increase stability
Regeneurin-C/O/F
Enchance CNS
penetration
H3C
Regeneurin-C/NMe
Block metabolism;
Increase stability
Enchance CNS
penetration
H3C
Regeneurin-C/NMe/F

FIG. 54

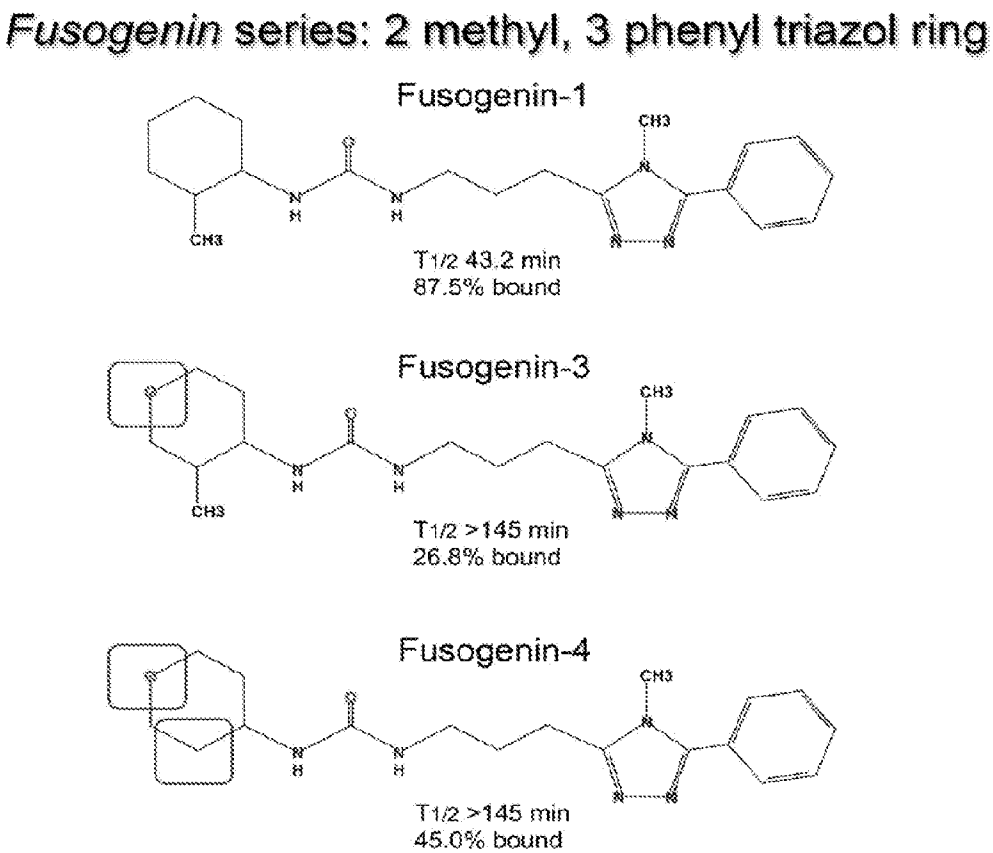
Fusogenin series: 2 methyl, 3 phenyl triazol ring
Fusogenin-1
CH3
CH3
N
H
N
H
N
N
T1/2 43.2 min
87.5% bound
Fusogenin-3
CH3
CH3
N
H
N
H
N
N
T1/2 >145 min
26.8% bound
Fusogenin-4
CH3
N
H
N
H
N
N
T1/2 >145 min
45.0% bound

FIG. 55

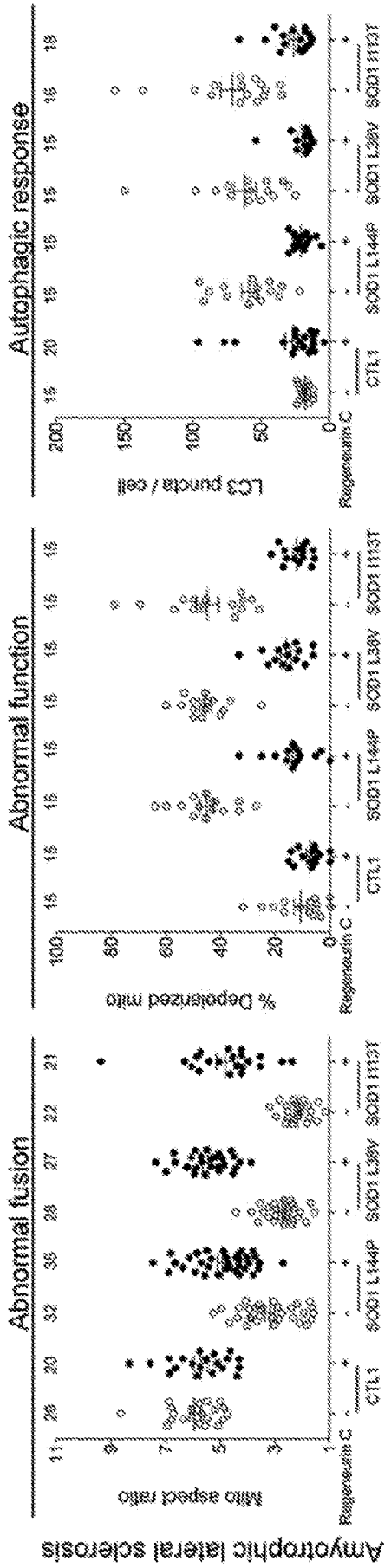
Amyotrophic lateral sclerosis
Abnormal fusion
Mito aspect ratio
Abnormal function
% Depolarized mito
Autophagic response
LC3 punda / cell
Rapamycin
CTL1
SOD1 L144P
SOD1 L38V
SOD1 I113T

FIG. 56A

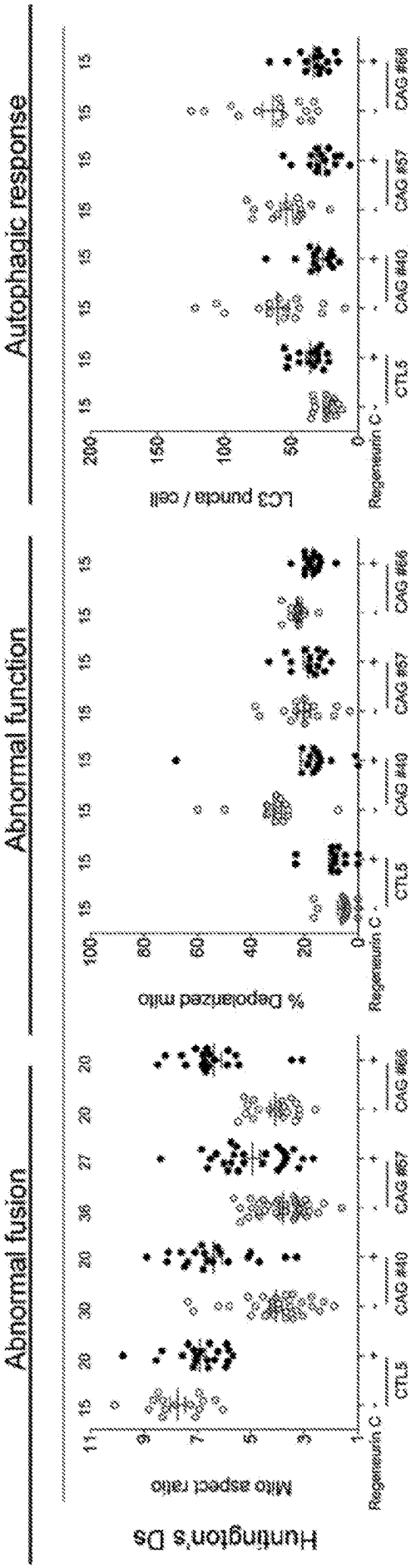
Huntington's Ds
Abnormal fusion
Abnormal function
Autophagic response
Ratio aspect ratio
% Depolarized mito
LC3 punda / cell
Regenerum C
CTLS
CAG #40
CAG #57
CAG #66

FIG. 56B

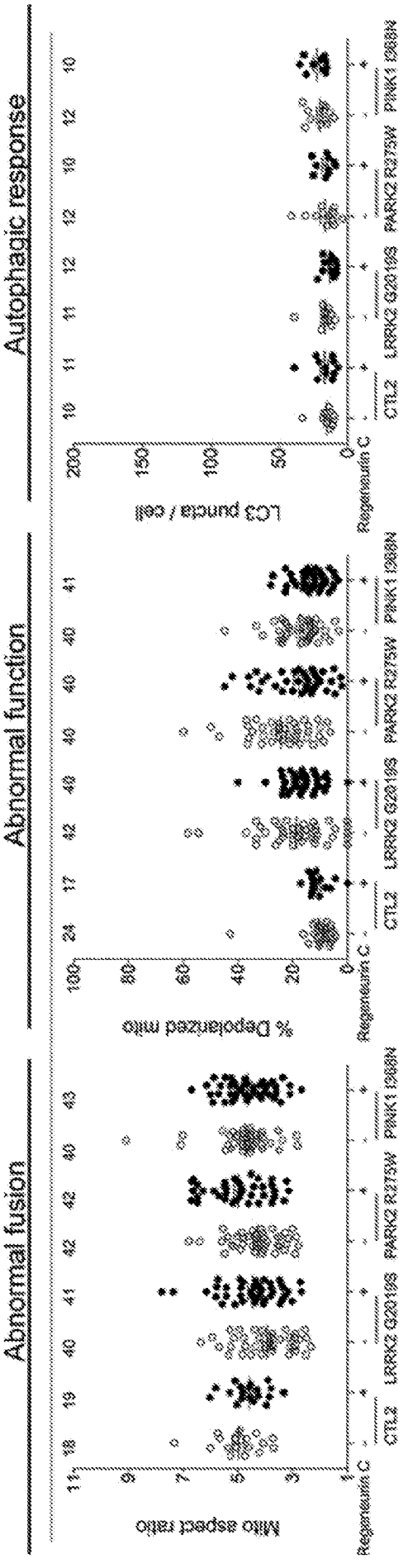
Abnormal fusion
Mito aspect ratio
Abnormal function
% Depolarized mito
Autophagic response
LC3 puncta / cell
Regenerin C
CTL2
LRRK2 G2019S
PARK2 R275W
PINK1 I368N

FIG. 56C

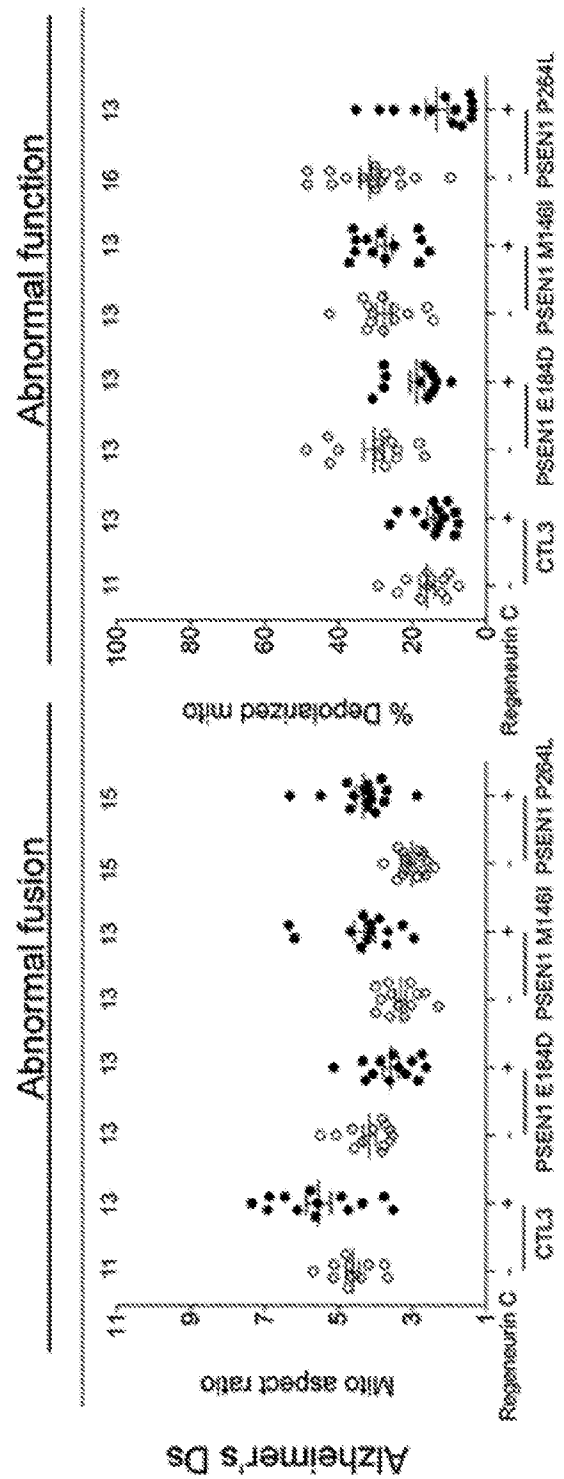
Alzheimer's Ds
Abnormal fusion
Abnormal function
Mito aspect ratio
% Depolarized mito
Rapamycin
CTL3
PSEN1 E184D
PSEN1 M146I
PSEN1 P284L

FIG. 56D

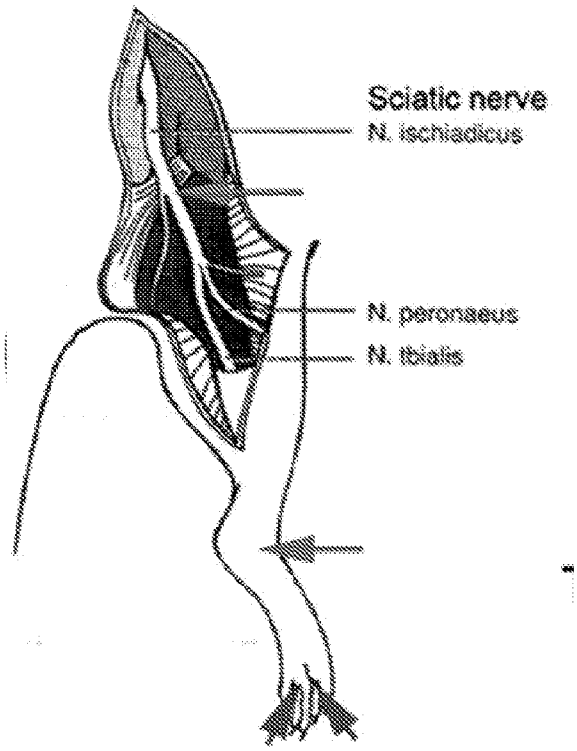

FIG. 57A

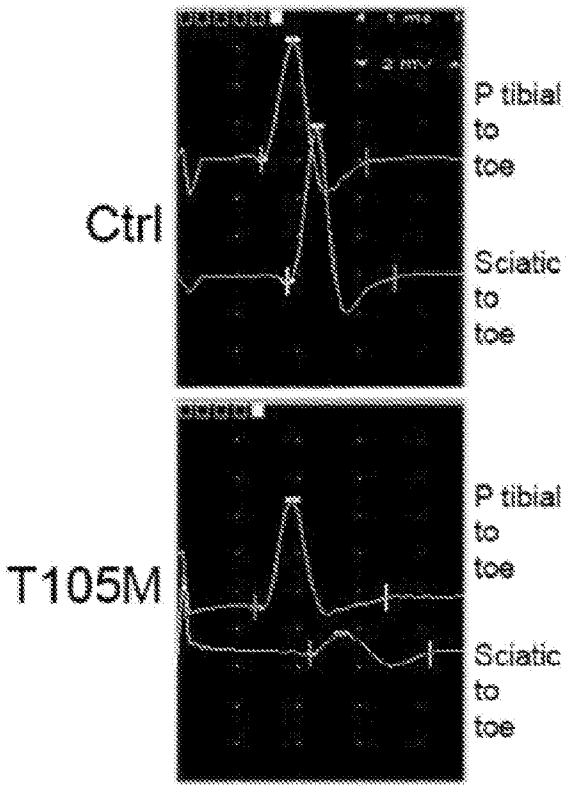

FIG. 57B

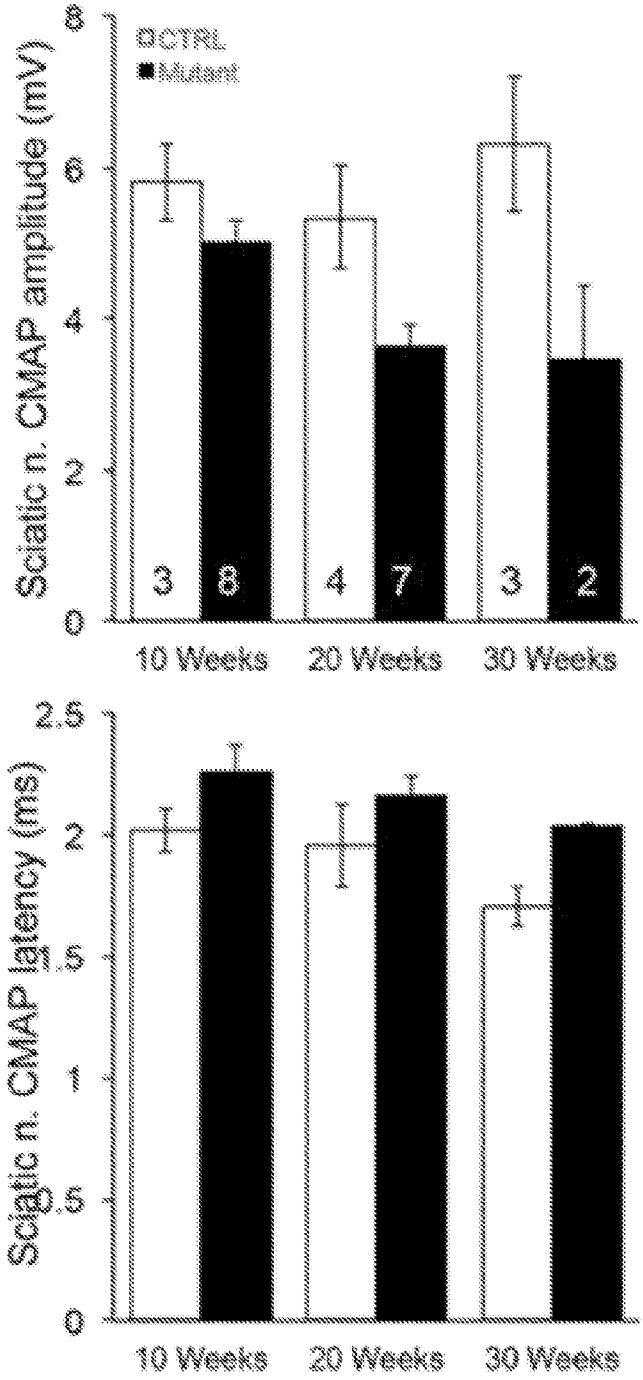
CTRL
Mutant
Sciatic n. CMAP amplitude (mV)
0
2
4
6
8
3
8
4
7
3
2
10 Weeks
20 Weeks
30 Weeks
Sciatic n. CMAP latency (ms)
0
0.5
1
1.5
2
2.5
10 Weeks
20 Weeks
30 Weeks

FIG. 57C

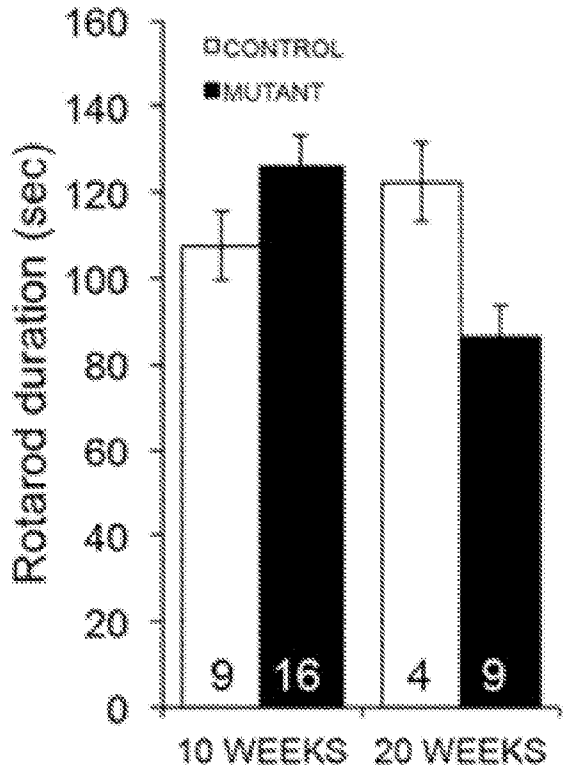

FIG. 57D

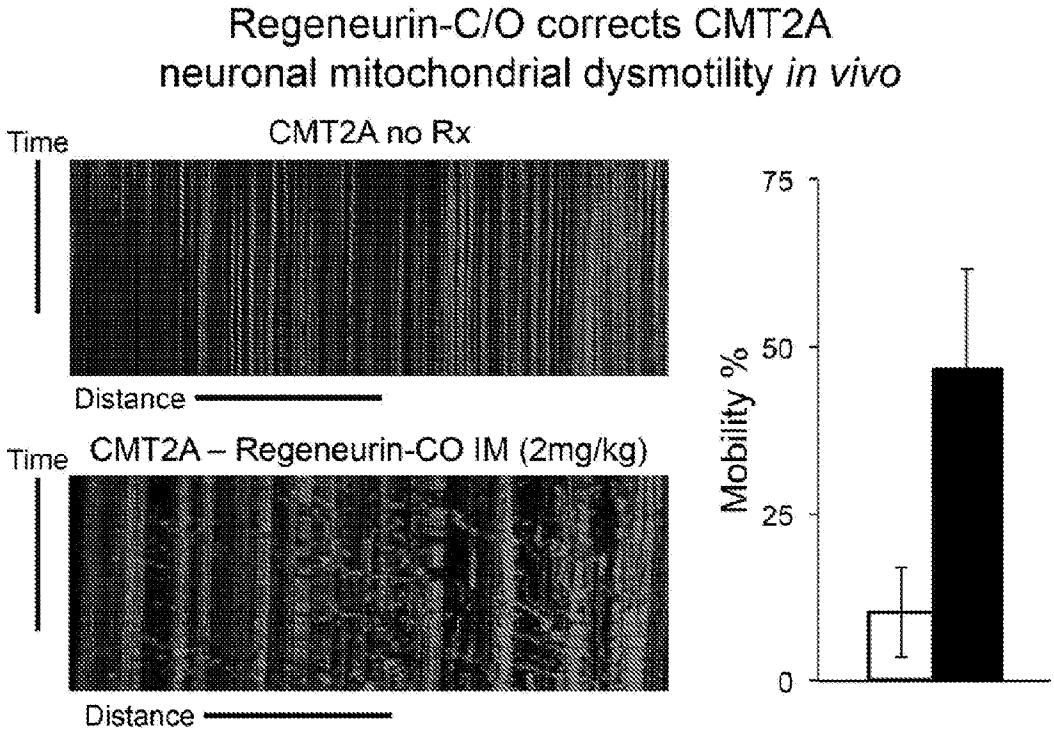

FIG. 58

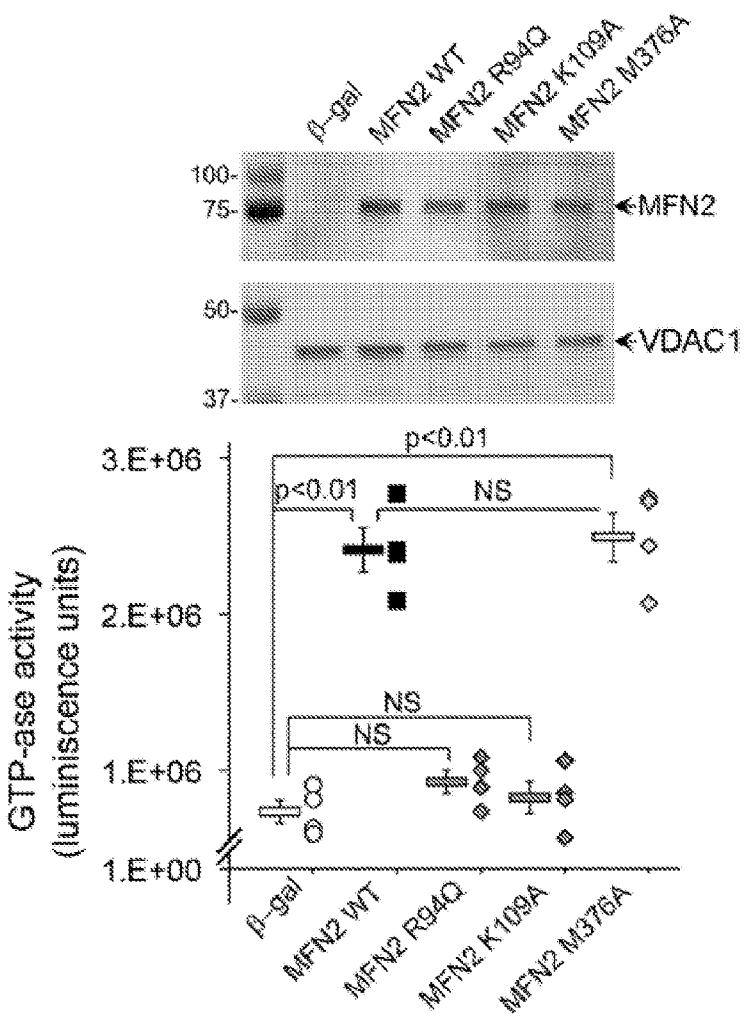
β-gal
MFN2 WT
MFN2 R94Q
MFN2 K109A
MFN2 M376A
100-
75-
MFN2
50-
VDAC1
37-
p<0.01
p<0.01
NS
NS
NS
3.E+06
2.E+06
1.E+06
1.E+00
GTP-ase activity
(luminiscence units)
β-gal
MFN2 WT
MFN2 R94Q
MFN2 K109A
MFN2 M376A

FIG. 59A

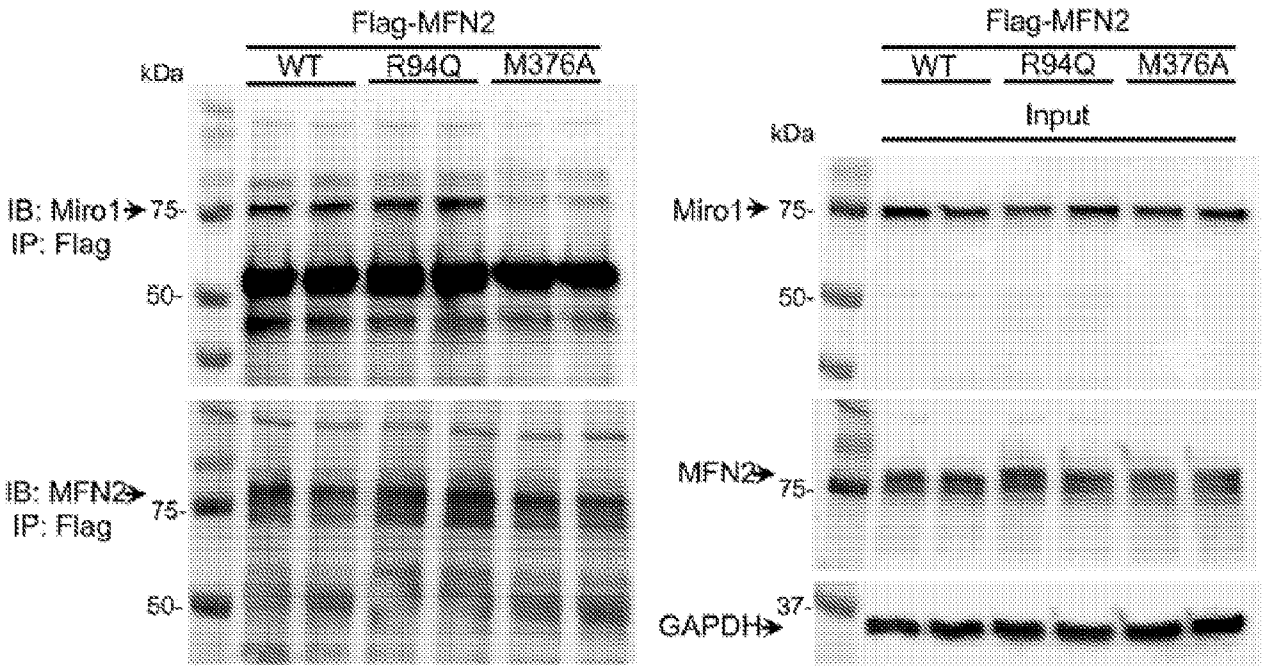
Flag-MFN2
WT
R94Q
M376A
kDa
IB: Miro1
IP: Flag
75-
50-
IB: MFN2
IP: Flag
75-
50-
Flag-MFN2
WT
R94Q
M376A
Input
kDa
Miro1
75-
50-
MFN2
75-
GAPDH
37-

FIG. 59B

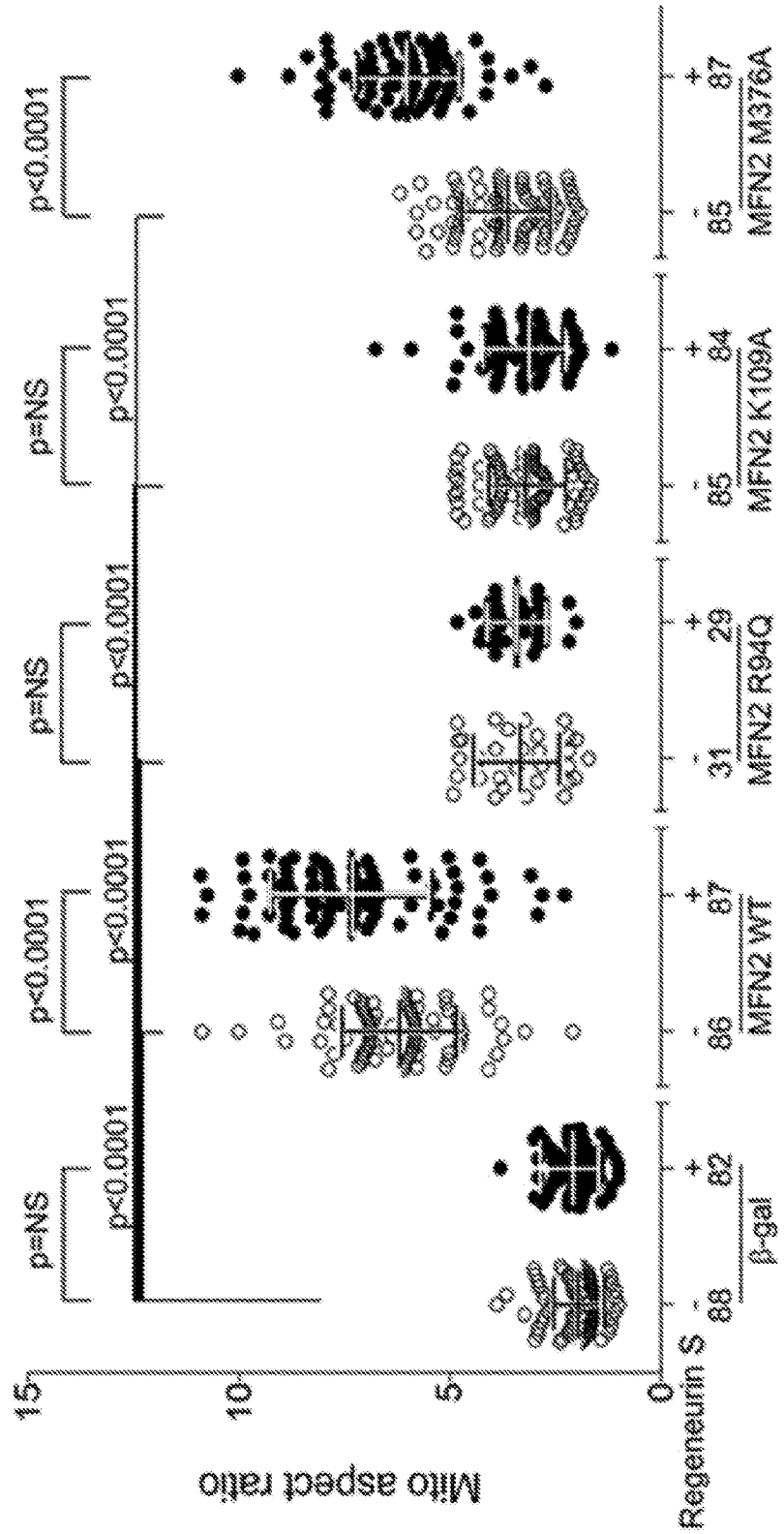
Mito aspect ratio
15
10
5
0
p=NS
p<0.0001
p<0.0001
p<0.0001
p=NS
p<0.0001
p=NS
p<0.0001
Regeneurin S
-
+
88
82
β-gal
-
+
86
87
MFN2 WT
-
+
31
29
MFN2 R94Q
-
+
85
84
MFN2 K109A
-
+
85
87
MFN2 M376A

FIG. 59C

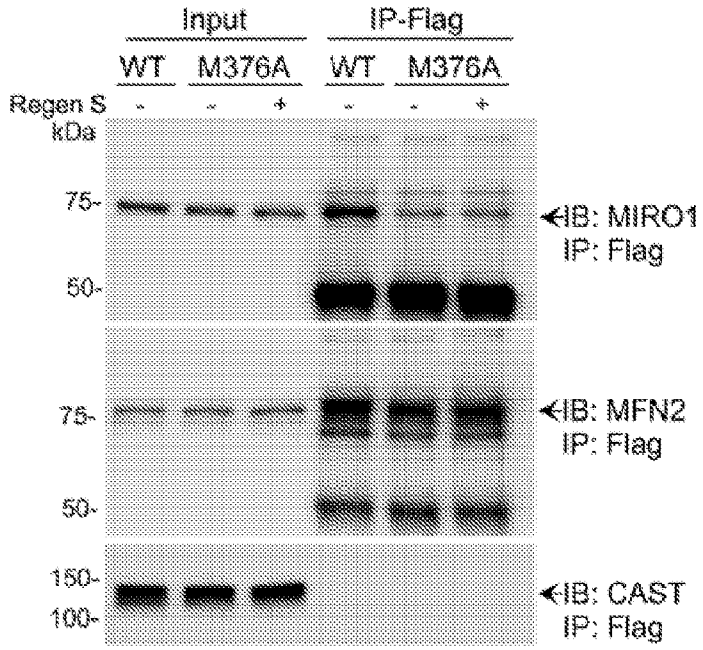

FIG. 59D

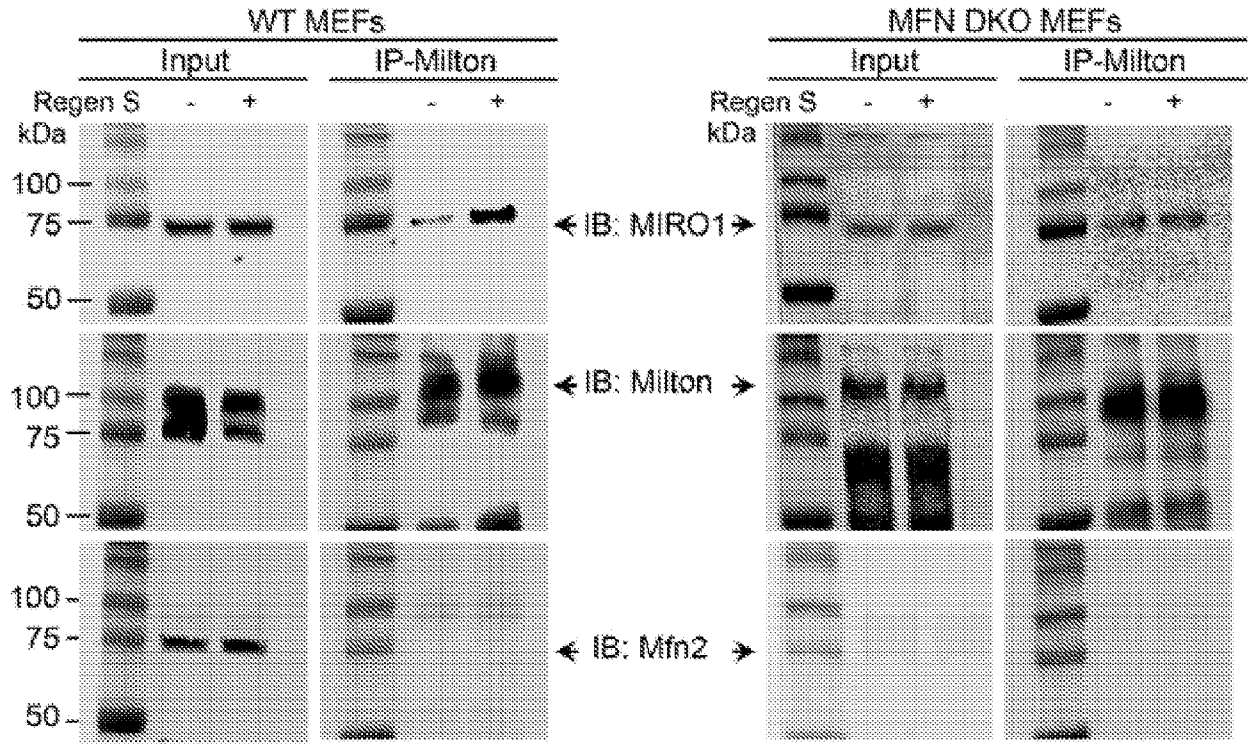

FIG. 59E

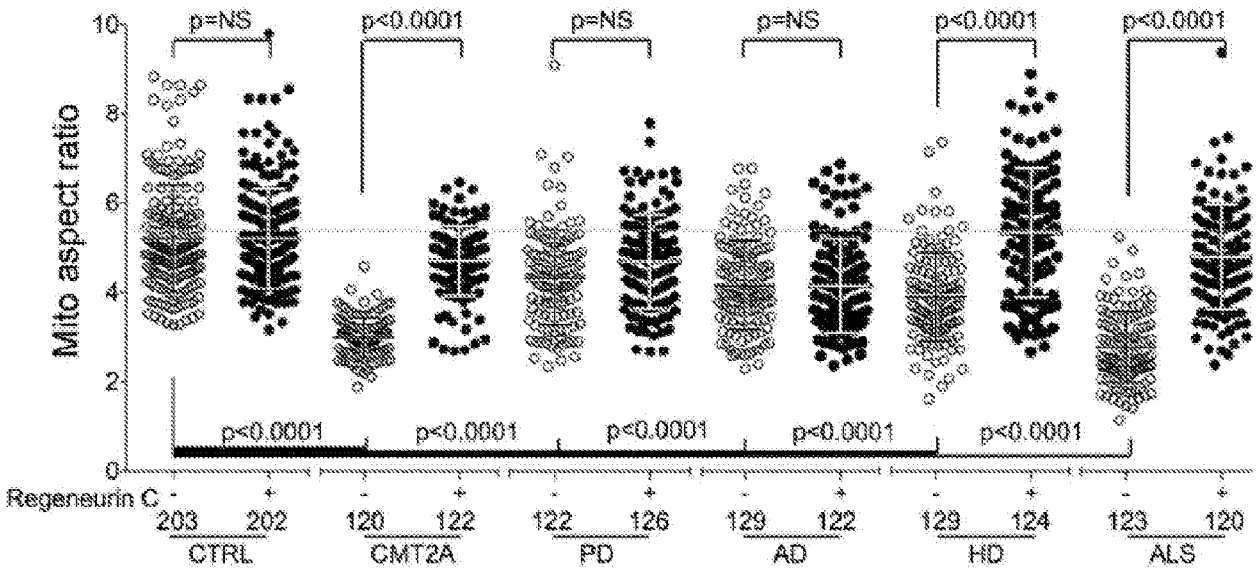

FIG. 60A

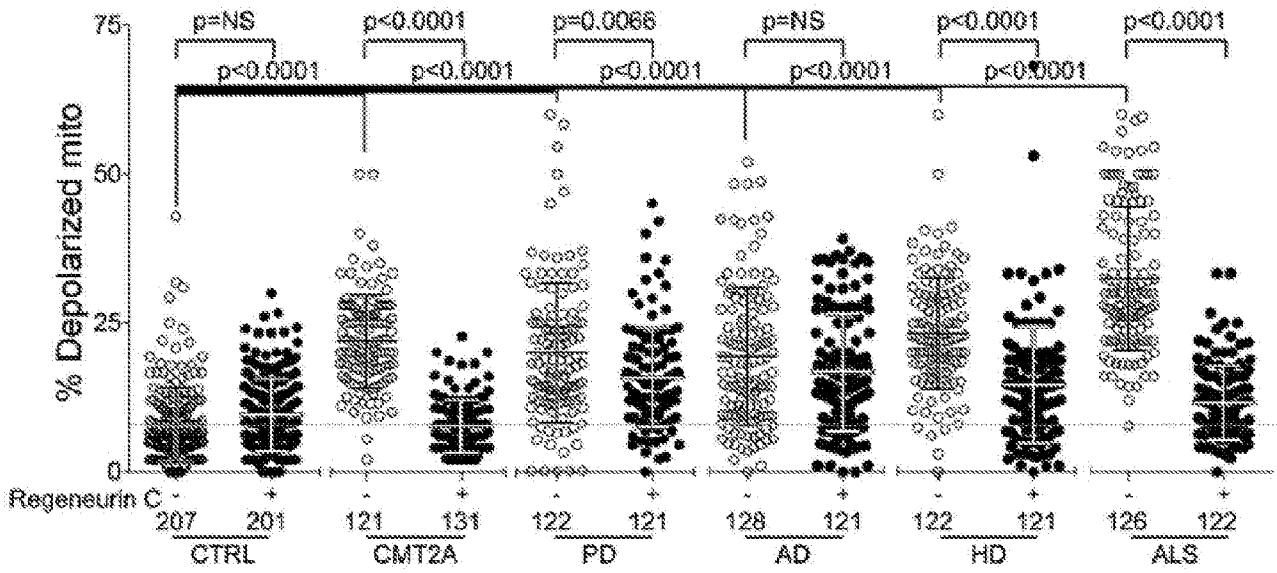

FIG. 60B

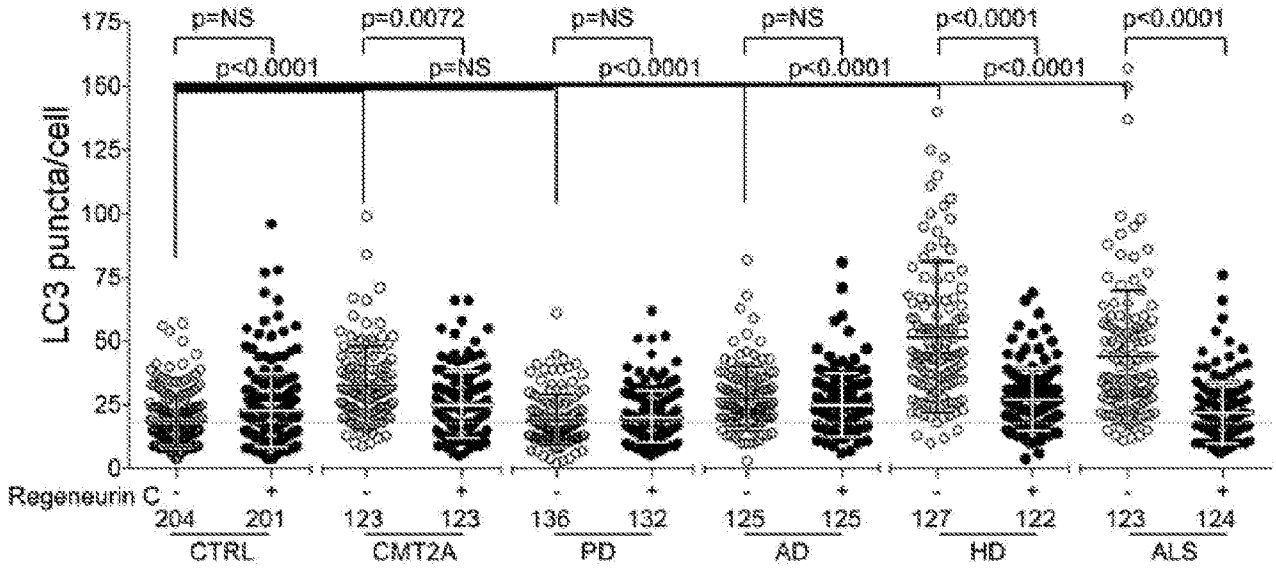

FIG. 60C

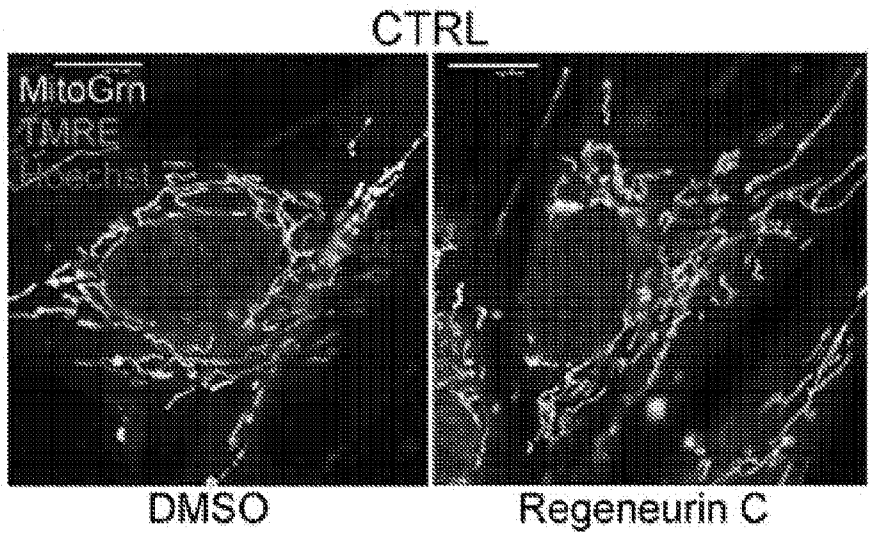

FIG. 60D

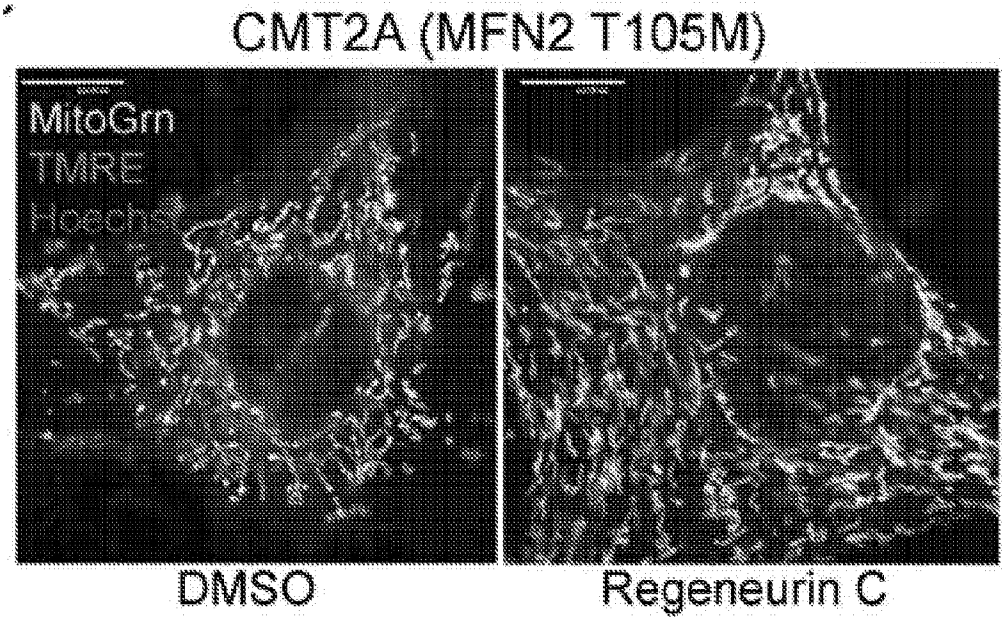

FIG. 60E

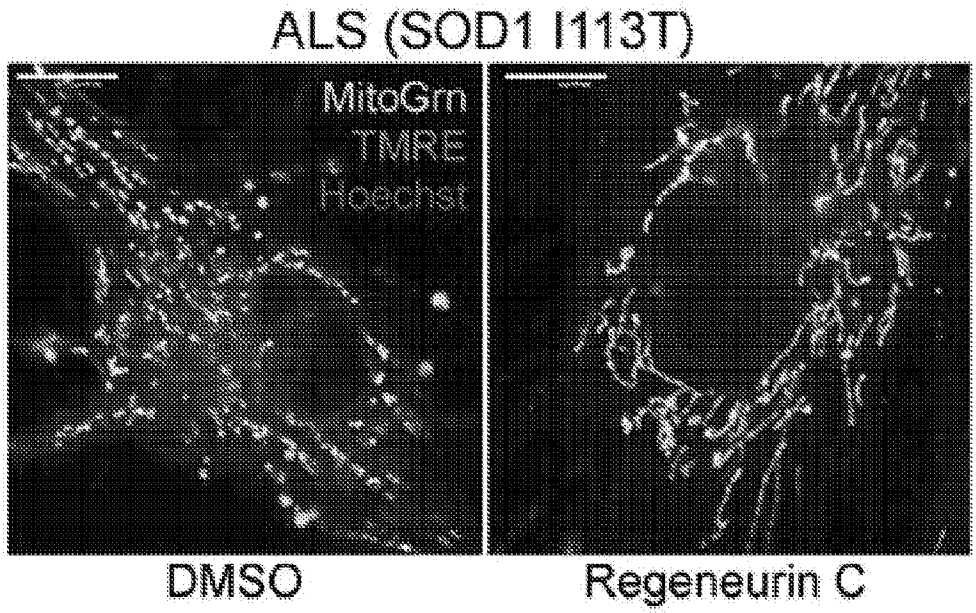

FIG. 60F

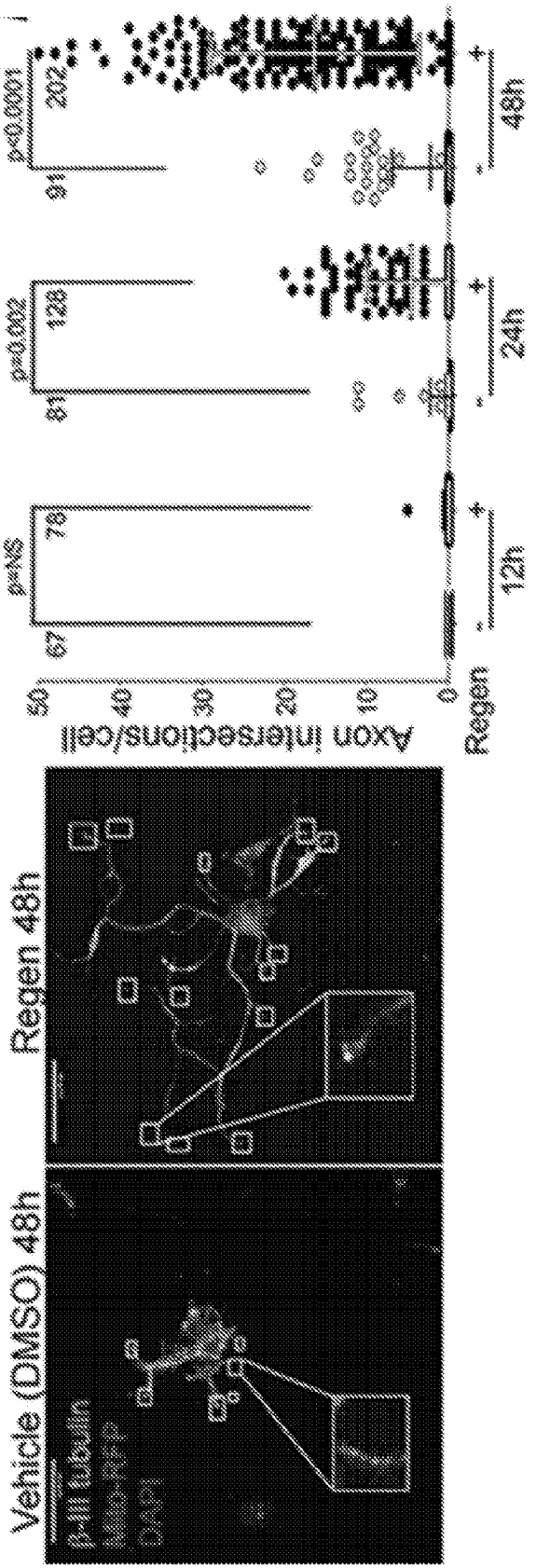
Axon intersections/cell
50
40
30
20
10
0
Regen
p=NS
67
78
12h
p=0.002
61
128
24h
p<0.0001
91
202
48h
Regen 48h
Vehicle (DMSO) 48h
β-III tubulin
GAP43
DAPI

FIG. 61A

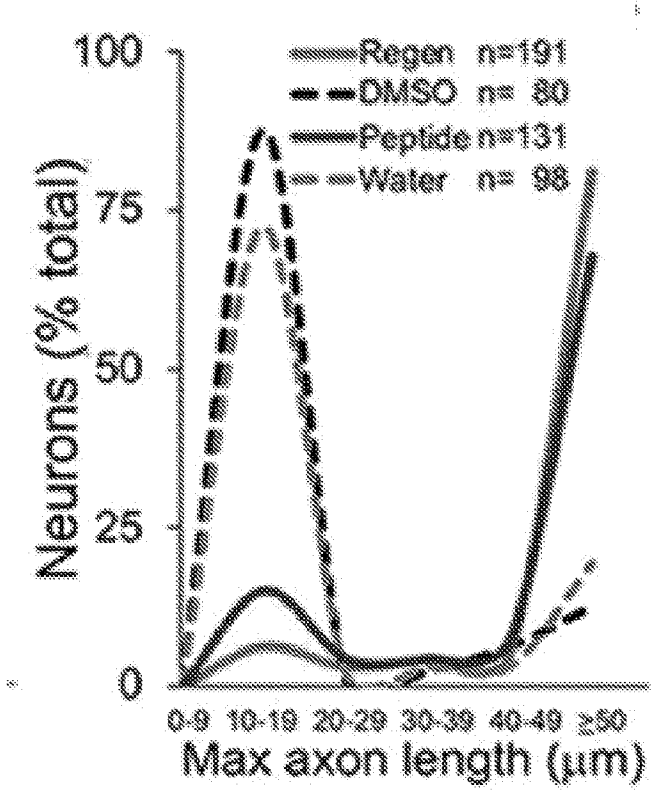

FIG. 61B

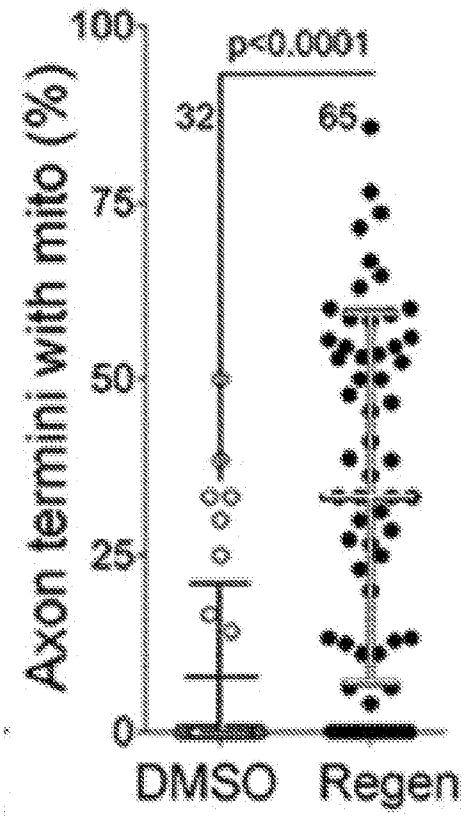

FIG. 61C

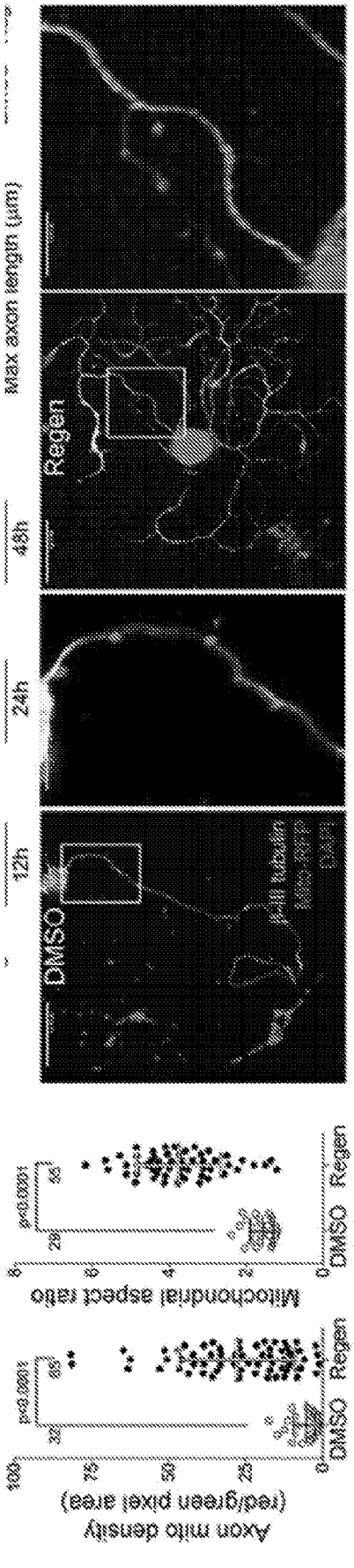
DMSO
Regen
12h
24h
48h
Max axon length (μm)
Axon mito density
(red/green pixel area)
Mitochondrial aspect ratio
p<0.0001
p<0.0001
DMSO
Regen

FIG. 61D

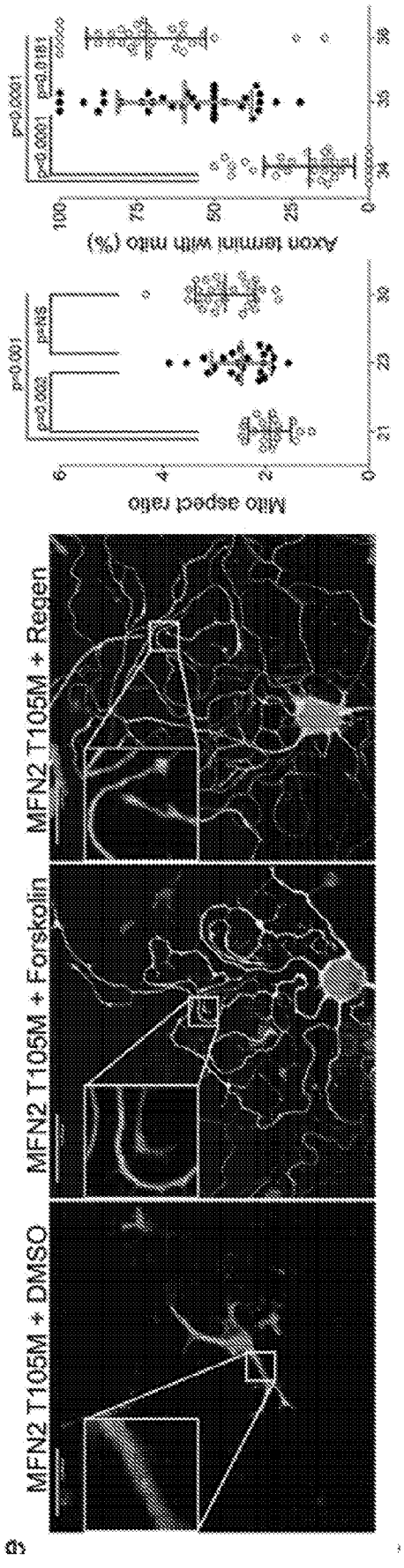
MFN2 T105M + DMSO
MFN2 T105M + Forskolin
MFN2 T105M + Regen
Mito aspect ratio
Axon lemmt with mito (%)

FIG. 61E

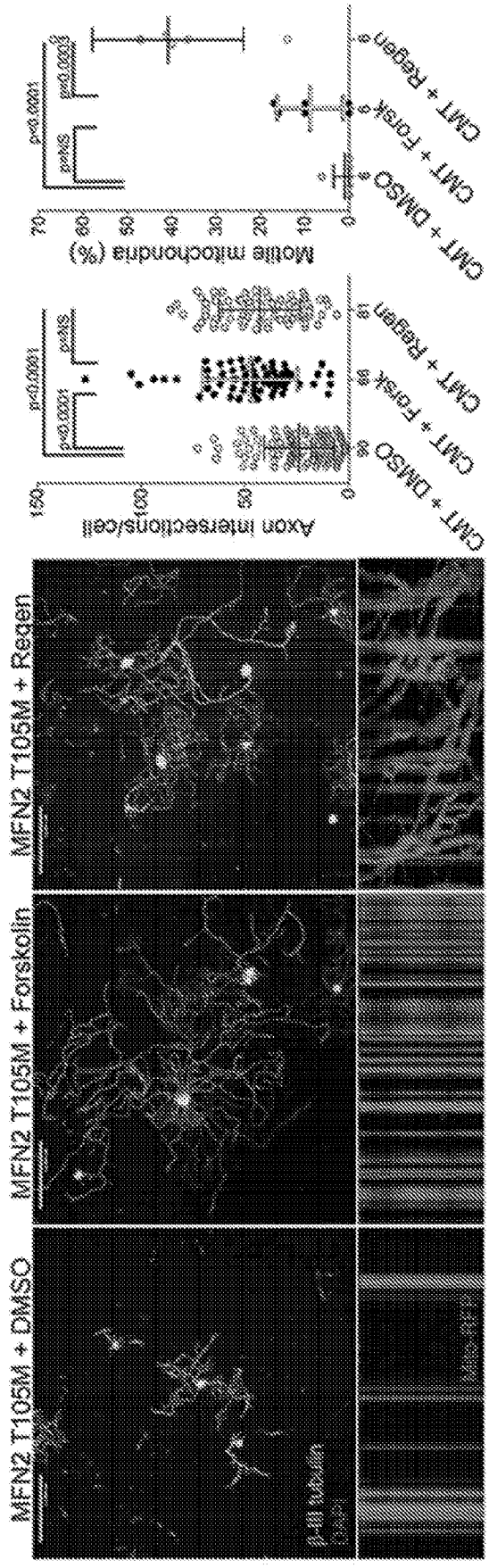
MFN2 T105M + DMSO
MFN2 T105M + Forskolin
MFN2 T105M + Regen
CMT + DMSO
CMT + Forsk
CMT + Regen
Axon intersections/cell
Motile mitochondria (%)
p<0.0001
p=NS

FIG. 61F

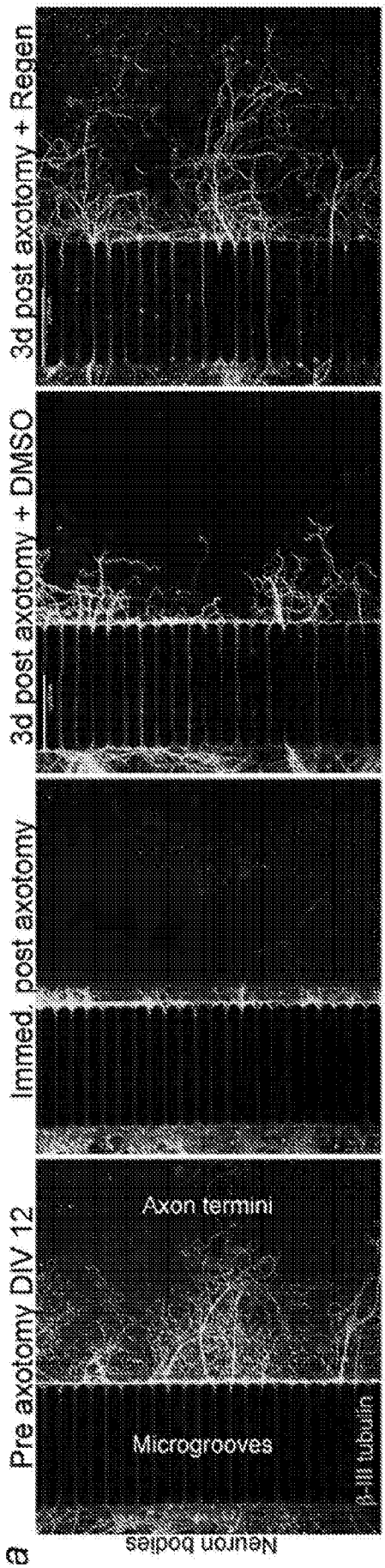
3d post axotomy + Regen
3d post axotomy + DMSO
Immed. post axotomy
Pre axotomy DIV 12
Axon termini
Microgrooves
β-III tubulin
Neuron bodies
a

FIG. 62A

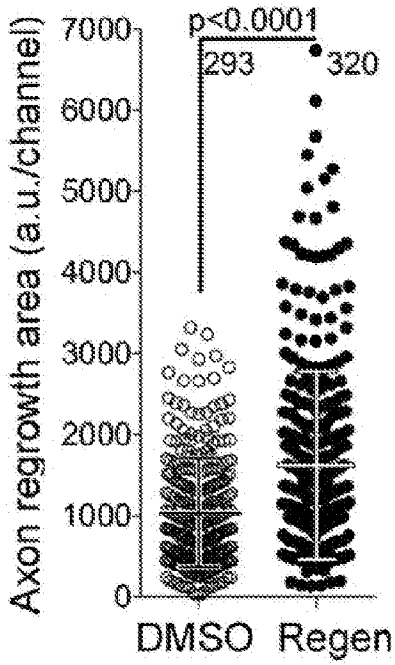

FIG. 62B

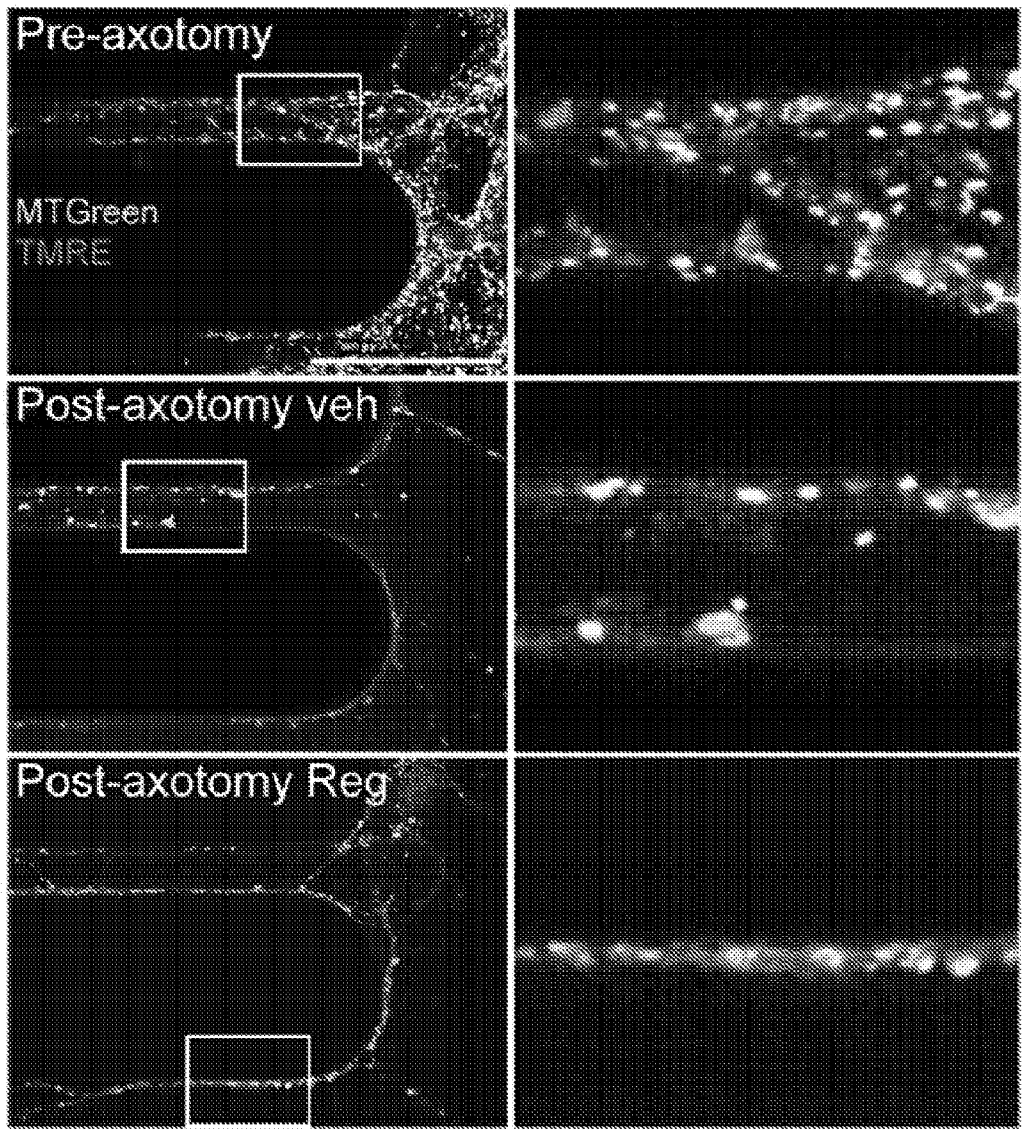

FIG. 62C

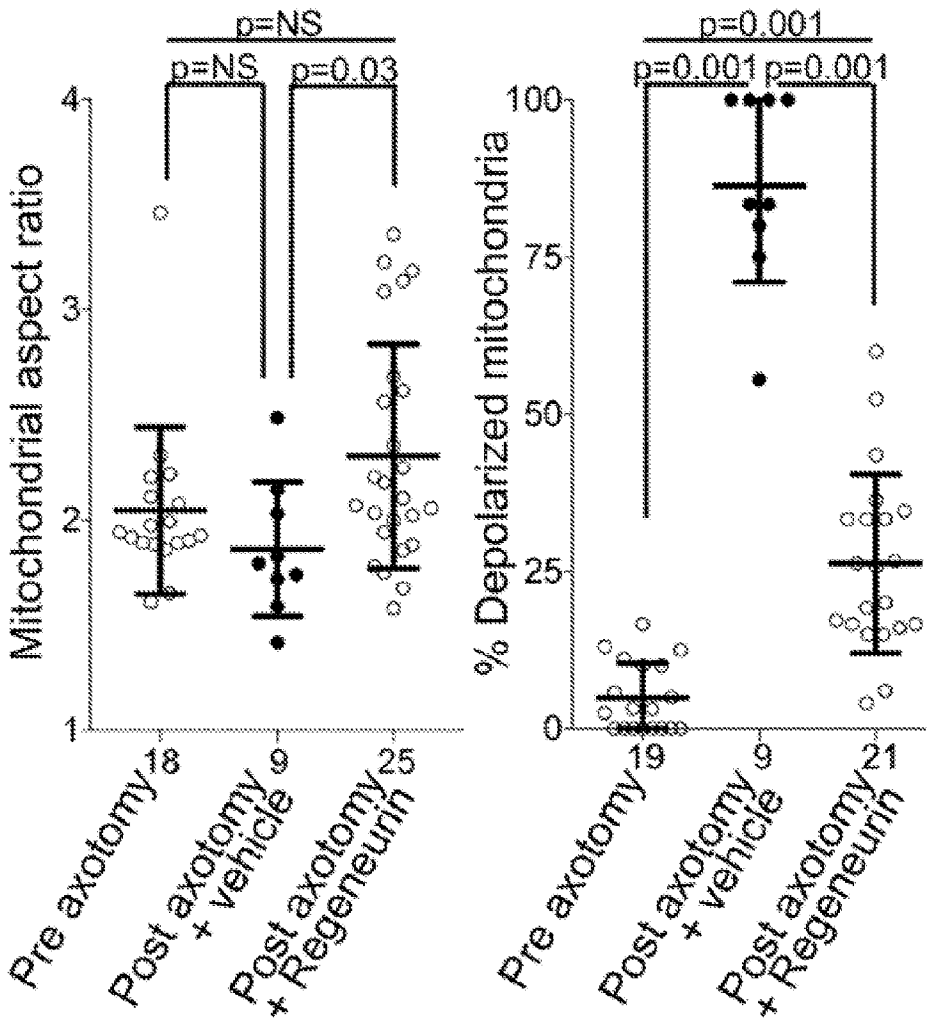
p=NS
p=NS
p=0.03
Mitochondrial aspect ratio
4
3
2
1
18
9
25
Pre axotomy
Post axotomy + vehicle
Post axotomy + Regeneurin
p=0.001
p=0.001
p=0.001
% Depolarized mitochondria
100
75
50
25
0
19
9
21
Pre axotomy
Post axotomy + vehicle
Post axotomy + Regeneurin

FIG. 62D

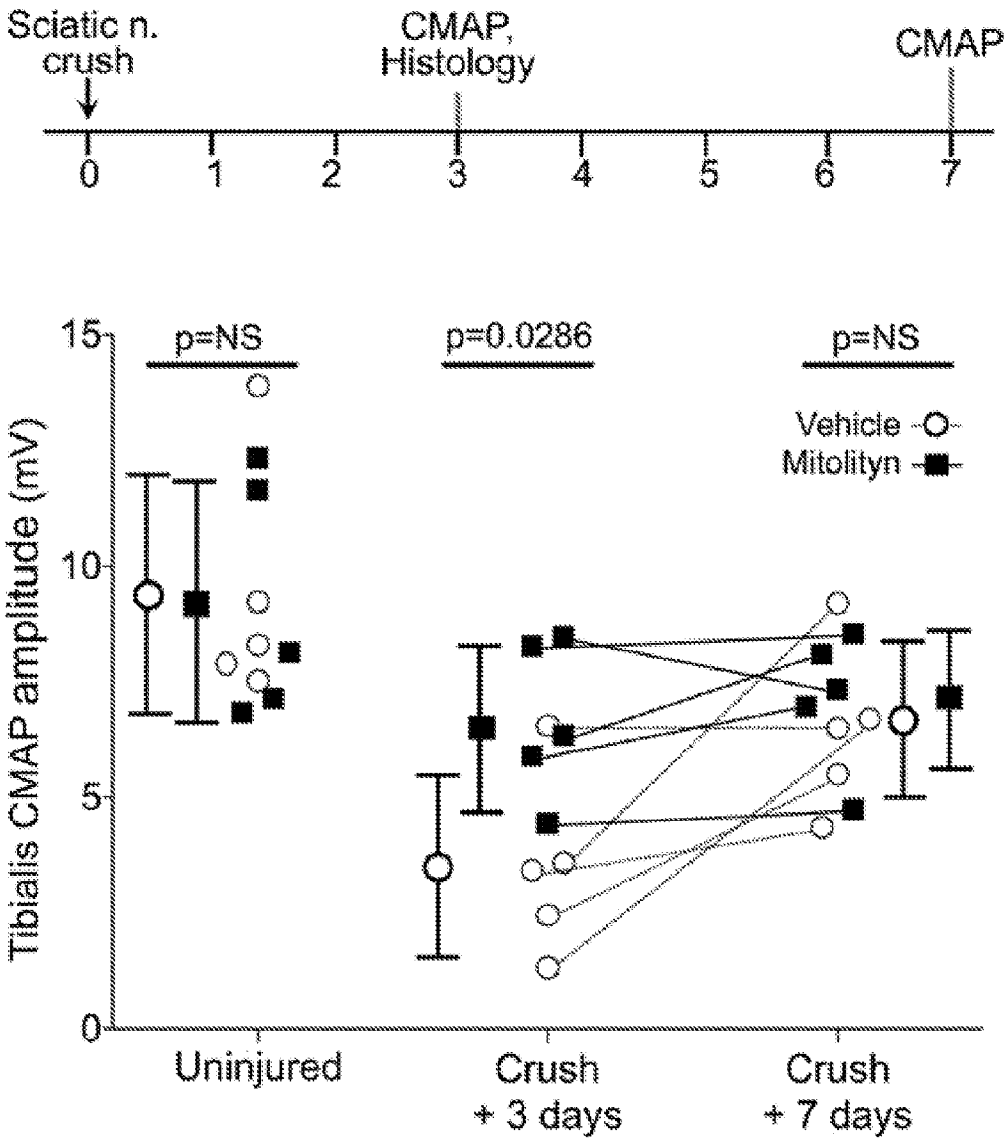
Sciatic n. crush
CMAP, Histology
CMAP
0
1
2
3
4
5
6
7
p=NS
p=0.0286
p=NS
Vehicle
Mitolityn
Tibialis CMAP amplitude (mV)
15
10
5
0
Uninjured
Crush + 3 days
Crush + 7 days

FIG. 62E

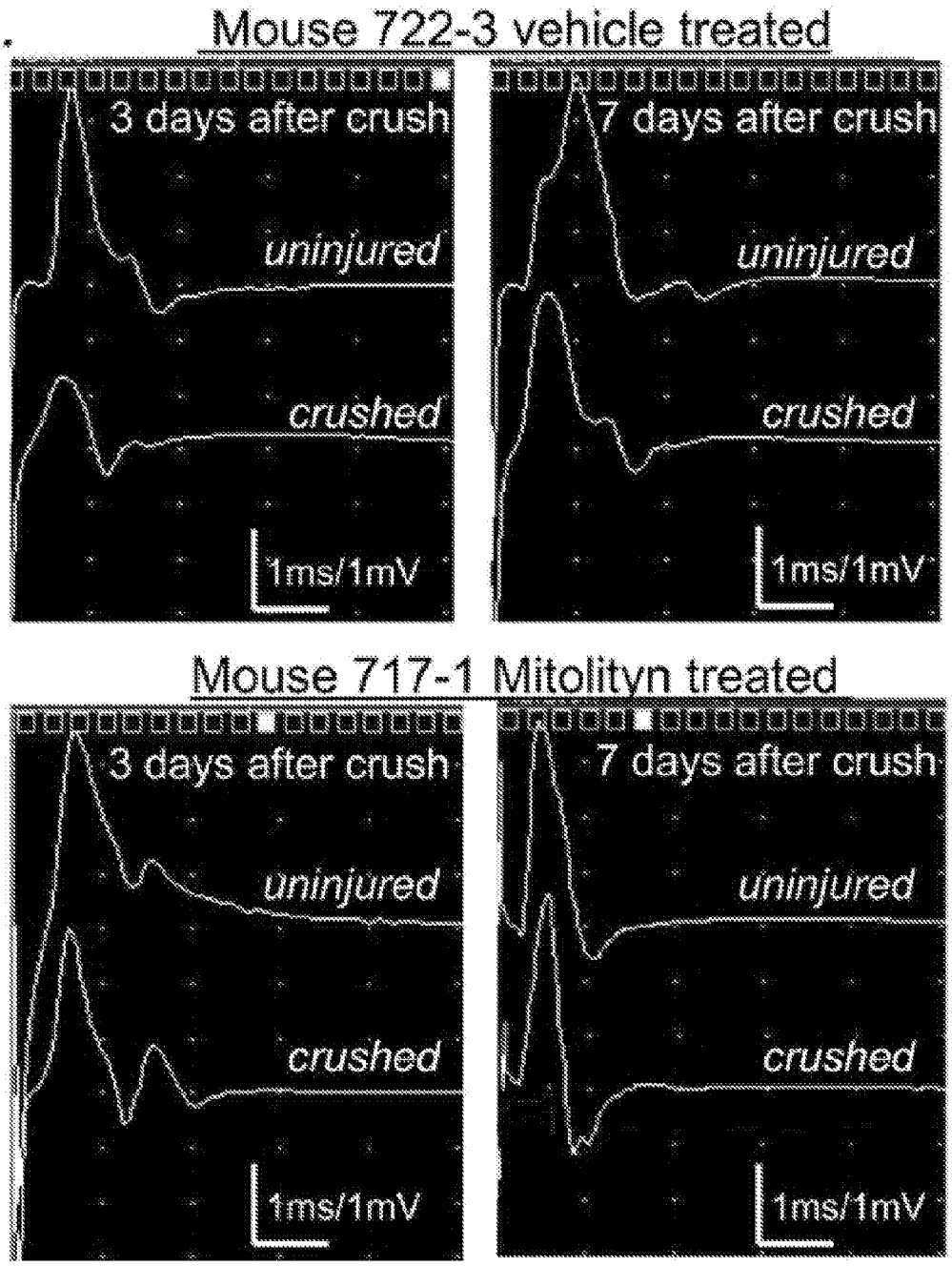
Mouse 722-3 vehicle treated
3 days after crush
uninjured
crushed
1ms/1mV
7 days after crush
uninjured
crushed
1ms/1mV
Mouse 717-1 Mitolityn treated
3 days after crush
uninjured
crushed
1ms/1mV
7 days after crush
uninjured
crushed
1ms/1mV

FIG. 62F

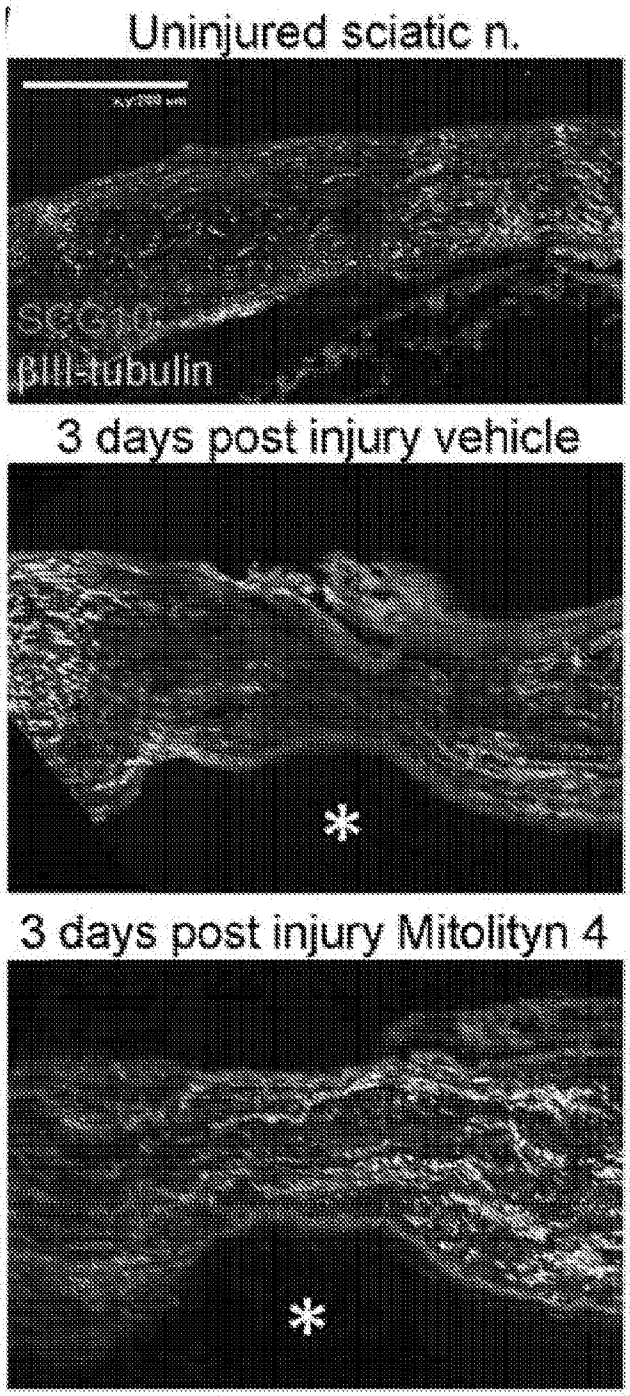
Uninjured sciatic n.
βIII-tubulin
3 days post injury vehicle
*
3 days post injury Mitolityn 4
*

FIG. 62G

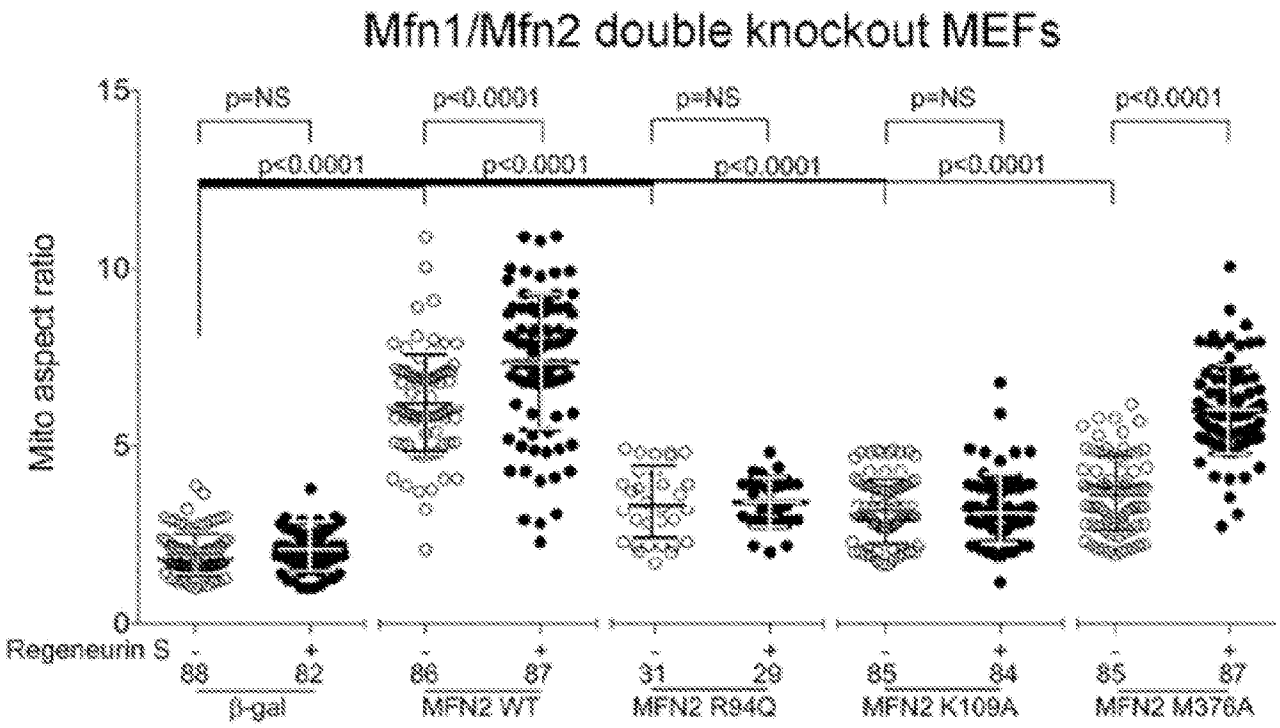

FIG. 63A

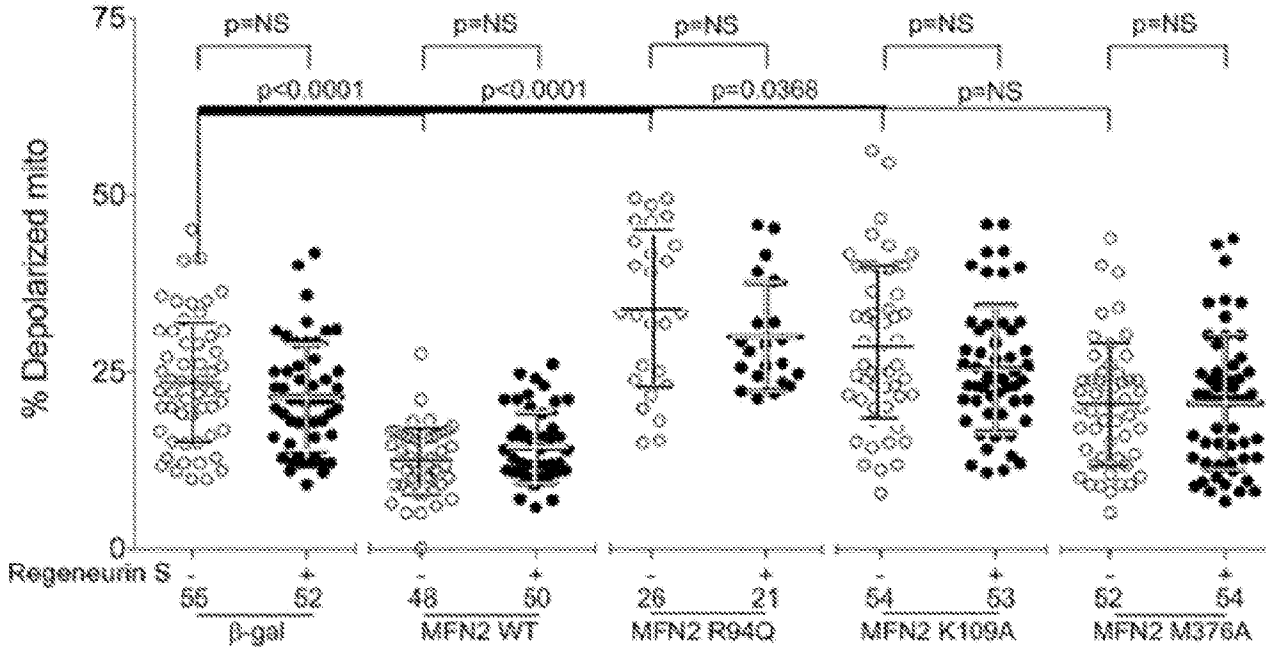

FIG. 63B

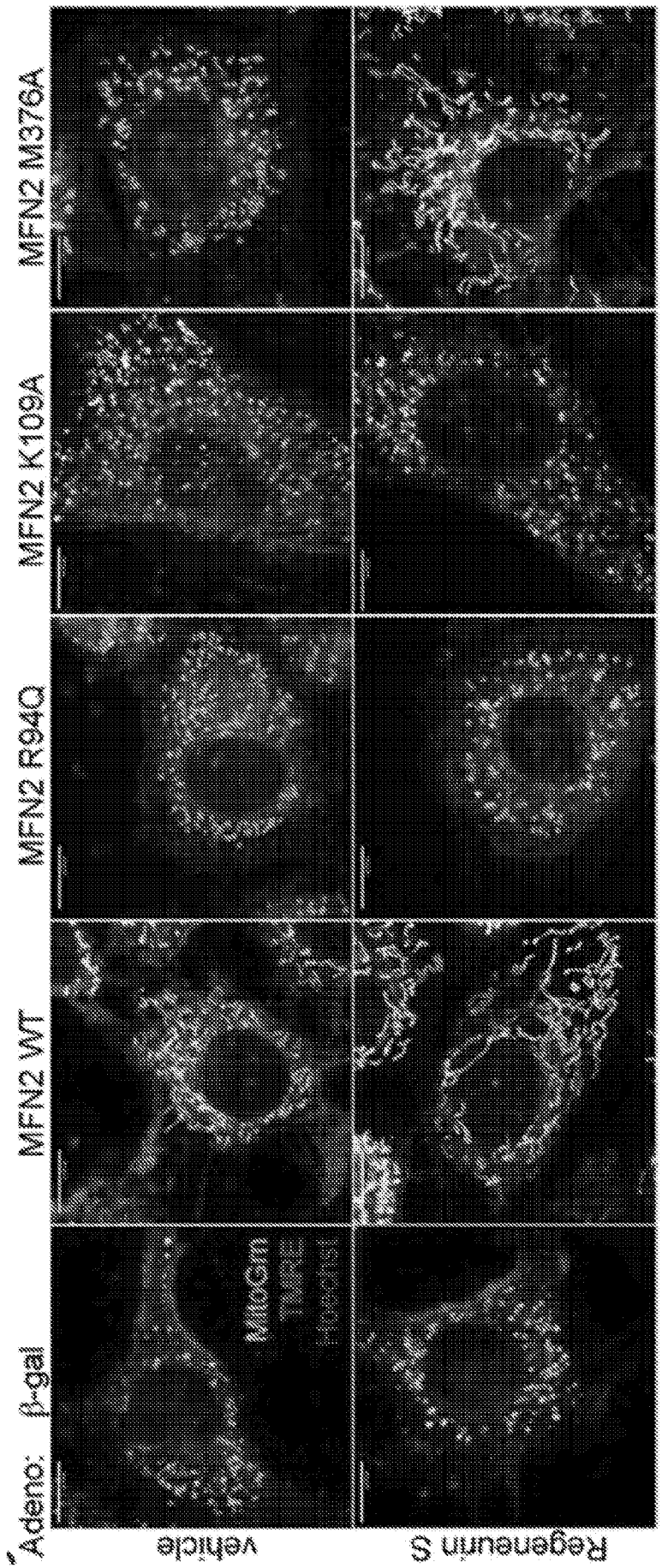
Adeno:
β-gal
MitoGm
TUNEL
Hoechst
MFN2 WT
MFN2 R94Q
MFN2 K109A
MFN2 M376A
vehicle
Regenerin S

FIG. 63C

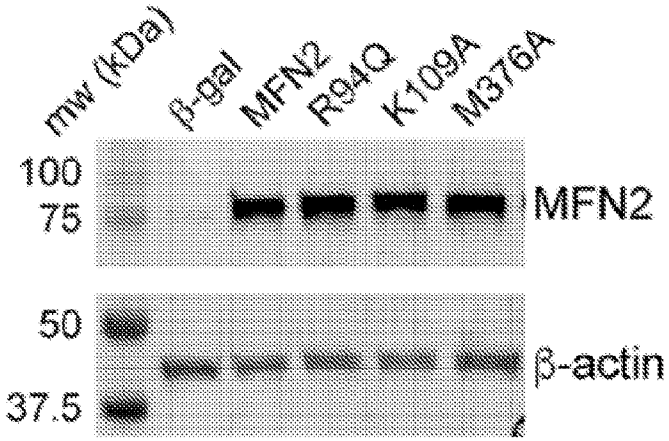

FIG. 64A

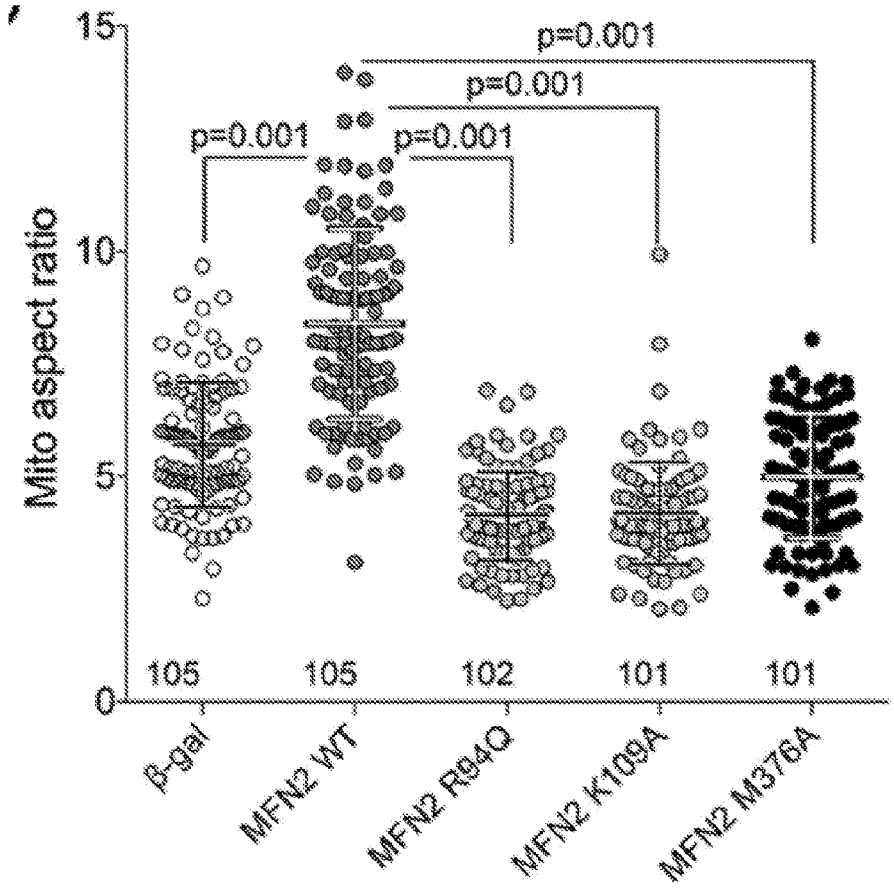

FIG. 64B

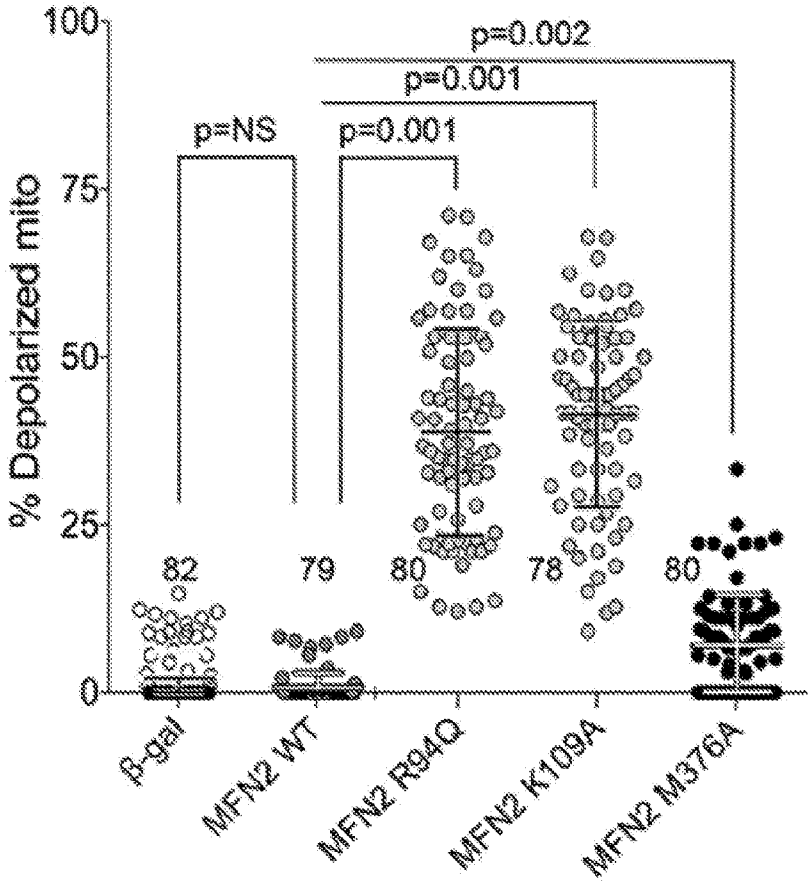
100
75
50
25
0
% Depolarized mito
p=0.002
p=0.001
p=NS
p=0.001
82
79
80
78
80
β-gal
MFN2 WT
MFN2 R94Q
MFN2 K109A
MFN2 M376A

FIG. 64C

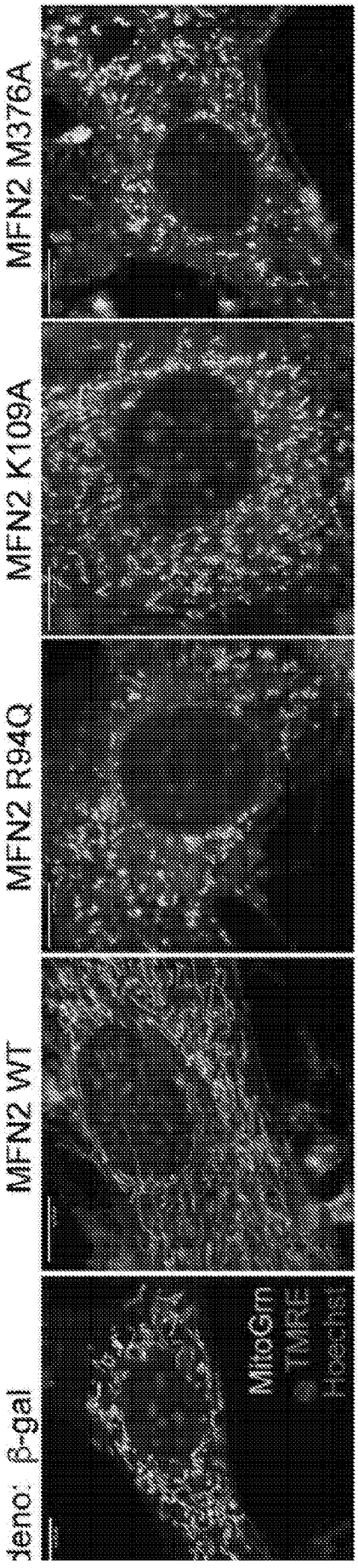
Adeno: β-gal
MFN2 WT
MFN2 R94Q
MFN2 K109A
MFN2 M376A
MitoGm
TMRE
Hoechst

FIG. 64D

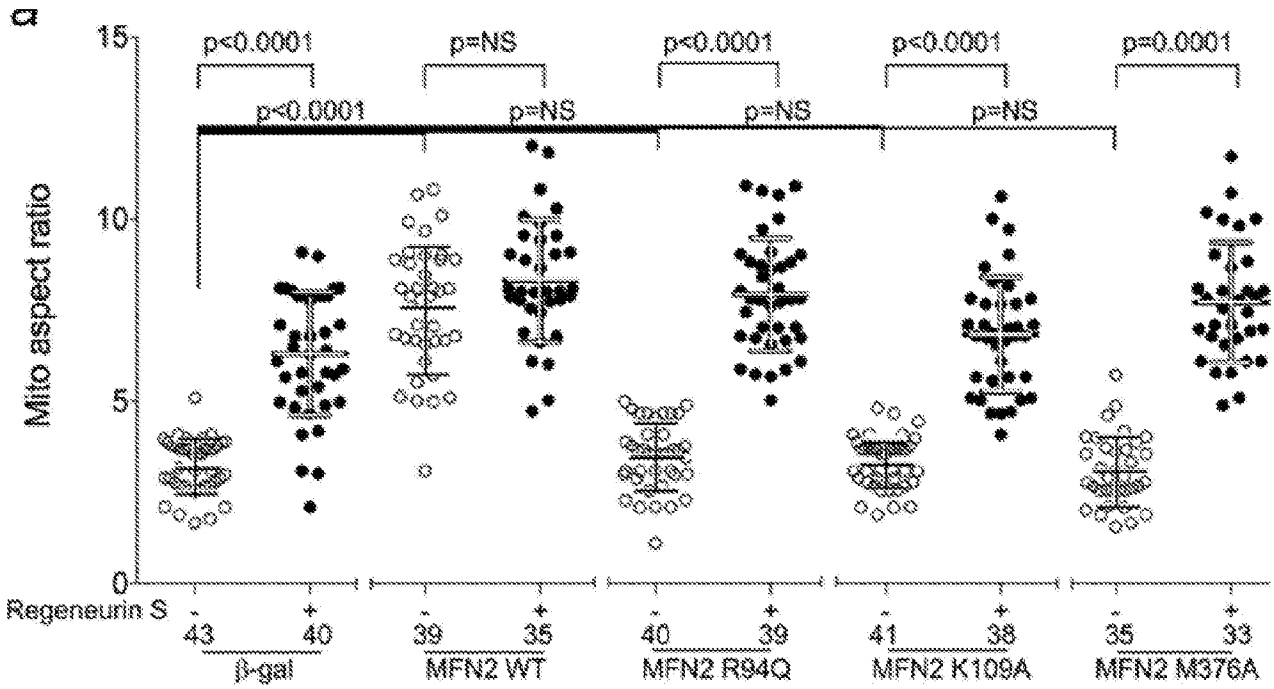

FIG. 65A

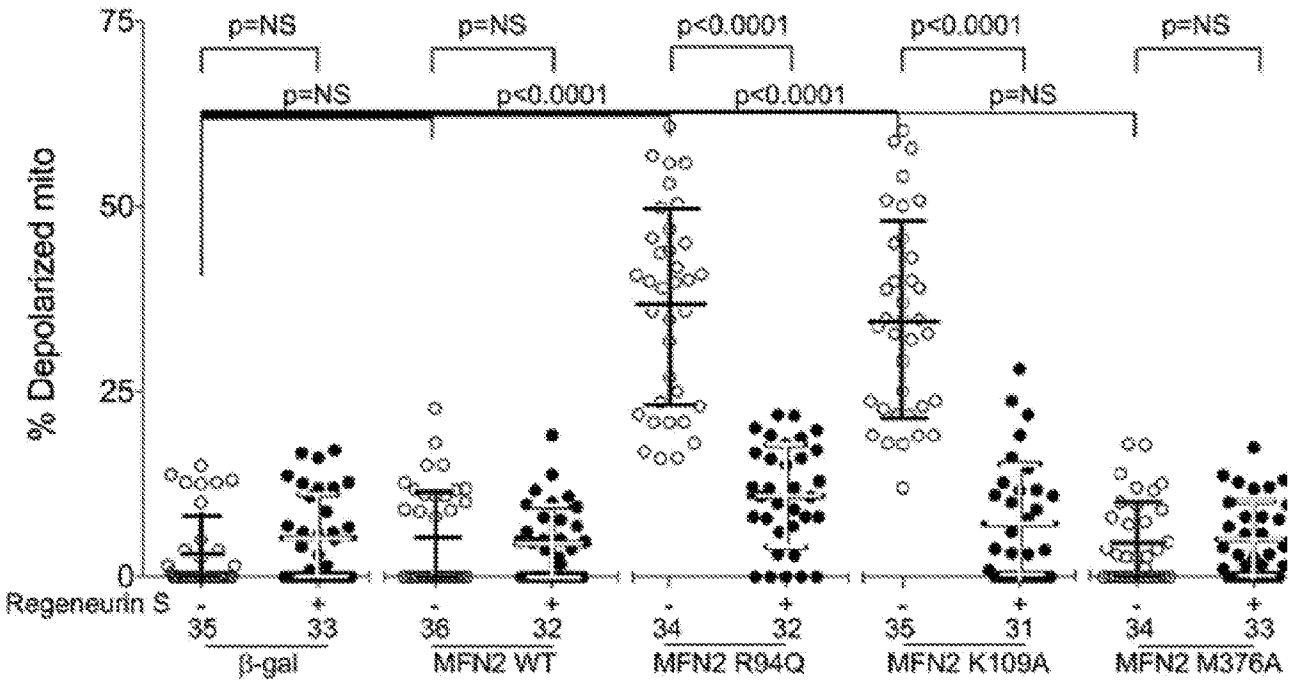

FIG. 65B

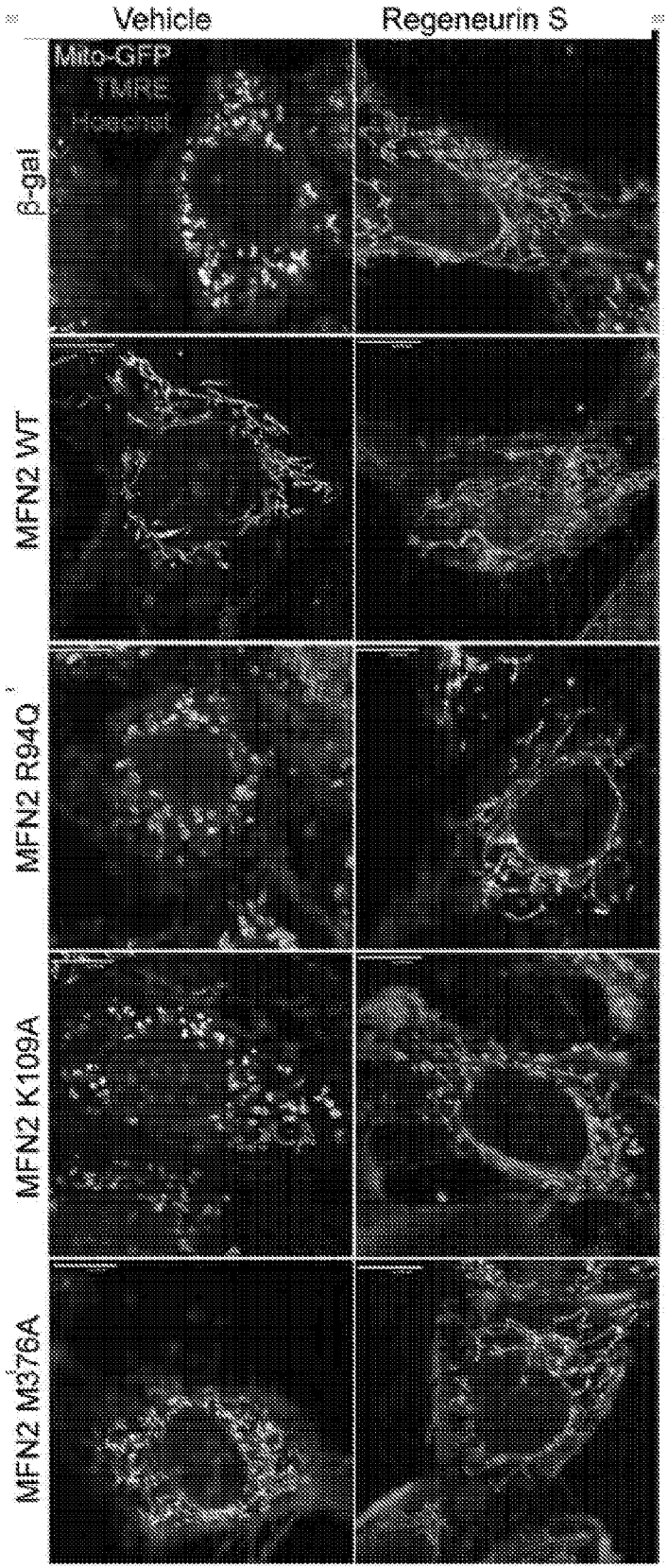
Vehicle
Regeneurin S
Mito-GFP
TMRE
Hoechst
β-gal
MFN2 WT
MFN2 R94Q
MFN2 K109A
MFN2 M376A

FIG. 65C

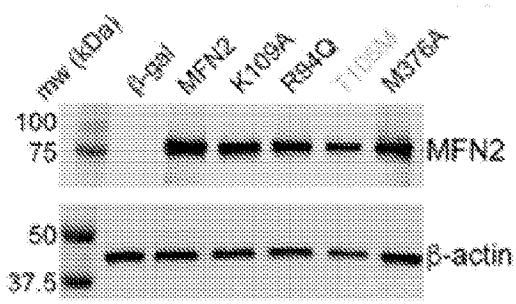

FIG. 66A

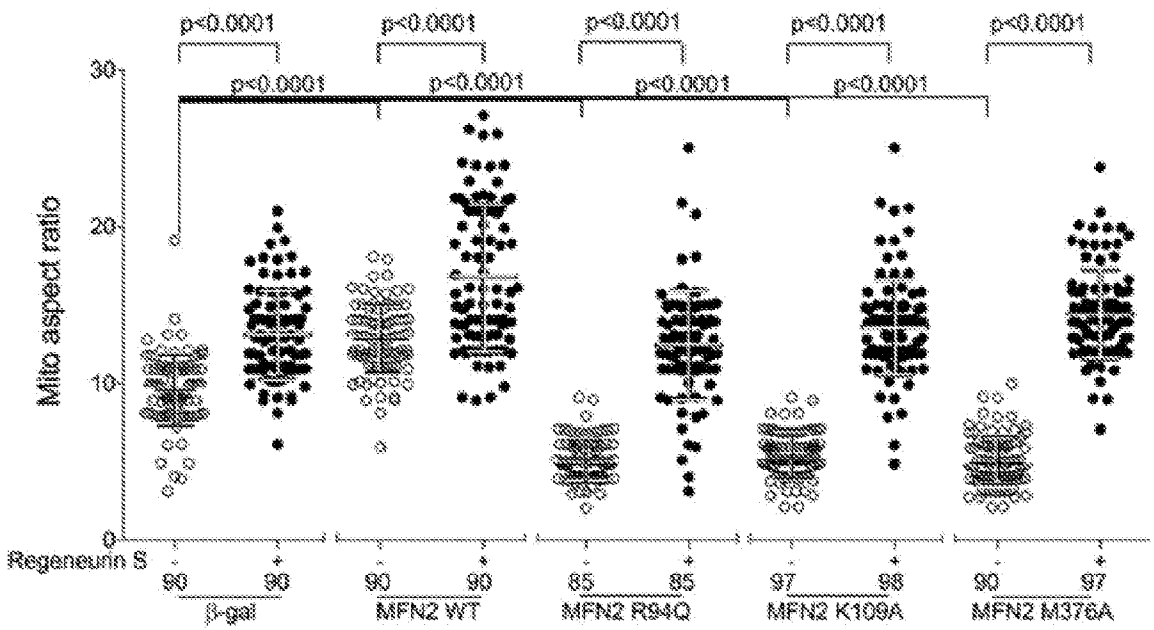

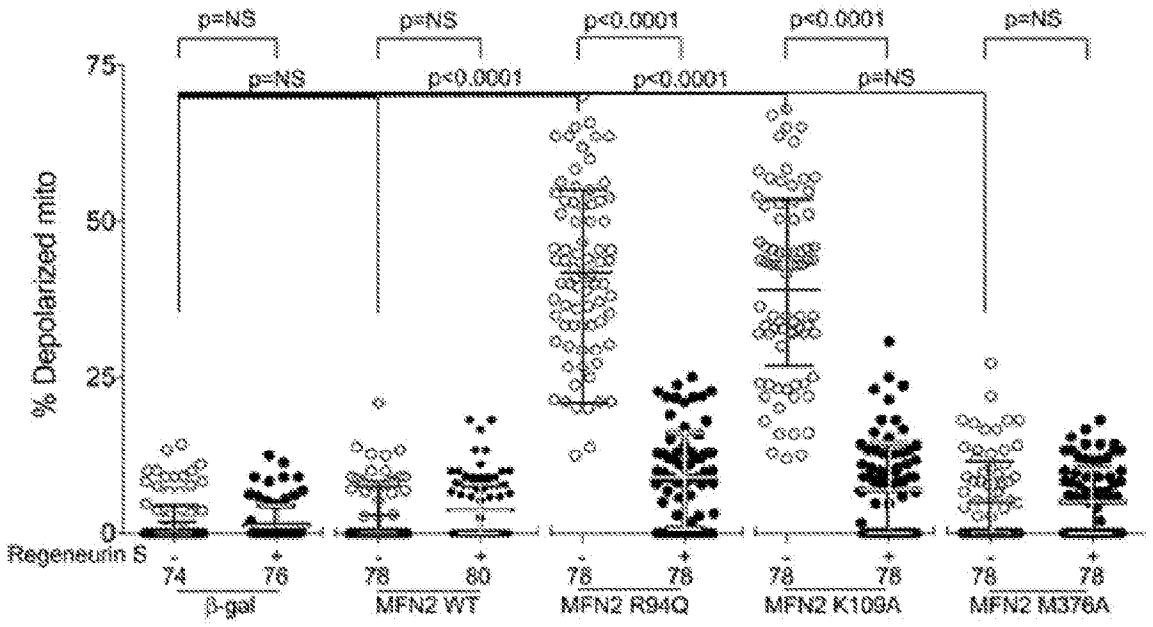

FIG. 66B

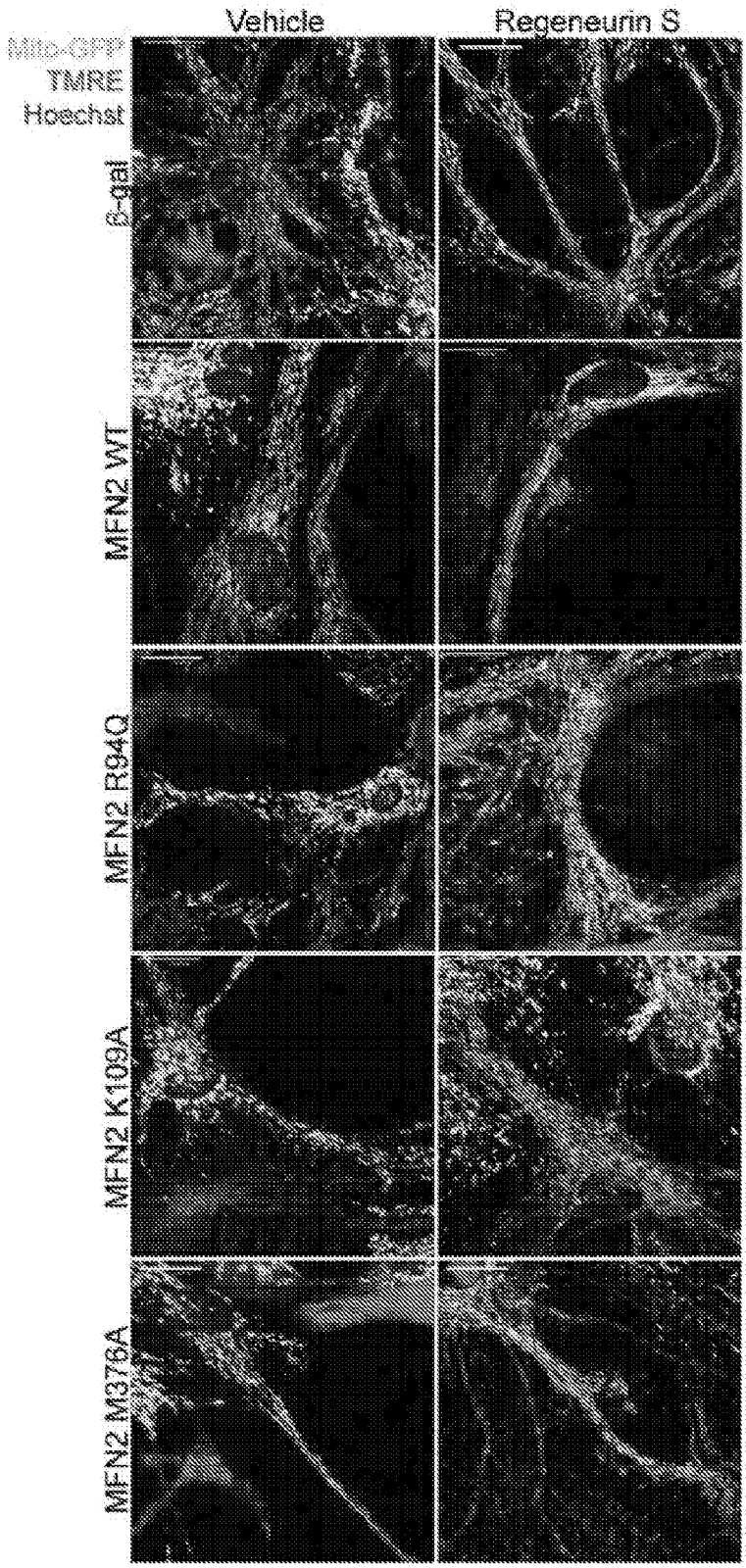
Vehicle
Regeneurin S
Mito-GFP
TMRM
Hoechst
β-gal
MFN2 WT
MFN2 R94Q
MFN2 K109A
MFN2 M376A

FIG. 66C

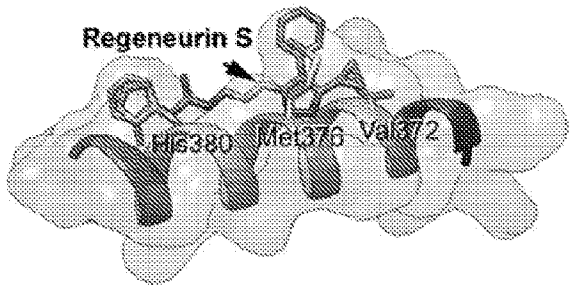

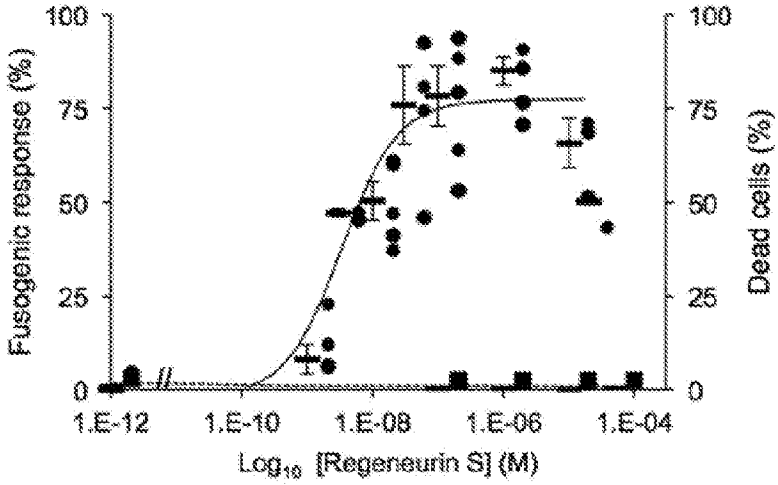

FIG. 67A

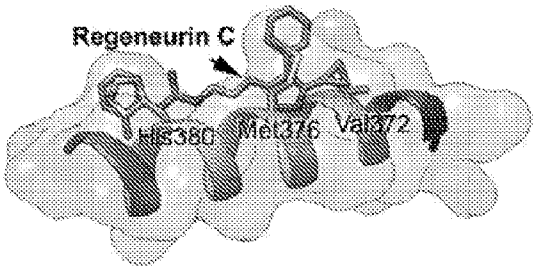

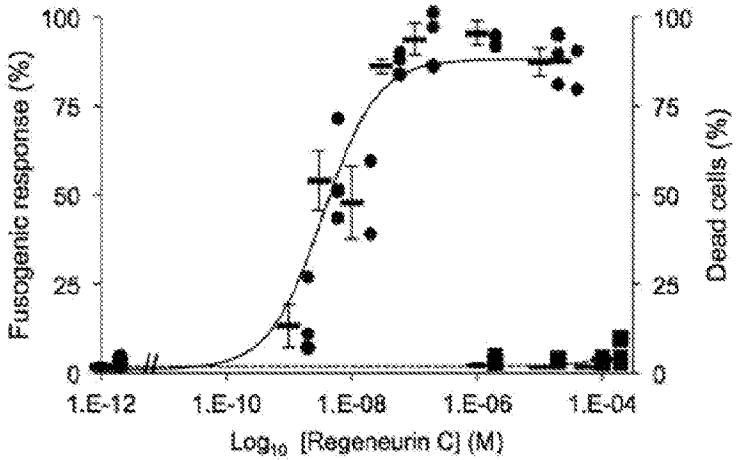

FIG. 67B

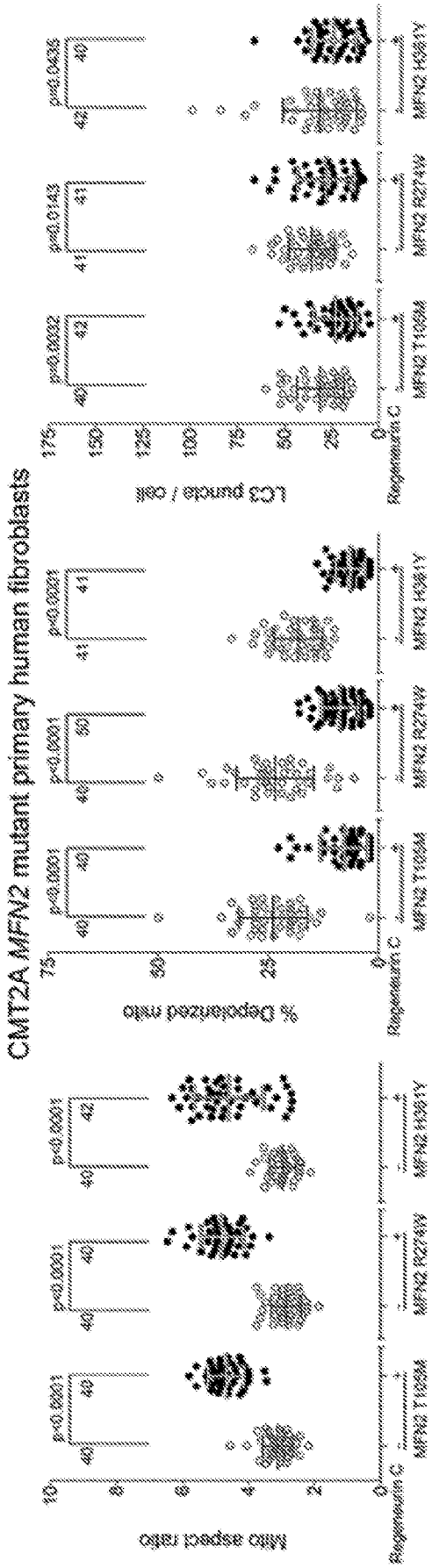
CMT2A MFN2 mutant primary human fibroblasts
Ratio aspect ratio
% Depolarized mito
LC3 puncta / cell
Rapamycin
MFN2 T105M
MFN2 R274W
MFN2 H361Y
p<0.0001
p=0.0032
p=0.0143
p=0.0436
p=0.0021

FIG. 68A

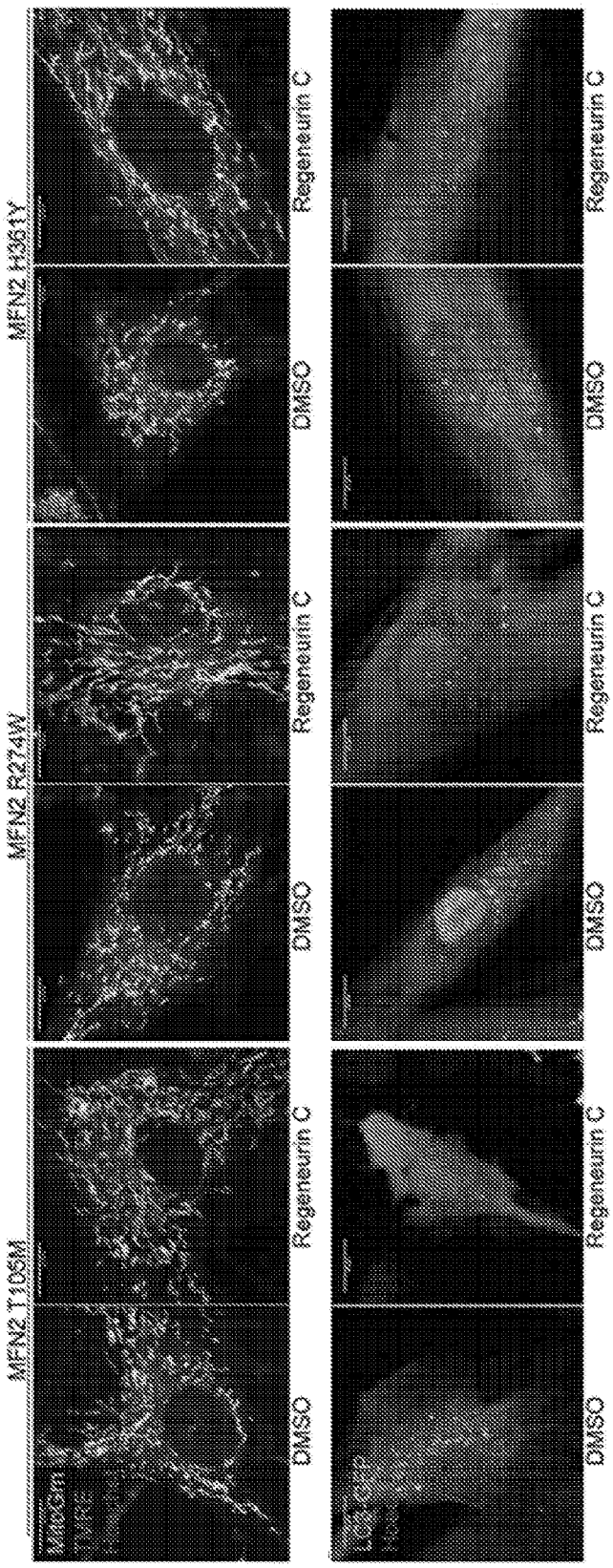

FIG. 68B

FIG. 68C

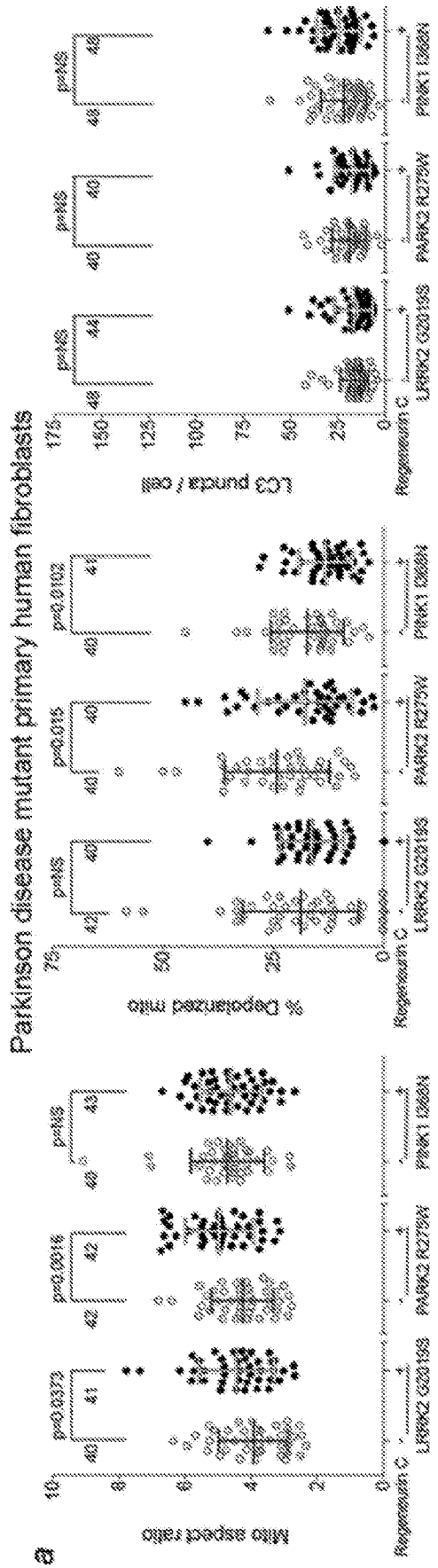
a
Parkinson disease mutant primary human fibroblasts
Mito aspect ratio
% Depolarized mito
LC3 puncta / cell
Rotenone C
LRRK2 G2019S
PARK2 R275W
PINK1 E98IN
p=0.0373
p=0.0016
p=0.015
p=0.0103
p=NS

FIG. 69A

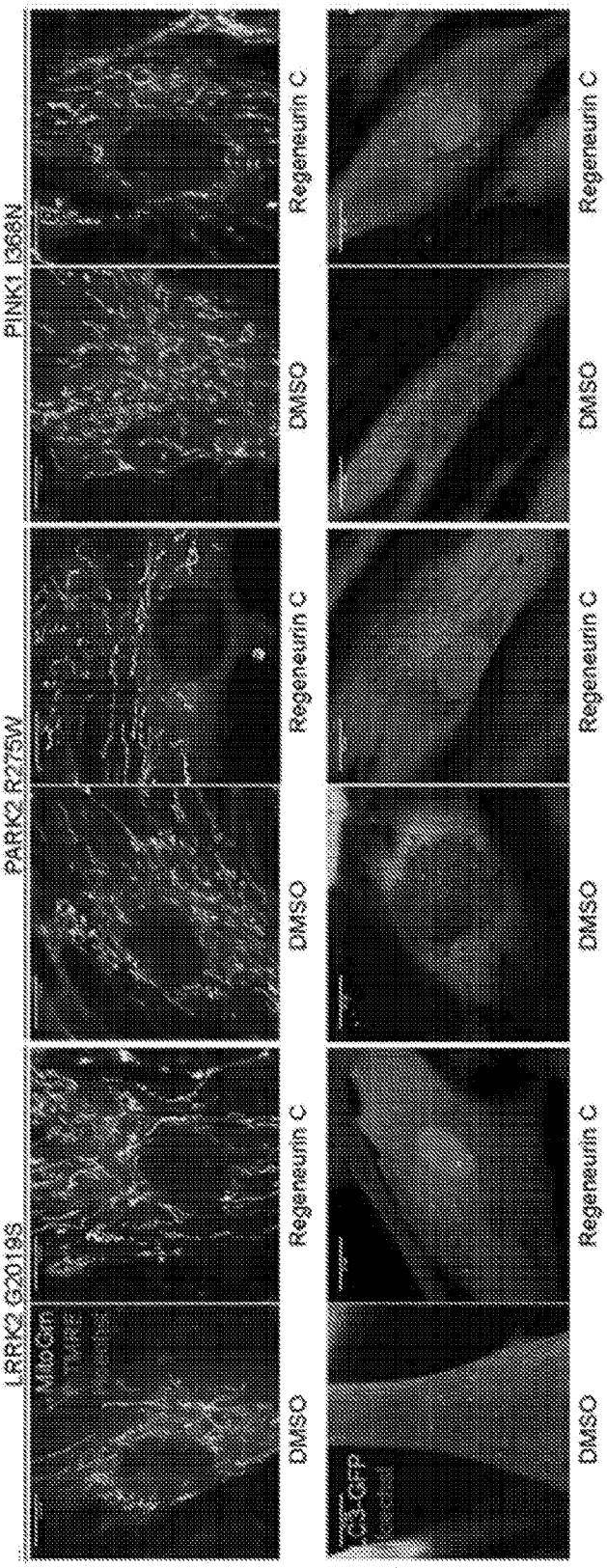

FIG. 69B

FIG. 69C

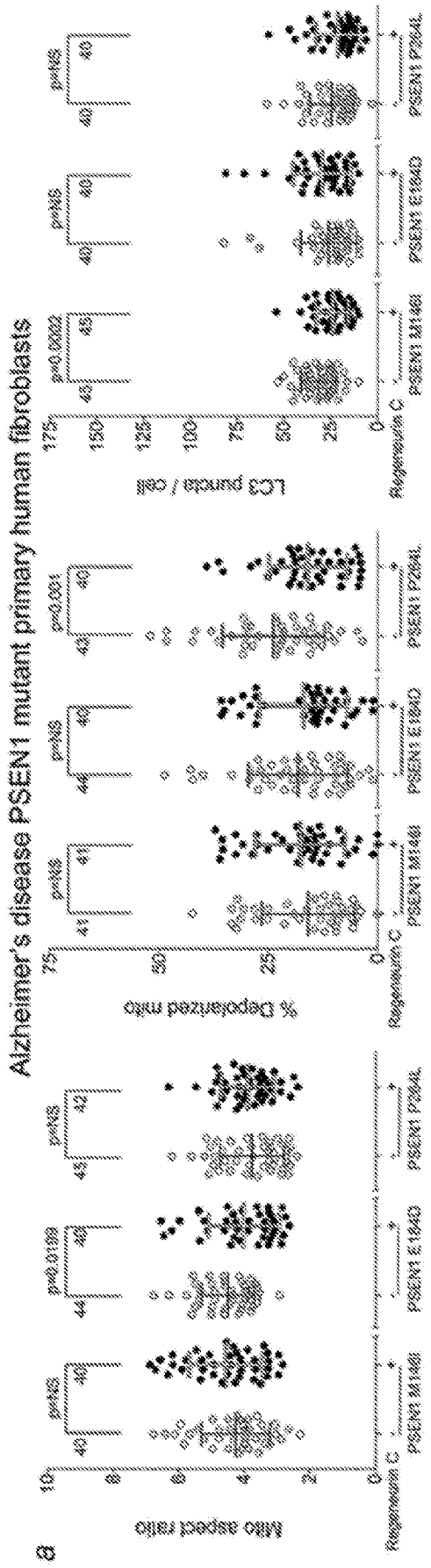
a
Alzheimer's disease PSEN1 mutant primary human fibroblasts
Mito aspect ratio
% Depolarized mito
LC3 puncta / cell
Regenerin C
PSEN1 M146I
PSEN1 E184D
PSEN1 P264L
p<0.0001
p<0.0002
p<0.0159
p<NS

FIG. 70A

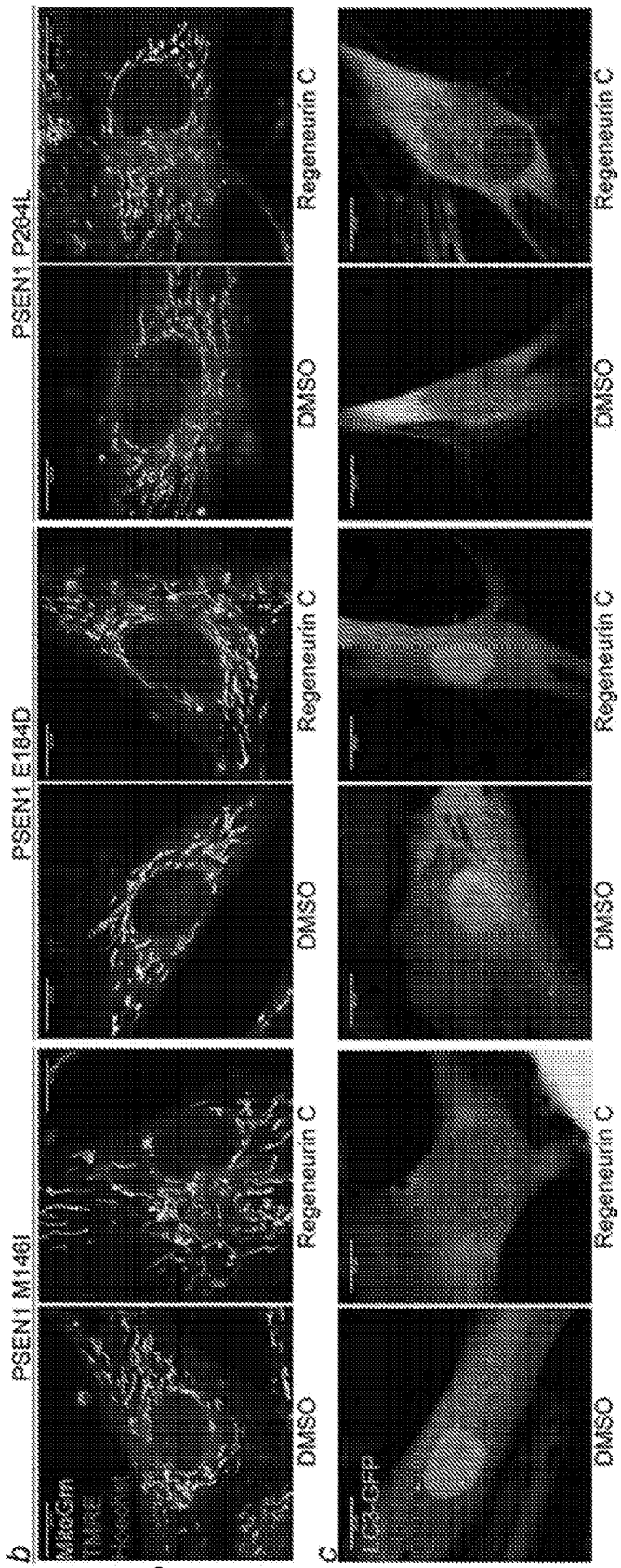

FIG. 70B

FIG. 70C

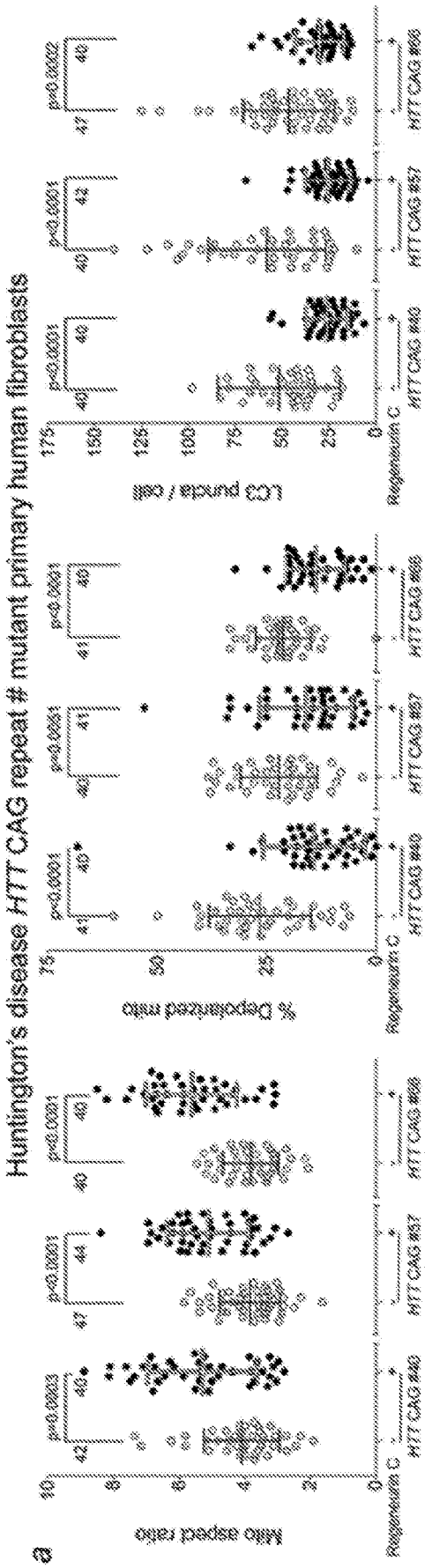
a
Huntington's disease HTT CAG repeat # mutant primary human fibroblasts
Ratio aspect ratio
% Depolarized mito
LC3 punda / cell
Rapamycin C
HTT CAG #40
HTT CAG #57
HTT CAG #66
p<0.0003
p<0.0001
p<0.0002

FIG. 71A

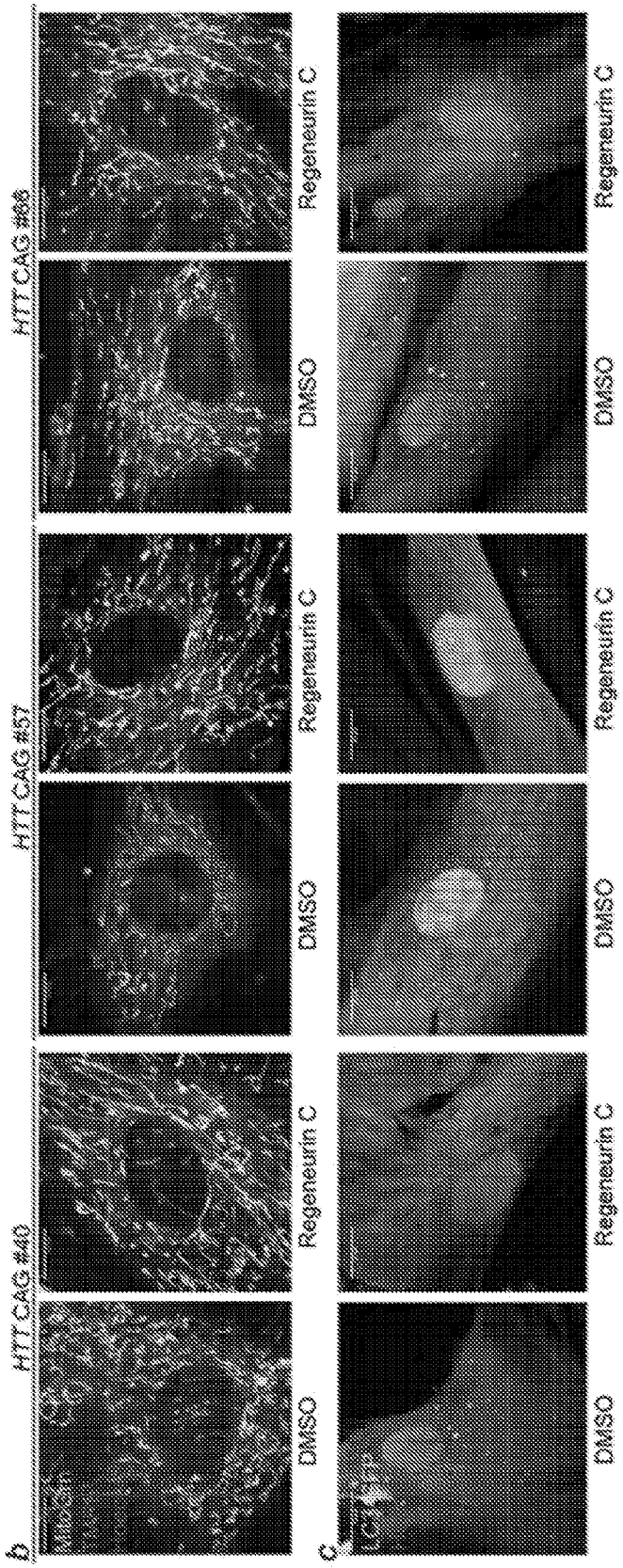

FIG. 71B

FIG. 71C

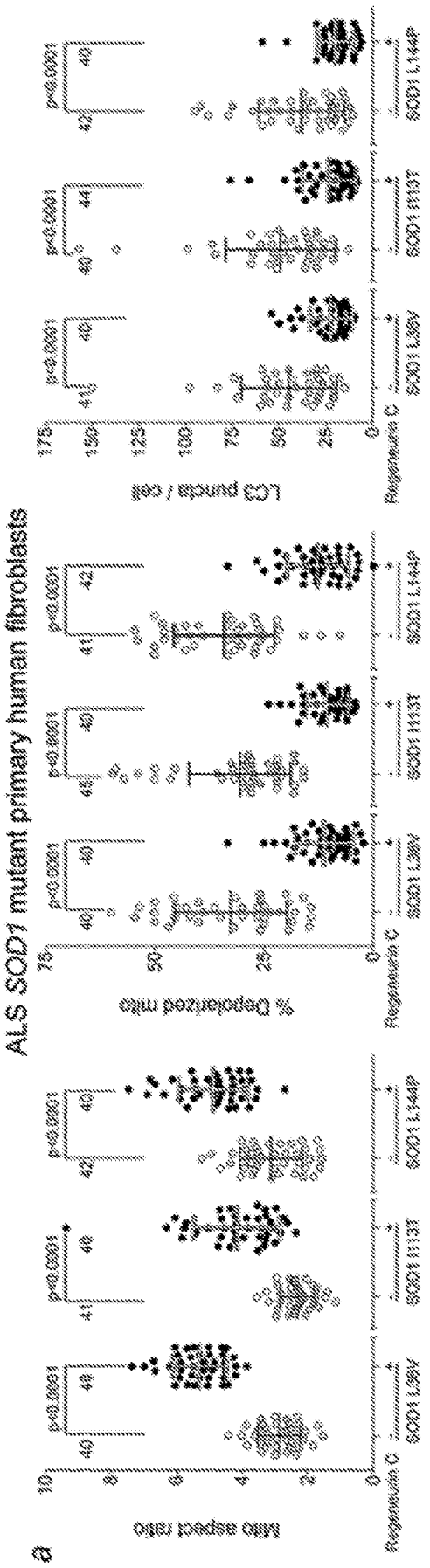
a
ALS SOD1 mutant primary human fibroblasts
Mito aspect ratio
% Depolarized mito
LC3 puncta / cell
Rapamycin
SOD1 L38V
SOD1 I113T
SOD1 L144P
p<0.0001

FIG. 72A

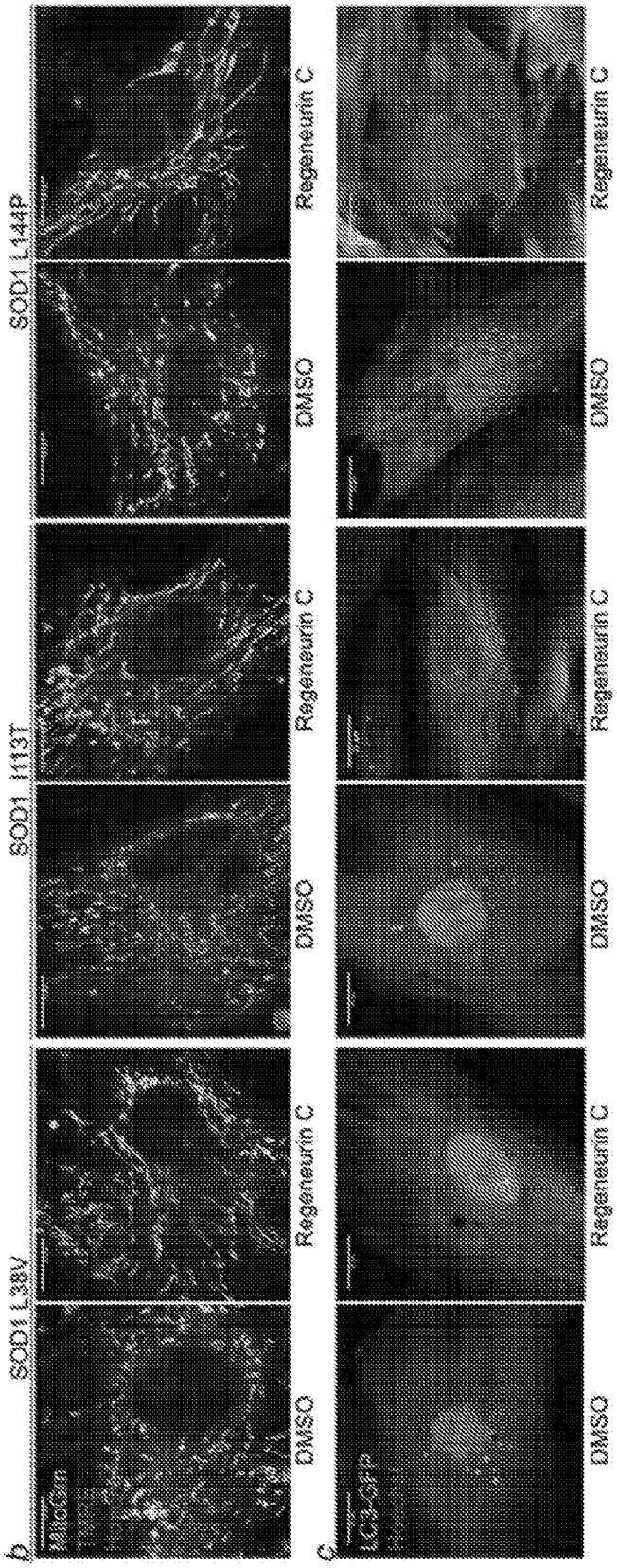

FIG. 72B

FIG. 72C

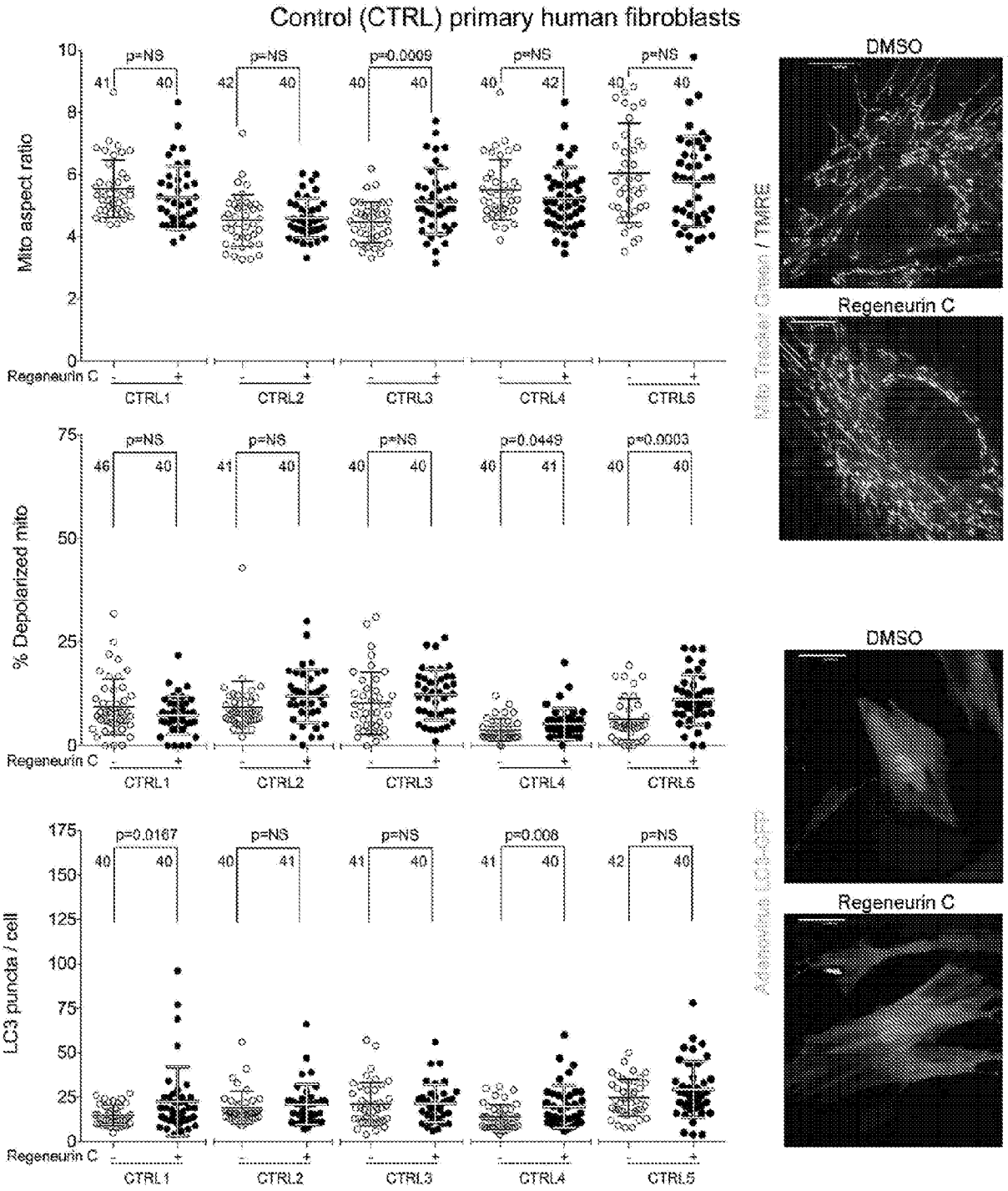
Control (CTRL) primary human fibroblasts
Mito aspect ratio
% Depolarized mito
LC3 puncta / cell
Regeneurin C
CTRL1
CTRL2
CTRL3
CTRL4
CTRL5
p=NS
p=0.0009
p=0.0449
p=0.0003
p=0.0167
p=0.006
Mito Tracker Green / TMRE
Adenovirus LC3-GFP
DMSO
Regeneurin C

FIG. 73

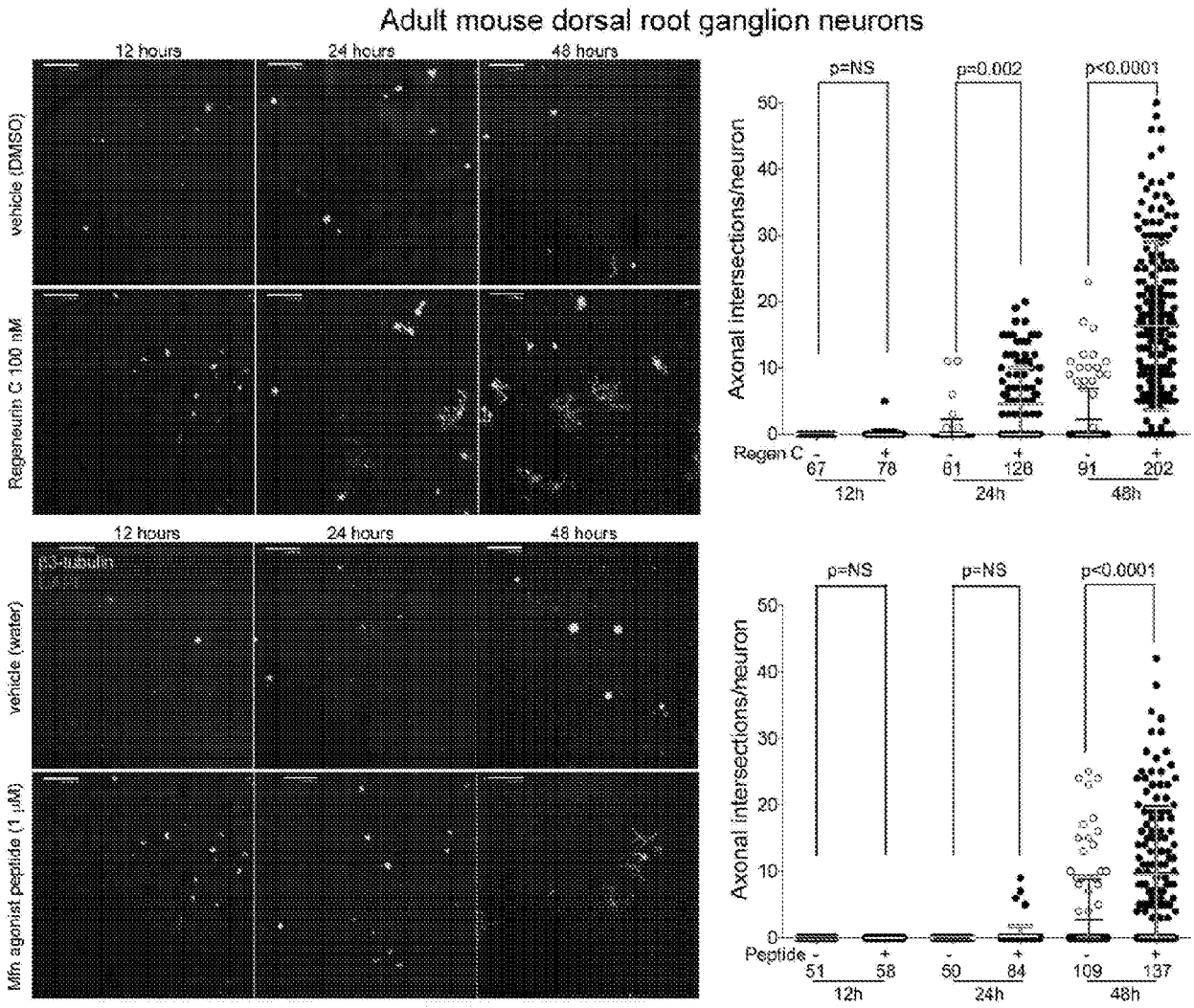
Adult mouse dorsal root ganglion neurons
12 hours
24 hours
48 hours
vehicle (DMSO)
Regeneurin C 100 nM
vehicle (water)
Mfn agonist peptide (1 μM)
Axonal intersections/neuron
p=NS
p=0.002
p<0.0001
Regen C
67
78
81
126
91
202
12h
24h
48h
p=NS
p=NS
p<0.0001
Peptide
51
58
50
84
109
137

FIG. 74

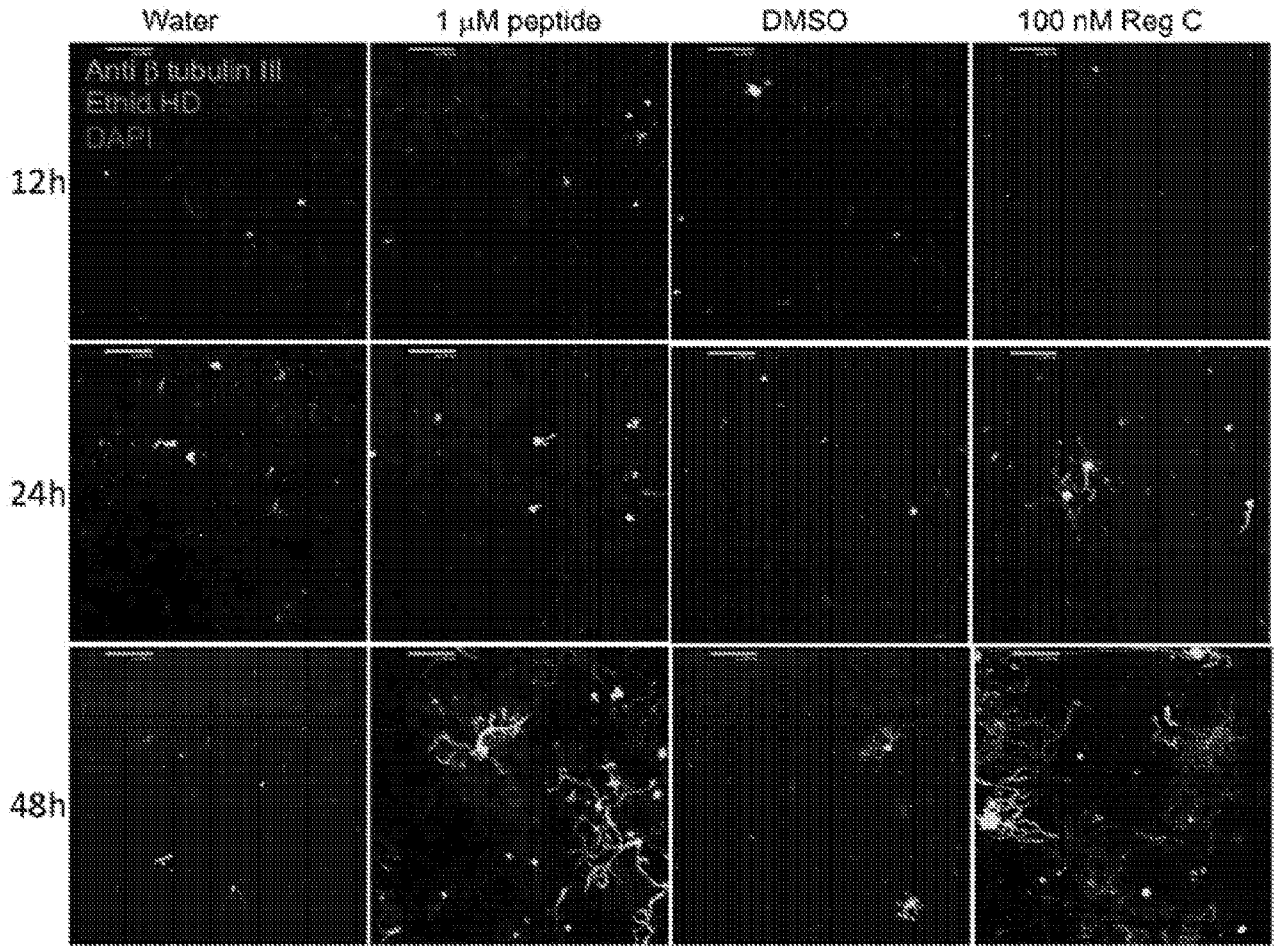
Water
1 μM peptide
DMSO
100 nM Reg C
Anti β tubulin III
Sytox NO
DAPI
12h
24h
48h

FIG. 75A

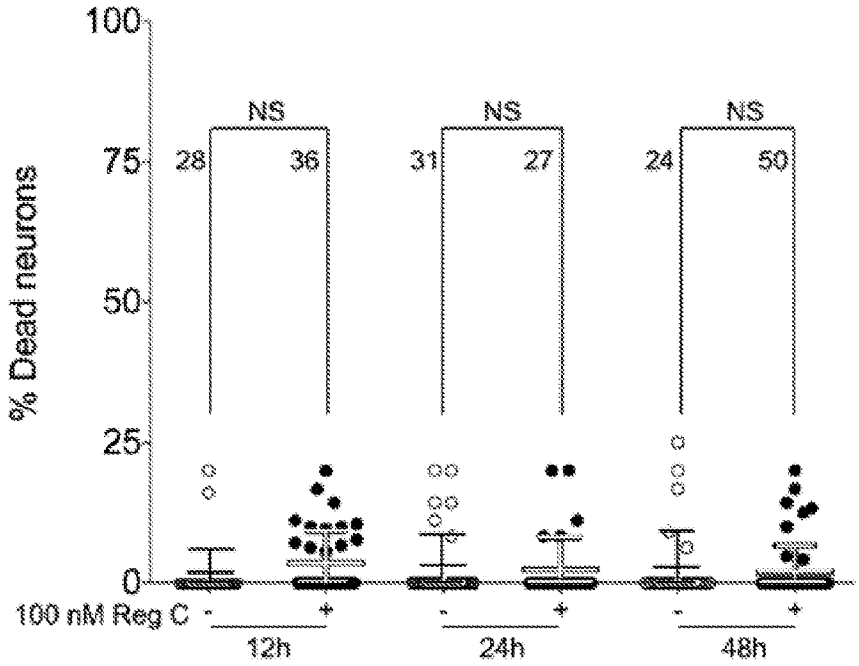

FIG. 75B

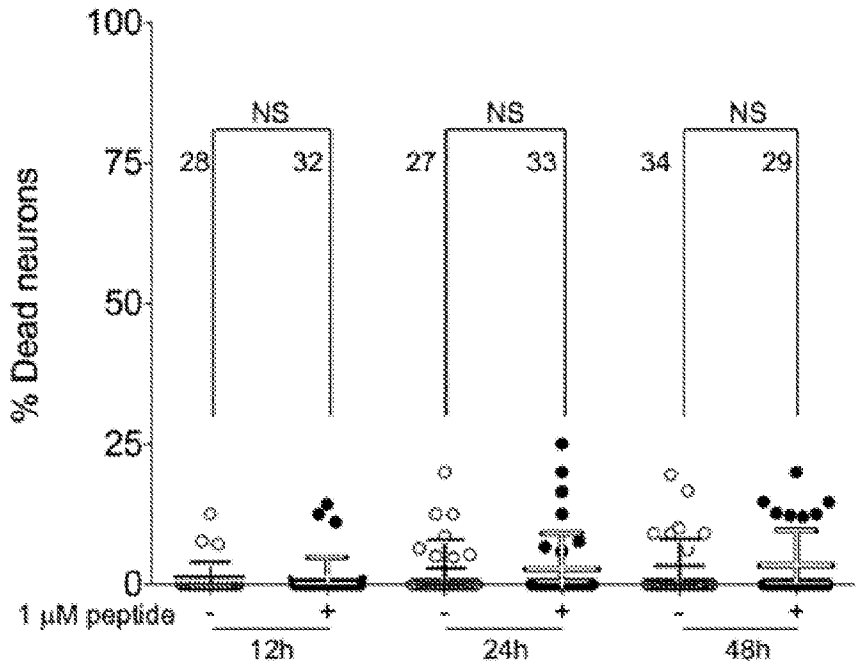

FIG. 75C

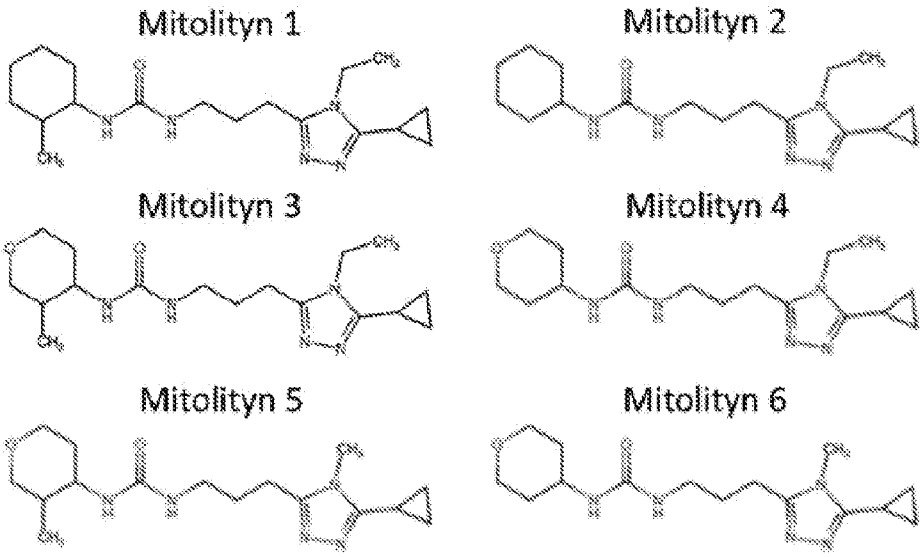

FIG. 76A

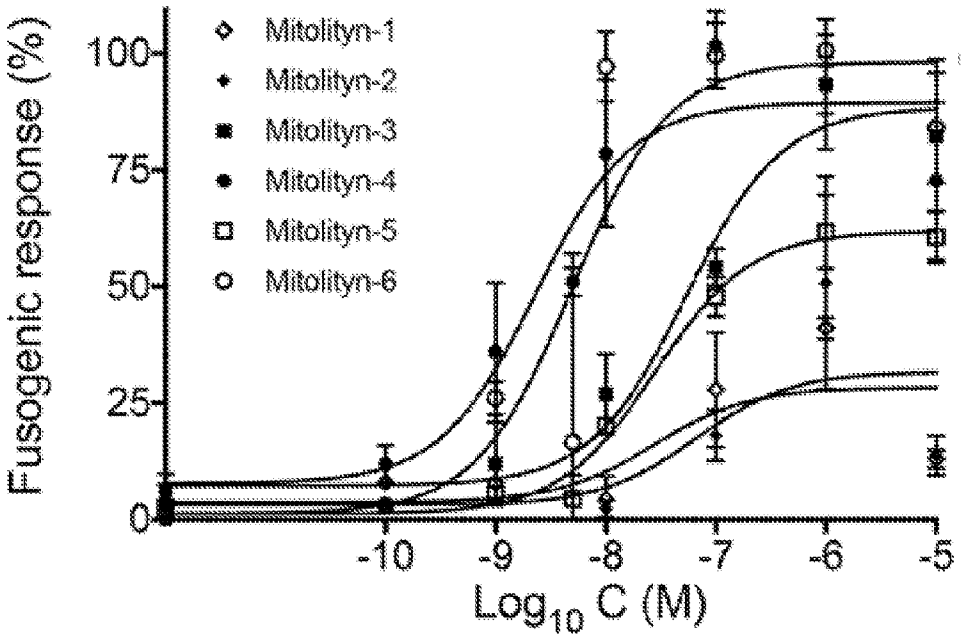

FIG. 76B

	EC_{50} (nM)	n
Mitolityn-1	inactive	2
Mitolityn-2	inactive	2
Mitolityn-3	60 ± 15	3
Mitolityn-4	3 ± 1	3
Mitolityn-5	147 ± 52	3
Mitolityn-6	7 ± 4	3

FIG. 76C

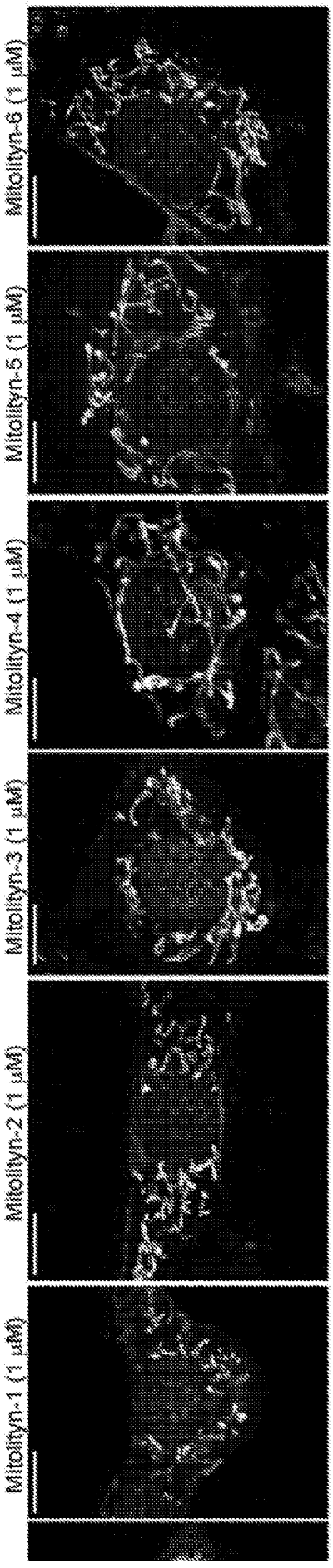

FIG. 76D

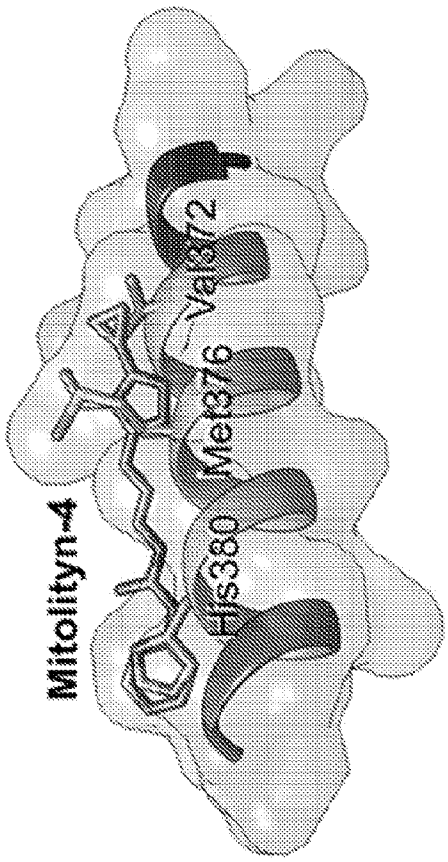

FIG. 76E

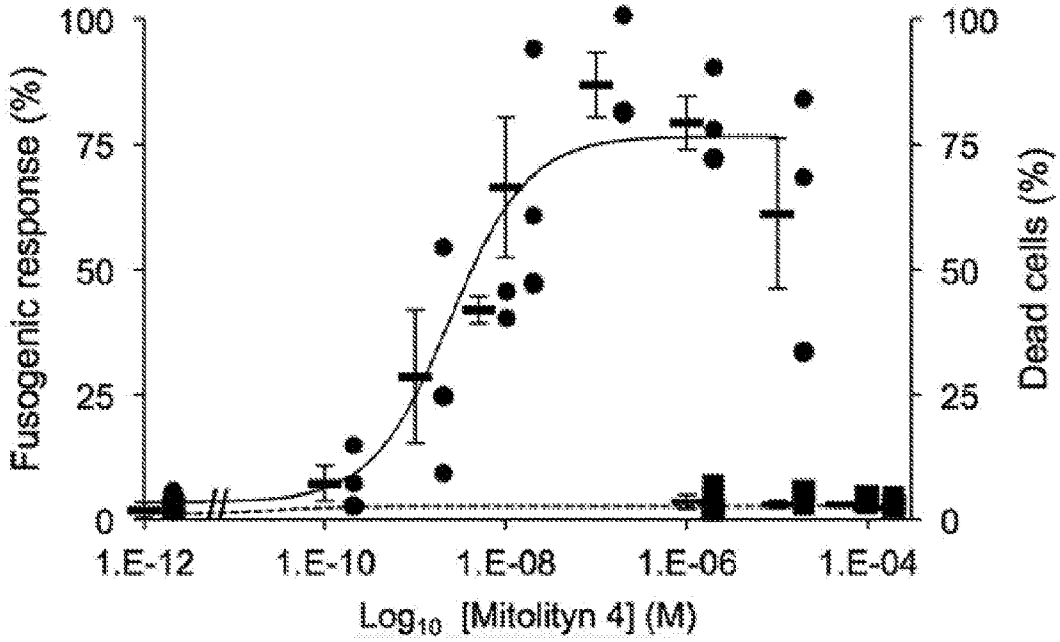
100
75
50
25
0
Fusogenic response (%)
100
75
50
25
0
Dead cells (%)
1.E-12
1.E-10
1.E-08
1.E-06
1.E-04
Log10 [Mitolityn 4] (M)

FIG. 76F

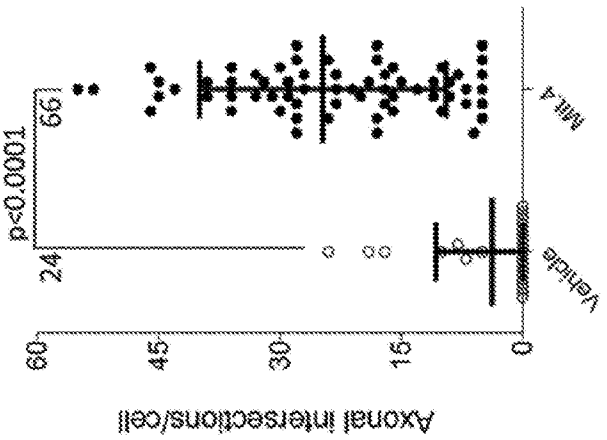
Axonal intersections/cell
60
45
30
15
0
Vehicle
Mit-4
p<0.0001
66
24

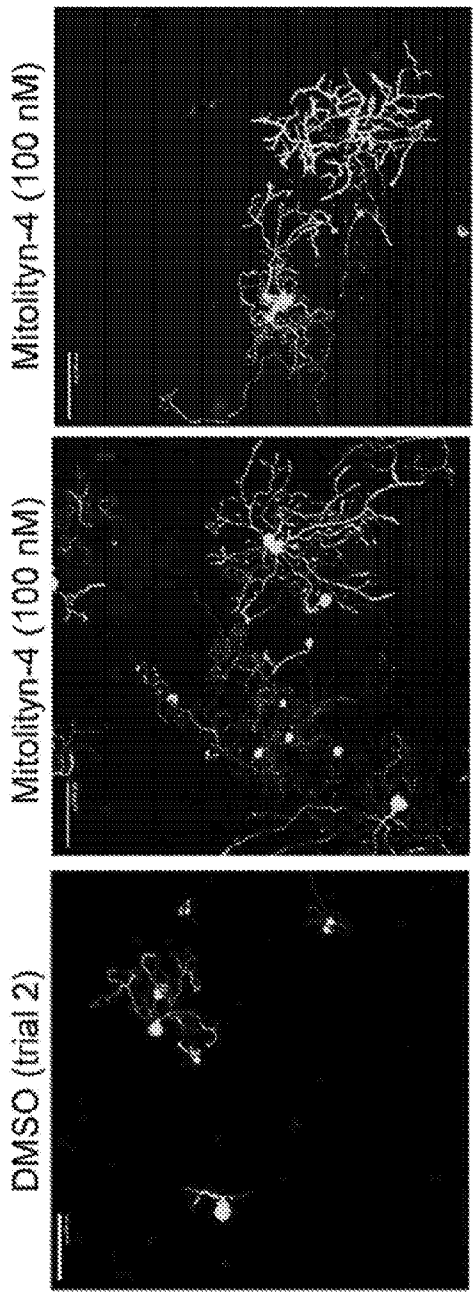
DMSO (trial 2)
Mitolityn-4 (100 nM)
Mitolityn-4 (100 nM)

FIG. 76G

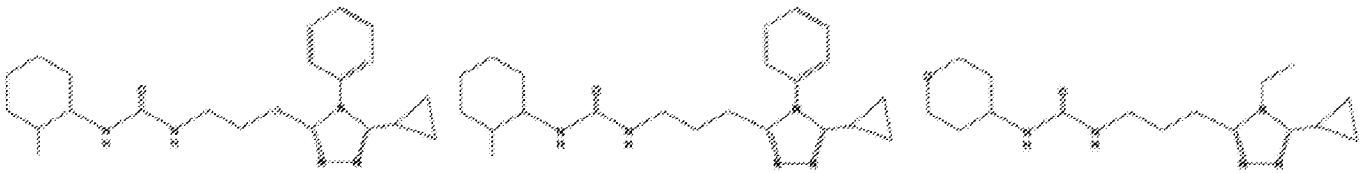

	Regeneurin-S	Regeneurin-C	Mitolityn-4
Molecular weight	399.6 g/mol	381.5 g/mol	321.4 g/mol
Solubility	67 μM	>200 μM	196.19 μM
Plasma protein binding			
human	98.20%	94.40%	19.60%
CD-1 mouse	92.10%	86.80%	11.20%
Plasma stability [120 min]			
human	94.60%	95%	91%
mouse	93.00%	>95%	97%
Microsome stability (T1/2)			
human liver	3.1 min	5.9 min	>145 min
rat liver	ND	4.5 min	>145 min
mouse liver	0.7 min	1.6 min	>145 min

FIG. 77

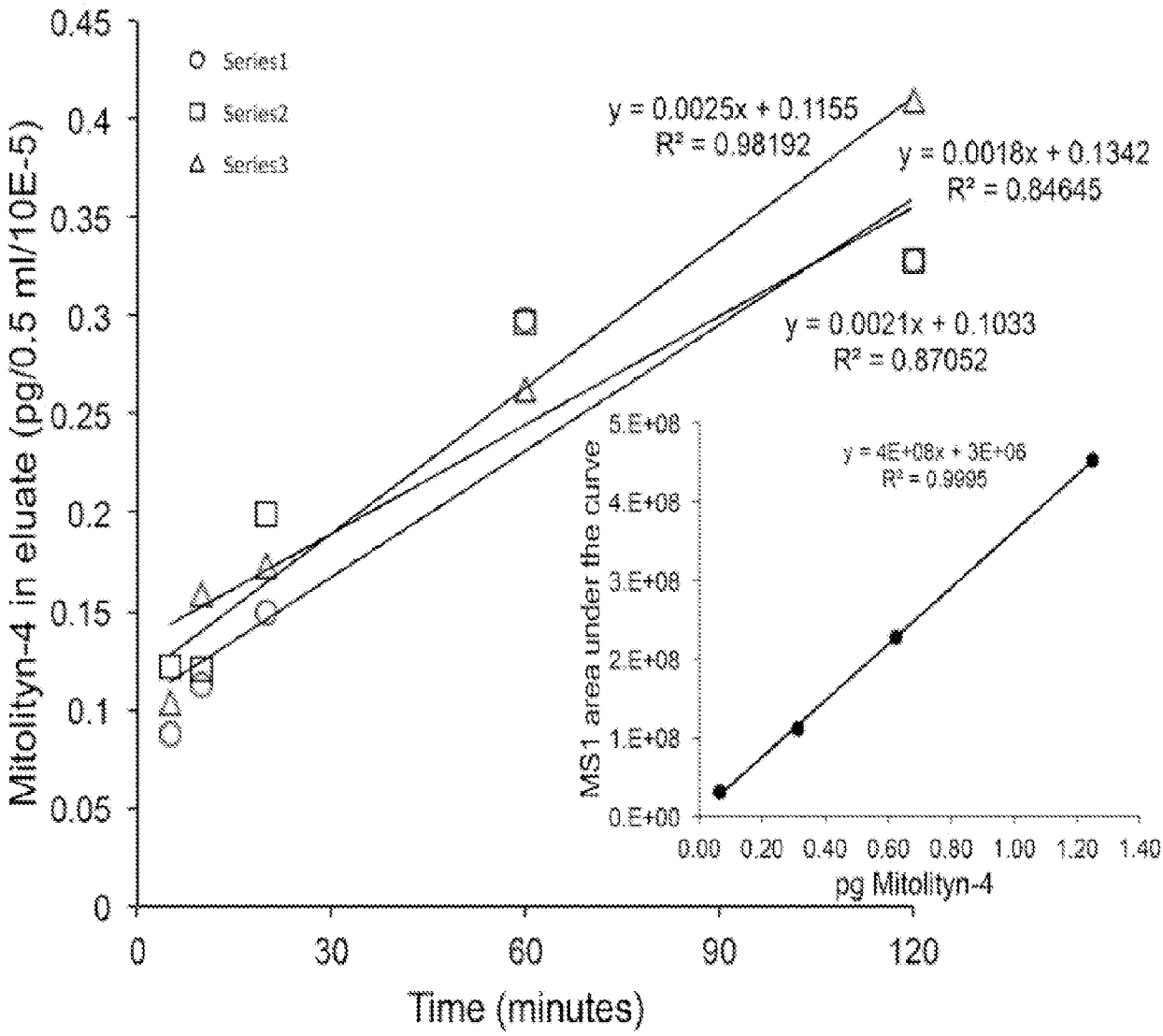
Mitolityn-4 in eluate (pg/0.5 ml/10E-5)
Time (minutes)
Series1
Series2
Series3
y = 0.0025x + 0.1155
R² = 0.98192
y = 0.0018x + 0.1342
R² = 0.84645
y = 0.0021x + 0.1033
R² = 0.87052
MS1 area under the curve
y = 4E+08x + 3E+06
R² = 0.9995
pg Mitolityn-4

FIG. 78

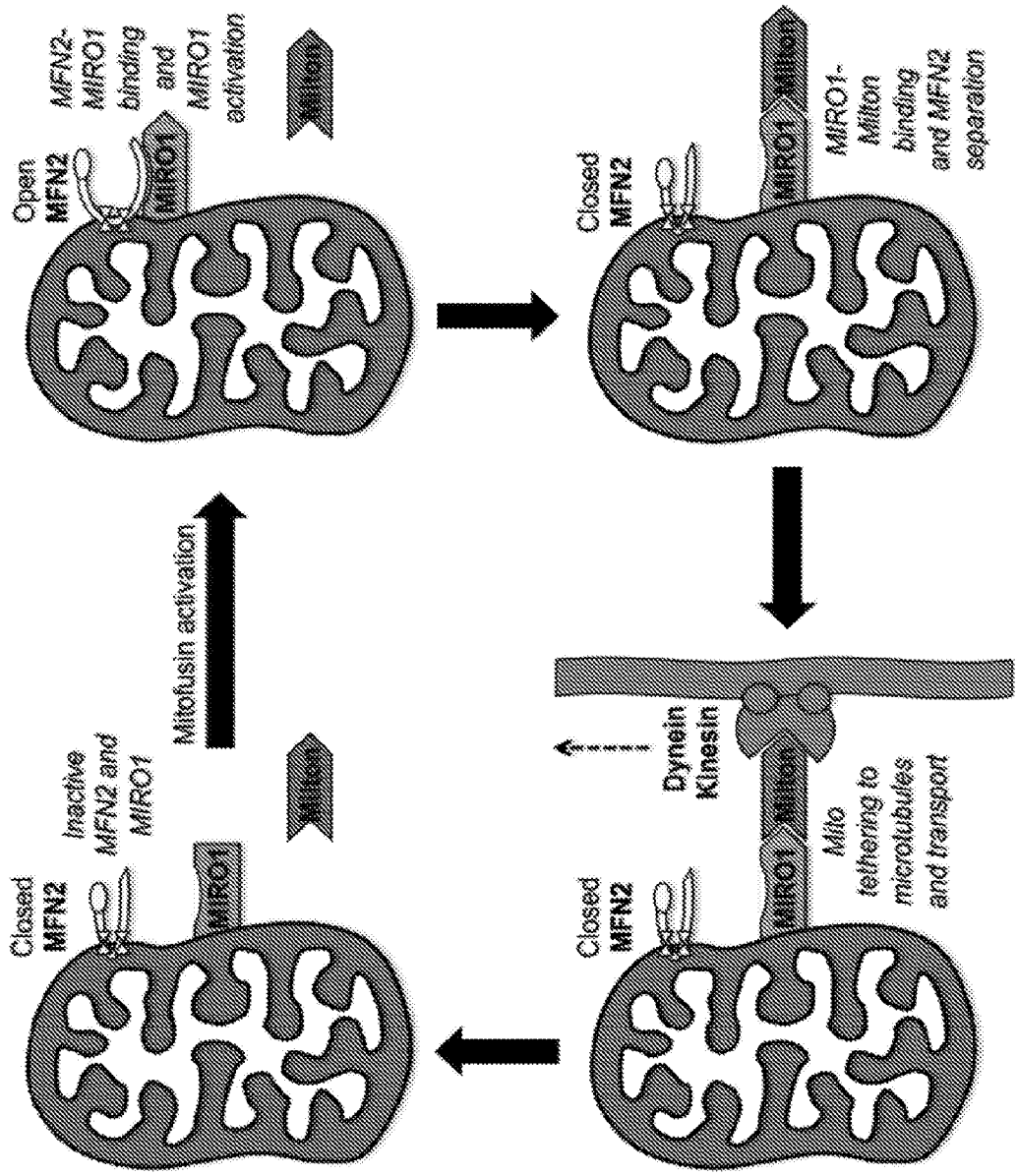

FIG. 79B

FIG. 79D

FIG. 79A

FIG. 79C

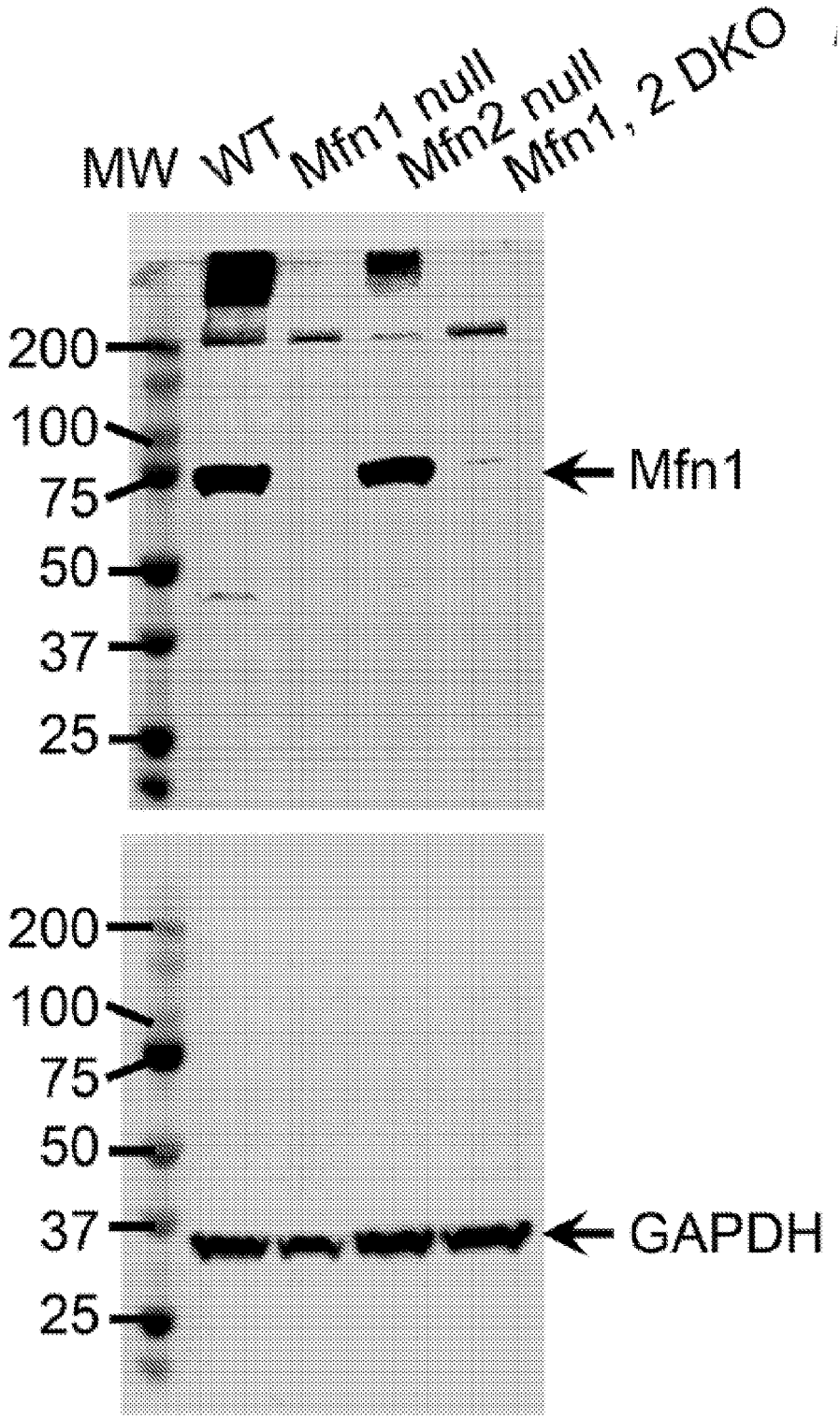
MW
WT
Mfn1 null
Mfn2 null
Mfn1, 2 DKO
200
100
75
50
37
25
Mfn1
200
100
75
50
37
25
GAPDH

FIG. 80A

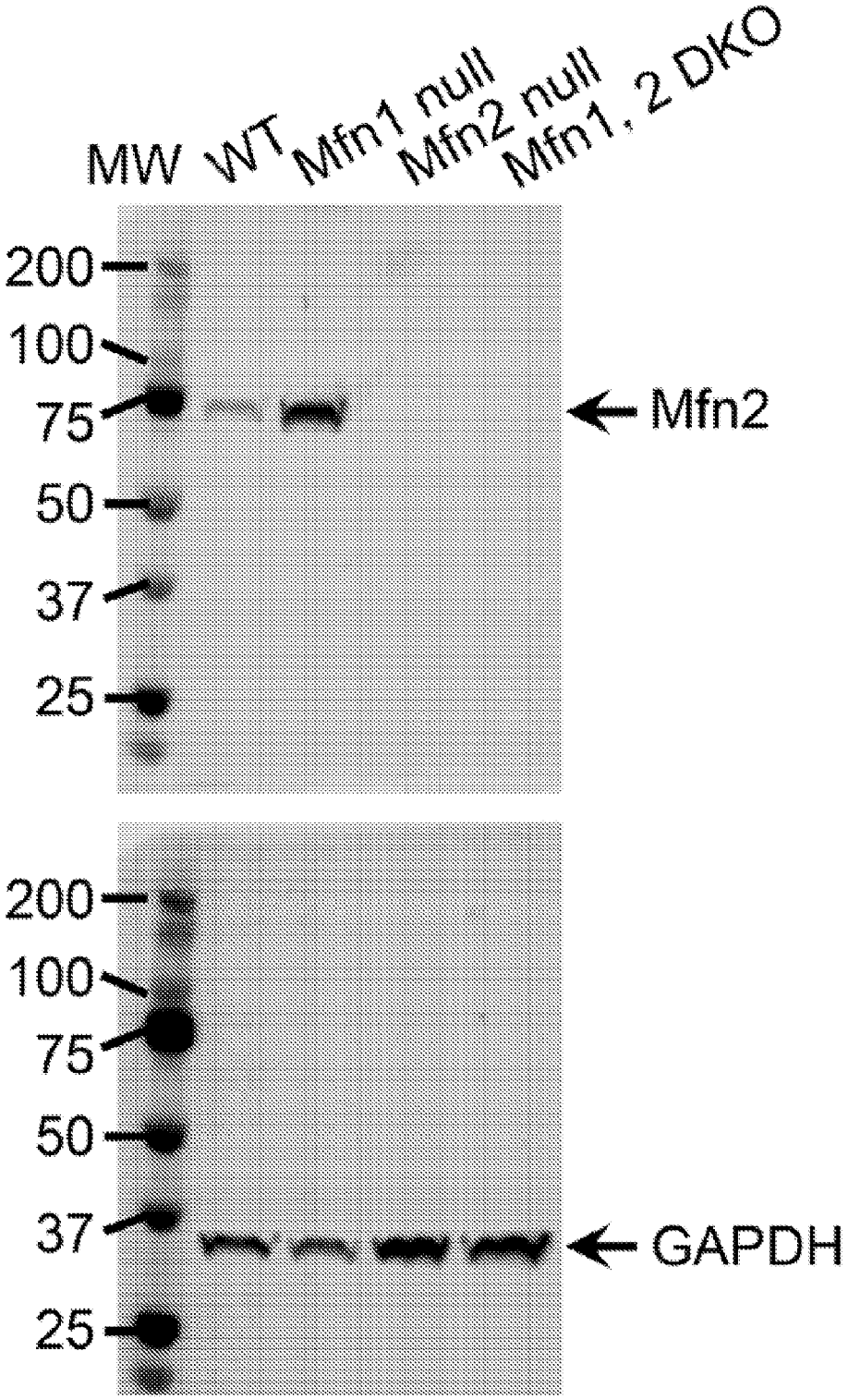
MW
WT
Mfn1 null
Mfn2 null
Mfn1, 2 DKO
200
100
75
50
37
25
Mfn2
200
100
75
50
37
25
GAPDH

FIG. 80B

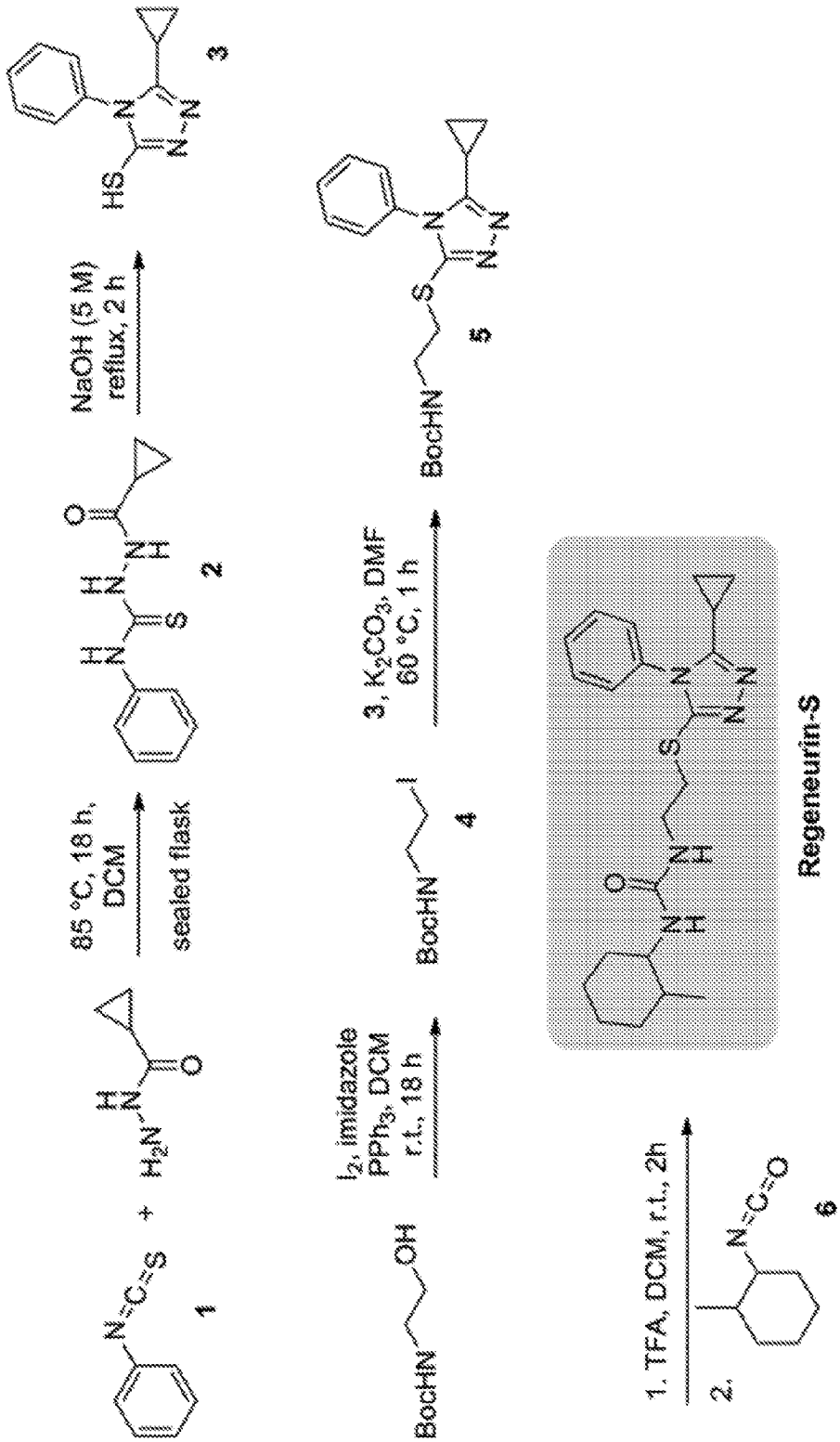
1
2
3
4
5
6
Regeneurin-S
85 °C, 18 h,
DCM
sealed flask
NaOH (5 M)
reflux, 2 h
I2, imidazole
PPh3, DCM
r.t., 18 h
3, K2CO3, DMF
60 °C, 1 h
1. TFA, DCM, r.t., 2h
2.
BocHN
OH
HS

FIG. 81

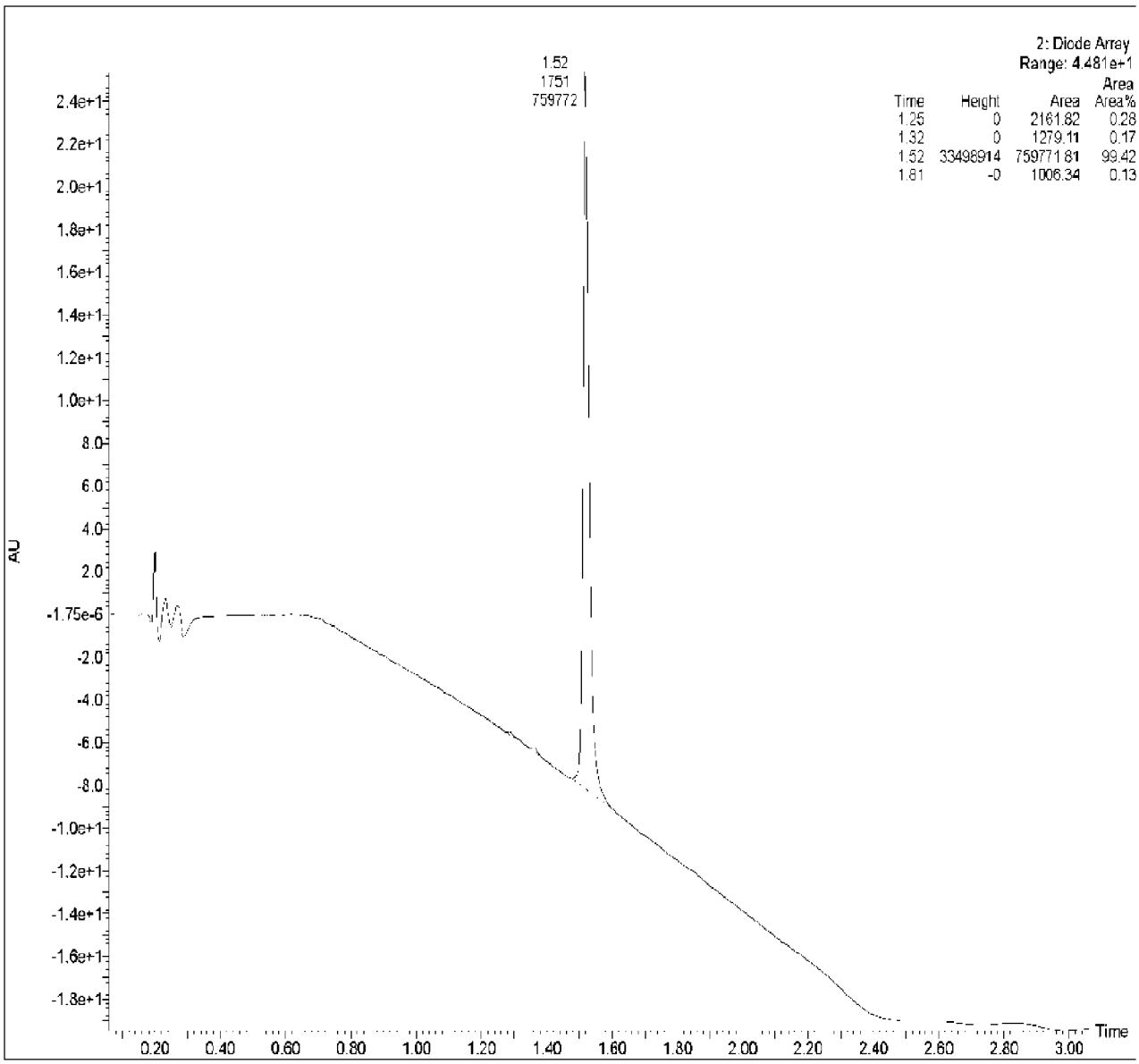
1.52
1751
759772
2: Diode Array
Range: 4.481e+1
Time Height Area Area%
1.25 0 2161.82 0.28
1.32 0 1279.11 0.17
1.52 33498914 759771.81 99.42
1.81 -0 1006.34 0.13
AU
2.4e+1
2.2e+1
2.0e+1
1.8e+1
1.6e+1
1.4e+1
1.2e+1
1.0e+1
8.0
6.0
4.0
2.0
-1.75e-6
-2.0
-4.0
-6.0
-8.0
-1.0e+1
-1.2e+1
-1.4e+1
-1.6e+1
-1.8e+1
0.20 0.40 0.60 0.80 1.00 1.20 1.40 1.60 1.80 2.00 2.20 2.40 2.60 2.80 3.00
Time

FIG. 82

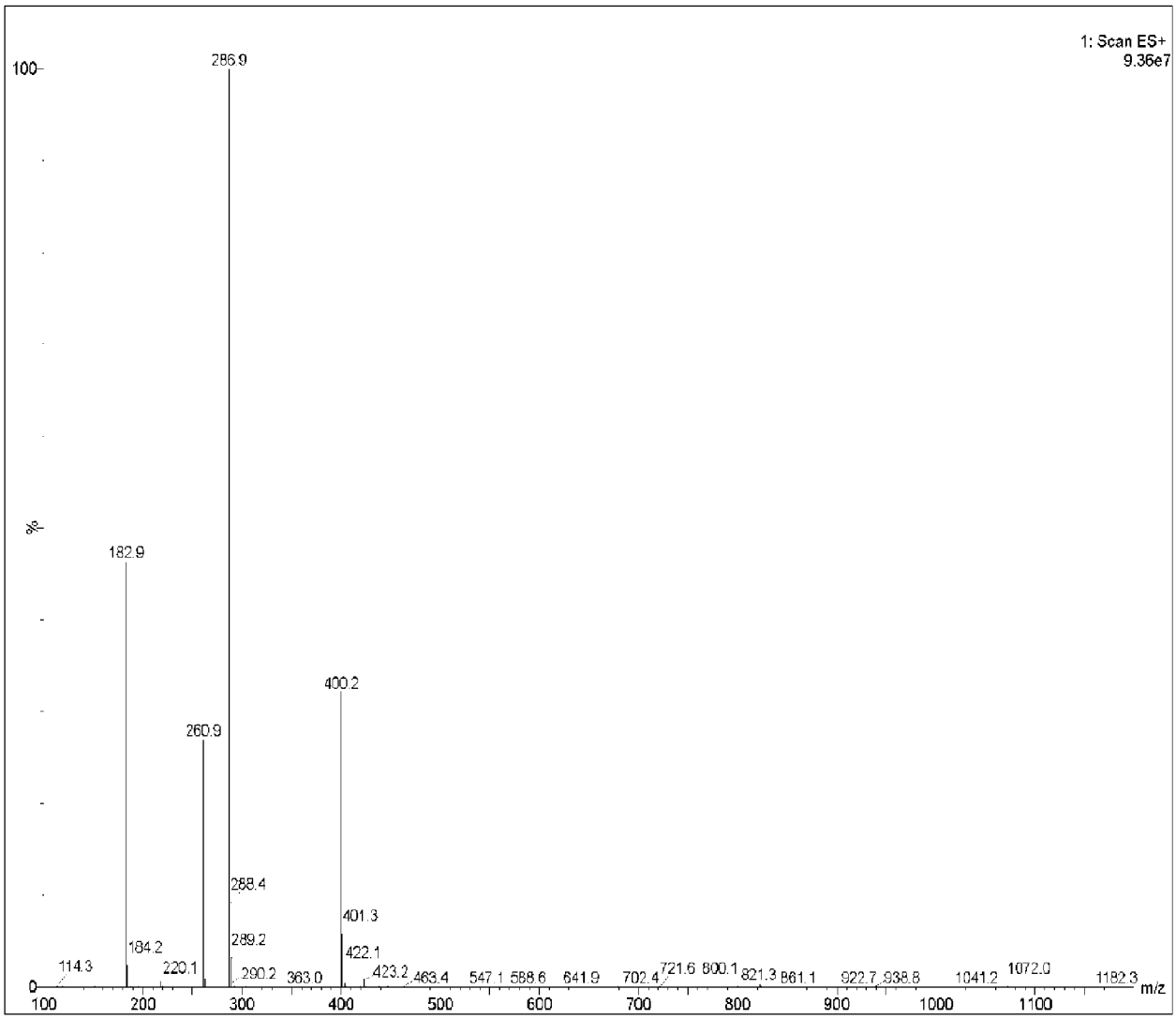
1: Scan ES+
9.36e7
100
%
0
286.9
182.9
260.9
400.2
288.4
401.3
289.2
422.1
184.2
114.3
220.1
290.2
363.0
423.2
463.4
547.1
588.6
641.9
702.4
721.6
800.1
821.3
861.1
922.7
938.8
1041.2
1072.0
1182.3
100
200
300
400
500
600
700
800
900
1000
1100
m/z

FIG. 83

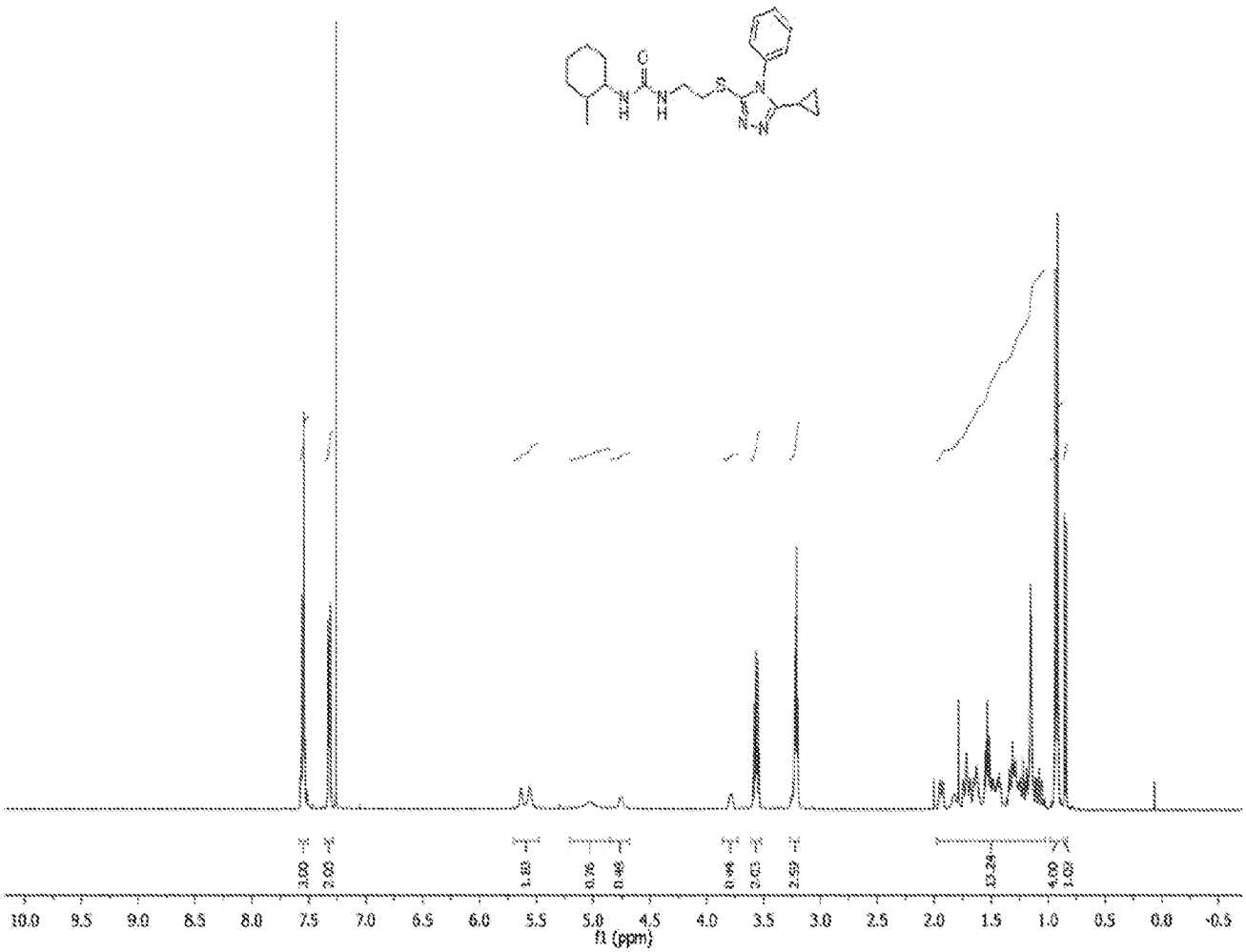
3.00
2.03
1.85
0.96
0.98
0.94
0.93
2.59
13.24
4.00
1.03
10.0
9.5
9.0
8.5
8.0
7.5
7.0
6.5
6.0
5.5
5.0
4.5
4.0
3.5
3.0
2.5
2.0
1.5
1.0
0.5
0.0
-0.5
f1 (ppm)

FIG. 84

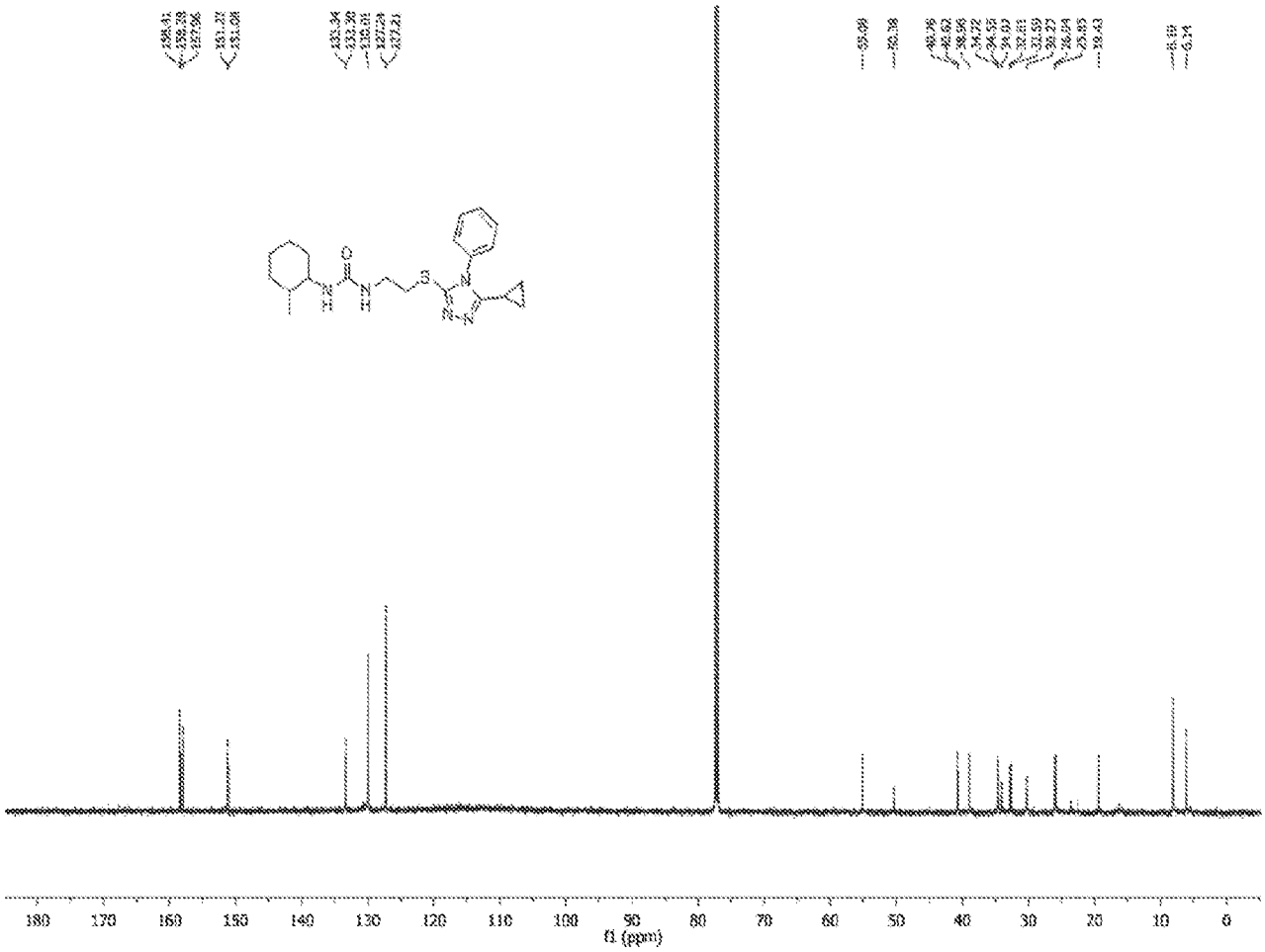

FIG. 85

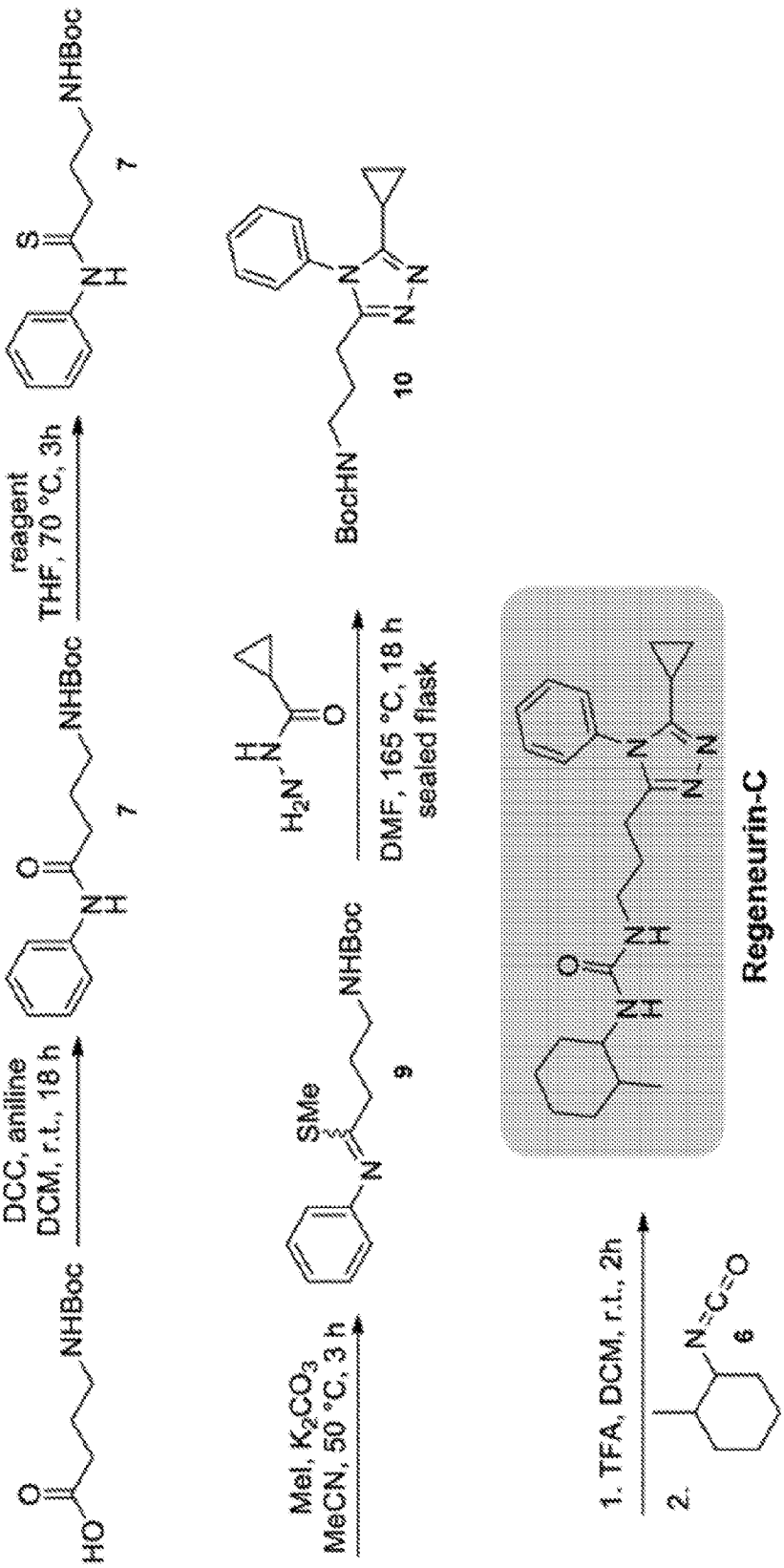
DCC, aniline
DCM, r.t., 18 h
Lawesson's reagent
THF, 70 °C, 3h
MeI, K2CO3
MeCN, 50 °C, 3 h
DMF, 165 °C, 18 h
sealed flask
1. TFA, DCM, r.t., 2h
2.
Regeneurin-C

FIG. 86

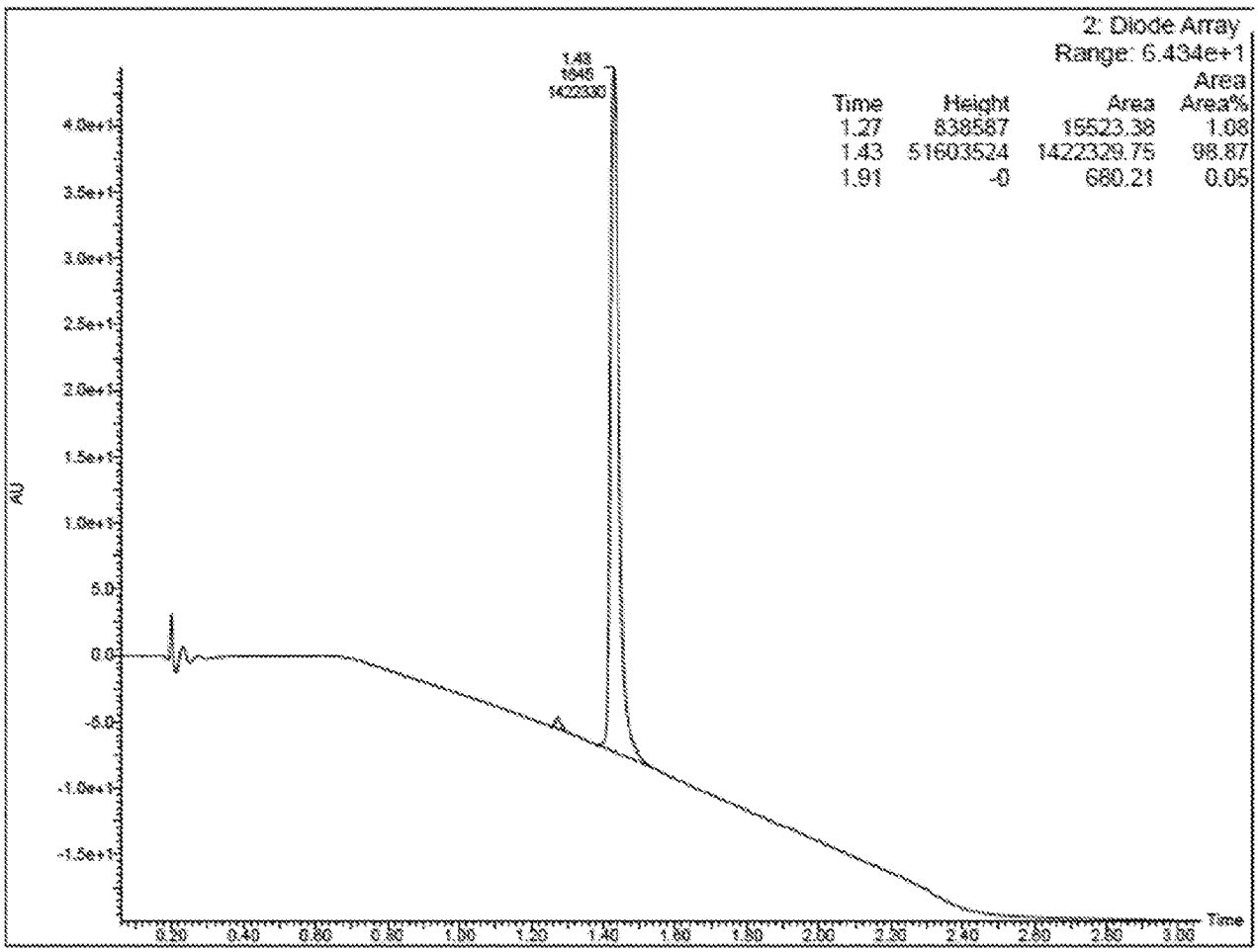
2: Diode Array
Range: 6.434e+1
Time Height Area Area%
1.27 838587 15523.38 1.08
1.43 51603524 14223329.75 98.87
1.91 -0 680.21 0.05
AU
Time

FIG. 87

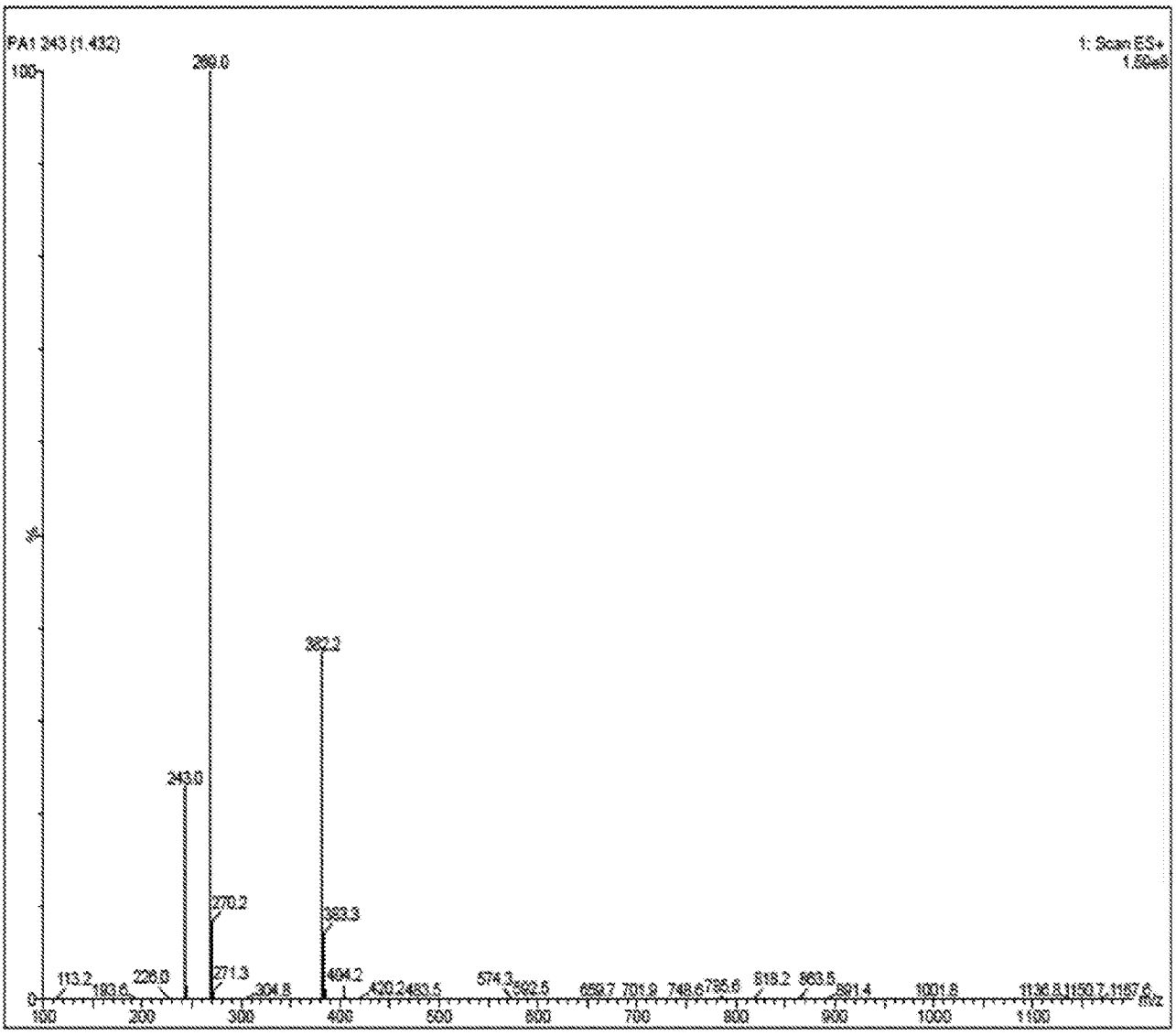
PA1 343 (1.432)
1: Scan ES+
100
%
0
260.0
382.3
343.0
270.2
383.3
271.3
404.2
113.2
226.0
m/z
100
200
300
400
500
600
700
800
900
1000
1100

FIG. 88

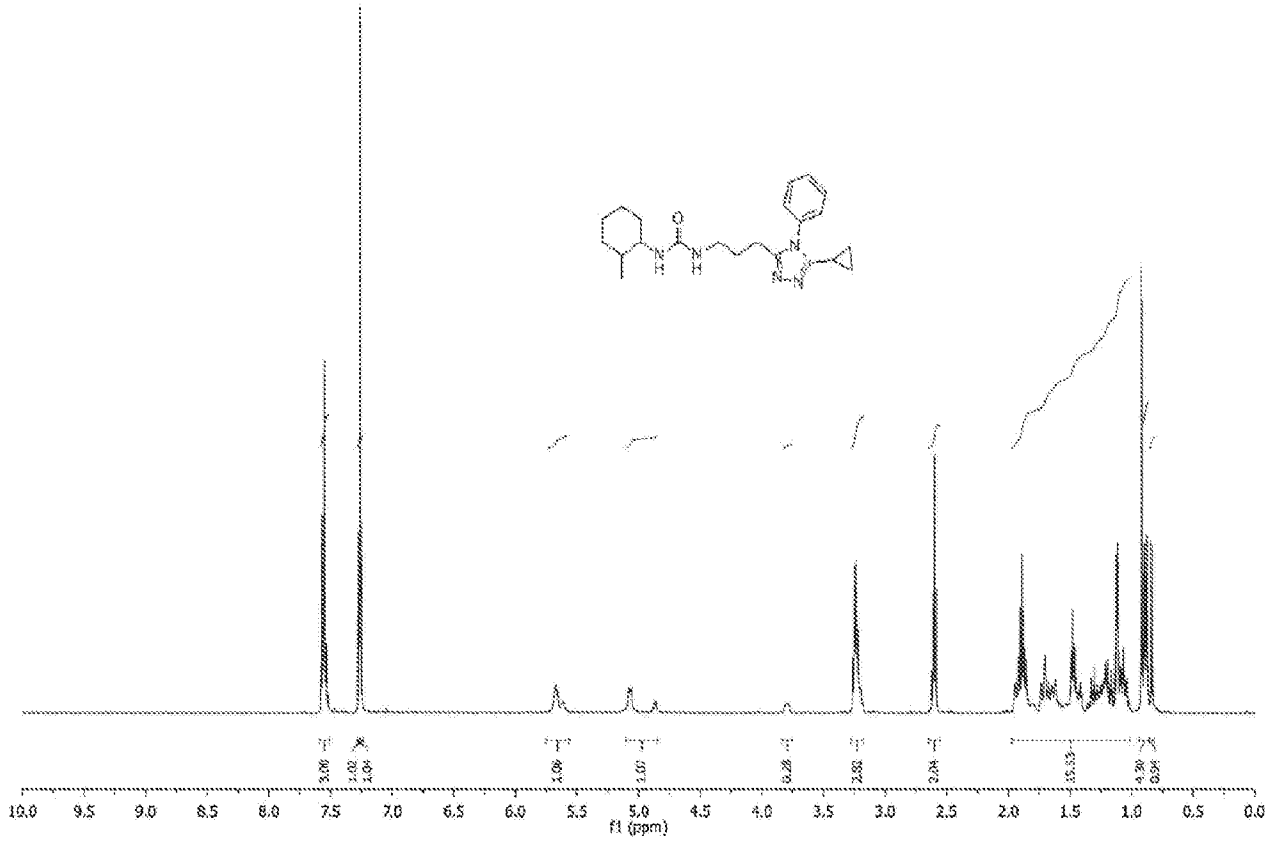

FIG. 89

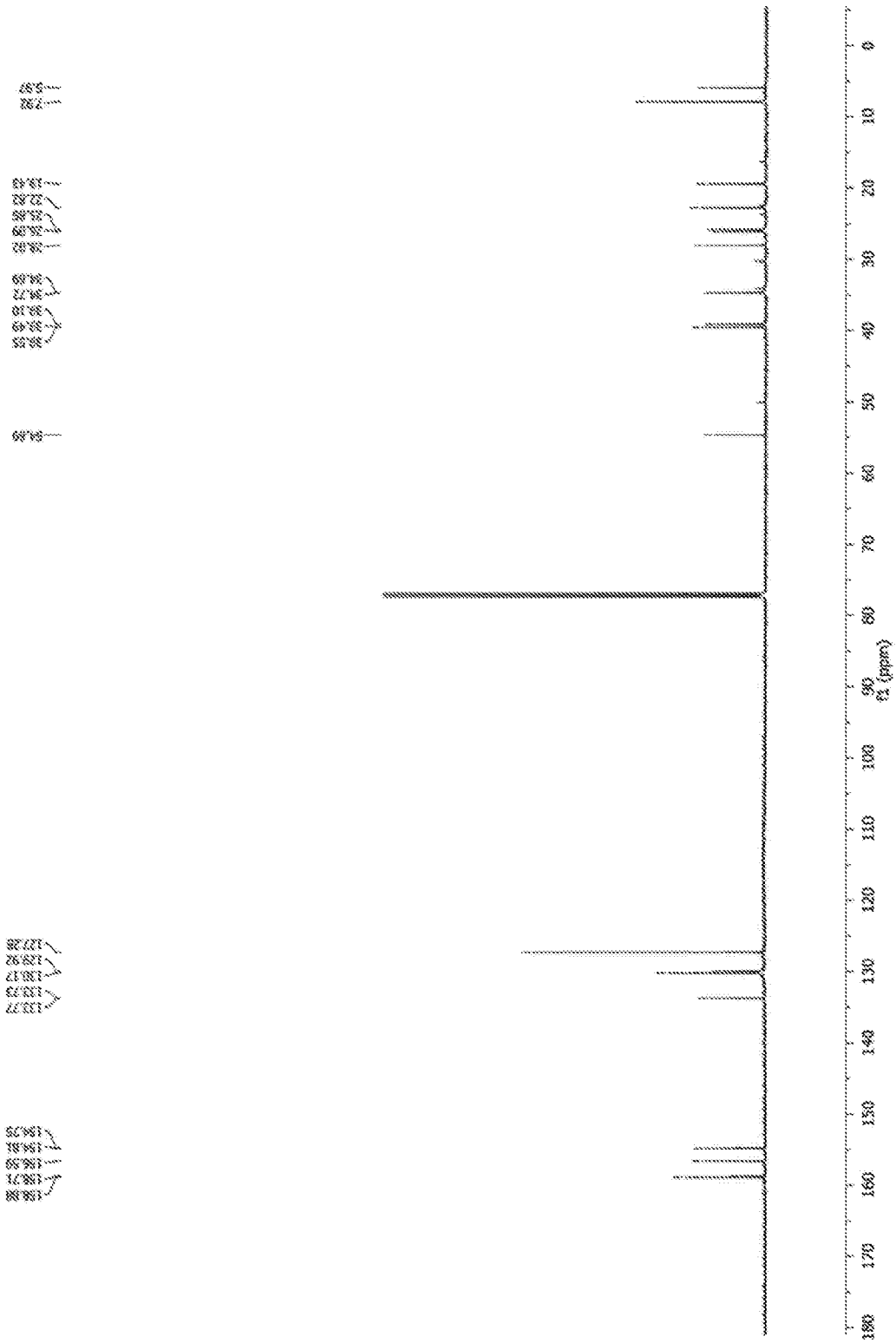

FIG. 90

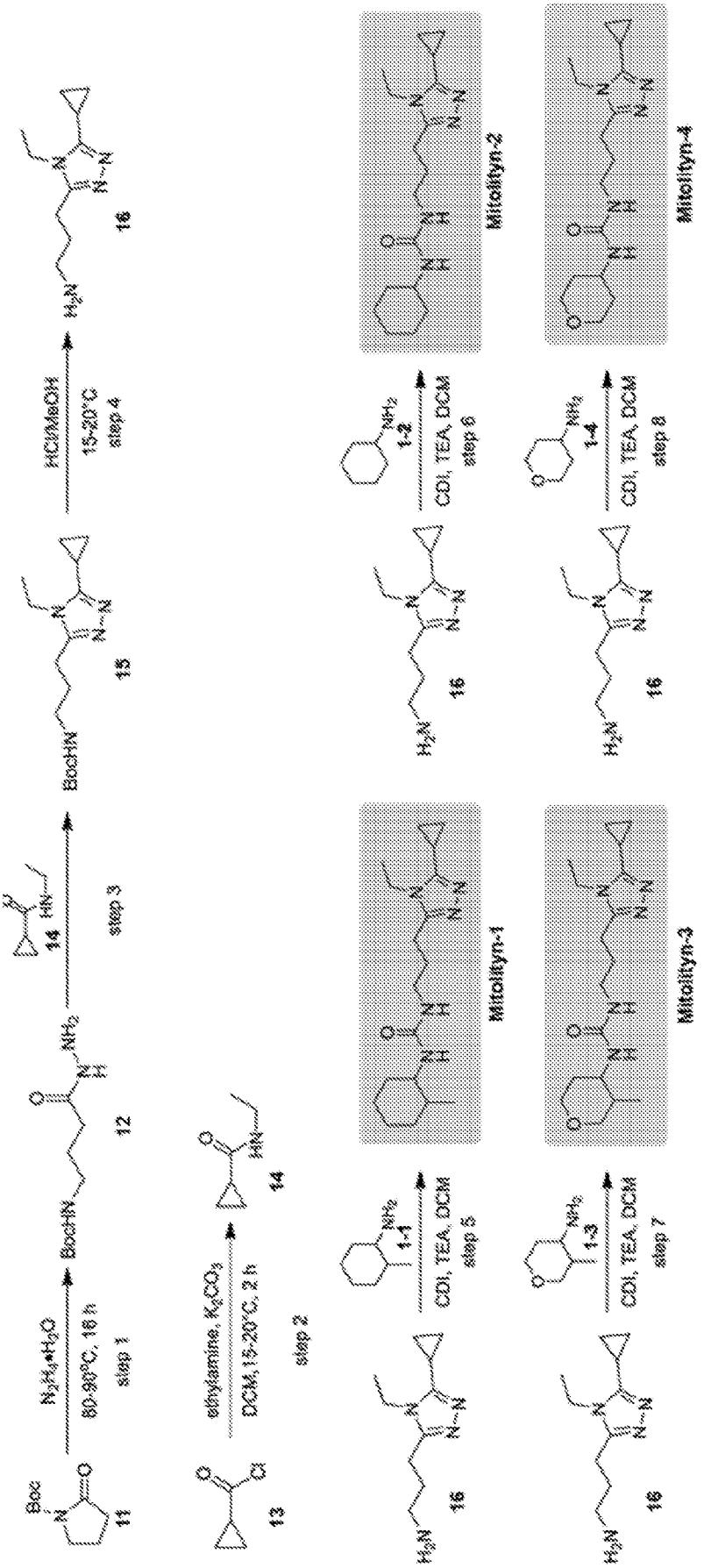
Boc
11
$N_2H_4 \cdot H_2O$
80-90°C, 16 h
step 1
BocHN
12
NH_2
O
Cl
13
ethylamine, K_2CO_3
DCM,15-20°C, 2 h
step 2
14
HN
step 3
BocHN
15
HCl/MeOH
15-20°C
step 4
H_2N
16
CDI, TEA, DCM
step 5
1-1
Mitolityn-1
step 6
1-2
Mitolityn-2
step 7
1-3
Mitolityn-3
step 8
1-4
Mitolityn-4

FIG. 91

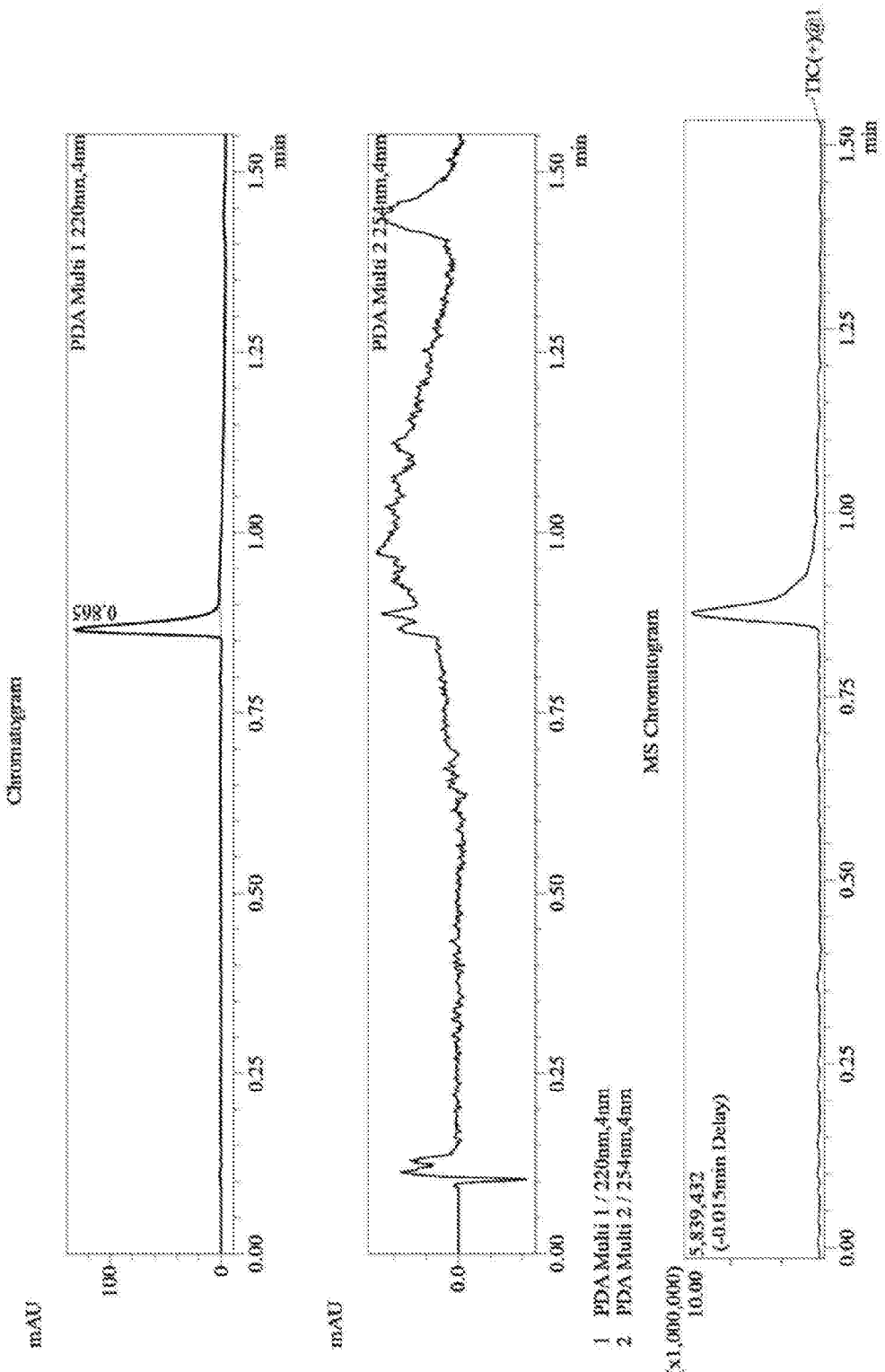
Chromatogram
mAU
PDA Multi 1 220nm,4nm
0.865
100
0
0.00
0.25
0.50
0.75
1.00
1.25
1.50
min
mAU
PDA Multi 2 254nm,4nm
0.0
1 PDA Multi 1 / 220nm,4nm
2 PDA Multi 2 / 254nm,4nm
MS Chromatogram
(x1,000,000)
10.00
5,839,432
(-0.015min Delay)
TIC(+)@1
PDA Ch1 220nm
Peak# Ret. Time Height Height% USP Width Area Area%
1 0.865 130939 100.000 0.030 139202 100.000
PDA Ch2 254nm

FIG. 92

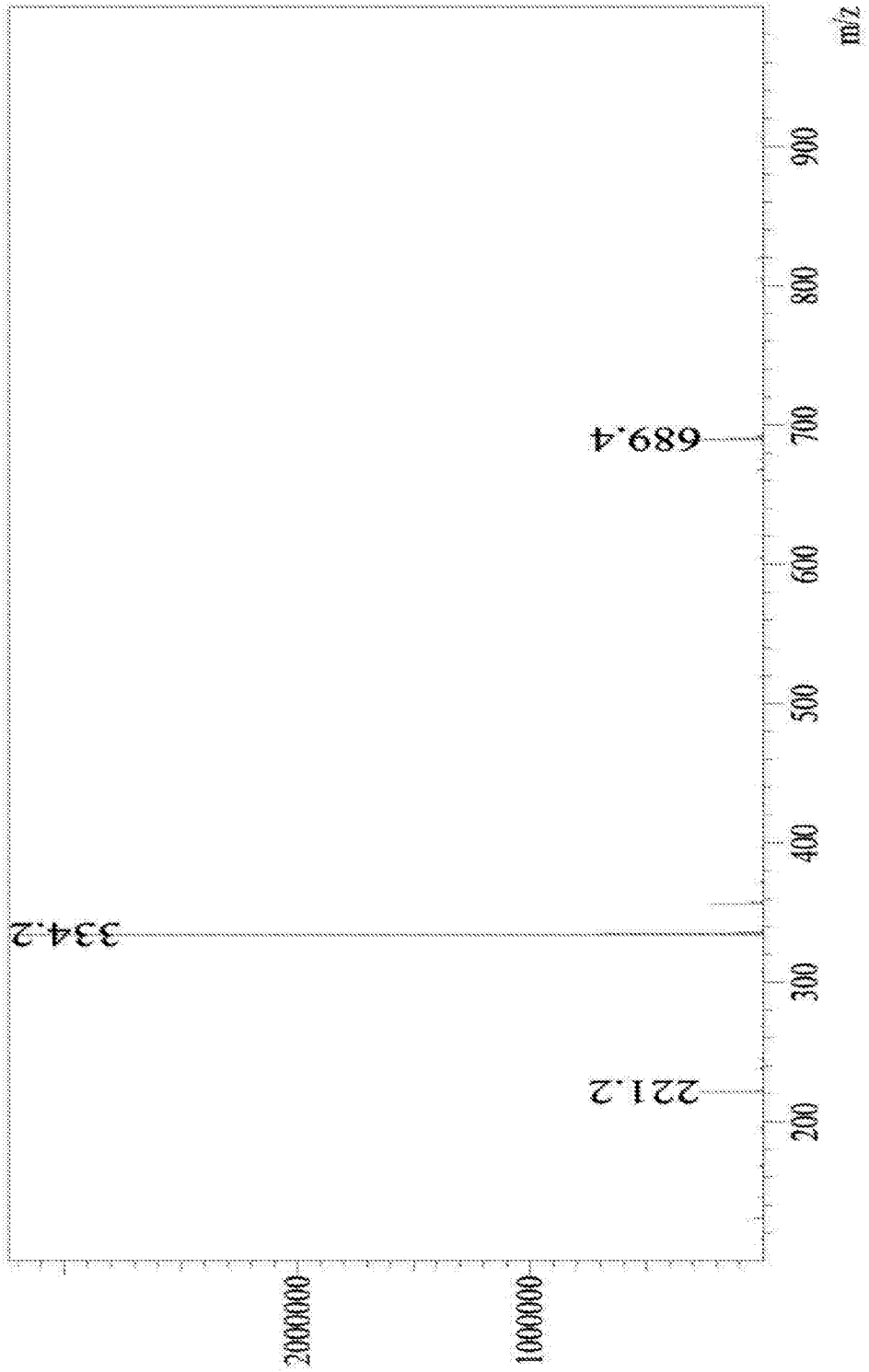
m/z
200
300
400
500
600
700
800
900
221.2
334.2
689.4
1000000
2000000

FIG. 93

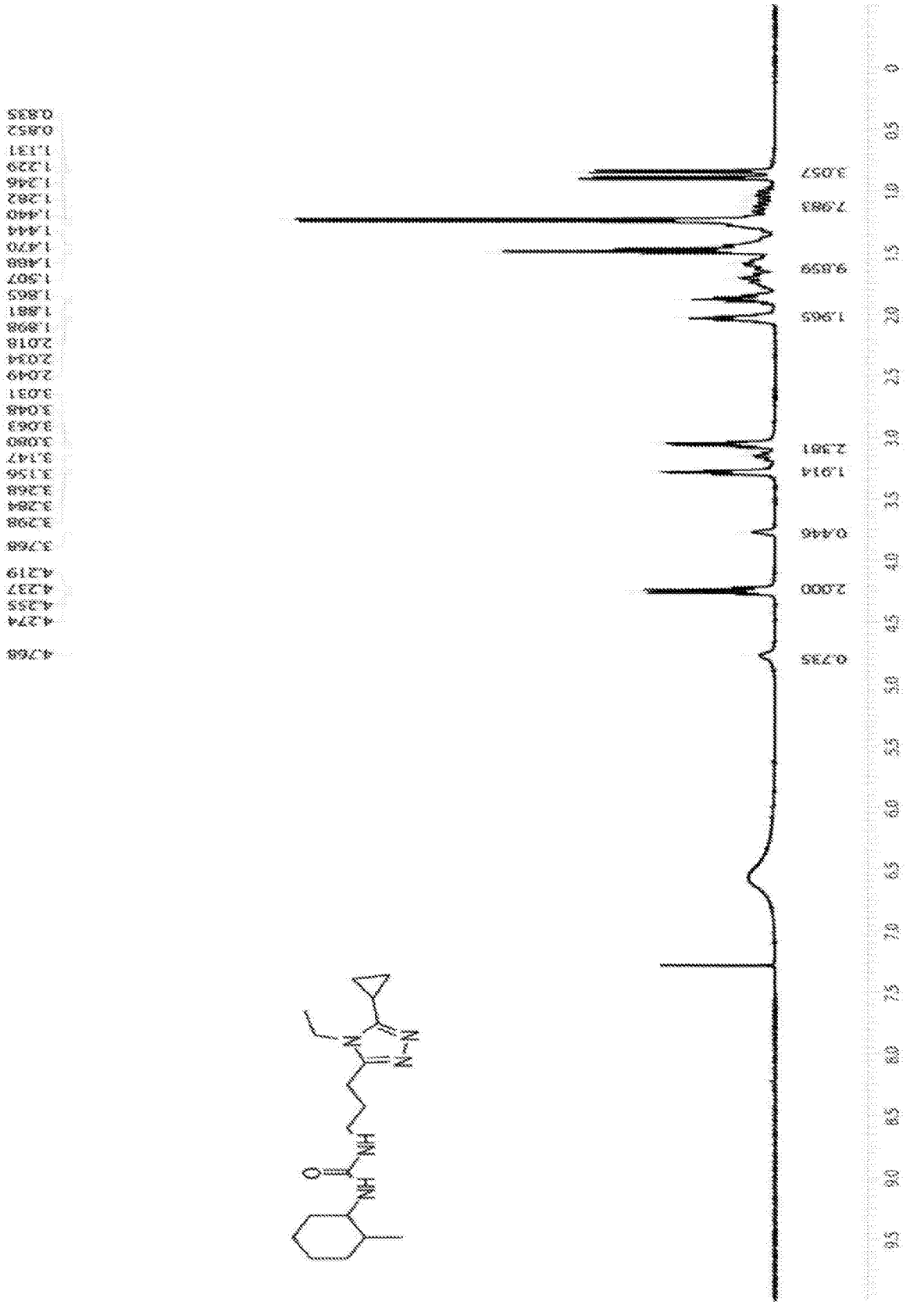

FIG. 94

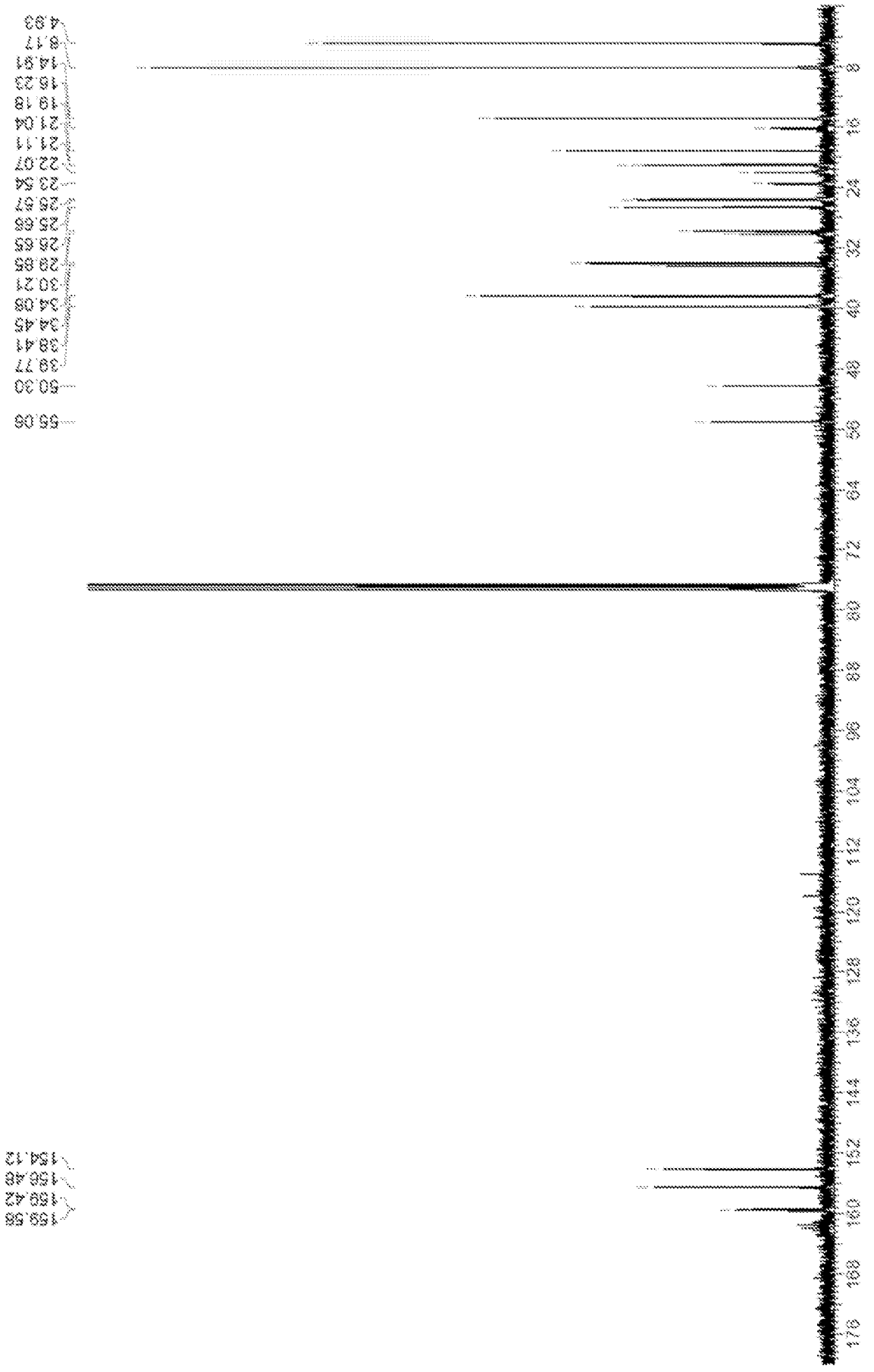
4.83
8.17
14.91
16.23
19.18
21.04
21.11
22.07
23.54
25.67
25.65
26.65
28.86
30.21
34.08
34.45
38.41
39.77
50.30
56.08
154.12
156.48
158.42
159.58
8
16
24
32
40
48
56
64
72
80
88
96
104
112
120
128
136
144
152
160
168
176

FIG. 95

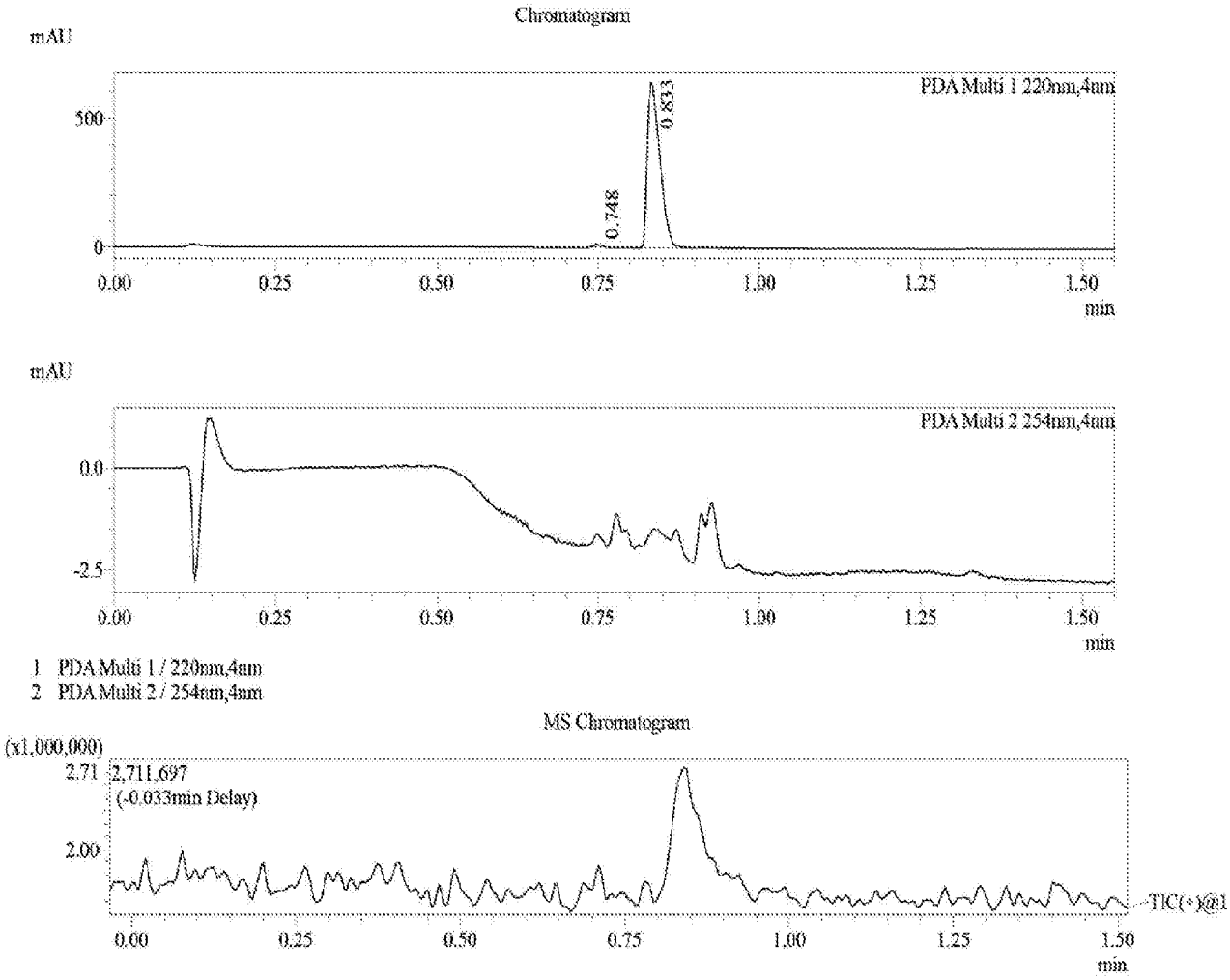

Peak Table

PDA Ch1 220nm

Peak#	Ret. Time	Height	Height%	USP Width	Area	Area%
1	0.748	12991	1.989	0.026	11389	1.308
2	0.833	639985	98.011	0.038	859346	98.692

Peak Table

PDA Ch2 254nm

FIG. 96

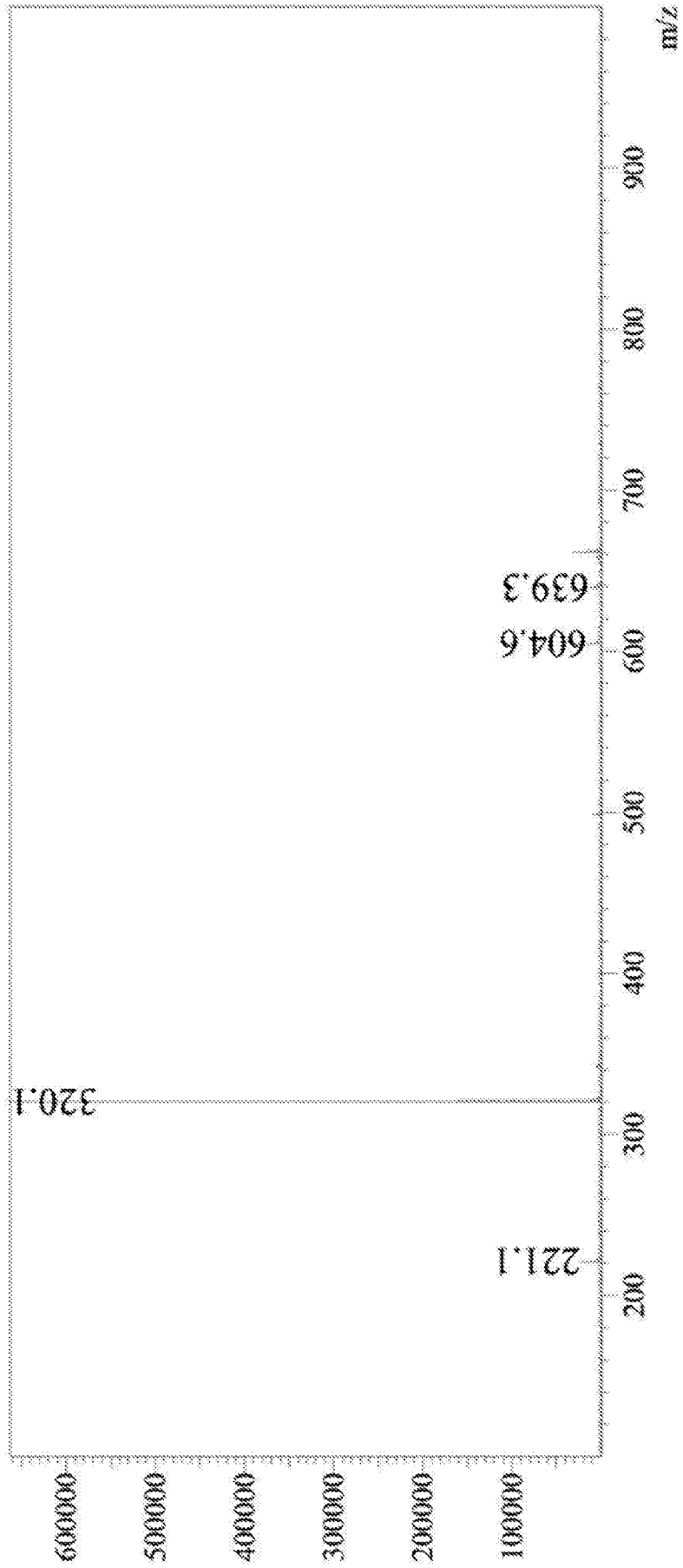
m/z
600000
500000
400000
300000
200000
100000
200
300
400
500
600
700
800
900
221.1
320.1
604.6
639.3

FIG. 97

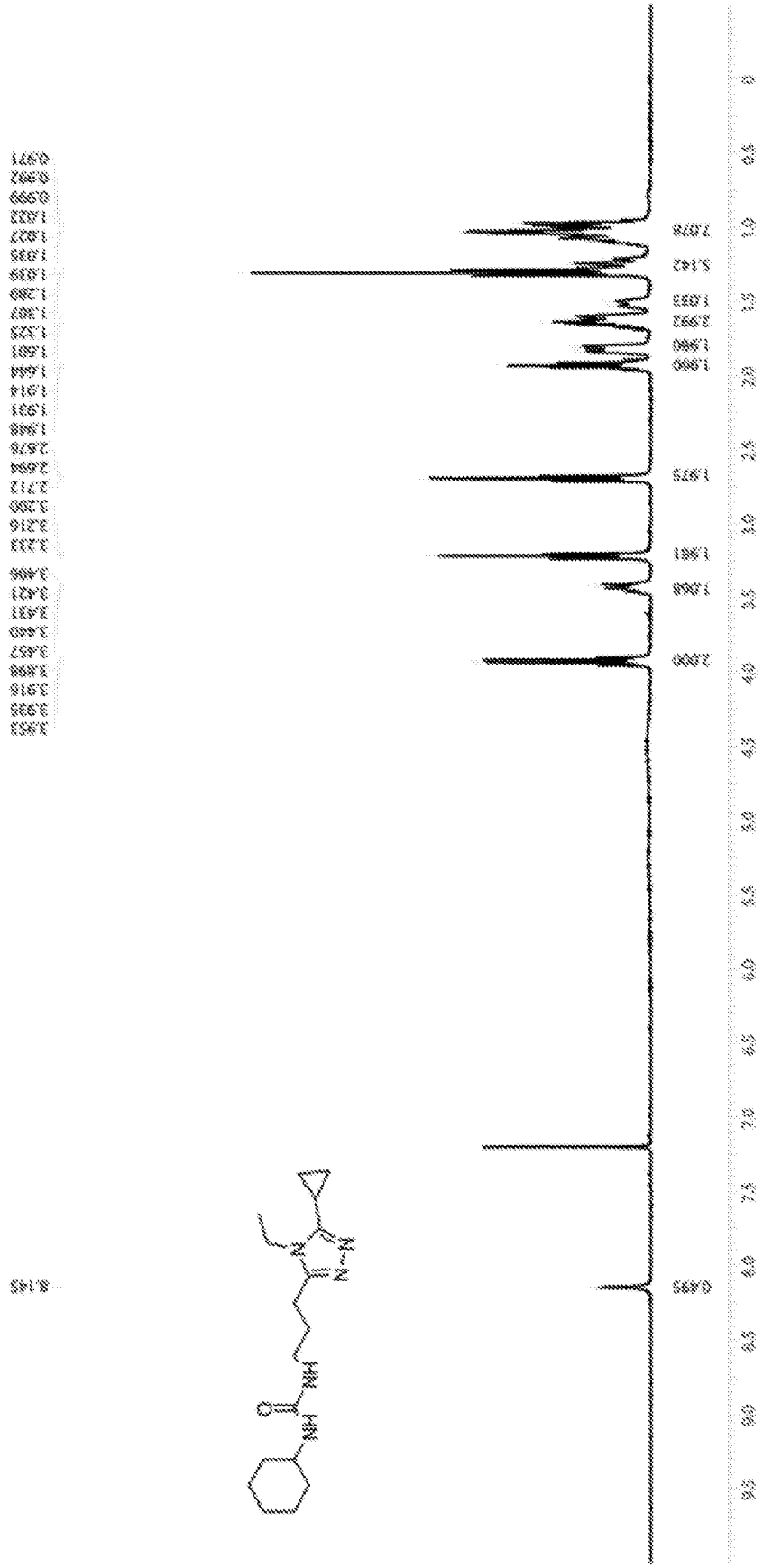

FIG. 98

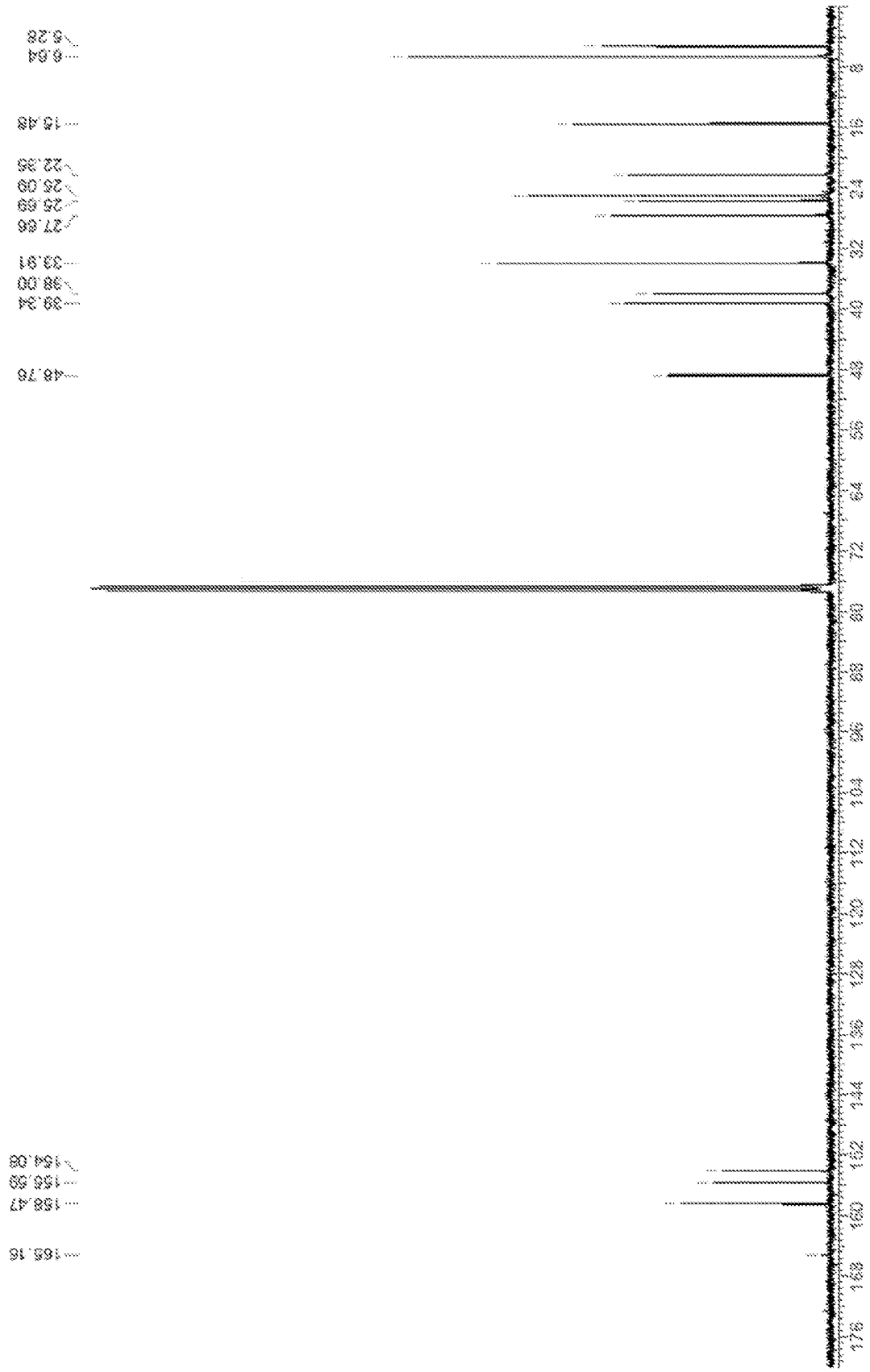
6.84
15.48
22.35
25.09
25.69
27.66
33.91
39.00
39.34
48.76
154.08
156.59
158.47
165.16

FIG. 99

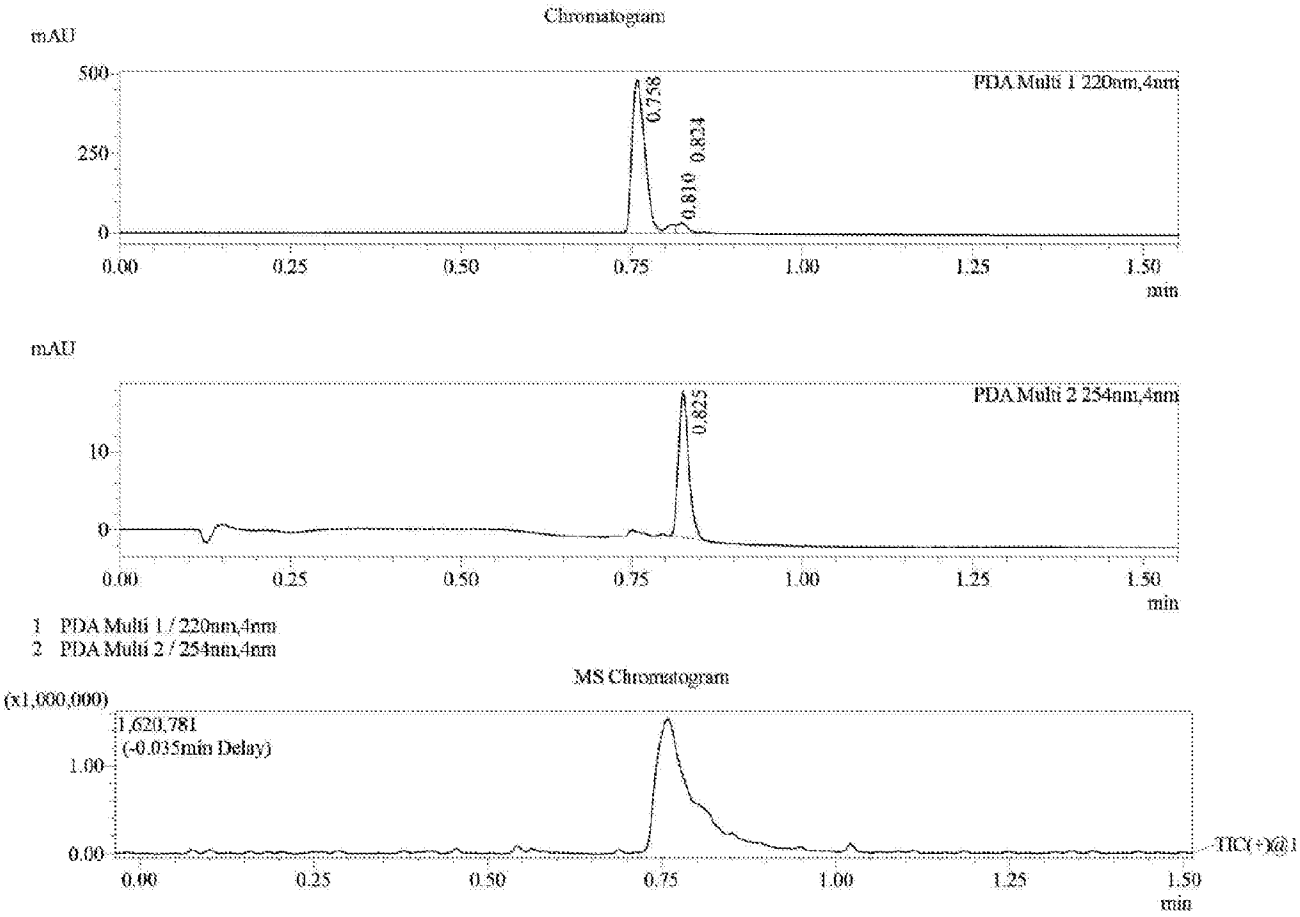

Peak Table

PDA Ch1 220nm

Peak#	Ret. Time	Height	Height%	USP Width	Area	Area%
1	0.758	482320	89.964	0.036	619255	92.203
2	0.810	24812	4.628	0.070	22492	3.349
3	0.824	28992	5.408	0.052	29876	4.448

Peak Table

PDA Ch2 254nm

Peak#	Ret. Time	Height	Height%	USP Width	Area	Area%
1	0.825	18799	100.000	0.029	19440	100.000

FIG. 100

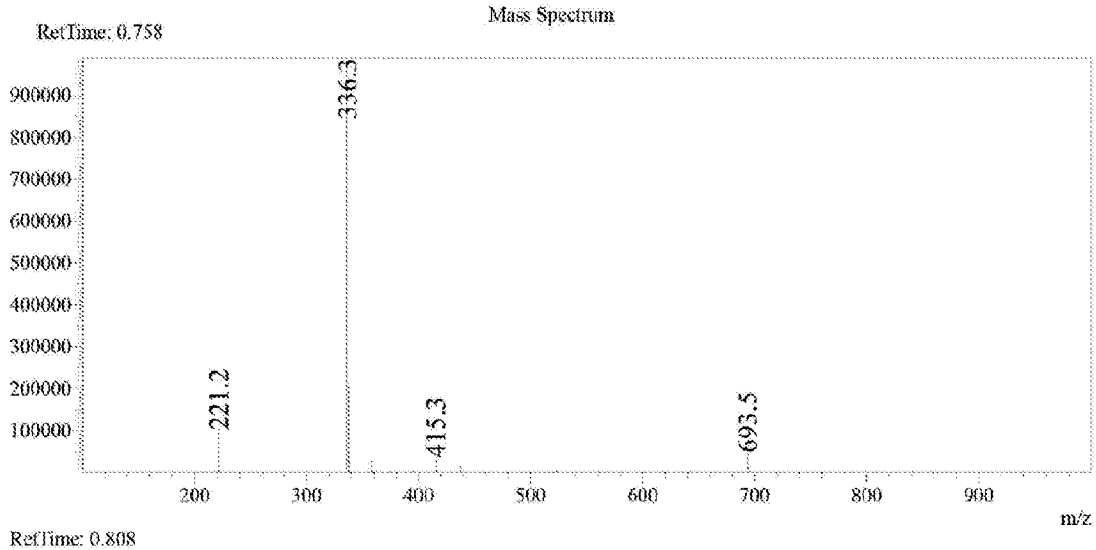

FIG. 101A

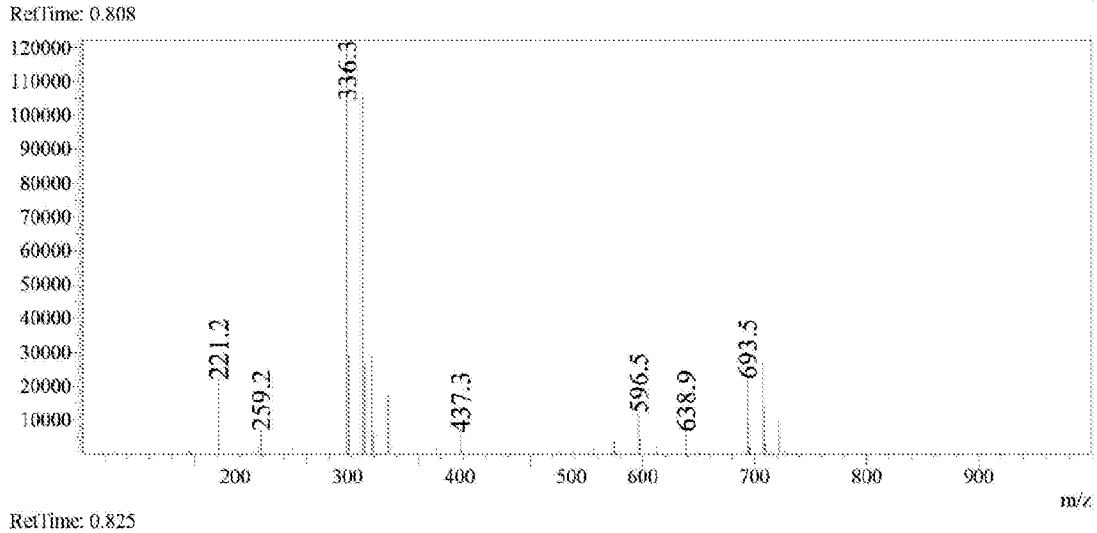

FIG. 101B

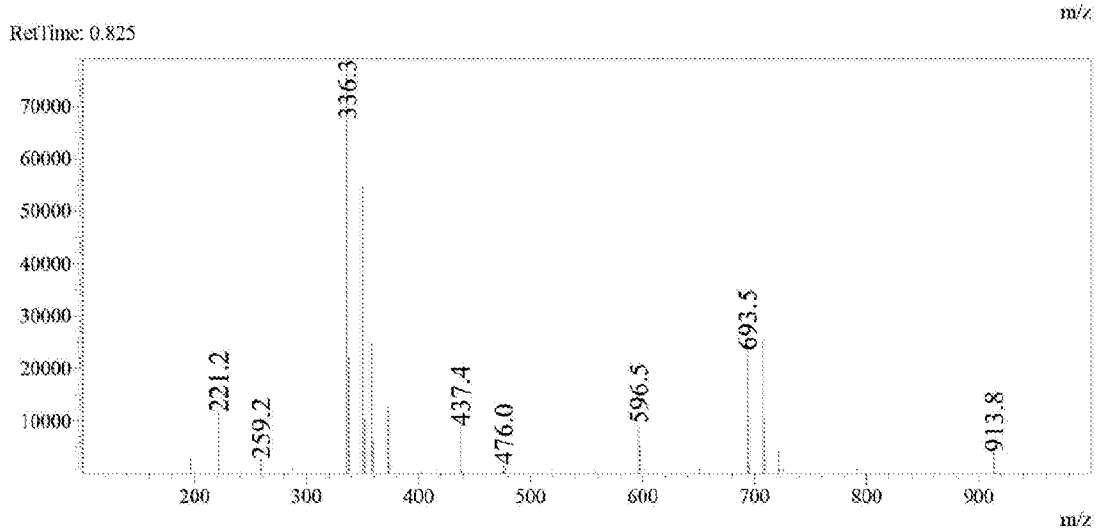

FIG. 101C

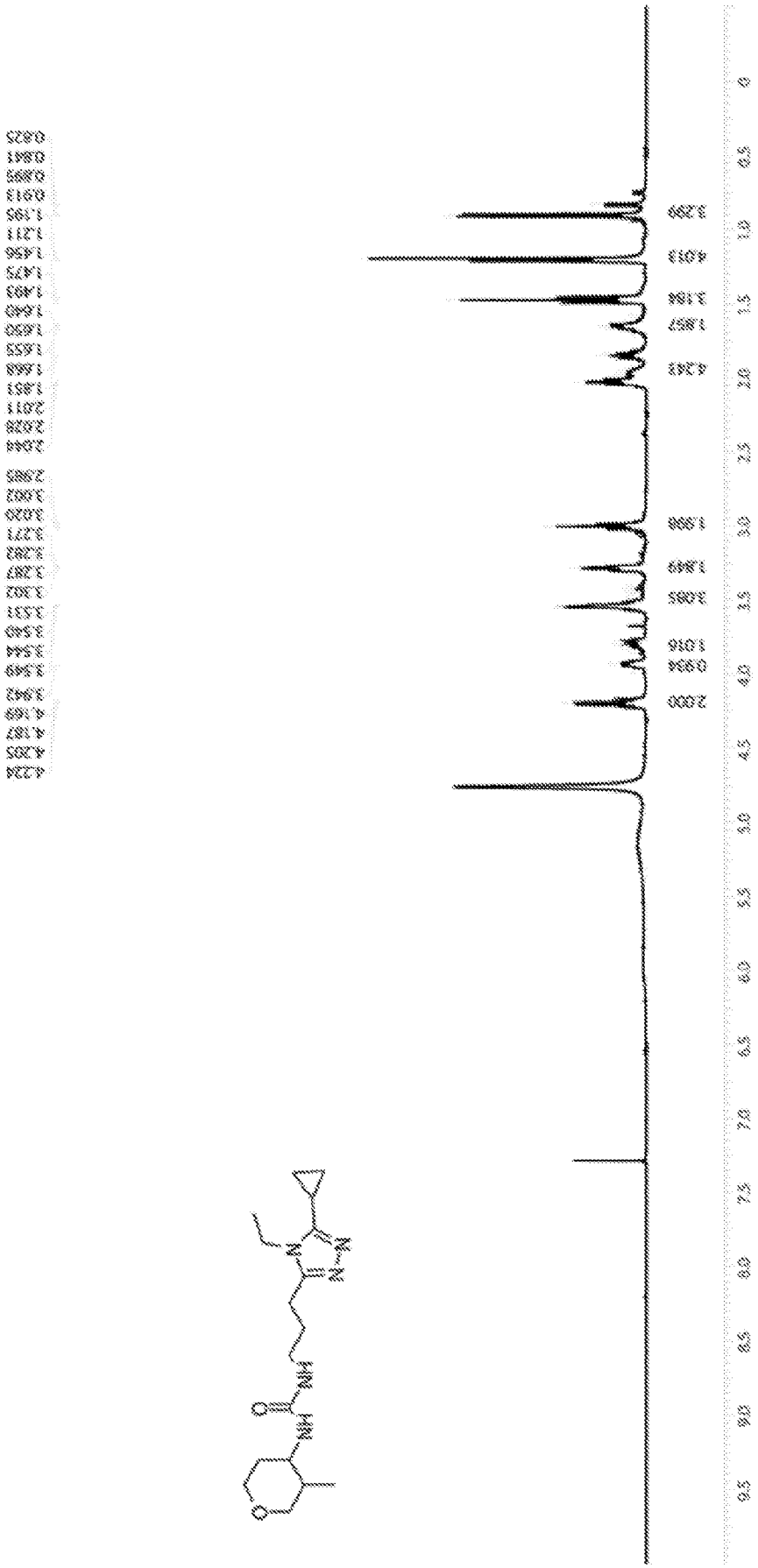

FIG. 102

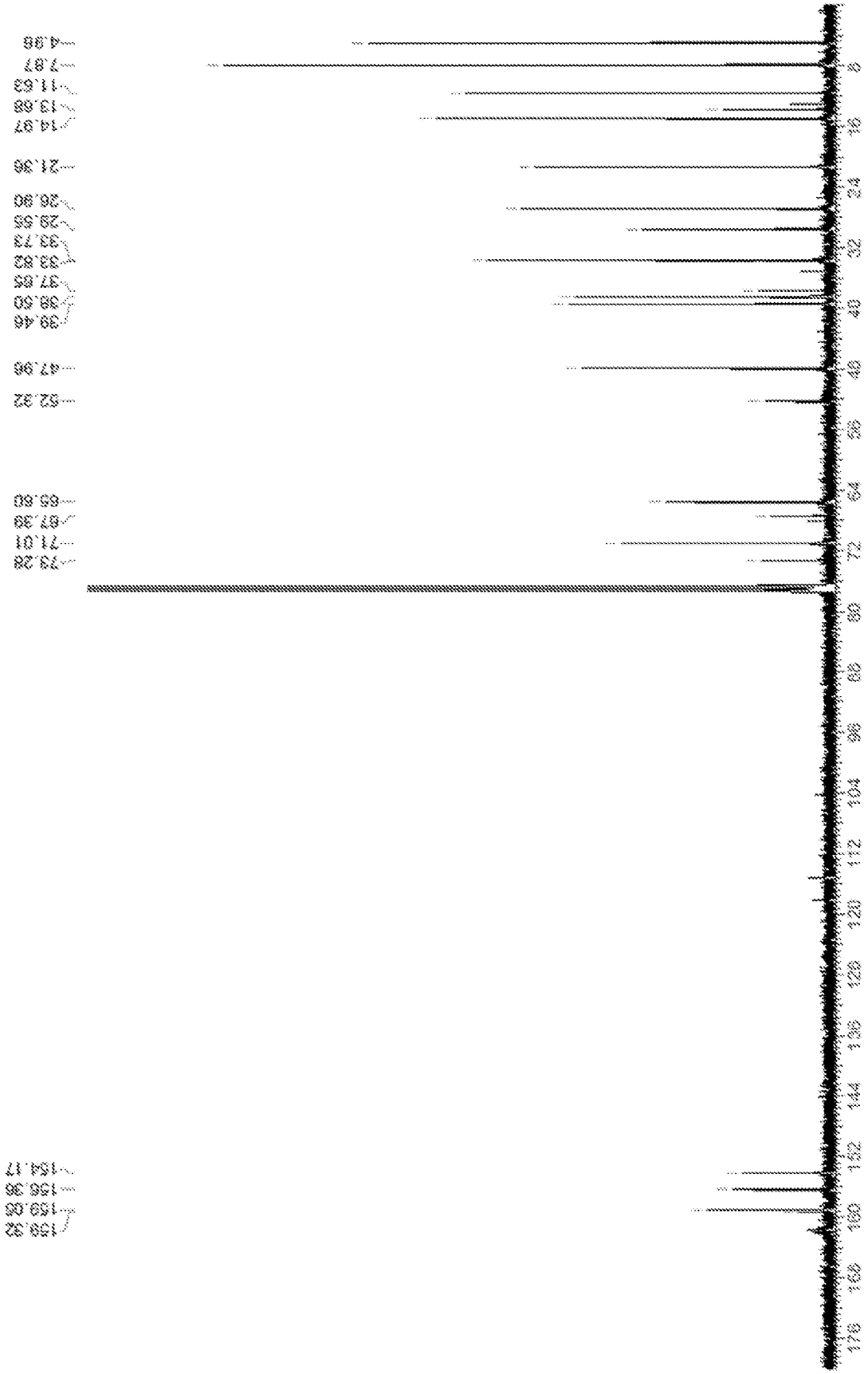
4.98
7.87
11.63
13.68
14.97
21.36
26.90
29.55
33.73
33.82
37.65
39.60
39.46
47.96
52.32
65.60
67.39
71.01
73.28
159.32
159.06
156.36
154.17

FIG. 103

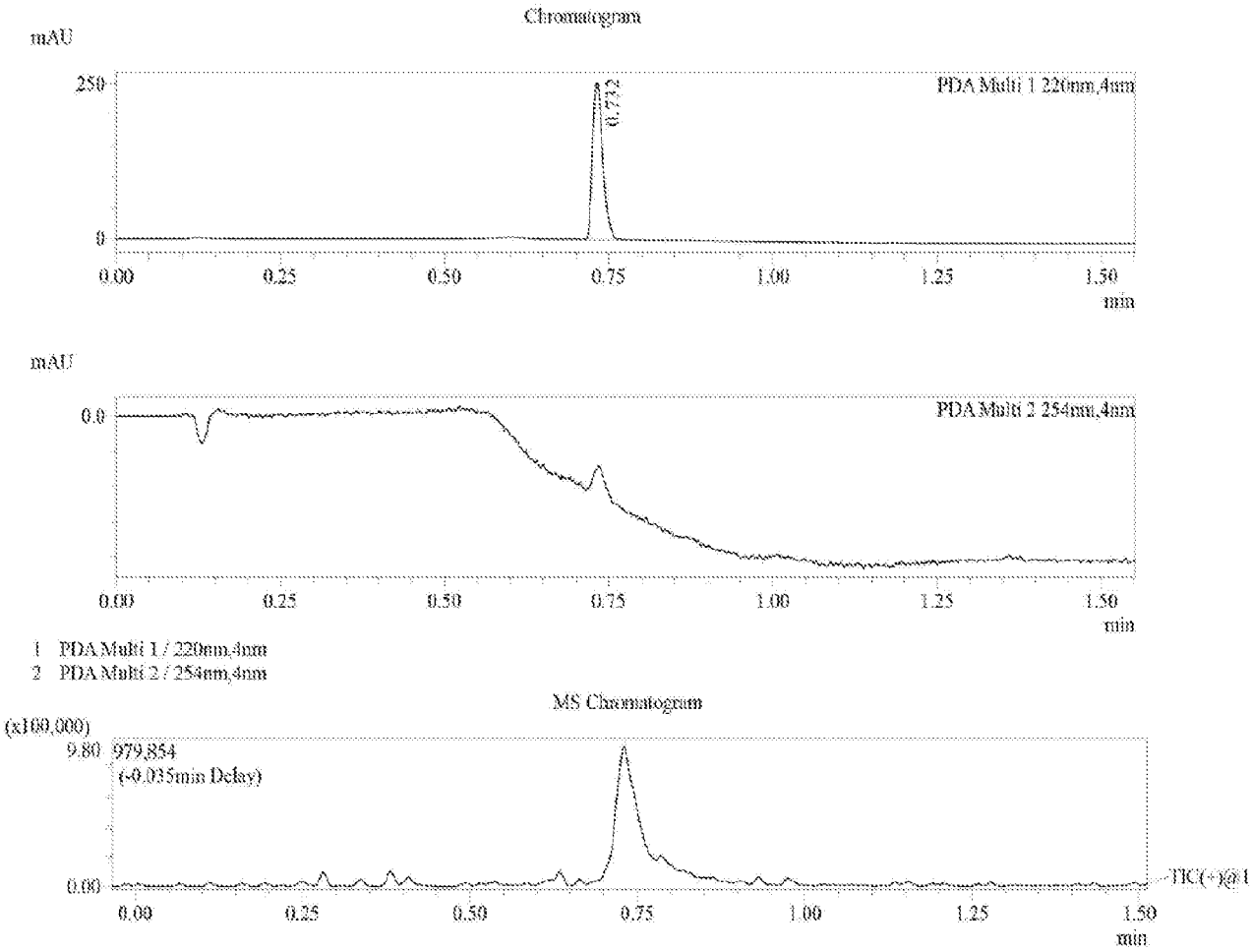

Peak Table

PDA Ch1 220nm

Peak#	Ret. Time	Height	Height%	USP Width	Area	Area%
1	0.732	253866	100.000	0.030	274862	100.000

Peak Table

PDA Ch2 254nm

FIG. 104

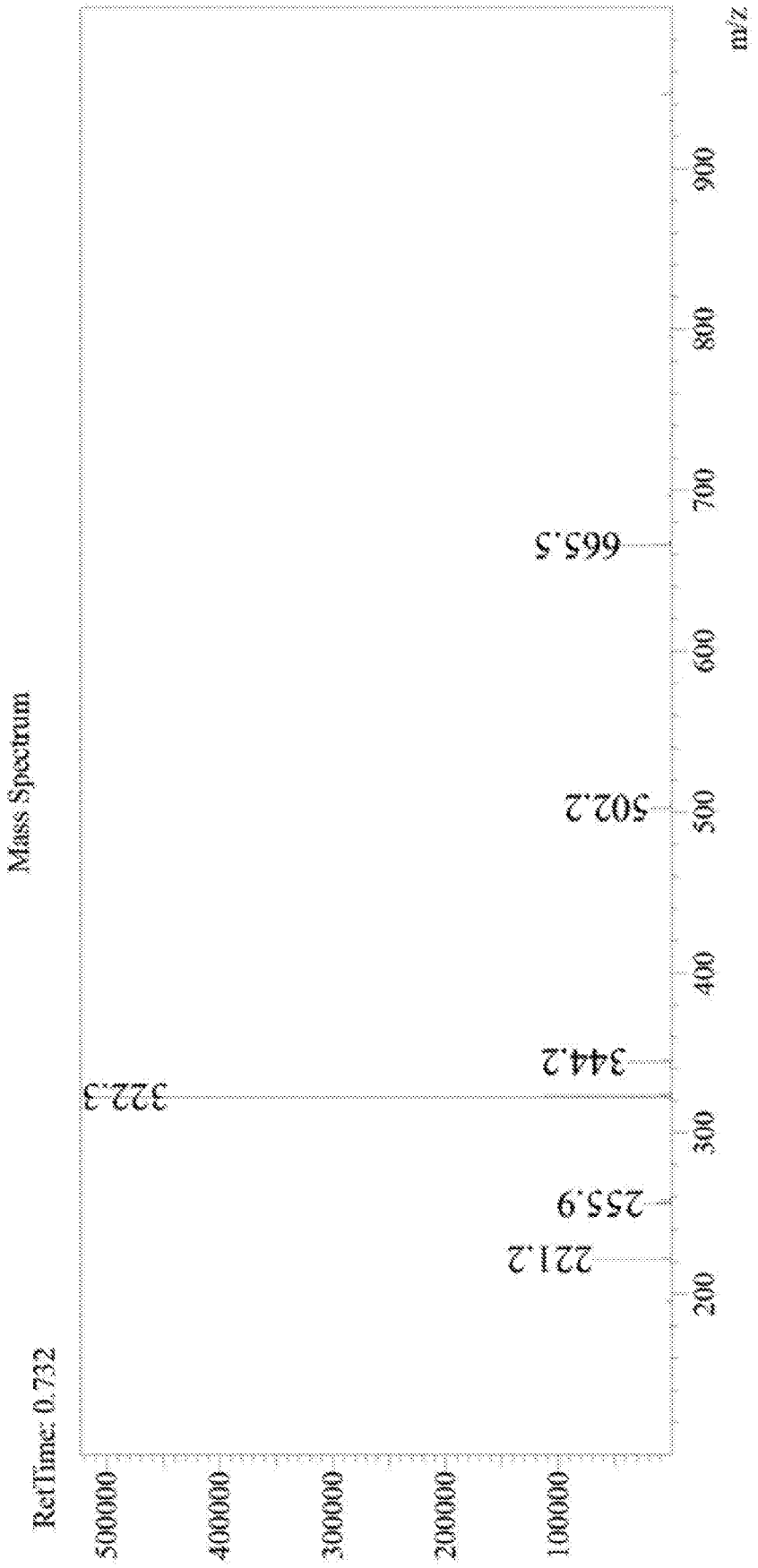
Mass Spectrum
RetTime: 0.732
500000
400000
300000
200000
100000
200
300
400
500
600
700
800
900
m/z
221.2
255.9
322.3
344.2
502.2
665.5

FIG. 105

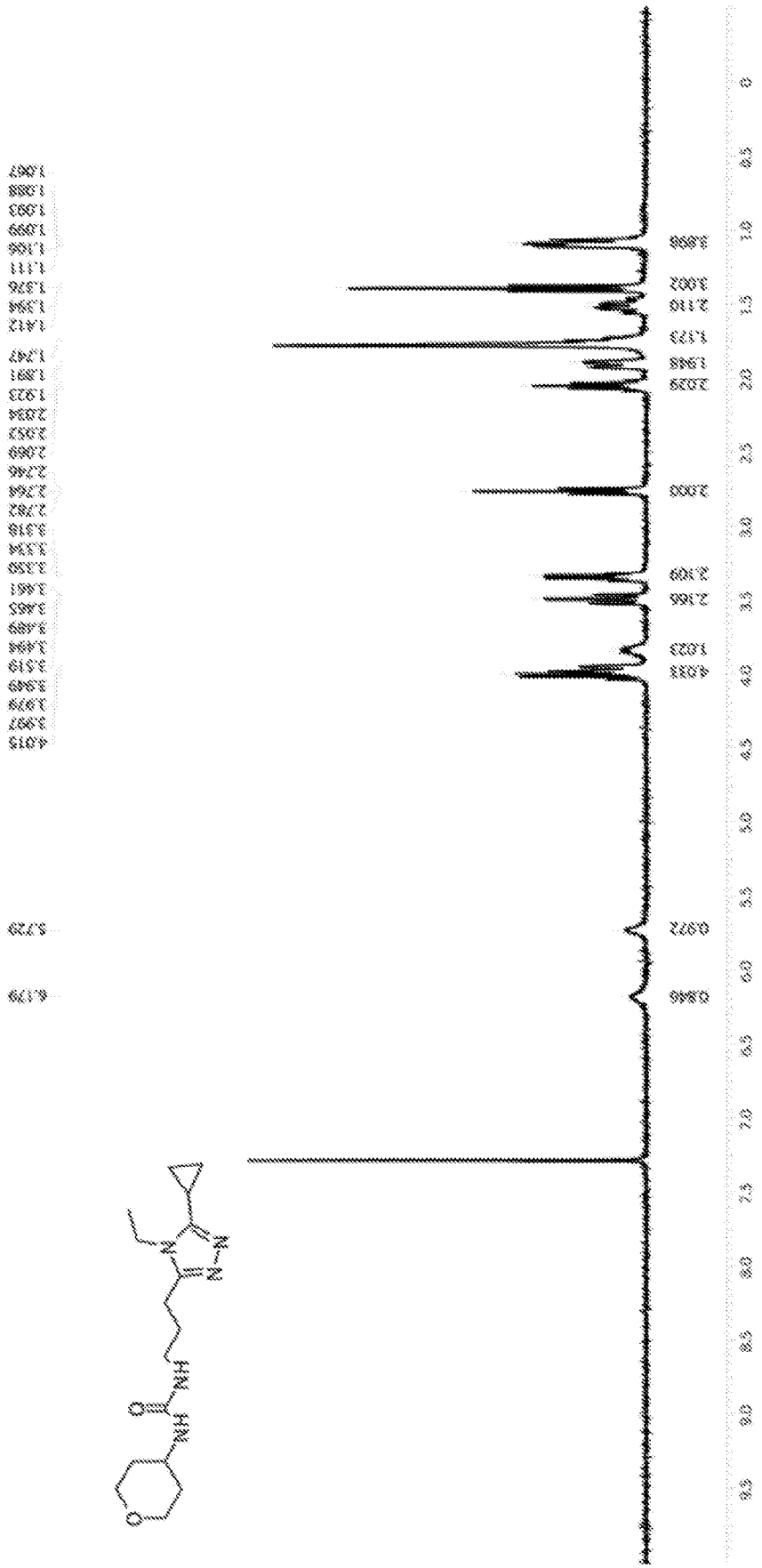

FIG. 106

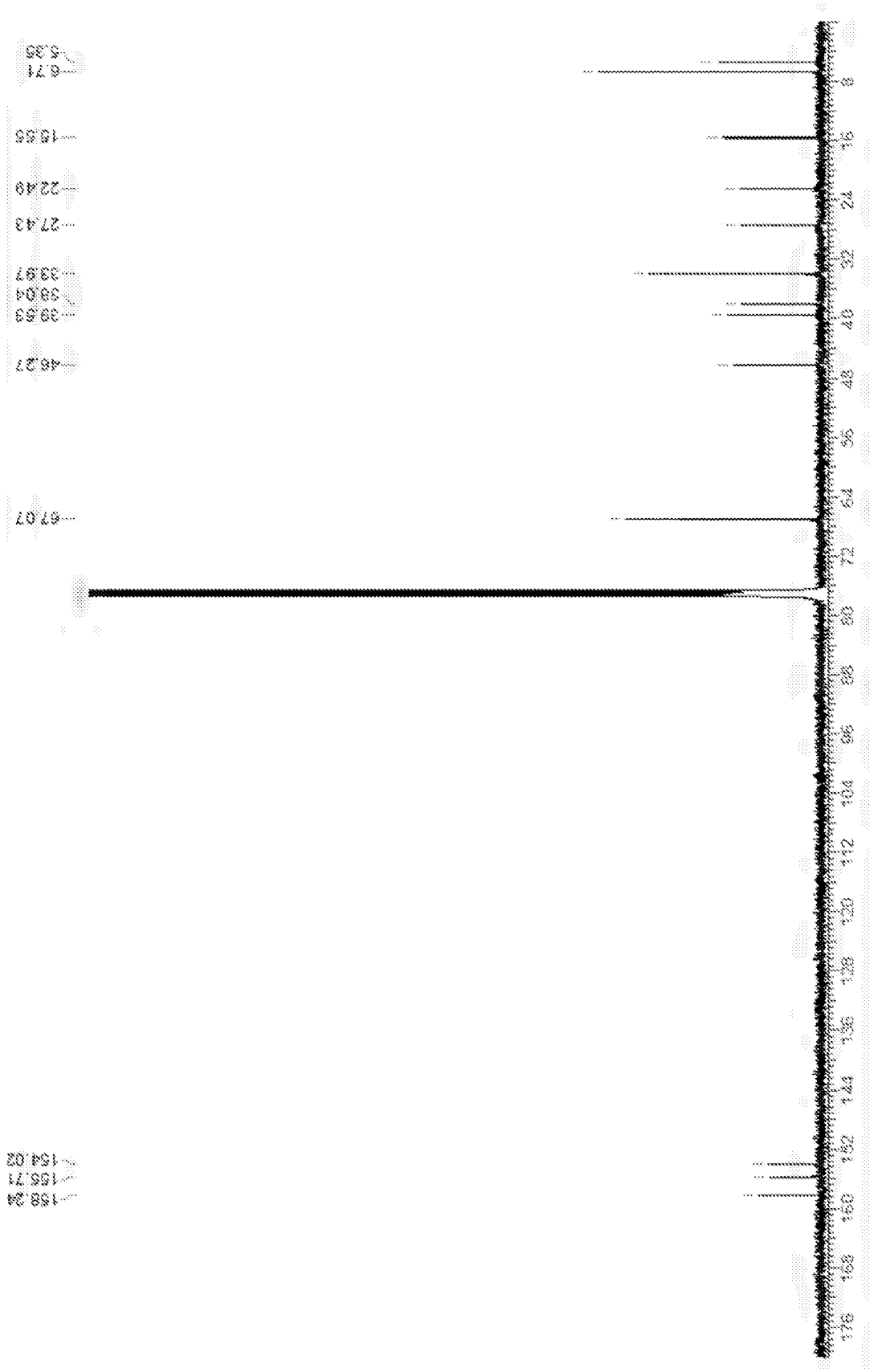
6.35
6.71
15.55
22.49
27.43
33.97
39.04
39.53
48.27
67.07
154.02
155.71
158.34
0
8
16
24
32
40
48
56
64
72
80
88
96
104
112
120
128
136
144
152
160
168
176

FIG. 107

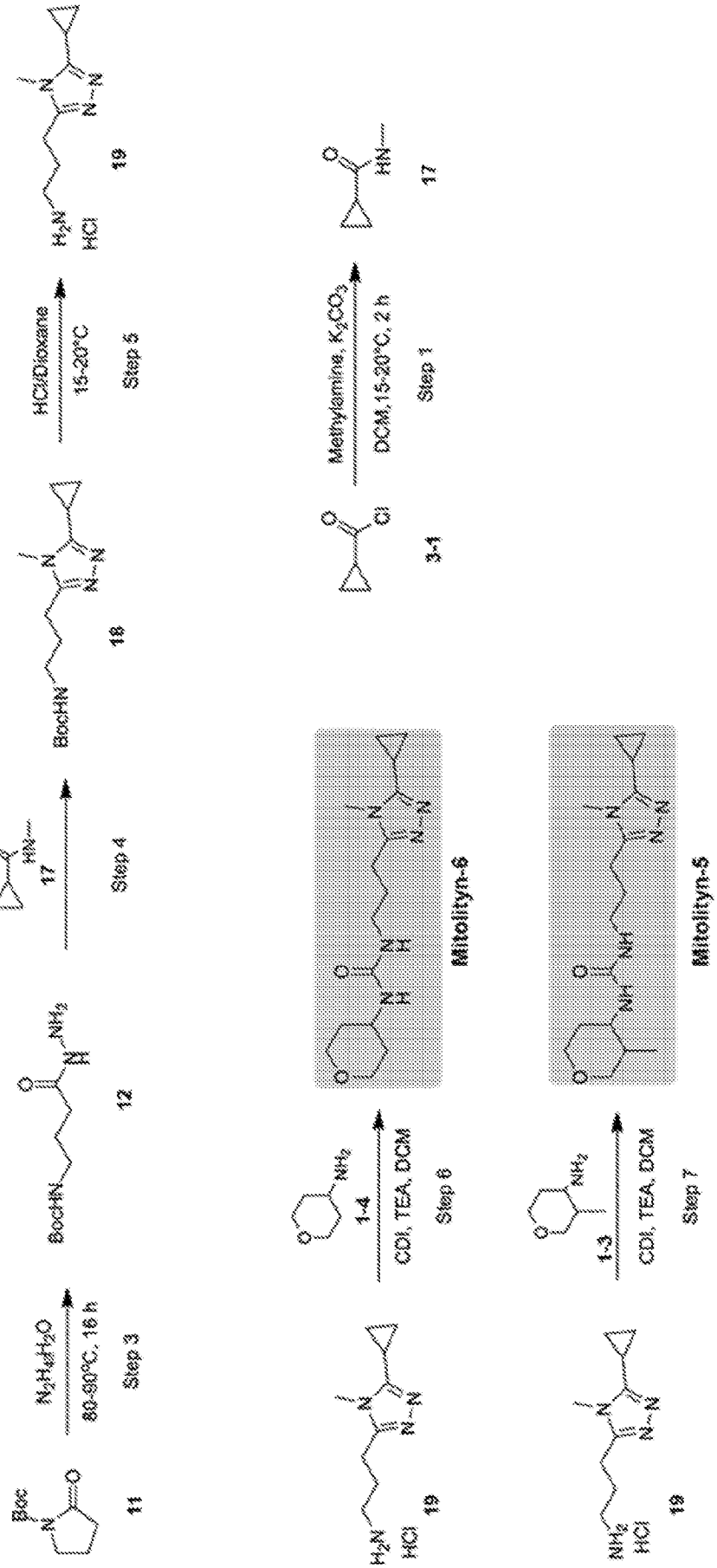
Boc
11
N2H4-H2O
80-90°C, 16 h
Step 3
BocHN
NH2
12
17
Step 4
BocHN
18
HCl/Dioxane
15-20°C
Step 5
H2N
HCl
19
Methylamine, K2CO3
DCM,15-20°C, 2 h
Step 1
Cl
3-1
17
1-4
CDI, TEA, DCM
Step 6
Mitolityn-6
1-3
CDI, TEA, DCM
Step 7
Mitolityn-5

FIG. 108

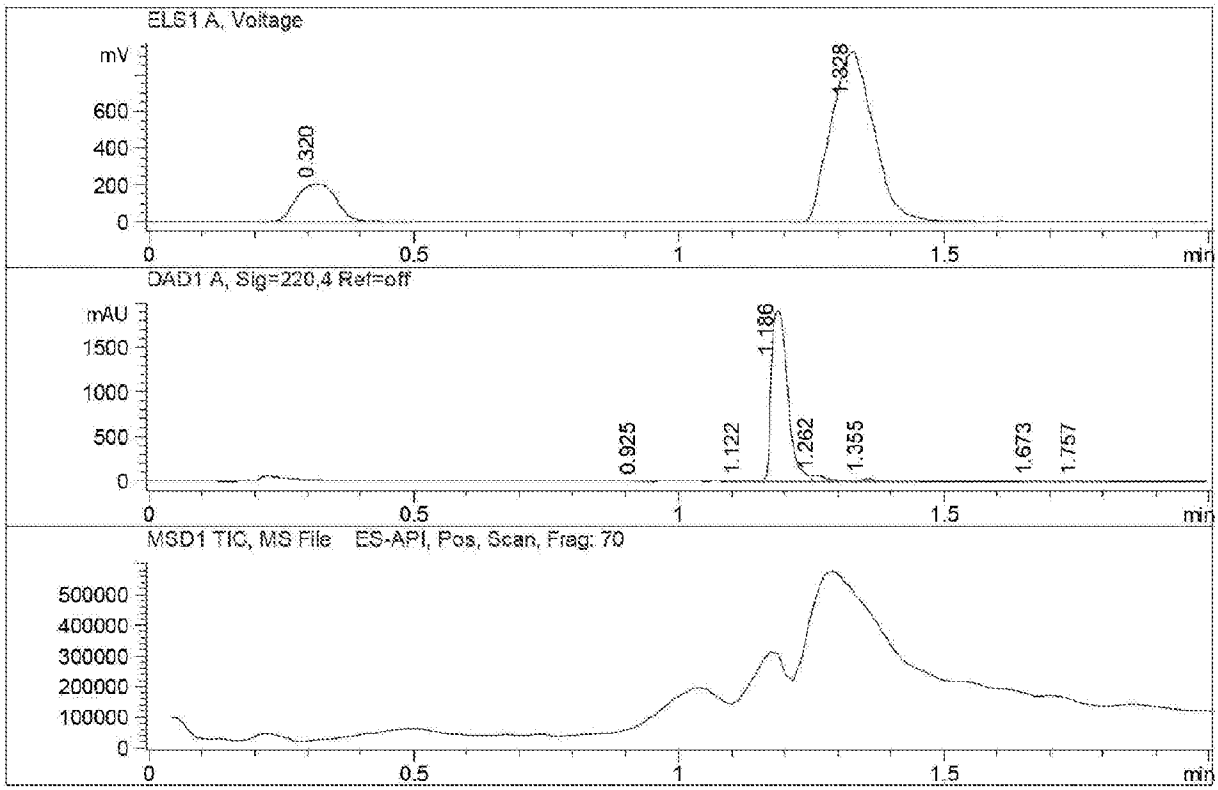

Signal 1 : ELS1 A, Voltage

#	Meas. Ret.	Height	Width	Area	Area %
1	0.320	204.565	0.087	1078.739	17.343
2	1.328	923.105	0.089	5141.298	82.657

Signal 2 : DAD1 A, Sig=220,4 Ref=off

#	Meas. Ret.	Height	Width	Area	Area %
1	0.925	2.258	0.020	2.861	0.067
2	1.122	11.342	0.027	21.845	0.509
3	1.186	1909.261	0.034	4068.285	94.759
4	1.262	66.941	0.029	137.275	3.197
5	1.355	29.089	0.025	49.116	1.144
6	1.673	5.070	0.027	9.127	0.213
7	1.757	2.738	0.027	4.768	0.111

FIG. 109

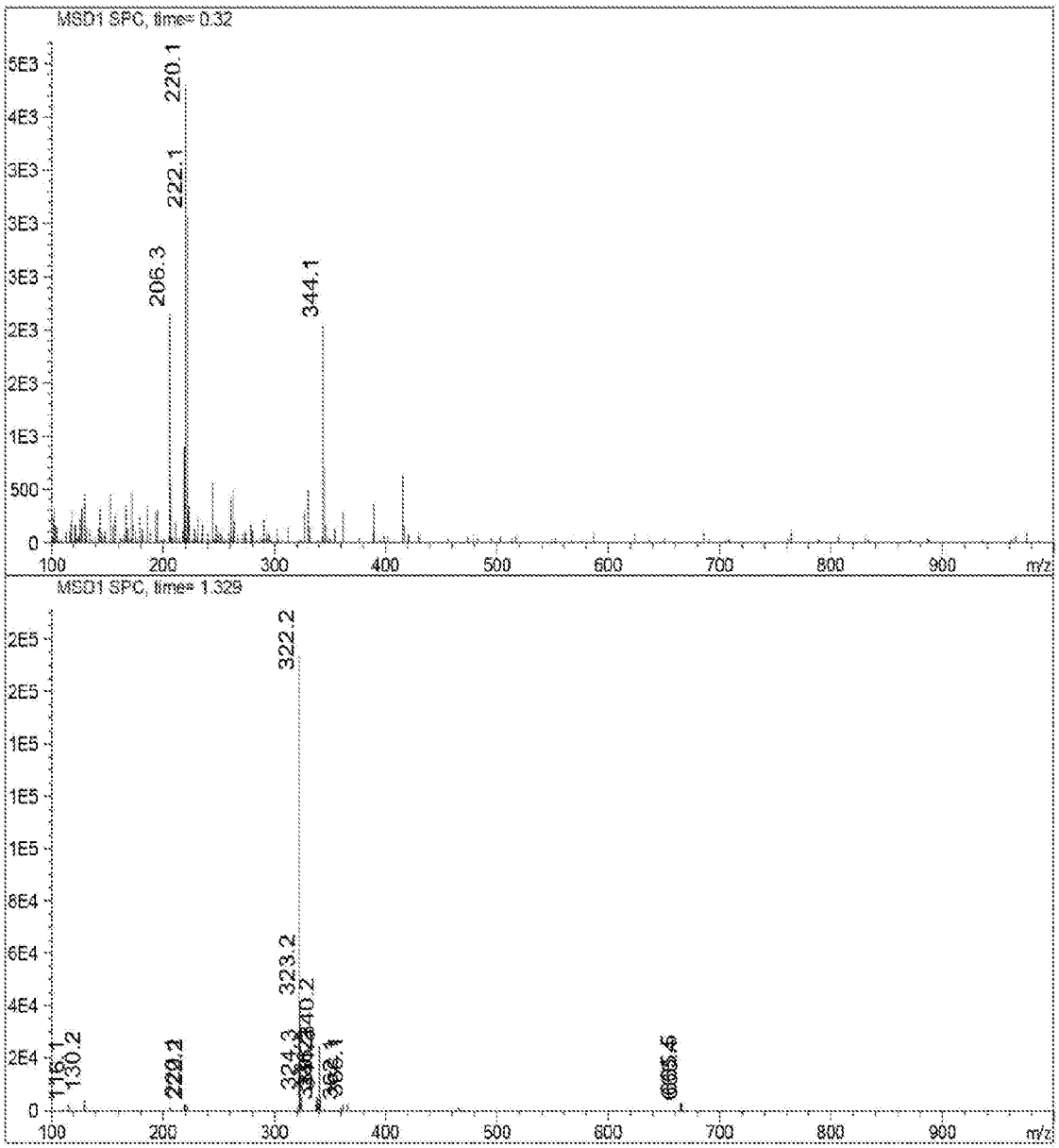
MSD1 SPC, time= 0.32
220.1
222.1
206.3
344.1
MSD1 SPC, time= 1.329
322.2
323.2
324.3
130.2
229.2
665.6
m/z

FIG. 110

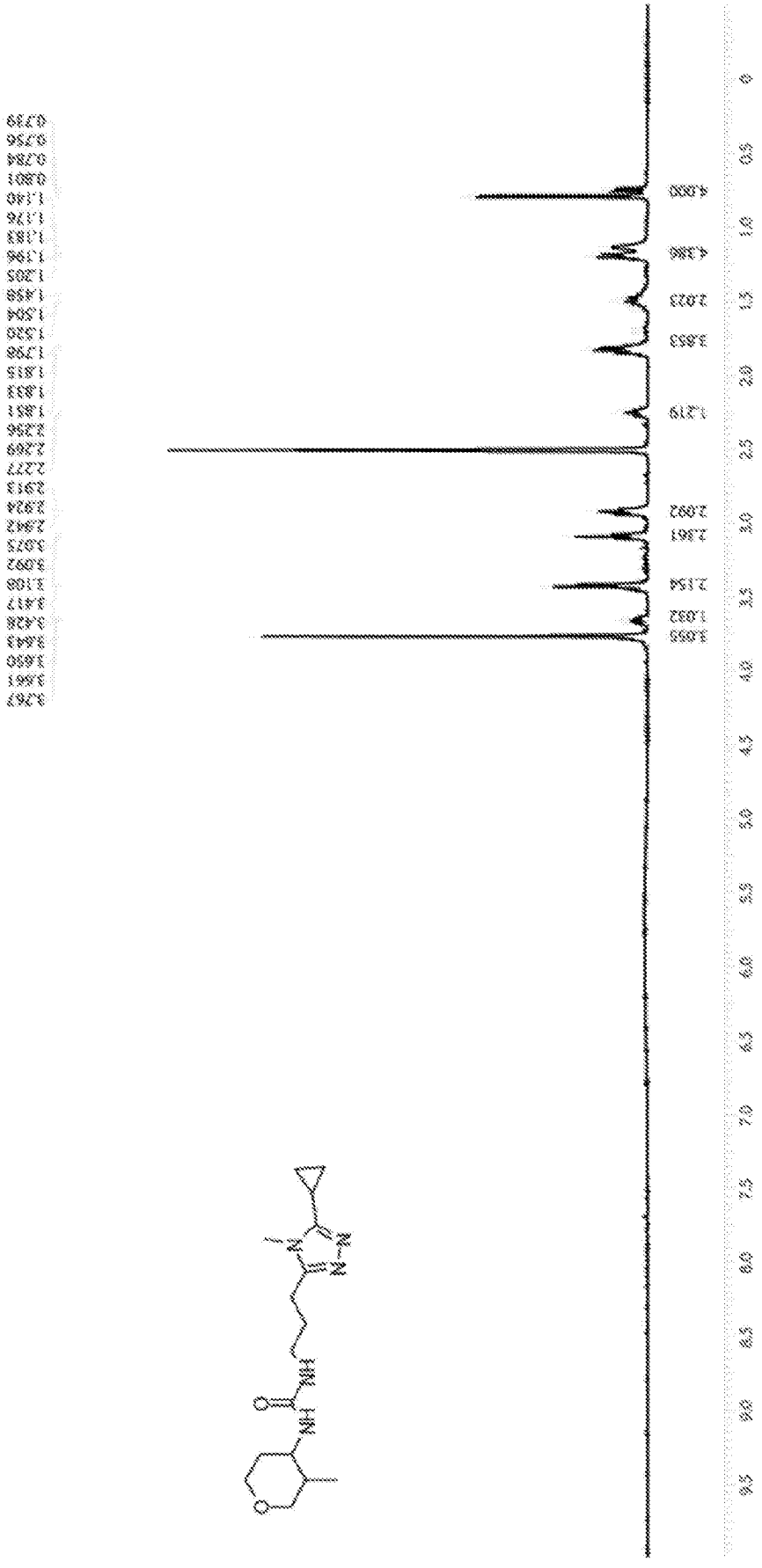

FIG. 111

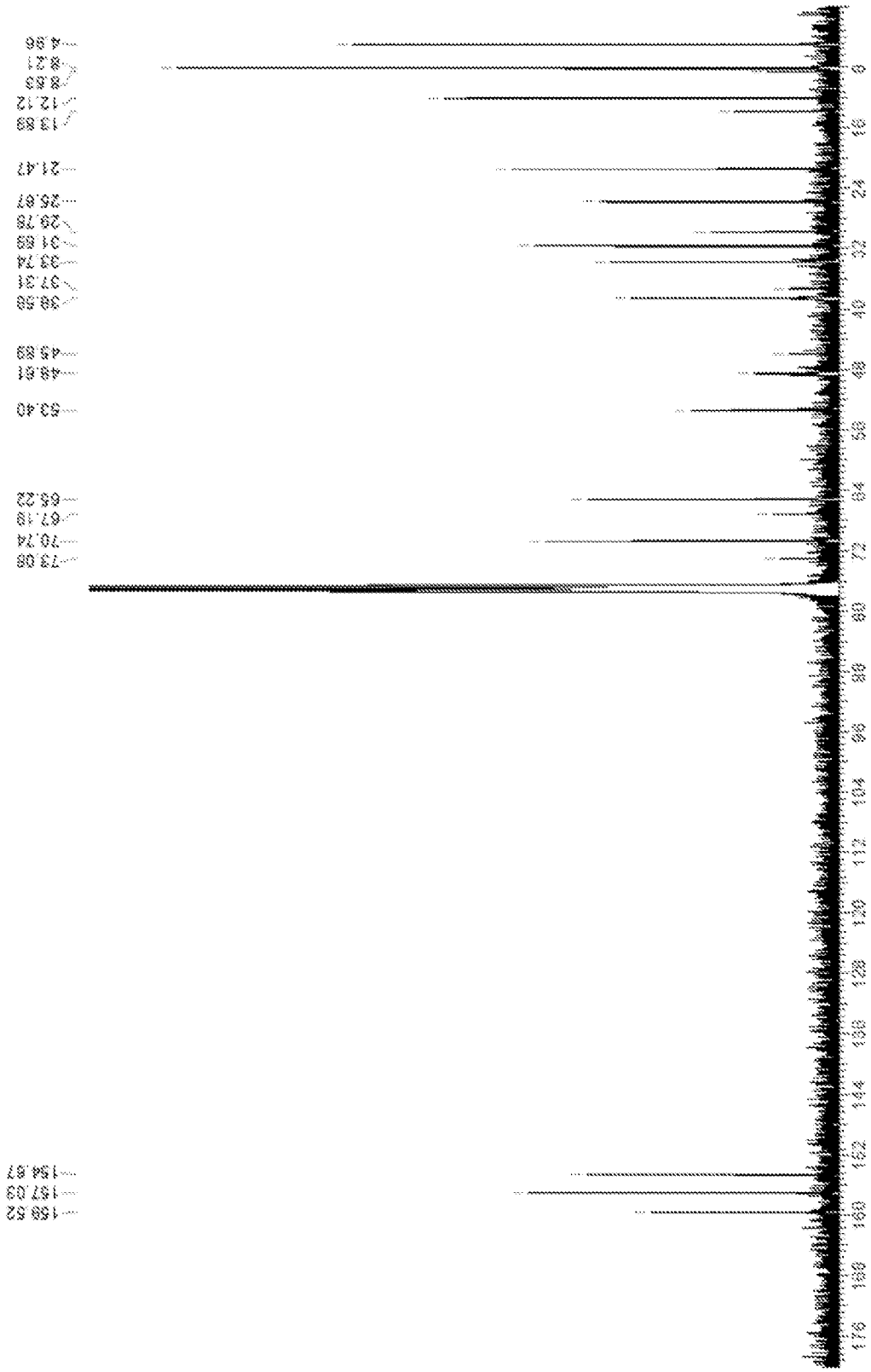
4.86
8.21
8.53
12.12
13.89
21.47
26.87
29.78
31.89
33.74
37.31
38.58
43.89
48.61
53.40
65.22
67.19
70.74
73.08
154.87
157.03
158.52
0
8
16
24
32
40
48
56
64
72
80
88
96
104
112
120
128
136
144
152
160
168
176

FIG. 112

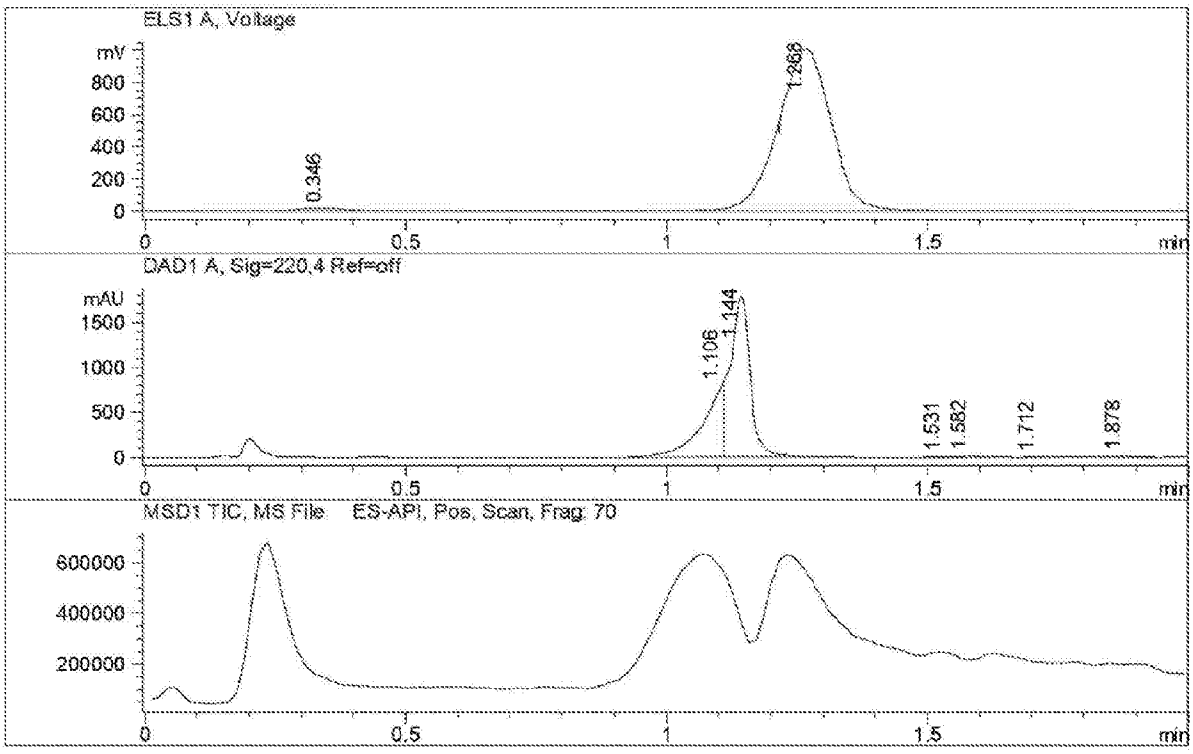

Signal 1 : EL51 A, Voltage

#	Meas. Ret.	Height	Width	Area	Area %
1	0.346	18.219	0.090	99.864	1.389
2	1.268	1005.521	0.116	7088.738	98.611

Signal 2 : DAD1 A, Sig=220,4 Ref=off

#	Meas. Ret.	Height	Width	Area	Area %
1	1.106	798.751	0.037	2277.742	32.730
2	1.144	1792.262	0.037	4600.015	66.100
3	1.531	5.382	0.033	12.710	0.183
4	1.582	17.826	0.027	32.263	0.464
5	1.712	5.725	0.024	8.833	0.127
6	1.878	12.827	0.033	27.610	0.397

FIG. 113

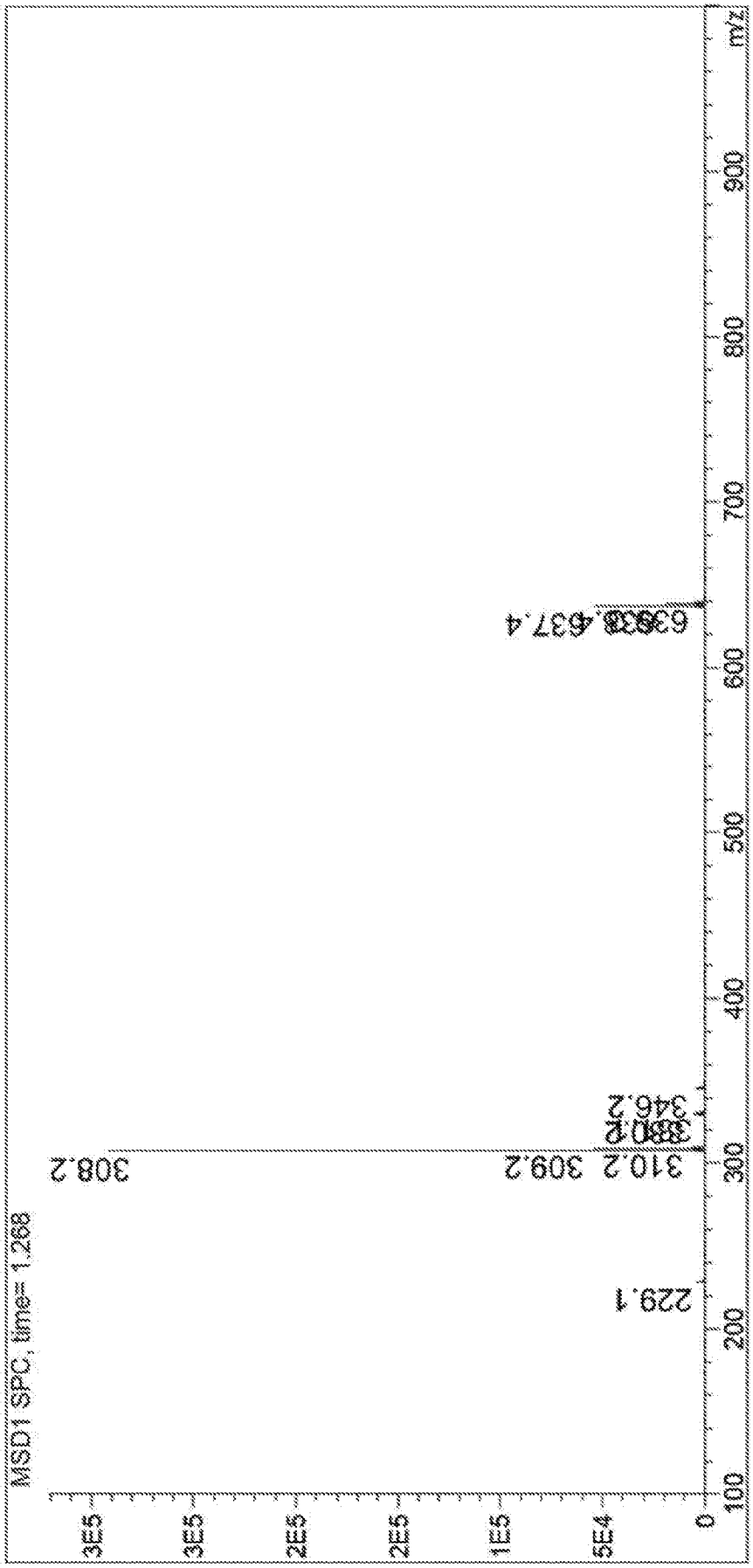
MSD1 SPC, time= 1.268
3E5
3E5
2E5
2E5
1E5
5E4
0
100
200
300
400
500
600
700
800
900
m/z
229.1
308.2
310.2
309.2
346.2
637.4

FIG. 114

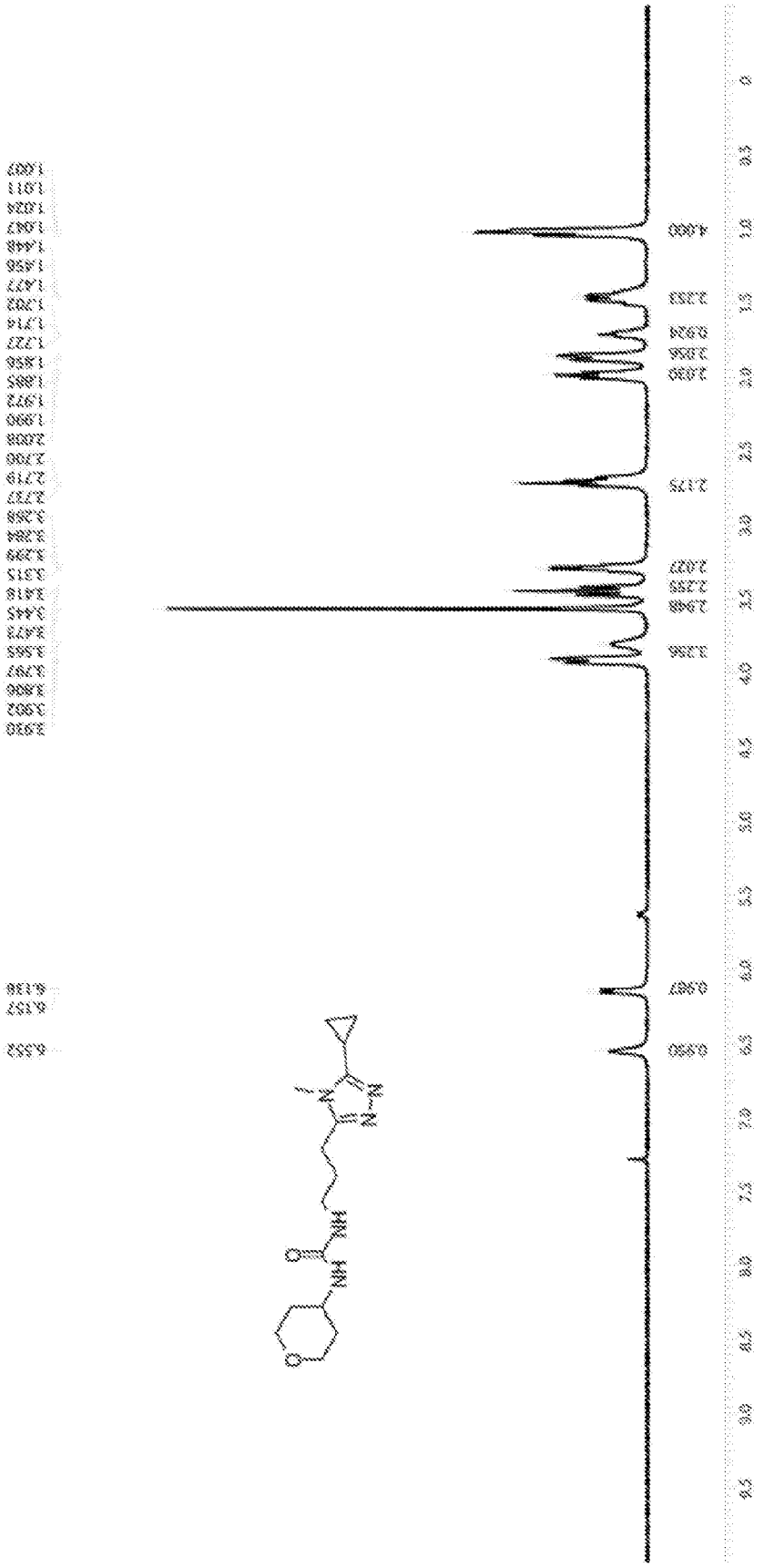

FIG. 115

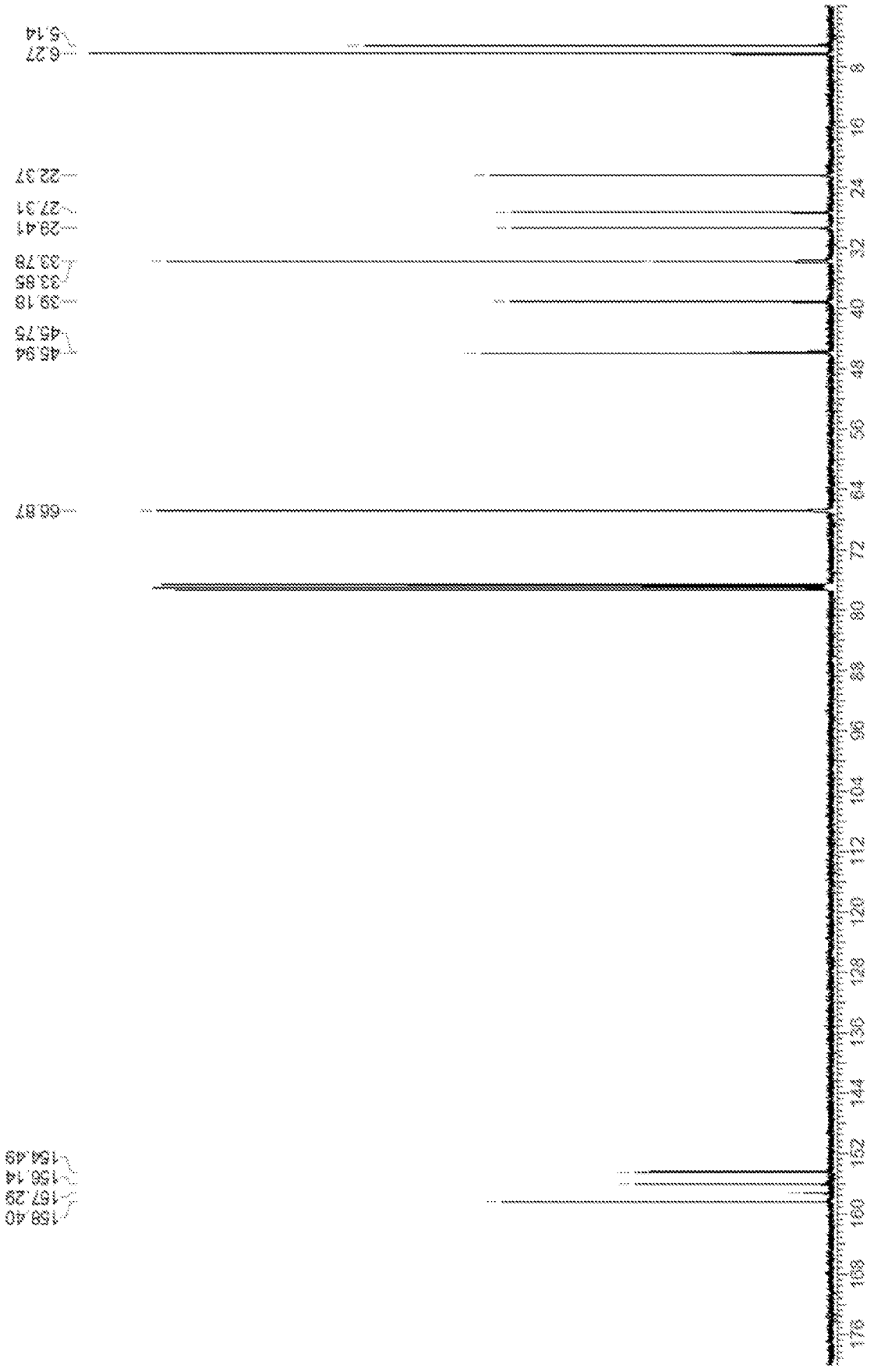
6.27
5.14
22.37
27.31
29.41
33.78
33.85
39.18
45.75
45.94
66.87
156.49
156.14
157.29
158.40
8
16
24
32
40
48
56
64
72
80
88
96
104
112
120
128
136
144
152
160
168
176

FIG. 116

Diseases	Mutation	Age	Sex	Passage	Source	Fibroblast ID
CMT2A	MFN2 Thr105Met	41	F	P4-P8	Dr. Robert H. Baloh	-
CMT2A	MFN2 Arg274Trp	23	M	P4-P8	Dr. Barbara Zablocka	-
CMT2A	MFN2 His361Tyr	41	M	P4-P8	Dr. Robert H. Baloh	-
PD	PARK2 Arg275Trp	61	F	P3-P7	NHCDR	ND29969
PD	PINK1 Ile368Asn	64	M	P3-P7	NHCDR	ND40066
PD	LRRK2 Gly2019Ser	66	F	P7-P10	NHCDR	ND33879
HD	*HTT* CAG #40	65	M	P3-P7	NHCDR	ND29970
HD	*HTT* CAG #57	29	F	P3-P7	NHCDR	ND33392
HD	*HTT* CAG #66	-	F	P3-P7	NHCDR	ND40536
AD	PSEN1 Met146Ile	-	F	P5-P9	NHCDR	ND34732
AD	PSEN1 Glu184Asp	-	M	P5-P9	NHCDR	ND34730
AD	PSEN1 Pro264Leu	-	M	P5-P9	NHCDR	ND34733
ALS	SOD1 Leu38Val	47	M	P3-P7	NHCDR	ND29523
ALS	SOD1 Ile113Thr	59	M	P9-P11	NHCDR	ND32969
ALS	SOD1 Leu144Pro	51	M	P3-P7	NHCDR	ND29415
CTRL 1	-	68	F	P3-P7	NHCDR	ND34769
CTRL 2	-	71	F	P3-P7	NHCDR	ND36320
CTRL 3	-	55	F	P3-P7	NHCDR	ND29510
CTRL 4	-	66	M	P8-P10	NHCDR	ND29178
CTRL 5	-	72	M	P3-P7	NHCDR	ND34770

FIG. 117

INTERNATIONAL SEARCH REPORT

International application No.
PCT/US2018/060177

A. CLASSIFICATION OF SUBJECT MATTER

IPC(8) - A61K 38/04; A61K 38/08; A61K 38/10; A61P 25/00; C07K 7/00; C07K 7/02; C07K 7/06 (2019.01)

CPC - A61K 38/005; A61K 38/04; A61K 38/08; A61K 38/10; A61P 25/00; C07K 7/00; C07K 7/02; C07K 7/06; C07K 7/08 (2019.02)

According to International Patent Classification (IPC) or to both national classification and IPC

B. FIELDS SEARCHED

Minimum documentation searched (classification system followed by classification symbols)

See Search History document

Documentation searched other than minimum documentation to the extent that such documents are included in the fields searched

USPC - 514/21.4; 514/21.5; 514/21.6; 514/21.7; 514/21.8; 530/325; 530/326; 530/327; 530/328; 530/329; 530/330 (keyword delimited)

Electronic data base consulted during the international search (name of data base and, where practicable, search terms used)

See Search History document

C. DOCUMENTS CONSIDERED TO BE RELEVANT

Category*	Citation of document, with indication, where appropriate, of the relevant passages	Relevant to claim No.
P, X	WO 2018/057648 A1 (THE BOARD OF TRUSTEES OF THE LELAND STANFORD JUNIOR UNIVERSITY et al) 29 March 2018 (29.03.2018) entire document	1-5, 7, 8, 16-25
P, X	WO 2018/200323 A1 (WASHINGTON UNIVERSITY) 01 November 2018 (01.11.2018) entire document	1-5, 7, 8, 16-25
P, X	ROCHA et al. "MFN2 agonists reverse mitochondrial defects in preclinical models of Charcot-Marie-Tooth disease type 2A," Science, 20 April 2018 (20.04.2018), Vol. 360, Iss. 6386, Pgs. 336-341. entire document	1-5, 7, 8, 16-25
P, X	ZACHARIOUDAKIS et al. "Direct Small Molecule Activation of Mitofusins," bioRxiv, 17 April 2018 (17.04.2018), Pgs. 1-30. Retrieved from the Internet:<https://www.biorxiv.org/content/early/2018/04/17/301713.full.pdf> on 25 February 2019 (25.02.2019). entire document	1-5, 7, 8, 16-25
A	US 2008/0267942 A1 (BOYLE et al) 30 October 2008 (30.10.2008) entire document	1-5, 7, 8, 16-25
A	US 2011/0275670 A1 (CHAPMAN et al) 10 November 2011 (10.11.2011) entire document	1-5, 7, 8, 16-25
A	US 2007/0021606 A1 (EGLE et al) 25 January 2007 (25.01.2007) entire document	1-5, 7, 8, 16-25
A	FRANCO et al. "Correcting mitochondrial fusion by manipulating mitofusin conformations," Nature, 24 October 2016 (24.10.2016), Vol 540, No. 7631, Pgs. 74-79. entire document	1-5, 7, 8, 16-25

☒ Further documents are listed in the continuation of Box C. ☐ See patent family annex.

* Special categories of cited documents:

"A" document defining the general state of the art which is not considered to be of particular relevance

"E" earlier application or patent but published on or after the international filing date

"L" document which may throw doubts on priority claim(s) or which is cited to establish the publication date of another citation or other special reason (as specified)

"O" document referring to an oral disclosure, use, exhibition or other means

"P" document published prior to the international filing date but later than the priority date claimed

"T" later document published after the international filing date or priority date and not in conflict with the application but cited to understand the principle or theory underlying the invention

"X" document of particular relevance; the claimed invention cannot be considered novel or cannot be considered to involve an inventive step when the document is taken alone

"Y" document of particular relevance; the claimed invention cannot be considered to involve an inventive step when the document is combined with one or more other such documents, such combination being obvious to a person skilled in the art

"&" document member of the same patent family

Date of the actual completion of the international search	Date of mailing of the international search report
25 February 2019	18 MAR 2019
Name and mailing address of the ISA/US Mail Stop PCT, Attn: ISA/US, Commissioner for Patents P.O. Box 1450, Alexandria, VA 22313-1450 Facsimile No. 571-273-8300	Authorized officer Blaine R. Copenheaver PCT Helpdesk: 571-272-4300 PCT OSP: 571-272-7774

INTERNATIONAL SEARCH REPORT

International application No.
PCT/US2018/060177

Box No. I Nucleotide and/or amino acid sequence(s) (Continuation of item 1.c of the first sheet)

1. With regard to any nucleotide and/or amino acid sequence disclosed in the international application, the international search was carried out on the basis of a sequence listing:

   a. ☒ forming part of the international application as filed:

      ☒ in the form of an Annex C/ST.25 text file.

      ☐ on paper or in the form of an image file.

   b. ☐ furnished together with the international application under PCT Rule 13*ter*.1(a) for the purposes of international search only in the form of an Annex C/ST.25 text file.

   c. ☐ furnished subsequent to the international filing date for the purposes of international search only:

      ☐ in the form of an Annex C/ST.25 text file (Rule 13*ter*.1(a)).

      ☐ on paper or in the form of an image file (Rule 13*ter*.1(b) and Administrative Instructions, Section 713).

2. ☐ In addition, in the case that more than one version or copy of a sequence listing has been filed or furnished, the required statements that the information in the subsequent or additional copies is identical to that forming part of the application as filed or does not go beyond the application as filed, as appropriate, were furnished.

3. Additional comments:

SEQ ID NOs: 1-20 were searched.

INTERNATIONAL SEARCH REPORT

International application No.
PCT/US2018/060177

C (Continuation). DOCUMENTS CONSIDERED TO BE RELEVANT

Category*	Citation of document, with indication, where appropriate, of the relevant passages	Relevant to claim No.
A	"SID 345345044," PubChem Substance Database, National Center for Biotechnology Information, 09 October 2017 (09.10.2017), Pgs. 1-5. Retrieved from the Internet: <https://pubchem.ncbi.nlm.nih.gov/substance/345345044> on 16 January 2019 (16.12.2019). entire document	1-5, 7, 8, 16-25
A	US 9,708,411 B2 (SHI) 18 July 2017 (18.07.2017) entire document	1-5, 7, 8, 16-25
A	US 2012/0141527 A1 (WALENSKY et al) 07 June 2012 (07.06.2012) entire document	1-5, 7, 8, 16-25

INTERNATIONAL SEARCH REPORT

International application No.
PCT/US2018/060177

Box No. II Observations where certain claims were found unsearchable (Continuation of item 2 of first sheet)

This international search report has not been established in respect of certain claims under Article 17(2)(a) for the following reasons:

1. ☐ Claims Nos.:
because they relate to subject matter not required to be searched by this Authority, namely:

2. ☐ Claims Nos.:
because they relate to parts of the international application that do not comply with the prescribed requirements to such an extent that no meaningful international search can be carried out, specifically:

3. ☒ Claims Nos.: 9-15
because they are dependent claims and are not drafted in accordance with the second and third sentences of Rule 6.4(a).

Box No. III Observations where unity of invention is lacking (Continuation of item 3 of first sheet)

This International Searching Authority found multiple inventions in this international application, as follows:
See extra sheet(s).

1. ☐ As all required additional search fees were timely paid by the applicant, this international search report covers all searchable claims.

2. ☐ As all searchable claims could be searched without effort justifying additional fees, this Authority did not invite payment of additional fees.

3. ☐ As only some of the required additional search fees were timely paid by the applicant, this international search report covers only those claims for which fees were paid, specifically claims Nos.:

4. ☒ No required additional search fees were timely paid by the applicant. Consequently, this international search report is restricted to the invention first mentioned in the claims; it is covered by claims Nos.:
1-5, 7, 8, and 16-25 to the extent that they read on a mitofusin modulating agent of 1-(3-(5-cyclopropyl-4-phenyl-4H-1,2,4-triazol-3-yl)propyl)-3-(2-methylcyclohexyl)urea, the Mfn2 protein receptor of SEQ ID NO:1, and the agonist ligand SEQ ID NO:2.

Remark on Protest

☐ The additional search fees were accompanied by the applicant's protest and, where applicable, the payment of a protest fee.

☐ The additional search fees were accompanied by the applicant's protest but the applicable protest fee was not paid within the time limit specified in the invitation.

☐ No protest accompanied the payment of additional search fees.

INTERNATIONAL SEARCH REPORT

International application No.
PCT/US2018/060177

Continued from Box No. III Observations where unity of invention is lacking

This application contains the following inventions or groups of inventions which are not so linked as to form a single general inventive concept under PCT Rule 13.1. In order for all inventions to be examined, the appropriate additional examination fees need to be paid.

Group I+: claims 1-8 and 16-25 are drawn to mitofusin modulatory agents, and methods comprising the same.

The first invention of Group I+ is restricted to a mitofusin modulatory agent, and methods comprising the same, wherein the mitofusin modulatory agent is selected to be 1-(3-(5-cyclopropyl-4-phenyl-4H-1,2,4-triazol-3-yl)propyl)-3-(2-methylcyclohexyl)urea. It is believed that claims 1-5, 7, 8, and 16-25 read on this first named invention and thus these claims will be searched without fee to the extent that they read on a mitofusin modulating agent of 1-(3-(5-cyclopropyl-4-phenyl-4H-1,2,4-triazol-3-yl)propyl)-3-(2-methylcyclohexyl)urea, the Mfn2 protein receptor SEQ ID NO:1, and the agonist ligand SEQ ID NO:2.

Applicant is invited to elect additional mitofusin modulating agents, each with specified chemical structure, to be searched in a specific combination by paying an additional fee for each set of election. An exemplary election would be a mitofusin modulatory agent, and methods comprising the same, wherein the mitofusin modulatory agent is selected to be 1-(3-(5-cyclopropyl-4-(4-fluorophenyl)-4H-1,2,4-triazol-3-yl)propyl)-3-(1-methylpiperidin-4-yl)urea. Additional mitofusin modulating agents will be searched upon the payment of additional fees. Applicants must specify the claims that read on any additional elected inventions. Applicants must further indicate, if applicable, the claims which read on the first named invention if different than what was indicated above for this group. Failure to clearly identify how any paid additional invention fees are to be applied to the "+" group(s) will result in only the first claimed invention to be searched/examined.

The inventions listed in Groups I+ do not relate to a single general inventive concept under PCT Rule 13.1, because under PCT Rule 13.2 they lack the same or corresponding special technical features for the following reasons:

The Groups I+ formulas do not share a significant structural element responsible for treating a peripheral nervous system or central nervous system injury, requiring the selection of alternatives for the mitofusin modulatory agents, where "the mitofusin modulating agent comprises a mitofusin mini peptide or formula (I); (II); or (III); or a pharmaceutically acceptable salt, tautomer, or stereoisomer thereof".

Additionally, even if Groups I+ were considered to share the technical features a method of treating a peripheral nervous system (PNS) or central nervous system (CNS) injury comprising: administering to a subject a therapeutically effective amount of a composition comprising one or more of a mitofusin modulating agent or a pharamaceutically acceptable salt thereof, wherein the mitofusin modulating agent regulates mitochondrial fusion, enhances axonal regeneration, neuronal regeneration, or enhances mitochondrial transport; a method of designing a peptide mimetic comprising: (i) providing an HR1-derived mini-peptide that competes with endogenous HR1-HR2 binding; (ii) functionally analyzing a complete series of alanine substituted peptides by structural modeling of functional amino acid side chains of mitofusin (Mfn)-derived mini-peptides, thereby identifying functionally-critical amino acid side chains; (iii) identifying a chemical structure that mimics the 3-dimensional spatial and charge characteristics of these functional amino acid side chains; and (iv) designing a peptide mimetic based on the identified chemical structure; a method of screening and evaluating one or more candidate molecules for mitochondrial fusion modulatory activity, the method comprising: (i) providing a Mfn2 protein receptor comprising a HR2 peptide sequence or a fragment of Mfn2 comprising an HR2 domain; (ii) immobilizing the receptor on a solid substrate to generate a bound substrate; (iii) contacting the immobilized receptor to amino-FITC-tagged agonist ligand or amino-FITC-tagged antagonist ligand; (iv) incubating at least one candidate molecule with a combination comprising a labeled peptide and a bound substrate to generate a test assay mixture; and (v) detecting or measuring a signal present at the location of a bound substrate; a method of screening one or more candidate molecules for mitochondrial fusion modulatory activity comprising: (i) labeling a first Mfn2 protein with an acceptor fluorophore within or near the HR2 domain to generate a first labeled Mfn2 protein; (ii) labeling a second Mfn2 protein with a donor fluorophore to generate a second labeled Mfn2 protein; (iii) combining the first labeled Mfn2 protein or fragment thereof with the second labeled Mfn2 protein or fragment thereof to generate a control mixture; (iv) combining the first labeled Mfn2 protein or fragment thereof with the second labeled Mfn2 protein or fragment thereof and at least one candidate molecule to generate a test mixture; and (v) measuring fluorescence of the test mixture and the fluorescence of the control mixture; a method for screening one or more candidate molecules for mitochondrial fusion modulatory activity, the method comprising: (i) labeling an Mfn2 protein with an acceptor fluorophore within or near the HR1 domain and labeling the Mfn2 protein with a donor fluorophore within or near the HR2 domain to generate a labeled Mfn2 protein; (ii) combining the labeled Mfn2 protein with one or more candidate molecules to generate a test mixture; and (iii) measuring the fluorescence of the test mixture and the fluorescence of a control mixture; and mitofusin modulating agent of formulas (I), (II), or (III); these shared technical features do not represent a contribution over the prior art.

Specifically, US 9,708,411 B2 to Shi discloses a method of treating a peripheral nervous system (PNS) or central nervous system (CNS) injury (a method of preventing or treating a patient suffering from a neurological disease or disorder comprises administering to a patient a therapeutically effective amount of one or more ALCAT1 modulators... include disorders that involve the central nervous system (brain, brainstem and cerebellum), the peripheral nervous system (including cranial nerves), Col. 18, Lns. 53-61) comprising: administering to a subject a therapeutically effective amount of a composition (administering to a patient in need thereof, a therapeutically effective amount of an inhibitor of acyl-CoA lysocardiolipin acyltransferase 1 (ALCAT1), Col 3, Lns. 23-25; a pharmaceutical composition, Col. 3, Ln. 30; a modulator of ALCAT1 regulates... mitofusins, Col. 17, Lns. 21-26) comprising one or more of a mitofusin modulating agent or a pharamaceutically acceptable salt thereof (administering to a patient in need thereof, a therapeutically effective amount of an inhibitor of acyl-CoA lysocardiolipin acyltransferase 1 (ALCAT1), Col 3, Lns. 23-25; a pharmaceutical composition, Col. 3, Ln. 30; a modulator of ALCAT1 regulates... mitofusins, Col. 17, Lns. 21-26), wherein the mitofusin modulating agent regulates mitochondrial fusion, enhances axonal regeneration, neuronal regeneration, or enhances mitochondrial transport (ALCAT1 impairs mitochondrial fusion, which can be rescued by MFN2 expression in C2C12 cells, Col. 4, Lns. 43-46).

"Correcting mitochondrial fusion by manipulating mitofusin conformations" to Franco et al. discloses a method of screening and evaluating one or more candidate molecules for mitochondrial fusion modulatory activity (Here we show that mitofusins adopt either a fusion-constrained or fusion-permissive molecular conformation directed by specific intramolecular binding interaction, Pg. 1, first paragraph; for screening and initial characterization, Pg. 8, bottom of second paragraph), the method comprising: (i) providing a Mfn2

protein receptor comprising a HR2 peptide sequence or a fragment of Mfn2 comprising an HR2 domain (The I-TASSER (Iterative Threading ASSEmbly Refinement) hierarchical approach to protein structure was used to derive a structural model of Mfn219, Pg. 9, top of third paragraph; two adjacent small transmembrane domains, and a carboxyl terminal second coiled-coiled heptad repeat region (HR2), Pg. 2, top of third paragraph); (ii) immobilizing the receptor on a solid substrate to generate a bound substrate (transferred onto nylon membranes, incubated with primary antibody and detected with peroxidase-conjugated anti-mouse secondary antibody, Pg. 7, second paragraph); (iii) contacting the immobilized receptor to amino-FITC-tagged agonist ligand or amino-FITC-tagged antagonist ligand (Additional studies validated the conformational shift mechanism of minipeptide action: FITC-labeled TAT-peptides decorated mitochondria in normal cells, Pg. 3, bottom of page); (iv) incubating at least one candidate molecule with a combination comprising a labeled peptide and a bound substrate to generate a test assay mixture (Binding of minipeptides to recombinant Mfn2 was positively cooperative (Figure 3b), consistent with destabilization of highly folded Mfn2 by 367-384Gly that facilitates 398-418Gly binding to newly extended carboxyl-terminal HR2 domains, bottom of page 3, top of page 4, first paragraph); and (v) detecting or measuring a signal present at the location of a bound substrate (we determined that TAT-398-418Gly promotes a more folded Mfn2 conformation using Forster resonance energy transfer (FRET) of hMfn2 tagged at the amino terminus with mCerulean1 and the carboxyl terminus with mVenus1, Pg. 4, first paragraph); a method of screening one or more candidate molecules for mitochondrial fusion modulatory activity (Here we show that mitofusins adopt either a fusion-constrained or fusion-permissive molecular conformation directed by specific intramolecular binding interaction, Pg. 1, first paragraph; for screening and initial characterization, Pg. 8, bottom of second paragraph) comprising: (i) labeling a first Mfn2 protein with an acceptor fluorophore within or near the HR2 domain to generate a first labeled Mfn2 protein (Additional studies validated the conformational shift mechanism of minipeptide action: FITC-labeled TAT-peptide, bottom of Pg. 3, Finally, we determined that TAT-398-418Gly promotes a more folded Mfn2 conformation using Forster resonance energy transfer (FRET) of hMfn2 tagged at the amino terminus with mCerulean1 and the carboxyl terminus with mVenus1, Pg. 4, first paragraph); (ii) labeling a second Mfn2 protein with a donor fluorophore to generate a second labeled Mfn2 protein (Additional studies validated the conformational shift mechanism of minipeptide action: FITC-labeled TAT-peptide, bottom of Pg. 3, Finally, we determined that TAT-398-418Gly promotes a more folded Mfn2 conformation using Forster resonance energy transfer (FRET) of hMfn2 tagged at the amino terminus with mCerulean1 and the carboxyl terminus with mVenus1, Pg. 4, first paragraph); (iii) combining the first labeled Mfn2 protein or fragment thereof with the second labeled Mfn2 protein or fragment thereof to generate a control mixture (For mitophagy studies MEFs were stained with MitoTracker Green and infected with adeno-mcherry Parkin or stained with LysoTracker Deep Red (50 nM, Invitrogen L-7528); carbonylcyanide p-trifluoromethoxyphenylhydrazone (FCCP, 10 μM for 1 hour) was applied as a positive control. Mitochondrial fusion was measured at 2 and 6 hours after PEG-mediated cell fusion of MEFs treated 48 hours previously with adeno-mitoGFP or adeno-mitoDsRed, Pg. 7, middle of fourth paragraph); (iv) combining the first labeled Mfn2 protein or fragment thereof with the second labeled Mfn2 protein or fragment thereof and at least one candidate molecule to generate a test mixture (These findings hinted at therapeutic potential of compelling endogenous normal mitofusins into their active unfolded conformation in order to overcome dominant inhibition by GTPase-defective Mfn2 mutants in diseases like CMT2A. We tested this notion in MEFs expressing the CMT2A-causal mutant hMfn2 T105M16,17 as a conditional flox/stop (fl/st) transgene, Pg. 4, top of third paragraph); and (v) measuring fluorescence of the test mixture and the fluorescence of the control mixture (was applied as a positive control. Mitochondrial fusion was measured at 2 and 6 hours after PEG-mediated cell fusion of MEFs treated 48 hours previously with adeno-mitoGFP or adeno-mitoDsRed14. Laser confocal fluorescence was excited with 561 nm (MitoTracker Green, GFP, FITC), 637 nm (TMRE, LysoTracker Red, mcherry-Parkin, MitoTracker Orange) or 408 nm (Hoechst) laser diodes, Pg. 7, bottom of page); a method for screening one or more candidate molecules for mitochondrial fusion modulatory activity (Here we show that mitofusins adopt either a fusion-constrained or fusion-permissive molecular conformation directed by specific intramolecular binding interaction, Pg. 1, first paragraph; for screening and initial characterization, Pg. 8, bottom of second paragraph), the method comprising: (i) labeling an Mfn2 protein with an acceptor fluorophore within or near the HR1 domain and labeling the Mfn2 protein with a donor fluorophore within or near the HR2 domain to generate a labeled Mfn2 protein (Additional studies validated the conformational shift mechanism of minipeptide action: FITC-labeled TAT-peptide, bottom of Pg. 3, Finally, we determined that TAT-398-418Gly promotes a more folded Mfn2 conformation using Forster resonance energy transfer (FRET) of hMfn2 tagged at the amino terminus with mCerulean1 and the carboxyl terminus with mVenus1, Pg. 4, first paragraph); (ii) combining the labeled Mfn2 protein with one or more candidate molecules to generate a test mixture (These findings hinted at therapeutic potential of compelling endogenous normal mitofusins into their active unfolded conformation in order to overcome dominant inhibition by GTPase-defective Mfn2 mutants in diseases like CMT2A. We tested this notion in MEFs expressing the CMT2A-causal mutant hMfn2 T105M16,17 as a conditional flox/stop (fl/st) transgene, Pg. 4, top of third paragraph); and (iii) measuring the fluorescence of the test mixture and the fluorescence of a control mixture (was applied as a positive control. Mitochondrial fusion was measured at 2 and 6 hours after PEG-mediated cell fusion of MEFs treated 48 hours previously with adeno-mitoGFP or adeno-mitoDsRed14. Laser confocal fluorescence was excited with 561 nm (MitoTracker Green, GFP, FITC), 637 nm (TMRE, LysoTracker Red, mcherry-Parkin, MitoTracker Orange) or 408 nm (Hoechst) laser diodes, Pg. 7, bottom of page).

US 2011/0275670 A1 to Chapman et al. discloses a compound of formula I, where R1 is C5 cycloalkyl, R2 is C6 heteroaryl, R3 is absent, R4 is H, X is N, Y is O, Z is CH2, and A is a bond (1-methylpiperidin-4-yl)methyl cyclopentylcarbamate hydrochloride, Para. [0134]); see structure, Para. [0133]).

US 2008/0267942 A1 to Boyle et al. discloses a compound of formula (II), where R5 is methyl, R6 is benzimidazole, and Z is ethyl (Specifically, as shown in Scheme I, the ketone of formula (XXXV) may be prepared, Para. [0082]; see structure (XXXV) in Scheme J, just above Para. [0082]).

"SID: 345345044" to PubChem discloses a compound of formula III, where R9 is methyl, and R8 and R7 form a cyclic group (3-methyl-5-(thiolan-2-yl)-1,2,4-oxadiazole, see structure Pg. 3).

The inventions listed in Groups I+ therefore lack unity under Rule 13 because they do not share a same or corresponding special technical features.